Journal of Chemistry

Innovations in Green Plant Protection and Food Storage Technology

Lead Guest Editor: Pei Li
Guest Editors: Lu Yu, Wenneng Wu, and Xiaotian Tang

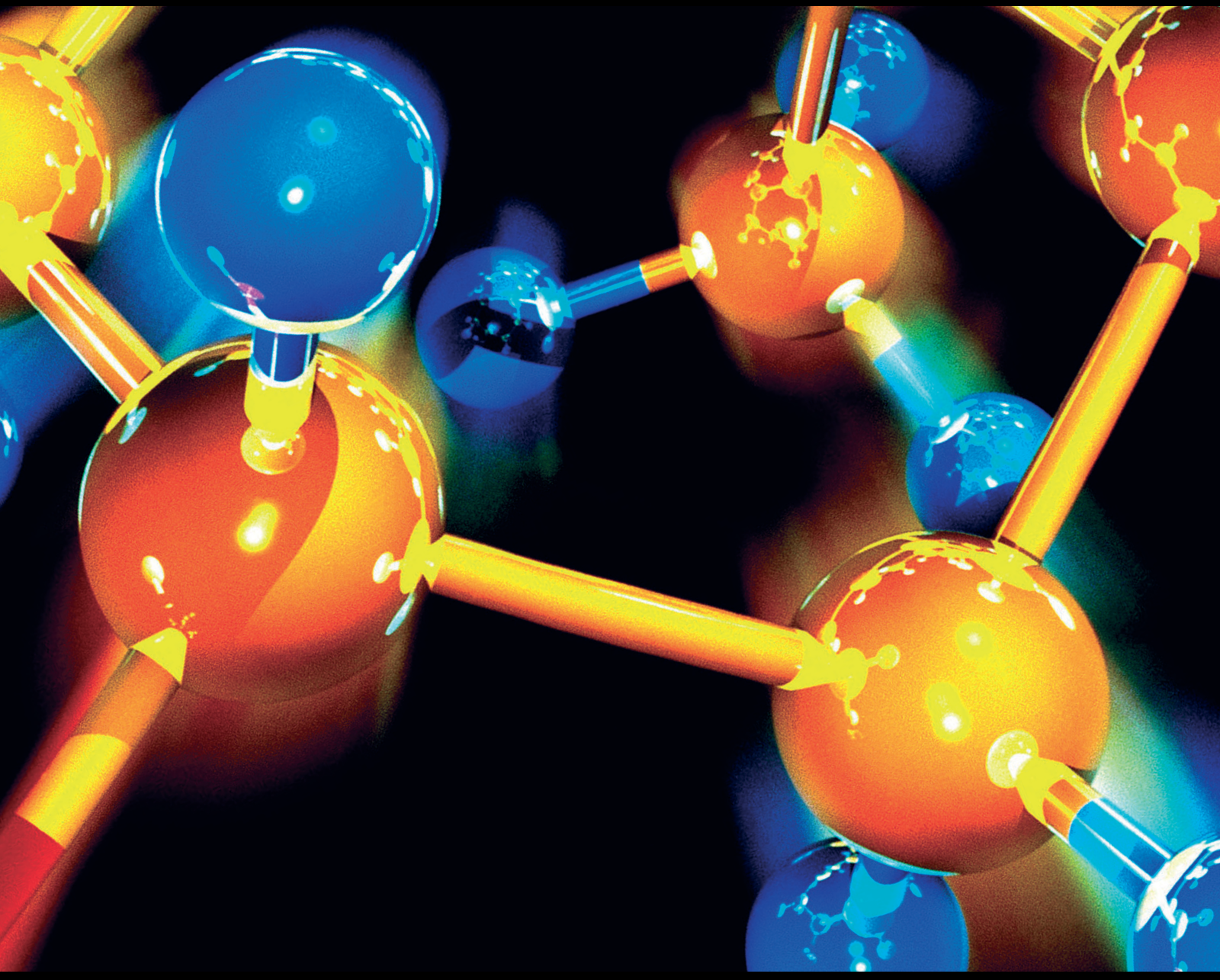

Innovations in Green Plant Protection and Food Storage Technology

Journal of Chemistry

Innovations in Green Plant Protection and Food Storage Technology

Lead Guest Editor: Pei Li
Guest Editors: Lu Yu, Wenneng Wu, and Xiaotian Tang

Contents

Transcriptome Profiling of Different State Callus Induced from Immature Embryo in Maize
Kaiwu zhang, Dengxiang Du, and Wei Wang
Research Article (12 pages), Article ID 6237298, Volume 2022 (2022)

Chemical Constituents of *Plectranthus tomentosa* Extract and Its Control Effect on *Tetranychus kanzawai*
Yuehua Sun, Tianlei Liu, Cuiying Sun, and Qing Luo
Research Article (6 pages), Article ID 5609391, Volume 2022 (2022)

Identification of Pathogens and Laboratory Activity Test of Kiwifruit Rot Disease in Guizhou Province, China
Tao Wang, Yanling Ren, Jinyu Zhao, Yingjie Jiang, Jian Tang, Yao Liu, Chao Liu, Juan Wang, Xiaolei Ji, and Mingyan Wang
Research Article (7 pages), Article ID 6893691, Volume 2022 (2022)

Metabolomics Study on the Resistance of Walnut Peel to *Colletotrichum gloeosporioides* under Prochloraz Treatment
Xia Yang, Liuyan Wu, Li Fu, Pin Fu, Jiamin Zhu, Yuxue Zhao, and Jing Liu
Research Article (7 pages), Article ID 7613285, Volume 2022 (2022)

Identification of the Pathogens and Laboratory Bioactivity Determination of the Rot Disease of Kiwifruit (*Actinidia* spp.)
Yanling Ren, Tao Wang, Jian Tang, Yingjie Jiang, Yaxin Huang, Chengping Zhang, Jing Peng, Juan Wang, Shanshan Wang, and Jing Wang
Research Article (9 pages), Article ID 2293297, Volume 2022 (2022)

A Systematic Review of Photolysis and Hydrolysis Degradation Modes, Degradation Mechanisms, and Identification Methods of Pesticides
Xingang Meng, Yuanjun Guo, Yihui Wang, Shijun Fan, Kaiqi Wang, and Wenhua Han
Review Article (13 pages), Article ID 9552466, Volume 2022 (2022)

Comparing the Transcriptomes of Two Different Tissues in *Helicoverpa assulta* (Guenée)
Hailing Zhang, Kuiyin Li, and Yubo Zhang
Research Article (7 pages), Article ID 3820942, Volume 2022 (2022)

The Efficacy of Chlorantraniliprole as a Seed Treatment for *Mythimna separata* (Walker) (Lepidoptera: Noctuidae)
Hongbo Li, Changgeng Dai, and Yang Hu
Research Article (6 pages), Article ID 3781567, Volume 2022 (2022)

Identification and Laboratory Fungicides Screening of the Pathogenic Fungus of Stem Spot of Pitaya (*Hylocereus* spp.) Stems
Hui Luo, Kun Guo, Xueying Shang, Lei Peng, Zhijun Peng, Jilin Jin, Bin Wang, and Xingwu Zhang
Research Article (4 pages), Article ID 3546266, Volume 2022 (2022)

Novel Karaya Gum Derivatives Produced by Alkaline Hydrolysis and Periodate Oxidation for Active Packaging with Cinnamaldehyde
Vinh Tien Nguyen, Nga Thi Vo, Hoan Thi Pham, Duy Quang Nguyen, Anh Thai Nguyen, and Khanh Son Trinh
Research Article (11 pages), Article ID 3939911, Volume 2022 (2022)

Analysis of Bacterial Community Composition and Ecological Function during Soft Rot Process in Pitaya (*Hylocereus* spp.) Stems
Zhijun Peng, Jingqiang Guan, Dan Mou, Xiao Zou, Bin Wang, Jilin Jin, Xingwu Zhang, and Hui Luo
Research Article (8 pages), Article ID 9169433, Volume 2022 (2022)

Design, Synthesis, and Antifungal Activity of Novel Benzimidazole Derivatives Bearing Thioether and Carbamate Moieties
Lei Yang
Research Article (4 pages), Article ID 8646557, Volume 2022 (2022)

Study on the Absorption and Conduction Properties of Vanisulfane in Tobacco
Xingang Meng, Fei Li, and Qian Huang
Research Article (9 pages), Article ID 6249042, Volume 2022 (2022)

Synthesis and Bioactivity Evaluation of Novel Thiochroman-4-One Derivatives Incorporating Carboxamide and 1, 3, 4-Thiadiazole Thioether Moieties
Lu Yu, Lingling Xiao, Pei Li, Jiyan Chi, Jie Li, and Shuming Tan
Research Article (7 pages), Article ID 5354088, Volume 2022 (2022)

Research on Crystal Structure and Fungicidal Activity of the Amide Derivatives Based on the Natural Products Sinapic Acid and Mycophenolic Acid
Zhanfang Chen, Hongbin Fang, Xuewen Hua, Wenrui Liu, Yi Liu, Chenmeng Xue, Bingxiang Wang, Dzmitry Bazhanau, Xiaohe Zhu, Man Yuan, Jing Ru, and Pengfei Chu
Research Article (10 pages), Article ID 1036199, Volume 2021 (2021)

Establishment of Tissue Culture System of *Actinidia deliciosa* Cultivar "Guichang"
Weimin Zhong, Junliang Zhou, Dongmei Tang, Yaxin Huang, Futao Liu, Min Zhang, Guoli Wang, Sufang Wu, Yue He, and Jingwen Tang
Research Article (9 pages), Article ID 9951949, Volume 2021 (2021)

Comparative Transcriptomic Analysis of Root Cadmium Responses in Two Chinese Rice Cultivars Yuzhenxiang and Xiangwanxian 12
Shangdu Zhang, Zhenliang Luo, Xiang Wu, Bangzhi Shi, Huidan Jiang, Leliang Zhou, and Lianyang Bai
Research Article (11 pages), Article ID 2166775, Volume 2021 (2021)

Study of the Physiological Dynamics of Cadmium Accumulation in Two Varieties of Rice with Different Cadmium-Accumulating Properties
Shangdu Zhang, Xiang Wu, Ju Peng, Xiufei Meng, Bangzhi Shi, Leliang Zhou, and Lianyang Bai
Research Article (12 pages), Article ID 6238893, Volume 2021 (2021)

Contents

Physiological Responses and Proteomic Analysis on the Cold Stress Responses of Annual Pitaya (*Hylocereus* spp.) Branches
Junliang Zhou, Lijuan Wang, Tujian Xiao, Zhuang Wang, Yongya Mao, and Yuhua Ma
Research Article (12 pages), Article ID 1416925, Volume 2021 (2021)

Hindawi
Journal of Chemistry
Volume 2022, Article ID 6237298, 12 pages
https://doi.org/10.1155/2022/6237298

Research Article

Transcriptome Profiling of Different State Callus Induced from Immature Embryo in Maize

Kaiwu zhang,[1] Dengxiang Du,[2] and Wei Wang [1]

[1]*Guizhou Institute of Upland Food Crops, Guizhou Academy of Agricultural Sciences, Guiyang 550006, China*
[2]*School of Life Science and Technology, Wuhan Polytechnic University, Wuhan 430023, China*

Correspondence should be addressed to Wei Wang; wwmaize@126.com

Kaiwu zhang and Dengxiang Du contributed equally to this work.

Received 5 May 2022; Accepted 2 August 2022; Published 13 September 2022

Academic Editor: Pei Li

Embryogenic and regenerable tissue cultures are widely used in plant transformation. To dissect the molecular mechanism of embryogenesis, we used inbred line A188 as the material; the immature embryo of kernels (15 day after pollination, 15DAP) was isolated and cultured in inducing medium and subjected to RNA-Seq. The results revealed that 5,076 differentially expressed genes (DEGs) were involved in morphological and histological changes and endogenous indole-3-acetic acid (IAA) alteration. Functional analysis showed that the DEGs were related to metabolic pathways and biosynthesis of secondary metabolites. In particular, ARF16 and ARF8 genes of auxin response factors (ARF) were upregulated from EC to IDC and EC to IRC. Meanwhile, BBM2, SERK1, and SERK2 genes of the embryogenic pathway were upregulated, and WIP2 and ESR genes of the wound-inducible were upregulated from EC to IDC and EC to IRC. These changes can improve conversion efficiency from EC to IRC, which is important for elucidating the underlying molecular mechanisms of callus formation.

1. Introduction

Maize is the main feed and food crop in the world and is very important for humans and livestock. In recent years, maize has changed from a single food crop and feed crop to a cash crop and industrial raw material. The genetic improvement of food crops, including conventional technology and biotechnology, is important for the needs of 8.3 billion people [1, 2]. Currently, most of the maize genetic engineering systems still greatly depend on callus induction from young embryos (called embryonic callus), which is the prerequisite for the genetic transformation of maize inbred lines [3]. The genetic transformation of maize mainly depends on the in vitro callus formation of young embryos, which is the process of plant cells to regain totipotency and is an important process of plant cell fate transformation. Callus induction from young embryos is strongly genotype-dependent; only specific genotypes have embryogenic competence in tissue culture and are able to develop callus [4]. The study shows that the callus induction rate of maize is related to the genotype of maize. Many maize inbred lines barely induce callus formation or the callus induction rate is very low [5–7]. Therefore, this genotype-dependent culture limits the application of crop improvement [8].

Callus formation is an important factor affecting maize genetic transformation efficiency, and the regulatory molecular mechanisms of embryogenesis remain unclear. It is commonly believed that embryogenesis mainly involves lots of cell reprogramming and signal activation [9, 10]. The efficiency of embryogenesis dedifferentiation is a quantitative trait, which is controlled by additive gene effects. Pan et al. mapped five QTLs (quantitative trait loci) on chromosomes 1, 3, 7, and 8 by composite interval mapping, which explained 5.25–23.4% of the phenotypic variation [11, 12].

Inbred line A188 has been widely used in genetic improvement due to its high embryogenic efficiency and regeneration ability [13–17]. To reveal the molecular mechanisms of callus induced and/or regeneration, immature embryo of A188 was cultured in the initiation and regeneration medium, and the transcriptome on callus (at

different states) of the A188 was analyzed by RNA-sequencing (RNA-Seq). We expect to find key genes of embryo-derived embryonic callus and provide a foundation for crop tissue culture.

2. Materials and Methods

2.1. Plant Material and Tissue Culture. The maize inbred line A188 was grown in an experimental field at the Huazhong Agricultural University (Wuhan, China). Ears were harvested at the 15th DAP (days after pollination), and the immature embryo was isolated and cultured in N6 medium (Table S1) at 28°C for 60 days [18, 19]. Callus can be divided into three types according to the characteristics of color, hardness, and granulation. The callus, with bright color and similar dryness, was embryogenic. The callus without complete dedifferentiation showed that most radicles and buds were present, and there were no small granular thin-wall callus cells. The other kind of callus was dark brown and could not be cultured in bands. The embryogenic callus was selected for further culture, and a large number of embryogenic calluses were transferred to the differentiation medium for differentiation. The culture conditions were 28°C and 16/8 h photoperiod, and regeneration seedlings were obtained after 30 days.

2.2. RNA-Seq Library Construction and Sequencing. Total RNA was isolated from callus after morphological classification using a plant RNA kit (OMEGA) [20]. RNA quality was checked by the Bioanalyzer (2100, Agilent Technologies, Palo Alto, CA, USA). The mRNA was enriched using oligo (dT) magnetic beads [21]. The target mRNA was reversely transcribed to cDNA, phosphorylated at the 5′ end, adhered to "A" base at the 3′ end, and ligated with adapters [22, 23]. The products were amplified by two specific primers and prepared using the Illumina TruSeq Stranded Total RNA HT Library Preparation Kit (Illumina). Transcriptional sequencing was performed on the Illumina HiSeqTM 2500 by Shanghai OE Biotech Co., Ltd.

2.3. Sequencing Analysis and Differential Expression Analysis. The B73 reference genomic and annotated files were used as the database [24]. The software HTSEQ-count was used to the reads of each gene [25, 26], and the software Cufflinks was used to calculate the FPKM (fragments per kilobase per million mapped fragments) values [27].

The reads containing ploy-N and the low-quality reads of raw data were removed using Trimmomatic [28, 29]. The resulting clean reads were mapped to the B73 reference genome [26]. DEGs were identified using the DESeq according to the following criteria-fold change >2 and corrected P value < 0.05 [30–36]. All DEGs were mapped to each term in the gene ontology database (http://www.geneontology.org/), and Gene Ontology (GO) enrichment analysis was performed using WEGO 2.0 [37–39]. Pathway enrichment analysis of DEGs was performed using the Kyoto Encyclopedia of Genes and Genomes (KEGG) database (http://www.genome.jp/kegg/) [40]. The GO terms and pathways with P value ≤ 0.05 and FDR≤0.01 were considered to be significantly enriched in DEGs [23].

2.4. Real-Time PCR Validation. Eight DEGs were selected for qRT-PCR verification. The primers were designed using Primer Premier 5.0. Total RNA was reversely transcribed into cDNA using a cDNA synthesis kit (Thermo Fisher Science). The qRT-PCR was performed using the CFX96 Real-time system [41, 42], according to the method used by Petersen [43], and actin was used as the internal reference. The standard error among the three biological replicates was calculated.

2.5. Accession Numbers. The raw data of RNA-Seq have been submitted to https://ngdc.cncb.ac.cn/:PRJCA009242. Temporary Submission ID: subPRO013562; PRJCA009242 records will be accessible upon publication on the indicated release date.

3. Results

3.1. Callus Culture and Phenotype Identification. According to transformation of morphological feature, after three cycles of induction culture, callus was produced in most of the immature embryo, and callus obtained can be divided into three categories, according to the morphological characteristics (Figure 1). A part of the callus which only expanded, accompanied by a large number of non-removable root bud structures, was named incomplete dedifferentiation callus (IDC). However, in the materials that produced callus, two kinds of callus exist simultaneously: callus that was yellow, loose, and small granular, and the other was the browning dead, which cannot be further cultured, which were named embryonic callus (EC) and browning dead callus (BDC), respectively. Regeneration plants were redifferentiated from the embryogenic callus, and incipient callus was produced. After 10 days of regeneration, incipient redifferentiation callus (IRC) was produced on the regeneration medium.

3.2. Statistical of Transcriptome Data. Thirty calluses with the same growth state were selected from each material, and RNA was extracted after mixing. The callus in each state was repeated twice. A total of eight libraries was established from four turntable callus for transcriptome sequencing analysis. Overall, 32.76 G of data was obtained in total, with Q30 bases distributed in 91.96–92.35%, and the average GC content was 54.41% (Table S2). The genome alignment ratio of each sample was 88.80–90.23%; after removing the low-quality tags, 35066073 (84.84%), 34749515 (83.76%), 34788501 (84.58%), 35596745 (86.45%), 35315481 (85.46%), 35923796 (86.50%), 35012769 (84.70%), and 35563113 (83.11%) clean tags were left. According to the comparison between the sequences and the exons of the reference genome, 60.78–62.77% of the sequences were completely compared to the exons, and 20.44–24.01% of the single-ended forces were compared to the exons. Reads mapped in proper pairs showed 78.70% (EC-1), 77.47% (EC-2), 77.60% (IDC-1), 79.91% (IDC-2), 78.82% (BDC-1), 80.25% (BDC-2), 78.08% (IRC-1), and 76.16% (IRC-2), separately.

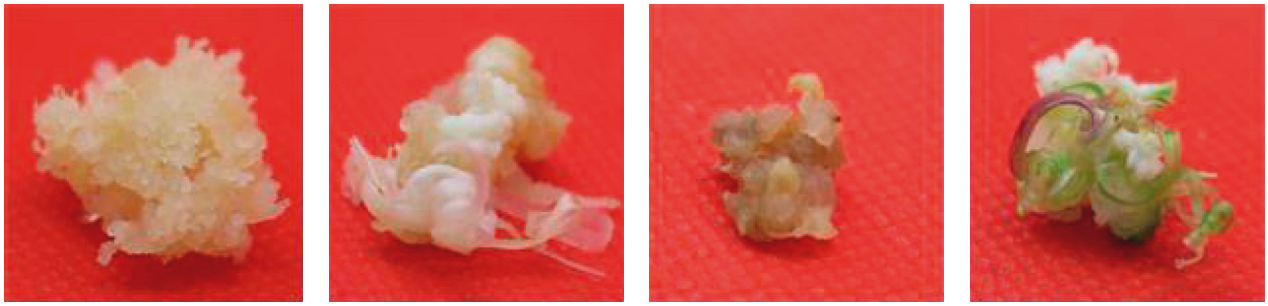

(a) (b) (c) (d)

Figure 1: Morphological stages of callus genesis in maize from immature embryos. (a) Embryonic callus (EC) that were yellow, loose, and small granular. (b) Callus, which only expanded (IDC), accompanied by a large number of nonremovable root bud structures. (c) Browning dead callus (BDC), which cannot be further cultured. (d) Incipient redifferentiation callus (IRC) produced on the regeneration medium.

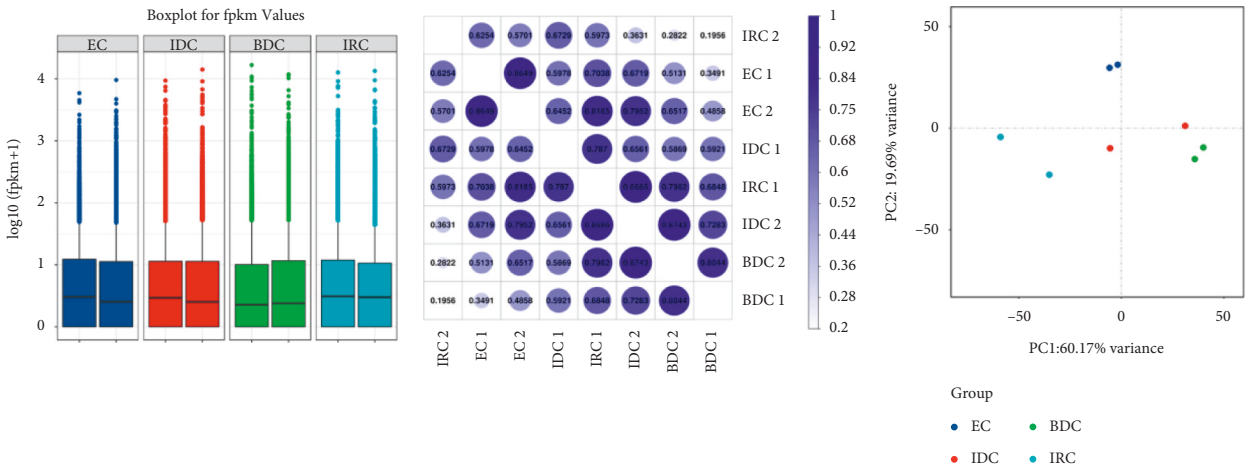

(a) (b) (c)

Figure 2: Gene expression changes in different states callus. (a) Boxplot of gene expression level. The x-coordinate is the sample name; the y-coordinate is log10 (FPKM +1). Gene expressions of each sample are shown in table under the boxplot. (b) Heat map of correlation coefficient between samples. (c) Principal component analysis for normalized reads for all 8 samples.

3.3. Gene Expression Level Analysis among Different State Callus. According to the differences in gene expression number and gene expression value distribution in samples (Figure 2(a)), the expression value (FPKM) was divided into four intervals (Table S3). There are 10,630 genes with more than 0.5–1(FPKM), 1,701 genes with 1–10 (FPKM), and 14,499 genes with FPKM≥10 in EC1. Meanwhile, in EC2, there were 10,409 genes with expression levels between 0.5 and 1, 1,768 genes with expression levels between 1 and 10, and 15,342 genes with expression levels greater than 10, using the FPKM value as the standard. In IDC callus, the number of genes in the expression range FPKM <0.5, 0.5 < FPKM <1, 1 < FPKM <10, and FPKM≥10 was 9516 and 9441, 11123 and 10328, 1835 and 1847, and 14457 and 15315, respectively. The number of genes expressed in BDC callus was between 8662 and 9639 (FPKM <0.5), 10582 and 9856 (0.5 < FPKM <1), 1984 and 1767 (1 < FPKM <10), and 15703 and 15669 (FPKM≥10), respectively. In the differentiated callus (IRC), with the FPKM value as parameter, 9831 and 8996 genes were expressed at less than 0.5, respectively, in the two groups of materials. There were 11094 genes and 11852 genes with 0.5–1 expression levels in the two groups of materials, respectively. The number of genes with expression levels between 1 and 10 (FPKM) was between 1797 and 1835, respectively. The number of genes with expression levels greater than or equal to 10 (FPKM) was between 14209 and 14284, respectively, in two replicates.

The function of highest expressed genes involves serine-type endopeptidase inhibitor activity, RNA binding, ATP binding, polysaccharide catabolic process, and DNA binding. *sci1* is annotated as a response to wounding by-product subtilisin-chymotrypsin inhibitor homolog 1. Another gene related to plant defense that was among the highest expressed genes was LOC100283098, which was with an FPKM value of 11648.33 at BDC, which decreased over 2-fold to IDC (5769.86) and IRC (5122.97), respectively. The highest expressed was about 4-fold to EC with an FPKM value of 2387.30. Finally, we obtained 28,076, 28,113, 27,776, and 28,707 unique labels for four states of callus, EC, IDC, BDC, and IRC, respectively.

Meanwhile, transcripts in the different samples were analyzed to perform a correlation analysis (Figure 2(b)). The correlation coefficients between two replicates of the same

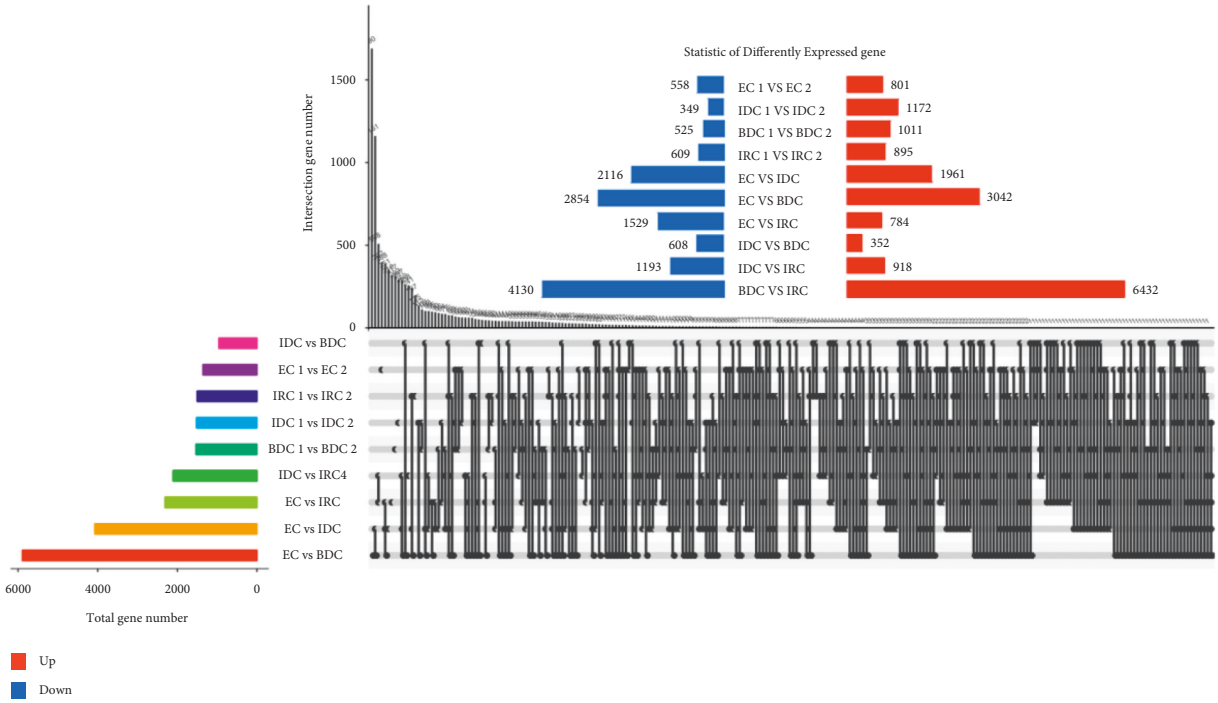

Figure 3: The statistic of DEGs counted in different tissues.

material were 0.8649 (EC 1 vs EC 2), 0.6561 (IDC 1 vs IDC 2), 0.8044 (BDC 1 vs BDC 2), and 0.5973 (IRC 1 vs IRC 2), respectively. The PCA results of the 8 samples showed a clear separation between the different stages of callus (Figure 2(c)). Additionally, the replicates of each treatment clustered together.

The trend of gene expression, the stability, and data reliability of transcriptome analysis by correlation analysis and PCA analysis were analyzed. Correlation analysis results also showed a similar trend, that is, there was a significant correlation between the same type of tissue samples, while the correlation between different tissues decreased, which was consistent with research expectations and consistent with the basis of this study. Finally, PCA analysis also showed a trend consistent with correlation analysis, with significant clustering among other materials except IDC. In general, the consistent results of the above three analyses indicated that the RNA-Seq data of all samples were credible and the differences between materials were significant, which was suitable for expression analysis of callus in different states.

3.4. Identification of Differentially Expressed Genes (DEGs). The number of DEGs between each pair of compared groups was analyzed using NOISeq [44, 45]. Venn diagrams show genes expressed consistently and differentially between repeats of different materials (Figure 3). As shown in the figure, the two groups of materials with the most DEGs were IRC and BDC, with 10,562 genes. EC and BDC followed, each with 5896 DEGs. The third largest group was 4077 DEGs in EC and IDC. Then, EC and IRC were with 2,313 DEGs. The least difference was expressed between IDC and BDC (960). The number of DEGs between different groups was 4077 genes between IDC and EC, 5896 genes between BDC and EC, 960 genes between BDC and IDC, and 2313 genes between IRC and EC.

3.5. Functional Analysis of DEGs of Callus Induction. DEGs were analyzed by Geno Ontology (GO) functional classification in IDC and BDC. These DEGs were grouped into the categories of BP (biological process, 23 GOs), CC (cellular component, 20 GOs), and MF (molecular function, 21 GOs) (Figure 4). For induced callus of different states, 1341 upregulated genes (Figure 4(a)) in IDC were significantly enriched in 49 ontologies and 1603 downregulated genes (Figure 4(a)) were significantly enriched in 52 ontologies (Figure 4(d)). The most abundant ontologies include biological regulation (GO:0065007), cellular process (GO:0009987), metabolic process (GO:0008152), and regulation of biological process (GO:0050791), single-organism process (GO:0044702), and binding (GO:0005488). Compared with EC, significantly enriched genes in BDC included 2118 upregulated genes and 2210 downregulated genes (Figure 4(b)), including 51 ontologies and 52 ontologies (Figure 4(d)), respectively. Ontology with a large number of enriched genes was highly consistent with EC vs IDC. Genes significantly differentially expressed between IDC and BDC were enriched in 47 ontologies and 50 ontologies (Figure 4(c) and Figure 4(d)). However, the number of enriched genes was significantly less than that between IDC and BDC and EC, respectively. The largest ontologies of the gene enrichment include the cellular process (GO:0009987), metabolic process (GO:0008152), and single-organism process (GO:0044702).

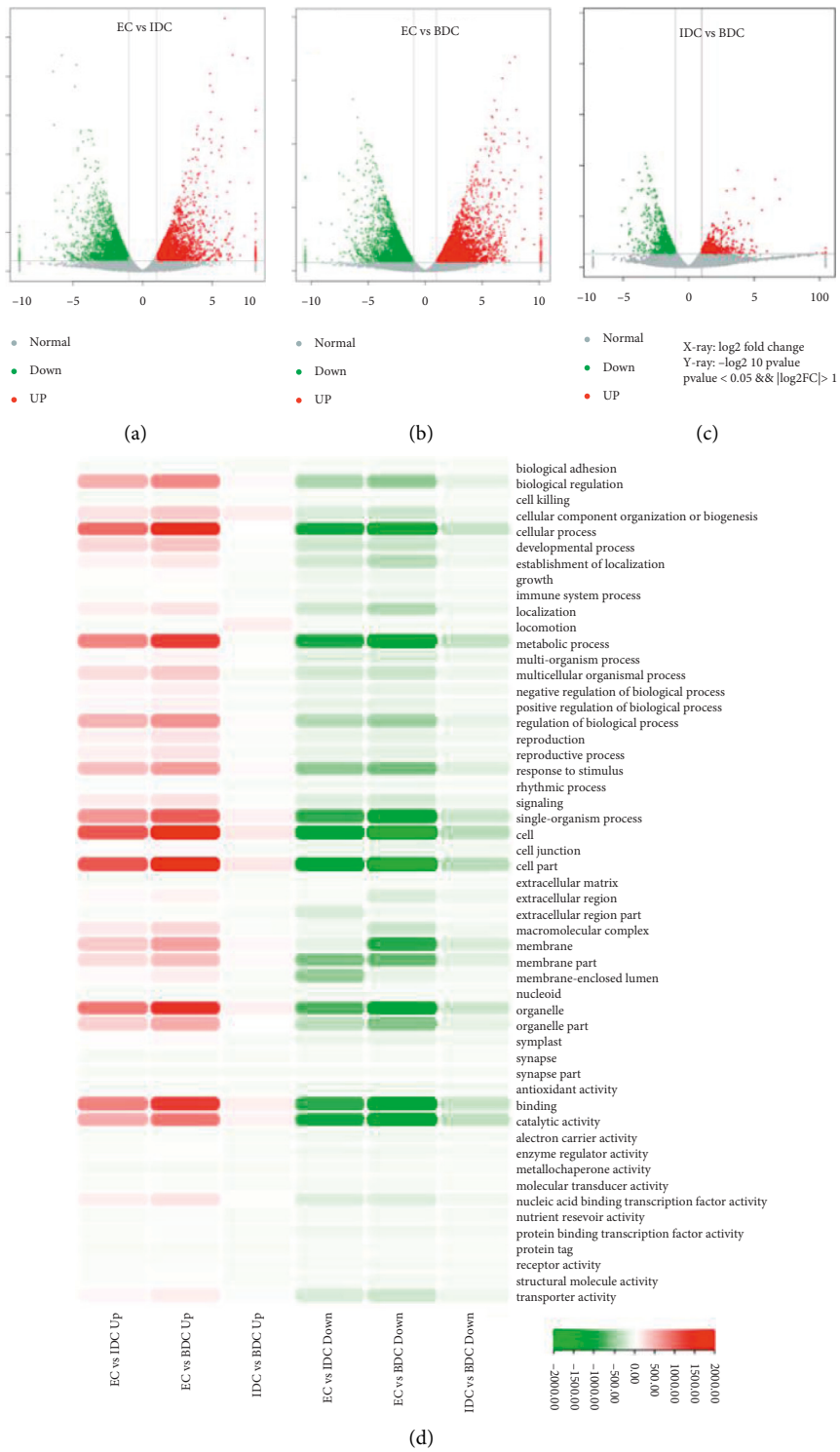

Figure 4: Identification of DEGs and Gene Ontology analysis among callus in different induction states. (a) Identification of DEGs between EC and IDC. The volcano plot presents the expression of the DEGs in different treatments, the red dots represent upregulated genes, and the green dots represent downregulated genes. (b) Identification of DEGs between EC and BDC. (c) Identification of DEGs between IDC and BDC. (d) Heat map of the gene numbers enriched of the DEGs in differential Gene Ontology. The color depth of the module represents the size of the contained genes. The darker the red, the more upregulated genes are enriched. The darker the green, the more downregulated genes are enriched.

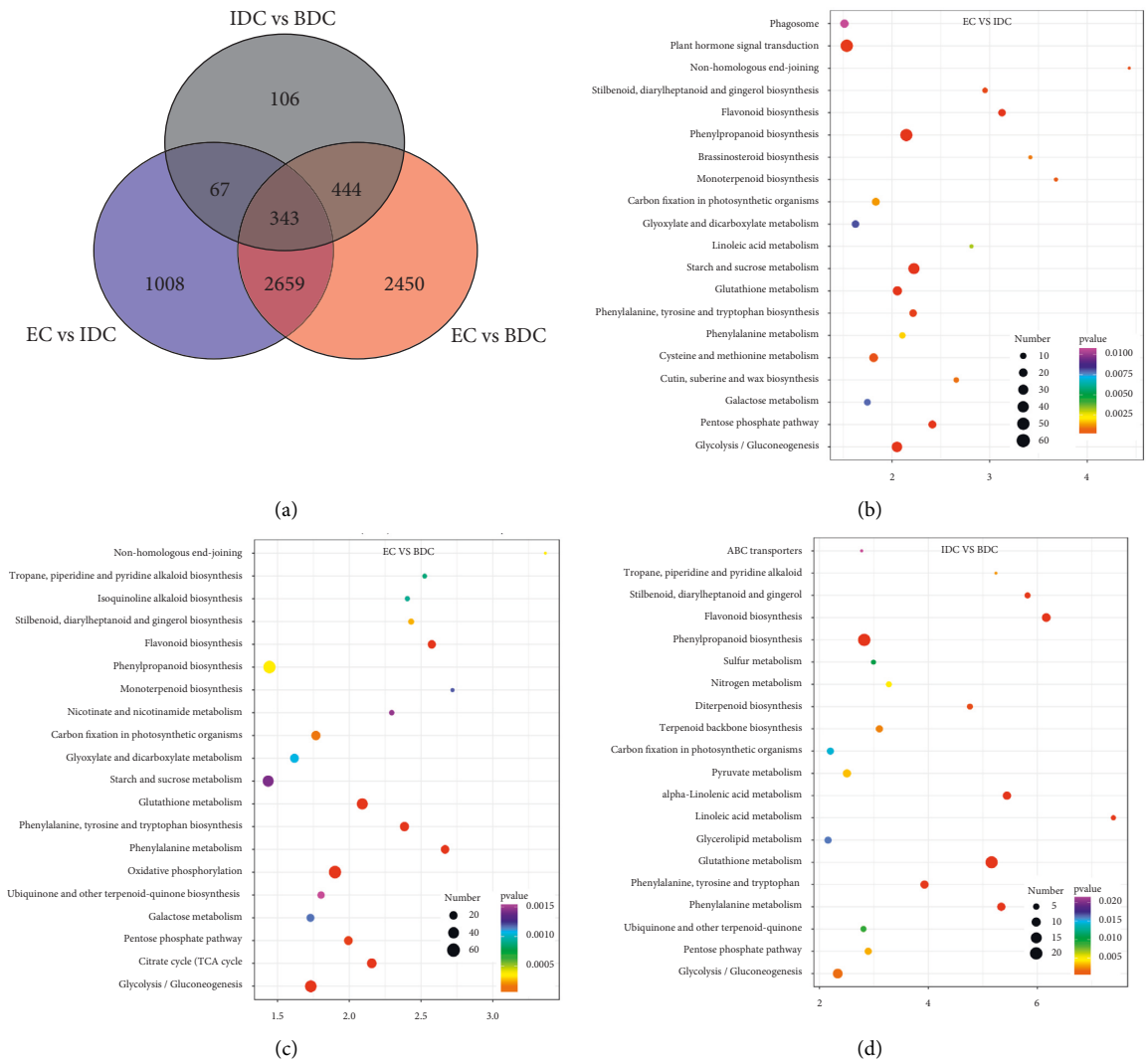

Figure 5: Functional analysis of DEGs among callus in different induction states. (a) Venn diagram of DEGs in three different states of callus. (b) KEGG analysis of DEGs between EC and IDC. The bubble map shows the KEGG enriched pathway. The larger the bubble, the more the genes; the darker the bubble color, the higher the Q-value of the DEGs. (c) KEGG analysis of DEGs between EC and BDC. (d) KEGG analysis of DEGs between IDC and BDC.

Overlap of DEGs in tissues under three different induced states is shown in Figure 5(a). There are 3002 overlaps of DEGs between EC vs IDC and EC vs BDC and 410 overlaps between EC vs IDC and IDC vs BDC. There were 787 genes that overlapped between EC vs BDC and IDC vs BDC. There were 343 DEGs in all three tissue materials. The expression levels of 343 genes are shown in Figure 5(e) and varied in different materials. In general, most of the genes maintained a low expression level in EC, and there was a certain upregulated expression level in IDC, while most of the genes in BDC showed a significant upregulated expression trend. Pathway analysis showed that DEGs were annotated into 20 KEGG pathways for each group comparison shown in Figures 5(b)–5(d). Pathways with the highest enrichment in EC vs IDC have plant hormone signal transduction, phenylpropanoid biosynthesis, starch and sucrose metabolism, and glycolysis gluconeogenesis. Between EC and BDC, pathways with the highest enrichment are glutathione metabolism and oxidative phosphorylation. Phenylpropanoid biosynthesis and glutathione metabolism are the most enriched pathways in IDC vs BDC.

3.6. Functional Analysis of DEGs of Callus Regeneration. A total of 2313 DEGs was identified between the EC and IRC tissues. GO classification analysis was related to BP, CC, and MF (Figure 6). Cellular process (GO:0009987), metabolic process (GO:0008152), single-organism process (GO: 0044702), response to stimulus (GO:0051869), and biological regulation (GO:0065007) were the top five classes in the BP. Cells (GO:0005623), cell parts (GO:0044464), organelles (GO:0043226), and membranes (GO:0016020) were the top four classes in the CC. Binding (GO:0005488) and catalytic activity (GO:0003824) were the top two classes in MF. Pathway analysis showed that DEGs were annotated into 20 pathways (Figure 6). The plant hormone signal transduction

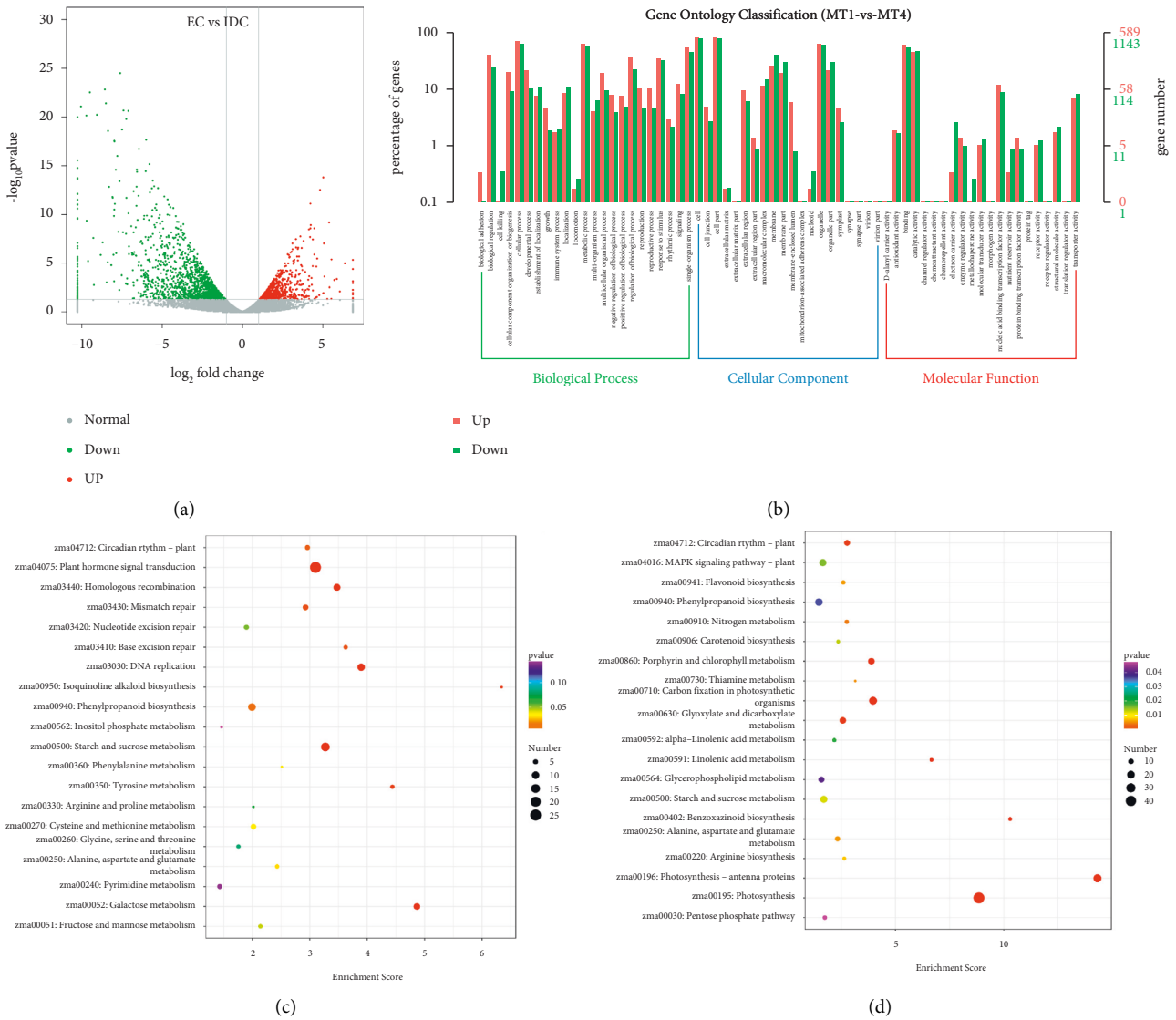

Figure 6: Statistics of functional analysis of DEGs between EC and IRC. (a) The volcano plot presenting the expression of the DEGs between EC and IRC. (b) Histogram of GO for significant clustering of DEGs in three processes. (c) KEGG analysis of upregulated gene between EC and IRC. (d) KEGG analysis of downregulated gene between EC and IRC.

and starch and sucrose metabolism were the top pathways of upregulated genes, and photosynthesis and carbon fixation in photosynthetic organisms were the down pathways of upregulated genes. For the GO analysis and KEGG enrichment, similar classes and trends were detected for newly detected transcripts.

3.7. qRT-PCR Validation. qRT-PCR was performed in order to verify the expression profile obtained by transcriptome analysis (Figure 7). A total of eight DEGs, reported to be related to callus induction, was compared with qRT-PCR and transcriptomes in the study. Overall, six DEGs showed the same trend in transcriptomes and qRT-PCR. The coincidence rate of RNA-Seq and qRT-PCR was 88.89%, indicating that RNA-Seq had high accuracy and the identified pathways and candidate genes were reliable.

4. Discussion

Maize is one of the most important crops in the world and plays an important role in agricultural production and economic life. From the establishment of DNA recombination technology in the 1970s to the emergence of the world's first transgenic plant-transgenic tobacco in 1983, the development of plant transgenic technology is changing rapidly [46]. With the development of the somatic cell regeneration system of corn and the development of transgenic technology [47, 48], based on the technology of genetically modified maize, genetic improvement technology has made a huge breakthrough, breaking reproductive isolation between species and directional import of the exogenous gene into the maize genome, so as to overcome the genetic improvement of specific traits the plight of insufficient resources [49–53]. At the same time, maize transgenic technology is still in the stage

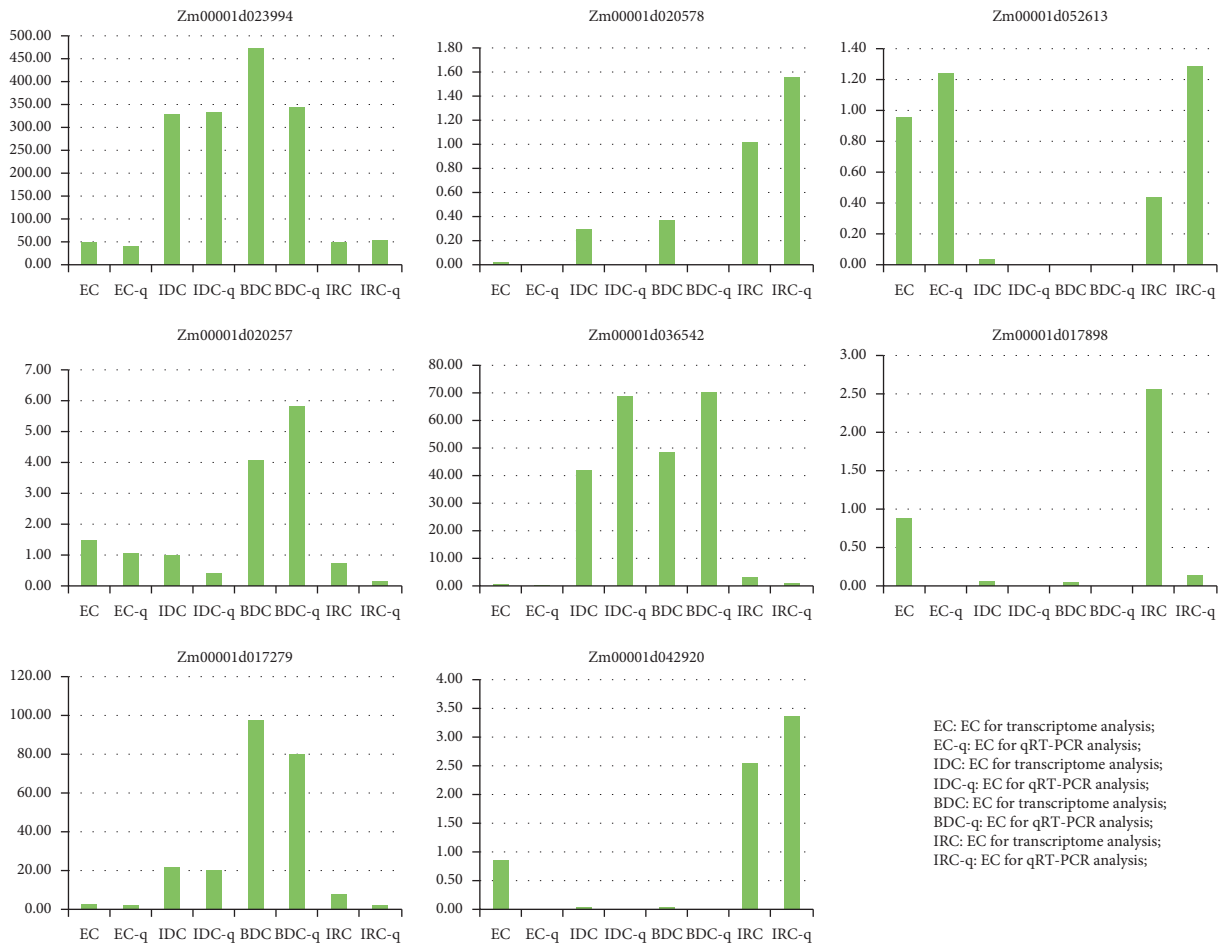

Figure 7: Expression profiles of DEGs selected based on the transcriptome analysis. qRT-PCR. EC, IDC, BDC, and IRC represent gene expression levels as a result of transcriptome analysis. EC-q, IDC-q, BDC-q, and IRC-q represent gene expression levels and were identified by qRT-PCR analysis.

of development and improvement, especially the overall domestic maize transgenic technology, which is still relatively backward, with difficult transformation operation, low transformation efficiency, limited source of transformed recipient materials, and less independently developed carrier system, which have a great impact on and limit the research and application of maize transgenic [49, 54, 55]. The establishment of a suitable transformation receptor system is a key link in maize genetic transformation. Effective somatic cell reproduction and regeneration system is one of the preconditions for plant genetic transformation, which is related to whether suitable transformation receptor materials can be provided and whether normal transgenic plants can be successfully regenerated after transformation. The establishment of a suitable transformation receptor system is a key link in maize genetic transformation [56, 57]. Effective somatic cell reproduction and regeneration system is one of the preconditions for plant genetic transformation, which is related to whether suitable transformation receptor materials can be provided and whether normal transgenic plants can be successfully regenerated after transformation [58–61].

Embryonic callus is induced by explants and can be regenerated by organogenesis and embryogenesis. Callus is a mass of parenchymal cells which can divide and proliferate continuously under hormone stimulation [62–65]. Embryonic callus can be cultured on a large scale in vitro, and it can divide continuously and remain undifferentiated in the proper medium under dark culture conditions. Studies have shown that induction of maize embryogenic callus is significantly limited by genotype, as well as affected by explant type, culture conditions, and exogenous hormones [8, 66]. The analysis of genetic mechanisms controlling embryonic callus cells is very important for understanding basic processes involved in plant tissue culture [67]. The research on the induction ability of embryonic callus has gradually become one of the focuses of researchers; embryogenesis-related genes have been authenticated in Arabidopsis [68]. To expound the molecular mechanism of somatic embryogenesis in maize, a large number of forward or reverse genetic studies have been carried out [69–71]. Previous studies showed that the callus induction ability of maize immature embryos was controlled by quantitative trait genes, and a series of QTLs loci were also identified in different maize populations [72].

RNA-Seq analyses are important for gene expression levels between different conditions [73]. In this study, transcriptome analysis was used to analyze the differential expression of callus in different induction states. The

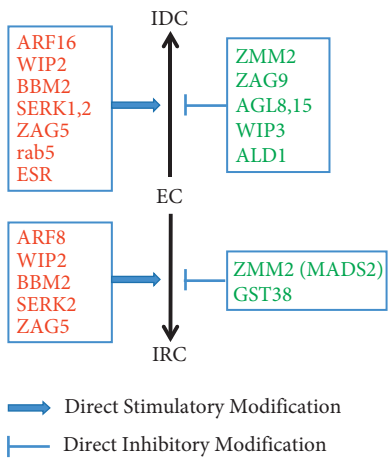

Figure 8: Expression of DEGs from EC to IDC and EC to IRC. Red means upregulated; the green means downregulated. ARF16, auxin response factors 16; wip2, wound inducible protein 2; BBM2, baby boom 2; ERK1, somatic embryogenesis receptor-like kinase 1; SERK2, somatic embryogenesis receptor-like kinase 2; ZAG5, zea agamous5; Rab5, responsive to abscisic acid 5; ESR, embryo surrounding region-related; ZMM2, *Zea mays* MADS2; ZAG9, zea agamous9; AGL8, Agamous-like 8; AGL15, Agamous-like 15; WIP3, wound-inducible protein 3; ALD1, aldolase 1; GST38, glutathione-S-transferase38; MADS2, MADS transcription factor 2.

number of DEGs between EC and IDC was 4077, 5896 DEGs between EC and BDC, and then EC and IRC, with 2,313 DEGs. In general, DEGs in EC and IDC are mainly concentrated in cell composition and biological processes, while DEGs in EC and BDC are mainly concentrated on the biological process, cellular process, and secondary metabolic process. In EC and IRC, DEGs are mainly concentrated on the biological processes, metabolic processes, and energy metabolism.

Embryogenesis is affected by many regulatory factors in maize. Auxin plays an important role in callus formation induced by embryogenesis [74] and activates the expression of downstream transcription factors, by mediating ARFs (auxin response factors) and inducing *E2Fα* (E2F transcription factor) to promote the formation of callus [75]. *ARF16* was upregulated from EC to IDC and *ARF8* was upregulated from EC to IRC in our study. Meanwhile, baby boom *(BBM)*, *SERK1,* and *SERK2* involved in the embryogenic pathway. Our results demonstrated that *BBM2,* SERK1, and SERK2 were upregulated from EC to IDC and EC to IRC. Mechanical damage has been recognized as a common stimulus of callus induction. *WIP2* and *ESR* were described as one of the wound-inducible genes, which were upregulated from EC to IDC and EC to IRC. These changes can improve conversion efficiency from EC to IRC, although the functions of these genes need to be further studied (Figure 8), which are important for elucidating the underlying molecular mechanisms of callus formation.

5. Conclusion

In this study, transcriptome analysis was used to analyze the differential expression of callus in different induction states. DEGs in EC and IDC are mainly concentrated in cell composition and biological process, while DEGs in EC and BDC are mainly concentrated on the biological process, cellular process, and secondary metabolic process. In EC and IRC, DEGs are mainly concentrated on the biological processes, metabolic processes, and energy metabolism. In particular, *ARF16* was upregulated from EC to IDC and *ARF8* was upregulated from EC to IRC. *BBM2*, *SERK1*, and *SERK2* were upregulated from EC to IDC and EC to IRC. These changes can improve conversion efficiency from EC to IRC, which is important for elucidating the underlying molecular mechanisms of callus formation [76].

Data Availability

The data used to support the results of this study are available from the corresponding author upon request.

Conflicts of Interest

The authors declare that they have no conflicts of interest.

Acknowledgments

This work was supported by the research project of the Science and Technology Department in the Guizhou Province (S20201Y050) and the special project of Animal and Plant Breeding in the Guizhou Province Agriculture department (B2018024).

Supplementary Materials

Supplementary Table 1: Compositions of the media used in callus tissue culture. Supplementary Table 2: Summary for RNA sequencing data of 8 samples. Supplementary Table 3: FPKM of all genes for morphological stages of callus genesis in maize. (*Supplementary Materials*)

References

[1] N. E. Borlaug, "Ending world hunger. The promise of biotechnology and the threat of antiscience zealotry," *Plant Physiol*, vol. 124, pp. 487–490, 2000.

[2] F. Delporte, J. M. Jacquemin, P. Masson, and B. Watillon, "Insights into the regenerative property of plant cells and their receptivity to transgenesis: wheat asa research case study," *Plant Signaling & Behavior*, vol. 7, pp. 1608–1620, 2012.

[3] S. Barampuram and Z. J. Zhang, "Recent advances in plant transformation," 2011, https://pubmed.ncbi.nlm.nih.gov/21181522/#:%7E:text=In%20particular%2C%20progress%20in%20Agrobacterium,gene%20targeting%2C%20and%20chromosomal%20engineering.

[4] A. Slater, N. W. Scott, and M. R. Fowler, *Plant Biotechnology: The Genetic Manipulation of Plants*, Plant Tissue Culture, Oxford University Press, New York, NY, USA, 2003.

[5] Y. Song, Y. Xia, X. Wei, Z. M. Zhang, M. J. Zhao, and T. Z. Rong, "Analysis on gene effect of four characters of immature embryo culture in maize," *Agriculatural sciences in china*, vol. 11, no. 6, pp. 1291–1296, 2006.

[6] S. Q. Ma L, Y. L. Zhou, C. L. Wu, and C. Q. Zhang, "Study on the relationship between inheritance and immature embryo

culturing capacity of maize inbreds," *Journal of Molecular Cell Biology*, vol. 40, pp. 164–171, 2007.

[7] M. Ahmadabadi, S. Ruf, and R. Bock, "A leaf-based regeneration and transformation system for maize (Zea mays L.)," *Transgenic Research*, vol. 16, no. 4, pp. 437–448, 2007.

[8] M. Targońska, A. Hromada-Judycka, H. Bolibok-Brągoszewska, and M. Rakoczy-Trojanowska, "The specificity and genetic background of the rye (Secale cereale L.) tissue culture response," *Plant Cell Reports*, vol. 32, no. 1, pp. 1–9, 2013.

[9] A. Feher, T. P. Pasternak, and D. Dudits, "Transition of somatic plant cells to an embryogenic state," *Plant Cell, Tissue and Organ Culture*, vol. 74, pp. 201–228, 2013.

[10] X. Y. Yang and X. L. Zhang, "Regulation of somatic embryogenesis in higher plants," *Critical Reviews in Plant Sciences*, vol. 29, pp. 36–57, 2010.

[11] G. T. Pan, Z. Yu, and T. Z. Rong, "Genetic variability analysis of Embryogenic callus inductivity from immature embryo culture in maize," *Acta Agronomica Sinica*, vol. 29, pp. 386–390, 2003.

[12] G. T. Pan, X. Wei, Y. Song, M. J. Zhao, and Y. L. Xia, "QTL analysis of maize (*Zea mays* L.) embryo culturing capacity," *Acta Agronomica Sinica*, vol. 32, no. 7–13, 2006.

[13] T. K. Hodges, K. K. Kamo, C. W. Imbrie, and M. R. Becwar, "Genotype specificity of somatic embryogenesis and regeneration in maize," *Nature Biotechnology*, vol. 4, no. 3, pp. 219–223, 1986.

[14] C. L. Armstrong, J. Romero-Severson, and T. K. Hodges, "Improved tissue culture response of an elite maize inbred through backcross breeding, and identification of chromosomal regions important for regeneration by RFLP analysis," *Theoretical and Applied Genetics*, vol. 84, no. 5, pp. 755–762, 1992.

[15] P. Landi, L. Chiappetta, S. Salvi, E. Frascaroli, and C. Lucchese, "Responses and allelic frequency changes associated with recurrent selection for plant regeneration from callus cultures in maize," *Maydica*, vol. 47, pp. 21–32, 2002.

[16] C. E. Green and R. L. Phillips, "Plant regeneration from tissue cultures of maize [1]," *Crop Science*, vol. 15, no. 3, pp. 417–421, 1975.

[17] D. D. Songstad, C. L. Armstrong, and W. L. Petersen, "AgNO3 increases type-II callus production from immature embryos of maize inbred B73 and its derivatives," *Plant Cell Reports*, vol. 9, no. 12, pp. 699–702, 1991.

[18] B. Frame, M. Main, R. Schick, and K. Wang, "Genetic transformation using maize immature zygotic embryos," *Methods in Molecular Biology*, vol. 710, pp. 327–341, 2011.

[19] D. Du, R. Jin, J. Guo, and F. Zhang, "Infection of embryonic callus with agrobacterium enables high-speed transformation of maize," *International Journal of Molecular Sciences*, vol. 20, no. 2, p. 279, 2019.

[20] D. Du, R. Jin, J. Guo, and F. Zhang, "Construction of marker-free genetically modified maize using a heat-inducible auto-excision vector," *Genes*, vol. 10, no. 5, p. 374, 2019.

[21] J. F. Hess, T. A. Kohl, M. Kotrová et al., "Library preparation for next generation sequencing: a review of automation strategies," *Biotechnology Advances*, vol. 41, Article ID 107537, 2020.

[22] J. Zhao, D. C. Dean, F. J. Hornicek, X. Yu, and Z. Duan, "Emerging next-generation sequencing-based discoveries for targeted osteosarcoma therapy," *Cancer Letters (Amsterdam, Netherlands)*, vol. 474, pp. 158–167, 2020.

[23] F. Ju, S. Liu, S. Zhang et al., "Transcriptome analysis and identification of genes associated with fruiting branch internode elongation in upland cotton," *BMC Plant Biology*, vol. 19, no. 1, pp. 415-416, 2019.

[24] Y. Jiao, P. Peluso, J. Shi et al., "Improved maize reference genome with single-molecule technologies," *Nature*, vol. 546, pp. 524–527, 2017.

[25] S. Anders, P. T. Pyl, and W. Huber, "HTSeq--a Python framework to work with high-throughput sequencing data," *Bioinformatics*, vol. 31, no. 2, pp. 166–169, 2015.

[26] D. Kim, G. Pertea, C. Trapnell, H. Pimentel, R. Kelley, and S. L. Salzberg, "TopHat2: accurate alignment of transcriptomes in the presence of insertions, deletions and gene fusions," *Genome Biology*, vol. 14, no. 4, pp. R36–R13, 2013.

[27] A. Roberts, H. Pimentel, C. Trapnell, and L. Pachter, "Identification of novel transcripts in annotated genomes using RNA-Seq," *Bioinformatics*, vol. 27, no. 17, pp. 2325–2329, 2011.

[28] A. M. Bolger, M. Lohse, and B. Usadel, "Trimmomatic: a flexible trimmer for Illumina sequence data," *Bioinformatics*, vol. 30, no. 15, pp. 2114–2120, 2014.

[29] S. Knyazev, L. Hughes, P. Skums, and A. Zelikovsky, "Epidemiological data analysis of viral quasispecies in the next-generation sequencing era," *Briefings in Bioinformatics*, vol. 22, no. 1, pp. 96–108, 2021.

[30] A. Grada and K. Weinbrecht, "Next-generation sequencing: methodology and application," *Journal of Investigative Dermatology*, vol. 133, no. 8, pp. 11–4, 2013.

[31] R. Pereira, J. Oliveira, and M. Sousa, "Bioinformatics and computational tools for next-generation sequencing analysis in clinical genetics," *Journal of Clinical Medicine*, vol. 9, no. 1, p. 132, 2020.

[32] A. Roberts, C. Trapnell, J. Donaghey, J. L. Rinn, and L. Pachter, "Improving RNA-Seq expression estimates by correcting for fragmentbias," *Genome Biology*, vol. 12, no. 3, p. 22, 2011.

[33] C. Trapnell, B. A. Williams, G. Pertea et al., "Transcript assembly and quantification by RNA-Seq reveals unannotated transcripts and isoform switching during cell differentiation," *Nature Biotechnology*, vol. 28, no. 5, pp. 511–515, 2010.

[34] Y. Liao, G. K. Smyth, and W. Shi, "The R package Rsubread is easier, faster, cheaper and better for alignment and quantification of RNA sequencing reads," *Nucleic Acids Research*, vol. 47, no. 8, p. 47, 2019.

[35] S. Anders and W. Huber, *Differential Expression of RNA-Seq Data at the Gene Level–The DESeq Package*, EMBL, Heidelberg, Germany, 2013.

[36] H. Guo, H. Guo, L. Zhang et al., "Dynamic transcriptome analysis reveals uncharacterized complex regulatory pathway underlying genotype-recalcitrant somatic embryogenesis transdifferentiation in cotton," *Genes*, vol. 11, no. 5, p. 519, 2020.

[37] M. Kanehisa, M. Araki, S. Goto et al., "KEGG for linking genomes to life and the environment," *Nucleic Acids Research*, vol. 36, no. Database, pp. 480–484, 2007.

[38] P. A. Auler, M. N. Do Amaral, G. d. S. Rodrigues et al., "Molecular responses to recurrent drought in two contrasting rice genotypes," *Planta*, vol. 246, no. 5, pp. 899–914, 2017.

[39] R. L. Tatusov, N. D. Fedorova, J. D. Jackson et al., "The COG database: an updated version includes eukaryotes," *BMC Bioinformatics*, vol. 4, no. 1, p. 41, 2003.

[40] Z. Avramova, "Transcriptional 'memory'of a stress: transient chromatin and memory (epigenetic) marks at stress-response genes," *The Plant Journal*, vol. 83, no. 1, pp. 149–159, 2015.

[41] C. Chen, B. He, X. Liu et al., "Pyrophosphate-fructose 6-phosphate 1-phosphotransferase (PFP 1) regulates starch

biosynthesis and seed development via heterotetramer formation in rice (*Oryza sativa* L.)," *Plant biotechnology journal*, vol. 18, no. 1, pp. 83–95, 2020.

[42] X. Zhang, Y. Wang, Y. Yan et al., "Transcriptome sequencing analysis of maize embryonic callus during early redifferentiation," *BMC Genomics*, vol. 20, no. 1, pp. 159–222, 2019.

[43] M. I. Petersen, I. Alvarez, K. G. Trono, and J. P. Jaworski, "Quantification of bovine leukemia virus proviral DNA using a low-cost real-time polymerase chain reaction," *Journal of Dairy Science*, vol. 101, no. 7, pp. 1–9, 2018.

[44] R. Lister, M. Pelizzola, R. H. Dowen et al., "Human DNA methylomes at base resolution show widespread epigenomic differences," *Nature*, vol. 462, no. 7271, pp. 315–322, 2009.

[45] X. Li, J. Zhu, F. Hu et al., "Single-base resolution maps of cultivated and wild rice methylomes and regulatory roles of DNA methylation in plant gene expression," *BMC Genomics*, vol. 13, no. 1, pp. 300–314, 2012.

[46] W. Li, D. Zhuang, H. Li et al., "Recombinant pseudorabies virus with gI/gE deletion generated by overlapping polymerase chain reaction and homologous recombination technology induces protection against the PRV variant PRV-GD2013," *BMC Veterinary Research*, vol. 17, no. 1, pp. 164–215, 2021.

[47] M. Ding, H. Dong, Y. Xue et al., "Transcriptomic analysis reveals somatic embryogenesis-associated signaling pathways and gene expression regulation in maize (Zea mays L.)," *Plant Molecular Biology*, vol. 104, no. 6, pp. 1–17, 2020.

[48] C. Wang, H. Ma, W. Zhu, J. Zhang, X. Zhao, and X. Li, "Seedling-derived leaf and root tip as alternative explants for callus induction and plant regeneration in maize," *Physiologia Plantarum*, vol. 172, no. 3, pp. 1570–1581, 2021.

[49] G. Hoerster, N. Wang, L. Ryan et al., "Use of non-integrating Zm-Wus2 vectors to enhance maize transformation," *In Vitro Cellular & Developmental Biology Plant*, vol. 56, no. 3, pp. 265–279, 2020.

[50] A. P. Kausch, K. Wang, H. F. Kaeppler, and W. Gordon-Kamm, "Maize transformation: history, progress, and perspectives," *Molecular Breeding*, vol. 41, no. 6, pp. 38–36, 2021.

[51] X. Liu, X. Feng, F. Liu, J. Peng, and Y. He, "Rapid identification of genetically modified maize using laser-induced breakdown spectroscopy," *Food and Bioprocess Technology*, vol. 12, no. 2, pp. 347–357, 2019.

[52] M. E. Otegui, M. Riglos, and J. L. Mercau, "Genetically modified maize hybrids and delayed sowing reduced drought effects across a rainfall gradient in temperate Argentina," *Journal of Experimental Botany*, vol. 72, no. 14, pp. 5180–5188, 2021.

[53] P. Steinberg, H. van der Voet, P. W. Goedhart et al., "Lack of adverse effects in subchronic and chronic toxicity/carcinogenicity studies on the glyphosate-resistant genetically modified maize NK603 in Wistar Han RCC rats," *Archives of Toxicology*, vol. 93, no. 4, pp. 1095–1139, 2019.

[54] Q. Que, S. Elumalai, X. Li et al., "Maize transformation technology development for commercial event generation," *Frontiers of Plant Science*, vol. 5, p. 379, 2014.

[55] P. Yadava, A. Abhishek, R. Singh et al., "Advances in maize transformation technologies and development of transgenic maize," *Frontiers of Plant Science*, vol. 7, p. 1949, 2016.

[56] C. Sell, G. Dumenil, C. Deveaud et al., "Effect of a null mutation of the insulin-like growth factor I receptor gene on growth and transformation of mouse embryo fibroblasts," *Molecular and Cellular Biology*, vol. 14, no. 6, pp. 3604–3612, 1994.

[57] G. Y. Wu and C. H. Wu, "Receptor-mediated in vitro gene transformation by a soluble DNA carrier system," *Journal of Biological Chemistry*, vol. 262, no. 10, pp. 4429–4432, 1987.

[58] I. Ghidoni, T. Chlapanidas, M. Bucco et al., "Alginate cell encapsulation: new advances in reproduction and cartilage regenerative medicine," *Cytotechnology*, vol. 58, no. 1, pp. 49–56, 2008.

[59] L. Heckmann, D. Langenstroth-Röwer, J. Wistuba et al., "The initial maturation status of marmoset testicular tissues has an impact on germ cell maintenance and somatic cell response in tissue fragment culture," *Molecular Human Reproduction*, vol. 26, no. 6, pp. 374–388, 2020.

[60] S. J. Murch and P. K. Saxena, "Somatic cell fusion: relevance to medicinal plants," in *Processing of The Development of Plant-Based Medicines: Conservation, Efficacy and Safety*, pp. 167–181, Springer, Dordrecht, 2001.

[61] J. C. Rink, "Stem cell systems and regeneration in planaria," *Development Genes and Evolution*, vol. 223, no. 1-2, pp. 67–84, 2013.

[62] F. Ge, H. Hu, X. Huang et al., "Metabolomic and proteomic analysis of maize embryonic callus induced from immature embryo," *Scientific Reports*, vol. 7, no. 1, pp. 1004–1016, 2017.

[63] L. Ma, M. Liu, Y. Yan et al., "Genetic dissection of maize embryonic callus regenerative capacity using multi-locus genome-wide association studies," *Frontiers of Plant Science*, vol. 9, no. 9, p. 561, 2018.

[64] V. Silveira, A. M. de Vita, A. F. Macedo, M. F. R. Dias, E. I. S. Floh, and C. Santa-Catarina, "Morphological and polyamine content changes in embryogenic and non-embryogenic callus of sugarcane," *Plant Cell, Tissue and Organ Culture*, vol. 114, no. 3, pp. 351–364, 2013.

[65] P. Zhang, Y. Jia, J. Shi et al., "The WY domain in the Phytophthora effector PSR 1 is required for infection and RNA silencing suppression activity," *New Phytologist*, vol. 223, no. 2, pp. 839–852, 2019.

[66] Y. Shen, Z. Jiang, X. Yao et al., "Genome expression profile analysis of the immature maize embryo during dedifferentiation," *PLoS One*, vol. 7, no. 3, 2012.

[67] F. Zeng, X. Zhang, L. Zhu, L. Tu, X. Guo, and Y. Nie, "Isolation and characterization of genes associated to cotton somatic embryogenesis by suppression subtractive hybridization and macroarray," *Plant Molecular Biology*, vol. 60, no. 2, pp. 167–183, 2006.

[68] Q. Zheng, Y. Zheng, and S. E. Perry, "AGAMOUS-Like15 promotes somatic embryogenesis in Arabidopsis and soybean in part by the control of ethylene biosynthesis and response," *Plant physiology*, vol. 161, no. 4, pp. 2113–2127, 2013.

[69] H. Bolibok and M. Rakoczy-Trojanowska, "Genetic mapping of QTLs for tissue-culture response in plants," *Euphytica*, vol. 149, no. 1-2, pp. 73–83, 2006.

[70] J. E. Cetz-Chel and V. M. Loyola-Vargas, "Transcriptome profile of somatic embryogenesis," in *Processing of the Somatic Embryogenesis," Fundamental Aspects And Applications*, pp. 39–52, 2016.

[71] S. A. G. D. Salvo, C. N. Hirsch, C. R. Buell, S. M. Kaeppler, and H. F. Kaeppler, "Whole transcriptome profiling of maize during early somatic embryogenesis reveals altered expression of stress factors and embryogenesis-related genes," *PLoS One*, vol. 9, no. 10, Article ID 111407, 2014.

[72] B. A. Lowe, M. M. Way, J. M. Kumpf et al., "Marker assisted breeding for transformability in maize," *Molecular Breeding*, vol. 18, no. 3, pp. 229–239, 2006.

[73] N. M. Doll, J. Just, V. Brunaud et al., "Transcriptomics at maize embryo/endosperm interfaces identifies a

transcriptionally distinct endosperm subdomain adjacent to the embryo scutellum," *The Plant Cell Online*, vol. 32, no. 4, pp. 833–852, 2020.

[74] M. Ikeuchi, K. Sugimoto, and A. Iwase, "Plant callus: mechanisms of induction and repression," *The Plant Cell Online*, vol. 25, no. 9, pp. 3159–3173, 2013.

[75] M. Z. Fan, C. Y. Xu, K. Xu, and Y. X. Hu, "Lateral organ boundaries domain transcription factors direct callus formation in Arabidopsis regeneration," *Cell Research*, vol. 22, no. 7, pp. 1169–1180, 2012.

[76] M. Kanehisa, "The KEGG database," *Novartis Found Symp*, vol. 247, pp. 91–101, 2002.

Hindawi
Journal of Chemistry
Volume 2022, Article ID 5609391, 6 pages
https://doi.org/10.1155/2022/5609391

Research Article

Chemical Constituents of *Plectranthus tomentosa* Extract and Its Control Effect on *Tetranychus kanzawai*

Yuehua Sun, Tianlei Liu, Cuiying Sun, and Qing Luo

School of Agricultural, Anshun University, Anshun 561000, Guizhou, China

Correspondence should be addressed to Yuehua Sun; 1270791568@qq.com

Received 4 May 2022; Accepted 16 June 2022; Published 12 July 2022

Academic Editor: Pei Li

The repellent and contact effects of *Plectranthus tomentosa* extracts of leaf and stem tissue on different stages of *Tetranychus kanzawai* were tested using the leaf-dip and insect-dip methods, and the constituents of the *Plectranthus tomentosa* extract were also determined. It was found that the repellent effect on *Tetranychus kanzawai* female adults has reached up to 84.43% after 60 min, with significant mortality of *Tetranychus kanzawai* at all growth stages. Sixty-nine components of the extract were identified by gas chromatography-mass spectrometry, of which limonene, followed by terpinolene, were present at the highest concentration. This research demonstrated that *Plectranthus tomentosa* has strong repellent and contact effects against *Tetranychus kanzawai*, offering potential natural strategies for the environmentally protective control of *Tetranychus kanzawai* in tea gardens and providing the foundation for the biomimetic synthesis of pesticides.

1. Introduction

In the era of "green food," "green agriculture," "sustainable agriculture," and integrated pest management (IPM), environmental standards of pesticides are becoming more and more stringent. Extracting substances with insecticidal activity from plants or directly processing them into new botanical pesticides and using them as leading compounds to synthesize new, safer, and more efficient pesticides have become hot topics of research.

Tetranychus kanzawai is one of the major pest mites that harm tea trees, strawberries, and vegetables, exploring pollution-free control methods to control the pest and is necessary to produce relevant green agricultural products. Botanical acaricides are of great interest recently, as they represent an important method for pollution-free control of mites. Grange and Ahmed have reported about 2400 species of plants with pest control activity early in 1988 [1]. Until now, the most studied acaricidal plants mainly belong to the Daphneaceae, Meliaceae, Solanaceae, Leguminosae, and Compositae families. Huang et al. screened acetone extracts of 121 species of plants in 51 families and 94 genera collected from Qinling Mountains and Inner Mongolia for aphidicidal and acaricidal activities [2]. Huo screened 117 species of plants in northwest China for acaricidal activity and found that acetone extracts of 71 species had good acaricidal activity against *Tetranychina harti* [3]. Jia et al. studied the biological activity of extracts of 8 indoor plants against *Tetranychus cinnabarinus* [4]. Liang et al. and Zhang et al. studied acaricidal substances of *Stellera chamaejasme* L. and found that daphnetin, daphnetin, squalene, β-sitosterol, and scopolactone were the key constituents responsible for the acaricidal activity [5–8]. Zhao et al. studied the components in volatile oil of hops and their acaricidal activity [9]. Zhou et al. studied the biological activity and mode of action of scoparone on different mite states of *Tetranychus cinnabarinus* [10]. Hu et al. studied the synergistic effect of abamectin and plant essential oils to kill *Tetranychus cinnabarinus* [11]. Onder et al. had proved that the essential oils of *Micromeria fruticosa* L., *Nepeta racemosa* L., and *Origanum vulgare* L. had biological activity against *Tetranychus urticae* Koch and *Bemisia tabaci* Genn [12]. Cavalcanti et al. measured the acaricidal effect of 20 chemical components in the plant essential oil of *Lippia sidoides* chain, and the results showed that thymol and carvacrol had a fumigation effect on *Tetranychus urticae* Koch [13]. Zou et al. found curcumin 2,4-dinitrophenylhydrazine

derivative showed a good control effect on *Tetranychus cinnabarinus* [14]. As for *Plectranthus tomentosa*, Zhao et al. and Meng et al. had explored the bacteriostatic effect of *Plectranthus tomentosa* [15, 16], and Xiong et al. had identified its volatile components [17]; however, there is no research study about the insecticidal or acaricidal activity of *Plectranthus tomentosa*. On the other hand, research on pollution-free control of *Tetranychus kanzawai* had been focused on predatory natural enemies of mites [18–22], while botanical pesticides for this pest have not been well studied.

In this study, the repellent and contact effect of *Plectranthus tomentosa* on *Tetranychus kanzawai* and the constituents of *Plectranthus tomentosa* extract were determined by GC-MS to provide references for the development of botanical acaricide and methods for pollution-free control of tea garden mites.

2. Materials and Methods

2.1. Sources of Test Insect and Plant. *Tetranychus kanzawai* was collected from the tea gardens in Huachu town, Puding County, Anshun City, Guizhou Province, and has been bred with strawberry leaves in the laboratory of Anshun College for more than three generations before use. After that, the adults, larvae, and eggs of *Tetranychus kanzawai* were produced according to the method introduced by IRAC (Insecticidal Resistance Action Committee, 2000). Fresh strawberry leaves were collected, washed, briefly dried, and placed in a humidified dish padded with a wet sponge and plastic wrap, with the petioles wrapped with wet cotton. Thirty female adult mites were released to the area with a #0 soft brush, and the dish was placed in the insect breeding room to allow the mites to lay eggs for 12 h; then, the adult mites were removed. The worms hatched from the eggs on the leaves were in the same worm state, so adult mites, larvae, and eggs at the same growth stage can be produced.

Plectranthus tomentosa was collected from the greenhouse of Anshun Academy of Agricultural Sciences. The plant was artificially propagated and cultivated to about 10 cm in height in Anshun College. The flesh stems and leaves were harvested and shattered with a multifunction food blender into a paste. The filtrate was centrifuged at 4000 rpm for 5 min at 20°C, and the *Plectranthus tomentosa* fresh juice was collected and stored in the refrigerator until use. While, the fully dried branches and leaves of *Plectranthus tomentosa* were pulverized into powder and filtered with an 80-mesh sieve. Fifty grams of the dry powder and 500 mL of acetone were added to a conical flask and irradiated with a microwave oven at 400 W power for 50 s. The mixture was filtered to get the solution, and the residue was reextracted twice with the same method. The filtrates were combined and concentrated under reduced pressure with a rotary evaporator at 40°C till the organic solvent was completely evaporated, and the extract was stored at 4°C for later use.

Table 1: Repellent rate of *Plectranthus tomentosa* fresh juice on *Tetranychus kanzawai*.

Time (min)	Repellent rate (%) (mean ± SE)*
5	72.23 ± 5.08^{bc}
30	81.10 ± 1.91^{ab}
60	84.43 ± 1.96^{a}

*Different lowercase letters in the same column revealed that the difference is significant with $p < 0.05$.

2.2. Experimental Method

2.2.1. Repelling Effect on Female Adult Mites of Tetranychus kanzawai Fresh Juice. The repellent effect of *Plectranthus tomentosa* fresh juice on *Tetranychus kanzawai* was tested by using the leaf-dipping method. Briefly, filter paper with a diameter of 9 cm was cut in half along the midline, one half was soaked in 10 mL 10% *Plectranthus tomentosa* fresh juice diluted with pure water, and the other half was soaked in 10 mL pure water served as a control. Both halves were naturally dried, stuck together along the cut with transparent tape, and fixed to the bottom of a clear Petri dish (9.0 cm × 2.0 cm) with double-sided tape. Vaseline was applied around the filter paper to prevent the adult mites from escaping. Thirty adult female mites were placed at the junction of the juice-soaked area and the control area. After 15, 30, and 60 min, the distribution of female adult mites on the two sides was recorded, and the repellent rate was calculated.

$$\text{Repellent rate} = \frac{(\text{number of test mites in the control area} - \text{number of test mites in the tjuice} - \text{soaked area})}{\text{number of test mites in the control area}} \times 100\%. \quad (1)$$

2.2.2. The Contact Effect of the Extract of Plectranthus tomentosa on Tetranychus kanzawai. The contact effect of the extract of *Plectranthus tomentosa* on *Tetranychus kanzawai* was determined using the insect-dipping method. Briefly, the *Plectranthus tomentosa* extract was dissolved and diluted with 0.1% Tween-80 aqueous solution to prepare 1000, 100, and 50 mg/mL concentrations. Thirty adult mites at the same growth stage on the same tea leave were immersed into the extract solution for 5 s and then naturally dried and put back into the humidified dish in an incubator with 25 ± 1°C, 60%–80% humidity, and a 16/8 light/dark cycle. For adult and larvae mites, the total number and death number were recorded to calculate the survival rate, and the hatching rate was calculated for eggs. Three duplicates were set for each test, and a 0.1% Tween-80 aqueous solution served as a control.

2.2.3. Determination of the Constituents in Plectranthus tomentosa Extract. *Plectranthus tomentosa* extract was

Table 2: The contact effect of *Plectranthus tomentosa* extract on *Tetranychus kanzawai*.

Concentration (mg/mL)	Mortality rate (%) (mean ± SE)*				
	Female adult		Larval		Eggs
	24 h	48 h	24 h	48 h	
1000	61.11 ± 1.93^{bc}	66.67 ± 3.34^{bc}	64.44 ± 1.93^{bc}	66.67 ± 3.34^{bc}	72.22 ± 2.09^{c}
100	65.56 ± 1.93^{b}	67.78 ± 1.92^{b}	66.67 ± 3.33^{b}	70.00 ± 3.33^{b}	77.78 ± 2.09^{b}
50	77.77 ± 5.09^{a}	83.33 ± 3.34^{a}	82.22 ± 5.09^{a}	86.67 ± 3.34^{a}	85.56 ± 1.92^{a}

*Different lowercase letters in the same column revealed the significant difference with $p < 0.05$.

Table 3: Composition and relative contents of *Plectranthus tomentosa* extract.

No.	Retention time	Compound name	Molecular weight	Relative content
1	7.41	Limonene	136	34.69
2	7.62	2 (3H)-Furanone, 5-ethenyldihydro-5-methyl-	126	0.08
3	8.63	Bicyclo [3.1.0] hexan-2-ol, 2-methyl-5-(1-methylethyl)-, (1.alpha., 2.beta., 5.alpha.)-	154	0.13
4	9.02	*trans*-p-Mentha-2,8-dienol	152	0.51
5	9.28	*cis*-p-Mentha-2,8-dien-1-ol	152	0.17
6	9.37	Bicyclo [3.1.1] heptan-3-ol, 6,6-dimethyl-2-methylene-	152	0.04
7	9.89	Bicyclo [3.3.0] oct-2-en-7-one, 6-methyl-	136	0.16
8	10.02	Benzene, 1,3-dimethyl-5-(1-methylethyl)-	148	0.06
9	10.27	Terpineol	154	0.14
10	10.59	7-Methyl-1,2,3,5,8,8a-hexahydronaphthalene	148	0.06
11	10.78	*trans*-Carveol	152	0.14
12	10.95	*cis*-p-Mentha-1 (7), 8-dien-2-ol	152	0.52
13	11.28	D-carvone	150	0.07
14	11.82	1,7-Octadiene-3,6-diol, 2,6-dimethyl-	170	0.73
15	12.15	Bornyl acetate	196	2.20
16	12.31	(1S, 2R, 4R, 7R)-4-Isopropyl-7-methyl-3,8-dioxatricyclo [5.1.0.02, 4] octane	168	0.08
17	12.42	Cyclohexasiloxane, dodecamethyl-	444	0.21
18	12.59	alpha.-Cubebene	204	1.07
19	13.00	Terpinolene	136	8.66
20	13.33	alpha.-Copaene	204	0.77
21	13.62	Bicyclosesquiphellandrene	204	4.10
22	13.83	Methyl eugenol	178	1.12
23	14.29	Caryophyllene	204	1.13
24	14.64	alpha.-Guaiene	204	0.08
25	14.94	Valerena-4,7 (11)-diene	204	0.07
26	15.44	Alloaromadendrene	204	0.49
27	16.01	Benzene, 1-(1,5-dimethyl-4-hexenyl)-4-methyl-	202	0.09
28	16.18	(3R, 3aR,3bR,4S,7R,7aR)-4-Isopropyl-3,7-dimethyloctahydro-1h-cyclopenta [1, 3] cyclopropa [1,2] benzen-3-ol	222	0.77
29	16.37	*trans*-Calamenene	202	0.12
30	16.48	Pacifigorgiol	222	0.12
31	17.30	(1aR, 4S, 7R, 7aS, 7bR)-1,1,4,7-Tetramethyl-1a,2,3,4,6,7,7a,7b-octahydro-1h-cyclopropa[e]azulen-4-ol	220	0.08
32	18.13	(-)-Spathulenol	220	1.09
33	18.36	(-)-Globulol	222	1.36
34	18.97	(1R,2R,4S,6S,7S,8S)-8-Isopropyl-1-methyl-3-methylenetricyclo[4.4.0.02,7]decan-4-ol	220	0.35
35	19.72	Ledol	222	0.76
36	20.02	Muurola-4,10 (14)-dien-1.beta.-ol	220	0.22
37	20.31	2-Naphthalenemethanol, decahydro-.alpha.,.alpha.,4a-trimethyl-8-methylene-, [2R-(2.alpha.,4a.alpha.,8a.beta.)]-	222	0.52
38	20.44	(1R, 4S)-4-Isopropyl-1,6-dimethyl-1,2,3,4-tetrahydronaphthalen-1-ol	218	0.60
39	20.52	1 (2H)-Naphthalenone, octahydro-4a, 8a-dimethyl-7-(1-methylethyl)-, [4aR-(4a.alpha., 7.beta., 8a.alpha.)]-	222	3.28
40	20.81	(1R, 7S, E)-7-Isopropyl-4,10-dimethylenecyclodec-5-enol	220	0.60
41	21.00	(E)-3-((4S, 7R, 7aR)-3,7-Dimethyl-2,4,5,6,7,7a-hexahydro-1h-inden-4-yl)-2-methylacrylaldehyde	218	1.29
42	21.58	(-)-Aristolene	204	0.86

Table 3: Continued.

No.	Retention time	Compound name	Molecular weight	Relative content
43	21.83	Cycloheptane, 4-methylene-1-methyl-2-(2-methyl-1-propen-1-yl)-1-vinyl-	204	0.06
44	22.82	Megastigma-4, 6 (Z),8 (E)-triene	176	0.09
45	22.98	2-Pentadecanone, 6,10,14-trimethyl-	268	0.72
46	23.34	Biphenylene, 1,2,3,6,7,8,8a,8b-octahydro-4,5-dimethyl-	188	0.83
47	23.79	Phthalic acid, 7-bromoheptyl butyl ester	398	1.60
48	23.90	1H-Indene-4-acetic acid, 6-(1,1-dimethylethyl)-2,3-dihydro-1,1-dimethyl-	260	0.39
49	24.45	7-Isopropyl-1,1,4a-trimethyl-1,2,3,4,4a,9,10,10a-octahydrophenanthrene	270	0.06
50	25.74	Hexadecane, 2,6,10,14-tetramethyl-	282	0.21
51	26.10	Octadecane	254	2.23
52	26.50	Heptadecane	240	2.83
53	26.83	Docosane	310	0.20
54	27.65	1-(2-Methoxyphenyl)-2,5-dihydro-1H-pyrrole-2,5-dione	203	1.29
55	27.82	2-Hydroxy-3,4-tetramethylene-6-methoxy quinoline	229	0.06
56	27.90	Hentriacontane	437	1.92
57	28.19	Ferruginol	286	0.29
58	28.47	3-Bromobenzyl alcohol, TMS derivative	258	0.89
59	28.69	Tetracosane	338	0.48
60	29.19	1-Phenanthrenemethanol, 1,2,3,4,4a,9,10,10a-octahydro-1,4a-dimethyl-7-(1-methylethyl)-	328	0.18
61	30.10	Aristolene epoxide	220	0.08
62	30.86	(2Z, 4E)-3,7,11-Trimethyl-2,4,10-dodecatriene	206	0.07
63	32.18	Davana ether	234	0.05
64	32.74	Heneicosane	296	4.17
65	33.29	Nonadecane, 9-methyl-	282	0.48
66	33.72	9,10-Dihydrodeoxynivalenol	298	0.05
67	34.15	Heptacosane	380	2.83
68	34.61	Octacosane	394	0.69
69	35.27	Triacontane	422	0.69

redissolved with 2 mL *n*-hexane and filtered with a 0.22 μm organic filter. The constituents in *Plectranthus tomentosa* extract were analyzed using a gas chromatography-mass spectrometer (Agilent GC-MS 7890B 5977A, Agilent Technologies, Palo Alto, CA).

2.3. Statistical Analysis. SPSS 24.0 was used for the statistical analysis of the data. The data of parallel tests were expressed by mean ± standard error ($X \pm$ SE), and Duncan's new complex range test was used for multiple comparisons.

3. Results and Discussion

3.1. Repellent Effect Test of Plectranthus tomentosa Fresh Juice on Tetranychus kanzawai. The results of the repellent effect of the *Plectranthus tomentosa* fresh juice on the female adults of *Tetranychus kanzawai* are given in Table 1. As given in Table 1, *Plectranthus tomentosa* fresh juice showed a good repellent effect on female *Tetranychus kanzawai*. The repellent rate reached 70% early at 15 min and was up to 84% at 60 min. The difference in repellent rate was not statistically significant between 15 min and 30 min or between 30 min and 60 min, but was statistically significant between 15 min and 60 min.

3.2. Contact Effect of Plectranthus tomentosa Extract on Tetranychus kanzawai. The contact effect of *Plectranthus tomentosa* extract on *Tetranychus kanzawai* at different growth stages is given in Table 2. As given in Table 2, *Plectranthus tomentosa* extract at 50 mg/mL killed 77.77% and 83.33% of the female adults at 24 and 48 h, respectively; the mortality rate was significantly higher than that at either 1000 mg/mL or 100 mg/mL. Meanwhile, Table 2 provides that extract at 50 mg/mL revealed the strongest contact effect on the larval of *Tetranychus kanzawai*, with the mortality rate of 82.22% and 86.67%, respectively, which were significantly higher than that at either 1000 mg/mL or 100 mg/mL. In addition, Table 2 provides that the extract at 50 mg/mL showed the strongest effect, killing 85.56% of the eggs, which was significantly higher than that at either 1000 mg/mL or 100 mg/mL, although the two latter concentrations still achieved greater than 72% egg mortality.

3.3. Determination of Chemical Constituents in the Extract. The chemical constituents in the extract were determined using GC-MS and the results are given in Table 3 and Figure 1. Table 3 and Figure 1 show that a total of 69 constituents were identified in the extract, accounting for 93.03% of the total mass. The extract contained 14 alkanes, 14 alkenes, 23 alcohols, 6 aldehydes, 1 ketone, 1 acid, 2 esters, 1 ether, and 7 aromatic hydrocarbons accounting for 17.08%, 52.28%, 10.06%, 5.60%, 1.29%, 0.39%, 3.8%, 0.05%, and 2.48% of the total volatile components, respectively. Limonene was the most abundant single constituent (34.69% of the total), followed by terpinolene (8.66%). It had been

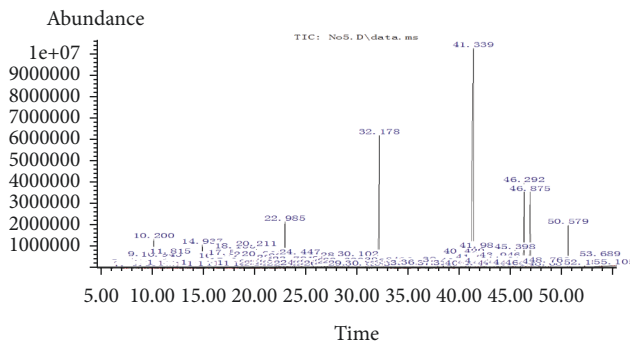

Figure 1: Ion current spectrum of the extract of *Plectranthus tomentosa*.

reported previously that limonene was also the key constituent responsible for the repellent effect of *P. tomentosa* [23], whereas the constituents responsible for the antibiosis effect were not identified.

4. Conclusion

The current research has demonstrated significant repellent and contact effects of *Plectranthus tomentosa* extract on *Tetranychus kanzawai*, with the level of control increasing with time, suggesting that intercropping *Plectranthus tomentosa* with tea bushes in commercial tea gardens may help control *Tetranychus kanzawai*, as may an acaricide-like extract from *Plectranthus tomentosa*. Such strategies may play a major role in the future in achieving pollution-free prevention and control of mites (possibly also mites other than *Tetranychus kanzawai*) in tea gardens, providing references for the large-scale planting of insecticidal plants and the biomimetic synthesis of pesticides.

Data Availability

The data used to support the results of this study are included within the article.

Conflicts of Interest

The authors declare that they have no conflicts of interest.

Acknowledgments

This work was supported by the Anshun Key Laboratory of Green Prevention and Control of Agriculture Diseases and Insect Pests ([2020]2), the Guizhou Province Educational Science and Technology Research Foundation (KY [2016] 279 and KY [2016]278), the Anshun University Foundation (Asxyxkpt201902), and the Capacity Building of Innovation Center for Efficient Agricultural of Guizhou Mountain Characteristics (QKZYD[2019]4010).

References

[1] M. Grange and S. Ahmed, *Handbook of Plants with Pest Control Properties*, John Wiley and Sons Inc, New York, NY, USA, 1988.

[2] Q. L. Huang, *Screening of Aphidicidal and Acaricidal Compounds from Extracts of 121 Plants*, Northwest A&F University, Xianyang, China, 2012.

[3] Y. B. Huo, *Screening of Acaricidal Activity in 117 Plants in Northwest China*, Northwest A&F University, Xianyang, China, 2013.

[4] F. L. Jia, Y. J. Chen, J. Chen, D. D. Wang, and G. Dai, "Screening of biological activity against *Tetranychus cinnabarinus* in extracts of 8 plants," *China Agricultural Science Bulletin*, vol. 27, no. 24, p. 286, 2011.

[5] W. Liang, G. L. Shi, and J. Cheng, "The killing effect of three acaricidal ingredients in Stellera chamaejasme L," *China Agricultural Science Bulletin*, vol. 27, no. 9, pp. 372–376, 2011.

[6] W. Liang, X. N. Bai, and J. Cheng, "Isolation and identification of acaricidal substances in *Stellera chamaejasme* L," *Journal of Horticulture*, vol. 38, no. 5, pp. 947–954, 2011.

[7] W. Liang, J. Cheng, and C. Y. Bu, "Chemical constituents and acaricidal activity of supercritical extracts from *Stellera chamaejasme* L," *Forestry Sciences*, vol. 48, no. 1, pp. 181–185, 2012.

[8] D. H. Zhang, E. Chen, and S. Y. Yang, "Isolation and identification of acaricidal substances in the root of *Stellera chamaejasme* L," *Journal of Gansu Agricultural University*, vol. 53, no. 1, pp. 95–101, 2018.

[9] N. N. Zhao, W. J. Fu, and W. Lu, "Chemical composition and toxicity of the essential oil derived from *Humulus lupulus* against *Tetranychus turkestani*," *Xinjiang Agricultural Sciences*, vol. 57, no. 6, pp. 1142–1150, 2020.

[10] H. Zhou, T. Guo, and F. Y. Guo, "Study on the biological activity of *Artemisia Lactone* on different mite states of *Tetranychus cinnabarinus* and the mode of action," *Plant Doctor*, vol. 33, no. 3, pp. 18–24, 2020.

[11] Y. Hu, H. Y. Zhou, and L. C. Tian, "Study on the synergistic effect of abamectin and plant essential oil in killing Tetranychus cinnabarinus," *Plant Doctor*, vol. 34, no. 1, pp. 57–61, 2021.

[12] Onder, A. Irfan, and S. Fikrettin, "Insectieidal and acaricidal effect of three Lamiaceae plant essential oils against Tranychus urticae Koch and Bemisia tabaci Genn," *Industrial Crops and Products*, vol. 23, pp. 140–146, 2005.

[13] S. C. H. Cavaleanti, E. S. Nieulau, A. F. Blank, C. A. Câmara, I. N. Araújo, and P. B. Alves, "Composition and acarieidal activity of Lippia sidoides essential oil against two-spotted spider mite (Tetranychus urtieae Koch)," *Bioresource Technology*, vol. 101, pp. 829–832, 2010.

[14] H. B. Zou, W. Ding, and G. Zhou, "Synthesis of Curcumin Bis (2,4-Dinitrophenylhydrazine) and its acaricidal activity," *Research on Prevention and Control of Agricultural Biohazards*, pp. 792–795, 2005.

[15] P. Meng, Y. X. Hu, L. Fan et al., "Analysis of volatile oil components and antibacterial activity of *Plectranthus tomentosa*," *Journal of Heilongjiang Ecological Engineering College*, vol. 27, no. 6, pp. 29-30, 2014.

[16] X. Z. Zhao, C. Li, and X. D. Cui, "GC-MS analysis of the chemical constituents of the essential oil of Plectranthus tomentosa and evaluation of its antibacterial activity," *Natural Product Research and Development*, vol. 28, no. 3, pp. 377–381, 2016.

[17] W. Xiong, H. X. Jin, and B. Z. Cai, "Chemical components of volatile compounds in *Plectranthus tomentosa*," *Journal of Zhejiang A&F University*, vol. 28, no. 4, pp. 680–684, 2011.

[18] Y. X. Zhang, J. Z. Lin, and Y. B. Chi, "Application of *Phytoseiulus persimilis* to control *Tetranychus kanzawai* in open-

air strawberry fields," *China Biological Control*, vol. 12, no. 4, pp. 188-189, 1996.

[19] Y. X. Zhang, J. Z. Lin, and Z. K. Weng, "Predation effect of *Amblyseius longhairi* on *Tetranychus kanzawai*," *Chinese Journal of Plant Protection*, vol. 23, no. 3, pp. 287-288, 1996.

[20] Z. Q. Yang, F. L. Tao, and H. G. Cao, "Field experiment of predatory control of *Tetranychus kanzawai* on vegetables with *Phytoseiulus persimilis*," *Bulletin of Biological Control*, vol. 6, no. 2, pp. 88-89, 1990.

[21] B. Y. Lin and Y. B. Chi, "Controlling *Tetranychus kanzawai* on strawberry using predatory *Amblysei longhair*," *Plant Protection*, vol. 27, no. 2, pp. 44-45, 2001.

[22] F. Y. Chen, Z. Q. Yang, and H. G. Cao, "Preliminary study on predatory control of *Tetranychus kanzawai* on kidney bean with *Phytoseiulus persimilis*," *Biohazard Science*, vol. 2, pp. 39–41, 1991.

Hindawi
Journal of Chemistry
Volume 2022, Article ID 6893691, 7 pages
https://doi.org/10.1155/2022/6893691

Research Article

Identification of Pathogens and Laboratory Activity Test of Kiwifruit Rot Disease in Guizhou Province, China

Tao Wang, Yanling Ren, Jinyu Zhao, Yingjie Jiang, Jian Tang, Yao Liu, Chao Liu, Juan Wang, Xiaolei Ji, and Mingyan Wang

Guizhou Light Industry Technical College, Guiyang 550032, China

Correspondence should be addressed to Yanling Ren; lingling00111@126.com and Jian Tang; tang123tang456jian@163.com

Received 1 May 2022; Accepted 3 June 2022; Published 29 June 2022

Academic Editor: Pei Li

Kiwifruit (*Actinidia* spp.) postharvest decay is common in China, which can cause serious economic losses to kiwifruit industry. In order to further clarify the pathogen of kiwifruit rot disease in Guizhou Province, the rotten fruits of kiwifruit (cultivar "Jinyan") were collected, and the pathogenic fungi were identified by isolation and purification, pathogenicity test, morphological characteristics, and analysis of rDNA-ITS sequences. The results showed that the pathogenic fungi of kiwifruit rot disease were *Diaporthe phaseolorum* and *Fusarium tricinctum*. Meanwhile, the results showed that all the tested agents had a certain inhibitory effect on *Diaporthe phaseolorum* and *Fusarium tricinctum*. Among them, 33.5% quinolone SC had the best inhibitory effect on *Diaporthe phaseolorum* with an EC_{50} value of 9.67 mg/L, and 25% fludioxonil SC had the best inhibitory effect on *Fusarium tridentatus* with the EC_{50} value of 13.13 mg/L. The results will provide a reference for the control of kiwifruit rot disease.

1. Introduction

Kiwifruit (*Actinidia* spp.) has soft meat, sour and sweet taste, rich in vitamin C, sugars, and a variety of essential amino acids for human body. It has a high nutritional and economic value and is deeply loved by consumers, which is known as "super fruit" and "king of fruit." Kiwifruit is native to China, and more than 30 countries have engaged in large scale and industrialized artificial cultivation of kiwifruit industry. In 2020, the planting area of kiwifruit in China was about 193000 hectares and the output was about 2.291 million tons, accounting for more than 68% and 50% of the world, respectively [1]. Guizhou Province is located in the west of China, and its geographical and climatic conditions are suitable for the growth of kiwifruit and have been one of the main kiwifruit planting areas in China. By 2020, the cultivated area has reached $4.51 \times 10^4\,hm^2$ [2].

In recently years, with the rapid expansion of the kiwifruit planting area, the problem of rot disease has become increasingly prominent [3–5]. At present, postharvest rot disease of kiwifruit occurs widely around the world, causing serious economic losses during fruit storage, transportation, and sales [6, 7]. Kiwifruit rot disease mainly occurs in the postharvest period and storage stage of the fruit. Its main symptoms are the formation of round or oval brown lesions on the peel, a water-stained ring on the edge of the lesion, and the color of the flesh of the lesion. It is milky white, and the pulp at the junction between disease and health is water-stained, often forming perforated rot. In severe cases, the whole fruit rots completely [8, 9]. The pathogenic microorganism of kiwifruit rot is rich in diversity. At present, the pathogenic microorganism that have been reported are mainly *Botryosphaeria dothidea* [10, 11], *Phomopsis* spp. [12, 13], and *Pestalotiopsis* spp. [7, 10]. *Alternaria alternata*, *Plectosphaerella cucumerina*, *Neofusicoccum parvum*, *Phomopsis* spp., and *Fusarium oxysporum* have been reported as pathogens of kiwifruit rot in Guizhou Province, China [10, 14–17]. However, research studies on rot disease of Guizhou kiwifruit are basically concentrated on "Guichang" kiwifruit and "Hongyang" kiwifruit varieties, and there are few reports on Guizhou "Jinyan" kiwifruit varieties.

2. Materials and Methods

2.1. Isolation and Purification of the Pathogens. The rotten kiwifruit was collected from Gubao town (106.525230°E,

26.852491°N), Maijia town (106.626288°E, 26.711823°N), and Machang town (106.223953°E, 26.447156°N) in Guizhou Province, China. A total of 290 samples were collected, packaged in a clean ziplock bag, and then taken back to the laboratory store in a 4°C refrigerator for pathogen isolation. The kiwifruit is first rinsed with tap water and then dried. The infected tissues (0.5 × 0.5 cm size) were soaked in 75% alcohol for about 30 s, rinsed with sterile water 3 s, and then plated the tissues on the PDA plates. After that, the PDA plates were maintained in a constant temperature incubator at 26°C without light. After culturing for 3 days, all the strains were cultured three times on the new PDA plates using a single spore technique to ensure purity. Finally, the purified strains were stored at 4°C for further use.

2.2. Pathogenicity Test. Pathogenicity tests were performed by inoculating the fungus on the puncture site of the surface of healthy and nearly mature kiwifruits, and the kiwifruits were incubated in an incubator in a 26°C constant temperature incubator with a humidity of 60% and a photoperiod of 14 L : 10 D. The surface of healthy and nearly mature kiwifruits inoculated with sterile water served as a control. After 12 days of inoculation, some symptoms have been observed on the surface. The causal fungus in the infected kiwifruit surface was reisolated on the PDA plate as described above. The characteristics of the reisolated fungus were used to compare with its original culture.

2.3. Morphological and Molecular Identification. Individual colony was inoculated on the PDA plate and maintained in a constant temperature incubator at 26°C without light for 8 days. Then, the morphology was identified by both eyes and an inverted microscopy (ECLIPSE Ni-E, Nikon Corporation, Japan). The total DNA of the tested strain was extracted with the Ezup column fungal genomic DNA extraction kit (B518259-0050, Sangon Corporation Shanghai, China), and the rDNA-ITS sequence was amplified by primers ITS1 (5′-TCCGTAGGTGAACCTG CGG-3′) and ITS4 (5′-TCCTCCGCTTATTGATATGC-3′). The total reaction volume is 25 μL: 12.5 μL 2xEs Taq Mix, 1 μL each primer, 1 μL DNA, and 9.5 μL ddH_2O. The polymerase chain reaction (PCR) reaction conditions were predenaturation at 94°C for 5 min, 35 cycles of 94°C for 30 s, 56°C for 1 min, 72°C for 1 min, and final extension at 72°C for 7 min. After amplification, the PCR product was sequenced at Sangon Corporation (Shanghai, China) and searched for sequence similarity with the National Center of Biotechnology Information (NCBI) database.

2.4. In Vitro Antifungal Activity Test. The in vitro antifungal activities of 11 kinds of fungicides, 33.5% quinolone SC (Shanghai Hulian biopharmaceutical Co., Ltd., China), 250 g/L propiconazole EC (Shandong Xinxing pesticide Co., Ltd., China), 25% myclobutanil EC (Zhejiang Yifan Biotechnology Group Co., Ltd., China), 25% fludioxonil SC (Jiangsu Syngenta Nantong crop protection Co., Ltd., China), 0.3% eugenol AP (Jiangsu Nantong Shenyu green Pharmaceutical Co., Ltd., China), 80% ethylicin EC (Henan Kebang Chemical Co., Ltd., China), 100 g/L cyazofamid SC (Henan Guangnong pesticide factory, China), 1% Osthol AP (Inner Mongolia Qingyuanbao Biological Technology Co., Ltd., China) 25% cupric-ammonium complexion (Henan Anyang Guofeng Pesticide Co., Ltd., China), 430 g/L tebuconazole SC (Jiangsu Renxin Crop Protection Technology Co., Ltd., China), and 80% zineb WP (Shandong Xinxing Pesticide Co., Ltd., China) and 5 kinds of essential oils (patchouli essential oil (Guangzhou Biotechnology Co., Ltd., China), fennel essential oil (Beijing Maosi Trading Co., Ltd.), garlic essential oil (Beijing Maosi Trading Co., Ltd.), clove essential oil (Beijing Maosi Trading Co., Ltd.), and benzoin essence oil (Beijing Maosi Trading Co., Ltd.) were tested [18]. The inhibition rates I (%) are calculated by the following formula, where C (cm) and T (cm) represent the fungi diameters of the CK and treated PDA plates, respectively. Meanwhile, the EC_{50} values of 11 kinds of fungicides and 5 kinds of plant essential oils against *Diaporthe phaseolorum* and *Fusarium tricinctum* were calculated with the SPSS 19.0 software.

$$\text{Inhibition rate, } I\ (\%) = \frac{(C - T)}{(C - 0.4)} \times 100. \quad (1)$$

3. Result

3.1. Morphological Identification. The hyphae of strain F1 are fluffy and white in the early stage of growth. The center of the hyphae appears yellowish-brown, and the edges are white on the 3rd day. On the 8th day, the diameter of the colony is overgrown in the Petri dish. The hypha on the front is dark gray (Figure 1(a)), the back of the PDA medium is dark brown (Figure 1(b)), and the hyphae are transparent with many branches and segments (Figure 1(c)).

The hyphae of strain F2 are fluffy, appearing white at the initial stage of growth, with irregular edges and slow growth. On the 3rd day, the mycelium produces pink pigment. Then, on the 10th day, the diameter of the colony grows over the Petri dish, and the color of the bottom of the medium gradually changes to rose red on the front (Figure 1(d)), with yellow on the back (Figure 1(e)) and many hyphae branches (Figure 1(f)).

3.2. ITS Sequence Identification. The sequences of F1 and F2 strains were uploaded to NCBI to obtain the GenBank numbers of ON566024 and ON566025. Phylogenetic trees of the ITS sequence were constructed based on the N-J and M-L methods, as shown in Figure 2, and the strain F1 was classified as *Diaporthe phaseolorum* with the similarity of 99% and 85%, respectively. Meanwhile, Figure 3 shows that the strain F2 was classified as *Fusarium tricinctum* with bootstrap values of both 100% ((N-J method) and (M-L method)).

3.3. Pathogenicity Determination. Pathogenicity was determined by the stab inoculation method, and the results are shown in Figure 4. Figure 4 shows that the *Diaporthe phaseolorum* (strain F1) and *Fusarium tricinctum* (strain F2) can cause kiwifruit rot. Among them, the diameter of kiwifruit rot disease caused by F1 was 3.93 cm (Figure 4(b)),

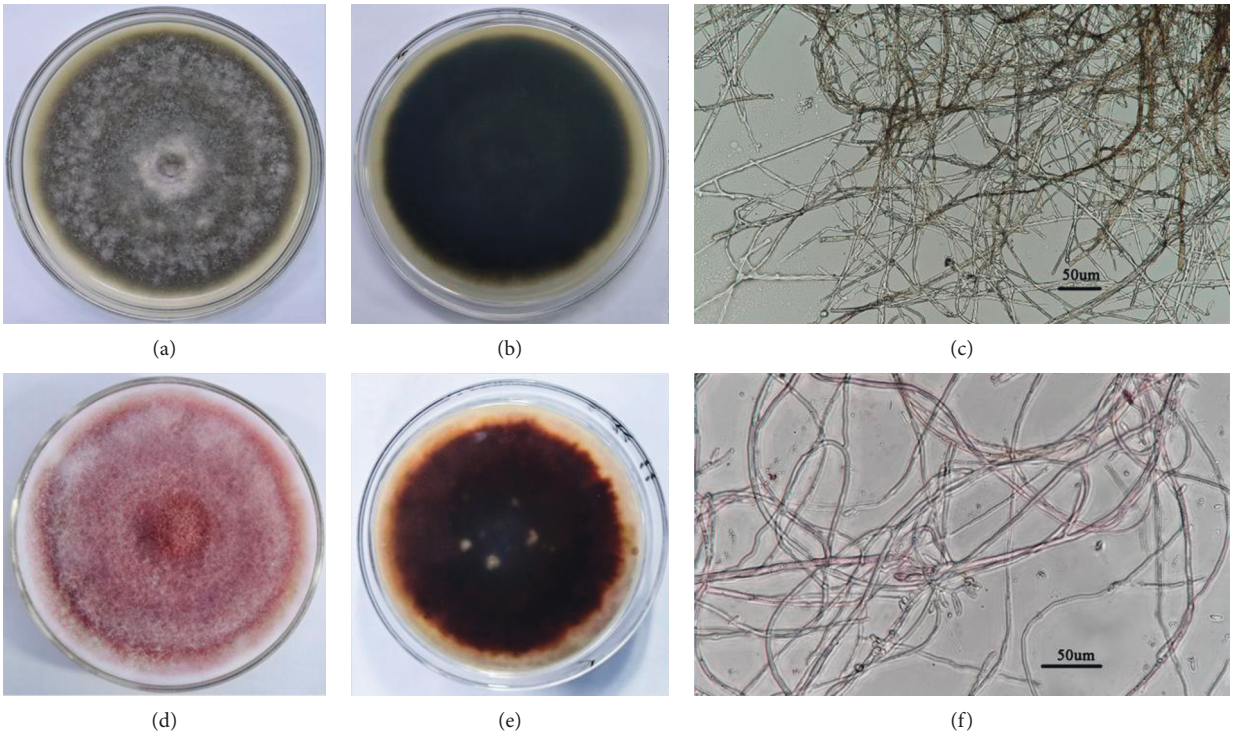

Figure 1: Morphological characteristics of F1 and F2 strains. (a)–(c) The front, back, and hyphal morphology of F1 colonies, respectively; (d)–(f) The front, back, and hyphal morphology of F2 colonies, respectively.

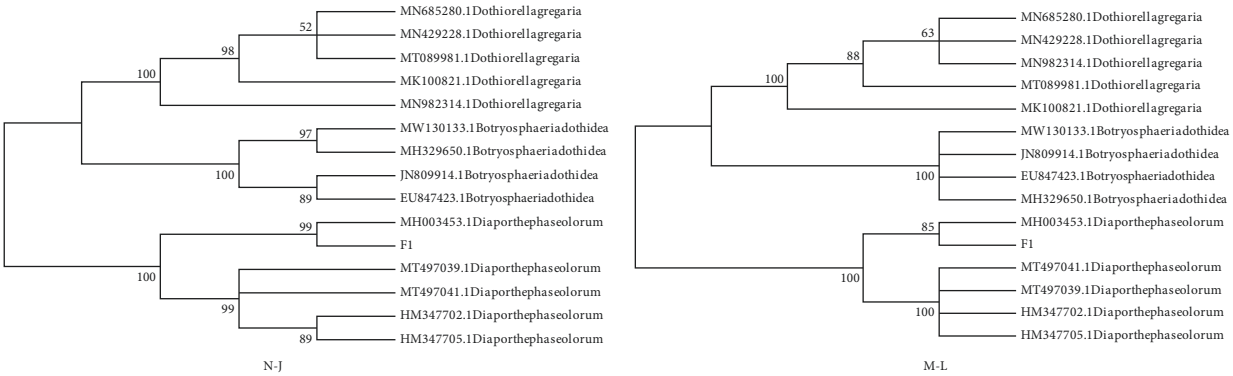

Figure 2: Phylogenetic trees of the ITS sequence of strain F1 constructed based on the N-J and M-L methods.

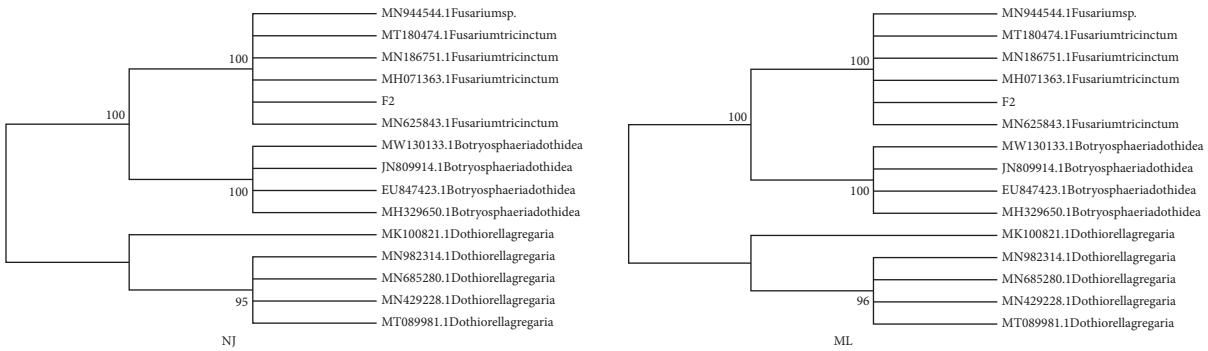

Figure 3: Phylogenetic trees of the ITS sequence of strain F2 constructed based on the N-J and M-L methods.

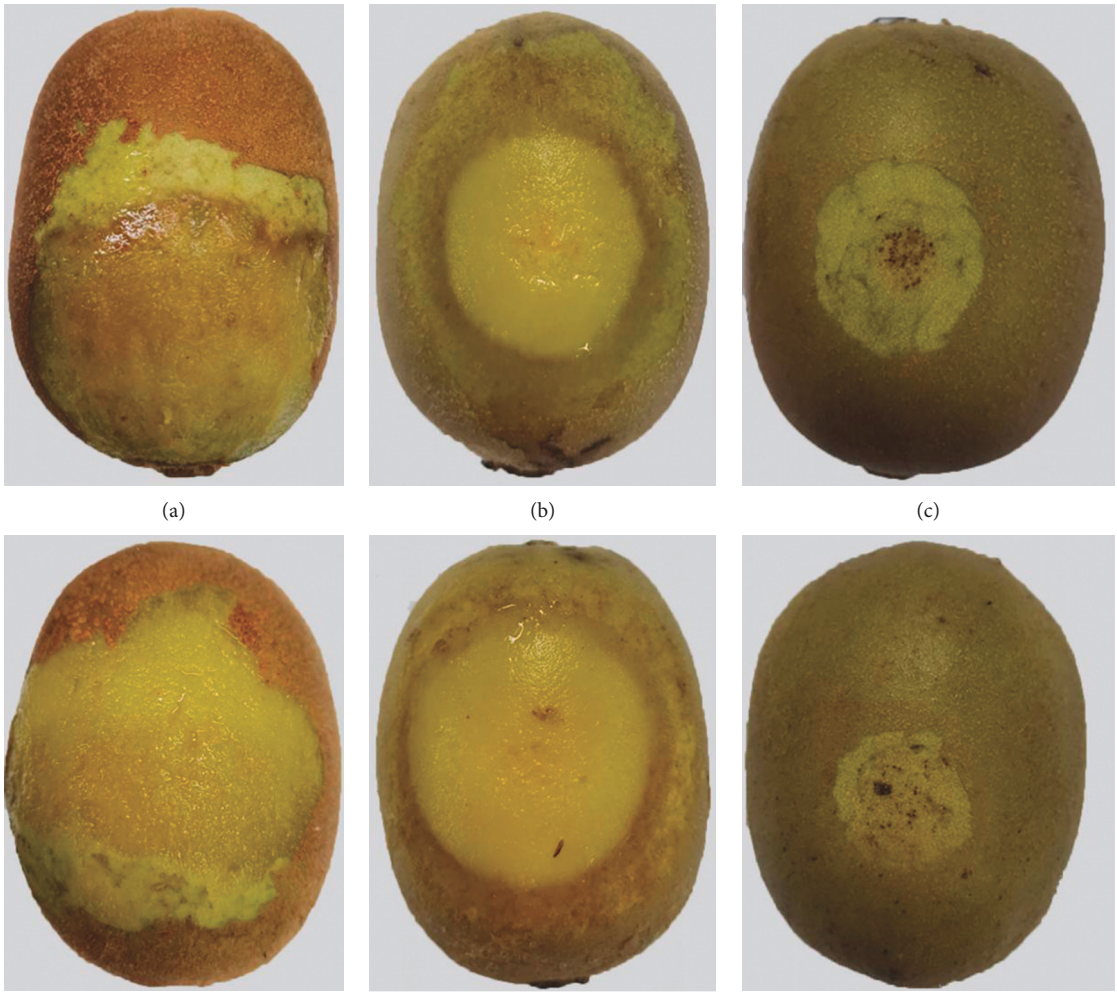

Figure 4: The symptoms of F1 and F2 strains in the pathogenicity test. (a)-(b) The pathogenicity test by F1 strain. (c) CK group for strain F1. (d)-(e) Pathogenicity test by F2 strain. (f) CK group for strain F2.

and F2 caused kiwifruit rot disease with a diameter of 4.25 cm (Figure 4(e)). The diseased kiwifruit was reisolated, and the strains with the same morphological characteristics as the original inoculated strains were obtained, which met the requirements of Koch's law.

3.4. In Vitro Antifungal Activity. It can be seen from Table 1 that the test fungicides and plant essential oils revealed different degrees of inhibition on the growth of *Diaporthe phaseolorum* and *Fusarium tricinctum*. Especially, 33.5% quinolone SC showed the best inhibitory effect against *Diaporthe phaseolorum* with the EC_{50} value of 9.67 mg/L; meanwhile, 25% fludioxonil SC had an EC_{50} value of 13.13 mg/L against *Fusarium tricinctum*, which were even better than those of other fungicides and plant essential oils.

4. Discussion

Postharvest rot disease of kiwifruit occurs globally, which has a significant impact on the quality and flavor of kiwifruit.

Table 1: The EC_{50} values of the test fungicides and plant essential oils against *Diaporthe phaseolorum* and *Fusarium tricinctum*.

Treatment	EC_{50} (mg/L)	
	Diaporthe phaseolorum	*Fusarium tricinctum*
33.5% quinolone SC	9.67	34.53
250 g/L propiconazole EC	12.55	59.71
25% myclobutanil EC	16.54	13.66
25% fludioxonil SC	18.54	13.13
0.3% eugenol AP	48.81	111.32
80% ethylicin EC	85.10	82.55
100 g/L cyzzofamid SC	91.66	30.83
430 g/L tebuconazole SC	103.78	58.89
80% zineb	106.27	642.17
1% osthol AP	215.36	15.52
25% cupric-ammonium complexion	430.73	49.04
Patchouli essential oil	115.00	122.89
Fennel essential oil	131.48	109.57
Garlic essential oil	156.11	101.74
Clove essential oil	163.87	132.96
Benzoin essence oil	163.96	136.67

At present, it has caused significant economic losses to the kiwifruit industry. Therefore, the identification of pathogens of kiwifruit postharvest rot disease is of great significance for industrial development. In this study, 2 pathogens classified as *Diaporthe phaseolorum* and *Fusarium tricinctum* were obtained from the rotten fruits of kiwifruit (cultivar "Jinyan") which were collected from Guizhou Province, China. *Diaporthe phaseolorum* has a higher separation rate, and the asexual form of the fungus is *Phomopsis* spp. [19]. *Phomopsis* spp. has also been reported many times in other varieties in Guizhou Province, for example, "Guichang" kiwifruit [12, 20] and "Hongyang" kiwifruit [21]. Our results showed that the main pathogen of kiwifruit (cultivar "Jinyan") rot disease in Guizhou Province was related to other strains. In addition, *Phomopsis* spp. was an important pathogen of kiwifruit rot disease in other regions, such as "Xuxiang" kiwifruit in Hubei and Shaanxi [22], "Jinyu" kiwifruit in Hubei, and "Golden" kiwifruit in Wuhan. The "Jinmei" kiwifruit [23] detected *Phomopsis* spp. as an important pathogen. It indicated that *Phomopsis* spp. was an important pathogen of kiwifruit rot disease among different strains and regions, and it caused harm to various strains of kiwifruit in the whole country.

Fusarium tricinctum is the first pathogenic fungus found in the identification of kiwifruit rot disease pathogens in Guizhou Province. This pathogen has not been found to infect kiwifruit in previous studies. *Fusarium* is widely distributed in nature and is one of the most important phytopathogens discovered so far [24]. It can cause a variety of plants and their fruits to rot. Among them, *Fusarium tricinctum* can cause apple moldy heart disease [25], garlic root rot [26], lily *Fusarium* wilt [27], and potato dry rot [28]. Yang et al. [29] found that there were significant differences in the pathogenicity and severity of *Fusarium* in different provinces and between different places in the same province. Because *Fusarium tricinctum* are more harmful to fruits and fruit trees and have a wide range of damage; they should be paid attention to in field prevention and control.

In recent years, the prevention and treatment of kiwifruit fruit rot disease gradually attracted the attention of the world kiwifruit industry. In this study, the in vitro inhibitory effects of 16 kinds of fungicides and plant essential oils against *Diaporthe phaseolorum* and *Fusarium tricinctum* were determined. The results showed that all the tested agents had a certain inhibitory effect on the four pathogenic fungi. Among them, 33.5% quinolone SC had the best inhibitory effect on *Diaporthe phaseolorum* and 25% fludioxonil SC had the best inhibitory effect on *Fusarium tricinctum*. At present, there are many screening studies on the prevention and control of kiwifruit rot disease. The commonly used agents are mainly carbendazim, tebuconazole, prohydan, flusilazole, benomyl, and thiophanate-methyl. Previous studies have shown that ethylicin could significantly inhibit the mycelial growth of *P. macrospore*, *Botryotinia fuckeliana*, *Botryosphaeria dothidea*, and *Fusarium proliferatum* [30]. 42.4% azole ether-fluranil SC, 40% flusilazole EC, and other three kinds of fungicides had a significant inhibitory effect on *Pestalotiopsis gracilis* [31]. Curcumin has a significant inhibitory effect on the growth of *Diaporthe phaseolorum* mycelium [32]. But serious pesticide residue problems will come with the long-term use of pesticides [33], for example, pesticide residues are the main bottleneck for my country's kiwifruit export volume and price increase [34]. Therefore, there is an urgent need for research and development to find alternatives to pesticides [35]. To sum up, the optimal control agents for various pathogens are different; this may be related to kiwifruit varieties and local geographic climate. Based on the results of the abovementioned in vitro screening of fungicides against kiwifruit rot pathogens, the field control effect tests of 33.5% quinolone SC and 25% fludioxonil SC against kiwifruit rot disease can be carried out in our next work, so as to provide an effective prevention and control method of kiwifruit rot disease in Guizhou Province.

5. Conclusion

In conclusion, our results showed that *Diaporthe phaseolorum* and *Fusarium tricinctum* were the pathogenic fungi of kiwifruit (cultivar "Jinyan") rot disease in Guizhou Province. Meanwhile, 33.5% quinolone SC had the best inhibitory effect on *Diaporthe phaseolorum* and 25% fludioxonil SC had the best inhibitory effect on *Fusarium tricinctum*. Our study could provide a theoretical basis for the effective control method of kiwifruit rot disease in Guizhou Province.

Data Availability

The data used to support this study are available from the corresponding author upon request.

Conflicts of Interest

The authors declare that they have no conflicts of interest.

Authors' Contributions

Tao Wang and Yanling Ren contributed equally to this work.

Acknowledgments

The study was supported by the Science and Technology Project of China Tobacco Guizhou Provincial Corporation grant number (201918), the Science and Technology Foundation of General Administration of Quality Supervision, Inspection and Quarantine of the People's Republic of China grant number (2017IK257, 2017IK261, 2016IK075, and 2014IK022), the Science and Technology Foundation of Guizhou Province grant number (J(2013)2149), the 2021 Humanities and Social Sciences Research Project of Guizhou Provincial Department of Education, grant number [2022ZC016], and the 2021 Guizhou Province Theoretical Innovation Project (Joint Project), grant number [GZLCLH-2021-169]. This research is the achievement of Guizhou Province Academic Pioneer and Academic Pioneer Construction.

References

[1] Z. W. Jiang and C. H. Zhong, "A comprehensive understanding with the importance of popular science knowledge to the kiwifruit quality improvement," *China Fruits*, vol. 1, pp. 1–8, 2020.

[2] W. M. Zhong, Y. X. Huang, D. M. Tang, X. Zhang, and Y. Qi, "Adaptability comparison of twenty of introduced kiwifruit varieties in central Guizhou," *Northern Horticulture*, vol. 8, pp. 29–37, 2021.

[3] R. L. Wang, *Research on Postharvest Disease Physiology and Ozone Preservation Technology of Hongyang Kiwifruit*, Sichuan Agricultural University, Chengdu, China, 2020.

[4] Y. J. Koh, J. S. Hur, and J. S. Jung, "Postharvest fruit rots of kiwifruit (*Actinidia deliciosa*) in Korea," *New Zealand Journal of Crop and Horticultural Science*, vol. 33, no. 3, pp. 303–310, 2005.

[5] G. Kim, Y. Koh, Y. J. Koh, J. S. Jung, and J. S. Hur, "Control of postharvest fruit rot diseases of kiwifruit by antagonistic bacterium *Bacillus subtilis*," *Acta Horticulturae*, vol. 1096, pp. 377–382, 2015.

[6] M. Manning, J. Burdon, N. De Silva et al., "Maturity and postharvest temperature management affect rot expression in "hort16a" kiwifruit," *Postharvest Biology and Technology*, vol. 113, pp. 40–47, 2016.

[7] L. Li, H. Pan, M. Y. Chen, and C. H. Zhong, "First report of pestalotiopsis microspora causing postharvest rot of kiwifruit in Hubei province, China," *Plant Disease*, vol. 100, no. 10, p. 2161, 2016.

[8] S. R. Pennycook, "Fungal fruit rots of *Actinidia deliciosa* (kiwifruit)," *New Zealand Journal of Experimental Agriculture*, vol. 13, no. 4, pp. 289–299, 1985.

[9] Y. Zhou, G. Gong, Y. Cui et al., "Identification of botryosphaeriaceae species causing kiwifruit rot in Sichuan province, China," *Plant Disease*, vol. 99, no. 5, pp. 699–708, 2015.

[10] L. Li, H. Pan, M. Chen, S. Zhang, and C. Zhong, "Isolation and identification of pathogenic fungi causing postharvest fruit rot of kiwifruit (*Actinidia chinensis*) in China," *Journal of Phytop athology*, vol. 165, no. 11-12, pp. 782–790, 2017.

[11] C. Li, J. X. Jiang, J. H. Leng, B. M. Li, and Q. Yu, "Isolation and identification of pathogenic bacteria of kiwifruit fruit rot disease in Fengxin county," *Acta Agriculturae Universitatis Jiangxiensis*, vol. 34, no. 2, pp. 259–263, 2012.

[12] L. Feng, H. Wei, Y. L. Huang, H. Xu, X. H. Sun, and J. Jiang, "Infection route and isolation and identification of rot fungus in kiwifruit Guichang," *China Brewing*, vol. 37, no. 2, pp. 66–70, 2018.

[13] W. W. Su, D. Wu, and Z. C. Han, "Identification and analysis of pathogenic bacteria of kiwifruit fruit rot disease in Guizhou," *Henan Agricultural Science*, vol. 50, no. 3, pp. 97–102, 2021.

[14] X. Y. Zhang and W. J. Li, "Inhibitory effect of artemisia annua tobacco vinegar on the growth of fusarium trilinea," *China Agricultural Science Bulletin*, vol. 36, no. 1, pp. 131–134, 2020.

[15] Y. Sun, Z. Ye, Y. Xia, X. M. Liu, J. J. Pu, and H. Zhang, "Research progress on stem-end rot of mango," *China Fruit & Vegetable*, vol. 40, no. 12, pp. 79–84, 2020.

[16] H. Pan, Q. L. Hu, S. J. Zhang, D. Zu, L. Li, and C. H. Zhong, "Kiwifruit disease investigation and pathogen identification in liupanshui city, guizou province," *Plant Protection*, vol. 44, no. 4, pp. 125–131, 2018.

[17] T. Q. Li, Y. X. Huang, and X. J. Wang, "Comprehensive prevention and control measures of kiwifruit canker in Xiuwen county," *Plant Doctor*, vol. 28, no. 1, pp. 37-38, 2015.

[18] Y. Zhou, Y. H. Ou, B. M. Li, and Q. Q. Li, "Indoor virulence determination of 10 fungicides against *Botryosphaeria dothidea*," *South China Fruits*, vol. 45, no. 6, pp. 124-125, 2016.

[19] L. Luongo, A. Santori, L. Riccioni, and A. Belisario, "Phomopsis sp. associated with post-harvest fruit rot of kiwifruit in Italy," *Journal of Plant Pathology*, vol. 93, no. 1, pp. 205–209, 2011.

[20] Y. H. Yang, J. Y. Wu, J. Ren, W. Yang, and Y. L. Zheng, "Isolation and identification of pathogenic bacteria of kiwifruit soft rot," *Plant Doctor*, vol. 33, no. 3, pp. 67–71, 2020.

[21] J. Q. Lei, W. N. Wu, Y. Liu, X. Q. Long, W. J. Li, and R. Wang, "Isolation, identification and pathogenicity difference of pathogenic bacteria of "hongyang" kiwifruit soft rot in liupanshui area of Guizhou province," *Northern Horticulture*, vol. 4, pp. 31–38, 2019.

[22] P. P. Zuo, S. Fu, L. T. Peng, G. Fan, S. Z. Yang, and J. Li, "Identification of the pathogenic bacteria of postharvest soft rot of kiwifruit and the control effect of carvacrol on it," *Journal of Huazhong Agricultural University*, vol. 39, no. 6, pp. 15–22, 2020.

[23] L. Deng, H. Pan, Y. H. Zhang et al., "Field validation of efficient control agents for kiwifruit fruit rot disease," *Fruit Trees in South China*, vol. 49, no. 4, pp. 127–129+132, 2020.

[24] B. A. Summerell, B. Salleh, and J. F. Leslie, "A utilitarian approach to *Fusarium* identification," *Plant Disease*, vol. 87, no. 2, pp. 117–128, 2003.

[25] L. L. Gao, *Study on Pathogen Diversity of Fuji Apple Mycoheart Disease in Shaanxi Province*, Northwest University of Agriculture and Forestry Science and Technology, Xianyang, China, 2003.

[26] L. J. Zhang, W. X. Wang, and Q. Yu, "Isolation and identification of pathogenic bacteria of garlic root rot in jimusar, Xinjiang," *Xinjiang Agricultural Sciences*, vol. 54, no. 4, pp. 725–734, 2017.

[27] W. Y. Li, Z. P. Liu, and X. F. He, "Isolation, identification and pathogenicity of pathogen of lily fusarium wilt," *Journal of Shenyang Agricultural University*, vol. 47, no. 2, pp. 153–158, 2016.

[28] N. N. Ning, Q. Liu, W. R. Xian, and W. H. Wang, "Determination of indoor toxicity of five fungicides to potato dry rot," *Journal of Qinghai University*, vol. 39, no. 1, pp. 31–37, 2020.

[29] B. Yang, *Damage Invertigation of Potato Root Rot Caused by Fusarium and its Pathogenic Identification and ISSR Analysis of Genetic Diversity in Northwest China*, Ningxia University, Ningxia, China, 2019.

[30] X. J. Wang, S. Y. Li, Y. W. Li, R. He, L. W. Zhu, and P. Liu, "Pathogen identification of kiwifruit soft rot and fungicide screening for control of the disease," *Journal of Plant Protection*, vol. 44, no. 5, pp. 826–832, 2017.

[31] C. Li, *Identification and Control of the Pathogen of Kiwifruit Ripening and Rot in Fengxin Nanchang: College of Agriculture*, Jiangxi Agricultural University, Nanchang, China, 2014.

[32] K. K. Kai, W. Bi, Y. Sui, C. Hua, Y. Liu, and D. Zhang, "Curcumin inhibits diaporthe phaseolorum and reduces postharvest decay in kiwifruit," *Scientia Horticulturae*, vol. 259, Article ID 108860, 2020.

[33] Y. L. Ren, T. Wang, Y. Wang, Q. Q. Cao, and H. J. Huang, "Research on the maximum residue limits of pesticides in fresh kiwifruit at home and abroad," *World Agriculture*, vol. 6, pp. 49–56, 2018.

[34] T. Wang, X. N. Wang, J. Tang, W. Li, Q. Q. Cao, and J. Peng, "Research on the response of kiwifruit industry to technical barriers to trade," *Public Standardization*, vol. 16, pp. 181–184+187, 2021.

[35] Y. L. Ren, T. Wang, Q. Q. Cao et al., "Research on the response of kiwifruit to technical trade barriers to pesticide residues in the high-end market—taking Japan and the European union as examples," *Jiangsu Agricultural Sciences*, vol. 46, no. 21, pp. 366–370, 2018.

Hindawi
Journal of Chemistry
Volume 2022, Article ID 7613285, 7 pages
https://doi.org/10.1155/2022/7613285

Research Article

Metabolomics Study on the Resistance of Walnut Peel to *Colletotrichum gloeosporioides* under Prochloraz Treatment

Xia Yang, Liuyan Wu, Li Fu, Pin Fu, Jiamin Zhu, Yuxue Zhao, and Jing Liu

Guizhou Institute of Walnut, Guiyang, Guizhou 550006, China

Correspondence should be addressed to Jing Liu; liujing1989202253@126.com

Received 29 April 2022; Accepted 25 May 2022; Published 28 June 2022

Academic Editor: Pei Li

Anthracnose, caused by *Colletotrichum gloeosporioides*, is highly harmful for walnut production in the world. To better control this disease, the inhibitory effects of 3 fungicides against *Colletotrichum gloeosporioides* were determined, and the results showed that prochloraz had better inhibitory activity. Through comparative metabolomics analysis, 311 metabolites might be associated with the walnut peel response to *Colletotrichum gloeosporioides* under prochloraz treatment. Furthermore, we supposed that the phenylpropanoid pathway might be induced by prochloraz to resist *Colletotrichum gloeosporioides* infection. In conclusion, the upregulated metabolites in the phenylpropanoid pathway might be related to synthesize lignin to further form a cell wall against *Colletotrichum gloeosporioides* infection.

1. Introduction

Colletotrichum gloeosporioides (*C. gloeosporioides*) is a plant pathogen highly harmful for many genus plants [1–3]. It can cause anthracnose disease which is a crucial constraint to walnut production in many areas in the world and results in significant yield and economic losses [4, 5]. Some reports demonstrated that some fungicides can inhibit anthracnose disease caused by *C. gloeosporioides* [6, 7], and prochloraz is a good fungicide to control diseases, which can inhibit the ergosterol synthesis of pathogen. However, there was a difference pathogenicity from different isolates. It should consider that the pathogenicity of the genus *Colletotrichum* from different sources [8] and these strains isolates from different plant or place had different fungicides sensitivities too [1, 2]. Therefore, any differences in fungicide sensitivities of isolates causing walnut anthracnose remain unknown [9]. Walnut anthracnose caused walnut production economy loss in Guizhou province every year, and the main pathogen is *C. gloeosporioides*, in which fungicide fit for this strain on walnut is unknown. It is known that prochloraz can inhibit the ergosterol synthesis of pathogen, but how it effects metabolic changes of walnut peels is unknown. This study was conducted to compare the control effect on *C. gloeosporioides* of walnut and analyze metabolomics of walnut peel against *C. gloeosporioides* under prochloraz treatment.

2. Materials and Methods

2.1. Experimental Materials. The *C. gloeosporioides* was isolated from walnut orchard in Qingzhen City and identified by Guizhou Academy of Forestry. 45% prochloraz EW was purchased from Hunan Xinchangshan Agricultural Development Co., Ltd. (Hunan, China); 50% fluazinam EC was purchased from Mengzhou Nonghuize Biological Technology Co., Ltd. (Henan, China); 80% ethylicin SC was purchased from Shandong Zouping pesticide Co., Ltd. (Shandong, China). The walnut peel was collected from walnut orchard located at Qingzhen City, Guizhou, China (106.276520N, 26.643765E, altitude 1294.77 m).

2.2. Antifungal Activity Test. The effects of three fungicides on the mycelial growth were detected according to the method described by Hua et al. with slight modifications [10]. The fungicides (200, 100, 50, 25, 12.5, and 6.25 mg/L) were prepared using sterile water. The *C. gloeosporioides*

mycelial disks (5 mm in diameter) taken from one-week-old cultures of *C. gloeosporioides* were placed at the center of Petri dishes (90 mm in diameter) containing 20 mL of PDA amended with different concentrations of fungicides. A control experiment was carried out by adding the corresponding volume of sterile water into PDA. Colony diameters were measured after incubation for 7 days at 25°C. Each treatment composed of three replicates. The inhibition rates of fungicides on the colony growth of *C. gloeosporioides* were calculated. The data were presented as the mean ± SD and analyzed to detect significant differences by ANOVA with SPSS version 24.0 software.

2.3. Fungicides Control Efficiency against C. gloeosporioides in the Field. Three fungicides were used to control *C. gloeosporioides* on walnut in Qingzhen City, Guizhou, China (106.276520N, 26.643765E, altitude 1294.77 m). These fungicides were sprayed on 10 walnut trees that were 10 years old; the application time was April 20, May 20, and June 20, 2021, respectively. The drug concentration of fungicides was 1 g/L and water served as blank control (CK). Randomly surveyed one branch from the east, south, north, and west of the trees and counted the area of fruit disease spots on each branch on April 19 and July 20, 2021. At least 20 fruits were surveyed with each tree; each treatment composed of 10 trees. The disease index was calculated according to the disease level. The disease grades were classified as follows. Grade I: no disease spots on the fruit, assigned a value of 0. Grade II: disease spots were less than 10% of the fruit area, assigned a value of 1. Grade III: disease spots were between 10% and 30% of the fruit area, assigned a value of 2. Grade IV: disease spots are between 30% and 50% of the fruit area, assigned a value of 3. Grade V: disease spots are more than 50% of the entire fruit area, assigned a value of 4. Incidence rate = (number of diseased branches/total number of fruits under investigation) × 100; disease index = (∑(disease grades × number of fruits in each grade)/(highest disease grade × total number of investigated fruits)) × 100. Control effect (%) = (1−(disease index after treating−disease index before treating)/control experiment disease index change) × 100. All data were calculated by Excel 2007.

2.4. Metabolomics Analysis. The walnut peels were collected on July 20, 2021. Choose infected fruits with the same symptoms to test. Untargeted metabolomics was used to analysis of the different metabolites of walnut peel between blank control (yunxin1, yunxin2, and yunxin3 named CK) and prochloraz treatment (yunxin4, yunxin5, and yunxin6 named PT). The freeze-dried sample was crushed, and 50 mg of powder was extracted overnight at 4°C with 1 mL of methanol-acetonitrile water (2 : 2 : 1). In addition, quality control (QC) samples were made by mixing the extracts of each sample. The sample extracts were tested by using a Waters Acquity I-Class PLUS/Xevo G2-XS QT of system. The analytical conditions were as follows: column, Waters Acquity UPLC HSS T3 (1.8 μm, 2.1 mm × 100 mm). The following gradient profile was used: 0–2 min, 98% A; 2–11 min, 2%–98% B; 11–13 min, 98% B; and 13–15 min, 2%–98% A. The flow rate was 0.2 mL/min, and the injection volume for each sample was 10 μL. The column temperature was maintained at 40°C, and the sample temperature was 10°C. The injection volume was 3 μL. The effluent was alternatively connected to an Xevo G2-XS QTOF mass spectrometer. Applied a high-resolution tandem mass spectrometer Xevo G2-XS QTOF (Waters, USA), equipped with an ESI Turbo ion-spray interface, operating in positive and negative ion modes, and controlled by Analyst MassLynx V4.2. The ESI source operation parameters were as follows: ion source, turbo spray; source temperature, 150°C; ion spray voltage, 2000 V (positive ion mode)/−1500 V (negative ion mode); the sampling cone voltage was set at 30 V; reverse blowing flow rate 50 L/h; and the flow rate of desolvation gas is 800 L/h.

The identification is based on the Progenesis QI software according to the sample type using online databases such as METLIN and self-compiled database (Biomarker, Beijing, China), and the mass deviation of fragment ion identification was within 100 μg/L. Compounds were identified based on second-level mass spectrum and retention time. Quantitative analysis was carried out in the MRM mode. The corresponding relative metabolite contents were expressed as chromatographic peak area integrals. The data were statistically analyzed and plotted using SPSS Statistics version 20.0 (SPSS Inc., Chicago, IL, USA). A principal component analysis (PCA) was performed in R package (version 3.5.0). Orthogonal partial least-squares discriminant analysis (OPLS-DA) was conducted by MetaboAnalystR package (version1.0.1), and the variable importance in projection (VIP) value was generated. Differentially accumulated metabolites (DAMs) were screened by VIP ≥ 1, $P < 0.05$, and |fold change| > 1. The functions of DAMs were further annotated using the KEGG compound database to determine the metabolic pathways that are most highly correlated with the resistance of walnut peel under prochloraz treatment against *C. gloeosporioides*.

3. Results and Discussion

3.1. The In Vitro Antifungal Activity Test. Table 1 provides that 45% prochloraz EW had the best in vitro inhibitory effect on the mycelial growth, with the EC_{50} value of 0.067 μg/mL; it was similarly reported by Ding et al. [7, 11]. The 80% ethylicin SC had the lowest inhibitory effect against *C. gloeosporioides* (EC_{50} = 31.62 μg/mL), which is consistent with Shi et al. report [12].

3.2. Control Efficiency of 3 Fungicides against C. gloeosporioides in the Field. Three fungicides were used to control *C. gloeosporioides* in the field, and the results are given in Table 2. The 45% prochloraz EC had the best control efficiency with 73.28%, 50% fluazinam EC had the control efficiency with 60.34%, and 80% ethylicin SC had the control

Table 1: The in vitro inhibitory effect of 3 fungicides.

Treatment	Concentration (μg/mL)	Colony diameter (cm)	Inhibition rate (%)	EC_{50} (μg/mL)
45% prochloraz EW	200	0.50 ± 0.00	100.00 ± 12.51	0.067
	100	0.65 ± 0.05	97.34 ± 6.57	
	50	0.77 ± 0.07	95.27 ± 5.92	
	25	0.89 ± 0.06	93.08 ± 12.82	
	12.5	0.95 ± 0.05	92.01 ± 4.53	
	6.25	1.18 ± 0.09	87.87 ± 4.18	
50% fluazinam EC	200	0.73 ± 0.07	95.95 ± 6.19	12.76
	100	1.13 ± 0.14	88.76 ± 5.27	
	50	1.70 ± 0.10	78.70 ± 3.09	
	25	2.32 ± 0.11	67.75 ± 2.40	
	12.5	3.38 ± 0.09	48.82 ± 1.10	
	6.25	4.25 ± 0.13	33.43 ± 1.23	
80% ethylicin SC	200	1.20 ± 0.08	87.57 ± 2.57	31.62
	100	2.37 ± 0.12	66.86 ± 1.92	
	50	2.98 ± 0.13	55.92 ± 1.69	
	25	3.78 ± 0.07	41.72 ± 0.83	
	12.5	4.38 ± 0.07	31.07 ± 0.75	
	6.25	4.78 ± 0.09	23.96 ± 0.86	
CK	—	6.13 ± 0.20	—	

Table 2: Control efficiency of 3 fungicides against *C. gloeosporioides* in the field.

Fungicides	Total branches	Disease branches	Disease branch rate (%)	Disease index (%)	Prevention and control effect (%)
45% prochloraz EW	40	30	75	15.50	73.28
50% fluazinam EC	40	36	90	23.00	60.34
80% ethylicin SC	40	40	100	38.00	34.48
CK	40	40	100	58.00	

efficiency with 34.48%. The control efficiency test in the field was consistent with the indoor toxicity test.

The 45% prochloraz EC and 50% fluazinam EC had a better control effect in the field, prochloraz often mixed with other fungicides to obtain better efficiency in the field [13, 14], and fluazinam showed a better inhibition against mycelial growth, but it was unstable and affected by the environment in the field experiment [15]. The ethylicin was the biopesticides; it can inhibit *Botrytis cinerea* effectively but have a little effect on *Colletotrichum* spp. [16].

3.3. Metabolome Analysis Resistance of Walnut under Prochloraz Treatment against C. gloeosporioides. Untargeted metabolomics was performed on samples taken from CK and PT walnut peel after treating on the 30th dpi. A total of 1256 metabolites were obtained in all samples, as presented in the heatmap visualization, which showed distinct hierarchical clustering of samples by different treatment of walnut peel (Figure 1, Table S1). In the PCA plot, CK and PT were divided into two parts by PCA1; it showed different metabolites under two treatments (Figure 2). Based on the quantitative analyses of all detected metabolites (Table S2) and the fold change threshold, a total of 311 DAMs were obtained for the comparison of CK versus PT, of which 68 metabolites were downregulated and 243 metabolites were upregulated in PT. A heatmap of DAM confirmed the significant differences in the metabolome of CK and PT walnut peels following *C. gloeosporioides* infection (Figure 1(b)) [17].

KEGG pathway analysis showed that DAMs were mainly enriched in the following 4 pathways: "biosynthesis of various secondary metabolites," "phenylpropanoid biosynthesis," "folate biosynthesis," and "Biosynthesis of unsaturated fatty acids" (Figure 3). Of these, metabolites involved in the pathways of "phenylpropanoid biosynthesis" showed the highest accumulation.

3.4. DAMs Analysis Dominated Resistance of Walnut under Prochloraz against C. gloeosporioides. All the number of DAMs enriched in the KEGG pathway were 51. Compared DAMs in CK with PT were mainly enriched in the phenylpropanoid pathway. The phenylpropanoid pathway is a well-known metabolite pathway that plays important roles in the plant disease resistance pathway [18]. There were 7 compounds of DAMs in the phenylpropanoid pathway had been detected, and they were all upregulated (Figure 4). The phenylpropanoid KEGG pathway is shown in Figure 5 (Figure S1); sinapic acid, caffeoyl quinic acid, caffeic acid, 5-hydroxyconiferyl alcohol, sinapyl alcohol, ferulic acid, and scopoletin were upregulated in this pathway. These compounds can further synthesize scopoline, sinapoyl malate, syringin, and syringyl lignin.

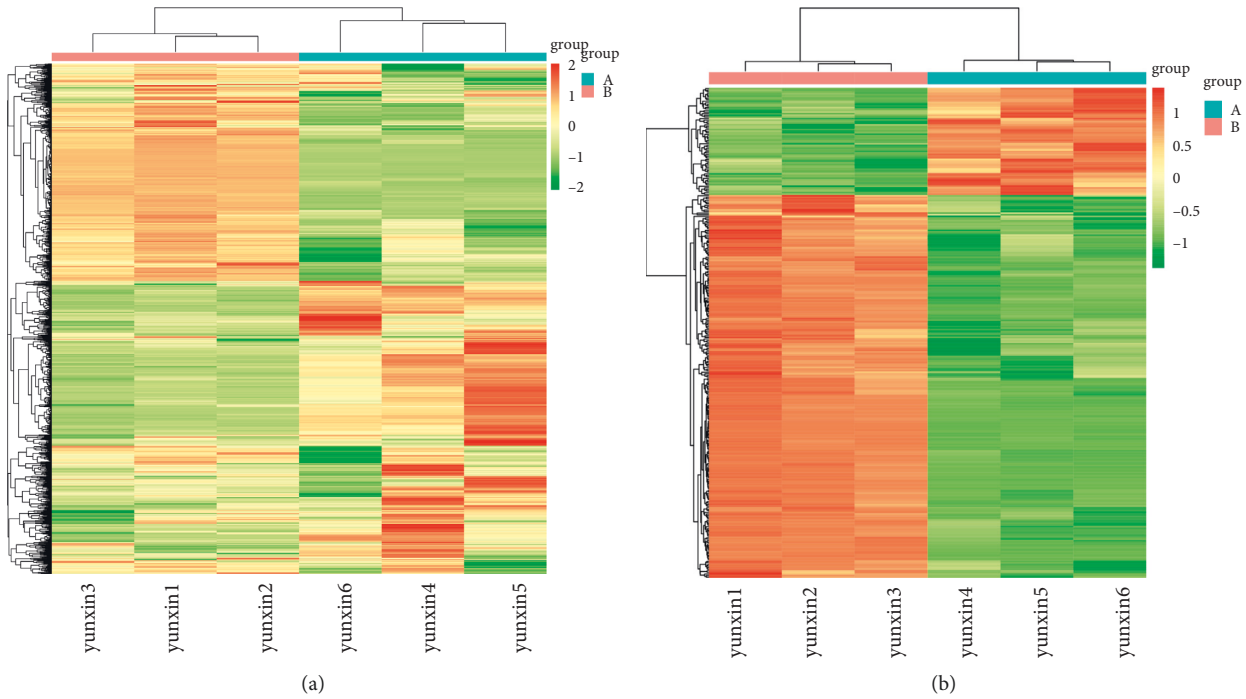

Figure 1: (a) Heatmap visualization of metabolites. (b) Heatmap of DAMs. The content of each metabolite was normalized with complete linkage hierarchical clustering. Each example was visualized in a single column, and each metabolite is represented by a single row. Red indicates high abundance, whereas low relative metabolites are shown in green.

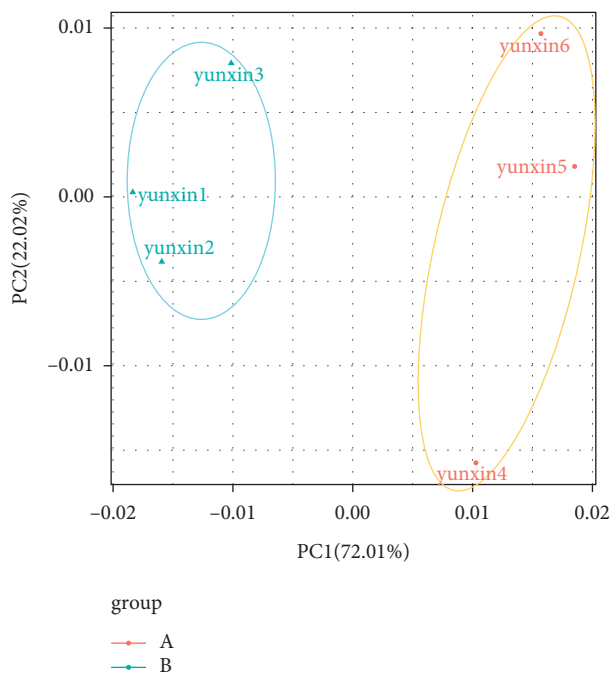

Figure 2: PCA of metabolites.

According to the KEGG pathway enrichment, the phenylpropanoid pathway may have been induced by prochloraz treatment. The phenylpropanoid pathway is an important antidisease pathway of plants; it bifurcates into the production of an enormous array of compounds based on the intermediates of the shikimate pathway in response to cell wall breach by pathogens. The whole metabolomic pathway is a complex network regulated by multiple gene

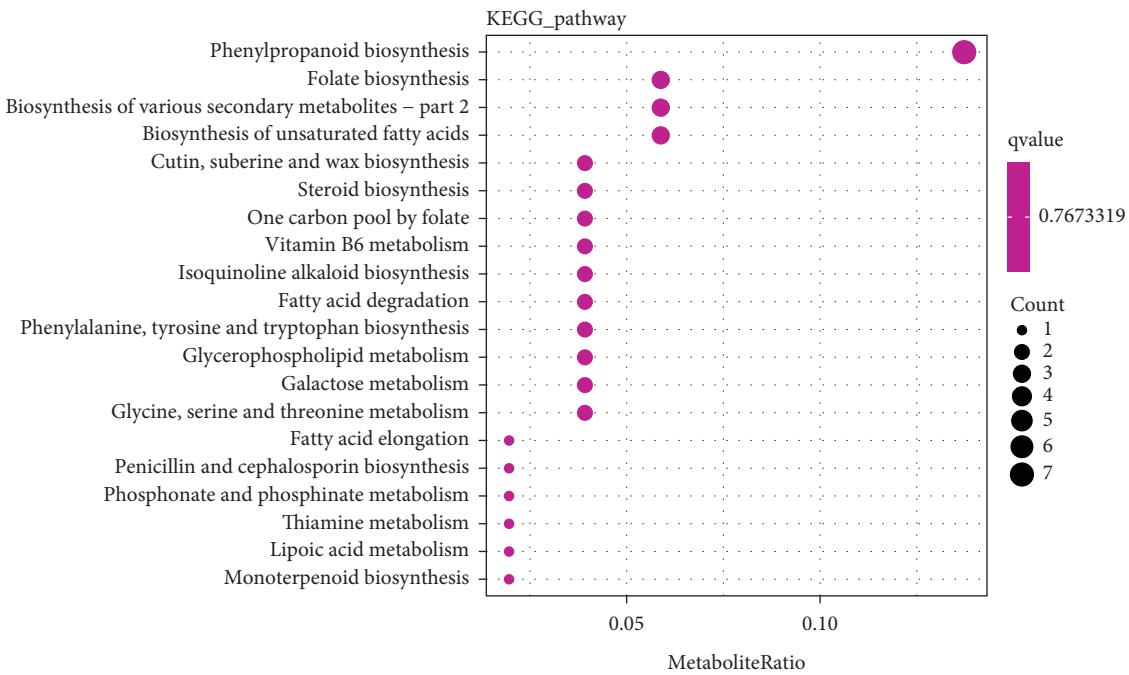

Figure 3: KEGG enrichment pathway of DAMs.

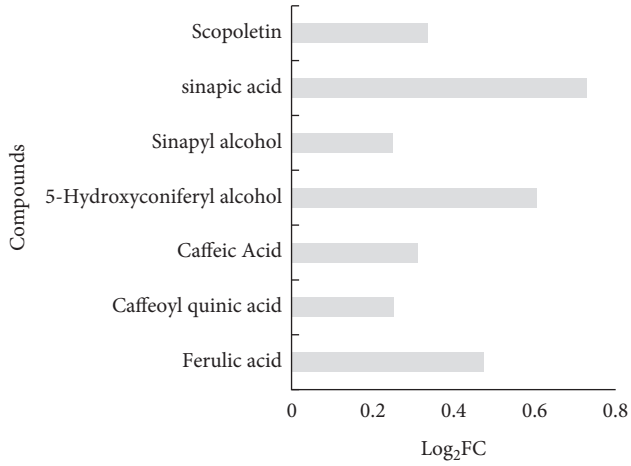

Figure 4: Metabolites of phenylpropanoid biosynthesis.

families, and it exhibits refined regulatory mechanisms at the transcriptional level [19]. The phenylpropanoid is serving as a starting point for the production of many other important compounds, such as flavonoids, coumarins, and lignans [20]; it can regulate downstream metabolite synthesis to respond to pathogen infection. When a pathogen infected plants, the microbe-associated molecular pattern (MAMP)-triggered immunity (PTI) activates a basal defense response, such as the biosynthesis of antimicrobial secondary metabolites or cell wall lignifications, protease inhibitor expression, and hormone biosynthesis [21, 22], and the lignin metabolism in plants regulated defense response that induced by pathogen [23]. According to this research, the content of sinapic acid, caffeoyl quinic acid, caffeic acid, 5-hydroxyconiferyl alcohol, sinapyl alcohol, ferulic acid, and scopoletin increased after treating and may lead to the content of lignin increase to resistant plant pathogen. As known to all, lignin plays an important role in the composition of plant cell walls [24–26]; therefore, prochloraz treatment may induce the synthesis of lignin in the cell wall to resist *C. gloeosporioides* infection expected, inhibiting the synthesis of ergosterol of pathogen.

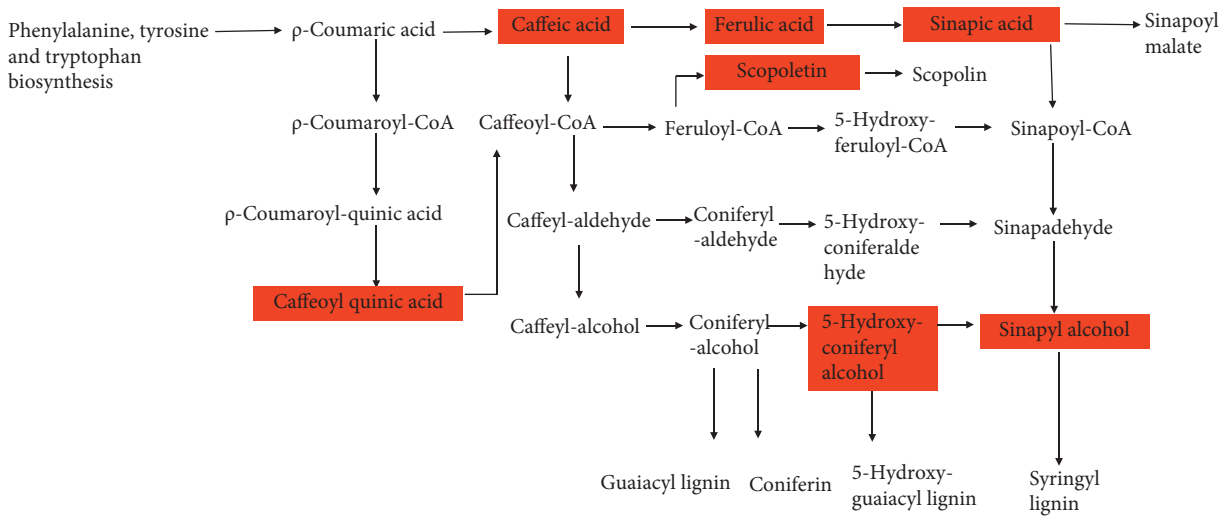

Figure 5: Expression profiles of metabolites involved in phenylpropanoid biosynthesis in CK and PT. The rectangle patterns represent the metabolites for the comparison of CK versus PT. Red indicates upregulation. Green indicates downregulation. White indicates the metabolites that were not annotated.

4. Conclusions

In conclusion, 45% prochloraz EW had the best in vitro and in vivo bioactivities against *C. gloeosporioides* with the EC_{50} values and control efficiency of 0.067 μg/mL and 73.28%, respectively. Meanwhile, metabolome analysis showed that the phenylpropanoid pathway may be induced by prochloraz to increase the metabolites of lignin to resist *C. gloeosporioides* infection.

Data Availability

The datasets used and analyzed during the current study are available from the corresponding author upon request.

Conflicts of Interest

The authors declare that they have no conflicts of interest.

Acknowledgments

This work was supported by the Guizhou Province Science and Technology Plan Project Natural Science ((2020) Y129), Guizhou Province Forestry Bureau Young Talent Found ((2019)12), and Guizhou Province Walnut Engineering Technology Research Center ((2019) 5202).

Supplementary Materials

Table S1: all metabolites in samples. Table S2: differentially accumulated metabolites in samples. Figure S1: phenylpropanoid biosynthesis, KEGG pathway. (*Supplementary Materials*)

References

[1] D. Chen, H. J. Shi, H. M. Wu, Z. H. Xu, and C. Q. Zhang, "Resistance of *Colletorichum gloeosporioides* causing grape ripe rot to thiophanate-methyl and tebuconazole in Zhejiang," *Journal of Fruit Science*, vol. 30, pp. 665–668, 2013.

[2] X. Y. Zhang, X. Li, and Z. Y. Gao, "Carbendazim resistance of *Colleotrichum gloeosporioides* on tropical and subtropical fruits," *Chinese Journal of Tropical Agriculture*, vol. 34, pp. 71–74, 2014.

[3] W. P. Deng, F. Du, M. Yang et al., "The genetic diversity of *Colletotrichum* spp. population isolated from grapes in Yunnan province," *Journal of Yunnan Agricultural University*, vol. 30, pp. 173–184, 2015.

[4] D. Da Lio, J. F. J. F. Cobo-Dıaz, C. Masson et al., "Combined metabarcoding and multi-locus approach for genetic characterization of *Colletotrichum* species associated with common walnut (*Juglans regia*) anthracnose in France," *Scientific Reports*, vol. 8, no. 1, Article ID 10765, 2018.

[5] Q. H. Wang, X. H. Liu, K. Fan, C. H. Duan, S. G. Niu, and X. Q. Wu, "Identification and biological characteristics of pathogen from *Colletotrichum gloeosporioides*," *Journal of Shandong Agricultural University (Natural Science Edition)*, vol. 47, pp. 9–14, 2016.

[6] X. X. Wang, J. G. Wei, and Z. D. Yang, "Investigation on fungal disease of Walnut in Northwest Guangxi and control experiment of Walnut anthracnose," *Journal of Southern Agriculture*, vol. 49, no. 8, pp. 1531–1540, 2018.

[7] K. Meng, Y. B. Zhan, J. Chang et al., "Toxicity test with 8 fungicides against 9 pathogens of pecan anthracnose (*Colletotrichum* spp.)," *Forest Research*, vol. 34, no. 1, pp. 153–164, 2021.

[8] X. C. Zhang, Q. Xiao, Z. Y. Gao, and J. B. Wang, "The detection of pathogenicity for Colletotrichum from different litchi cultivars and regions," *Journal of Fruit Science*, vol. 31, pp. 296–301, 2014.

[9] Q. H. Wang, K. Fan, D. W. Li et al., "Identification, virulence and fungicide sensitivity of *Colletotrichum gloeosporioides* ss responsible for walnut anthracnose disease in China," *Plant Disease*, vol. 104, no. 5, pp. 1358–1368, 2020.

[10] C. Hua, K. Kai, X. Wang, W. Shi, D. Zhang, and Y. Liu, "Curcumin inhibits gray mold development in kiwifruit by targeting mitogen-activated protein kinase (MAPK) cascades in botrytis cinerea," *Postharvest Biology and Technology*, vol. 151, pp. 152–159, 2019.

[11] W. X. Ding, X. Q. Li, C. X. Pan, J. Geng, and Y. T. Duan, "Selection of fungicides for controlling anthracnose of walnut," *Northern Horticulture*, vol. 2, pp. 30–36, 2021.
[12] J. Shi, B. Y. Li, B. H. Luan, L. Y. Li, Y. Y. Tian, and Y. Z. Wang, "Efficacy of five biological agents against grape anthracnose," *China Friuts*, vol. 1, pp. 74–76, 2021.
[13] X. Yang, Y. K. Wu, L. Fu, P. Fu, and Y. Jinyong, "Biopesticides and chemical pesticides against diaporthe vaccinii shear," *Agrochemicals*, vol. 56, no. 08, pp. 609–612, 2017.
[14] S. K. Li, F. He, Z. Chen et al., "Effective fungicides screening and field application for litchi anthracnose," *Agrochemicals*, vol. 58, no. 10, pp. 773–776, 2019.
[15] B. Zhang, W. L. Li, Q. Wu, J. Lü, and H. Li, "Evaluation of the effectiveness of fluazinam against citrus black spot," *Plant Protection*, vol. 46, 2020.
[16] R. T. Fu, Y. X. Ke, C. Chen et al., "Tocixity test and field control effect of ethylicin against several plant pathogens," *Agrochemicals*, vol. 57, no. 8, pp. 611–613, 2018.
[17] P. Li, Z. Ruan, Z. X. Fei, J. Yan, and G. Tang, "Integrated transcriptome and metabolome analysis revealed that flavonoid biosynthesis may dominate the resistance of *Zanthoxylum bungeanum* against stem canker," *Journal of Agricultural and Food Chemistry*, vol. 69, no. 22, pp. 6360–6378, 2021.
[18] R. A. Dixon, L. Achnine, P. Kota, C. J. Liu, M. S. S. Reddy, and L. Wang, "The phenylpropanoid pathway and plant defence—a genomics perspective," *Molecular Plant Pathology*, vol. 3, no. 5, pp. 371–390, 2002.
[19] V. Yadav, Z. Wang, C. Wei et al., "Phenylpropanoid pathway engineering: an emerging approach towards plant defense," *Pathogens*, vol. 9, no. 4, p. 312, 2020.
[20] C. M. Fraser and C. Chapple, "The phenylpropanoid pathway in arabidopsis," *The Arabidopsis Book/American Society of Plant Biologists*, vol. 9, 2011.
[21] C. Denoux, R. Galletti, N. Mammarella et al., "Activation of defense response pathways by OGs and Flg22 elicitors in arabidopsis seedlings," *Molecular Plant*, vol. 1, no. 3, pp. 423–445, 2008.
[22] R. Galletti, C. Denoux, S. Gambetta et al., "The atrbohD-mediated oxidative burst elicited by oligogalacturonides in arabidopsis is dispensable for the activation of defense responses effective against botrytis cinerea," *Plant Physiology*, vol. 148, no. 3, pp. 1695–1706, 2008.
[23] C. Yang, Y. Liang, D. Qiu, H. Zeng, J. Yuan, and X. Yang, "Lignin metabolism involves botrytis cinerea BcGs1- induced defense response in tomato," *BMC Plant Biology*, vol. 18, no. 1, 2018.
[24] R. Whetten and R. Sederoff, "Lignin biosynthesis," *The Plant Cell Online*, vol. 7, no. 7, p. 1001, 1995.
[25] J. H. Grabber, "How do lignin composition, structure, and cross linking affect degradability? a review of cell wall model studies," *Crop Science*, vol. 45, no. 3, pp. 820–831, 2005.
[26] Q. Zhao, H. Wang, Y. Yin, Y. Xu, F. Chen, and R. A. Dixon, "Syringyl lignin biosynthesis is directly regulated by a secondary cell wall master switch," *Proceedings of the National Academy of Sciences*, vol. 107, no. 32, pp. 14496–14501, 2010.

Hindawi
Journal of Chemistry
Volume 2022, Article ID 2293297, 9 pages
https://doi.org/10.1155/2022/2293297

Research Article

Identification of the Pathogens and Laboratory Bioactivity Determination of the Rot Disease of Kiwifruit (*Actinidia* spp.)

Yanling Ren,[1] Tao Wang,[1] Jian Tang,[1] Yingjie Jiang,[1] Yaxin Huang,[2] Chengping Zhang,[1] Jing Peng,[1] Juan Wang,[1] Shanshan Wang,[1] and Jing Wang[1]

[1]*Guizhou Light Industry Technical College, Guiyang 550025, China*
[2]*Agricultural Bureau of Xiuwen, Guiyang 550200, China*

Correspondence should be addressed to Tao Wang; wangtaotougao@126.com and Yingjie Jiang; jmulinsen@outlook.com

Received 3 May 2022; Accepted 2 June 2022; Published 27 June 2022

Academic Editor: Pei Li

Kiwifruit is an important economic crop in the world today with a high nutritional value. It can cause huge damage by causing kiwifruit rot disease; however, at present, the control methods for this disease are limited. In this study, the rotten fruits of kiwifruit (Cultivar "Jinyan") were collected from Pujiang city (Sichuan province), Xixia city, (Henan province), Zhouzhi (Shaanxi province), Meixian city (Shaanxi province), and Bijie (Guizhou province), China, and the pathogenic fungi were identified by isolation and purification, pathogenicity test, morphological characteristics, and analysis of ribosomal DNA internal transcribed spacer (rDNA-*ITS*) sequences. The results showed that the pathogenic fungi of kiwifruit rot disease were *Botryosphaeria dothidea* and *Dothiorella gregaria*. Meanwhile, the in vitro antifungal activity of 11 kinds of fungicides and 5 kinds of plant essential oils against *B. dothidea* and *D. gregaria* were determined and the results showed that all the tested fungicides and plant essential oils had a certain inhibitory effect on *B. dothidea* and *D. gregaria*. Among them, propiconazole had the best inhibitory effect on *B. dothidea* with an EC_{50} value of 4.10 mg/L, and quinolinone had the best inhibitory effect on *D. gregaria* with the EC_{50} value of 10.05 mg/L. Moreover, the pesticides and essential oils have practical application values for prevention and treatment of fruit rot diseases pathogens.

1. Introduction

Kiwifruit (*Actinidia* spp.) is rich in nutrients [1, 2], and it is one of the wild fruit trees that have been domesticated and cultivated 100 years ago [3–5]. The first record of it seem appears to be in the Book of "Shijing" before AD 1000–500 [1], while the definitive first record is in a poem written by Censen. However, the taxonomic studies, that is, to distinguish between varieties and species were still in 1984 [6]. Although it is an indigenous fruit in China [7, 8], its large-scale cultivation only started in 1978 [5], while the commercial cultivation in New Zealand began in 1930 [9]. However, because of its origin, even if it started late, China is still the largest producer of kiwifruit in the world along with New Zealand and Italy [10], and China is also the region with the highest kiwifruit diversity [11]. According to statistics, there are more than 60 species of *Actinidia* spp. in the world, with China as the center, the distribution involves latitude 500N to the equator, from cold temperate or arctic to tropical and many other countries [11–14]. As of 2019, a total of 23 countries in the world are planting kiwifruit, with a total harvest area of about 270,000 hm^2, and accounting for 67.92% (182,000 hm^2) in China [10]. In China, 40% of the kiwifruit grown in China is green pulp, followed by yellow pulp (30%) and red pulp (30%). The yellow pulp kiwifruit is mainly "Jinyan," "Jintao," "Jinyuan," "Huayou," "Jinmei," etc. [10]. "Jinyan" kiwifruit was crossed with *Actinidia chinensis* as the female parent and *Actinidia eriantha* as the male parent by the Wuhan Botanical Garden of the Chinese Academy of Sciences in 1984 [15]. It is a kind of the kiwifruit with the characteristics of high yield, beautiful and tidy fruit, smooth skin, less hairy, high content of ascorbic acid in fruit, good quality, and good storage resistance [16, 17]. It has been promoted and planted in various regions of China, including Yunnan [17], Jiangxi [16], Sichuan [18], and Guizhou [19].

The fruit rot disease can harm many fruits, such as, apple [20], sweet pepper [21], watermelon [22], areca nut [23], tomato [24], etc. It is also one of the main diseases of kiwifruit after the near-ripening stage. The damaged kiwifruit will form lesions during severe periods and emit an alcohol smell, making it inedible. The fungi of *Botryosphaeraceae* (Ascomycota: *Dothideomycetes*) degrade and passivate pollutants are a type of fungi with great potential in environmental remediation [25, 26]. But at present, its harms outweigh its benefits. This type of fungus generally parasitizes or grows in the fruits, roots, stems, and leaves of plants, causing a variety of plant diseases [27–29]. *Botryosphaeria dothidea* belong to *Botryosphaeraceae*. It is currently recognized by domestic and foreign scholars as the main pathogen causing the kiwifruit fruit rot disease [30, 31]. It is distributed in many countries and regions: New Zealand [32–34], Iran [35], Japan [36], Chile [37], Italy [38], United States [39], South Korea [40, 41], and China [42–45]. In addition to infecting kiwifruit and causing fruit rot disease, this fungus can also cause other diseases [46–49]. With the increasingly serious damage of the fruit rot disease, the prevention and control of fruit rot disease has gradually attracted the attention of the world. For example: 11% metalaxyl-M·fludioxonil·azoxystrobin, 43% Tebuconazole, Atailin, Carbendazim, and *Bacillus polymyxa,* cuminaldehyde, geraniol, and β-citronellol have a good inhibitory effect on *B. dothidea* [50–54]. However, there are fewer repots about the rot disease in kiwifruit (Cultivar "Jinyan") [55].

In order to avoid the development of related fungal resistance and ensure the diversity of fungicides, research studies on other fungicides for fruit rot disease pathogens and new fungicides of botanical origin are necessary. Therefore, in this study, the rotten fruits of kiwifruit (Cultivar "Jinyan") were collected and the pathogenic fungi were identified. Meanwhile, the in vitro antifungal activity of 11 kinds of fungicides and 5 kinds of plant essential oils against *B. dothidea* and *D. gregaria* was determined.

2. Materials and Methods

2.1. Pathogen Identification and Pathogenicity Test. The rotten kiwifruit was collected from Pujiang city (Sichuan province), Xixia city, (Henan province), Zhouzhi (Shaanxi province), Meixian city (Shaanxi province), and Bijie (Guizhou province), China (Figure 1), and packaged in a clean Ziplock bag, then was taken back to the Guizhou Engineering Research Center for Mountain Featured Fruits and Products, Guizhou Light Industry Technical College, and stored at 4°C.

The kiwifruits are first rinsed with tap water and ultrapure water 3 times, respectively, and then ventilated for 30 min to dry. The infected tissues ($1 \times 1 \times 0.5$ cm size) were soaked in 75% alcohol for about 30 s, rinsed with sterile water 3 s, and then the tissues were plated on the PDA plates. After that, the PDA plates were maintained in a constant temperature incubator at 26°C without light. After 3 days, all the strains were cultured on the new PDA plates using a single spore technique to ensure purity. Finally, the purified strains were stored at 4°C for further use.

Pathogenicity determination of pathogenic fungus was performed according to Koch's law. The healthy and near-ripe kiwifruits (Cultivar "Jinyan") were soaked in 75% alcohol for 60 s, washed with sterile water 2-3 times, and then placed on the filter papers for 15 s to absorb moisture. A sterile inoculation needle was used to pierce the middle epidermis of the cleaned kiwifruits to form a 0.2 mm wound, and a 0.5 cm sterile punch was used to make a fungus cake, and the mycelial surface of the fungus cake was attached to the wound. The sterile distilled water served as a negative control. Each treatment was repeated three times. After that, the kiwifruits were incubated in a 26°C constant temperature incubator with a humidity of 60% and a photoperiod of 12L : 12D. The surface of healthy and nearly mature kiwifruits inoculated with sterile water served as a control. After 7 days of inoculation, some symptoms have been observed on the surface. The causal fungus in the infected kiwifruit surface was re-isolated on the PDA plate as described above. The characteristics of the re-isolated fungus was used to compare with its original culture. The pathogenic fungi separation rate and the disease severity index (DSI) of Koch's test were calculated according to the following formulas. In the formulas, 0, 1, 3, 5, and 7 represent different disease levels (0: no disease; 1 : 0% < disease plaque size < 10%; 3 : 10% < disease plaque size < 25%; 5 : 25% < disease plaque size < 50%; 7 : 50% < disease plaque size), and A, B, C, D, and E represent the number of seedlings within each disease severity levels [56].

$$\text{Separation rate}\,(\%) = \frac{\text{Number of separate pathogenic fungi kiwifruits}}{\text{Total number of test kiwifruits}} \times 100,$$

$$\text{DSI} = \left(\frac{(0A + 1B + 3C + 5D + 7E)}{4\,(A + B + C + D + E)}\right) \times 100. \quad (1)$$

2.2. Morphological and Molecular Identification. Individual colony was inoculated on the PDA plate and maintained in a constant temperature incubator at 26°C without light for 8 days. Then, the morphology was identified by both eye and an inverted microscopy (ECLIPSE Ni-E, Nikon Corporation, Japan).

The fungus DNA extraction was performed using the DP336 kit (Beijing Tsingke Biotechnology Co., Ltd. Chengdu Branch (BT)), and the steps were referred to the kit's instructions. The extracted DNA is amplified by PCR reaction to obtain the target gene fragment. The reaction system: 12.5 μL 2xEs Taq Mix (BT), 1 μL forward primer (ITS1: 5′-TCCGTAGGTGAACCTGCGG-3′), 1 μL reward primer (ITS4: 5′-TCCTCCGCTTATTGATATGC-3′) [57], 1 μL DNA, and 9.5 μL ddH_2O. Reaction conditions were as follows: pre-denaturation at 94°C for 5 min, 35 cycles (denaturation at 94°C for 30 s, annealing at 56°C for 1 min, extension at 72°C for 1 min), extension at 72°C for 7 min, and

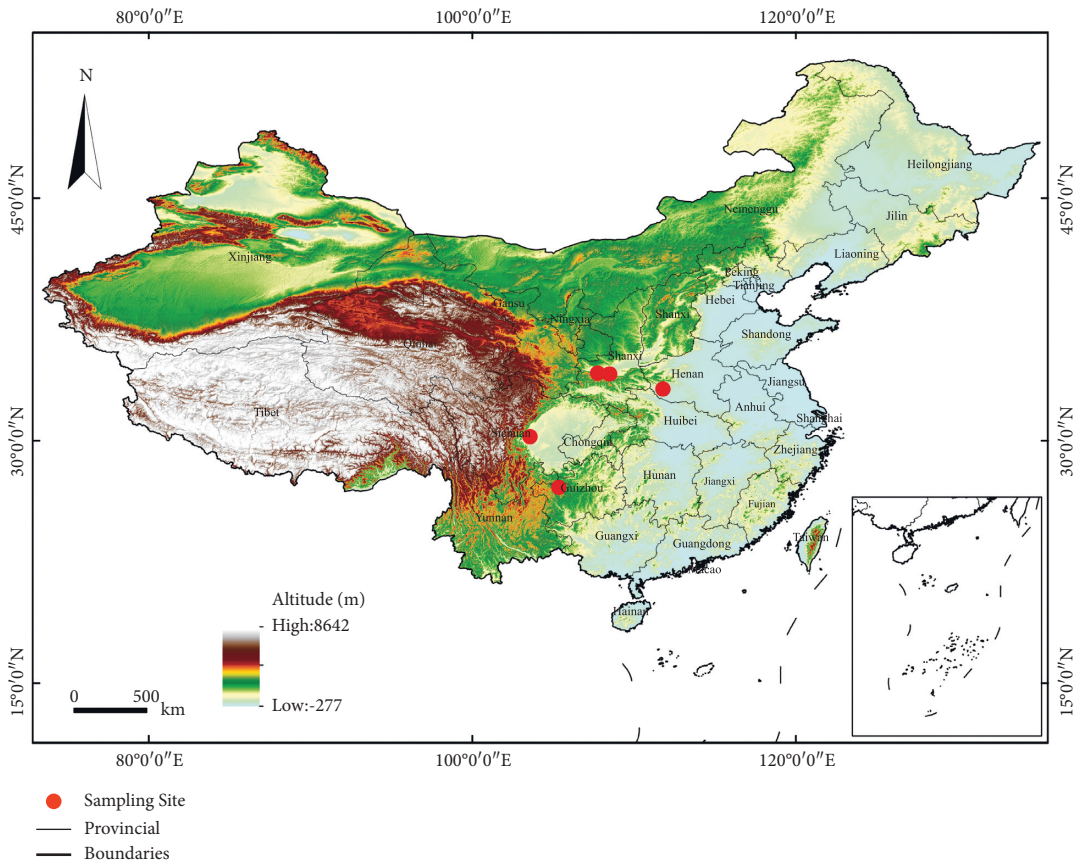

Figure 1: Distribution map of kiwifruit sample collection points.

stored at 4°C. The amplified products were sequenced by Applied Biosystems (3730XL) equipment.Viewing and calibration of sequences were performed in BioEdit (version 7.0.9.0) to obtain high-quality sequences. The obtained high-quality sequences were aligned and identified in the NCBI (https://www.ncbi.nlm.nih.gov/). Moreover, the sequences were upload to the Genbank database to obtain the accession numbers of ON566021 and ON566022.

2.3. Phylogenetic Tree Construction. Referring to the research of Zheng et al. [47], *Tiarosporella graminis* (Genbank: KC769962.1) was selected as the outgroup comparison. High-quality sequences were aligned by MAFFT (version 7.149b) [58]. The aligned sequences were edited in gBlocks (version 0.91b) software to obtain conserved sequences [59]. The ML tree of all sequences was reconstructed in MEGA (version 7.0.26), and the base substitution model used GTR + G + I clade support was estimated by bootstrap analyses with 1,000 replicates [60].

2.4. In Vitro Antifungal Activity Test. In this study, 11 kinds of fungicides and 5 kinds of plant essential oils (Table 1) against *B. dothidea* and *D. gregaria* were determined according to the reported method [53]. The inhibition rates I (%) are calculated after 7 days by the following formula, where C (cm) and T (cm) represent the fungi diameters of the CK and treated PDA plates, respectively. Meanwhile, the EC_{50} values of 11 kinds of fungicides and 5 kinds of plant essential oils against *B. dothidea* and *D. gregaria* were calculated with SPSS 19.0 software.

$$\text{Inhibition Rate } I\,(\%) = \left(\frac{(C-T)}{C}\right) \times 100. \quad (2)$$

3. Result

3.1. Pathogenicity Determination. Figure 2 shows that the strain F1 and strain F4 can cause kiwifruit rot disease. Moreover, 7 days after the pathogenicity test, the pathogenic rates of F1 and F4 strains are both 100%, and the DSI is 10.7% (Table 2). Therefore, the F1 and F4 strains are the pathogens of kiwifruit rot disease. The diseased kiwifruit was re-isolated, and the strains with the same morphological characteristics as the original inoculated strains were obtained, which met the requirements of Koch's law.

3.2. Morphological Identification and Sequence Identification. Figure 3(a) shows that the hyphae of strain F1 were initially transparent and grew in an irregular circular shape with a fast growth rate. The color gradually changed to white and off-white with time and began to appear light gray on the 3rd day (Figures 3(a) and 3(c)). In the later stage of observation, the color of the hyphae was dark green and the hyphae branched more and intertwined with each other

Table 1: List of 11 kinds of fungicides and 5 kinds of plant essential oils.

Names	Source
33.5% quinolinone SC	Shanghai hulian biological pharmaceutical co., Ltd
250 g/L propiconazole EC	Shandong xinxing pesticide co. Ltd
25% myclobutanil EC	Zhejiang yifan biotechnology group co., Ltd
25% bromothalonil WP	Jiangsu tuoqiu agrochemical co. Ltd
3% zhongshengmycin WP	Fujian kaili bio-product co., Ltd
80% ethylicin EC	Henan kebang chemical co, Ltd
100 g/L cyazofamid SC	Henan guangnong pesticide factory
10% polyoxin WP	Shanghai hulian biological pharmaceutical co., Ltd
1% osthol AP	Inner Mongolia qingyuanbao biological technology co., Ltd
0.3% eugenol AP	Jiangsu nantong shenyu green medicine co., Ltd
20% triazolone EC	Chongqing yiershuangfeng technology co., Ltd
75% chlorothalonil WP	Shandong luobang biopesticides co. Ltd
66% dithianon WG	Jiangxi heyi chemical co., Ltd
Patchouli essential oil	Beijing maosi trading co., Ltd
Ylang-ylang essential oil	Beijing maosi trading co., Ltd
Garlic essential oil	Beijing maosi trading co., Ltd
Cedarwood essential oil	Beijing maosi trading co., Ltd

Figure 2: The symptoms of F1 and F4 strains in pathogenicity test. (a) and (d): Natural occurrence characteristics of kiwifruit fruit rot disease, (b) and (e): pathogenicity test CK group, (c) and (f): pathogenicity test characteristics; (a)–(c) F1 strain. (d)–(f) F4 strain. Scale bar: 10 mm.

(Figures 3(a) and 3(c)). Its morphology was consistent with the descriptions of Liang and Ferguson [6] and He et al. [61].

Figure 3(d) shows that the hyphae of strain F4 were felt-like and the hyphae were gray in the early stage of growth. The hyphae were pale yellow-green and the center was dark gray on the 4th day. On the 8th day, the diameter of the fungus covered the petri dish (diameter = 90 mm) (Figure 3(e)). Figure 3(d) shows that the hyphae had more branches, thinner hyphae, and vigorous hyphae growth. As the growth days increased, the hyphae were dark gray in the

Table 2: Separation rate of pathogenic fungi of kiwifruit fruit rot and pathogenic rate and DSI of pathogenicity test.

Strain	Separation rate (%)	Pathogenic rate (%)	DSI (%)
F1	50	100	10.7
F4	5	100	10.7

Data statistics after seven days of pathogenicity test.

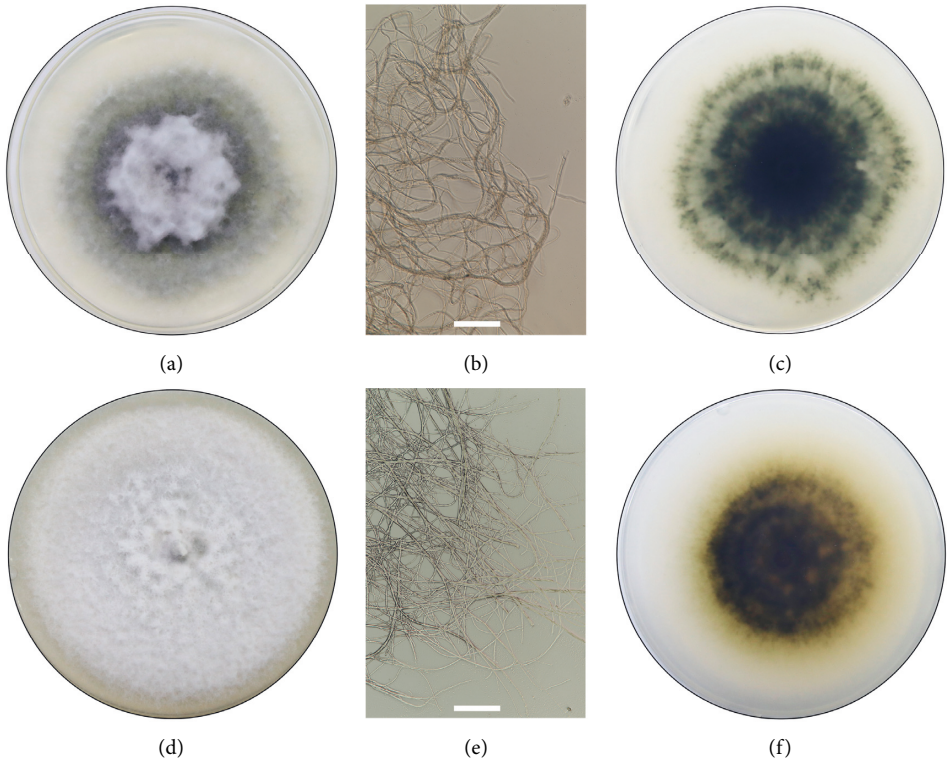

Figure 3: Morphological characteristics of pathogenic fungus of kiwifruit fruit rot disease. (a) and (d) observe surface of colony (front), (c) and (f) observe surface of colony (back), (b) and (e) mycelial morphology. (a)–(c) F1 strain. (d)–(f) F4 strain. Scale bar: 100 nm.

middle, white at the edges, and black at the bottom of the medium (Figure 3(f)). The morphology is basically consistent with the descriptions of Saccardo [62] and Zhao and Huang [63].

The phylogenetic tree was constructed using the MEGA 7.0 based on the *ITS* sequence and the results shown in Figure 4. As shown in Figure 4, the F1 and F4 strains were classified as *Botryosphaeria dothidea* and *Dothiorella gregaria*, respectively.

3.3. In Vitro Antifungal Activity. It can be seen from Table 3, the test fungicides and plant essential oils revealed different degrees of inhibition on the growth of *B. dothidea* and *D. gregaria*. Especially, quinolinone showed the best inhibitory effect against *D. gregaria* with the EC_{50} value of 10.05 mg/L; meanwhile, propiconazole had an EC_{50} value of 4.10 mg/L against *B. dothidea*, which was even better than those of other fungicides and plant essential oils.

4. Discussion

Since the first report of kiwifruit fruit rot in 1985 [64], it has been studied by various scholars one after another. At present, a variety of pathogens have been found, such as *B. dothidea*, *Botryotinia fuckeliana*, *Alternaria alternata*, *Cylindrocarpon candidum*, etc [33, 43, 64, 65]. However, *D. gregaria* is the first report that can cause fruit rot in kiwifruit. It was previously reported as the causative agent of poplar canker [66, 67], jujube fruit shrink disease [68, 69], jujube fruit black rot disease [70], cedar dieback disease [71, 72], citrus [73]. In previous studies, there are fewer control methods for this fungus: the combination of 20.67% Wanxing EC + 68.75% Yibao dispersible granules + 72% streptomycin soluble powder had a good control effect on the fungus, and the field control effect on jujube shrinkage fruit disease reached 86.9% [68]. Among the substances screened in this study, quinolinone has the lowest EC_{50} value, reaching 10.05 mg/L, such that the agent should be able to achieve a good effect in the field control of rhesus monkey fruit rot.

Among the agents we screened against *B. dothidea*, propiconazole has the best effect, and its EC_{50} reached 4.10 mg/L after 7 days, so propiconazole is recommended as an effective control agent for kiwifruit fruit rot caused by *B. dothidea*. Besides, the antifungal effect of monoterpenes on *B. dothidea* showed that cuminaldehyde had the best

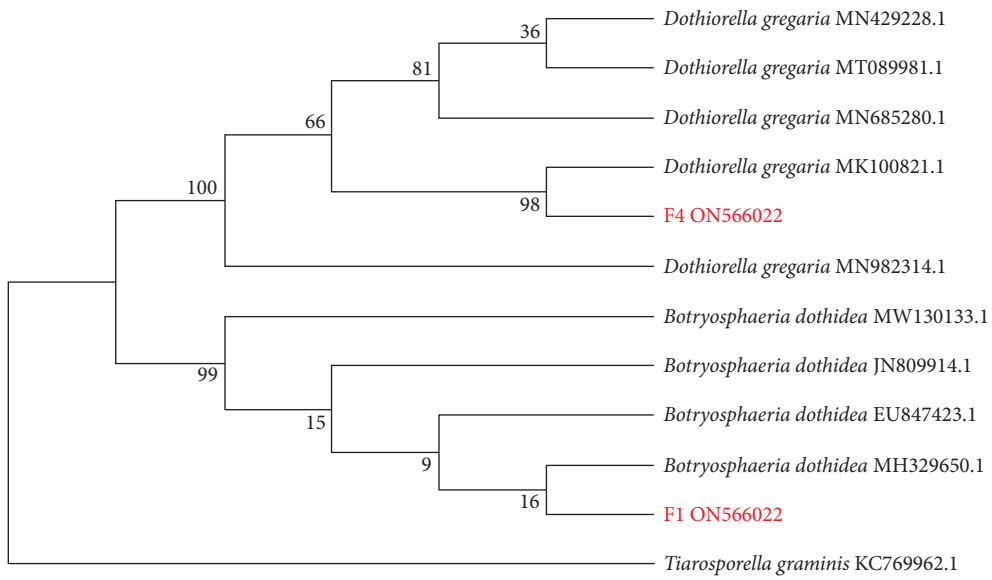

Figure 4: ML Phylogenetic tree based on *ITS*-rDNA gene sequence of kiwifruit fruit rot disease pathogen. Posterior probabilities from 1,000 bootstraps inferences are given node dates. The out group is *Tiarosporella graminis*.

Table 3: The EC_{50} values of the test fungicides and plant essential oils against *Botryosphaeria dothidea* and *Dothiorella gregaria*.

Treatment	*Dothiorella gregaria*		*Botryosphaeria dothidea*	
	Regression equation	EC_{50} (mg/L)	Regression equation	EC_{50} (mg/L)
Quinolinone	$Y = 3.9521 + 1.0456\ X$	10.05	$Y = 2.8548 + 0.9647\ X$	167.40
Propiconazole	$Y = 3.8706 + 1.1022\ X$	10.58	$Y = 4.4247 + 0.9394\ X$	4.10
Cyazofamid	$Y = 3.7769 + 0.9738\ X$	18.03	$Y = 3.1692 + 1.0047\ X$	66.40
Myclobutanil	$Y = 3.6815 + 1.0232\ X$	19.44	$Y = 3.9907 + 1.1013\ X$	8.25
Bromothalonil	$Y = 3.4510 + 0.9517\ X$	42.43	$Y = 3.6706 + 1.0776\ X$	17.12
Eugenol	$Y = 2.9490 + 1.2041\ X$	50.51	$Y = 3.2386 + 1.1044\ X$	39.34
Zhongshengmycin	$Y = 2.8882 + 1.0207\ X$	117.24	$Y = 3.5394 + 1.0988\ X$	21.35
Osthol	$Y = 2.5885 + 1.1629\ X$	118.52	$Y = 2.7987 + 1.4142\ X$	36.02
Polyoxin	$Y = 2.7142 + 1.0970\ X$	121.27	$Y = 2.4053 + 1.2884\ X$	103.25
Ethylicin	$Y = 2.5530 + 1.1350\ X$	143.22	$Y = 2.1970 + 1.4658\ X$	81.72
Chlorothalonil	$Y = 2.7630 + 0.8777\ X$	353.73	$Y = 3.5119 + 0.8690\ X$	51.57
Triazolone	$Y = 1.9850 + 1.1435\ X$	433.08	$Y = 2.8361 + 1.0914\ X$	96.10
Dithianon	$Y = 1.4391 + 1.2688\ X$	640.33	$Y = 1.1043 + 1.4664\ X$	453.47
Patchouli essential oil	$Y = 2.6529 + 1.1907\ X$	93.56	$Y = 2.7897 + 1.0509\ X$	126.84
Cedarwood essential oil	$Y = 2.7182 + 1.1448\ X$	98.43	$Y = 2.7233 + 1.0809\ X$	127.73
Garlic essential oil	$Y = 2.4979 + 1.2248\ X$	110.37	$Y = 3.0058 + 1.0010\ X$	98.21
Ylang-ylang essential oil	$Y = 2.3641 + 1.2185\ X$	145.65	$Y = 2.9745 + 1.0192\ X$	97.14

effect with the EC_{50} of 105.2 mg/L [54]; however, the bioactivity was lower than that of ylang-ylang essential oil reported in our present study ($EC_{50} = 97.14$ mg/L). Although there are many studies on plant essential oils or their volatile substances to control pests [74–78], the current application needs to be accelerated to provide new pesticides for comprehensive pest control.

5. Conclusion

In conclusion, our results showed that *B. dothidea* and *D. gregaria* were the pathogenic fungi of kiwifruit (Cultivar "Jinyan") rot disease in China. Meanwhile, quinolone and propiconazole revealed the best inhibitory effect on *D. gregaria* and *B. dothidea*, respectively. Our study could provide a theoretical basis for the effective control method of kiwifruit rot disease in China.

Data Availability

All data included in this study are available upon request by contacting the corresponding author.

Disclosure

This research is the achievement of Guizhou Province Academic Pioneer and Academic Pioneer Construction.

Conflicts of Interest

The authors declare that they have no conflicts of interest.

Authors' Contributions

Tao Wang and Yanling Ren contributed equally to this article.

Acknowledgments

The study was supported by the Science and Technology Project of China Tobacco Guizhou Provincial Corporation, grant number (201918), the Science and Technology Foundation of General Administration of Quality Supervision, Inspection and Quarantine of the Peoples Republic of China, grant number (2017IK257, 2017IK261, 2016IK075, and 2014IK022), the Science and Technology Foundation of Guizhou Province, grant number J(2013)2149, the 2021 Humanities and Social Sciences Research Project of Guizhou Provincial Department of Education, grant number (2022ZC016), and the 2021 Guizhou Province Theoretical Innovation Project (Joint Project), grant number (GZLCLH-2021-169). This research is the achievement of Guizhou Province Academic Pioneer and Academic Pioneer Construction.

References

[1] C. Huang, C. C. Zhou, and W. Li, "Nutrition and health care function of kiwi fruit and its processing technique," *Food Science and Technology*, vol. 4, pp. 51–55, 2007.

[2] D. P. Richardson, J. Ansell, and L. N. Drummond, "The nutritional and health attributes of kiwifruit: a review," *European Journal of Nutrition*, vol. 57, no. 8, pp. 2659–2676, 2018.

[3] H. Huang and A. R. Ferguson, "Genetic resources of kiwifruit: domestication and breeding," *Horticultural Reviews*, vol. 33, pp. 1–12, 2007.

[4] Y. Song and Z. X. Liu, "A review of studies on kiwifruit planting and meteorological conditions in my country," *Jiangsu Agricultural Sciences*, vol. 48, no. 8, pp. 41–47, 2020.

[5] Z. W. Jiang and C. H. Zhong, "A comprehensive understanding with the importance of popular science knowledge to the kiwifruit quality improvement," *China Fruits*, vol. 1, pp. 1–8, 2020.

[6] C. F. Liang and A. R. Ferguson, "Emendation of the latin name of *Actinidia chinensis P*1. var. hispida Guihaia," *New Zealand Journal of Botany*, vol. 4, pp. 181-182, 1984.

[7] A. R. F. Kiwifruit, "A botanical review," *Hartwick Review*, vol. 6, pp. 1–64, 1984.

[8] H. Huang and A. R. Ferguson, "Review: kiwifruit in China," *New Zealand Journal of Crop and Horticultural Science*, vol. 29, no. 1, pp. 1–14, 2001.

[9] B. N. Hazarika, T. Angami, and V. A. Parthasarathy, *Kiwifruit*, Daya Publishing House, Delhi, India, 2022.

[10] C. H. Zhong, W. J. Huang, and D. W. Li, "Development of world kiwifruit industry and dynamic analysis of fresh fruit trade," *China Fruits*, vol. 7, pp. 101–108, 2021.

[11] H. W. Huang, S. J. Gong, S. M. Wang, H. Zi-Can, Z. Zhong-Hui, and L. Jian-Qiang, "Genetic diversity in the genus *Actinidi*," *Chinese Biodiversity*, vol. 8, no. 1, pp. 1–12, 2000.

[12] C. F. Liang, "On the distribution of *Actinidias*," *Guihaia*, vol. 3, pp. 229–248, 1983.

[13] Z. X. Cui, H. Huang, and X. G. Xiao, *Actinidia in China*, Agricultural Science and Technology Press, Beijing, China, 2002.

[14] H. Rymbai, H. Talang, and D. V. Dayal, "Kiwifruit-a rich value crop for hilly ferrain," in *Natural Resource Management in Horticultural Crops*Publisher: Today & Tomorrow's Printers and Publishers, New Delhi, India, 2022.

[15] C. Zhong, S. Wang, Z. Jiang, and H. Huang, "'Jinyan', an interspecific hybrid kiwifruit with brilliant yellow flesh and good storage quality," *HortScience*, vol. 47, no. 8, pp. 1187–1190, 2012.

[16] S. S. Chen, Y. Q. He, and X. B. Xu, "Comparative analysis of fruit quality of "Jinyan" kiwifruit from different origins in Jiangxi Province," *South China Fruits*, vol. 51, no. 2, pp. 113–116, 2022.

[17] Y. C. Yang, Q. D. Nong, Y. X. Li et al., "Introduced performance of four kiwifruit varieties in rocky desertification areas of Yunnan Province," *South China Fruits*, vol. 51, no. 1, pp. 130–134, 2022.

[18] Z. J. Qian, T. Liu, and H. Wang, "Effects of harvest stage and storage temperature on quality of 'Jin Yan' kiwifruit (*Actinidia chinensis* × *A. eriantha*)," *Journal of Tropical and Subtropical Botany*, vol. 19, no. 2, pp. 127–134, 2011.

[19] M. Zhang, D. M. Tang, and Z. B. Zhao, "Evaluation of canker resistance on yellow-fleshed kiwifruit cultivars and superior lines in Guizhou," *Molecular Plant Breeding*, vol. 19, no. 23, pp. 7892–7899, 2021.

[20] M. Petreš, J. Kalajdžić, B. Milić et al., "Effect of hot water treatments on apple fruit rot caused by *Fusarium* spp," *Journal of Plant Diseases and Protection -New Series*, vol. 127, no. 5, pp. 651–655, 2020.

[21] M. R. L. Mallik, M. M. Sikder, M. K. Hossain, M. B. Billah, and N. Alam, "Molecular characterization and in vitro control measures of fruit rot disease of sweet pepper," *International Journal of Agricultural Research, Innovation and Technology*, vol. 11, no. 2, pp. 108–116, 2021.

[22] M. Z. Rahman, K. Ahmad, Y. Siddiqui et al., "First report of *Fusarium equiseti*, causing fruit rot disease of watermelon in Malaysia," *Plant Disease*, vol. 106, no. 1, pp. 1–7, 2021.

[23] P. Balanagouda, S. Sridhara, S. Shil et al., "Assessment of the spatial distribution and risk associated with fruit rot disease in *Areca catechu* L," *Journal of Fungi*, vol. 7, no. 10, p. 797, 2021.

[24] C. Mohana, H. K. N. Kumar, S. Mahadevakumar, R. Sowmya, K. R. Sridhar, and S. Satish, "First report of *Aspergillus versicolor* associated with fruit rot disease of tomato (*Solanum lycopersicum*) from India," *Plant Disease*, vol. 106, no. 4, pp. 1–3, 2022.

[25] Z. Y. Zhang, C. P. Wang, H. B. Liu, and H.-W. Sun, "Bioremediation of PAHs contaminated soil from beijing coking plant by *Lasiodiplodia theobromae*," *Environmental Sciences*, vol. 33, no. 8, pp. 2833–2839, 2012.

[26] Z. Deng, R. Zhang, Y. Shi, L. A. Hu, H. Tan, and L. Cao, "Characterization of cd-, pb-, zn-resistant endophytic *Lasiodiplodia sp*. MXSF31 from metal accumulating Portulaca oleracea and its potential in promoting the growth of rape in metal-contaminated soils," *Environmental Science and Pollution Research*, vol. 21, no. 3, pp. 2346–2357, 2014.

[27] X. Q. Wu, Q. Y. He, and Z. H. Liu, "Occurrence and progress on tree cankers caused by *Botryosphaeria* spp," *Journal of Nanjing Forestry University (Natural Sciences Edition)*, vol. 25, no. 1, pp. 61–66, 2001.

[28] B. Slippers, W. A. Smit, and P. W. Crous, "Taxonomy, phylogeny and identification of Botryosphaeriaceae associated with pome and stone fruit trees in South Africa and other

regions of the world," *Plant Pathology*, vol. 56, pp. 128–139, 2007, T. A. Coutinho B. D. Wingfield M. J. Wingfield.

[29] C. Y. Meng, *Molecular Phylogenetic Studies on Plant Pathogenic Fungi of Botryosphaeriaceae*, Guizhou University, Guiyang, China, 2021.

[30] Y. H. Ou, *Identifieation of Bacillus Siamensis Antagonistic to Fruit Ripe Rot of Kiwifruit and the Tentative Study of its Antimicrobical*, Jiangxi Agricultural University, Nanchang, China, 2017.

[31] L. Wei, *Studies on Mechanism of Citral in Preventing and Controlling Soft Rot of Kiwifruit and its Effect on Kiwifruit Postharvest Preservation*, Jiangxi Agricultural University, Nanchang, China, 2021.

[32] B. T. Hawthorne, J. Rees-George, and G. J. Samuels, "Fungi associated with leaf spots and post-harvest fruit rots of kiwifruit (*Actinidia chinensis*) in New Zealand," *New Zealand Journal of Botany*, vol. 20, no. 2, pp. 143–150, 1982.

[33] S. R. Pennycook, "Fungal fruit rots of *Actinidia deliciosa* (kiwifruit)," *New Zealand Journal of Experimental Agriculture*, vol. 13, no. 4, pp. 289–299, 1985.

[34] M. A. Manning, X. Meier, T. L. Olsen, and P. R. Johnston, "Fungi associated with fruit rots of *Actinidia chinensis* 'Hort16A' in New Zealand," *New Zealand Journal of Crop and Horticultural Science*, vol. 31, no. 4, pp. 315–324, 2003.

[35] E. Nazerian, M. Mirabolfathy, S. P. Ashnaei, and F. Beiki, "Characterization of *Botryosphaeria dothidea* as new pathogen of kiwifruit in Iran," *Journal of Plant Protection Research*, vol. 59, no. 1, pp. 134–137, 2019.

[36] T. S. Yong, "Soft rot of kiwi fruit," *Agriculture and Horticulture*, vol. 57, no. 12, pp. 33-34, 1982.

[37] J. Auger, I. Pérez, and M. Esterio, "*Diaporthe ambigua* associated with post-harvest fruit rot of Kiwifruit in Chile," *Plant Disease*, vol. 97, no. 6, 2013.

[38] L. Luongo, A. Santori, L. Riccioni, and A. Belisario, "*Phomopsis* sp. associated with post-harvest fruit rot of kiwifruit in Italy," *Journal of Plant Pathology*, vol. 93, pp. 205–209, 2011.

[39] L. Beraha, "Stem-end rot of Chinese gooseberry (*Actinidia chinensis*) on the market," *Plant Disease Reporter*, vol. 54, no. 5, pp. 422-423, 1970.

[40] Y. J. Koh, J. S. Hur, and J. S. Jung, "*Botrysphaeria dothidea*, the causal organism of ripe rot of kiwifruit (*Actinidia deliciosa*) in korea," *New Zealand Journal of Experimental Agriculture*, vol. 33, no. 3, pp. 303–310, 2003.

[41] Y. J. Koh, J. S. Hur, and J. S. Jung, "Postharvest fruit rots of kiwifruit (*Actinidia deliciosa*) in Korea," *New Zealand Journal of Crop and Horticultural Science*, vol. 33, no. 3, pp. 303–310, 2005.

[42] R. L. Wang, *Study on Physiology of Post-harvest Diseases on 'Red Sun' Kiwifruit and Preservation Technology by Ozone. Sichuan*, Sichuan Agricultural University, Yaan, China, 2010.

[43] C. Li, J. X. Jiang, and J. H. Leng, "Isolation and identification of pathogenic fungi causing fruit rot of kiwifruit in Fengxin county," *Acta Agriculturae Universitatis Jiangxiensis*, vol. 34, no. 2, pp. 259–263, 2014, L. I. Bang-ming Y. U. Qiang T. U. Gui-qing.

[44] Y. Zhou, G. Gong, Y. Cui et al., "Identification of *Botryosphaeriaceae* species causing kiwifruit rot in Sichuan province, China," *Plant Disease*, vol. 99, no. 5, pp. 699–708, 2015.

[45] L. Wang, H. Hou, Z. Zhou, H. Tu, and H. Yuan, "Identification and detection of *Botryosphaeria dothidea* from kiwifruit (*Actinidia chinensis*) in China," *Plants*, vol. 10, no. 2, p. 401, 2021.

[46] A. Marsberg, M. Kemler, F. Jami et al., "Botryosphaeria dothidea: a latent pathogen of global importance to woody plant health," *Molecular Plant Pathology*, vol. 18, no. 4, pp. 477–488, 2017.

[47] X. R. Zheng, M. J. Zhang, X. L. Shang, S.-Z. Fang, and F.-M. Chen, "Stem canker on *Cyclocarya paliurus* is caused by *Botryosphaeria dothidea*," *Plant Disease*, vol. 104, no. 4, pp. 1–9, 2019.

[48] T. M. Chen, X. C. Shi, S. Y. Wang, and P. Laborda, "First report of *Botryosphaeria dothidea* causing stem canker on soybean in China," *Plant Disease*, vol. 105, no. 4, pp. 1–6, 2020.

[49] Z. Polat, M. A. Gültekin, G. Palacıoğlu, and H. Bayraktar, "First report of *Botryosphaeria dothidea* causing stem canker of hazelnut in Turkey," *Journal of Plant Pathology*, vol. 104, no. 467, 2021.

[50] Y. Zhou, Y. H. Ou, and J. X. Jiang, "Indoor virulence determination of 10 fungicides against *Botryosphaeria dothidea*," *South China Fruits*, vol. 45, no. 6, pp. 124–130, 2016.

[51] W. N. Wu, Q. Zhang, and Q. Q. Lei, "Identification and pharmacentical screning of kiwifruit soft rot disease on 'guichang' gooseberry," *Northern Horticulture*, vol. 16, pp. 47–54, 2018.

[52] K. D. Zhang, Y. Qiang, and M. F. Zhou, "Field control effect test of six inducers against two fungal diseases of Fengxin kiwifruit," *South China Fruits*, vol. 49, no. 4, pp. 130–132, 2020.

[53] X. J. Wang, S. Y. Li, and Y. W. Li, "Pathogen identification of kiwifruit soft rot and fungicide screening for control of the disease," *Journal of Plant Protection*, vol. 44, no. 5, pp. 826–832, 2017.

[54] Z. L. Zhang, Y. J. Xie, X. Hu, H. Shi, M. Wei, and Z. Lin, "Antifungal activity of monoterpenes against *Botryosphaeria dothidea*," *Natural Product Communications*, vol. 13, no. 12, pp. 1721–1724, 2018.

[55] K. Li, H. J. Li, and H. Y. Yuan, "Isolation and identification of rot disease pathogens during storage of "Jinyan" kiwifruit," *Journal of Anhui Agricultural Sciences*, vol. 46, no. 1, pp. 160–164, 2018.

[56] T. A. Wheeler, S. A. Russell, M. G. Anderson, L. M. Serrato-Diaz, R. D. French-Monar, and J. E. Woodward, "Management of peanut pod rot *I*: disease dynamics and sampling," *Crop Protection*, vol. 79, pp. 135–142, 2016.

[57] T. J. White, T. Bruns, S. Lee, and J. Taylor, "Amplification and direct sequencing of fungal ribosomal RNA genes for phylogenetics," *PCR Protocols: A Guide to Methods and Amplifications*, Academic Press, San Diego, CA, USA, pp. 315–322, 1990.

[58] K. Katoh and D. M. Standley, "MAFFT multiple sequence alignment software version 7: improvements in performance and usability," *Molecular Biology and Evolution*, vol. 30, no. 4, pp. 772–780, 2013.

[59] G. Talavera and J. Castresana, "Improvement of phylogenies after removing divergent and ambiguously aligned blocks from protein sequence alignments," *Systematic Biology*, vol. 56, no. 4, pp. 564–577, 2007.

[60] S. Kumar, G. Stecher, and K. Tamura, "MEGA7: molecular evolutionary genetics analysis version 7.0 for bigger datasets," *Molecular Biology and Evolution*, vol. 33, no. 7, pp. 1870–1874, 2016.

[61] J. L. He, W. Qin, and X. Y. Liu, "Biocological characteristics and pathogenicity of *Botryosphaeria parva* isolated from "Hongyang" kiwifruit," *Food Machinery*, vol. 33, no. 12, pp. 115–124, 2017.

[62] P. A. Saccardo, *Sylloge Fungorum*, Patavii Sumptibus Auctoris, Typis seminarii, Iterum impressum apud R. Friedländer & Sohn, Berlin, Germany, 1884.

[63] G. H. Zhao and Z. Y. Huang, "NL895 poplar vesicular canker caused by the fungus conidial fungus," *Forest Protection*, vol. 12, pp. 28–39, 2011.
[64] S. R. Pennycook and G. J. Samuels, "*Botryosphaeria* and *Fusicoccum* species associated with ripe fruit rot of *Actinidia deliciosa* (kiwifruit) in New Zealand," *Mycotaxon*, vol. 24, pp. 445–458, 1985.
[65] X. M. Chen, Y. J. Peng, and J. L. Tang, "Isolation of postharvest pathogenic bacteria from kiwifruit and preliminary study on the antibacterial effect of Chinese herbal medicine extracts," *Hunan Agricultural Sciences*, vol. 5, pp. 81–83, 2015.
[66] Y. Jing, J. J. Wang, and W. F. Zhou, "A study on the latent infection of poplar canker," *Forest Science*, vol. 27, no. 2, pp. 173–178, 1991.
[67] Y. Zhang, *Effects of Arbuscular Mycorrhizal Fungi Inoculation on Resistance of Populus Cathayana to Canker Disease*, Northwest Agriculture and Forestry University, Xianyang, China, 2021.
[68] H. J. Liu, X. Q. Liu, and S. C. Liu, "Research on function of seven germicides to inhibit pathogens of fruit shrink disease in jujube," *Journal of Shanxi Agricultural Sciences*, vol. 35, no. 3, pp. 66–68, 2007.
[69] H. X. Wu, H. X. Li, and J. Gao, "Study on pathogens of jujube fruit shrink disease in Shanxi province," *Shanxi Forestry Science and Technology*, vol. 41, no. 4, pp. 34–36, 2012.
[70] J. X. Qu, R. X. Shen, and Z. Q. Li, "Study on the pathogen of jujube black rot," *Forest Pest and Disease*, vol. 2, pp. 1–4, 1992.
[71] W. M. Zheng, G. L. Ren, and Y. F. Wang, "A preliminary study on top blight of cedar," *Acta Agriculturatis Henanensis*, vol. 30, no. 1, pp. 46–49, 1996.
[72] Z. H. Gao, Y. G. Wang, and L. Han, "Morphological and biological characteristic of the pathogen of cedar branch withering," *Journal of Northwest Forestry University*, vol. 20, no. 3, pp. 127–130, 2005.
[73] W. D. S. Moraes, H. A. D. Castro, J. D. Lima, E. A. d. G. Leite, and M. d. Souza, "Suscetibilidade de três espécies cítricas à *Dothiorella gregaria* Sacc. em função do estado nutricional," *Ciência Rural*, vol. 37, no. 1, pp. 7–12, 2007.
[74] O. L. Sun, G. J. Choi, and K. S. Jang, "Antifungal activity of five plant essential oils as fumigant against postharvest and soilborne plant pathogenic fungi," *Plant Pathology Journal*, vol. 23, no. 2, pp. 97–102, 2007.
[75] A. Marchese, C. Arciola, R. Barbieri et al., "Update on monoterpenes as antimicrobial agents: a particular focus on p-cymene," *Materials*, vol. 10, no. 8, p. 947, 2017.
[76] H. Shirzad, A. Hassani, A. Abdollahi, Y. Ghosta, and S. R. Finidokht, "Assessment of the preservative activity of some essential oils to reduce postharvest fungal rot on kiwifruits (*Actinidia deliciosa*)," *Journal of Essential Oil Bearing Plants*, vol. 14, no. 2, pp. 175–184, 2011.
[77] Y. L. Ren, T. Wang, and Y. J. Jiang, "Behavioral response, fumigation activity, and contact activity of plant essential oils against tobacco beetle (*Lasioderma serricorne* (F.)) adults," *Frontiers of Chemistry*, vol. 10, pp. 1–6, 2011.
[78] H. Shirzad, A. Hassani, Y. Ghosta, A. Abdollahi, R. Finidokht, and M. Meshkatalsadat, "Assessment of the antifungal activity of natural compounds to reduce postharvest gray mould (*Botrytis cinerea* Pers.: FR.) of kiwifruits (*Actinidia Deliciosa*) during storage," *Journal of Plant Protection Research*, vol. 51, no. 1, pp. 1–6, 2011.

Hindawi
Journal of Chemistry
Volume 2022, Article ID 9552466, 13 pages
https://doi.org/10.1155/2022/9552466

Review Article

A Systematic Review of Photolysis and Hydrolysis Degradation Modes, Degradation Mechanisms, and Identification Methods of Pesticides

Xingang Meng,[1,2] **Yuanjun Guo**,[1] **Yihui Wang**,[3] **Shijun Fan**,[1] **Kaiqi Wang**,[1] **and Wenhua Han**[1,2]

[1]*College of Biological and Environmental Engineering, Jingdezhen University, Jingdezhen 333000, Jiangxi, China*
[2]*Jiangxi Key Laboratory of Plant Resources and Biodiversity, Jingdezhen 333400, Jiangxi, China*
[3]*Anshun Ecological Environment Monitoring Center, Monitoring of Four Departments, Anshun 561000, Guizhou, China*

Correspondence should be addressed to Xingang Meng; 15885007970@163.com

Received 23 March 2022; Accepted 18 May 2022; Published 6 June 2022

Academic Editor: Wenneng Wu

The degradation modes and characteristics of different pesticides were introduced. In addition, this paper also describes the degradation mechanism of different pesticides, classifies, and summarizes the methods of degradation products identification. For the sake of human life health and better biological environment, we should have a familiar knowledge of the natural degradation of pesticides and understand the photo-hydrolysis and its influencing factors (temperature, pH, light, etc.). Through the degradation mechanism and influencing factors, the degradation time could be accelerated and it also provides a theoretical basis and basic support for the treatment of pesticide residues in the future.

1. Introduction

Pesticide, as a chemical synthetic substance or a natural substance from the other bionts, used to prevent, destroy or control diseases, insects, grasses, and other harmful organisms that endanger agriculture, forestry plants and their products, and purposefully regulate the growth and development of plants and insects. As an important agricultural means of production, the primarily function of pesticides is to ensure crop yield, quality, and safety. They are divided into several major types depending on their control objects, such as insecticide, fungicide, acaricide, herbicide, nematicide, and plant growth regulator. The development and application of pesticides had played a very important role in promoting the harvest of agricultural food crops. However, excessive dependence on pesticides and irrational use of pesticides had a certain negative impact on agricultural production. With the mass production and widespread use of pesticides, the application of pesticides inevitably causes residues and pollution in the environment and has caused a widespread concern in countries around the world [1–4]. Pesticides must be residual when used, these residues will have incalculable implications for food, the environment, biomes, and even humans. The ecological effects of pesticide residues and the fate of these residues in the environment are urgently needed to be solved for both the scientific community and the general public. Therefore, it is necessary for us to explore the photolysis, hydrolysis mechanism, and identification method of pesticide degradation mode to provide a theoretical basis and technical support for multitudinous pesticide detection technology and residue solution in the future.

There are many reasons for causing and affecting pesticide residues. The properties of pesticides, environmental factors, and the application methods of pesticides are the main factors affecting pesticide residues. The pollution of pesticides to the water environment mainly come from (I) direct application to the water environment; (II) migration of pesticides applied to the farmland with rainwater or irrigation water; (III) discharge of wastewater from pesticide

production and processing enterprises; (IV) during the use of pesticides, the droplets, or dust particles migrating with the wind and settle into the water body and the cleaning of the application tools and instruments. For example, some pesticides were found in the water environment with extensive agricultural activity [5, 6]. Furthermore, many pesticides were found in urban streams [7], lakes [8–11], underground water [12], and rivers [13–16]. After the pesticides were applied, some of them adhered to the plant body, or part infiltrated into the body of the plant, and the other part was scattered on the soil or evaporates, dissipates into the air, or flows into the lake with rainwater and farmland drainage, thereby polluting the water body. Pesticide residues mainly enter the human body through the atmosphere, water, soil and food, and cause various chronic or acute diseases.

Both photolysis and hydrolysis are important ways in the degradation of pesticides in the environment. Hydrolysis is a hydrolysis reaction of pesticides because there are chemical structures in the pesticide molecules that can be hydrolyzed, such as ester bonds, ether bonds, amide bonds, cyano group, and acyl chloride group. Photolysis of pesticides is a process in which a pesticide molecule gets light radiation energy, and light energy is converted into a molecular bond of the compound to break the bond and generate an internal reaction. Pesticide molecules must absorb a certain wavelength of light energy in an excited state in order to carry out a photochemical reaction. Due to the structural properties of the pesticide itself, most pesticides are very sensitive to photolysis. In the past few decades, a large number of studies have been conducted on the photolysis of pesticides and the effects of organic and inorganic constituents in natural world on the degradation of pesticides in water [17–33].

In this paper, the literature on pesticide degradation in recent years is reviewed, the degradation methods of photolysis and hydrolysis are introduced, the degradation mechanism of pesticides is discussed, and the identification methods of degradation products are summarized. Finally, this review provides some useful data and recommendations for future research that will be urgently needed to inform pesticide users, developers, and governmental regulators as well as will have a more thorough reference point from which the future of these widely applied pesticides can be determined.

2. Types and Characteristics of Pesticides

Pesticides are divided into several major types depending on their control objects, such as insecticides, fungicides, acaricides, herbicides, nematicides, and plant growth regulators. Insecticides were agents that control the chemical or biological sources of insects. Insecticides could control insects which may be due to killing the insect or otherwise preventing it from engaging in a considered destructive behavior. Historically, humans have had long experience using pesticides [34, 35]. Compared with insecticides, fungicides have a short development history. It was not until 1807 that the first practical chemical used for disease control, the first fungicide, was discovered [36, 37]. In recent years, the development of Strobilurin fungicides was remarkable. The mechanism of action was to block electron transmission, inhibit mitochondrial respiration, and inhibit fungal growth [38]. Ammoniacides have been developed due to the economic losses caused by the rampant reproduction of herbivorous mites affecting fruits, cotton, and vegetables. Today, to achieve the goal of drug resistance, most of the new acaricides can be classified as mitochondrial respiratory inhibitors, growth inhibitors, and neurotoxins [39, 40]. Herbicides act on large numbers of metabolic functions and energy transfer sites in plant cells [41]. The first commercial synthetic herbicide was created in the 1940s [42]. Herbicides are divided into three categories: the first, biochemical pathways and physiological processes related to photosynthesis; the second, inhibit bioconstruction or assemble into biopolymers; and the third, other modes of action [43]. Plant parasitic nematodes cause huge economic losses to agriculture around the world annually [44]. Compounds controlling nematodes began synthesis only in the 19th century [45, 46]. Plant hormones play regulatory roles in growth and development, while synthetic chemicals with similar physiological activities, or compounds capable of otherwise modifying plant growth, are called plant growth regulators [47]. Plant growth regulators play a mainly active regulatory role in plant development and affect the balance of plant body hormones generally [48].

3. Pesticide Degradation Mode

The degradation mode of pesticides in the environment is divided into biological degradation and nonbiological degradation. Nonbiological degradation is also divided into hydrolysis and photolysis.

3.1. Hydrolysis. Hydrolysis reactions are important processes when many pesticides are degraded. Because of adsorption catalytic reactions, pesticide hydrolysis is faster in soil than in soil-free systems. This is more significant for the degradation of chlorotriazine herbicides and organophosphate insecticides [49]. We take organophosphorus insecticides as an example. Its hydrolysis reaction can occur by homogenization machine production. Water and hydroxide ions participate as nucleophiles in bimolecular nucleophilic replacement reactions. Iron and aluminum oxides as well as different clays can increase the hydrolysis rates by providing the surface positions of the nucleophiles and the hydrolysis reactions. Despite much speculation about the hydrolysis mechanisms, there is still uncertainty [50, 51].

3.2. Photolysis. The light-induced chemical reactions of pesticides on the surface of the atmosphere, water bodies, or objects (e.g., plants and soil) are an important nonbiodegradation pathway of pesticides and has a significant impact on pesticide residues, efficacy, toxicity, and the environment. Photocatalytic degradation is a relatively cheap and effective degradation method and has good potential [52–55]. Photodegradation requires absorption of light energy and only pesticides that absorbed light above 285 nm

could be decomposed by natural sunlight. Therefore, photocatalytic degradation experiments are usually carried out under high intensity light. Pesticides absorbed light radiation and produced hydroxyl, superoxide, and ozone radicals, which ultimately lead to degradation products. Photocatalytic degradation reactions might be isomerization, substitution, or oxidation. The reaction type is affected by the physical properties of pesticides, environmental factors, reactants, and so on [56, 57]. Photocatalytic degradation reactions generally required photocatalysts. The ideal material for photocatalysts should have high photoactivity, photocorrosion resistance, chemical inertia, low cost, and low environmental toxicity in the near ultraviolet and visible regions of the electromagnetic spectrum [58]. Titanium dioxide and zinc oxide were the main catalysts in photocatalytic reaction experiments [59–62]. However, recent research using semiconductors as catalysts has emerged [63].

3.3. Biodegradation. Biodegradation has the advantages of efficiency, economy, flexibility, wide range of degradation objects, stable degradation ability, and no secondary pollution to the environment [64]. The main reactions involved in microbial degradation include hydrolysis, oxidation, alkylation, and dealkylation [65]. Biodegradation might be thought of as the transformation of a complex substance into one or more simpler substances by biological machinery, through the production of enzymes that broke a chemical bond, and the degradation of large compounds into small ones, rendering them inactive. In addition to degrading enzymes, biodegradation could also be influenced by environmental factors, including the soil type, water content, temperature, and pH [66–68]. The role of oxygen in pesticide biodegradation was complex; for example, as an oxygenase substrate involved in biodegradation reactions. If oxygen was sufficient, the end products of degradation will be carbon dioxide, water, sulfate, nitrate, phosphate, chloride ions, etc. If oxygen was insufficient, anoxic conditions can stimulate the activity of potential anaerobic microorganisms, which may directly or indirectly affect the transformation of pesticides [69].

3.4. Factors Affecting the Degradation. The factors affecting pesticide degradation in the water environment and soil were generally related to the nature of soil and water itself, such as water soil pH, temperature, soil water content, soil organic matter content, and different soil types (the actual essence was related to the organic matter content) [70, 71]. Some influencing factors were related to the nature of the pesticide itself; for example, the effectiveness of pesticides on soil pests was also the main factor affecting the pesticide degradation in the soil. There were other environmental factors, such as other soil phenomena (adsorption) and environmental exposure of nontarget organisms [72].

4. Pesticide Degradation Mechanism

4.1. Insecticide. In the study of nonbiodegradation of insecticides in nature (soil or water), the experimenter will explore the consistency of hydrolyzed photolysis products through comparative experiments and will compare the effects of natural light and man-made radiation sources on photolysis. The main photolysis mechanism of insecticide was ester group breaking (Figure 1(a)) [73, 74]. However, the photolysis pathway of pesticides was not only the breaking of the ester group. There were many kinds of pesticides with different components. Some pesticides have only one degradation pathway, some have two, and some even have a variety of degradation pathways. For example, the photolysis of the organophosphorus insecticides-ethyl parathion, methyl parathion, and phenylthiophosphorus in water and soil was found to include oxidation, hydrolysis, isomerization, and reduction (Figures 1(b)–1(d)) [75]. Pesticide hydrolysis was also the same. In the experiment of hydrolysis of chlorpyrifos (*O*,*O*-diethyl-*O*-(3,5,6-trichloro-2-pyridyl) phosphorothioate), nucleophilic attack was done by water of ethoxy carbon degradation products (Figures 1(e) and 1(f)) [76]. The effect of environmental factors on the photolysis and hydrolysis of pesticides was also a subject worthy of study. It was found that three insecticides were stable under acidic conditions. Dealkylation occurred in a neutral medium. In the alkaline medium, the ether bond broke to form phenol derivatives and dialkyl phosphoric acid (Figures 1(g)–1(j)) [77].

4.2. Fungicide. Like insecticides, the degradation pathways of fungicides were diverse. When the main degradation reaction occurs, it will be accompanied by parallel reactions. For example, the main photoproducts of azoxystrobin fungicides were produced by ether bond breaking. The secondary photolysis products might be due to demethylation. Photoisomerization and cleavage of acrylate double bonds were parallel pathways of degradation (Figures 2(a)–2(e)) [78]. For the degradation of fungicides, the researchers also considered the influence of environmental factors on the reaction. For example, the common humus in soil, acid-base environment, and the effect of micellar medium on degradation. The research showed that humus as the oxidant extracts electrons or hydrogen atoms from bactericides to form oxidation products. In the acidic environment, the disulfide bond and carbon-nitrogen bond in bactericide were destroyed, and there will be byproducts in the absence of metal tin ions. In nonionic micelles, the loss of the ethyl ester group and the opening of a dihydrocarbon ring will be inhibited. In the alkaline hydrolysis of benzoic acid and benzyl fungicides, the degradation mechanism was inferred to be a carboxyl fracture (Figures 2(f)–2(k)) [79–82].

4.3. Acaricide. For acaricides with a relatively complex structure, its degradation pathway also has many routes. For example, the photolysis pathway of abamectin, an acaricide composed of two colorless homologs with the same macrolide structure included oxygenation, demethylation, and isomerization (Figures 3(a) and 3(b)) [83]. In order to understand the degradation of acaricides under different conditions, the experimenters will design the degradation of acaricide under different light conditions in different solutions to master the possible different degradation

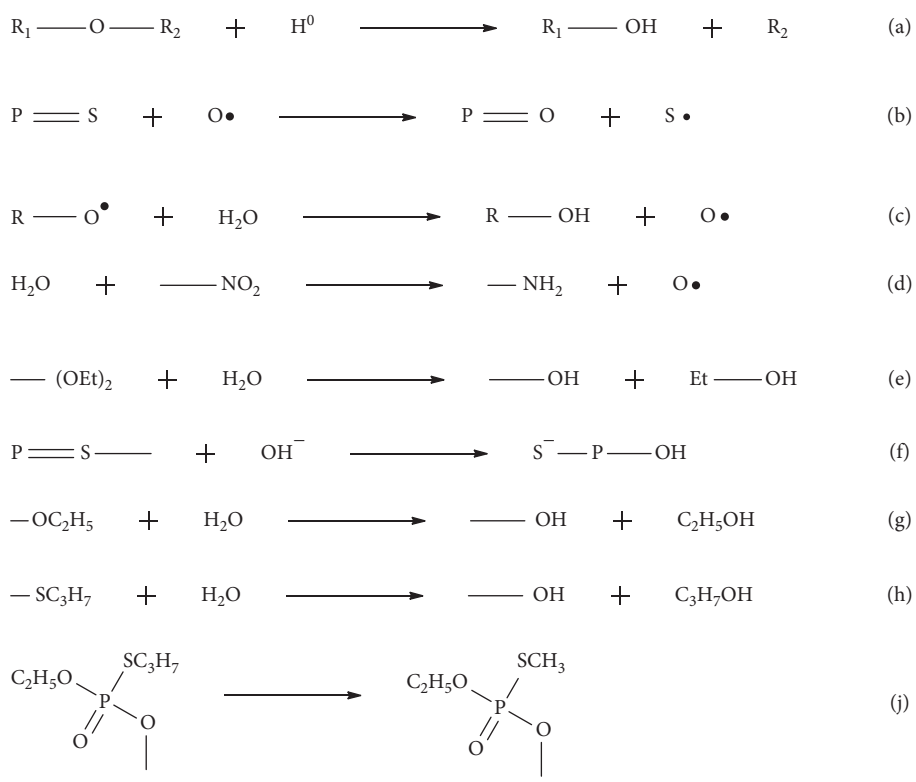

Figure 1: Main photolysis mechanism of insecticides.

mechanisms. For example, in the study of photolysis of nonnaphthoquine, it was found that the degradation mechanism was the cleavage of ether bond between quinazoline and the phenyl ring system, the oxidation of a tert-butyl substituent and the oxidation of the heterocyclic part of a quinazoline ring (Figures 3(c)–3(e)) [84]. Even if the possible degradation mechanism was mastered, the renewal of acaricides was changing with each passing day. This means that it is very important to study the degradation of the new mechanism. In the study of a new benzoyl acetamide acaricide cyflumetofen (CYF), it was found that the electrophilic group carbon atoms on the CYF were found to be easily damaged by a nucleophilic attack, producing a hydrolysate 1. When the carbon-carbon single bond breaks, it binds with an amino group to produce hydrolysate 2 (Figures 3(f) and 3(g)) [85].

4.4. Herbicide. In the study of herbicide degradation, photolysis and hydrolysis were also studied by changing the light. It was found that Sulfuron could cause the sulfonyl group to fall off under neutral and alkaline conditions. Photooxidation and photoisomerization were the main reactions of triketone herbicides (Figure 4(a)) [86, 87]. Of course, herbicides were mostly organic, and their degradation reactions were complex and changeable, and there were many degradation products. There were nine photolysis products of ketene herbicides. It was conceivable that there were many photolysis pathways, including isomerization and cracking of the oxime ether bond, cracking of dechlorinated isopropyl group, sulfoxide, and oxidative cracking of the dechlorinated epoxy group (Figures 4(b) and 4(c)) [88]. Water molecules play an indispensable role in the hydrolysis of herbicides. They often attack compounds as nucleophiles, as do other types of pesticides. For example, the hydrolysis of sulfonyl herbicides. The hydrolysis mechanism was similar to the nucleophilic substitution reaction in which water molecules attack carbon groups from the aryl or heterocyclic side (Figure 4(d)) [89].

4.5. Nematicide. The most of degradation products detected in the degradation of nematicides were sulfoxides and sulfones because sulfur ions or methyl groups would undergo oxidative desulfurization and sulfur oxidation. The degradation of amine (4-methylisopropyl phosphoramide) nematicide and thiazole phosphorus were taken as an example (Figure 5) [90, 91]. It has also been shown above that titanium dioxide often participates in photolysis as a photocatalyst. The photolysis of fenamiphos nematicide has two steps under the action of catalyst, the first was oxidation and the second was mineralization [92].

4.6. Plant Growth Regulator. Photoisomerization often occurs under photolysis and plant growth regulators are no exception. The photolysis mechanism of gibberellin A3 derivatives was photoinduced aromatization of a ring (Figures 6(a) and 6(b)) [93]. Generally, the degradation of plant growth regulators is also needed to be considered as the influence of environmental factors. In the study of the degradation of methyl phosphonate (MPN), the effects of

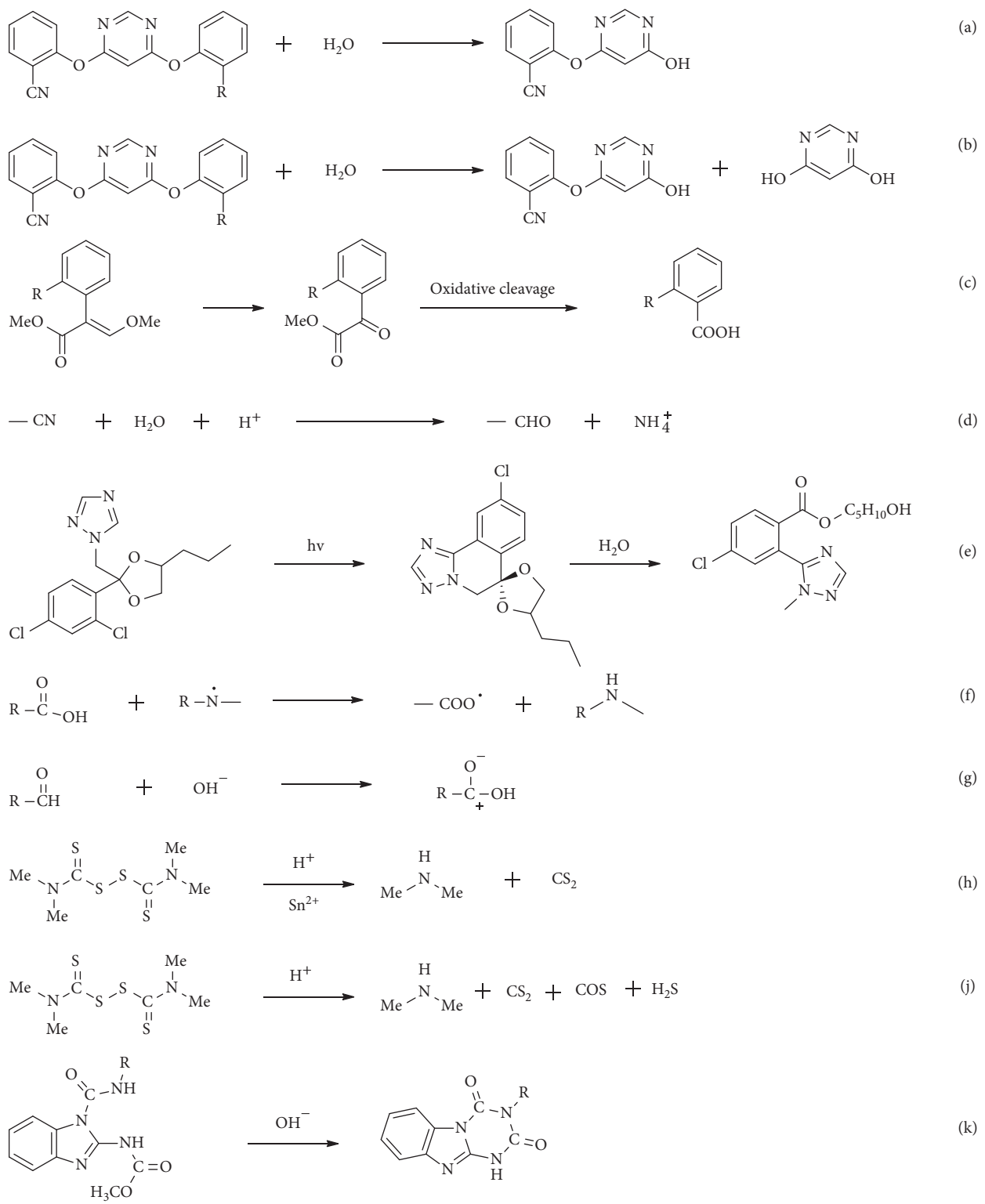

Figure 2: Degradation pathways of fungicides.

different environmental factors on its degradation were compared. It was found that the degradation mechanism was that electron transfer produces free radicals, reacts with oxygen to form peroxy radicals, and finally decomposes into hydroxyl radicals to attack methyl in MPN (Figure 6(c)) [94]. The degradation of plant growth regulators also involved many ways. For example, the photolysis pathway of malehydrazine included carbon-carbon double bond

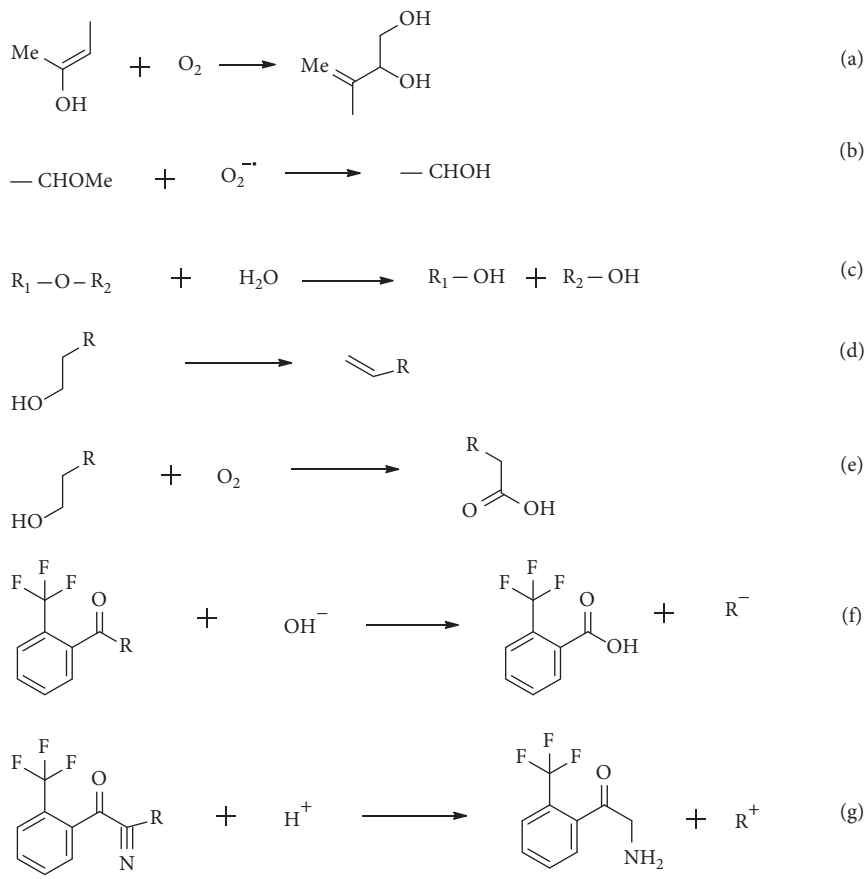

Figure 3: Degradation pathways of acaricides.

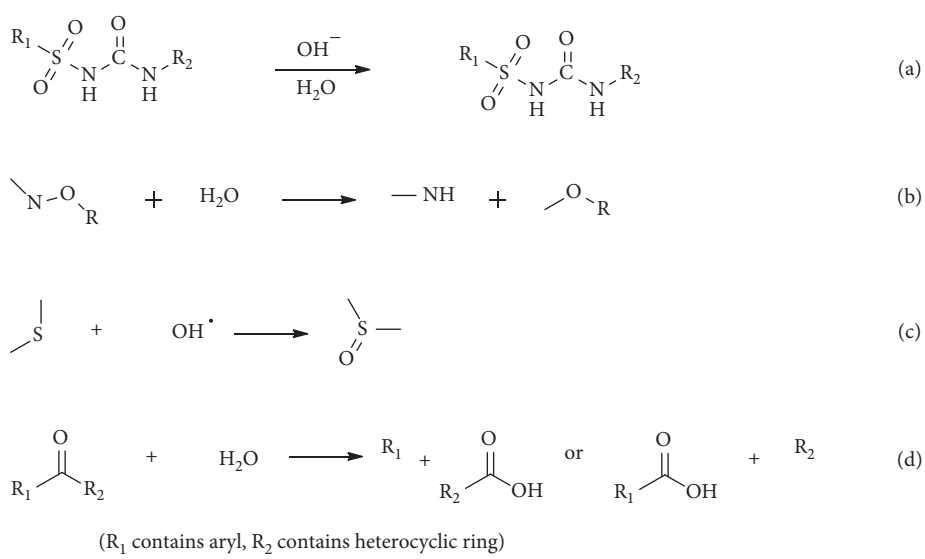

(R_1 contains aryl, R_2 contains heterocyclic ring)

Figure 4: Main photolysis mechanism of herbicides.

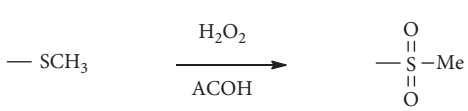

Figure 5: Degradation mechanism of nematicides.

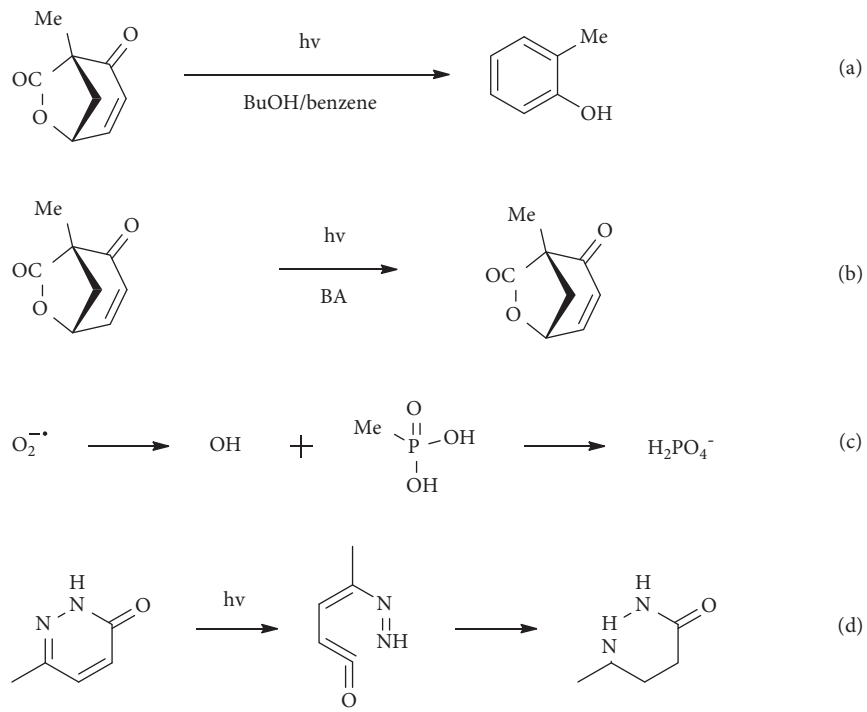

Figure 6: Degradation mechanism of plant growth regulators.

transfer site, ketone group, and amino group cleavage (Figure 6(d)) [95].

5. Identification Methods

In recent years, the methods and techniques for quantitative and qualitative analysis of pesticides were constantly updated. The critical methods and techniques were very useful for the residue analysis of pesticides and the identification of degradation products, degradation mechanism, and reaction pathway of the pesticides. Many technologies, such as gas chromatography-mass spectrometry (GC-MS/MS) [96–98], liquid chromatography-mass spectrometry (HPLC-MS/MS) [99–102], ultraperformance liquid chromatography-quadrupole-time-of-flight mass spectrometry (UPLC-Q-TOF-MS) [103–109], ultraperformance liquid chromatography-orbitrap mass spectrometry (UPLC-Orbitrap MS/MS) [110–114], and high-resolution mass spectrometry (UPLC-HRMS) [115–117] were used to separate the degradation products and identify the structure of products. So far, the high-resolution mass spectrometry combined with UPLC is increasingly used in the qualitative screening and degradation mechanism of pesticide metabolites, for its high-resolution ensures high sensitivity, accuracy, and high specificity required for complex sample analysis. Through these techniques, the degradation mechanisms and reaction pathways of many pesticides in the environment were identified. Pesticide may undergo physical and chemical processes in the soil. Therefore, a combination of physical and chemical unit processes was required and actually employed to ensure the removal of pesticide residues and byproducts from the environment. The mode and mechanism of chemical degradation were closely related to the molecular structure of pesticides. Generally, pesticides with functional groups such as haloalkyl, amide, amine, carbamate, epoxy, cyano, phosphate, and sulfate were easily hydrolyzed.

5.1. High-Performance Liquid Chromatography. High-performance liquid chromatography (HPLC) used a liquid as the mobile phase and high pressure infusion system. Single solvent or mixed solvent with different polarities and buffer were pumped into the chromatographic column. After being separated in the column, the sample was detected by the detector. High-performance liquid chromatography was used to study the degradation rate of fenpyroximate in apples, oranges, and grapes. The classical QuEChERS method was used for pretreatment. The C_{18} column was used for separation and HPLC-PDA was used for detection [118].

5.2. Liquid Chromatography-Mass Spectrometry. Liquid chromatography-mass spectrometry (LC-MS). Pesticide residues were mainly detected by liquid chromatography tandem mass spectrometry, high performance liquid chromatography tandem mass spectrometry, and ultrahigh liquid chromatography tandem mass spectrometry.

Of course, in the experiment, the experimental method was not single and unchanging. There will be different methods in sample extraction, such as ultrasonic extraction,

solid phase extraction, and so on. For example, ultrasonic extraction and HPLC-APCI-MS were used to determine antifouling pesticides and their degradation products in the sea. Solid phase extraction combined with liquid chromatography-mass spectrometry was used to determine benzophenone, carbazine, and their degradation products in water samples [119, 120]. However, overly complex experimental methods will consume a lot of human, material, and financial resources. Liquid chromatography tandem mass spectrometry was used to determine pesticides and their degradation products [121, 122]. With the development of science and technology, the identification and determination experiments of pesticides were constantly innovated. In the experiment of studying the photo-hydrolysis and degradation products of neonicotine insecticides, the absorbance of each neonicotine was determined by spectrophotometer, and the reaction products were determined by UPLC-MS/MS. There are also technologies such as ultrahigh liquid chromatography time of flight mass spectrometry (UPLC-Q-TOF-MS) and high-resolution mass spectrometry (UPLC-HRMS) to separate degradation products and identify the structure of products [123–125].

5.3. Gas Chromatography and Gas Chromatography-Mass Spectrometry. Gas chromatography was a chromatographic separation and analysis method using a gas as mobile phase. The vaporized sample was carried into the column by the carrier gas. The molecular forces of each component were different and the outflow time was different, so that the components were separated from each other. In pesticide degradation experiments, solid phase microextraction was often used to treat samples, regardless of the final detection method. This was the case in the experiment of studying the degradation residues of amitraz, which was treated by solid-phase microextraction and detected by gas chromatography ion trap detector (GC-ITD) [126].

In terms of gas chromatography-mass spectrometry, mass spectrometry has a unique ability to identify unknown compounds with extremely high sensitivity, making GC-MS one of the most powerful tools for separating and detecting complex compounds. Sometimes, the toxicity of degradation products will also be determined in the experiment because it is impossible to distinguish whether the degradation products of pesticides are still toxic. For example, the disappearance of methyl organophosphorus, toxic phosphorus, and malathion in aqueous solution and the formation of photodegradation products were detected by gas chromatography-mass spectrometry (GC-MS). The toxicity was determined by FIA-ache-TLS bioassay [127].

5.4. Other Methods. Isotope labeling was a method to understand the detailed process of chemical reactions by tracing compounds labeled by tracer elements. Carbon elements were used as tracer elements in pesticide degradation product recognition. Pesticide degradation research methods using carbon 13 and carbon 14 isotope markers have emerged and have gradually been widely used. This technique could be readily seen in studies of the degradation pathways and the identification of the degradation products of multiple pesticides [128, 129].

6. Concluding Remarks

Mentioned in this article are the different types of pesticide and its effects on human health and biological environment. Not only that, but also for pesticide degradation model, different kinds of pesticide degradation mechanisms and methods to identify degraded products are mentioned.

In today's world, the widespread use of pesticides and pesticide residues did become a hot topic. For the health of human life and better biological environment, degradation of pesticide in nature should be familiar with the cognitive method and understand the photolysis hydrolysis and influencing factors (temperature, pH, light, etc.). Through the degradation mechanism and influencing factors, the degradation time could be accelerated, and the theoretical basis and basic support for pesticide residues could be provided in the future. In this paper, the biodegradation of pesticides was not described too much, mainly focusing on the photolysis and hydrolysis of pesticides. However, in recent years, there were more and more research studies on the biodegradation of pesticides. In the future development, the biodegradation of pesticides is also crucial to the development of pesticide degradation residues.

The identification method of pesticide degradation products was also mentioned in this paper. Through consulting data, the author found that high-performance liquid chromatography-mass spectrometry was mostly used in research experiments, mainly because of its advantages of high efficiency, high sensitivity, and wide application. With the development of technology, identification methods would be gradually updated, including UPLC-Q-TOF-MS and ultraperformance liquid chromatography-orbitrap mass spectrometry (UPLC-Orbitrap MS/MS).

Data Availability

The data that support the findings of this study are available from the corresponding author upon reasonable request.

Conflicts of Interest

The authors declare that they have no conflicts of interest.

Acknowledgments

This study was supported by the Key Project of the Science and Technology Research Project of the Education Department of Jiangxi Province (GJJ202803), Subject Construction Project of Jingdezhen Science and Technology Plan (20202GYZD015-07), and the Education Department of Jiangxi Province (GJJ212801).

References

[1] W. J. Brill, "Safety concerns and genetic engineering in agriculture," *Science*, vol. 227, no. 4685, pp. 381–384, 1985.

[2] R. L. Metcalf, "An increasing public concern," in *The Pesticide Question*, pp. 426–430, Springer, Heidelberg, Germany, 1993.

[3] W. W. Stone, R. J. Gilliom, and K. R. Ryberg, "Pesticides in U.S. Streams and rivers: occurrence and trends during 1992-2011," *Environmental Science and Technology*, vol. 48, no. 19, pp. 11025–11030, 2014.

[4] F. P. Carvalho, "Pesticides, environment, and food safety," *Food and Energy Security*, vol. 6, no. 2, pp. 48–60, 2017.

[5] S. Z. Lari, N. A. Khan, K. N. Gandhi, T. S. Meshram, and N. P. Thacker, "Comparison of pesticide residues in surface water and ground water of agriculture intensive areas," *Journal of environmental health science and engineering*, vol. 12, no. 1, pp. 11–17, 2014.

[6] S. Arora, I. Mukherjee, and T. P. Trivedi, "Determination of pesticide residue in soil, water and grain from IPM and non-IPM field trials of rice," *Bulletin of Environmental Contamination and Toxicology*, vol. 81, no. 4, pp. 373–376, 2008.

[7] Z. Xing, L. Chow, H. Rees et al., "Influences of sampling methodologies on pesticide-residue detection in stream water," *Archives of Environmental Contamination and Toxicology*, vol. 64, no. 2, pp. 208–218, 2013.

[8] G. Darko, O. Akoto, and C. Oppong, "Persistent organochlorine pesticide residues in fish, sediments and water from Lake Bosomtwi, Ghana," *Chemosphere*, vol. 72, no. 1, pp. 21–24, 2008.

[9] S. M. Gitahi, D. M. Harper, S. M. Muchiri, M. P. Tole, and R. N. Ng'ang'a, "Organochlorine and organophosphorus pesticide concentrations in water, sediment, and selected organisms in Lake Naivasha (Kenya)," *Lake Naivasha, Kenya*, vol. 488, no. 1, pp. 123–128, 2002.

[10] E. D. Caldas, R. Coelho, L. C. K. R. Souza, and S. C. Silva, "Organochlorine pesticides in water, sediment, and fish of paranoá lake of brasilia, Brazil," *Bulletin of Environmental Contamination and Toxicology*, vol. 62, no. 2, pp. 199–206, 1999.

[11] K. Feng, B. Y. Yu, D. M. Ge, M. H. Wong, X. C. Wang, and Z. H. Cao, "Organo-chlorine pesticide (DDT and HCH) residues in the Taihu Lake Region and its movement in soil-water system," *Chemosphere*, vol. 50, no. 6, pp. 683–687, 2003.

[12] G. Shukla, A. Kumar, M. Bhanti, P. E. Joseph, and A. Taneja, "Organochlorine pesticide contamination of ground water in the city of Hyderabad," *Environment International*, vol. 32, no. 2, pp. 244–247, 2006.

[13] T. A. Albanis and D. G. Hela, "Multi-residue pesticide analysis in environmental water samples using solid-phase extraction discs and gas chromatography with flame thermionic and mass-selective detection," *Journal of Chromatography A*, vol. 707, no. 2, pp. 283–292, 1995.

[14] I. Osuna-Flores and M. C. Riva, "Organochlorine pesticide residue concentrations in shrimps, sediments, and surface water from Bay of Ohuira, Topolobampo, Sinaloa, Mexico," *Bulletin of Environmental Contamination and Toxicology*, vol. 68, no. 4, pp. 532–539, 2002.

[15] R. Jayashree and N. Vasudevan, "Organochlorine pesticide residues in ground water of Thiruvallur district, India," *Environmental Monitoring and Assessment*, vol. 128, no. 1, pp. 209–215, 2007.

[16] G. A. Idowu, "Organochlorine pesticide residue levels in river water and sediment from cocoa-producing areas of Ondo State central senatorial district, Nigeria," *Journal of Environmental Chemistry and Ecotoxicology*, vol. 5, no. 9, pp. 242–249, 2013.

[17] B. Sevilla-Morán, C. López-Goti, J. L. Alonso-Prados, and P. Sandín-España, "Aqueous photodegradation of sethoxydim herbicide: qtof elucidation of its by-products, mechanism and degradation pathway," *The Science of the Total Environment*, vol. 472, pp. 842–850, 2014.

[18] J. Chang, Z. L. Chen, Z. Wang et al., "Ozonation degradation of microcystin-LR in aqueous solution: intermediates, byproducts and pathways," *Water Research*, vol. 63, pp. 52–61, 2014.

[19] L. Qin, Y.-L. Lin, B. Xu et al., "Kinetic models and pathways of ronidazole degradation by chlorination, UV irradiation and UV/chlorine processes," *Water Research*, vol. 65, pp. 271–281, 2014.

[20] L. Pareja, A. Pérez-Parada, A. Agüera, V. Cesio, H. Heinzen, and A. R. Fernández-Alba, "Photolytic and photocatalytic degradation of quinclorac in ultrapure and paddy field water: identification of transformation products and pathways," *Chemosphere*, vol. 87, no. 8, pp. 838–844, 2012.

[21] P. C. Rúa-Gomez and W. Püttmann, "Degradation of lidocaine, tramadol, venlafaxine and the metabolites O-desmethyltramadol and O-desmethylvenlafaxine in surface waters," *Chemosphere*, vol. 90, no. 6, pp. 1952–1959, 2013.

[22] X. Liu, T. Zhang, Y. Zhou, L. Fang, and Y. Shao, "Degradation of atenolol by UV/peroxymonosulfate: kinetics, effect of operational parameters and mechanism," *Chemosphere*, vol. 93, no. 11, pp. 2717–2724, 2013.

[23] B. Abramović, S. Kler, D. Sojić, M. Laušević, T. Radović, and D. Vione, "Photocatalytic degradation of metoprolol tartrate in suspensions of two TiO2-based photocatalysts with different surface area. Identification of intermediates and proposal of degradation pathways," *Journal of Hazardous Materials*, vol. 198, pp. 123–132, 2011.

[24] K. Azrague, V. Pradines, E. Bonnefille, C. Claparols, M.-T. Maurette, and F. Benoit-Marquié, "Degradation of 2,4-dihydroxibenzoic acid by vacuum UV process in aqueous solution: kinetic, identification of intermediates and reaction pathway," *Journal of Hazardous Materials*, vol. 237-238, pp. 71–78, 2012.

[25] X. H. Lin, S. N. Lee, W. Zhang, and S. F. Y. Li, "Photocatalytic degradation of terephthalic acid on sulfated titania particles and identification of fluorescent intermediates," *Journal of Hazardous Materials*, vol. 303, pp. 64–75, 2016.

[26] G. Su, Y. Liu, L. Huang et al., "Synergetic effect of alkaline earth metal oxides and iron oxides on the degradation of hexachlorobenzene and its degradation pathway," *Chemosphere*, vol. 90, no. 1, pp. 103–111, 2013.

[27] P. Chelme-Ayala, M. G. El-Din, and D. W. Smith, "Kinetics and mechanism of the degradation of two pesticides in aqueous solutions by ozonation," *Chemosphere*, vol. 78, no. 5, pp. 557–562, 2010.

[28] J. Švrček, A. Marhoul, P. Kačer, M. Kuzma, L. Panek, and L. Cerveny, "The influence of operating conditions on the efficiency of vapor phase hydrogen peroxide in the degradation of 4-(dimethylamino) benzaldehyde," *Chemosphere*, vol. 81, no. 5, pp. 617–625, 2010.

[29] X. Liu, X. Xu, C. Li et al., "Degradation of chiral neonicotinoid insecticide cycloxaprid in flooded and anoxic soil," *Chemosphere*, vol. 119, pp. 334–341, 2015.

[30] H.-F. Miao, M. Cao, D.-Y. Xu et al., "Degradation of phenazone in aqueous solution with ozone: influencing factors and degradation pathways," *Chemosphere*, vol. 119, pp. 326–333, 2015.

[31] E. Koumaki, D. Mamais, C. Noutsopoulos et al., "Degradation of emerging contaminants from water under natural

sunlight: the effect of season, pH, humic acids and nitrate and identification of photodegradation by-products," *Chemosphere*, vol. 138, pp. 675–681, 2015.

[32] L. Xin, Y. Sun, J. Feng, J. Wang, and D. He, "Degradation of triclosan in aqueous solution by dielectric barrier discharge plasma combined with activated carbon fibers," *Chemosphere*, vol. 144, pp. 855–863, 2016.

[33] P. N. Patil, S. D. Bote, and P. R. Gogate, "Degradation of imidacloprid using combined advanced oxidation processes based on hydrodynamic cavitation," *Ultrasonics Sonochemistry*, vol. 21, no. 5, pp. 1770–1777, 2014.

[34] G. W. Ware and D. M. Whitacre, "An introduction to insecticides," in *The Pesticide Book*Edu-Ware, Agoura Hills, CA, USA, 2004.

[35] V. Oberemok, K. V. Laikova, Y. I. Gninenko, Z. Aleksei, P. M. Nyadar, and T. A. Adeyemi, "A short history of insecticides," *Journal of Plant Protection Research*, vol. 55, no. 3, pp. 221–226, 2015.

[36] P. E. Russell, "A century of fungicide evolution," *The Journal of Agricultural Science*, vol. 143, no. 1, pp. 11–25, 2005.

[37] C. J. Klittich, "Milestones in fungicide discovery: chemistry that changed agriculture," *Plant Health Progress*, vol. 9, no. 1, 2008.

[38] D. W. Bartlett, J. M. Clough, J. R. Godwin, A. A. Hall, M. Hamer, and B. Parr-Dobrzanski, "The strobilurin fungicides," *Pest Management Science*, vol. 58, no. 7, pp. 649–662, 2002.

[39] P. Jeschke, "Status and outlook for acaricide and insecticide discovery," *Pest Management Science*, vol. 77, no. 1, pp. 64–76, 2021.

[40] M. A. Dekeyser, "Acaricide mode of action," *Pest Management Science*, vol. 61, no. 2, pp. 103–110, 2005.

[41] S. O. Duke, "Overview of herbicide mechanisms of action," *Environmental Health Perspectives*, vol. 87, pp. 263–271, 1990.

[42] F. E. Dayan, "Current status and future prospects in herbicide discovery," *Plants*, vol. 8, no. 9, p. 341, 2019.

[43] F. E. Dayan, A. Barker, R. Bough, M. Ortiz, H. Takano, and S. O. Duke, "Herbicide mechanisms of action and resistance," *Comprehensive Biotechnology*, vol. 4, pp. 36–48, 2019.

[44] J.-x. Chen and B.-a. Song, "Natural nematicidal active compounds: recent research progress and outlook," *Journal of Integrative Agriculture*, vol. 20, no. 8, pp. 2015–2031, 2021.

[45] L. A. Ebone, M. Kovaleski, and C. C. Deuner, "Nematicides: history, mode, and mechanism action," *Plant Science Today*, vol. 6, no. 2, pp. 91–97, 2019.

[46] P. Warrior, L. A. Rehberger, M. Beach, P. A. Grau, G. W. Kirfman, and J. M. Conley, "Commercial development and introduction of DiTeraTM, a new nematicide," *Pesticide Science*, vol. 55, no. 3, pp. 376–379, 1999.

[47] E. F. George, M. A. Hall, and K. G. J. De, "Plant growth regulators i: introduction; auxins, their analogues and inhibitors," in *Plant Propagation by Tissue Culture*, pp. 175–204, Springer, Heidelberg, Germany, 2008.

[48] W. Rademacher, "Plant growth regulators: backgrounds and uses in plant production," *Journal of Plant Growth Regulation*, vol. 34, no. 4, pp. 845–872, 2015.

[49] D. E. Armstrong and J. G. Konrad, "Nonbiological degradation of pesticides," in *Pesticides in Soil and Water*, pp. 123–131, Wiley, Hoboken, NJ, USA, 1974.

[50] S. O. Pehkonen and Q. Zhang, "The degradation of organophosphorus pesticides in natural waters: a critical review," *Critical Reviews in Environmental Science and Technology*, vol. 32, no. 1, pp. 17–72, 2002.

[51] A. Dannenberg and S. O. Pehkonen, "Investigation of the heterogeneously catalyzed hydrolysis of organophosphorus pesticides," *Journal of Agricultural and Food Chemistry*, vol. 46, no. 1, pp. 325–334, 1998.

[52] D. S. Bhatkhande, V. G. Pangarkar, and A. A. C. M. Beenackers, "Photocatalytic degradation for environmental applications - a review," *Journal of Chemical Technology and Biotechnology*, vol. 77, no. 1, pp. 102–116, 2002.

[53] F. Akbal and A. Nur Onar, "Photocatalytic degradation of phenol," *Environmental Monitoring and Assessment*, vol. 83, no. 3, pp. 295–302, 2003.

[54] D. Chatterjee and S. Dasgupta, "Visible light induced photocatalytic degradation of organic pollutants," *Journal of Photochemistry and Photobiology C: Photochemistry Reviews*, vol. 6, no. 2-3, pp. 186–205, 2005.

[55] G. M. Zuo, Z. X. Cheng, H. Chen, G. Li, and T. Miao, "Study on photocatalytic degradation of several volatile organic compounds," *Journal of hazardous materials*, vol. 128, no. 2-3, pp. 158–163, 2006.

[56] S. Ahmed, M. G. Rasul, R. Brown, and M. A. Hashib, "Influence of parameters on the heterogeneous photocatalytic degradation of pesticides and phenolic contaminants in wastewater: a short review," *Journal of Environmental Management*, vol. 92, no. 3, pp. 311–330, 2011.

[57] S. Devipriya and S. Yesodharan, "Photocatalytic degradation of pesticide contaminants in water," *Solar Energy Materials and Solar Cells*, vol. 86, no. 3, pp. 309–348, 2005.

[58] W. Li, "Photocatalysis of oxide semiconductors," *Journal of the Australian Ceramic Society*, vol. 49, no. 2, pp. 41–46, 2013.

[59] J.-M. Herrmann and C. Guillard, "Photocatalytic degradation of pesticides in agricultural used waters," *Comptes Rendus de l'Academie des Sciences - Series IIC: Chemistry*, vol. 3, no. 6, pp. 417–422, 2000.

[60] S. H. Khan and B. Pathak, "Zinc oxide based photocatalytic degradation of persistent pesticides: a comprehensive review," *Environmental Nanotechnology, Monitoring and Management*, vol. 13, Article ID 100290, 2020.

[61] A. Marinas, C. Guillard, J. M. Marinas, A. Fernández-Alba, A. Aguëra, and J.-M. Herrmann, "Photocatalytic degradation of pesticide-acaricide formetanate in aqueous suspension of TiO2," *Applied Catalysis B: Environmental*, vol. 34, no. 3, pp. 241–252, 2001.

[62] D. D. Dionysiou, A. P. Khodadoust, M. T. Suidan, A. M. Kern, I. Baudin, and J. M. Laine, "Continuous-mode photocatalytic degradation of chlorinated phenols and pesticides in water using a bench-scale TiO2 rotating disk reactor," *Applied Catalysis B: Environmental*, vol. 24, no. 3-4, pp. 139–155, 2000.

[63] D. Vaya and P. K. Surolia, "Semiconductor based photocatalytic degradation of pesticides: an overview," *Environmental Technology and Innovation*, vol. 20, Article ID 101128, 2020.

[64] K. Nawaz, K. Hussain, and N. Choudary, U. llyas, F. Lin, Eco-friendly role of biodegradation against agricultural pesticides hazards," *African Journal of Microbiology Research*, vol. 5, no. 3, pp. 177–183, 2011.

[65] G. K. Sidhu, S. Singh, V. Kumar, D. S. Dhanjal, S. Datta, and J. Singh, "Toxicity, monitoring and biodegradation of organophosphate pesticides: a review," *Critical Reviews in Environmental Science and Technology*, vol. 49, no. 13, pp. 1135–1187, 2019.

[66] M. Alexander, "Biodegradation of pesticides," *Pesticides and Their Effects on Soils and Water*, vol. 8, pp. 78–84, 1966.

[67] I. F. Lalrintluangi, V. Kumar, and D. Bisarya, "Biodegradation of pesticides: A review," *Biodegradation*, vol. 8, no. 11, 2020.

[68] J. Aislabie and G. Lloyd-Jones, "A review of bacterial-degradation of pesticides," *Soil Research*, vol. 33, no. 6, pp. 925–942, 1995.

[69] G. K. Sims and R. G. Kanissery, "Anaerobic biodegradation of pesticides," *Microorganisms for Sustainability*, vol. 10, pp. 33–54, 2019.

[70] R. L. Jones and F. A. Norris, "Factors affecting degradation of aldicarb and ethoprop," *Journal of nematology*, vol. 30, no. 1, 1998.

[71] R. H. Bromilow, A. A. Evans, and P. H. Nicholls, "Factors affecting degradation rates of five triazole fungicides in two soil types: 2. Field studies," *Pesticide Science*, vol. 55, no. 12, pp. 1135–1142, 1999.

[72] K. D. Racke, K. P. Steele, R. N. Yoder, W. A. Dick, and E. Avidov, "Factors affecting the hydrolytic degradation of chlorpyrifos in soil," *Journal of Agricultural and Food Chemistry*, vol. 44, no. 6, pp. 1582–1592, 1996.

[73] N. Burkhard and J. A. Guth, "Photolysis of organophosphorus insecticides on soil surfaces," *Pesticide Science*, vol. 10, no. 4, pp. 313–319, 1979.

[74] M. Tamimi, S. Qourzal, A. Assabbane, J.-M. Chovelon, C. Ferronato, and Y. Ait-Ichou, "Photocatalytic degradation of pesticide methomyl: determination of the reaction pathway and identification of intermediate products," *Photochemical and Photobiological Sciences*, vol. 5, no. 5, pp. 477–482, 2006.

[75] T. M. Sakellarides, M. G. Siskos, and T. A. Albanis, "Photodegradation of selected organophosphorus insecticides under sunlight in different natural waters and soils," *International Journal of Environmental Analytical Chemistry*, vol. 83, no. 1, pp. 33–50, 2003.

[76] D. L. Macalady and N. L. Wolfe, "New perspectives on the hydrolytic degradation of the organophosphorothioate insecticide chlorpyrifos," *Journal of Agricultural and Food Chemistry*, vol. 31, no. 6, pp. 1139–1147, 1983.

[77] O. A. Aly and M. I. Badawy, "Hydrolysis of organophosphate insecticides in aqueous media," *Environment International*, vol. 7, no. 6, pp. 373–377, 1982.

[78] A. Boudina, C. Emmelin, A. Baaliouamer, O. Païssé, and J. M. Chovelon, "Photochemical transformation of azoxystrobin in aqueous solutions," *Chemosphere*, vol. 68, no. 7, pp. 1280–1288, 2007.

[79] D. Vialaton, J.-F. Pilichowski, D. Baglio, A. Paya-Perez, B. Larsen, and C. Richard, "Phototransformation of propiconazole in aqueous media," *Journal of Agricultural and Food Chemistry*, vol. 49, no. 11, pp. 5377–5382, 2001.

[80] J. C. Villedieu, A. de Savignac, and J. P. Calmon, "Kinetics and mechanisms of hydrolysis of dicarboximide fungicides in micellar media," *Journal of Agricultural and Food Chemistry*, vol. 43, no. 7, pp. 1948–1953, 1995.

[81] W. Schwack and S. Nyanzi, "Analysis of dithiocarbamate fungicides. Reaction products of the thiuram disulphide fungicide thiram (TMTD) during acid hydrolysis," *Zeitschrift fur Lebensmittel-Untersuchung und -Forschung*, vol. 198, no. 1, pp. 8–10, 1994.

[82] E. R. White, E. A. Bose, J. M. Ogawa, B. T. Manji, and W. W. Kilgore, "Thermal and base-catalyzed hydrolysis products of the systemic fungicide, benomyl," *Journal of Agricultural and Food Chemistry*, vol. 21, no. 4, pp. 616–618, 1973.

[83] J. P. Escalada, J. Gianotti, A. Pajares, W. A. Massad, F. Amat-Guerri, and N. A. García, "Photodegradation of the Acaricide abamectin: a kinetic study," *Journal of Agricultural and Food Chemistry*, vol. 56, no. 16, pp. 7355–7359, 2008.

[84] J. Bhattacharyya, H. Banerjee, and A. Bhattacharyya, "Photodecomposition of an acaricide, fenazaquin, in aqueous alcoholic solution," *Journal of Agricultural and Food Chemistry*, vol. 51, no. 14, pp. 4013–4016, 2003.

[85] M. Li, R. Wang, Z. Kong, T. Gao, F. Wang, and B. Fan, "Cyflumetofen degradation in different aquatic environments and identification of hydrolytic products," *Journal of Environmental Chemical Engineering*, vol. 8, no. 6, Article ID 104512, 2020.

[86] L. Scrano, S. A. Bufo, P. Perucci, P. Meallier, and M. Mansour, "Photolysis and hydrolysis of rimsulfuron," *Pesticide Science*, vol. 55, no. 9, pp. 955–961, 1999.

[87] A. Trivella, M. Stawinoga, F. E. Dayan, C. L. Cantrell, P. Mazellier, and C. Richard, "Photolysis of natural β-triketonic herbicides in water," *Water Research*, vol. 78, pp. 28–36, 2015.

[88] J. J. Villaverde, B. Sevilla-Morán, C. Calvo, J. L. Alonso-Prados, and P. Sandín-España, "Photolysis of clethodim herbicide and a formulation in aquatic environments: fate and ecotoxicity assessment of photoproducts by QSAR models," *The Science of the Total Environment*, vol. 615, pp. 643–651, 2018.

[89] Q. Luo, G. Li, J. Xiao et al., "DFT study on the hydrolysis of metsulfuron-methyl: a sulfonylurea herbicide," *Journal of Theoretical and Computational Chemistry*, vol. 17, no. 8, Article ID 1850050, 2018.

[90] S. Walia and P. Dureja, "Chemical and photochemical transformation of fenamiphos—an organophosphorus nematicide," *Toxicological and Environmental Chemistry*, vol. 28, no. 2-3, pp. 189–194, 1990.

[91] S. Qin, J. Gan, W. Liu, and J. O. Becker, "Degradation and adsorption of fosthiazate in soil," *Journal of Agricultural and Food Chemistry*, vol. 52, no. 20, pp. 6239–6242, 2004.

[92] A. El Yadini, B. Marouane, A. Ahmido et al., "Photolysis and photodegradation of fenamiphos insecticide by using slurry and supported TiO_2," *Journal of Materials and Environmental Science*, vol. 4, no. 6, pp. 973–980, 2013.

[93] L. A. Gurvich, N. S. Kobrina, E. P. Serebryakov, and V. F. Kucherov, "Photochemical transformations of gibberellin A3 derivatives aromatization of ring A," *Tetrahedron*, vol. 27, no. 23, pp. 5901–5909, 1971.

[94] C. Zhang and H. B. Ji, "Effects of Environmental parameters on the ultraviolet Degradation of methylphosphonate," *Applied Ecology and Environmental Research*, vol. 17, no. 4, pp. 9473–9482, 2019.

[95] A. Stoessl, "The photolysis of maleic hydrazide: evidence for an intermolecular hydrogen transfer," *Canadian Journal of Chemistry*, vol. 43, no. 8, pp. 2430–2432, 1965.

[96] I. K. Konstantinou, T. M. Sakellarides, V. A. Sakkas, and T. A. Albanis, "Photocatalytic degradation of selected s-triazine herbicides and organophosphorus insecticides over aqueous TiO2 suspensions," *Environmental Science and Technology*, vol. 35, no. 2, pp. 398–405, 2001.

[97] E.-S. Hwang, J. N. Cash, and M. J. Zabik, "Determination of degradation products and pathways of mancozeb and ethylenethiourea (ETU) in solutions due to ozone and chlorine dioxide treatments," *Journal of Agricultural and Food Chemistry*, vol. 51, no. 5, pp. 1341–1346, 2003.

[98] P. P. Choudhury, S. Roy, K. K. Somyajulu, and P. Dureja, "Light induced transformation of isoprothiolane on glass,

soil, and plant surface," *Toxicological and Environmental Chemistry*, vol. 90, no. 5, pp. 873–878, 2008.

[99] S.-S. Chou, E. Taniguchi, and M. Eto, "Photodegradation of dialkyl 1,3-Dithiolan-2-ylidenemalonates and some other pesticides on solid particles," *Agricultural and Biological Chemistry*, vol. 44, no. 9, pp. 2169–2177, 1980.

[100] B. Gupta, M. Rani, and R. Kumar, "Degradation of thiram in water, soil and plants: a study by high-performance liquid chromatography," *Biomedical Chromatography*, vol. 26, no. 1, pp. 69–75, 2012.

[101] O. M. S. Filipe, S. A. O. Santos, M. R. M. Domingues et al., "Photodegradation of the fungicide thiram in aqueous solutions. Kinetic studies and identification of the photodegradation products by HPLC-MS/MS," *Chemosphere*, vol. 91, no. 7, pp. 993–1001, 2013.

[102] C. Sirtori, A. Agüera, I. Carra, and J. A. Sanchéz Pérez, "Identification and monitoring of thiabendazole transformation products in water during Fenton degradation by LC-QTOF-MS," *Analytical and Bioanalytical Chemistry*, vol. 406, no. 22, pp. 5323–5337, 2014.

[103] L. Yu, L. Wang, Y. Zhao, and B. Wang, "Identification and dissipation of omethoate and its main metabolite DMP in wheat determined by UPLC-QTOF/MS," *Journal of Agricultural and Food Chemistry*, vol. 67, no. 20, pp. 5891–5898, 2019.

[104] J. M. Wolfand, G. H. LeFevre, and R. G. Luthy, "Metabolization and degradation kinetics of the urban-use pesticide fipronil by white rot fungus Trametes versicolor," *Environmental Sciences: Processes and Impacts*, vol. 18, no. 10, pp. 1256–1265, 2016.

[105] D. D. Dionysiou, A. P. Khodadoust, M. T. Suidan, A. M. Kern, I. Baudin, and J. M. Laine, "Identification of sethoxydim degradation products in natural waters under different light sources by HPLC-QTOF-MS," *Microchemical Journal*, vol. 119, pp. 6–10, 2015.

[106] G. Chen, Y. Qiao, X. Zhang et al., "Identification and characterization of herbicide penoxsulam transformation products in aqueous media by UPLC-QTOF-MS," *Bulletin of Environmental Contamination and Toxicology*, vol. 102, no. 6, pp. 854–860, 2019.

[107] K. Chen, F. Tian, C. Wu et al., "Degradation products and pathway of ethiprole in water and soil," *Water Research*, vol. 161, pp. 531–539, 2019.

[108] I. Ferrer and E. M. Thurman, *Mass Spectrometry for the Analysis of Pesticide Residues and Their Metabolites*, Wiley-Blackwell, Hoboken, NJ, USA, pp. 207–229, 2015.

[109] M. Jović, D. Manojlović, D. Stanković et al., "Degradation of triketone herbicides, mesotrione and sulcotrione, using advanced oxidation processes," *Journal of Hazardous Materials*, vol. 260, pp. 1092–1099, 2013.

[110] A. Tawk, M. Deborde, J. Labanowski, and H. Gallard, "Chlorination of the β-triketone herbicides tembotrione and sulcotrione: kinetic and mechanistic study, transformation products identification and toxicity," *Water Research*, vol. 76, pp. 132–142, 2015.

[111] A. Lozano, S. Uclés, A. Uclés, C. Ferrer, and A. R. Fernández-Alba, "Pesticide residue analysis in fruit- and vegetable-based baby foods using GC-orbitrap MS," *Journal of AOAC International*, vol. 101, no. 2, pp. 374–382, 2018.

[112] C. I. Nannou, V. I. Boti, and T. A. Albanis, "Trace analysis of pesticide residues in sediments using liquid chromatography-high-resolution orbitrap mass spectrometry," *Analytical and Bioanalytical Chemistry*, vol. 410, no. 7, pp. 1977–1989, 2018.

[113] M. Jović, D. Manojlović, D. Stanković et al., "Electrochemical degradation of triketone herbicides and identification of their main degradation products," *CLEAN–soil, Air, Water, vool.*vol. 43, no. 7, pp. 1093–1099, 2014.

[114] J. Cotton, F. Leroux, S. Broudin et al., "Development and validation of a multiresidue method for the analysis of more than 500 pesticides and drugs in water based on on-line and liquid chromatography coupled to high resolution mass spectrometry," *Water Research*, vol. 104, pp. 20–27, 2016.

[115] A. López, V. Yusà, and M. Millet, "Retrospective screening of pesticide metabolites in ambient air using liquid chromatography coupled to high-resolution mass spectrometry," *Talanta*, vol. 150, pp. 27–36, 2016.

[116] A. López, C. Coscollà, V. Yusà, S. Armenta, M. de la Guardia, and F. A. Esteve-Turrillas, "Comprehensive analysis of airborne pesticides using hard cap espresso extraction-liquid chromatography-high-resolution mass spectrometry," *Journal of Chromatography.A*, vol. 1506, pp. 27–36, 2017.

[117] A. López, P. Dualde, and V. Yusà, "Retrospective analysis of pesticide metabolites in urine using liquid chromatography coupled to high-resolution mass spectrometry," *Talanta*, vol. 160, pp. 547–555, 2016.

[118] S. H. Abd Al-Rahman, M. M. Almaz, and I. A. Osama, "Determination of degradation rate of acaricide fenpyroximate in apple, citrus, and grape by HPLC-DAD," *Food Analytical Methods*, vol. 5, no. 2, pp. 306–311, 2012.

[119] K. Martínez and D. Barceló, "Determination of antifouling pesticides and their degradation products in marine sediments by means of ultrasonic extraction and HPLC-APCI-MS," *Fresenius' Journal of Analytical Chemistry*, vol. 370, no. 7, pp. 940–945, 2001.

[120] X. Wang, R. Jia, Y. Song, M. Wang, Q. Zhao, and S. Sun, "Determination of pesticides and their degradation products in water samples by solid-phase extraction coupled with liquid chromatography-mass spectrometry," *Microchemical Journal*, vol. 149, Article ID 104013, 2019.

[121] A. Farran, J. De Pablo, and D. Barceló, "Identification of organophosphorus insecticides and their hydrolysis products by liquid chromatography in combination with UV and thermospray-mass spectrometric detection," *Journal of Chromatography A*, vol. 455, pp. 163–172, 1988.

[122] K. Sinderhauf and W. Schwack, "Photolysis experiments on phosmet, an organophosphorus insecticide," *Journal of Agricultural and Food Chemistry*, vol. 51, no. 20, pp. 5990–5995, 2003.

[123] S. A. Todey, A. M. Fallon, and W. A. Arnold, "Neonicotinoid insecticide hydrolysis and photolysis: rates and residual toxicity," *Environmental Toxicology and Chemistry*, vol. 37, no. 11, pp. 2797–2809, 2018.

[124] S. Song, C. Zhang, Z. Chen, J. Wei, H. Tan, and X. Li, "Hydrolysis and photolysis of bentazone in aqueous abiotic solutions and identification of its degradation products using quadrupole time-of-flight mass spectrometry," *Environmental Science and Pollution Research*, vol. 26, no. 10, pp. 10127–10135, 2019.

[125] X. Meng, N. Wang, X. Long, and D. Hu, "Degradation of a novel pesticide antiviral agent vanisulfane in aqueous solution: kinetics, identification of photolysis products, and pathway," *ACS Omega*, vol. 5, no. 38, pp. 24881–24889, 2020.

[126] M. Jović, D. Manojlović, D. Stanković et al., "Solid phase microextraction and gas chromatography with ion trap detector (GC-ITD) analysis of amitraz residues in beeswax after hydrolysis to 2, 4-dimethylaniline" *Analytica chimica acta*," *Vool*, vol. 571, no. 1, pp. 40–44, 2006.

[127] M. Bavcon Kralj, M. Franko, and P. Trebše, "Photodegradation of organophosphorus insecticides - investigations of products and their toxicity using gas chromatography-mass spectrometry and AChE-thermal lens spectrometric bioassay," *Chemosphere*, vol. 67, no. 1, pp. 99–107, 2007.

[128] S. Wang, A. Miltner, and K. M. Nowak, "Identification of degradation routes of metamitron in soil microcosms using 13C-isotope labeling," *Environmental Pollution*, vol. 220, pp. 927–935, 2017.

[129] C. Poßberg, B. Schmidt, K. Nowak, M. Telscher, A. Lagojda, and A. Schaeffer, "Quantitative identification of biogenic nonextractable pesticide residues in soil by 14C-analysis," *Environmental Science and Technology*, vol. 50, no. 12, pp. 6415–6422, 2016.

Hindawi
Journal of Chemistry
Volume 2022, Article ID 3820942, 7 pages
https://doi.org/10.1155/2022/3820942

Research Article

Comparing the Transcriptomes of Two Different Tissues in *Helicoverpa assulta* (Guenée)

Hailing Zhang, Kuiyin Li, and Yubo Zhang

Key Laboratory of Insect Information System and Resource Utilization, Development of Guizhou Province, Anshun University, Anshun, Guizhou 561000, China

Correspondence should be addressed to Hailing Zhang; asxyhailing@163.com

Received 10 March 2022; Accepted 9 May 2022; Published 27 May 2022

Academic Editor: Lu Yu

Helicoverpa assulta (Guenée), a moth species belonging to the Noctuidae (Lepidoptera) family, is a destructive agricultural pest that infests multiple cash crops. To assess differences in the gene expression profiles of different tissues in *H. assulta*, we analyzed the transcriptomes of two tissue types (midgut and hemocytes) using the Illumina Hiseq 2000 platform, on the basis of which we obtained 52076750 and 53404200 high-quality clean reads, respectively. De novo assembly yielded 46146 and 33707 unigenes from the midgut and hemocytes, respectively. After screening, we identified 23726 unigenes differentially expressed between the midgut and hemocytes. Taking the midgut as the control, we detected 7448 and 16278 unigenes that were up- and downregulated in hemocytes, respectively. Gene Ontology functional annotation divided the differentially expressed unigenes (DEUs) into three categories (biological process, cellular component, and molecular function) and 51 branches, whereas the Kyoto Encyclopedia of Genes and Genomes metabolic pathway annotation assigned the DEUs to six categories, mapping these to 258 pathways. In addition, we detected 224918 single-nucleotide polymorphic sites. Our findings based on transcriptome sequencing, data assembly, and functional gene annotation of two different tissues in *H. assulta* will provide a valuable reference for further excavation and study of functional genes in *H. assulta*.

1. Introduction

The moth species *Helicoverpa assulta*, belonging to the family Noctuidae (Lepidoptera), is an important polyphagous pest of agricultural crops, causing potentially widespread damage and immeasurable economic losses. The larvae generally feed on the buds, flowers, and fruits of crop plants, and consume tender stems and leaf buds, with fruit decay being the primary source of yield reductions. *H. assulta* is widely distributed in numerous Asian countries, wherein addition to tobacco and pepper [1, 2], its hosts include tomato, pumpkin, cowpea, cabbage, and cauliflower. Currently, the control of *H. assulta* is primarily based on applying chemical insecticides, which pollute the environment and disrupt ecosystem balance to varying extents. Consequently, it is particularly desirable to identify less environmentally damaging prevention and control measures. In this regard, recent developments in high-throughput sequencing technology have witnessed the application of transcriptome sequencing technology to the study of insects. For example, the molecular mechanisms associated with pesticide detoxification by *Spodoptera frugiperda* have been studied based on second-generation sequencing technology [3], and transcriptome sequencing has been used to solve the problem of sex identification in *Helicoverpa armigera* [4]. Similarly, transcriptome sequencing has been used to study differences in the expression of different tissues of *Agrotis ipsilon* to reveal the mechanisms underlying wing development [5]. In contrast, Illumina sequencing has been used to characterize differences in gene alterations, signal pathways, and gene expression patterns associated with the infection of rice by *Nilaparvata lugens* and *Chilo suppressalis* [6]. To date, transcriptome sequencing-based studies on *H. assulta* have primarily focused on the following aspects: gender-related olfactory system differentiation [7], functional

characterization of chemosensory genes [8], and host selection and adaptation [9]. However, the accumulated biological information resources for *H. assulta* are main comparatively limited. To augment these resources, we adopted a high-throughput transcriptome sequencing approach to analyze the transcriptomes of two types of tissues in *H. assulta*, namely, those of the midgut and hemocytes. Based on Trinity software assembly, functional database annotation, analysis of differential gene expression, and single-nucleotide polymorphism (SNP) site screening, we performed a comprehensive molecular genetic characterization of *H. assulta*. The information thus obtained will provide a valuable basis for further study of functional genes and differential gene expression in *H. assulta* and contribute to augmenting its biological information databases. Moreover, gaining new insights into genetic mechanisms underlying the responses of *H. assulta* may contribute to developing novel strategies for controlling and preventing this important agricultural pest.

2. Materials and Methods

2.1. Acquisition of Insect Tissues and Extraction of RNA. Midgut and hemocyte material was obtained from fourth-instar larvae of *H. assulta* raised in our laboratory. The larvae were placed on ice and decapitated using scissors. Midguts were extracted from the head-less bodies and immediately immersed in liquid nitrogen for preservation. Having excised the larval gastropods, hemocytes were collected into precooled Eppendorf tubes. Total RNA was extracted from the two tissue types using TriZol reagent according to the manufacturer's instructions. The purity and integrity of the isolated RNA were determined using an Agilent 2100 Bioanalyzer and 1% agarose gel electrophoresis, respectively, and samples of the qualified preparations were used as templates for transcriptome sequencing.

2.2. Construction of cDNA Libraries and RNA Sequencing. To isolate poly-A mRNAs from total RNA, we used Oligo (dT) magnetic beads. The mRNA was randomly denatured at 94°C for 5 min to obtain small fragments of approximately 200 bp in size, and these mRNA fragments were used as templates for synthesizing first-strand cDNA using random hexamer primers. Subsequent synthesis of second-strand cDNA was performed using a mixture of dNTPs, DNA polymerase I, and buffer solution. The purified double-stranded cDNA thus obtained was then subjected to terminal repair, followed by the addition of poly-A tails and the ligation of sequencing adapters. Finally, cDNA libraries were constructed for each type by enriching the amplified products and subsequently sequenced using the Illumina HiseqTM 2000 platform.

2.3. De Novo Assembly and Functional Annotation. Prior to sequence assembly, the raw reads were cleaned by removing low-quality reads (those with a quality value of less than 20), adaptor reads, and reads containing N (ambiguous) bases using Filter software. The clean reads were then de novo assembled into unigenes using Trinity software [10, 11], for which we calculated Q20 values and GC and N contents. Clean reads with a certain overlap length are initially combined to generate longer fragment contigs. Thereafter, we mapped the read data to contigs based on peer-to-peer mapping, thereby enabling us to determine contigs from the same transcriptome and inter-contig distances. Finally, the contigs were assembled into sequences that could be extended no further at either end. These sequences were defined as single unigenes. The unigene sequences thus obtained were functionally annotated based on searches of the Gene Ontology (GO) and Kyoto Encyclopedia of Genes and Genomes (KEGG) databases using BlastX software.

2.4. Identification of Differentially Expressed Unigenes (DEUs). The expression of single unigene was normalized using the fragments per kb per million fragments (FPKM) method [12]. Differential expression levels were analyzed based on false detection rate (FDR) [13], with $FDR \leq 0.001$ and $|\log2 \text{ ratio}| \geq 1$ being used as thresholds values for determining the significance of differential gene expression. Based on GO database searches, we performed functional classification annotation and enrichment analysis of differentially expressed unigenes (DEUs) in different tissues, with a P value of ≤ 0.05 used as a threshold indicating the DEU enrichment. In addition, based on a significant enrichment of KEGG pathways, we identified the main biochemical, metabolic, and signal transduction pathways associated with these DEUs.

3. Results

3.1. Transcriptome Assembly. By sequencing the transcriptomes of two different tissues from *H. assulta*, we obtained 52076750 and 53404200 clean reads for midgut and hemocytes tissues, respectively, with respective Q20 and GC content values of 98.71% and 98.64% and 46.09% and 49.13%, indicating that the amount and quality of transcriptome sequencing data were high. These read fragments were accordingly used for subsequent transcriptome assembly (Table 1).

As a consequence of assembly, we obtained 46146 midgut unigenes, among which 27717 were of lengths between 200 and 500 bp, accounting for 60.06% of the total unigenes. Moreover, 1905 of these had lengths exceeding 3000 bp, accounting for 4.13% of the total (Figure 1). Comparatively, 33707 unigenes were obtained for hemocytes, among which 20827 were between 200 and 500 bp and 4318 had lengths ranging from 1000–2000 bp, accounting for 61.79% and 12.81% of the total unigenes, respectively (Figure 2). The sequence datasets described in this manuscript have been deposited in the National Center for Biotechnology Information Sequence Read Archive (https://www.ncbi.nlm.nih.gov/sra) under accession number PRJNA789178.

3.2. Analysis of Differentially Expressed Unigenes. A comparative analysis of the differential expression in the midgut and hemocyte unigenes revealed altered expression profiles for 23726 unigenes, among which 7448 were upregulated

Table 1: Summary of transcriptome sequencing for different *Helicoverpa assulta* tissues.

Parameter	Midgut	Hemocyte
Total raw reads	54 622916	57 007 970
Total clean reads	52 076750	53 404 200
Total clean nucleotides	4686907500	4 806 378 000
Q20/%	98.71	98.64
N/%	0	0
GC/%	46.09	49.13
Total length of contig (nt)	30 338 537	22 561 513
Mean size of contig (nt)	393	352
Total length of unigene (nt)	35 741 176	22 561 814
Mean size of unigene (nt)	775	669
Number of contigs	77 182	64 112
Number of unigenes	46 146	33 707
N50 of contig (nt)	787	696
N50 of unigene (nt)	1 494	1 140

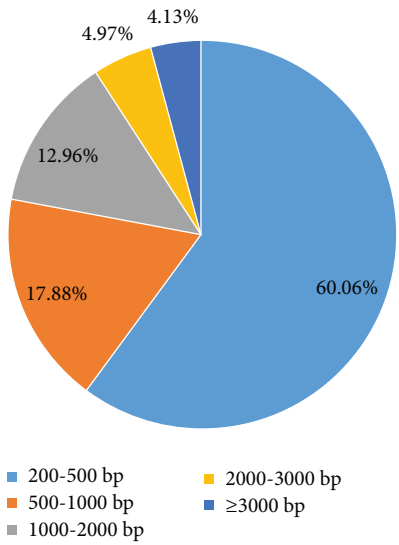

Figure 1: Size distribution of the lengths of *Helicoverpa assulta* midgut unigenes.

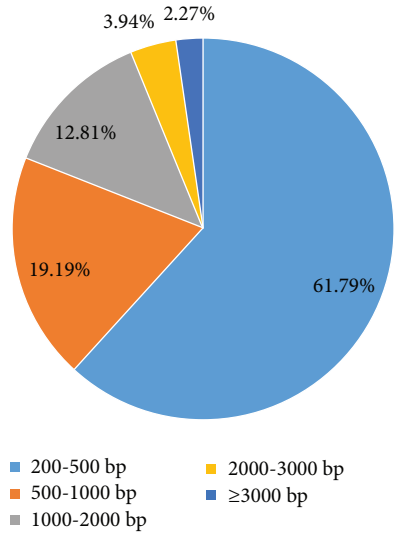

Figure 2: Size distribution of the lengths of *Helicoverpa assulta* hemocyte unigenes.

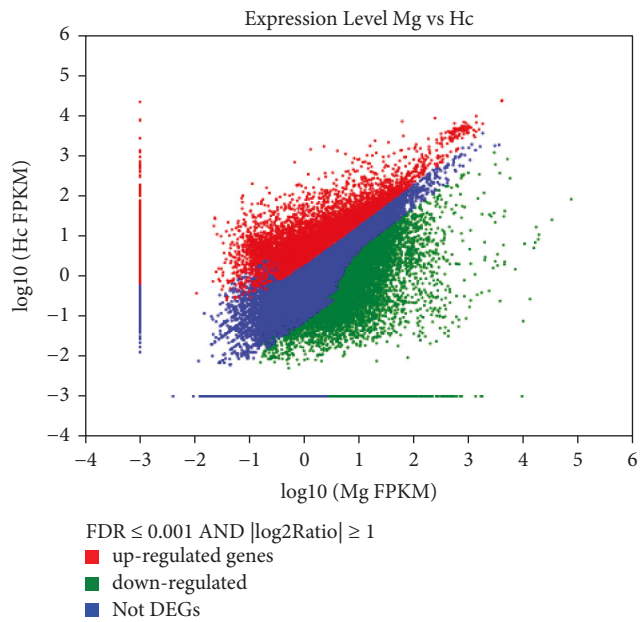

Figure 3: Comparison of unigene expression between the midgut and hemocytes of *Helicoverpa assulta*. The differentially expressed unigenes are shown in red and green, whereas those shown in blue were not differentially expressed between midgut and hemocytes. Red and green represent the rising and declining expression, respectively. With respect to expression profiles, midgut and hemocyte genes are considered the control and treatment groups, respectively.

and 16278 were downregulated in hemocytes compared with those in the midgut (Figure 3). For example, the expression levels of cytochrome P450 and cathepsin in hemocytes were higher than those in the midgut. In contrast, those of carboxypeptidase inhibitor and disintegrin metalloproteinase were higher in the midgut than in hemocytes.

3.3. Gene Ontology (GO) Annotation of DEUs. GO functional annotation classified midgut and hemocytes unigenes into the three primary GO categories, namely, biological process, cellular component, and molecular function, among which the annotated proteins were found to be mainly grouped into the following subcategories: cellular process (3871), cell (2849), cell part (2848), binding (2975), and catalytic activity (2872) (Figure 4).

3.4. KEGG Pathway Analysis of Differentially Expressed Unigenes. We identified 9270 DEUs that were functionally annotated with respect to KEGG pathways based on enrichment analysis. Among the six KEGG categories, organismal systems, metabolism, human diseases, genetic information processing, environmental information processing, and cellular processes, DEUs were mapped to 258 pathways, with bile secretion, metabolic pathways, amoebiasis, RNA transport, neuroactive ligand-receptor interaction, and regulation of actin cytoskeleton, having the

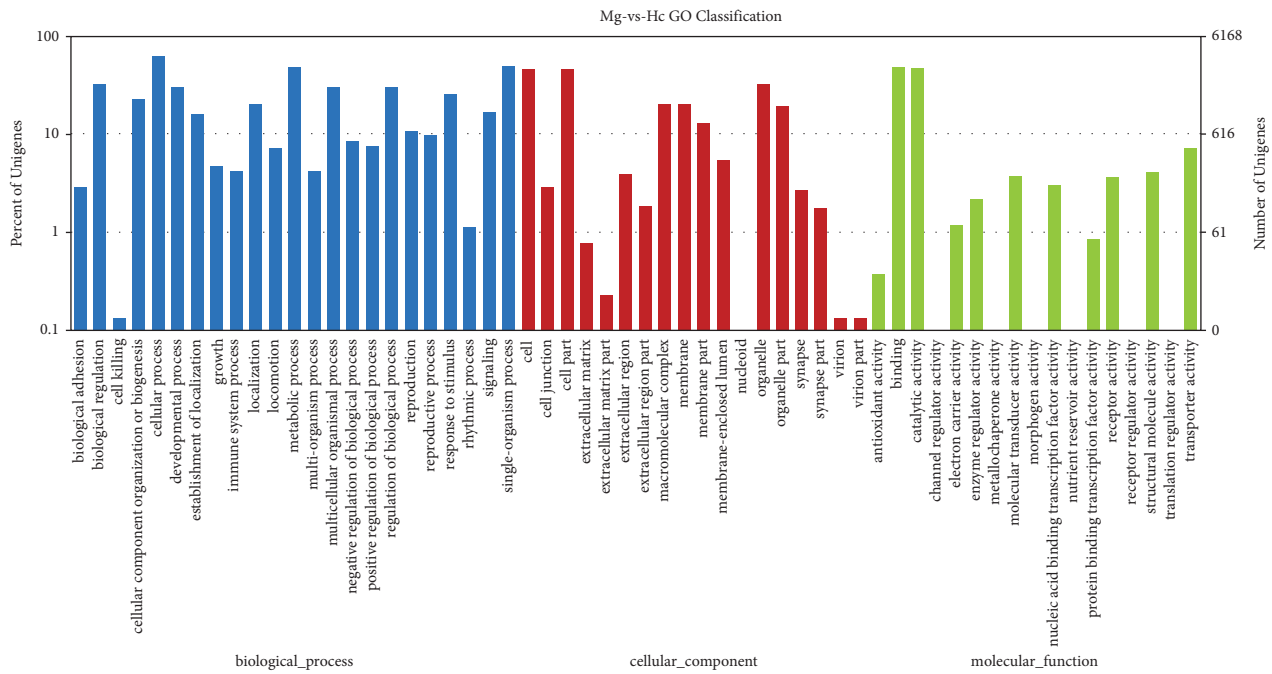

Figure 4: Gene Ontology (GO) classification of *Helicoverpa assulta* unigenes.

respective highest representations (Figure 5). Among these, 1988, 1331, 829, and 1580 DEUs were annotated to metabolic, signal, immune, and infectious disease pathways, respectively. Moreover, 1541, 605, 146, and 733 unique DEUs were, respectively, annotated to these four pathways (Figure 6). The category immune pathway comprises two pathway types, namely, immune system and immune disease, to which 77.8% and 8% of DEUs were annotated, respectively (Figure 7).

3.5. Analysis of Single-Nucleotide Polymorphisms. Our analysis of SNPs revealed 224918 polymorphic sites of six types (A-G, C-T, A-C, A-T, C-G, and G-T), among which types A-G and C-T accounted for the highest proportion (64.6%) of all markers, with the remaining four types having similar smaller proportions. Furthermore, we identified base transitions as being more common than transversions. Comparative tissue analysis indicated a larger number of SNPs in hemocytes than in midgut tissues. For each tissue type, the proportions of the SNP types and transition/transversion were similar to those of the total SNPs (Table 2).

4. Discussion

Based on our transcriptome sequencing of two different tissue types (midgut and hemocytes) from larvae of the *H. assulta* moth, we identified a large number of genes differentially expressed between these two tissues, with differences in the expression profiles of 23726 unigenes (7448 up- and 16278 downregulated in hemocytes compared with those in the midgut) being detected. For example, genes encoding cytochrome P450 and cathepsin were upregulated, whereas carboxypeptidase inhibitor and disintegrin metalloproteinase were downregulated. In insects, the cytochrome P450 enzyme system serves as a vital metabolic enzyme system, which plays functional roles in detoxifying and metabolizing exogenous chemicals, including plant secondary metabolites and pesticides. By enhancing P450 gene expression and enzyme activity, insects can regulate their defense state, thereby bolstering resistance to toxic compounds or adverse environmental conditions [14–16]. Disintegrin metalloproteinases play roles in cell proliferation, migration, and invasion [17]. In contrast, carboxypeptidase inhibitors inhibit carboxypeptidase activity in the insect intestine [18]. Furthermore, metallocarboxypeptidases are crucial enzymes involved in food digestion and absorption in the digestive tracts of insects. They may also play important roles in insect metamorphosis, development, disease resistance, and immunity. For example, upregulated expression of five midgut metallocarboxypeptidase genes in response to pathogen infection was observed within 24 h of infecting silkworm larvae with *Bombyx mori* nuclear polyhedrosis virus [19, 20]. In addition, cathepsin has been established to play a significant role in regulating the fecundity and pathogen response of insects [21].

Although we could functionally annotate many of the identified DEUs with reference to the GO and KEGG databases, many genes remain unannotated. We speculate that this could be attributable to an insufficient sequence length and lack of sequence information for comparable species, thereby precluding annotation via homologous sequence alignment.

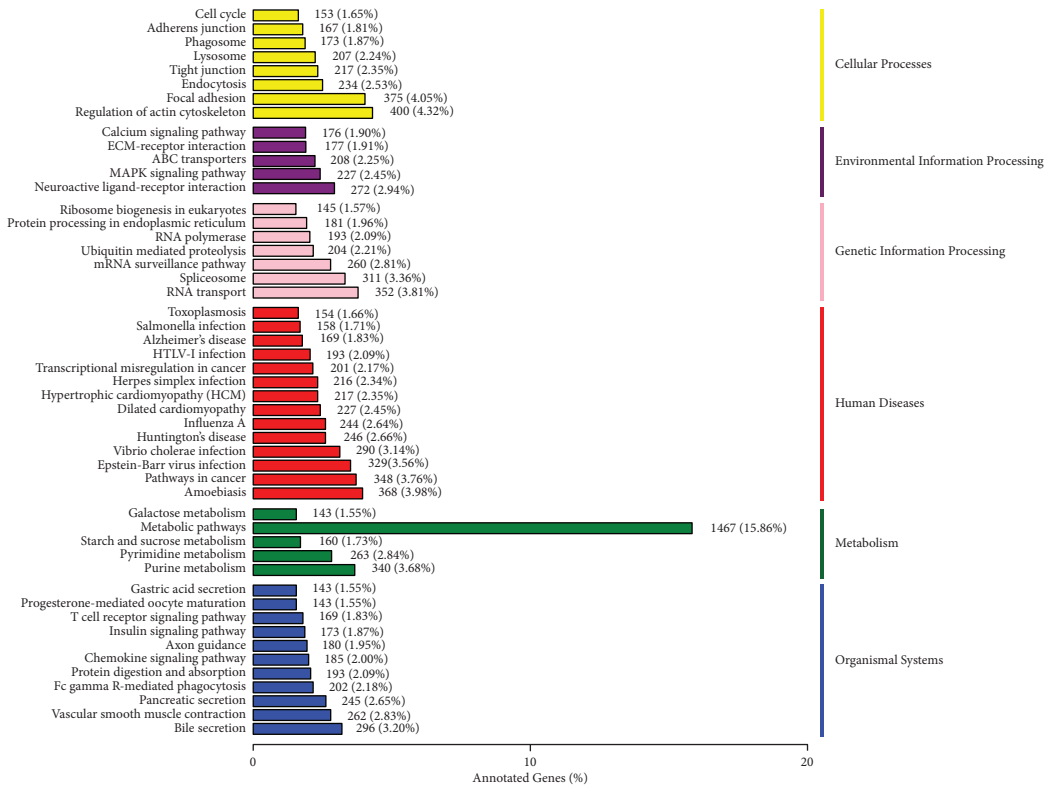

Figure 5: List of KEGG pathways.

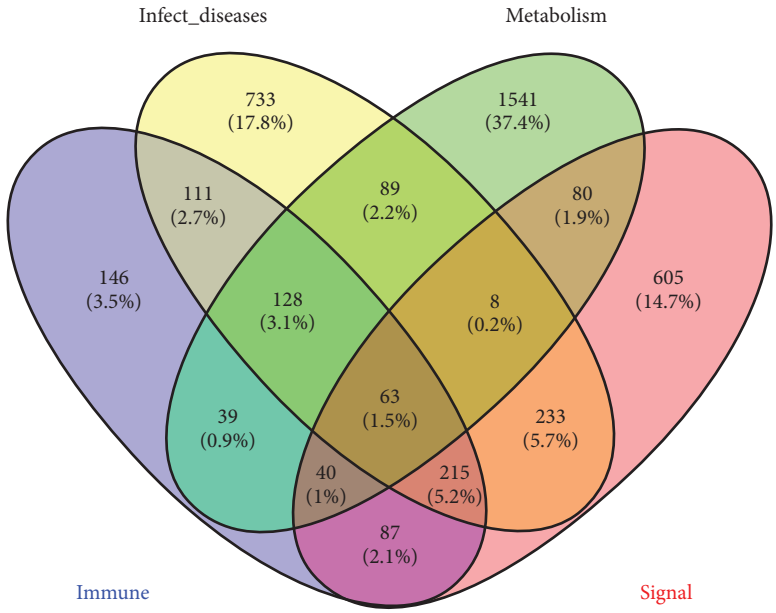

Figure 6: A Venn diagram depicting the results of KEGG pathway analysis.

Based on our KEGG analysis of the transcriptomes of different tissues in *H. assulta*, we annotated 9270 DEUs to KEGG pathways (metabolic, signal, immune, and infectious disease pathways), among which the largest number were assigned to metabolic pathways, followed by infectious disease pathways, with immune pathways having the fewest annotations. Furthermore, among the genes annotated to immune pathways, 92% were associated with immune system pathways, whereas 22.2% were involved in immune disease pathways. In this regard, the hemolymph system of insects facilitates the transport of nutrients and metabolic wastes as well as plays functional roles in cellular immune regulation [22, 23]. Insects are characterized by an innate mode of immunity, comprising humoral and cellular

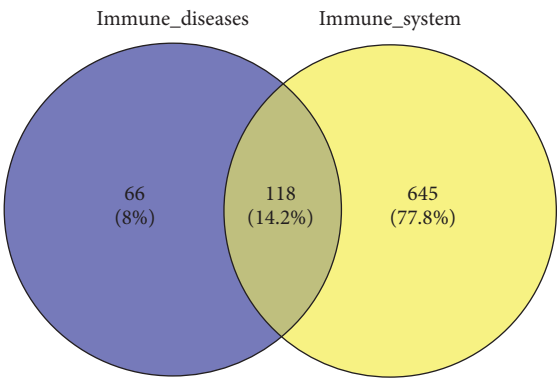

Figure 7: Venn diagram depicting the results of KEGG immune pathway analysis.

Table 2: Distribution of different single-nucleotide polymorphism types between the different tissues.

Type	Mg	Hc	Total
Transition			
A-G	27.268	44.618	71.886
C-T	27.993	45.495	73.488
Transversion			
A-C	6.981	10.966	17.947
A-T	10.509	16.405	26.914
C-G	6.140	10.656	16.796
G-T	6.826	11.061	17.887
Total	85.717	139.201	224.918

mechanisms, in which hemocytes are mainly involved in targeting invasive pathogens via phagocytosis, nodules and coating.

Our findings regarding the differential expression of genes in two different tissue types in *H. assulta*, along with the identification of several SNPs, will provide a valuable scientific basis for further studies examining the growth and development, life metabolism, defense, and pesticide resistance mechanisms of *H. assulta*. Moreover, they will contribute to the further excavation and characterization of functional genes in *H. assulta*.

5. Conclusion

High-throughput sequencing is an effective approach for obtaining gene resources for nonmodel organisms. In this study, we used this technique to sequence the transcriptomes of the midgut and hemocytes of *H. assulta* larvae. We obtained the total unigenes associated with these two tissue types, many of which were successfully annotated based on reference to the GO and KEGG databases. These data will accordingly augment the resources of insect gene databases. We also identified and characterized several SNP sites, thereby significantly contributing to the future development of molecular markers for *H. assulta*. Moreover, our findings will provide a valuable reference source for the further excavation, development, and utilization of functional genes in *H. assulta*.

Data Availability

Availability of data 1. The data that support the findings of this study are openly available in the National Center for Biotechnology Information Sequence Read Archive (https://www.ncbi.nlm.nih.gov/sra) under accession number PRJNA789178. 2. The data that support the findings of this study are included within the article. 3. The data that support the findings of this study are available from the corresponding author by request. 4. Some data are not publicly available due to the information they contain that could compromise the privacy of research participants.

Conflicts of Interest

The authors declare that they have no conflicts of interest.

Authors' Contributions

Kuiyin Li and Yubo Zhang contributed equally to this work.

Acknowledgments

This work was supported by the special fund of Guizhou Province to Support the City (Prefecture) College Education Quality Improvement Project (Qian Cai Jiao [2021] No. 78), the Science and Technology Foundation of Guizhou Province (Qiankehe foundation [2017] 1001), and Guizhou Province Educational Science and Technology Research (Guizhou Province KY Character [2016] 279, [2016] 278).

References

[1] S. Cao, Y. Liu, M. B. Guo, and G. Wang, "A conserved odorant receptor tuned to floral volatiles in three *Heliothinae* species," *PLoS One*, vol. 11, no. 5, Article ID e0155029, 2016.

[2] H. Chang, M. Guo, B. Wang, Y. Liu, S. Dong, and G. Wang, "Sensillar expression and responses of olfactory receptors reveal different peripheral coding in two *Helicoverpa* species using the same pheromone components," *Scientific Reports*, vol. 6, Article ID 18742, 2016.

[3] H. L. Chen, M. H. Xie, L. L. Lin, Y. Zhong, F. Zhang, and W. Su, "Transcriptome analysis of detoxification-related genes in *Spodoptera frugiperda* (Lepidoptera: noctuidae)," *Journal of Insect Science*, vol. 22, no. 1, p. 11, 2022.

[4] Z. Y. Deng, Y. K. Zhang, M. Zhang et al., "Characterization of the first W-specific protein-coding gene for sex identification in *Helicoverpa armigera*," *Frontiers in Genetics*, vol. 11, p. 649, 2020.

[5] W. G. Zheng, M. H. Le, S. Chakrabarty, B. Xiao, Y. Xiao, and H. Yuan, "Difference expression analysis in different tissues of *Agrotis ipsilon* reveals the possible mechanism of wing development," *Biotechnology Bulletin*, vol. 35, no. 10, pp. 102–110, 2019.

[6] H. P. Li, Z. H. Zhou, H. X. Hua, and W. Ma, "Comparative transcriptome analysis of defense response of rice to *nilaparvata lugens* and *chilo suppressalis* infestation," *International Journal of Biological Macromolecules*, vol. 163, pp. 2270–2285, 2020.

[7] H. C. Li, W. Z. Li, C. J. Miao et al., "Identification of the differences in olfactory system between male and female oriental tobacco budworm *Helicoverpa assulta*," *Archives of Insect Biochemistry and Physiology*, vol. 107, no. 4, Article ID e21829, 2021.

[8] J. Zhang, B. Wang, S. L. Dong et al., "Antennal transcriptome analysis and comparison of chemosensory gene families in two closely related noctuidae moths, *Helicoverpa armigera* and *H. assulta*," *PLoS One*, vol. 10, no. 2, Article ID e0117054, 2015.

[9] H. C. Li, H. Zhang, R. B. Guan, and X. Miao, "Identification of differential expression genes associated with host selection and adaptation between two sibling insect species by transcriptional profile analysis," *BMC Genomics*, vol. 14, no. 1, p. 582, 2013.

[10] M. G. Grabherr, B. J. Haas, M. Yassour et al., "Full-length transcriptome assembly from RNA-seq data without a reference genome," *Nature Biotechnology*, vol. 29, no. 7, pp. 644–652, 2011.

[11] B. J. Haas, A. Papanicolaou, M. Yassour et al., "De novo transcript sequence reconstruction from RNA-seq using the Trinity platform for reference generation and analysis," *Nature Protocols*, vol. 8, no. 8, pp. 1494–1512, 2013.

[12] A. Mortazavi, K. Mccue, L. Schaeffer, and B. Wold, "Mapping and quantifying mammalian transcriptomes by RNA-Seq," *Nature Methods*, vol. 5, no. 7, pp. 621–628, 2008.

[13] S. Audic and J. M. Claverie, "The significance of digital gene expression profiles," *Genome Research*, vol. 7, no. 10, pp. 986–995, 1997.

[14] Z. Y. Qiu, F. Liu, H. M. Lu, H. Yuan, Q. Zhang, and Y. Huang, "De novo assembly and characterization of the transcriptome of grasshopper *Shirakiacris shirakii*," *International Journal of Molecular Sciences*, vol. 17, no. 7, p. 1110, 2016.

[15] C. L. Yin, X. H. Ye, M. Y. Chen, Y. Mei, H. M. Xiao, and F. Li, "Evolution analysis of cytochrome P450 gene family in *parasitoid wasps*," *Chinese Journal of Biological Control*, vol. 35, no. 3, pp. 335–342, 2019.

[16] H. Peng and H. M. Liu, "Development of cytochrome P450 in mediating metabolic resistance and applications for mosquito control," *China Tropical Medicine*, vol. 22, no. 1, pp. 79–83, 2022.

[17] J. Q. Zhou, S. J. Xu, L. R. Gao, and Z. Y. Liu, "Disintegrin metalloproteinase 15 promotes the proliferation, migration and invasion of lung cancer cells via AKT/ERK pathway and MMP9," *Journal of Clinical Lung*, vol. 26, no. 11, pp. 1707–1712, 2021.

[18] W. B. Chen, Z. X. Zang, L. L. Sun, X. Gao, and G. Xie, "Effects of potato carboxypeptidases inhibitor combined with cry 1 Ac toxin on protease activities and insecticidal activity against cotton bollworm *Helicoverpa armigera*," *Rotection*, vol. 48, no. 5, pp. 1147–1155, 2021.

[19] Y. P. Zhu, M. J. Han, X. L. Cha, Y. Chen, and Y. H. Shen, "Identification and expression analysis of metallocarboxypeptidase gene family in silkworm, *Bombyx mori*," *Science of Sericulture*, vol. 42, no. 3, pp. 393–403, 2016.

[20] J. F. Xiu, C. C. Wei, X. L. Shang, Q. Wu, and J. Wu, "Cloning and prokaryotic expression of Musca domestica carboxypeptidase gene," *Guangdong Agricultural Science*, vol. 41, no. 10, pp. 152–154, 2014.

[21] Y. Y. Pan, L. Huang, and X. Q. Wu, "Study on function of cathepsin bmcath1 in *Bursaphelenchus mucronatus* using method of RNA interference," *Journal of Nanjing Forestry University (Natural Sciences Edition)*, vol. 42, no. 5, pp. 65–70, 2018.

[22] E. H. Zhao, K. Zhang, J. J. Su et al., "Structure and function of BmIntegrin $\beta 2$ in silkworm, *Bombyx mori*," *Chinese journal of biotechnology*, vol. 34, no. 10, pp. 1620–1630, 2018.

[23] H. H. Liang, H. Y. Gao, M. Xu, P. Tan, and H. Cui, "Cloning and characterization of BmBrat in silkworm, *Bombyx mori*," *Chinese journal of biotechnology*, vol. 32, no. 3, pp. 375–384, 2016.

Hindawi
Journal of Chemistry
Volume 2022, Article ID 3781567, 6 pages
https://doi.org/10.1155/2022/3781567

Research Article

The Efficacy of Chlorantraniliprole as a Seed Treatment for *Mythimna separata* (Walker) (Lepidoptera: Noctuidae)

Hongbo Li, Changgeng Dai, and Yang Hu

Institute of Plant Protection, Guizhou Academy of Agricultural Sciences, Guiyang 550006, China

Correspondence should be addressed to Hongbo Li; gzlhb2017@126.com

Received 21 April 2022; Accepted 13 May 2022; Published 26 May 2022

Academic Editor: Pei Li

The oriental armyworm (OAW), *Mythimna separata* (Walker) (Lepidoptera: Noctuidae), is an important pest in China and causes serious economic losses in corn. The anthranilic diamide, chlorantraniliprole (CHL), has been widely used as a seed treatment to control corn pests; however, no information is available on the efficacy of this insecticide as a seed treatment for OAW. In this study, the efficacy of seed treatment with CHL alone and CHL combined with the neonicotinoid insecticide clothianidin (CHL + CLO) was evaluated for controlling OAW larvae in the laboratory and field conditions. Pot experiments demonstrated that seed treatment with CHL and CHL + CLO (both 240 g a.i. 100 kg^{-1} seeds) resulted in >79% mortality of OAW larvae and a damage rate <20% in corn at 14 days after seed emergence (DAE). Similar to results obtained in pots, the residual toxicity of CHL and CHL + CLO to OAW larvae in the field declined with DAE and larval development. The control efficacy of field plots treated with CHL and CHL + CLO was >70% within 14 DAE, which was significantly higher than CLO alone. These results suggest that CHL and CHL + CLO as seed treatments could effectively reduce OAW larval infestation in corn. This study validates the effectiveness of corn seed treatment for OAW as an alternative to conventional foliar applications.

1. Introduction

The oriental armyworm (OAW), *Mythimna separata* (Walker) (Lepidoptera: Noctuidae), is a polyphagous pest on various crops in Asia and Australia [1–3]. In China, OAW has a long history and occurs throughout the country. OAW larvae feed on multiple grain crops, including corn, wheat, and rice [3, 4]. In corn, larvae feed on leaves and strip them to the midrib, which reduces yield [5, 6]. Damage occurs as a result of adult moth migration, and there are four or more migration events per year in China [3]. Approximately 20 OAW outbreaks occurred from 1950 to 2014 [7], the area was affected, and the amount of damage was staggering. For example, the OAW occurrence area in corn was about 7.00×10^7 hm^2 in 2013, and the estimated yield losses were approximately 9.92×10^5 tons [7].

For many years, the management of OAW relied on spraying chemical insecticides [8–10]; however, *M. separata* has developed resistance to several conventional insecticides, including lambda-cyhalothrin, chlorfenapyr, phoxim, and chlorpyrifos [11–13]. A further study showed that lambda-cyhalothrin significantly stimulated reproduction of OAW moths, thus promoting population growth in the field [4]. Furthermore, the biological characteristics of OAW, especially larval feeding inside the corn whorl, hinder control by spraying foliage. Therefore, the management of OAW requires novel pesticides with a more precise application strategy.

Chlorantraniliprole (CHL) is an anthranilic diamide insecticide that targets insect ryanodine receptors (RyRs) channels and affects the functioning of calcium channels [14]. This insecticide can control a wide range of sucking and chewing insects and is particularly effective against lepidopteran pests, including *Spodoptera frugiperda* [15, 16], *Helicoverpa zea* [17], *Mythimna unipuncta* [18], *Spodoptera exigua* [19], and *Athetis lepigone* [20].

Treatment of seeds with insecticides facilitates the precise targeting of pests [21]. In China, chlorantraniliprole has been widely used as a seed treatment to control corn pests, including *Agrotis ipsilon*, *Pleonomus canaliculatus*, and

Anomala corpulenta [21, 22]; however, no information is available on the efficacy of chlorantraniliprole as a seed treatment for controlling OAW larvae. In this study, we evaluate the efficacy of seed treatments with CHL alone and in combination with neonicotinoid insecticide clothianidin (CHL + CLO). We examined the effects of CHL and CHL + CLO on mortality of OAW larvae and determined residual toxicity of the insecticides to OAW in the laboratory. Finally, we evaluated the effect of these insecticides on corn growth and efficacy for controlling OAW in the field.

2. Materials and Methods

2.1. Insect Rearing. M. separata was originally collected in June 2014 from infested corn fields in Qianxi City (27.00°N, 106.03°E), China. Insects were maintained at the Institute of Plant Protection, the Guizhou Academy of Agricultural Sciences. Larvae were reared on a diet of corn leaves at 25°C under a 16 : 8 h light : dark photoperiod as described previously [23]. Second, third, and fourth instar larvae were used in this study.

2.2. Seed Treatments. Seeds of corn cv. Jinyu 818 (non-transgenic) were provided by Guizhou Jinlong Technology Co., Ltd. Seeds were treated with recommended rates (Table 1) of CHL, CHL + CLO, and CLO as described previously [21]; untreated seeds were used as a control. Fifty treated seeds per treatment were sown in plastic pots (30 × 20 × 20 cm) containing a mixture of sand/clay/organic matter (4 : 4 : 2) in a climate-controlled room at 25°C, 70% RH with a 14 : 10 h (L : D) photoperiod. Water was provided during seed emergence and growth, as necessary.

2.3. Pot Experiments. Laboratory assays were conducted in April 2020. At 3, 7, 14, 21, and 28 d after seedling emergence (DAE), 20 newly molted 3rd instar larvae of *M. separata* larvae were transferred to corn plants. To prevent escape, corn plants and larvae were placed in nylon cages (60 × 60 × 60 cm). Each cage was considered as one replication, and each treatment included four replications. After 3 d, the number of dead OAW larvae and the proportion of corn plants damaged by OAW larvae (defined as the damage rate) were recorded. Plants were considered damaged if the feeding spot caused by FAW larvae was found on corn leaves. Larvae were considered dead if they failed to move when stimulated with a moist brush.

2.4. Residual Toxicity of Insecticides to OAW. Seeds were planted in fields located at the Guizhou Academy of Agricultural Sciences (26.48°N, 106.65°E) on 23 May 2020; the treatment area was 20 m^2. Plants were watered as needed and fertilized with a controlled release fertilizer. To prevent feeding by other insects, pots were caged with a nylon net after seedling emergence. Residual toxicity was measured on treated corn plants collected at 3, 7, 14, 21, and 28 DAE.

Twenty newly molted 2nd, 3rd, and 4th instar larvae were collected, transferred to plastic containers (diameter, 12 cm; height, 6 cm), and starved for 2 h prior to experiments. The larvae were fed on insecticide-treated corn leaves at each sampling date. Larval mortality was evaluated after three days, and larvae were considered dead if they were unable to move when stimulated with a moist brush. Each treatment was replicated four times.

2.5. Field Experiments. Field studies were conducted in Luodian County (25.62°N, 106.63°E) in 2021. Sixteen plots were arranged in a randomized, complete block design with four treatments and four replications. Treated corn seeds were sown on June 3, 2021, and a controlled release fertilizer was applied. Each plot was 30 m^2 (5 × 6 m) and consisted of 10 rows separated by 60 cm of uncultivated ground. The emergence rate of corn seeds was recorded by counting the number of emerged plants in each plot at 7 DAE, and plant height was determined by measuring random plants ($n = 20$) in each plot at 14 DAE. Each treatment included four replications.

The density of *M. separata* larvae in the field was generally low; therefore, the efficacy of insecticidal formulations was also evaluated by inoculating field-grown corn with larvae reared in the laboratory. A single newly molted 3rd instar larva was inoculated into corn whorls at 7 and 14 DAE, respectively, and fifty individuals were included in each plot. The plot was caged with nylon netting to prevent escape. Each plot was considered as on replication, and each treatment included four replications. The damage rate of corn and the number of survived larvae were recorded 3 d after inoculation.

2.6. Statistical Analysis. The damage rate of corn, corrected mortality, and control efficacy were calculated as follows:

$$\text{Damage rate (\%)} = \frac{\text{number of corn with OAW damage}}{\text{total number of investigated corn plants}} \times 100, \quad (1)$$

$$\text{Corrected mortality (\%)} = \frac{\text{mortality in treatment} - \text{mortality in control}}{100 - \text{mortality in control}} \times 100, \quad (2)$$

$$\text{Control efficacy (\%)} = \frac{\text{\#OAW in control plot} - \text{\#OAW in treated plot}}{\text{\#OAW in control plot}} \times 100. \quad (3)$$

Variables evaluated include the damage rate of corn, corrected mortality of larvae, seed emergence rate, plant height, and control efficacy of insecticides. One-way ANOVA was used to determine the statistical difference among treatments at each sampling date, followed by Tukey's test.

Table 1: Insecticides and dosages used in this study.

Treatment	Insecticide	Dose (g a.i.100 kg^{-1} corn seed)	Producer
CHL	Chlorantraniliprole	CHL 240	DuPont Crop Protection (USA)
CHL + CLO	Chlorantraniliprole + clothianidin	CHL 60 + CLO 180	Guangdong Kairuifeng Technology Co., Ltd. (China)
CLO	Clothianidin	CLO 120	Hebei Lishijie Technology Co., Ltd. (China)
CK	Control	—	—

Results were considered significant at $P < 0.05$. All statistical analyses were performed using DPS v. 17.0 software [24].

3. Results

3.1. Efficacy of CHL and CHL + CLO Seed Treatments for OAW Larvae in Pot Experiments. Overall, the corrected mortality of OAW larvae fed on corn plants treated with CHL and CHL + CLO declined with increasing days of seed emergence (Figure 1(a)). At 3 and 7 DAE, OAW mortality in CHL and CHL + CLO treatments exceeded 90%, which was significantly higher than mortality in CLO treatment. Beginning at 14 DAE, OAW in CHL and CHL + CLO treatments began to decline and was 79.74% and 79.55%, respectively; at 21 DAE, mortality in CHL and CHL + CLO treatments was below 60% but remained higher than CLO. At 28 DAE, OAW mortality in CHL, CHL + CLO, and CLO treatments was below 30.00% with no significant difference among three treatments.

The percentage of corn plants damaged by OAW in the untreated control was about 80% and remained stable and high throughout the experiment (Figure 1(b)). From 3 to 14 DAE, damage rates in CHL and CHL + CLO treatments ranged from 11.00 to 17.10%, respectively, and values in the CLO treatment ranged from 49.00 to 63.50%. All damage rates were lower than the control at each sampling date. Beginning at 21 DAE, damage rates in CHL and CHL + CLO treatments increased but remained lower than the CLO treatment and untreated control. Damage rates of corn plants in CLO and control treatments were not significantly different at 21 and 28 DAE (Figure 1(b)).

3.2. Determination of Residual Insecticide Toxicity. The residual toxicity of CHL and CHL + CLO treatments to *M. separata* gradually declined with the number of days after seed emergence (Figure 2). Mortality of 2nd and 3rd instar larvae in CHL and CHL + CLO treatments exceeded 67% when OAW fed on plants at 3–14 DAE. Although there was no significant difference in mortality rates between CHL and CHL + CLO treatments, they were, generally, higher than mortality in CLO treatment. As corn plants grew, mortality in CHL and CHL + CLO treatments decreased; for example, mortality of 2nd and 3rd instar larvae was below 50% beginning at 21 DAE (Figures 2(a) and 2(b)). Furthermore, OAW mortality declined as larvae developed; for example, mortality of 2nd and 3rd instar larvae in CHL and CHL + CLO treatments ranged from 82.35 to 89.24% at 3–7 DAE, but was only 70.01–73.16% in 4th instar larvae for the same time period (Figure 2(c)). Similarly, CHL and CHL + CLO treatments resulted in over 67% mortality in the 2nd and 3rd instar larvae at 14 DAE and declined to less than 48% in 4th instar larvae (Figures 2(a)–2(c)).

3.3. Efficacy of CHL and CHL + CLO Seed Treatments for OAW Larvae in the Field. The emergence rates of corn seeds were above 90% in the four treatments, and no significant differences were observed among treatments (Table 2). At 14 DAE, corn plants in plots treated with CHL + CLO and CLO were significantly taller than in plots treated with CHL and CK treatments. The percentage of corn seedlings with OAW damage in CHL and CHL + CLO treatments was below 20% at both 7 and 14 DAE, and these values were significantly lower than CLO and CK treatments. At 7 DAE, control efficacy of CHL and CHL + CLO treatments was 86.59% and 84.91%, respectively, and was significant than CLO treatment (36.87%). At 14 DAE, control efficacy of CHL (72.14%) and CHL + CLO (74.56%) decreased but remained higher than CLO treatment (34.91%).

4. Discussion

Insecticide resistance is a challenge in integrated pest management [25]. Although seed treatments with insecticides are excellent choices for pest control, the efficacy of seed treatments for OWA has not been previously reported. Our study clearly shows that seed treatments with CHL and CHL + CLO can reduce OAW-mediated damage to corn plants and can result in control levels exceeding 70% up to 14 DAE. These results indicate that CHL alone or in combination with CLO can effectively control early stage OAW larvae on corn seedlings and has relatively good persistence.

Insecticide treatments can effectively reduce feeding injuries inflicted by insects [18]. The percentage of corn plants with OAW damage in CHL and CHL + CLO treatments was less than 20% up to 14 DAE and was significantly lower than damage in CLO and CK treatments. These results are consistent with a prior study conducted on seed treatments for *M. unipuncta* [18]. Prior studies have shown that CHL can result in rapid feeding cessation of several insect species; for example, the lepidopteran species, *Plutella xylostella*, *Trichoplusia ni*, and *H. zea*, stopped feeding within 30 min after exposure to plants grown from CHL-treated seed [26]. The damage rate in CHL-treated plants was reduced by 50–99% [18,26]. Similarly, *Coptotermes gestroi* feeding stopped within five minutes after exposure to CHL-treated plant materials [27]. In our study, CHL treatment alone or in combination with CLO reduced the damage rate caused by OAW larval feeding.

In previous studies, CHL showed a systemic insecticidal activity against various pests when applied as a seed

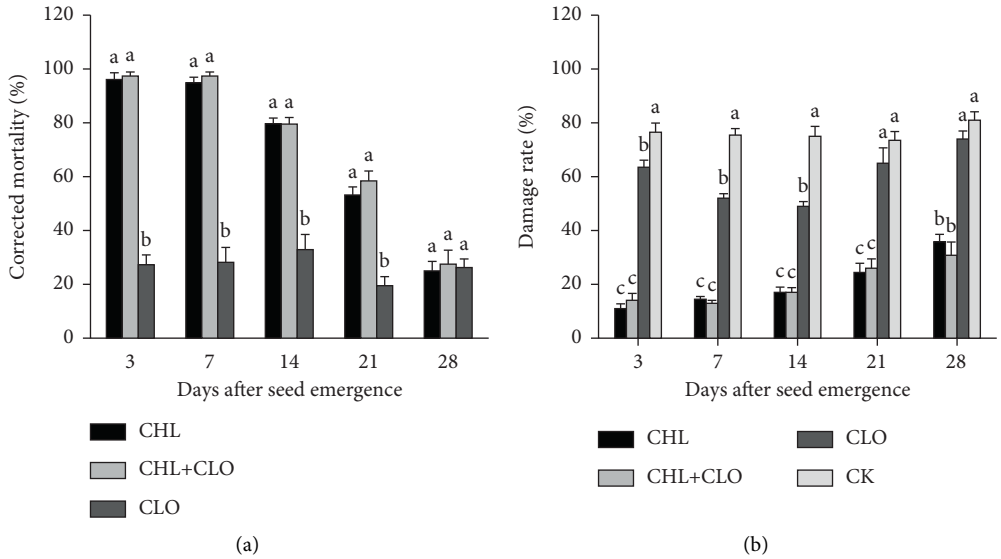

Figure 1: Corrected mortality and damage rates of OAW fed on corn plants treated with CHL, CHL + CLO, and CLO. (a) Corrected mortality. (b) Damage rate. CHL, chlorantraniliprole; CHL + CLO, chlorantraniliprole + clothianidin; CLO, clothianidin; CK, untreated control. All data are expressed as mean ± SE. Different letters above bars indicate significant difference by Tukey's test ($P < 0.05$).

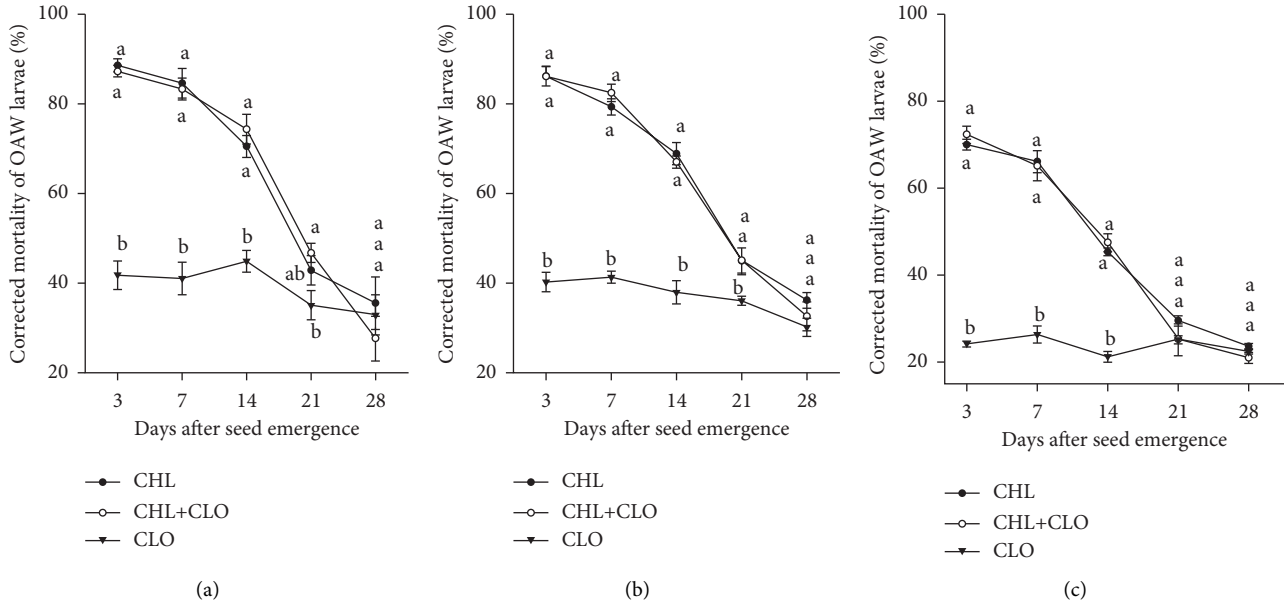

Figure 2: Mortality of OAW larvae fed on field-grown plants treated with CHL, CHL + CLO, and CLO. Panels show mortality for 2nd (a), 3rd (b), and 4th (c) instar larvae. CHL, chlorantraniliprole; CHL + CLO, chlorantraniliprole + clothianidin; CLO, clothianidin. Data are analyzed using one-way ANOVA followed by Tukey's test at each sampling date, and different letters indicate significance at $P < 0.05$.

Table 2: Control efficiency and growth indices of corn seedlings treated with CHL, CHL + CLO, and CLO in the field*.

Treatment	Concentration (g a.i.100 kg^{-1} corn seed)	Emergence rate (%)	Plant height (cm)	7 DAE Damage rate (%)	7 DAE Control efficacy (%)	14 DAE Damage rate (%)	14 DAE Control efficacy (%)
CHL	240	91.62 ± 2.33^a	59.22 ± 3.90^b	$11.62 + 1.52^c$	86.59 ± 2.04^a	16.84 ± 1.50^c	72.19 ± 2.02^a
CHL + CLO	240	90.38 ± 0.97^a	69.30 ± 0.81^a	12.76 ± 1.93^c	84.91 ± 2.30^a	15.15 ± 1.75^c	70.56 ± 2.44^a
CLO	120	92.47 ± 1.56^a	68.91 ± 0.25^a	39.29 ± 3.37^b	36.87 ± 3.34^b	43.36 ± 2.90^b	34.91 ± 2.46^b
CK	—	90.89 ± 1.64^a	56.61 ± 0.68^b	73.16 ± 4.74^a	—	71.50 ± 2.98^a	—

*CHL, chlorantraniliprole; CHL + CLO, chlorantraniliprole + clothianidin; CLO, clothianidin; CK, untreated control. Data are analyzed using one-way ANOVA followed by Tukey's test, and different lowercase letters indicated significance at $P < 0.05$.

treatment. For example, seed treatment with CHL at 25 μg a.i. seed^{-1} resulted in 90.4% suppression of immature water weevils approximately 25 d after flooding [28]. A corn seed treated with CHL at 2 g a.i. kg^{-1} provided 76.02% control efficacy against *A. ipsilon* larvae at 19 DAE [21]. Similarly, Pes et al. found that CHL applied at 45 g a.i. per 60,000 corn seeds significantly reduced infestation by *S. frugiperda* larvae up to 30 d after planting [15]. The current study indicated that seed treatments with CHL and CHL + CLO caused systemic insecticidal activity against OAW larvae. High mortality rates (70%) were observed up to 14 DAE and began to decline thereafter, suggesting that the efficacy declined due to the dilution of active ingredients. Furthermore, the control efficacy decreased in the 4th instar larval stage, which suggests that insecticide concentrations were insufficient to kill older larval instars.

Interestingly, CHL and CHL + CLO treatments showed similar efficacy for controlling OAW larvae, although the concentration of CHL in the CHL + CLO treatment was lower than the concentration of CHL alone. In this respect, our results were similar to those reported previously [18], where CHL and CHL + THI (thiamethoxam) had similar efficacy in reducing foliar injury to corn by *M. unipuncta* [18]. Our results suggests that CHL and CLO function synergistically when combined, although the underlying mechanism is unclear and warrants a further study. Potential synergism could reduce both the amount and cost of pesticide applications and may delay the onset of insecticide resistance.

In recent years, the subterranean pests *A. ipsilon*, *Proxenus lepigone*, *P. canaliculatus*, and *A. corpulenta* caused serious damage to corn seedlings in China, and diamide insecticides have been used to manage these pests as seed treatments [21, 22, 29]. Neonicotinoid insecticides, such as CLO, are considered effective for controlling aphids and thrips on various crops [30–32]. Thus, the use of CHL and CHL + CLO as seed treatments can control both OWA and other target pests on corn. Furthermore, seed treatment reduces insecticide exposure to nontarget organisms and has fewer side effects to nontargets residing on corn plants and in soil. Finally, we found that treating a corn seed with CHL + CLO promotes corn growth, which is consistent with previous studies [21, 33].

5. Conclusion

In summary, our results indicate that CHL and CHL + CLO seed treatments effectively control OAW larvae on corn seedlings up to 14 DAE. The OAW-induced damage rate was low in both CHL and CHL + CLO treatments as compared to the untreated control. Thus, the use of CHL and CHL + CLO as seed treatments offers potential alternatives to conventional foliar sprays in the management of OAW on corn.

Data Availability

The data used to support this study are included within the article.

Conflicts of Interest

The authors declare that they have no conflicts of interest.

Authors' Contributions

H.L. conceptualized, supervised, validated, visualized, and investigated the study, performed data curation, formal analysis, funding acquisition, and project administration, collected resources, and developed software. H.L. and C.D. performed the methodology. H.L. and Y.H wrote and reviewed the article. All authors have read and agreed to the published version of the manuscript and contributed equally to this study.

Acknowledgments

This work was supported and funded by the supplementary project of National Natural Science Foundation of China (202102), Science & Technology Support Program of Guizhou Province (2021218), and Youth Foundation of Guizhou Academy of Agricultural Sciences (202013).

References

[1] H. C. Sharma and J. C. Davies, *The Oriental Armyworm, Mythimna Separata (Walker) Distribution, Biology and Control: A Literature Review*, Center for Oversea Pest Research, London, UK, 1983.

[2] H. C. Sharma, D. J. Sullivan, and V. S. Bhatnagar, "Population dynamics and natural mortality factors of the oriental armyworm, *Mythimna separata* (Lepidoptera: Noctuidae), in South-Central India," *Crop Protection*, vol. 21, no. 9, pp. 721–732, 2002.

[3] X. Jiang, "Current status and trends in research on the oriental armyworm, *Mythimna separata* (Walker) in China," *Chinese Journal of Applied Entomology*, vol. 51, no. 4, pp. 881–889, 2014.

[4] X. R. Li, Y. Li, W. Wang, N. He, X. L. Tan, and X. Q. Yang, "LC_{50} of lambda-cyhalothrin stimulates reproduction on the moth *Mythimna separata* (Walker)," *Pesticide Biochemistry and Physiology*, vol. 153, pp. 47–54, 2019.

[5] G. Li, "Mythimna separata (walker)//compiled by institute of plant protection," *Academy of Agricultural Sciences of China. "Main Diseases and Pests of Chinese Crops"*, China Agriculture Press, Beijing, China, 1996.

[6] A. W. Schaafsma, M. L. Holmes, J. Whistlecraft, and S. A. Dudley, "Effectiveness of three Bt corn events against feeding damage by the true armyworm (*Pseudaletia unipuncta* Haworth)," *Canadian Journal of Plant Science*, vol. 87, no. 3, pp. 599–603, 2007.

[7] Y. Jiang, J. Li, J. Zeng, and J. Liu, "Population dynamics of the armyworm in China: a review of the past 60 years' research," *Chinese Journal of Applied Entomology*, vol. 51, no. 4, pp. 890–898, 2014.

[8] H. Pei, X. Ou, Y. Wang, X. Lin, and K. Yu, "Synergism of organophosphorous insecticides with monosultap against *Mythimna separata* walker," *Pesticide Science and Administration*, vol. 28, no. 7, pp. 35–37, 2007.

[9] Y. Duan, H. Li, Q. Chen, Z. Li, Y. Xing, and Y. Wu, "Susceptibility of *Mythimna separata* field populations collected from Xinyang and Luohe city of Henan province to six insecticides," *Plant Protection*, vol. 47, no. 3, pp. 247–249, 2021.

[10] Q. Huang, T. Jiang, X. Jiang, Y. Lin, Y. Chen, and L. Long, "Oviposition ability of *Mythimna separata* (Walker) and its sensitivity to eleven insecticides in Guangxi," *Journal of Environmental Entomology*, vol. 39, no. 6, pp. 1363–1368, 2017.

[11] J. Dong, X. Liu, J. Yue et al., "Resistance of *Mythimna separata* (Lepidoptera: Noctuidae) to five different types of insecticides in Beijing," *Chinese Journal of Pesticide Science*, vol. 16, no. 6, pp. 687–692, 2014.

[12] Y. Zhao, L. Su, S. Li et al., "Insecticide resistance of the field populations of oriental armyworm, *Mythimna separata* (Walker) in Shaanxi and Shanxi provinces of China," *Journal of Integrative Agriculture*, vol. 17, no. 7, pp. 1556–1562, 2018.

[13] X. Yang, X. Li, X. Cang, J. Guo, X. Shen, and K. Wu, "Influence of seasonal migration on the development of the insecticide resistance of oriental armyworm (*Mythimna separata*) to λ-cyhalothrin," *Pest Management Science*, vol. 78, no. 3, pp. 1194–1205, 2022.

[14] G. P. Lahm, T. M. Stevenson, T. P. Selby et al., "Rynaxypyr: a new insecticidal anthranilic diamide that acts as a potent and selective ryanodine receptor activator," *Bioorganic & Medicinal Chemistry Letters*, vol. 17, no. 22, pp. 6274–6279, 2007.

[15] M. P. Pes, A. A. Melo, R. S. Stacke et al., "Translocation of chlorantraniliprole and cyantraniliprole applied to corn as seed treatment and foliar spraying to control *Spodoptera frugiperda* (Lepidoptera: Noctuidae)," *PLoS One*, vol. 15, no. 4, Article ID e0229151, 2020.

[16] M. Kulye, S. Mehlhorn, D. Boaventura et al., "Baseline Susceptibility of *Spodoptera frugiperda* populations collected in India towards different chemical classes of insecticides," *Insects*, vol. 12, no. 8, p. 758, 2021.

[17] A. Adams, J. Gore, A. Catchot et al., "Susceptibility of *Helicoverpa zea* (Lepidoptera: Noctuidae) neonates to diamide insecticides in the midsouthern and southeastern United States," *Journal of Economic Entomology*, vol. 109, no. 5, pp. 2205–2209, 2016.

[18] G. E. Carscallen, S. V. Kher, and M. L. Evenden, "Efficacy of Chlorantraniliprole seed treatments against Armyworm (*Mythimna unipuncta* [Lepidoptera: Noctuidae]) larvae on corn (Zea mays)," *Journal of Economic Entomology*, vol. 112, no. 1, pp. 188–195, 2019.

[19] C. Zhou, H. Wang, X. Li, W. Wang, and W. Mu, "Comparison of the toxicity of chlorantraniliprole and flubendiamide to different developmental stages of Spodoptera exigua," *Journal of Plant Protection*, vol. 38, no. 4, pp. 344–350, 2011.

[20] Z. Zhang, J. Zhong, R. Han, and C. Liu, "Sublethal effects of echlorantraniliprole on *Athetis lepigone. Southwest*," *China Journal Agricultural Science*, vol. 27, no. 5, pp. 1949–1952, 2014.

[21] Z. Zhang, C. Xu, J. Ding et al., "Cyantraniliprole seed treatment efficiency against *Agrotis ipsilon* (Lepidoptera: Noctuidae) and residue concentrations in corn plants and soil," *Pest Management Science*, vol. 75, no. 5, pp. 1464–1472, 2019.

[22] F. He, S. Sun, H. Yu et al., "Control effect of chlorantraniliprole on three kinds of underground pests in the maize field by seed treatment," *Plant Protection*, vol. 46, no. 1, pp. 253–261, 2020.

[23] H. B. Li, C. G. Dai, C. R. Zhang, Y. F. He, H. Y. Ran, and S. H. Chen, "Screening potential reference genes for quantitative real-time PCR analysis in the oriental armyworm, *Mythimna separata*," *PLoS One*, vol. 13, no. 4, Article ID e0195096, 2018.

[24] Q. Y. Tang and C. X. Zhang, "Data Processing System (DPS) software with experimental design, statistical analysis and data mining developed for use in entomological research," *Insect Science*, vol. 20, no. 2, pp. 254–260, 2013.

[25] M. A. I. Ahmed and C. F. A. Vogel, "The synergistic effect of octopamine receptor agonists on selected insect growth regulators on *Culex quinquefasciatus* Say (Diptera: Culicidae) mosquitoes," *One Health*, vol. 10, Article ID 100138, 2020.

[26] G. T. Hannig, M. Ziegler, and P. G. Marçon, "Feeding cessation effects of chlorantraniliprole, a new anthranilic diamide insecticide, in comparison with several insecticides in distinct chemical classes and mode-of-action groups," *Pest Management Science*, vol. 65, no. 9, pp. 969–974, 2009.

[27] K. B. Neoh, J. Hu, B. H. Yeoh, and C. Y. Lee, "Toxicity and horizontal transfer of chlorantraniliprole against the Asian subterranean termite *Coptotermes gestroi* (Wasmann): effects of donor:recipient ratio, exposure duration and soil type," *Pest Management Science*, vol. 68, no. 5, pp. 749–756, 2012.

[28] J. Hamm, S. Lanka, and M. Stout, "Influence of rice seeding rate on efficacies of neonicotinoid and anthranilic diamide seed treatments against Rice Water Weevil," *Insects*, vol. 5, no. 4, pp. 961–973, 2014.

[29] H. Zhang, J. Shi, N. Guo, Y. Hu, Y. Yang, and P. Li, "A method for using seed treatment to control Proxenus lepigone under greenhouse conditions," *China Plant Protection*, vol. 36, no. 10, pp. 63–67, 2016.

[30] P. Zhang, X. Zhang, Y. Zhao, Y. Wei, W. Mu, and F. Liu, "Effects of imidacloprid and clothianidin seed treatments on wheat aphids and their natural enemies on winter wheat," *Pest Management Science*, vol. 72, no. 6, pp. 1141–1149, 2016.

[31] Z. Zhang, X. Zhang, Y. Wang et al., "Nitenpyram, dinotefuran, and thiamethoxam used as seed treatments act as efficient controls against *Aphis gossypii* via high residues in cotton leaves," *Journal of Agricultural and Food Chemistry*, vol. 64, no. 49, pp. 9276–9285, 2016.

[32] J. Ding, H. Li, Z. Zhang, J. Lin, F. Liu, and W. Mu, "Thiamethoxam, clothianidin, and imidacloprid seed treatments effectively control thrips on corn under field conditions," *Journal of Insect Science*, vol. 18, no. 6, p. 19, 2018.

[33] A. Horii, P. Mccue, and K. Shetty, "Enhancement of seed vigour following insecticide and phenolic elicitor treatment," *Bioresource Technology*, vol. 98, no. 3, pp. 623–632, 2007.

Hindawi
Journal of Chemistry
Volume 2022, Article ID 3546266, 4 pages
https://doi.org/10.1155/2022/3546266

Research Article

Identification and Laboratory Fungicides Screening of the Pathogenic Fungus of Stem Spot of Pitaya (*Hylocereus* spp.) Stems

Hui Luo, Kun Guo, Xueying Shang, Lei Peng, Zhijun Peng, Jilin Jin, Bin Wang, and Xingwu Zhang

Institute of Fruit Science, Guizhou Academy of Agricultural Sciences, Guiyang 550006, China

Correspondence should be addressed to Hui Luo; luohui8732@163.com

Received 18 April 2022; Accepted 3 May 2022; Published 17 May 2022

Academic Editor: Pei Li

In this study, the pathogenic fungus of stem spot disease of pitaya (*Hylocereus* spp.) stems was identified by isolation and purification, pathogenicity test, morphological characteristics, and analysis of rDNA-ITS sequences. The results turned out that the rDNA-ITS sequences of the H1 strain showed 100% of identity with *Botryosphaeria dothidea*, indicating that the pathogenic fungus of stem spot disease of pitaya stems was *Botryosphaeria dothidea*. Meanwhile, the H1 strain was then used as a reference strain to screen some commercial fungicides. The bioassay test results indicated that prochloraz had an obvious inhibitory effect on *Botryosphaeria dothidea* with the EC_{50} value of 0.0798 μg/mL. Our study could provide a theoretical basis for the effective control method of stem spot disease of pitaya.

1. Introduction

Pitaya (*Hylocereus* spp.), a famous fruit in tropical and subtropical regions of Central America, has been planted in Hainan, Guangdong, Guizhou, Guangxi, Yunnan, Fujian, and other regions, and has become one of the important sources of farmers' income in southern China. However, since cultivation and further domestication on commercial plantations, some symptoms of decay and spots have been observed in stems and fruits [1–4]. Meanwhile, the yields could be diminished due to such decay and spot diseases, which may induce economic losses reach 44% [1, 5]. For these reasons, since 1990s, some studies on stem spot disease and the crop protection had been initiated [6, 7]. Hong et al. reported that the stem rot on Wilford Swallowwort was caused by *Stemphylium lycopersici* in Korea [8]. Meanwhile, Edwards et al. found that *Fusarium agapanthi* sp. nov. was a novel bikaverin- and fusarubin-producing leaf and stem spot pathogen of *Agapanthus praecox* (African lily) from Australia and Italy [9]. Moreover, in 2008, Culbreath et al. showed that the incidence of stem rot for all penthiopyrad treatments was usually less than that of tebuconazole or azoxystrobin [10].

The aim of this work was to identify the pathogenic fungus of stem spot disease of pitaya stems and then screen some commercial fungicides on the pathogenic fungus to provide a theoretical basis for the effective control method of stem spot disease of pitaya stems.

2. Materials and Methods

2.1. Fungus Isolation and Purification. Pitaya stems with the symptoms of spots collected from Luodian county, Guizhou Province, China, were sterilized using sterile 75% ethanol and sterile distilled water for three times, excised the infected tissues with a sterile scalpel, plated the infected tissues on the sterile potato dextrose agar (PDA) plates, and then incubated the PDA plates in a sterile incubator at 28°C for 3 days. All isolations were cultured twice on a new PDA plate using a single spore technique to ensure purity [11]. Then, the pure cultures were maintained in a 4°C refrigerator for further use.

2.2. Morphological and Molecular Identification. Individual colony was inoculated on the PDA plate in a sterile incubator (28°C) for 7 days, and the morphology was

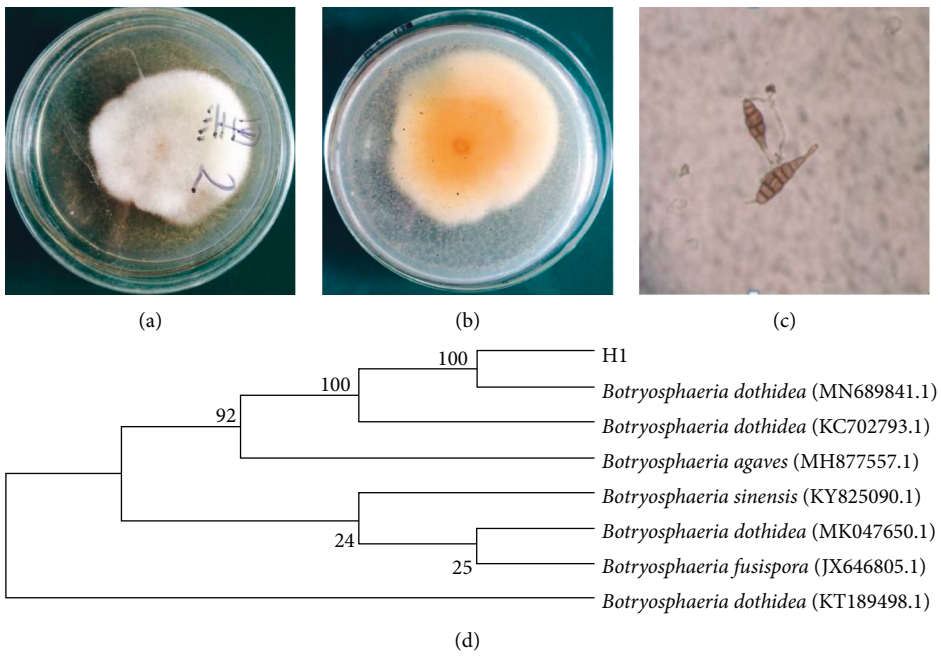

Figure 1: Morphology of H1 isolate cultures on PDA: (a) Observe surface of colony (front), (b) observe surface of colony (back), (c) microstructure of conidia, and (d) phylogenetic analysis based on sequence analysis.

identified by both eye and a Model EX30 inverted microscopy (Ningbo Shunyu Tech. Co. Ltd., Zhejiang, China) [12]. Approximately, 100 mg fungal mycelia were collected to extract DNA using a TIANamp fungal DNA kit (Tiangen-Biotech Co. Ltd., Beijing, China) [13–15]. Polymerase chain reactions (PCRs) were conducted using a Premix Taq ver. 2.0 plus dye kit (Takara, Dalian, China) according to the manufacturer's instructions with the universal primer ITS1 and ITS4 [16–18] and the following amplification program: 98°C for 5 min; 30 cycles of 95°C for 35 s, 55°C for 35 s and 72°C for 40 s; 72°C for 8 min. After that, the PCR products were sequenced at Sangon Corporation (Shanghai, China) and searched for sequence similarity with the NCBI database. The phylogenetic tree was constructed using the MEGA 7.0 software [19–21].

2.3. Pathogenicity Test. Pathogenicity tests were performed by injecting the 1.0×10^6 conidia/L conidial suspension on the surface of the pitaya stems, and the pitaya stems were incubated in an incubator at 28°C with 95% relative humidity for 14 days [22]. Pitaya stems inoculated with sterile water served as a control. After 14 days of inoculation, some symptoms of spots have been observed in stems. The causal fungus in the infected pitaya stems was reisolated on the PDA plates as described above. The characteristics of the reisolated fungus was used to compare with its original culture.

2.4. Laboratory Fungicides Screening. The *in vitro* antifungal activity of thiophanate-methyl (content: 99%), difenoconazole (content: 99%), pyraclostrobin (content: 98%), and prochloraz (content: 99%), which were mainly registered to control stem spot disease, against *Botryosphaeria dothidea* was tested according to the reported method [23, 24]. Each drug (5.0 mg) was dissolved in 1 mL DMSO, 9 mL Tween 20 aqueous solution (0.1%), 90 mL PDA medium, and poured into 6 sterilized dishes to prepare PDA plates. Mycelia dishes (0.4 cm diameter) were inoculated on the middle of PDA plates and fostered in an incubator at 28°C. After the mycelia diameter of control group (CK) reached 6–7 cm, the inhibition rates I (%) are calculated by the following formula, where C (cm) and T (cm) represent the fungi diameters of the CK and treated PDA plates, respectively. Meanwhile, the EC_{50} values of thiophanate-methyl, difenoconazole, pyraclostrobin, and prochloraz against *Botryosphaeria dothidea* were calculated with the SPSS 19.0 software (SPSS Inc., IL, USA).

$$\text{Inhibition rate } I\,(\%) = \frac{(C - T)}{(C - 0.4)} \times 100. \quad (1)$$

3. Results and Discussion

3.1. Fungal Isolation and Identification. Figure 1 showed that the fungal strain H1 appearance was white in front (Figure 1(a)) and claybank in back (Figure 1(b)). The conidia (Figure 1(c)) were fusiform and septate, with the length and width ranging of 18.00–30.00 μm and 4.00–11.00 μm, respectively. Meanwhile, based on the ITS sequences and phylogenetic analysis, as shown in Figure 1(d), the fungal strain H1 isolated from rotting pitaya stems was classified as *Botryosphaeria dothidea* (accession no. MN689841.1) with the similarity of 100%.

3.2. Pathogenicity Test. After 14 days of pathogenicity test, the symptoms of the stem disease (Figure 2) caused by H1

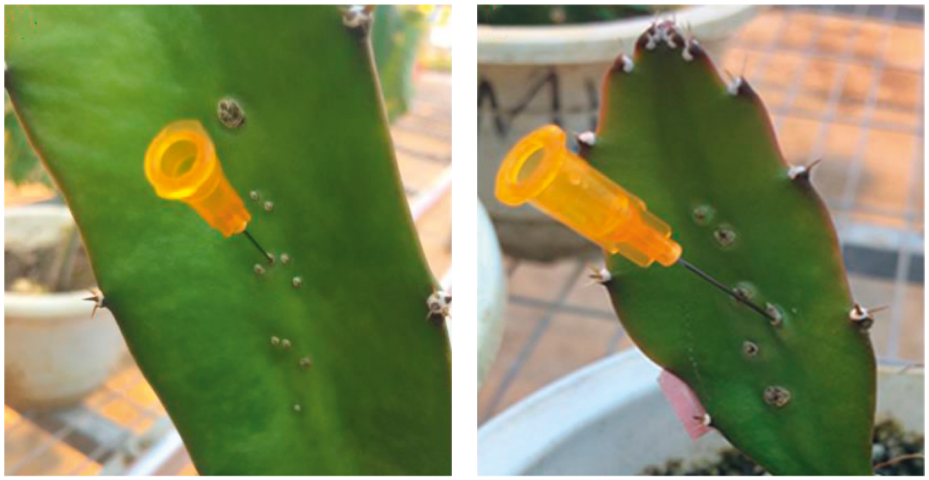

(a) (b)

Figure 2: The symptoms of H1 strain in the pathogenicity test. (a) CK group; (b) treatment group.

Table 1: The EC_{50} values of 5 fungicides against *Botryosphaeria dothidea*.

Fungicides	Toxicity regression equation	EC_{50} (μg/mL)
Thiobacillam-methyl	$y = 0.857x + 10.638$	0.2640
Difenoconazole	$y = 0.761x + 10.136$	0.1795
Pyraclostrobin	$y = 0.851x + 10.127$	0.9466
Prochloraz	$y = 1.212x + 13.606$	0.0798

strain were consistent with the initial symptoms appeared on the collected pitaya stems, and the strains isolated again had the same culture characteristics as the original strain, proving that the obtained strain was the pathogen of stem spot disease.

3.3. In Vitro Antifungal Activity. The antifungal activity against *Botryosphaeria dothidea* of thiophanate-methyl, difenoconazole, pyraclostrobin, and prochloraz were determined and listed in Table 1. The results showed that the EC_{50} values of four fungicides were in descending order as follows: prochloraz < difenoconazole < thiobacillam-methyl < pyraclostrobin, indicating that prochloraz had the best inhibitory effect on *Botryosphaeria dothidea* with an EC_{50} value of 0.0798 μg/mL.

4. Conclusion

In conclusion, our study demonstrated that the pathogen causing the stem disease of pitaya stems in Guizhou was *Botryosphaeria dothidea*. Bioassay results showed that prochloraz had the best in vitro inhibitory effect on *Botryosphaeria dothidea*. Our study could provide a theoretical basis for choosing the effective pesticide for controlling the stem spot disease of pitaya.

Data Availability

All data included in this study are available upon request by contact with the corresponding author.

Conflicts of Interest

The authors declare no conflicts of interest.

Acknowledgments

This research was funded by the Platform Project of Guizhou Science and Technology Department (grant no. QKHFQ [2021]2), Guizhou Fine Fruit Modern Agricultural Industrial Technology System (grant no. GZCYTX2018), and Guizhou Outstanding Young Scientific and Technological Talents Training Program (grant no. [2019]5642).

References

[1] A. J. Valencia-Botín, H. Kokubu, and Y. D. Ortíz-Hernández, "A brief overview on pitahaya (Hylocereus spp.) diseases," *Australasian Plant Pathology*, vol. 42, no. 4, pp. 437–440, 2013.

[2] H. S. Kim, W. Cheon, Y. Lee et al., "Identification and characterization of xanthomonas arboricola pv. juglandis causing bacterial blight of walnuts in Korea," *The Plant Pathology Journal*, vol. 37, no. 2, pp. 137–151, 2021.

[3] M. D. A. Mohamed, M. H. A. Moharam, and H. A. M. Ahmed, "In vitro and in vivo toxicity of nano chitosan against curvularia lunata, the causal microorganism of fruit rot and blight, a new disease of olive (O. europaea L.)," *European Journal of Plant Pathology*, vol. 161, no. 4, pp. 881–894, 2021.

[4] C. Zhi, M. M. Ali, J. Y. Zhang, M. Shi, S. Ma, and F. Chen, "Effect of paper and aluminum bagging on fruit quality of loquat (eriobotrya japonica lindl.)," *Plants*, vol. 10, no. 12, p. 2704, 2021.

[5] A. J. Valencia-Botín, J. S. Sandoval-Islas, E. Cárdenas-Soriano, T. J. Michailides, and G. Rendón-Sánchez, "A new stem spot disease of pitahaya (Hylocereus undatus H.) caused by

fusicoccum-like anamorph of botryosphaeria dothidea in Mexico," *Revista Mexicana Fitotecnia*, vol. 22, pp. 40–42, 2004.

[6] I. K. Toth, J. M. van der Wolf, G. Saddler et al., "Dickeya species: an emerging problem for potato production in Europe," *Plant Pathology*, vol. 60, no. 3, pp. 385–399, 2011.

[7] A. J. Valencia-Botín, J. S. Sandoval-Islas, E. Cárdenas-Soriano, T. J. Michailides, and G. Rendón-Sánchez, "Botryosphaeria dothidea causing stem spots on Hylocereus undatus in Mexico," *Plant Pathology*, vol. 52, no. 6, p. 803, 2003.

[8] S. K. Hong, H. W. Choi, Y. K. Lee, H. S. Shim, and S. Y. Lee, "Leaf spot and stem rot on wilford swallowwort caused by stemphylium lycopersici in Korea," *Mycobiology*, vol. 40, no. 4, pp. 268–271, 2012.

[9] J. Edwards, D. Auer, S. K. de Alwis et al., "Fusarium agapanthi sp. nov., a novel bikaverin and fusarubin-producing leaf and stem spot pathogen of agapanthus praecox (African lily) from Australia and Italy," *Mycologia*, vol. 108, no. 5, pp. 981–992, 2016.

[10] A. K. Culbreath, T. B. Brenneman, R. C. Kemerait Jr., and G. G. Hammes, "Effect of the new pyrazole carboxamide fungicide penthiopyrad on late leaf spot and stem rot of peanut," *Pest Management Science*, vol. 65, no. 1, pp. 66–73, 2009.

[11] J. H. Kwon, M. G. Cheon, O. Choi, and J. Kim, "First report of botrytis cinerea as a postharvest pathogen of blueberry in Korea," *Mycobiology*, vol. 39, no. 1, pp. 52-53, 2011.

[12] M. Qiu, C. Wu, G. R. Ren, X. Liang, X. Wang, and J. Huang, "Effect of chitosan and its derivatives as antifungal and preservative agents on postharvest green asparagus," *Food Chemistry*, vol. 155, pp. 105–111, 2014.

[13] Y. L. Tian, Y. Q. Zhao, T. Sun et al., "Identification and characterization of phomopsis amygdali and botryosphaeria dothidea associated with peach shoot blight in Yangshan, China," *Plant Disease*, vol. 102, no. 12, pp. 2511–2518, 2018.

[14] F. Yang, R. Zhang, X. Y. Wu et al., "An endophytic strain of the genus bacillus isolated from the seeds of maize (Zea mays L.) has antagonistic activity against maize pathogenic strains," *Microbial Pathogenesis*, vol. 142, Article ID 104074, 2020.

[15] X. Liang, Y. Peng, Y. Liu, M. Wang, Y. Yang, and Y. Zhang, "First report of bipolaris bicolor causing a leaf spot disease on rubber tree," *Journal of Phytopathology*, vol. 167, no. 10, pp. 553–557, 2019.

[16] H. N. Li, J. J. Jiang, N. Hong, G. P. Wang, and W. X. Xu, "First report of colletotrichum fructicola causing bitter rot of pear (Pyrus bretschneideri) in China," *Plant Disease*, vol. 97, no. 7, p. 1000, 2013.

[17] Y. P. Cui, B. Wu, A. T. Peng, Z. L. Li, J. F. Lin, and X. B. Song, "First report of nigrospora leaf blight on sugarcane caused by nigrospora sphaerica in China," *Plant Disease*, vol. 102, no. 4, p. 824, 2018.

[18] R. Q. Cui and X. T. Sun, "First report of curvularia lunata causing leaf spot on lotus in China," *Plant Disease*, vol. 96, no. 7, p. 1068, 2012.

[19] M. Amir, A. Hussain, M. Asif et al., "Full-length genome and partial viral genes phylogenetic and geographical analysis of dengue serotype 3 isolates," *Microorganisms*, vol. 9, no. 2, p. 323, 2021.

[20] L. Zhou, Y. Sun, T. Lan et al., "Retrospective detection and phylogenetic analysis of swine acute diarrhoea syndrome coronavirus in pigs in southern China," *Transboundary and Emerging Diseases*, vol. 66, no. 2, pp. 687–695, 2019.

[21] F. F. Zhang, S. X. Luo, J. Gu et al., "Prevalence and phylogenetic analysis of porcine diarrhea associated viruses in southern China from 2012 to 2018," *BMC Veterinary Research*, vol. 15, no. 1, p. 470, 2019.

[22] E. H. Achbani, A. Benbouazza, and A. Douira, "First report of olive anthracnose, caused by colletotrichum gloeosporioides, in Morocco," *Atlas Journal of Biology*, vol. 2, no. 3, pp. 171–174, 2013.

[23] L. Yu, L. L. Xiao, J. Y. Chi et al., "Design, synthesis, and bioactivity evaluation of novel thiochromanone derivatives containing an oxime or oxime ether moiety," *Journal of Heterocyclic Chemistry*, vol. 58, no. 11, pp. 2124–2131, 2021.

[24] L. Yu, L. L. Xiao, P. Li, J. Chi, J. Li, and S. Tan, "Synthesis and bioactivity evaluation of novel thiochroman-4-one derivatives incorporating carboxamide and 1, 3, 4-thiadiazole thioether moieties," *Journal of Chemistry*, vol. 2022, Article ID 5354088, 7 pages, 2022.

Hindawi
Journal of Chemistry
Volume 2022, Article ID 3939911, 11 pages
https://doi.org/10.1155/2022/3939911

Research Article

Novel Karaya Gum Derivatives Produced by Alkaline Hydrolysis and Periodate Oxidation for Active Packaging with Cinnamaldehyde

Vinh Tien Nguyen,[1] Nga Thi Vo,[1] Hoan Thi Pham,[1] Duy Quang Nguyen,[1] Anh Thai Nguyen,[2,3] and Khanh Son Trinh[1]

[1]*Faculty of Chemical and Food Technology, Ho Chi Minh City University of Technology and Education, Vietnam*
[2]*Faculty of Environment and Natural Resources, Ho Chi Minh City University of Technology (HCMUT), 268 Ly Thuong Kiet St., Dist. 10, Ho Chi Minh City, Vietnam*
[3]*Vietnam National University Ho Chi Minh City, Linh Trung Ward, Thu Duc City, Ho Chi Minh City, Vietnam*

Correspondence should be addressed to Khanh Son Trinh; sontk@hcmute.edu.vn

Received 4 April 2022; Accepted 20 April 2022; Published 11 May 2022

Academic Editor: Pei Li

This study aims to produce novel derivatives of karaya gum using chemical modification and then apply them for active packaging with cinnamaldehyde as the main active component. Native karaya gum (NKG) was hydrolyzed using sodium hydroxide to yield hydrolyzed karaya gum (HKG), which then was oxidized using sodium periodate to yield hydrolyzed-oxidized karaya gum (HOKG). For comparison, NKG was also directly oxidized using sodium periodate to produce oxidized karaya gum (OKG). FTIR spectra confirmed the removal of acetyl groups after alkaline hydrolysis and the formation of carbonyl groups with subsequent formation of hemiacetal and acetal structures after periodate oxidation. The alkaline hydrolysis and the periodate oxidation resulted in opposite effects on the hydrophilicity of the gum: hydrolysis increased solubility, moisture uptake, and viscosity, while periodate oxidation decreased these properties. We then produced films from corn starch and these gums (5% *w*/*w* gum/starch) and properties of the films were studied. Hydrolysis of KG resulted in higher tensile strength, higher transparency but lower puncture strength and antifungal activity against of the films, while periodate oxidation exerted the opposite effects. The incorporation of 5% cinnamaldehyde (*w*/*w* of starch) exerted strong antifungal and antibacterial effects on the films against *Colletotrichum gloeosporioides* and *Escherichia coli*, which are useful in active packaging. The active packages based on the novel derivatives of KG can find applications in the agricultural, food, and pharmaceutical industries.

1. Introduction

Karaya gum is produced from *Sterculia* trees in the form of dried tears. Native karaya gum (NKG) is a natural branched, partially acetylated rhamnogalacturonan-type polysaccharide with molecular masses of 9-16 MDa [1]. Its main structure is made of α-D-galacturonic acid and α–L-rhamnose units bonded alternately by $1 \rightarrow 2$ and $1 \rightarrow 4$ linkages (Figure 1). There are two types of sidechains on the main structure: (i) β-D-glucuronic acid sidechains linked by $1 \rightarrow 3$-bonds to the galacturonic acid and (ii) β-D-galactose sidechains linked by $1 \rightarrow 4$-bonds to the rhamnose part and by $1 \rightarrow 2$-bonds to the galacturonic part. Neutral sugars rhamnose and galactose compose 55-60% of NKG, while galacturonic and glucuronic acid sugars compose 37-40%, and acetyl groups—about 8% [2]. NKG exists in the form of calcium and magnesium salts of the sugar acids. The acetyl groups and the 2+ cations make NKG insoluble and highly swellable in water [1]. Alkaline hydrolysis using ammonia or alkali metal hydroxides is a simple way to remove the acetyl groups and precipitate the 2+ cations to increase the solubility of KG and widen its applications [3]. The structure of NKG and hydrolyzed karaya gum (HKG) is presented in Figure 1.

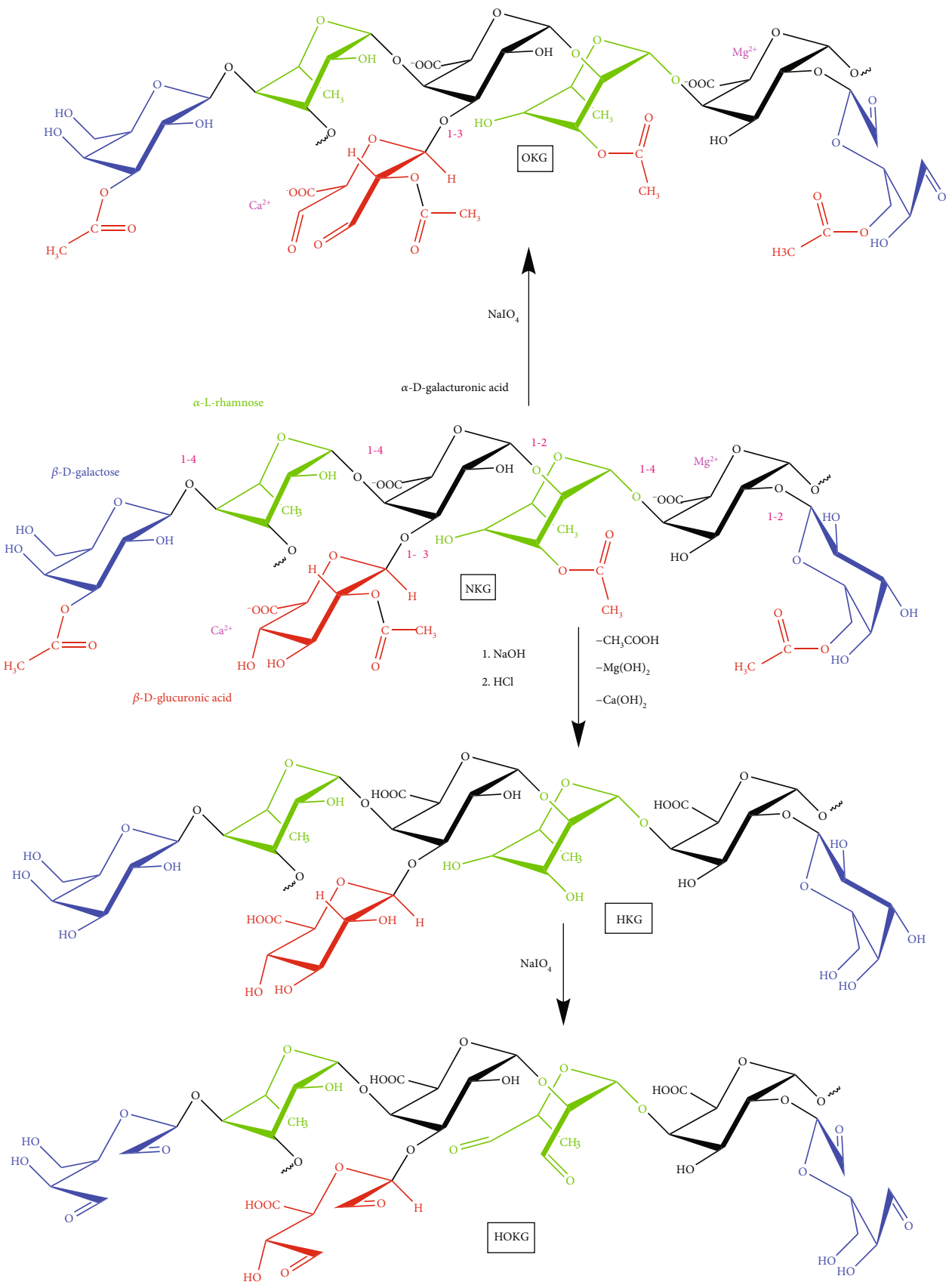

Figure 1: Structures of native (NKG), hydrolyzed (HKG), periodate oxidized (OKG), and hydrolyzed-periodate oxidized (HOKG) karaya gums.

Periodate oxidation is a popular method in structural carbohydrate chemistry. In this method, the periodate ion selectively oxidizes 1,2-dihydroxyl groups to paired aldehyde groups without significant side reactions. Sodium periodate $NaIO_4$ is the most common reagent and has been used to oxidize several polysaccharides such as starch [4, 5], cellulose [6, 7], alginate [8, 9], chitosan [10, 11], and hyaluronic acid [12, 13]. The dialdehyde derivatives of these polysaccharides are commonly used as a crosslinker with other polymers in films and gels. To the best of our knowledge, there was no study using periodate to oxidize karaya gum. Therefore, we used the periodate oxidation to modify the structure of NKG and HKG to convert the vicinal hydroxyl groups to carbonyl groups and obtained oxidized karaya gum (OKG) and hydrolyzed-oxidized karaya gum (HOKG), respectively (Figure 1). Compared to the instinct carboxyl and hydroxyl groups in KG and HKG, the carbonyl groups can participate in more chemical reactions, such as nucleophile addition with a wide range of nucleophiles, oxidation-reduction, and bisulphite reaction. Therefore, OKG and HOKG can be potential intermediates to several derivatives of KG.

This study intended to produce novel derivatives of KG and apply them in active food packaging. Active packaging is a growing research interest in producing packages that have active functions such as antibacterial, antifungal, and antioxidant activities by releasing active components to protect and prolong the shelf life of the packaged food [14]. The active components should be natural, such as essential oils, plant extracts, or compounds isolated from them. Cinnamaldehyde is a yellowish oil extracted from cinnamon oils and is commonly used to give a cinnamon flavour to food, cosmetics, medicines, and perfumes [15]. Cinnamaldehyde inhibits bacterial growth [16], molds [15], and insects [17] by inhibiting ATPase synthesis [18] and cell wall biosyntheses [19] and altering cell wall structure and integrity [20]. Cinnamaldehyde has been incorporated into several natural polymeric films from natural sources such as starch [21], gliadin [22], soy protein isolate [23], and synthetic polymers [24, 25] for antifungal and antibacterial applications.

In this study, after producing hydrolyzed and oxidized KG and incorporating them into starch films, we also added 5% cinnamaldehyde and tested the antibacterial, antifungal, and antioxidant properties of the composite films.

2. Experimental Methods

2.1. Chemicals and Materials. Karaya gum and corn starch were purchased from Xuan Hong Ltd. (Vietnam). Analytical-grade chemicals including NaOH, HCl, $NaIO_4$, $NH_2OH.HCl$, and cinnamaldehyde were purchased from Xilong Ltd. (China), 95% ethanol from Chemsol (Vietnam).

2.2. Alkaline Hydrolysis of Karaya Gum. HKG was prepared according to a published procedure [3]. Two grams of NKG were left swelling in 100 mL of distilled water for 24 h. The swelled gum was hydrolyzed and solubilized by adding 33.3 mL of 1 M NaOH solution and stirring the mixture for 30 min. The excess NaOH was then neutralized using 1 M HCl solution until the suspension pH reached approximately 3. To precipitate NKG, 95% ethanol was added to the solution with a 3 : 1 *v*/*v* ratio. The precipitated gum was collected using a stirring rod, washed twice using 75% ethanol, dried at 50°C for 24 h, and ground to powder.

2.3. Periodate Oxidation of NKG and HKG. Dialdehyde derivatives of NKG and HKG were prepared based on a method for carboxymethyl cellulose [26]. Each type of gum (1 g) was stirred in 20 mL of distilled water for 24 h. Then, 2 mL of 0.11 g/mL $NaIO_4$ solution was added, and the pH was adjusted to 3 using 1 M HCl solution. The mixture was stirred for 4 h at room temperature in the dark. The oxidized product was precipitated by adding 95% ethanol with a 3 : 1 *v*/*v* ratio. The filtered precipitate was then washed using 75% ethanol until the washing water did not change the color of a solution containing KI and soluble starch. The filtered solid was dried at 50°C for 8 h, ground to powder, and stored for further uses.

2.4. Characterization of Gum Powders

2.4.1. Content of Carbonyl Groups [5]. Each oxidized gum powder (0.2 g) was dispersed in 25 mL of 0.25 M $NH_2OH.HCl$ solution (pH = 5.0) by stirring for 15 min. The mixture was then heated in a water bath at 50°C under stirring and continuously titrated with a standard 0.100 M NaOH solution to maintain the solution pH at 5.0. The same procedure was conducted for the NKG as the control.

The mass percentage (%) of carbonyl groups in the oxidized gum was calculated using the following formula:

$$\%\text{CHO} = \frac{29 \times 0.1 \times (V_s - V_c)}{0.2 \times 1000} \times 100 = 14.5 \times (V_s - V_c), \quad (1)$$

where V_s and V_c (mL) were the volumes of the standard 0.100 NaOH solution used to titrate the oxidized gum and the NKG control, respectively.

2.4.2. FTIR Spectra. The dried gum powders were pressed on an attenuated total reflection (ATR) support of an FT/IR—4700 spectrophotometer (Jasco, Japan). The spectra were scanned from 400 to 4000 cm^{-1} with a resolution of 2 cm^{-1}.

2.4.3. Solubility. An excess amount of each gum was stirred for 24 h in 100 mL of distilled water for complete solubilization. The mixture was then centrifuged at 3000 rpm for 15 min. The clear supernatant was poured on a Petri dish, weighed, and dried at 105°C for 24 h to obtain the dissolved gum portion. The procedure was triplicated for each gum. The solubility was calculated using the following formula:

$$S\% = \frac{m_{\text{solid}}}{m_{\text{so ln}}} \times 100, \quad (2)$$

where m_{soln} was the mass of clear supernatant, and m_{solid} was the mass of remaining solid after complete drying of the supernatant.

2.4.4. Relative Viscosity. The relative viscosity of gum solutions (concentrations from 0.025 to 0.100 g/L) was determined with an Ostwald viscosimeter (Ø = 0.3 mm) and using distilled water as the reference.

2.4.5. Moisture Uptake. Each dried gum powder was spread on a Petri dish and put in a closed container with 75% relative humidity (by a saturated NaCl solution put inside). The mass of the Petri dish with gum was recorded every hour for 2 days to calculate the moisture of the gum over time.

2.5. Film Preparation. Starch-gum films were prepared based on a published procedure [27]. A dispersion containing 0.1 g of gum and 20 mL water was prepared and left for 24 h. Two grams of corn starch, 0.6 g glycerol, and a predetermined amount of cinnamaldehyde were dispersed in 40 mL of distilled water. The mixture was heated to 95°C and kept for 20 min for complete gelatinization of starch. The swelled gum dispersion was then added to the gelatinized starch solution. This film-forming mixture was stirred for 10 min and then poured into Petri dishes and left 48 h for drying at room temperature. The dried films were then peeled off the Petri dishes and conditioned in a vessel containing a saturated NaCl solution (75% relative humidity) at least 48 h before film characterizations.

2.6. Film Characterization. The thickness of each film was measured at 10 positions using a digital caliper (Mitutoyo, Japan) with an accuracy of 0.01 mm.

2.6.1. Texture Analysis. Puncture and tensile tests for the films were conducted using a CT3 Texture Analyzer (Brookfield, USA) according to a published study [28]. For puncture tests, each film was cut to 40 × 40 mm strips and conditioned in the 75% RH container for at least 48 h before the test. Each strip was gripped and punctured perpendicularly using a 4.0 mm probe with a 1.0 mm/s speed until completely penetrated (Figure 2(a)).

The puncturing penetration stress (MPa) was calculated using the following formula:

$$P = \frac{F}{A}, \tag{3}$$

where F is the maximum resistance force (N), and $A = 12.56\,\text{mm}^2$ is the contact area between the film and the penetration probe.

For tensile tests, the films were cut to 120 × 15 mm strips and glued and wrapped around the 17.8 mm probes at an initial distance of 45 mm (Figure 2(b)). The upper probe was then moved upward at a 1.0 mm/s speed until the film is completely broken.

The tensile strength of the films (N/mm^2) was calculated using the following formula:

$$P = \frac{F}{S}, \tag{4}$$

where F was the maximum resistance force (N), and S was the initial cross-section area (mm^2).

2.6.2. Moisture, Water Uptake, and Solubility of Films. The moisture, water uptake, and solubility of the films were determined based on a published procedure with minor modifications [29]. The films were cut into 30 × 30 mm pieces, weighed (m_o), dried at 105°C for 24 h, and weighed again (m_1). The dried films were then immersed in 20 mL of distilled water for 24 h, dried using a filter paper, and weighed (m_2). The films were subsequently dried at 105°C for 24 h and weighed again (m_3). The moisture content (MC, %), water uptake (WU, %), and solubility in water (S, %) were calculated using the following formulae:

$$\begin{aligned} \text{MC} &= \frac{m_0 - m_1}{m_0} \times 100\,(\%), \\ \text{WU} &= \frac{m_2 - m_3}{m_3} \times 100\,(\%), \\ S &= \frac{m_1 - m_3}{m_1} \times 100\,(\%). \end{aligned} \tag{5}$$

Water vapor permeability (WVP) of films was determined according to method ASTM E-96.

2.6.3. Antibacterial and Antifungal Activities. Antibacterial and antifungal activities of the films were evaluated based on the disc diffusion method [30]. The bacteria *Escherichia coli* and the mold *Colletotrichum gloeosporioides* were supplied by the Vietnam Type Culture Collection. The culture medium contained 2% agar and 2% nutrient broth. For antifungal tests, the antibiotic chloramphenicol (8 ppm) was used to inhibit the growth of bacteria. The medium was autoclaved, left cooling, and then poured into Petri dishes. When the medium was cooled to room temperature, 100 μL of the microorganism suspension (5 log cfu/mL of *E. coli* or mycelia of *C. gloeosporioides)* was spread onto the medium surface. The films were cut into 10 mm diameter circles and put on the dry contaminated agar surface. The growth of microorganisms was then observed every 4, 48, and 52 h.

2.7. Statistical Analysis. All experiments were triplicated, and the results were analyzed with the one-way analysis of variance (ANOVA) using SPSS software. The differences between mean values were evaluated using Ducan's multiple range test with a 95% significance level.

3. Results and Discussion

3.1. Characterization of Native and Modified Karaya Gum Powders

3.1.1. Carbonyl Content. The carbonyl contents in OKG (5.12 ± 0.44%) and HOKG (4.01 ± 0.33%) determined by titration with hydroxylamine were significantly different ($p < 0.05$). HOKG had a lower free carbonyl content probably because it had a higher content of hydroxyl groups, hence, more readily reacted with carbonyl groups to form hemiacetal and acetal groups and could not react with hydroxylamine [31].

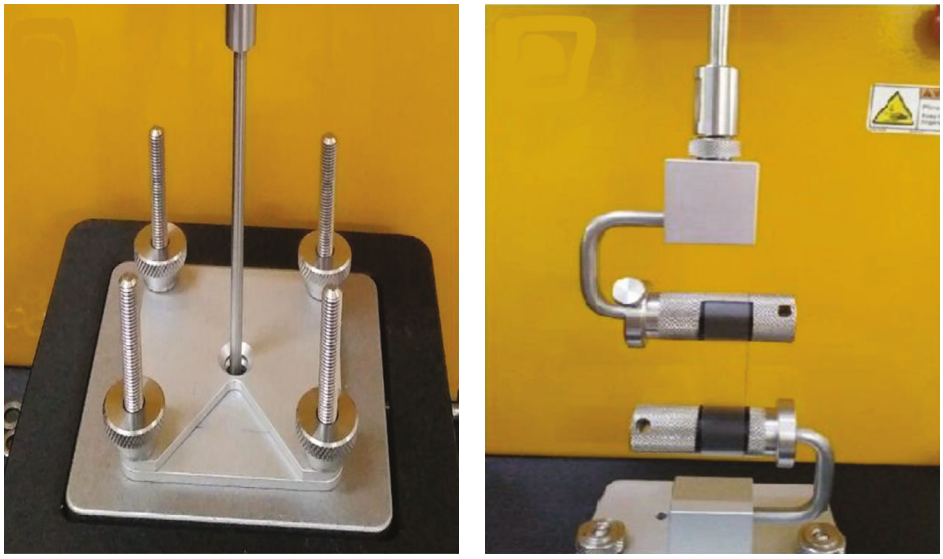

(a) (b)

Figure 2: Experimental setups for the puncture (a) and tensile (b) strength tests.

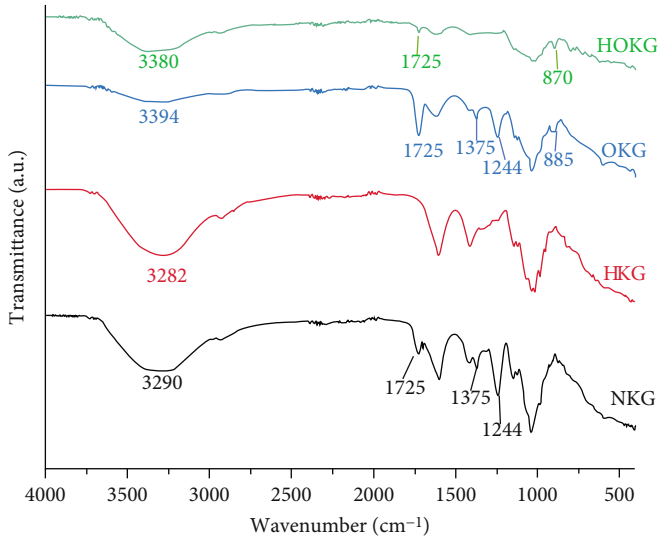

Figure 3: FTIR spectra of KG samples.

Table 1: Some characteristic peaks in FTIR spectra of the KG types.

Wavenumber (cm^{-1})	3282-3394	1725, 1244	1375	885, 887
Bond	-OH	Carbonyl/ester C=O	Methyl C-H	(Hemi)acetal C-O

3.1.2. FTIR Spectra. The FTIR spectra of the four KG types are presented in Figure 3, and their major peaks are listed in Table 1.

The broad peaks at 3282-3394 cm^{-1} in FTIR spectra of the native and modified KG characterize hydroxyl groups in KG structure and the absorbed moisture (Figure 3). This peak for oxidized KG was significantly lower, indicating a low content of hydroxyl in its structure. The reason for this low hydroxyl content is the peroxidation that converted the turned adjacent hydroxyl groups to carbonyl groups, which

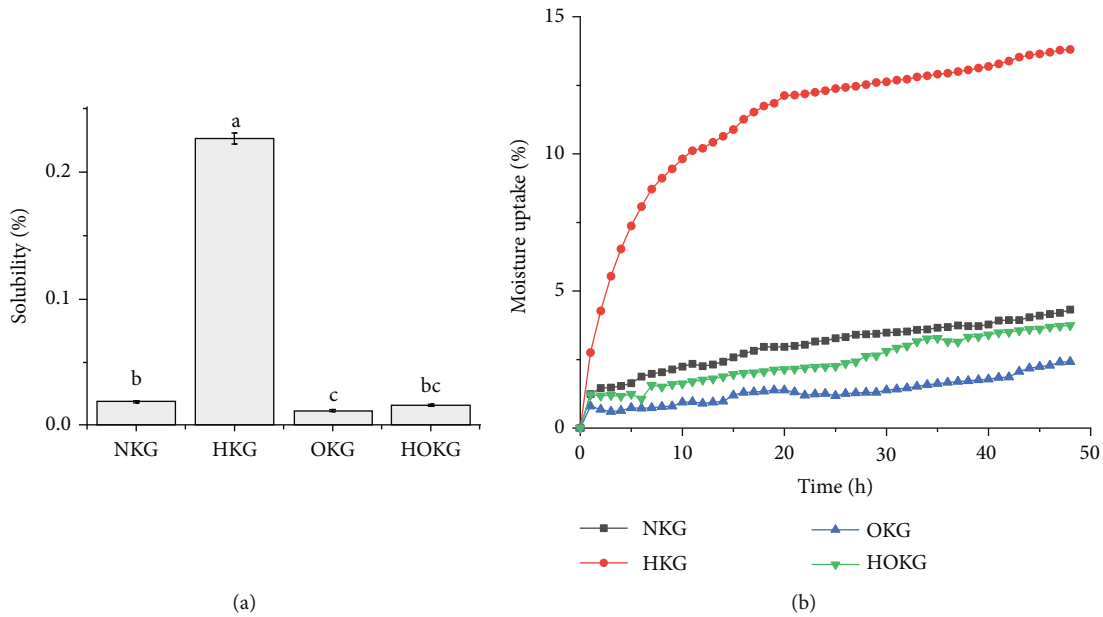

Figure 4: Solubility (a) and moisture uptake (b) of KG powders.

could further react with other hydroxyl groups in the KG backbone to form hemiacetal and acetal.

The peaks of C=O bond at 1725 cm^{-1} and 1244 cm^{-1} and methyl C-H at 1375 cm^{-1} groups, which were present in NKG spectrum, disappeared in the spectrum of HKG due to the removal of acetyl groups by alkaline hydrolysis [3]. After periodate oxidation of HKG, the 1725 cm^{-1} peak appeared again in the spectrum of OKG and HOKG due to the formation of carbonyl groups [32]. Moreover, the intensity of this 1725 cm^{-1} peak was significantly lower for HOKG because HOKG has more hydroxyl groups due to the hydrolysis step, thus, facilitating the formation of hemiacetal and acetal groups and lowering the number of free carbonyl groups. The peaks of hemiacetal groups were at 885 cm^{-1} for OKG and 887 cm^{-1} for HOKG [26].

3.1.3. Solubility, Moisture Uptake, and Relative Viscosity. Because of the presence of acetyl groups and Mg^{2+}/Ca^{2+} cations in the structure, NKG has a low aqueous solubility of 0.018% (Figure 4(a)), which is closed to a reported value of 0.02% [3]. After alkaline hydrolysis that replaced the hydrophobic acetyl groups with the hydrophylic hydroxyl ones and 2+ cations with Na^{+}, the solubility of HKG increased 10-fold compared to NKG [26]. OKG has a lower solubility (0.011%) compared to NKG because some hydroxyl groups were converted to the carbonyl groups. Interestingly, HOKG has a solubility comparable with that of NKG and significantly lower than that of HKG. This result indicates that the conversion of hydroxyl to carbonyl groups and the formation of hemiacetal and acetal strongly decreased the hydroxyl content and hence lowered the solubility of the gum.

The order of moisture uptake by the gum powders was **HKG** > >**NKG** > **HOKG** > **OKG** (Figure 4(b)), which is the same as the order of the aqueous solubility. The explanation of this order remained the same with that for solubility because these two properties are determined by hydrophilicity.

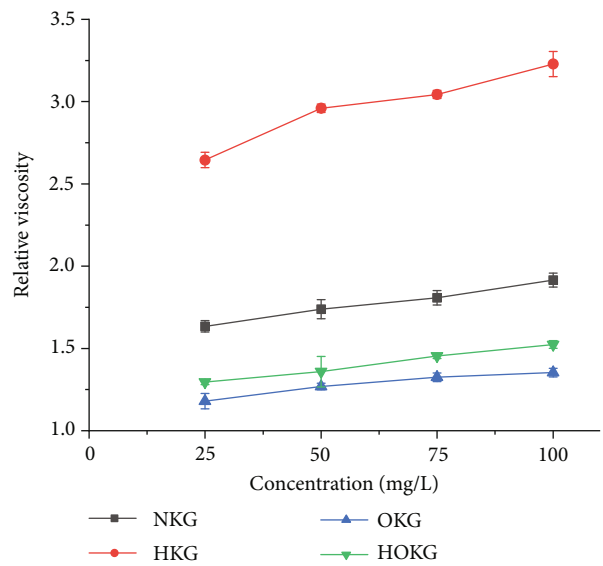

Figure 5: Relative viscosity of KG solutions at room temperature.

The order of relative viscosity of KG samples was **HKG** > >**NKG** > **HOKG** > **OKG** (Figure 5). This order is the same as the order of aqueous solubility. HKG solution has a high viscosity due to the high content of hydroxyl groups, which increased the hydrogen bonds between its molecules in solution. This result is in line with another report that the viscosity of KG solution increased with higher concentration, lower temperature, and higher deacetylation degree [33].

3.2. Properties of Starch Films Incorporated with Native and Modified KG

3.2.1. Puncture and Tensile Strength. Table 2 shows that starch films containing 5% KG had puncture strengths increasing in the order HKG < NKG < HOKG < OKG and

Table 2: Results of puncture and tensile tests of the films.

Starch film with	Elongation at puncture (%)	Puncture strength (N/mm^2)	Elongation-at-break (%)	Tensile strength (N/mm^2)
NKG	53.29 ± 3.02^{bc}	0.316 ± 0.005^{c}	36.64 ± 0.46^{d}	3.00 ± 0.19^{bcd}
HKG	47.72 ± 1.47^{c}	0.279 ± 0.008^{d}	49.45 ± 1.66^{b}	3.55 ± 0.31^{a}
OKG	66.67 ± 1.78^{a}	0.411 ± 0.025^{a}	19.47 ± 0.07^{g}	2.60 ± 0.24^{de}
HOKG	50.51 ± 0.80^{c}	0.372 ± 0.011^{b}	32.65 ± 0.56^{e}	2.84 ± 0.41^{cde}

Results are expressed as mean ± standard deviation ($n = 3$). Means with different superscripts in a column are significantly different ($p < 0.05$).

Table 3: Results of moisture, water uptake, solubility, and moisture permeability of the films.

Starch film with	Moisture content (%)	Water uptake (%)	Solubility (%)	Moisture permeability ($\times 10^{-10}$ g/Pa.m.s)
NKG	21.72 ± 0.54^{b}	124.80 ± 0.77^{b}	19.62 ± 1.04^{b}	1.736 ± 0.066^{ab}
HKG	24.90 ± 0.80^{a}	151.77 ± 2.26^{a}	21.44 ± 0.24^{a}	1.882 ± 0.054^{a}
OKG	18.53 ± 0.66^{e}	104.73 ± 3.56^{c}	16.78 ± 0.51^{d}	1.589 ± 0.037^{bc}
HOKG	20.15 ± 0.38^{cd}	119.32 ± 2.64^{b}	18.06 ± 0.70^{c}	1.670 ± 0.061^{bc}

Results are expressed as mean ± standard deviation ($n = 3$). Means with different superscripts in a column are significantly different ($p < 0.05$).

elongation at break decreasing in the same order. This result means that alkaline hydrolysis plasticized, while periodate oxidation hardened the films. The reason of plasticizing effect of alkaline hydrolysis was possibly the removal of metallic cations crosslinking $-COO^-$ groups in the KG backbones. Moreover, hydrophilic hydroxyl groups released after hydrolysis of KG attracted more moisture that acted as a plasticizer. The plasticizing effect of alkaline hydrolysis was also observed in another study, in which deacetylation of xanthan gum increased deceased the strength and increase the elongation-at-break of its films [34].

The hardening effect of periodate oxidation on the films was due to the formation of carbonyl groups in KG molecules that can form hemiacetal and acetal crosslinks with hydroxyl groups in the molecules of starch and KG [35]. The crosslinking of carbonyl groups was also observed in collagen films incorporated with glutaraldehyde [36] and eggwhite films incorporated with oxidized starch [37].

Table 2 shows that the puncture strength and tensile strength of the films were inversely related to their EB: films with lower tensile strength/puncture strength had higher EB.

It is interesting to note that the alkaline hydrolysis and periodate oxidation oppositely affected the puncture and tensile strengths of the films: alkaline hydrolysis increased the tensile strength but lowered the puncture strength, while periodate oxidation decreased the tensile strength but increased the puncture strength. These results showed that the action mode of KG along the films in tensile tests was different from the action in the perpendicular direction in the puncture tests.

3.2.2. Hydrophilicity. Table 3 shows that moisture content, moisture permeability water uptake, and solubility of the films incorporated with KG had the same trend: HKG > NKG > HOKG > OKG. These three properties are related with the hydrophilicity of the films. Alkaline hydrolysis of KG produced more hydrophilic hydroxyl groups and hence increased the hydrophilicity of the films [3]. Oppositely, periodate oxidation converted hydroxyl groups to less hydrophilic carbonyl groups, which further produced hemiacetal and acetal with other hydroxyl groups [5]. Therefore, periodate oxidation significantly reduced the hydrophilicity of the OKG and HOKG films. Our results are consistent with other studies on dialdehyde starch-gelatin films [38] and dialdehyde carboxymethyl cellulose-gelatin films.

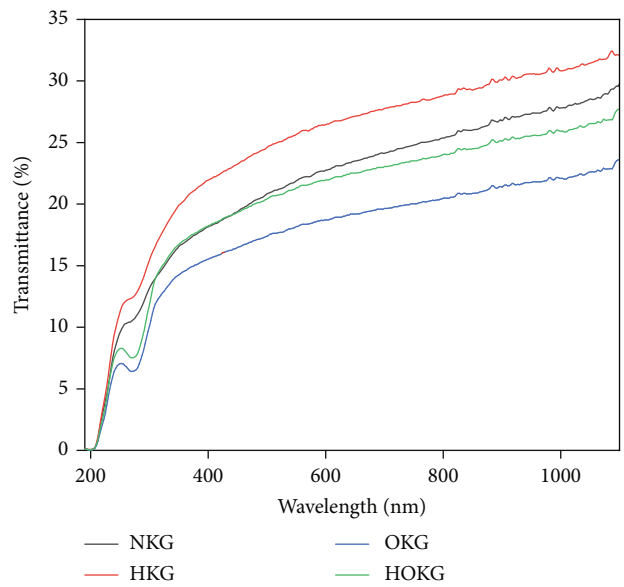

Figure 6: UV-vis spectra of starch-KG films.

3.2.3. UV-Vis Spectra and Transparency. UV-vis spectroscopy helps evaluate the visible transparency and UV barrier properties of films, which are important for food packaging applications. Figure 6 shows that the order of transparency of the films is the same in three regions (UV, visible, and IR): HKG > NKG > HOKG > OKG. This result indicates that hydrolysis enhanced but periodate oxidation lowered the film transparency.

Films containing OKG and HKG showed a strong absorption peak at 270 nm while the peak was weak for films containing NKG and HKG. This peak is due to the

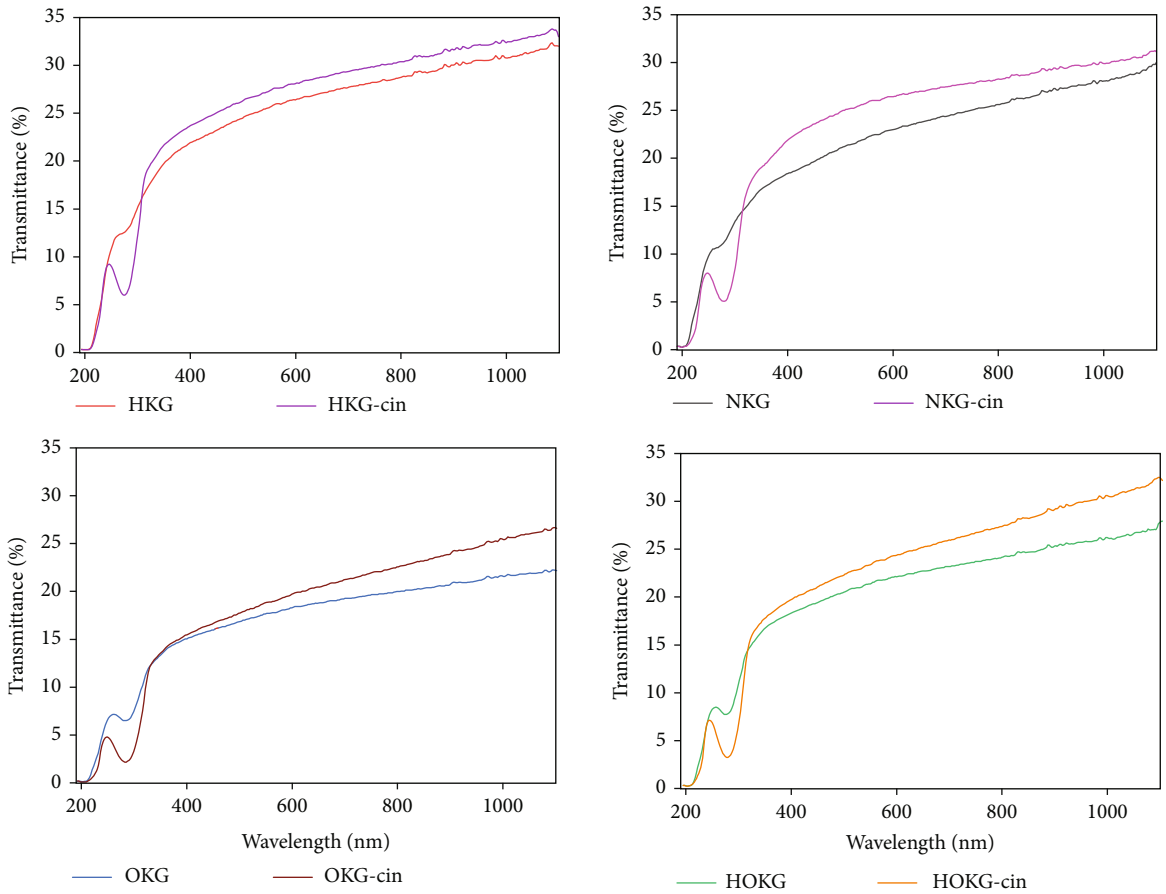

Figure 7: UV-vis spectra of starch-KG films with and without 5% cinnamaldehyde.

absorption of the –C=O bond in the aldehyde and ester groups in KG, which was also observed in gelatin films incorporated with dialdehyde CMC [26]. The strong absorption of starch films incorporated with OKG and HOKG can protect the packaged products from UV radiation.

It is interesting to note that when incorporated with 5% cinnamaldehyde, all the four films transmitted slightly more IR and visible radiation, but more strongly absorbed UV light (Figure 7) because the carbonyl group in aldehydes was reported to absorb radiations near 280 nm [39]. Therefore, the incorporation of cinnamaldehyde can enhance the protective effect of the films against UV- light.

3.2.4. Antifungal Activity. Figure 8 shows that *C. gloeosporioides* grew quickly on the Petri dishes with films not containing cinnamaldehyde. Except for OKG, the fungi grew on the surface of starch-KG films. However, the incorporation of 5% cinnamaldehyde significantly inhibited the growth of *C. gloeosporioides*. Several studies have shown the antifungal activity of cinnamaldehyde against several fungi such as *Colletotrichum gloeosporioides*, *Rhizoctonia solani*, *Fusarium solani*, and *Ganoderma austral* [22, 40]. The mechanism of the antifungal activity is related to the decrease of plasma membrane ATPase activity and ergosterol, a vital component of the fungal cell wall [41].

Based on the degree of invasion of fungi on the film surface, the antifungal activity of KG types is HKG < NKG < HOKG < OKG. Interestingly, the starch film with HKG (Figure…) facilitated the growth and spore production of *C. gloeosporioides* after even one day. The fact that the fungi strongly developed even outside the film indicates that HKG with high solubility diffused to the agar and promoted the growth of *C. gloeosporioides*. On the opposite side, the fungi grew normally outside the film with OKG but almost could not invade the film after 3 days (Figure 8). This result indicates that OKG can inhibit by direct contact with fungal cells possibly due to the carbonyl groups that can interact with the fungal cell wall.

3.2.5. Antibacterial Activity. Figure 9 shows that after 4 days *E.coli* grew fully on the agar and the films without cinnamaldehyde. Although KG has a slight antibacterial and enzyme degradation activity [42], its content in the films (3.7% on a dry basis) was too low to be effective. The incorporation of 5% cinnamaldehyde in the films resulted in an inhibition zone around each film from day 1 (images not shown), and the diameters of the inhibition zones did not change afterwards.

The antibacterial action of cinnamaldehyde is known to be dose-dependent and can differ for different bacteria. At low concentrations, cinnamaldehyde interacts and damages the bacterial cell walls while at high concentrations, it can

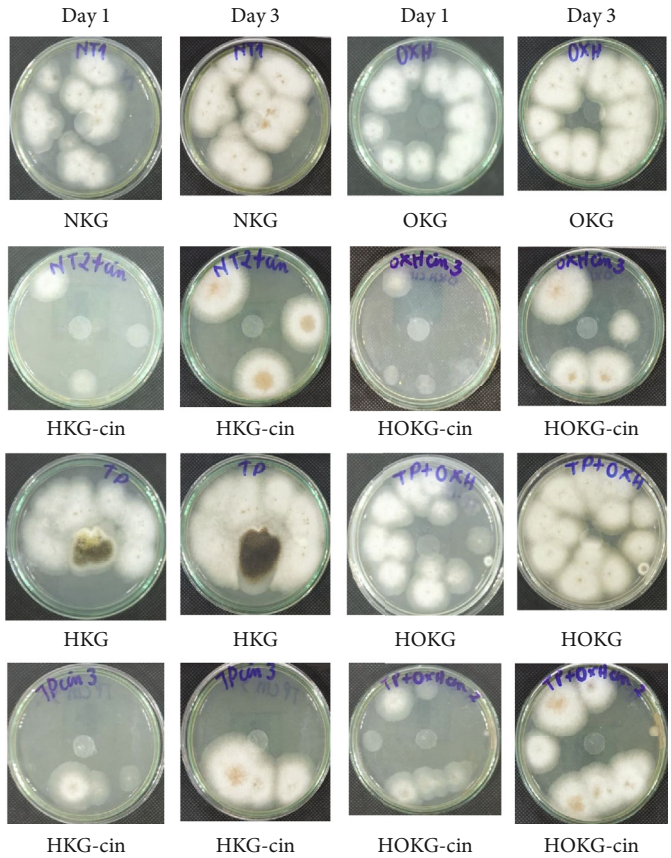

Figure 8: Antifungal activity of KG-starch films with and without cinnamaldehyde for 3 days against *C. gloeosporioides*.

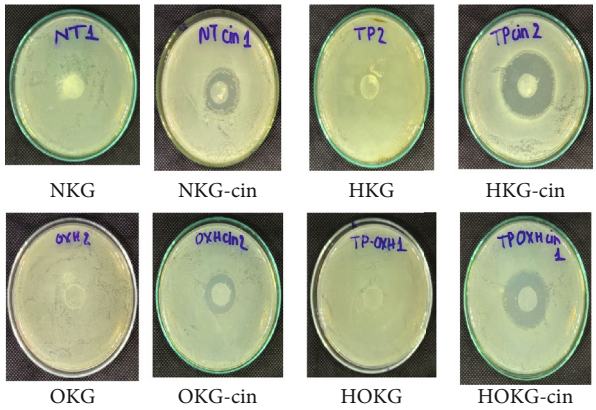

Figure 9: Disc diffusion test of KG-starch films with and without 5% cinnamaldehyde after 4 days.

diffuse into the cell and denature proteins in important enzymes in the cytoplasm, leading to cell death [43, 44].

4. Conclusion

This is the first report on periodate oxidation with and without alkaline hydrolysis to chemically modify karaya gum (KG) and develop new products from it. The hydrolysis increases while periodate oxidation decreases the hydrophilicity of KG. The carbonyl groups formed by periodate oxidation can give KG the possibility to be further modified by redox reactions or coupling with functional groups such as hydroxyl and amine. The modified KG can be blended with different biopolymers and active components to be used as packaging materials in the food and pharmaceutical industries.

Data Availability

The data used to support the findings of this study are available from the corresponding author upon request.

Conflicts of Interest

The authors declare that there are no conflicts of interest regarding the publication of this paper.

Acknowledgments

This work is financially supported by HCMUTE through the project T2021-36TĐ. The authors thank Ms. Tran Thi My Lanh (Student ID 16116041) and Ms. Nguyen Thi Thanh Trang (Student ID 16116092) for their helpful technical assistance.

References

[1] D. Le Cerf, F. Irinei, and G. Muller, "Solution properties of gum exudates from *Sterculia urens* (Karaya gum)," *Carbohydrate Polymers*, vol. 13, no. 4, pp. 375–386, 1990.

[2] V. Raj, J. H. Lee, J. J. Shim, and J. Lee, "Recent findings and future directions of grafted gum karaya polysaccharides and

their various applications: a review," *Carbohydrate Polymers*, vol. 258, article 117687, 2021.

[3] H. Postulkova, I. Chamradova, D. Pavlinak, O. Humpa, J. Jancar, and L. Vojtova, "Study of effects and conditions on the solubility of natural polysaccharide gum karaya," *Food Hydrocolloids*, vol. 67, pp. 148–156, 2017.

[4] M. Fiedorowicz and A. Para, "Structural and molecular properties of dialdehyde starch," *Carbohydrate Polymers*, vol. 63, no. 3, pp. 360–366, 2006.

[5] J. Yu, P. R. Chang, and X. Ma, "The preparation and properties of dialdehyde starch and thermoplastic dialdehyde starch," *Carbohydrate Polymers*, vol. 79, no. 2, pp. 296–300, 2010.

[6] E. Maekawa and T. Koshijima, "Preparation and structural consideration of nitrogen-containing derivatives obtained from dialdehyde celluloses," *Journal of Applied Polymer Science*, vol. 42, no. 1, pp. 169–178, 1991.

[7] U.-J. Kim, M. Wada, and S. Kuga, "Solubilization of dialdehyde cellulose by hot water," *Carbohydrate Polymers*, vol. 56, no. 1, pp. 7–10, 2004.

[8] Y. Hu, L. Liu, Z. Gu, W. Dan, N. Dan, and X. Yu, "Modification of collagen with a natural derived cross-linker, alginate dialdehyde," *Carbohydrate Polymers*, vol. 102, pp. 324–332, 2014.

[9] R. Aston, M. Wimalaratne, A. Brock, G. Lawrie, and L. Grøndahl, "Interactions between chitosan and alginate dialdehyde biopolymers and their layer-by-layer assemblies," *Biomacromolecules*, vol. 16, no. 6, pp. 1807–1817, 2015.

[10] X. Liu, N. Dan, W. Dan, and J. Gong, "Feasibility study of the natural derived chitosan dialdehyde for chemical modification of collagen," *International Journal of Biological Macromolecules*, vol. 82, pp. 989–997, 2016.

[11] J. Ren, M. Li, R. Yuan, A. Pang, Z. Lu, and L. Ge, "Adherent self-healing chitosan/dialdehyde starch coating," *Colloids and Surfaces A: Physicochemical and Engineering Aspects*, vol. 586, article 124203, 2020.

[12] A. Sionkowska, M. Michalska-Sionkowska, and M. Walczak, "Preparation and characterization of collagen/hyaluronic acid/chitosan film crosslinked with dialdehyde starch," *International Journal of Biological Macromolecules*, vol. 149, pp. 290–295, 2020.

[13] R. R. Vildanova, N. N. Sigaeva, O. S. Kukovinets, and S. V. Kolesov, "Preparation and rheological properties of hydrogels based on N-succinyl chitosan and hyaluronic acid dialdehyde," *Polymer Testing*, vol. 96, article 107120, 2021.

[14] I. Ahmed, H. Lin, L. Zou et al., "A comprehensive review on the application of active packaging technologies to muscle foods," *Food Control*, vol. 82, pp. 163–178, 2017.

[15] S. Shreaz, W. A. Wani, J. M. Behbehani et al., "Cinnamaldehyde and its derivatives, a novel class of antifungal agents," *Fitoterapia*, vol. 112, pp. 116–131, 2016.

[16] M. Friedman, P. R. Henika, and R. E. Mandrell, "Bactericidal activities of plant essential oils and some of their isolated constituents against Campylobacter jejuni, Escherichia coli, Listeria monocytogenes, and Salmonella enterica," *Journal of Food Protection*, vol. 65, no. 10, pp. 1545–1560, 2002.

[17] Y. Huang and S. Ho, "Toxicity and antifeedant activities of cinnamaldehyde against the grain storage insects, *Tribolium castaneum* (Herbst) and *Sitophilus zeamais* Motsch," *Journal of Stored Products Research*, vol. 34, no. 1, pp. 11–17, 1998.

[18] J. Usta, S. Kreydiyyeh, P. Barnabe, Y. Bou-Moughlabay, and H. Nakkash-Chmaisse, "Comparative study on the effect of cinnamon and clove extracts and their main components on different types of ATPases," *Human & Experimental Toxicology*, vol. 22, no. 7, pp. 355–362, 2003.

[19] K. H. Bang, D. W. Lee, H. M. Park, and Y. H. Rhee, "Inhibition of fungal cell wall synthesizing enzymes by trans-cinnamaldehyde," *Bioscience, Biotechnology, and Biochemistry*, vol. 64, no. 5, pp. 1061–1063, 2000.

[20] X. Xie, J. Fang, and Y. Xu, "Study of antifungal effect of cinnamaldehyde and citral on Aspergillus flavus," *Food Science*, vol. 25, no. 9, pp. 32–34, 2004.

[21] J. Ke, L. Xiao, G. Yu, H. Wu, G. Shen, and Z. Zhang, "The study of diffusion kinetics of cinnamaldehyde from corn starch-based film into food simulant and physical properties of antibacterial polymer film," *International Journal of Biological Macromolecules*, vol. 125, pp. 642–650, 2019.

[22] M. P. Balaguer, G. Lopez-Carballo, R. Catala, R. Gavara, and P. Hernandez-Munoz, "Antifungal properties of gliadin films incorporating cinnamaldehyde and application in active food packaging of bread and cheese spread foodstuffs," *International Journal of Food Microbiology*, vol. 166, no. 3, pp. 369–377, 2013.

[23] J. Wu, Q. Sun, H. Huang, Y. Duan, G. Xiao, and T. le, "Enhanced physico-mechanical, barrier and antifungal properties of soy protein isolate film by incorporating both plant-sourced cinnamaldehyde and facile synthesized zinc oxide nanosheets," *Colloids and Surfaces B: Biointerfaces*, vol. 180, pp. 31–38, 2019.

[24] A. Nostro, R. Scaffaro, M. D'Arrigo et al., "Study on carvacrol and cinnamaldehyde polymeric films: mechanical properties, release kinetics and antibacterial and antibiofilm activities," *Applied Microbiology and Biotechnology*, vol. 96, no. 4, pp. 1029–1038, 2012.

[25] A. Srisa and N. Harnkarnsujarit, "Antifungal films from trans-cinnamaldehyde incorporated poly(lactic acid) and poly(butylene adipate-co-terephthalate) for bread packaging," *Food Chemistry*, vol. 333, article 127537, 2020.

[26] C. Mu, J. Guo, X. Li, W. Lin, and D. Li, "Preparation and properties of dialdehyde carboxymethyl cellulose crosslinked gelatin edible films," *Food Hydrocolloids*, vol. 27, no. 1, pp. 22–29, 2012.

[27] A. Nawab, F. Alam, M. A. Haq, Z. Lutfi, and A. Hasnain, "Mango kernel starch-gum composite films: physical, mechanical and barrier properties," *International Journal of Biological Macromolecules*, vol. 98, pp. 869–876, 2017.

[28] A. Farahnaky, B. Saberi, and M. Majzoobi, "Effect of glycerol on physical and mechanical properties of wheat starch edible films," *Journal of Texture Studies*, vol. 44, no. 3, pp. 176–186, 2013.

[29] T. L. Cao and K. B. Song, "Effects of gum karaya addition on the characteristics of loquat seed starch films containing oregano essential oil," *Food Hydrocolloids*, vol. 97, article 105198, 2019.

[30] N. M. Zain, A. G. Stapley, and G. Shama, "Green synthesis of silver and copper nanoparticles using ascorbic acid and chitosan for antimicrobial applications," *Carbohydrate Polymers*, vol. 112, pp. 195–202, 2014.

[31] H. Li, B. Wu, C. Mu, and W. Lin, "Concomitant degradation in periodate oxidation of carboxymethyl cellulose," *Carbohydrate Polymers*, vol. 84, no. 3, pp. 881–886, 2011.

[32] S. D. Zhang, Y. R. Zhang, J. Zhu, X. L. Wang, K. K. Yang, and Y. Z. Wang, "Modified corn starches with improved comprehensive properties for preparing thermoplastics," *Starch-Stärke*, vol. 59, no. 6, pp. 258–268, 2007.

[33] Y. López-Franco, I. Higuera-Ciapara, J. Lizardi-Mendoza, W. Wang, and F. M. Goycoolea, "Other exudates: tragacanth, karaya, mesquite gum, and larchwood arabinogalactan," in *Handbook of Hydrocolloids*, pp. 673–727, Woodhead Publishing Series in Food Science, Technology and Nutrition, 2021.

[34] P. Veiga-Santos, L. M. Oliveira, M. P. Cereda, A. J. Alves, and A. R. P. Scamparini, "Mechanical properties, hydrophilicity and water activity of starch-gum films: effect of additives and deacetylated xanthan gum," *Food Hydrocolloids*, vol. 19, no. 2, pp. 341–349, 2005.

[35] S. Veelaert, D. de Wit, K. F. Gotlieb, and R. Verhé, "Chemical and physical transitions of periodate oxidized potato starch in water," *Carbohydrate Polymers*, vol. 33, no. 2-3, pp. 153–162, 1997.

[36] D. Simmons and J. Kearney, "Evaluation of collagen cross-linking techniques for the stabilization of tissue matrices," *Biotechnology and Applied Biochemistry*, vol. 17, no. 1, pp. 23–29, 1993.

[37] A. Gennadios, A. Handa, G. W. Froning, C. L. Weller, and M. A. Hanna, "Physical properties of egg white– dialdehyde starch films," *Journal of Agricultural and Food Chemistry*, vol. 46, no. 4, pp. 1297–1302, 1998.

[38] O. Moreno, J. Cárdenas, L. Atarés, and A. Chiralt, "Influence of starch oxidation on the functionality of starch-gelatin based active films," *Carbohydrate Polymers*, vol. 178, pp. 147–158, 2017.

[39] A. Asthana, D. Bose, S. Kulshrestha, S. P. Pathak, S. K. Sanghi, and W. T. Kok, "Determination of aldehydes in water samples by capillary electrophoresis after derivatization with hydrazino benzene sulfonic acid," *Chromatographia*, vol. 48, no. 11-12, pp. 807–810, 1998.

[40] H. C. Lee, S. S. Cheng, and S. T. Chang, "Antifungal property of the essential oils and their constituents from Cinnamomum osmophloeum leaf against tree pathogenic fungi," *Journal of the Science of Food and Agriculture*, vol. 85, no. 12, pp. 2047–2053, 2005.

[41] S. Shreaz, R. A. Sheikh, B. Rimple, A. A. Hashmi, M. Nikhat, and L. A. Khan, "Anticandidal activity of cinnamaldehyde, its ligand and Ni(II) complex: effect of increase in ring and side chain," *Microbial Pathogenesis*, vol. 49, no. 3, pp. 75–82, 2010.

[42] D. Verbeken, S. Dierckx, and K. Dewettinck, "Exudate gums: occurrence, production, and applications," *Applied Microbiology and Biotechnology*, vol. 63, no. 1, pp. 10–21, 2003.

[43] F. Mousavi, B. Bojko, V. Bessonneau, and J. Pawliszyn, "Cinnamaldehyde characterization as an antibacterial agent toward E. coli metabolic profile using 96-blade solid-phase microextraction coupled to liquid chromatography–mass spectrometry," *Journal of Proteome Research*, vol. 15, no. 3, pp. 963–975, 2016.

[44] N. Sanla-Ead, A. Jangchud, V. Chonhenchob, and P. Suppakul, "Antimicrobial activity of cinnamaldehyde and eugenol and their activity after incorporation into cellulose-based packaging films," *Packaging Technology and Science*, vol. 25, no. 1, pp. 7–17, 2012.

Hindawi
Journal of Chemistry
Volume 2022, Article ID 9169433, 8 pages
https://doi.org/10.1155/2022/9169433

Research Article

Analysis of Bacterial Community Composition and Ecological Function during Soft Rot Process in Pitaya (*Hylocereus* spp.) Stems

Zhijun Peng, Jingqiang Guan, Dan Mou, Xiao Zou, Bin Wang, Jilin Jin, Xingwu Zhang, and Hui Luo

Institute of Fruit Science, Guizhou Academy of Agricultural Sciences, Guiyang 550006, China

Correspondence should be addressed to Hui Luo; luohui8732@163.com

Received 9 April 2022; Accepted 25 April 2022; Published 6 May 2022

Academic Editor: Pei Li

The soft rot in pitaya (*Hylocereus* spp.) stems seriously affected the harvest of pitaya fruits, but the dynamic change characteristics of bacterial community in pitaya stems during soft rot stages had not been revealed. In this study, we analyzed the bacterial community composition of different soft rot stages and visualized functional annotations of the core bacterial community in five soft rot periods via the Illumina high-throughput sequencing technology, MetaCoMET online network platform, and FAPROTAX database. The results showed that the dominant bacteria in healthy and diseased pitaya stems were Proteobacteria and Firmicutes. *Pseudomonas*, *Enterobacter*, *Sphingomonas*, and *Sphingobacterium* were the core bacteria microbiomes during the infection stages. Meanwhile, the ecological function analysis results showed that the *Enterobacter* and *Pseudomonas* bacteria may play an important role in causing soft rot of pitaya stems. Therefore, the results shown in this paper could provide a useful reference for the study on microecological mechanism of soft rot of pitaya stems.

1. Introduction

Pitaya (*Hylocereus* spp.) is often planted in tropical and subtropical regions and has high economic and nutritional value. Hainan Province in China began to grow pitaya in the late 1990s, followed by Fujian, Guangdong, Guangxi, Guizhou, Yunnan, and other southern provinces (regions) began to large-scale introduction. In recently years, Guizhou Province is one of the major pitaya producing areas in China, and pitaya in Luodian County has become a national geographic landmark product.

At present, pitaya yield is threatened by many diseases; among which, soft rot is one of the main diseases. Various studies showed that a variety of fungi could produce soft rot on pitaya fruits, for example, *Scytalidium dimidiatum*, *Fusarium* spp., *F. dimerum*, *Gilbertella persicaria*, and *F. oxysporum* [1–6]. If the pitaya stem is infected by *F. semitectum*, *F. oxysporum*, *F. moniliforme*, and other *Fusarium* fungi, it will show symptoms of tissue softening, ulceration, and depression at the stem ridge [2, 7]. *Bipolaris* was a plant pathogenic fungus with strong distribution in the world, which could cause soft rot in cacti plants, for example, fruit rot of pitaya and stem rot of cactus [8, 9]. In addition, Liang et al. showed that *B. cactivora* could harm the stem of pitaya under natural conditions, which was the first report on the harm of stem rot of this fungus at home and abroad [10].

However, there are few reports about the bacterial diseases of pitaya. Yuan et al. found that *Erwinia* sp. could make the nodes of pitaya stems infected with soft rot in western Guangdong Province [11]. Sang et al. also confirmed that the soft rot of pitaya stem was mainly caused by *Erwenella* [12]. Meanwhile, Masyahit et al. [13] first sampled the pitaya stems of soft rot from 11 sample areas in Malaysia and found that *Enterobacter cloacae* could cause soft rot and yellow-brown of pitaya stems. Lin et al. [14] isolated the endogenous bacteria in pitaya seedlings, and the identification results showed that *Enterobacter* bacteria induced typical soft rot symptoms in pitaya plants. In

Table 1: Statistics of sequencing date and alpha diversity index in different soft rot stages.

Samples	Raw reads	Effective reads	Numbers	Coverage (%)	Simpson index	Shannon index	Sobs index	Ace index	Chao1 index
CK	36580	36024	56	99.953	0.627	0.705	49	67.360	68.429
B-1	41511	40771	56	99.968	0.690	0.632	50	68.989	57.800
B-2	41016	40002	80	99.955	0.546	0.897	70	86.786	82.750
B-3	36948	35749	139	99.964	0.566	1.130	121	127.709	128.091
B-4	38898	36044	185	99.989	0.090	3.287	152	153.213	152.667

addition to *Erwenella* and *Enterobacter*, Zhang et al. [15] found that *Paenibacillus polymyxa* could also cause soft rot in the stem of pitaya. When plant stems are affected by soft rot pathogens, this type of disease will further spread and eventually affect the fruit yield [16]. However, the change characteristics of endogenous bacterial community during soft rot of pitaya stem are not clear.

In this study, we analyzed the bacterial community composition in the pitaya stem tissue in different soft rot stages by the Illumina high-throughput sequencing technology and annotated the core bacterial microbiome to provide theoretical guidance for the prediction of pitaya soft rot disease in different soft rot stages.

2. Materials and Methods

2.1. Sample Collection. In July 2019, the stems of pitaya (variety "Purple Red Dragon") in five different soft rot stages were sampled from Luodian County, Guizhou Province, China. According to the methods of Masyahit et al. [13], the soft rot disease grade of pitaya stem was divided into five grades, which were normal (CK), early soft rot grade (B-1), middle soft rot grade (B-2), middle and late soft rot grade (B-3), and late soft rot grade (B-4), respectively. Three stems were collected at each period. The samples were encapsulated in sterile ziplock bags, stored in ice bags, and transported to the laboratory for further processing. Tissue blocks with a size of 5 mm × 5 mm were cut at the junction of the disease with a sterile scalpel, 3 tissue blocks were cut from each stem, and 9 tissue blocks were mixed evenly in each period. According to the treatment method of Xu et al. [17], tissue blocks in each period were disinfected: first soaked in 75% alcohol for 40 s, then soaked in 5% sodium hypochlorite solution for 1 min, and finally washed with sterile water for 4 times. The dried tissue was encapsulated in a sterile ziplock bag and stored in a -80°C refrigerator.

2.2. DNA Extraction, PCR Amplification, and Sequencing. Under aseptic conditions, plant tissue blocks were ground into a fine powder with liquid nitrogen. Approximately, 50 mg tissue powder was taken at each onset stage, and total microbial genomic DNA was extracted according to the instructions in the E.Z.N.A.® SoiL DNA Kit (Omega Bio-Tek, Norcross, GA, USA). According to the method of Wei et al. [18], the V3-V4 region of bacterial 16S rDNA was amplified by ABI Gene Amp®9700 (ABI, CA, USA). Polymerase chain reaction (PCR) reaction system is as follows: 0.4 μL of TransStart Fastpfu DNA Polymerase (2.5 U·μ/L), 4 μL of Fastpfu Buffer, 2 μL of dNTPs (2.5 mol/L), 0.8 μL of forward and reverse primers of 338F (5 μmol/L) and 806R (5 μmol/L), 0.2 μL of BSA (0.8 μg·μ/L), 10 μL of DNA template (1 ng/μL), and 20 μL of ddH_2O. PCR reaction procedure is as follows: predenaturation at 95°C for 3 min; denaturation at 98°C for 30 s, 55°C for 30 s, 72°C for 45 s, a total of 30 cycles; extended at 72°C for 10 min [19, 20]. PCR products were detected by 1% agarose gel electrophoresis and sequenced using the Illumina Miseq platform.

2.3. Data Analysis. In order to obtain effective Tags data, the sequence of each sample was splicing and quality optimization (Tags interception, filtering, and chimeric removal) by referring to the processing method of Robert [21]. The UPARSE software was used to cluster the 97% nonrepeating sequences (excluding single sequences) into operational taxonomic units (OTUs). Mothur method was used to compare OTUs with species in SSU rRNA database. Finally, α diversity analysis was performed on the obtained data.

The species abundance of each sample was counted at the taxonomic level of phylum and genus, and the bacterial communities of samples in each period were analyzed by using the Origin Pro 2018C software. The distribution differences of OTUs in different soft decay stages were analyzed by Venn diagram. At the genus level, the species annotation and abundance of each sample were analyzed. The top 26 groups with relative abundance were selected, and the changes of dominant bacterial groups in samples at different soft rot stages were analyzed by heat map.

Core microbiome is a key component of Holobionts, which is of great significance for the study of symbiotic and pathogenic microorganisms [22]. OTUs were uploaded to the MetaCoMET platform (http://probes.pw.usda.gov/MetaCoMETT). The membership definition method was used to obtain the core bacterial microbiomes of different soft decay stages.

FAPROTAX is a kind of database collected for culturable bacteria and is often used to predict the ecological function of the microbiome. The database has included more than 4600 culturable bacteria, including more than 80 functional groups and 7600 functional annotations, which can be applied to predict the ecological function of culturable bacteria [23]. Through the FAPROTAX database, the OTU function of the core bacterial microbiome in different soft decay stages was predicted.

3. Results

3.1. Sequence Data. As shown in Table 1, a total of 178,745 valid sequences and 516 OUTs were obtained, with an

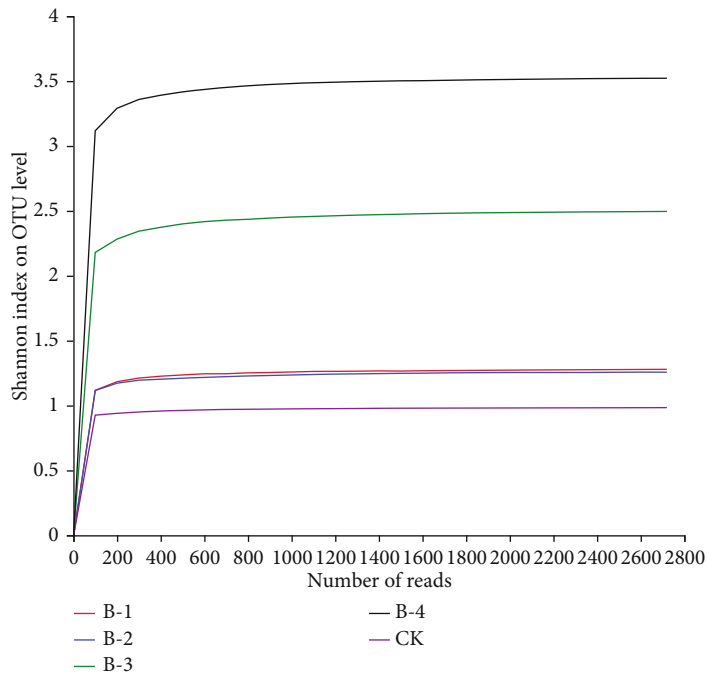

Figure 1: The Shannon-Wiener curves in different soft rot stages.

average of 103 OUTs per sample. Sequencing results showed that the coverage rate of each sample was above 99%, which could accurately reflect the real situation of the bacterial community of the sample [24]. According to the sobs index differences shown in Table 1, bacterial abundance in different onset periods was B-4 > B-3 > B-2 > B-1 > CK, indicating that the abundance and diversity of bacteria in stem tissue of pitaya changed with the progression of disease degree. Meanwhile, based on Simpson and Shannon indexes in Table 1, Simpson index was the lowest (0.090), and Shannon index was the highest (3.42) in B-4 stage (late onset), indicating that the bacterial community gradually tended to diversify during the soft rot of pitaya stem tissue. In addition, Shannon-Wiener index can reflect the relationship between species diversity and sequencing amount [25, 26]. As can be seen from Figure 1, Shannon-Wiener index curve becomes flatter with the increase of sample sequence number, indicating that the data depth of this experiment can fully reflect the microbial information in the sequenced samples. Analysis of OTUs of samples in 5 periods (Figure 2) revealed that 2, 4, 5, 20, and 34 endemic OTUs (Figure 2) were shared by the five samples of CK, B-1, B-2, B-3, and B-4, respectively.

3.2. Composition of Bacterial Community in Different Soft Rot Stages. As shown in Figure 3, except Proteobacteria and Firmicutes, Proteobacteria and Firmicutes have always been at the level of dominant phyla, while bacteria at other phyla levels have undergone great changes. From CK to B-4, Proteobacteria accounted for more than 70%, which was the dominant flora in the whole pathological process (>1%). Firmicutes were the dominant bacteria next to Proteobacteria; the abundance of Firmicutes was more than 2% in all periods. From B-2 to B-4, the abundance of Actinobacteria and Bacteroidetes showed an increasing trend and gradually established a dominant position in B-3 and B-4. Verrucomicrobia belonged to the dominant group in B-1 and B-2 stages, but with the development of disease (B-3 to B-4 stage), it gradually changed to non-dominant group (<1%).

As shown in Figure 4, a total of 116 genera of bacteria were detected in five samples. In the CK group, *Pseudomonas* was the main dominant groups accounting for 93.75%. From B-1 to B-4, *Pseudomonas*, *Enterobacter*, *Sphingomonas*, and *Sphingobacterium* were the dominant genera accounting for more than 2%. The bacterial community structure became more complex, and the species diversity became richer when the soft rot disease of pitaya stem was aggravated.

3.3. Dynamic Analysis of Bacterial Community in Different Soft Rot Stages. As shown in Figure 5, in the CK group, *Pseudomonas* of Bacteroidetes and *Enterococcus* of Firmicutes were obviously dominant. From B-1 to B-2, the abundance of *Pseudomonas*, *Enterobacter*, *Sphingosphinx*, and *Sphingosphinx* showed an increasing trend. With the soft rot grade rising to B-3 stage, *Sphingosphinx* of Bacteroides and *Enterobacter* of Firmicutes were the dominant genera. In B-4 stage, *Pseudomonas*, *Sphingomonas*, *Methylobacterium*, *Rhizobium*, *Devosia*, *Kineococcus*, *Enterobacter*, and *Aureimonas* had obvious dominant characteristics.

3.4. Core Bacterial Group and Functional Analysis during Soft Decay Period. MetaCoMET analysis of data sets from B-1 to B-4, as shown in Figure 6, showed that there were five core bacterial microbiomes at the genus level, namely,

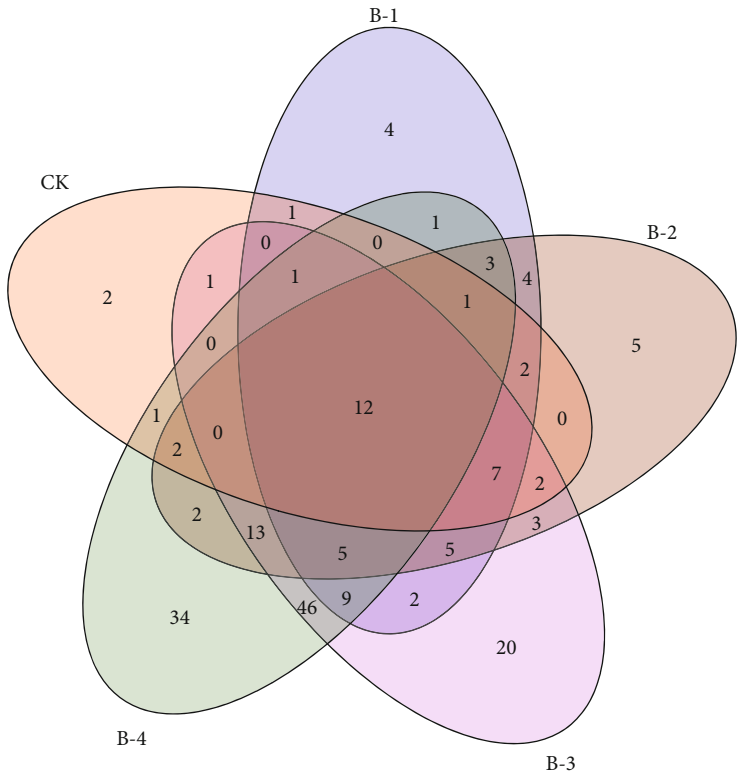

Figure 2: Analysis of OTUs from different soft rot process with Venn diagram.

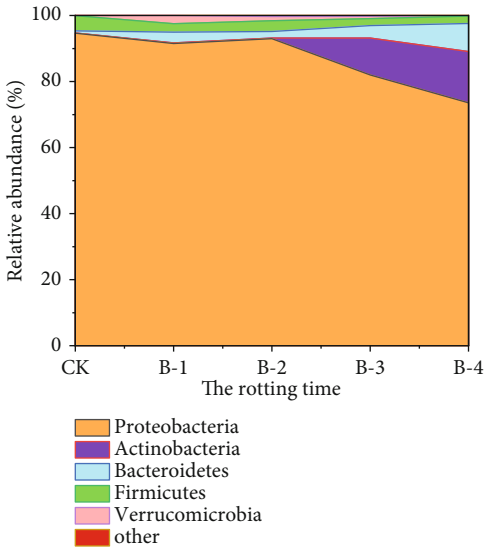

Figure 3: The stacked area graph of bacteria on phylum level.

Pseudomonas, *Sphingomonas*, *Enterobacter*, and *Sphingobacterium*. Meanwhile, Figure 7 showed that the main functional groups of the core bacterial groups in the different soft rot periods were chemoheterotrophy, aerobic chemoheterotrophy, animal parasites or symbiotics symbionts, and plant pathogens, among which chemoheterotrophs and oxidative functional groups dominated. This suggested that microbes needed to break down organic matter in the stem tissue to obtain a supply of nutrients. In the whole soft rot process, Pseudomonas played an important role in chemoheterotrophy, heterotrophy, animal parasitism, and symbiosis. It is noteworthy that, combined with the change process of species abundance, the change of species abundance of Enterobacter was synchronized with the change of plant pathogenic functional groups. With the increase of species abundance, the role of Enterobacter in plant pathogenic functional groups became more and more prominent. Therefore, the Enterobacter sequenced in this study may be a class of important plant pathogens, with certain functional potential for the occurrence of soft rot diseases.

4. Discussion

Microbial invasion is often the main cause of fruit and vegetable quality degradation. In natural ecosystems, the quality of fruit and vegetable crops is affected by soft rot pathogens from planting, harvesting to storage. Bruises, cuts, and insect bites of plants can increase the advantages of microbial colonization [27]. At present, there are few reports on the change of bacterial community in pitaya stem tissue during soft rot. Therefore, exploring and revealing the relationship between bacteria and stem soft rot can provide important reference value for the maintenance of pitaya fruit quality and disease prediction.

The occurrence of soft rot in pitaya stem changed the composition and distribution of bacterial community in stem tissue. Alpha diversity analysis showed that bacterial

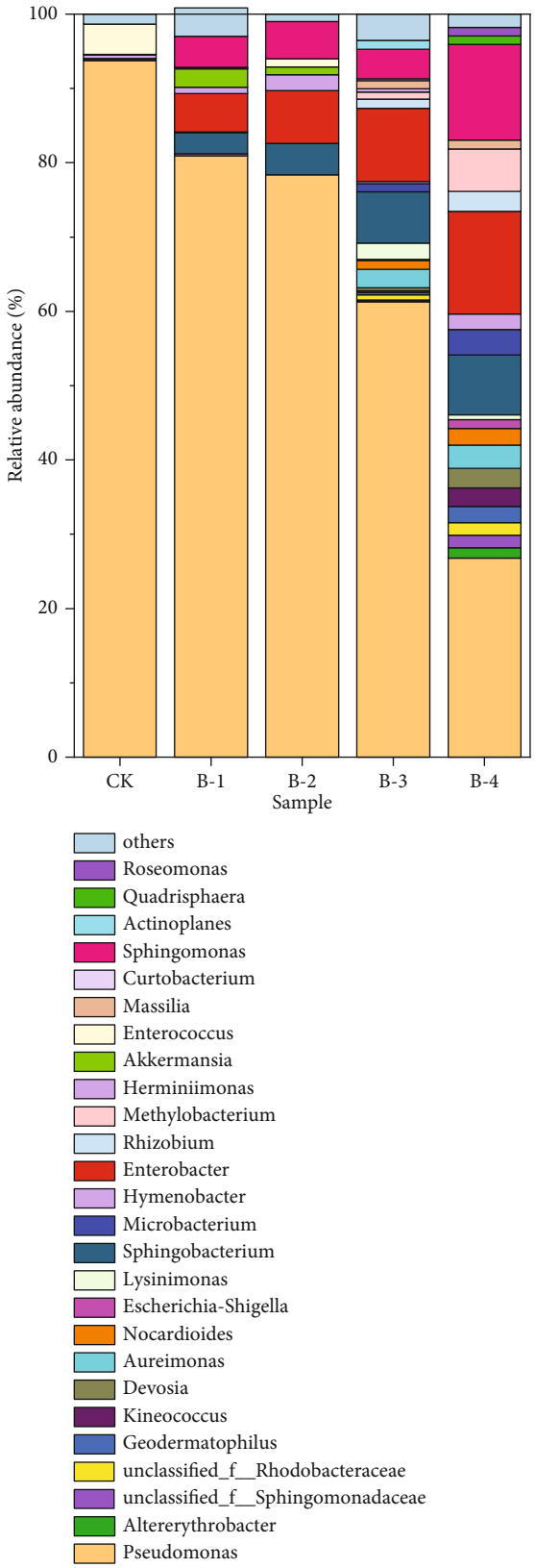

Figure 4: Histogram of sample's relative abundance on genus level.

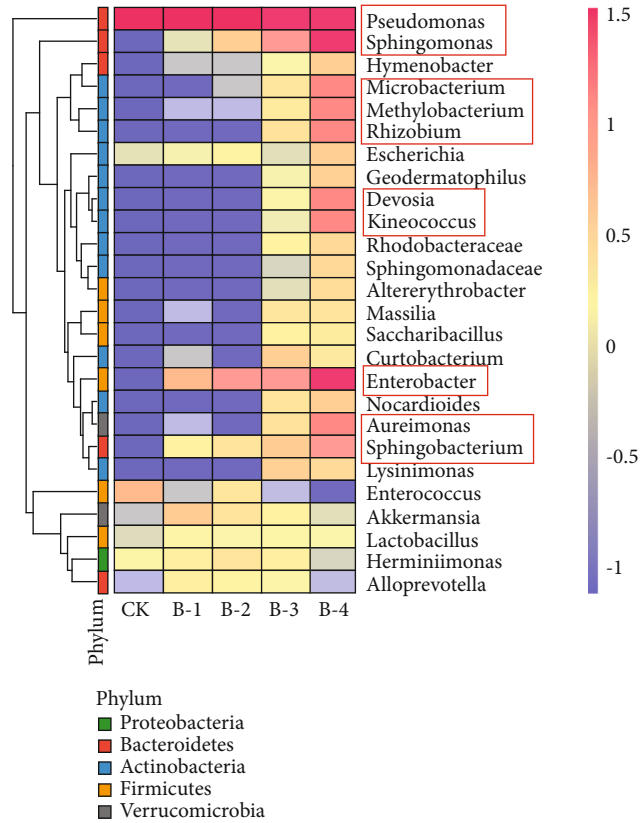

Figure 5: Heat map of the species abundance during different soft rot stages.

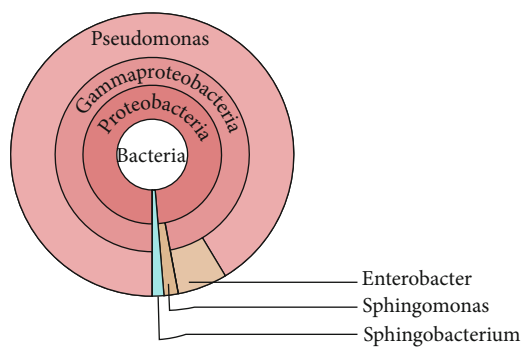

Figure 6: Core bacterial microbiota compositions during different soft rot stages.

community richness and diversity in stem tissues gradually increased with the deepening of the degree of soft rot disease. Welington et al. [28] believed that the healthy plants could only be colonized by a few dominant microorganisms, while the diseased plants without obvious diseases could recruit more community richness. This study also found a similar phenomenon: *Pseudomonas* and *Enterococcus* were the dominant bacteria in the stem tissue of the healthy pitaya. In the early stage of soft rot, there were not only Pseudomonas bacteria but also abundant *Enterobacter* and *Sphingomonas*. At the end of soft rot, the abundance and diversity of bacteria in stem tissue reached the maximum.

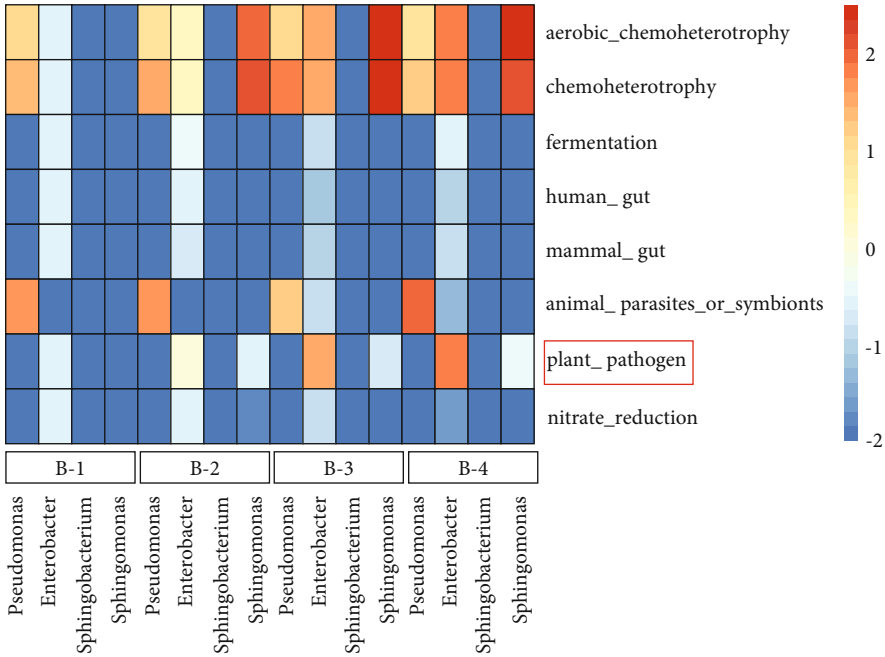

Figure 7: Changes of the functional groups of the core bacterial microbiota at different soft rot stages.

The distribution differences of OTUs in different soft rot stages indicated that there was a transient succession process in the bacterial community in the stem tissue of pitaya at different soft rot stages: the bacterial community structure was most complex when the bacterial community in the stem tissue succeeded to the end of soft rot. It can be seen that plants are a complex microecosystem, in which bacterial communities occupy a certain ecological niche and constantly compete with each other for nutrients and water in host tissues [29].

MetaCoMET analysis and FAPROTAX functional analysis showed that the functional groups of the core bacterial groups in the five soft decay stages were mainly dominated by chemoheterotrophic and oxidation-requiring functional groups. These results suggested that microorganisms need to decompose organic matter in the stem tissue to obtain a supply of nutrients. It should be noted that *Pseudomonas* and *Enterobacter* may play an important role in the occurrence of pitaya stem soft rot disease by analyzing the changes of bacterial community composition and the functional changes of core bacterial group. In healthy pitaya stem tissue, *Pseudomonas* was the dominant bacterium with the highest species abundance, accounting for 93.75%. However, with the aggravation of soft rot, the species abundance of *Pseudomonas* decreased gradually and reached the lowest value (26.8%) at the end of soft rot. Studies had showed that after inoculation with *Pseudomonas*, the fruit quality of grape and cotton can be well maintained and improved [30]. Based on this research significance, Pseudomonas bacteria can be used as an important indicator for the prediction of soft rot in pitaya in subsequent studies.

In the early stage of soft rot disease, *Enterobacter* began to colonize in the stem tissue, and its species abundance increased to the maximum (13.79%) in the late stage of soft rot disease. FAPROTAX functional analysis showed that *Enterobacter* played an increasingly important role in plant pathogenic functional groups with the increase of species abundance. *Enterobacter* was a common human pathogen in Enterobacteriaceae, which could often activate pectinase regulation pathway and cause the occurrence of plant soft rot. At present, *Enterobacter cloacae*, *Enterobacter nimipressuralis*, and *Enterobacter pyrinus* could cause soft rot in plants [14]. In recent years, studies on the harm of *Enterobacter* bacteria to fruits, vegetables, and other plants had been reported. Masyahit et al. [13] first found that *Enterobacter cloacae* could cause bacterial soft rot in stem segments of pitaya fruit and causes the disease in 36% of pitaya fruit. Lin et al. [14] first discovered *Enterobacter* bacteria in pitaya stems from Taiwan, China. According to morphological characteristics, molecular identification, pathogenicity determination, and other methods, the bacteria causing the soft rot of pitaya stem was *Enterobacter* group. Oniha and Egwari [16] isolated *Enterobacter* spp. bacteria that could cause soft rot from the fruit and stem of *Carica papaya* L. In addition to the harmful effects of *Enterobacter* bacteria on fruits, researchers had observed the symptoms of decay in cucumbers, carrots, cabbage, and onions inoculated with *Enterobacter* spp. [31]. The *Enterobacter* bacteria obtained in this test may play an important role in the occurrence of soft rot of pitaya stem, but whether it has the above soft rot pathogenic ability is not clear and needs to be isolated and identified. It is worth discussing that studying the change characteristics of bacterial community in plants can not only provide help for predicting plant diseases but also reveal the role of dominant microorganisms in orchard ecosystem.

5. Conclusion

In conclusion, the dominant bacterial genera with the stem samples of healthy pitaya were *Pseudomonas* and *Enterococcus*. From the initial infection stage to the late infection stage, the dominant bacteria in pitaya stems were *Pseudomonas*, *Enterobacter*, *Sphingomonas*, and *Sphingobacterium*. At the terminal stage, the bacterial genera with dominance in soft rot pitaya stems were *Pseudomonas*, *Sphingomonas*, *Sphingobacterium*, *Microbacterium*, *Methylobacterium*, *Rhizobium*, *Devosia*, *Kineococcus*, *Enterobacter*, and *Aureimonas*, of which *Pseudomonas*, *Enterobacter*, *Sphingomonas*, and *Sphingobacterium* were the core microbiota of bacteria during the stages of infection. Meanwhile, the functional groups of these core microbiomes were chemoheterotrophy, aerobic chemoheterotrophy, animal parasites or symbionts, and plant pathogen. The *Enterobacter* and *Pseudomonas* bacteria may play an important role in causing soft rot disease of pitaya stems.

Data Availability

All data included in this study are available upon request by contact with the corresponding author.

Conflicts of Interest

The authors declare no conflict of interest.

Acknowledgments

This research was funded by the Guizhou Outstanding Young Scientific and Technological Talents Training Program (grant number [2019]5642) and the Guizhou Fine Fruit Modern Agricultural Industrial Technology System (grant number GZCYTX2018).

References

[1] M. Li, M. J. Hu, Z. Y. Gao, D. R. Xue, D. P. Yang, and B. Yang, "Identification and biological characteristics of a pathogen causing fruit rot of *Hylocereus undatus* (Haw.) Britt. et. Rose," *Chinese Journal of Tropical Crop*, vol. 33, no. 11, pp. 2044–2048, 2012.

[2] T.-f. Ma, B. Yang, Y. Yu et al., "Market disease pathogens detection of imported fruits in Shanghai," *Agricultural Sciences in China*, vol. 8, no. 9, pp. 1087–1096, 2009.

[3] Z. Yingying, G. Zhaoyin, L. Min, C. Liang, and H. Meijiao, "Identification and biological characteristics of dragon fruit (Hylocereus undatus Britt) Fusarium rot pathogen," *Chinese Journal of Tropical Crop*, vol. 37, no. 1, pp. 164–171, 2016.

[4] L. W. Guo, Y. X. Wu, H. X. He, Z. C. Mao, P. B. He, and Y. Q. He, "A new fruit rot disease in *Hylocereus costaricensis* in Yunnan Province of China," *Journal of Fruit Science*, vol. 31, no. 1, pp. 111–114, 2014.

[5] F. Zheng, G. Xu, F. Qiu, F. Q. Zheng, L. Zheng, and C. P. Xie, "Identification and biological characteristics of the pathogenic fungus causing the soft rot of Hylocereus costaricensis in Hainan, China," *Plant Protection*, vol. 45, no. 4, pp. 137–142, 2019.

[6] Z. J. Cui, Y. W. Wang, Y. Yu, and L. Xu, "Pathogens analysis of soft rot disease of imported pitaya in Shanghai," *Microbiology China*, vol. 38, no. 10, pp. 1499–1506, 2011.

[7] W. Zheng, Y. Q. Cai, and L. Y. Dai, "Research progress on main diseases and insect pests of pitaya," *Guizhou Agricultural Sciences*, vol. 6, pp. 139–142, 2007.

[8] S. Taba, N. Miyahira, K. Nasu, T. Takushi, and Z. Moromizato, "Fruit rot of strawberry pear (pitaya) caused by Bipolaris cactivora," *Journal of General Plant Pathology*, vol. 73, no. 5, pp. 374–376, 2007.

[9] Z. L. Wang and Z. Z. Lin, "Fruit rot of pitaya and stem rot of cacti in Taiwan," *Plant Pathology Bulletin*, vol. 14, no. 4, pp. 269–274, 2005.

[10] Q. L. Liang, J. Wei, X. Y. Li, and L. Q. Wang, "Identification on causal agent of dragonfruit stem rot and indoor determination of fungicide toxicity," *South China Fruits*, vol. 40, no. 1, pp. 9–12, 2011.

[11] C. L. Yuan, W. F. Zhang, and H. X. Yuan, "Preliminary study on disease investigation and control measures of pitaya in Yuexi area," *South China Fruit*, vol. 33, no. 2, pp. 49-50, 2004.

[12] W. J. Sang, D. F. Wang, Q. Wei, R. Yang, G. Q. Fan, and Y. L. Jin, "Preliminary identification of pitaya disease in Guizhou province," *Journal of Mountain Agriculture and Biology*, vol. 26, no. 3, pp. 267–270, 2007.

[13] M. Masyahit, K. Sijam, Y. Awang, and M. Ghazali, "First report on bacterial soft rot disease on dragon druit (*Hylocereus* spp.) caused by Enterobacter cloacae in Peninsular Malaysia," *International Journal of Agriculture and Biology*, vol. 11, no. 6, pp. 1560–8530, 2009.

[14] W. Z. Lin, R. F. Liao, X. H. Chen et al., "Isolation and identification of the pathogen causing soft rot in *Hylocereus undatus*," *Acta Phytopathologica Sinica*, vol. 45, no. 2, pp. 220–224, 2015.

[15] R. Y. Zhang, X. S. Zhao, Q. Z. Tan, and C. H. Zhu, "First report of bacterial stem rot disease caused by *Paenibacillus polymyxa* on *Hylocereus undulatus* in China," *Plant Disease*, vol. 101, no. 6, p. 1031, 2017.

[16] M. Oniha and L. Egwari, "Fruit, leaf and stem diseases of *Carica papaya* L," *Journal of Agriculture and Food*, vol. 3, no. 1, article 398-4.7, 2015.

[17] L. Xu, X. W. Li, and K. N. Teng, "Detection and control of postharvest pathogenic fungi in fruits and vegetables," *Food Science*, vol. 7, pp. 155–158, 2003.

[18] D. Wei, Q. H. Wu, Y. P. Liu et al., "Microbial community diversity and its characteristics in Magnolia Officinalis Cortex "sweating" process based on high-throughput sequencing," *Zhongguo Zhong Yao Za Zhi*, vol. 44, no. 24, pp. 5405–5412, 2019.

[19] J. Walter, G. W. Tannock, A. Tilsala-Timisjarvi et al., "Detection and identification of gastrointestinal Lactobacillus species by using denaturing gradient gel electrophoresis and species-specific PCR primers," *Applied and Environmental Microbiology*, vol. 66, no. 1, pp. 297–303, 2000.

[20] Y. Youngseob, L. Changsoo, and K. Jaai, "Group-specific primer and probe sets to detect methanogenic communities using quantitative real-time polymerase chain reaction," *Biotechnology and Bioengineering*, vol. 89, no. 6, pp. 670–679, 2005.

[21] C. E. Robert, "UPARSE: highly accurate OTU sequences from microbial amplicon reads," *Nature Methods*, vol. 10, no. 10, pp. 996–998, 2013.

[22] C. B. Dong, Z. Y. Zhang, Y. F. Han, and Z. Q. Liang, "Research and application prospects of core microbiome," *Mycosystema*, vol. 38, no. 1, pp. 1–10, 2019.

[23] S. Louca, L. W. Parfrey, and M. Doebeli, "Decoupling function and taxonomy in the global ocean microbiome," *Science*, vol. 353, no. 6305, pp. 1272–1277, 2016.

[24] C. C. Liu, S. B. Feng, Q. Wu et al., "Flavor-related microbiota and their flavor metabolism during highland barley baijiu fermentation," *Microbiology China*, vol. 47, no. 1, pp. 151–161, 2020.

[25] W. H. Mao, S. L. Wu, and X. Zhang, "Establish and application of the high throughput sequencing method for soil microbial 16S rDNA using Ion Torrent PGM," *Acta Agriculturae Zhejiangensis*, vol. 27, no. 12, pp. 2165–2170, 2015.

[26] U. Kõljalg, R. H. Nilsson, K. Abarenkov et al., "Towards a unified paradigm for sequence-based identification of fungi," *Molecular Ecology*, vol. 22, no. 21, pp. 5271–5277, 2013.

[27] A. O. Charkowski, "Decaying signals: will understanding bacterial–plant communications lead to control of soft rot?," *Current Opinion in Biotechnology*, vol. 20, no. 2, pp. 178–184, 2009.

[28] W. L. Araújo, J. Marcon, W. Maccheroni Jr., J. D. Van Elsas, J. W. Van Vuurde, and J. L. Azevedo, "Diversity of endophytic bacterial populations and their interaction with Xylella fastidiosa in citrus plants," *Applied and Environmental Microbiology*, vol. 68, no. 10, pp. 4906–4914, 2002.

[29] M. M. Wei, X. C. Liu, Y. H. He et al., "Biochar inoculated with *Pseudomonas putida* improves grape (*Vitis vinifera* L.) fruit quality and alters bacterial diversity," *Rhizosphere*, vol. 16, pp. 100261–100269, 2020.

[30] L. X. Yao, Z. S. Wu, Y. Y. Zheng, I. Kaleem, and C. Li, "Growth promotion and protection against salt stress by Pseudomonas putida Rs-198 on cotton," *European Journal of Soil Biology*, vol. 46, no. 1, pp. 49–54, 2010.

[31] B. C. Adebayo-Tayo, N. N. Odu, C. U. Esen, and I. O. Okonko, "Microorganisms associated with spoilage of stored vegetables in Uyo Metropolis, Akwa Ibom State, Nigeria," *Nature and Science*, vol. 10, no. 3, pp. 23–32, 2012.

Hindawi
Journal of Chemistry
Volume 2022, Article ID 8646557, 4 pages
https://doi.org/10.1155/2022/8646557

Research Article

Design, Synthesis, and Antifungal Activity of Novel Benzimidazole Derivatives Bearing Thioether and Carbamate Moieties

Lei Yang

No. 1 Middle School Affiliated to Central China Normal University, Guiyang School, Guiyang 550014, China

Correspondence should be addressed to Lei Yang; leiyangchem@126.com

Received 17 March 2022; Revised 10 April 2022; Accepted 18 April 2022; Published 4 May 2022

Academic Editor: Pei Li

In this study, a series of benzimidazole derivatives bearing thioether and carbamate moieties have been synthesized and evaluated for their *in vitro* antifungal activity against *Cytospora mandshurica*, *Thanatephorus cucumeris*, *Botrytis cinerea*, *Verticillium daliae*, *Phytophthora infestans*, and *Gibberella zeae* by the mycelium growth rate method. The result of bioassay demonstrated that most of the compounds had certain antifungal activity. Especially, compound E11 revealed better antifungal activity against *Verticillium daliae* and *Phytophthora infestans* at 50 μg/mL, with the inhibition rates of 70% and 75%, respectively, than those of albendazole (38% and 61%, respectively). To the best of our knowledge, it is the first study on the synthesis and antifungal activity of benzimidazole derivatives containing thioether and carbamate moieties.

1. Introduction

In several decades, the fungal diseases are caused by fungal pathogens, leading to severe losses to agriculture and horticulture crop production worldwide and constitute an emerging threat to the global food security [1–5]. Among the drugs to treat fungal infection, benzimidazole derivatives as potent and safe antifungal agents have attracted more and more attention for a long time [6–8]. Carbendazol, Benomyl, Thiabendazole, *etc.*, have been widely used in antifungal therapy. However, the extensive use of those antifungal drugs has led to the resistance to drug treatment. Therefore, development of new benzimidazole drugs for antifungal treatment is pressing need.

Benzimidazole derivatives have received much attention in synthesis and bioassay investigations as a result of their extremely important role in medicinal chemistry and agrochemicals [9–12]. Many investigations on the structures and bioactivities of benzimidazole compounds have been carried out. In 2006, Madkour et al. synthesized a series of 2-substituent benzimidazole derivatives, and these compounds demonstrated good inhibitory effect against *Botrytis cinerea* and *Fusarium solani* [13]. In 2010, Mobinikhaledi et al. investigated 2-substituted benzimidazole derivatives through the mycelium growth rate method test in vitro, and the result indicated that most compounds displayed good inhibitory effect antifungal bioactivities [14]. In 2012, Zhang et al. found a series of novel 1*H*-benzimidazol-1-yl acetates and 1*H*-benzimidazol-1-yl propionates containing 1*H*-1,2,4-triazole moiety. The antifungal activities of the target compounds against *Botrytis cinerea* and *Sclerotinia sclerotiorum* were evaluated by mycelial growth rate method. All the target compounds exhibited higher activities against *Botrytis cinerea*, with the E C_{50} values of 7.96–21.74 mg/mL, than that of carbendazim [15]. In 2013, Bai et al. found that 2-chloromethyl-1*H*-benzimidazole derivatives showed strong growth inhibition of *Cytospora* sp., *Colletotrichum gloeosporioides*, *Botrytis cinerea*, *Alternaria solani*, and *Fusarium solani* [16]. In 2016, a series of novel *N*-alkylated benzimidazole derivatives were synthesized and bioassay results showed that the target compounds revealed excellent antifungal activity against *Bacillus subtilis* and *Bacillus proteus* [17].

Herein, inspired by those description facts above and in connection of our work on benzimidazole derivatives, using albendazole as the lead compound, we design and synthesize

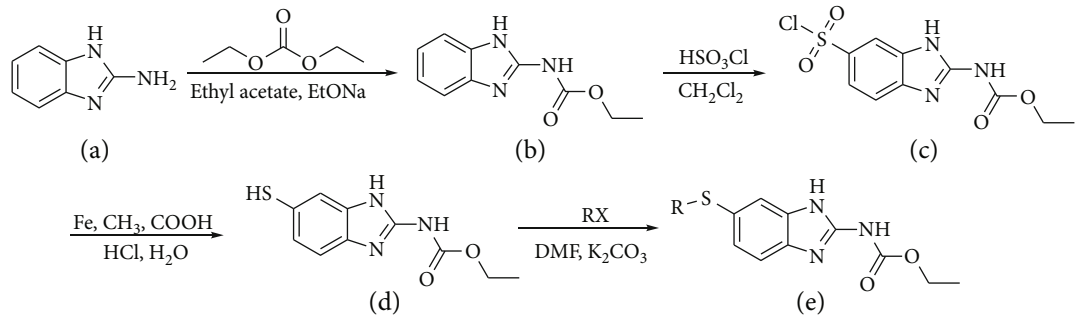

E1: R=CH_3
E2: R=CH_2H_5
E3: R=Ph_2CH_2
E4: R=3–CH_3–$PhCH_2$
E5: R=4–F–$PhCH_2$
E6: R=4–Cl–$PhCH_2$
E7: R=4–NO_2–$PhCH_2$
E8: R=2,4–2Cl–$PhCH_2$
E9: R=2–$PyCH_2$
E10: R=2–Cl–6–$PyCH_2$
E11: R=$COOCH_3$
E12: R=$COOCH_2CH_2$
E13: R=CH_2COOCH_3
E14: R=$CH_2COOCH_2CH_3$
E15: R=3,4,4–3F–$CCCH_2CH_2$

Scheme 1: Synthetic pathway for the target compounds.

a series of benzimidazole derivatives containing thioether and carbamate moieties and evaluated for their in vitro antifungal activity against *Cytospora mandshurica* (*C. mandshurica*), *Thanatephorus cucumeris* (*T. cucumeris*), *Botrytis cinerea* (*B. cinerea*), *Verticillium daliae* (*V. daliae*), *Phytophthora infestans* (*P. infestans*), and *Gibberella zeae* (*G. zeae*).

2. Materials and Methods

2.1. Synthesis. Melting points were determined using an XT-4 binocular microscope (Beijing Tech Instrument Co., China) and left uncorrected. The ^{1}H and ^{13}C NMR spectra (solvent DMSO-d_6) were measured with a JEOL-ECX 500 NMR spectrometer operating at room temperature with using TMS as an internal standard. The course of the reactions was monitored by thin-layer chromatography analysis on silica gel GF254. All solvents were freshly distilled or purified according to standard procedures. All reagents were purchased from Accela ChemBio Co., Ltd (Shanghai, China).

2.2. Preparation Procedure of Intermediate D. A mixture of 2-amino benzimidazole (0.01 mol), diethyl carbonate (10 mL), and EtONa (0.02 mol) was stirred in ethyl acetate (20 mL), and the reaction was reacted at 90°C and monitored by TLC. After complication of the reaction, the resulting mixture was filtrated and washed with ethyl acetate and dried under vacuum to get intermediate B.

A mixture of intermediate B (0.01 mol) and sulfonic acid chloride (5 mL) was stirred in ethylene dichloride (20 mL), and the reaction was reacted for 0.5 h at 0°C and then reacted for 3 h at 60°C and monitored by TLC. After complication of the reaction, the resulting mixture was washed with alcohol, filtrated, and dried under vacuum to get intermediate C.

A mixture of intermediate C (0.01 mol) and Fe (0.02 mol) was stirred in a mixture of HCl (5 mL), HCOOH (5 mL), and H_2O (10 mL). The reactions were reacted for 10 h at 60°C. Then, the pH values of the reaction mixture were regulated to 4-5 by 5% NaOH, solid precipitation, and filtration and dried under vacuum to obtain intermediate D.

Table 1: Effect of different reaction condition on the yields of intermediate C.

Entry	Solvent	Temp (°C)	Time (h)	Yield (%)
1	Ethyl acetate	0	8	10
2	DMF	0	8	0
3	CH_3CN	0	8	<10
4	Acetone	0	8	<10
5	THF	0	8	<10
6	CH_2Cl_2	0	3	100

Table 2: Effect of different reaction condition on the yields of intermediate D.

Entry	Reduction	Acid	Temp (°C)	Time (h)	Molar equivalent (C : reduction)	Yield (%)
1	Zn	HCl	60	8	1 : 4	-
2	Mg	HCl	60	8	1 : 4	-
3	Fe	HCl	60	8	1 : 4	27
4	Fe	HCl	20	8	1 : 4	13
5	Fe	H_2SO_4	60	8	1 : 4	18
6	Fe	HNO_3	60	8	1 : 4	12

2.3. Preparation Procedure of the Target Compounds E1-E15. A mixture of intermediate D (0.01 mol), K_2CO_3 (0.02 mol), and RX (0.012 mol) was stirred in DMF (20 mL). The reactions were reacted for 5 h at room temperature. Then, the residue was filtered, dried under vacuum, and recrystallized from ethanol to get the target compounds E1-E15.

Table 3: The in vitro antifungal activity of the target compounds against *C. mandshurica*, *T. cucumeris*, *B. cinerea*, *V. daliae*, *P. infestans*, and *G. zeae* at 50 μg/mL.

Compounds	Inhibition rate (%)				
	T. cucumeris	*V. daliae*	*P. infestans*	*G. zeae*	*C. mandshurica*
E1	17 ± 1.5	39 ± 0.7	3 ± 2.2	25 ± 1.4	26 ± 1.9
E2	19 ± 3.2	19 ± 2.5	0.00	4 ± 1.6	34 ± 1.4
E3	23 ± 1.0	0	1 ± 0.0	10 ± 3.0	18 ± 1.0
E4	42 ± 1.0	12 ± 0.9	27 ± 0.3	28 ± 2.9	9 ± 3.1
E5	7 ± 0.7	5 ± 0.9	8 ± 1.8	12 ± 5.5	29 ± 3.1
E6	6 ± 0.8	8 ± 1.4	24 ± 3.0	9 ± 0.6	23 ± 0.9
E7	17 ± 2.5	13 ± 1.8	7 ± 1.1	20 ± 2.5	10 ± 1.4
E8	10 ± 0.6	14 ± 4.0	14 ± 3.1	20 ± 2.8	16 ± 2.3
E9	15 ± 2.6	9 ± 0.9	2 ± 0.0	4 ± 0.7	1 ± 1.3
E10	2 ± 1.5	19 ± 1.5	7 ± 0.9	19 ± 3.1	30 ± 1.9
E11	9 ± 2.8	70 ± 0.1	75 ± 0.8	12 ± 0.6	11 ± 2.7
E12	3 ± 8.9	36 ± 1.2	22 ± 1.4	0	8 ± 2.3
E13	14 ± 2.8	43 ± 2.5	0.00	3 ± 1.7	2 ± 2.8
E14	17 ± 1.1	0	3 ± 10	0	0
E15	41 ± 2.9	69 ± 3.3	22 ± 3.4	15 ± 0.7	44 ± 1.8
Albendazole	61 ± 1.3	38 ± 0.1	61 ± 2.4	32 ± 1.4	32 ± 1.4

2.4. Bioactivity Assay. All the target compounds E1-E15 were evaluated for their in vitro antifungal activity against *C. mandshurica*, *T. cucumeris*, *B. cinerea*, *V. daliae*, *P. infestans*, and *G. zeae* by the growth rate method in comparison with albendazole at 50 μg/mL [18]. Each treatment was repeated 3 times. Inhibition rate I (%) is calculated by the following formula, where C represents the diameter of control group (not treated with compound) and T represents the diameter of treatment group.

$$I\,(\%) = \frac{(C - T)}{(C - 0.4)} \times 100. \quad (1)$$

3. Results and Discussion

3.1. Chemistry. Using 2-amino benzimidazole as the starting material, as shown in Scheme 1, a series of novel benzimidazole derivatives bearing thioether and carbamate moieties were synthesized with the yields of 16.7%-36.4%. Their structures were characterized by nuclear magnetic resonance (^{1}H NMR and ^{13}C NMR), and the physical characteristics ^{1}H NMR, and ^{13}C NMR data for all the target compounds E1-E15 can be found in the Supplemental Materials (available here).

High product yield, good molar equivalent, suitable reaction temperature, and short reaction time encouraged us to apply previously reported methods under the optimized reaction conditions with the aim of expanding their applications in synthesis and medicine field. Thus, we used the synthesis of intermediates C and D as the model reactions with some modifications about the reaction solvent, reaction reduction and acid, reaction temperature and time, and molar equivalent of intermediate C : reduction. As shown in Table 1, the highest yield (100%) of intermediate C was obtained when the reaction solvent, reaction temperature, and reaction time were CH_2Cl_2, 0°C, and 3 h, respectively. Meanwhile, Table 2 shows that the highest yield (27.4%) of intermediate D was obtained when the reduction, acid, and reaction temperature were Fe, HCl, and 60°C, respectively, at a reaction time of 8 h and a molar equivalent of intermediate C : reduction of 1 : 4.

3.2. Antifungal Activity Test. The results of the preliminary bioassays, as listed in Table 3, indicated that most of the compounds had certain in vitro antifungal activity against *C. mandshurica*, *T. cucumeris*, *B. cinerea*, *V. daliae*, *P. infestans*, and *G. zeae* at 50 μg/mL. Table 3 shows that compounds E11 and E15 showed better in vitro antifungal activity against *V. daliae*, with the inhibition rates of 70% and 69%, respectively, than albendazole (38%). Meanwhile, compound E11 showed superior in vitro antifungal activity against *P. infestans* (75%) to albendazole (61%). In addition, compound E15 showed good in vitro antifungal activity against *C. mandshurica* (44%), which were superior to albendazole (32%).

4. Conclusion

In this study, 15 new benzimidazole derivatives bearing thioether and carbamate moieties were synthesized. Bioassay results showed some of the target compounds revealed superior antifungal activity to that of albendazole. It was demonstrated that the benzimidazole derivatives bearing thioether and carbamate moieties can be used to develop potential agrochemicals.

Data Availability

All data included in this study are available upon request by contact with the corresponding author.

Conflicts of Interest

The author declares that no conflicts of interest.

Supplementary Materials

The supporting information contained ^{1}H NMR and ^{13}C NMR spectra data for all the target compounds E1–E15. *(Supplementary Materials)*

References

[1] R. S. Goswami and H. C. Kistler, "Heading for disaster: *Fusarium graminearum* on cereal crops," *Molecular Plant Pathology*, vol. 5, no. 6, pp. 515–525, 2004.

[2] M. C. Fisher, D. Henk, C. J. Briggs et al., "Emerging fungal threats to animal, plant and ecosystem health," *Nature*, vol. 484, no. 7393, pp. 186–194, 2012.

[3] A. Anna and K. Wolfgang, "Rhynchosporium commune: a persistent threat to barley cultivation," *Molecular Plant Pathology*, vol. 13, no. 9, pp. 986–997, 2012.

[4] R. Dean, J. A. L. Van Kan, Z. A. Pretorius et al., "The top 10 fungal pathogens in molecular plant pathology," *Molecular Plant Pathology*, vol. 13, no. 4, pp. 414–430, 2012.

[5] B. Scherm, V. Balmas, F. Spanu et al., "*Fusarium culmorum*: causal agent of foot and root rot and head blight on wheat," *Molecular Plant Pathology*, vol. 14, no. 4, pp. 323–341, 2013.

[6] H. Göker, R. Ertan, H. Akgün, and N. Yulug, "Synthesis and antifungal activity of some new benzimidazole derivatives," *Archiv der Pharmazie*, vol. 324, no. 5, pp. 283–286, 1991.

[7] L. Srikanth, V. Varun Raj, N. Raghunandan, and L. Venkateshwerlu, "ChemInform Abstract: Recent advances and potential pharmacological activities of benzimidazole derivatives," *ChemInform*, vol. 42, no. 40, 2011.

[8] F. Alasmary, A. Snelling, M. Zain, A. Alafeefy, A. Awaad, and N. Karodia, "Synthesis and evaluation of selected benzimidazole derivatives as potential antimicrobial agents," *Molecular Plant Pathology*, vol. 20, no. 8, pp. 15206–15223, 2015.

[9] S. Khabnadideh, Z. Rezaei, K. Pakshir, K. Zomorodian, and N. Ghafari, "Synthesis and antifungal activity of benzimidazole, benzotriazole and aminothiazole derivatives," *Research in Pharmaceutical Sciences*, vol. 7, no. 2, pp. 65–72, 2012.

[10] V. M. Reddy and K. R. Reddy, "Synthesis and biological evaluation of some novel-3-(5-substituted benzimidazol-2-yl)-5-arylisoxazolines," *Chinese Chemical Letters*, vol. 21, no. 10, pp. 1145–1148, 2010.

[11] J. M. Yi, X. L. Ni, X. Xiao et al., "Complexation of sym-bis(benzimidazole)-2,20-ethylene salts with cucurbit[6]uril derivatives: a potential axle molecule for pseudorotaxanes," *Chinese Chemical Letters*, vol. 24, no. 5, pp. 362–366, 2013.

[12] X. J. Wang, M. Y. Xi, J. H. Fu et al., "Synthesis, biological evaluation and SAR studies of benzimidazole derivatives as H_1-antihistamine agents," *Chinese Chemical Letters*, vol. 23, no. 6, pp. 707–710, 2012.

[13] H. M. F. Madkour, A. A. Farag, S. S. Remses, and N. A. A. Ibrahiem, "Synthesis and fungicial activity of new imidazoles from 2-(choloromethly)-1*H*-benzimidazole," *Phosphorus, Sulfur, and Silicon and the Related Elements*, vol. 181, no. 2, pp. 255–265, 2006.

[14] A. Mobinikhaledi, N. Foroughifar, M. Kalhor, and M. Mirabolfathy, "Synthesis and antifungal activity of novel 2-benzimidazoleyllimino-5-arylidene-4-thiazolidinonrs," *Journal of Heterocyclic Chemistry*, vol. 47, no. 1, pp. 77–80, 2009.

[15] P. Z. Zhang, S. F. Zhou, T. R. Li, and L. Jiang, "Efficient synthesis and in vitro antifungal activityof 1H-benzimidazol-1-yl acetates/propionates containing 1*H*-1,2,4-triazole moiety," *Chinese Chemical Letters*, vol. 23, no. 12, pp. 1381–1384, 2012.

[16] Y. B. Bai, A. L. Zhang, J. J. Tang, and J. M. Gao, "Synthesis and antifungal activity of 2-chloromethyl-1*H*-benzimidazole derivatives against phytopathogenic fungi in vitro," *Journal of Agricultural and Food Chemistry*, vol. 61, no. 11, pp. 2789–2795, 2013.

[17] J. Wen, Y. L. Luo, H. Z. Zhang, H. H. Zhao, C. H. Zhou, and G. X. Cai, "A green and convenient approach toward benzimidazole derivatives and their antimicrobial activity," *Chinese Chemical Letters*, vol. 27, no. 3, pp. 391–394, 2016.

[18] L. Yu, L. Xiao, P. Li, J. Chi, J. Li, and S. Tan, "Synthesis and bioactivity evaluation of novel thiochroman-4-one derivatives incorporating carboxamide and 1,3,4-thiadiazole thioether moieties," vol. 2022, Article ID 5354088, Journal of Chemistry, 2022.

Hindawi
Journal of Chemistry
Volume 2022, Article ID 6249042, 9 pages
https://doi.org/10.1155/2022/6249042

Research Article

Study on the Absorption and Conduction Properties of Vanisulfane in Tobacco

Xingang Meng,[1,2] **Fei Li**,[2] **and Qian Huang**[3]

[1]*College of Biological and Environmental Engineering, Jingdezhen University, Jiangxi 333000, China*
[2]*Jiangxi Key Laboratory of Plant Resources and Biodiversity, Jingdezhen 333400, China*
[3]*Jingdezhen Nursing School, Jingdezhen 333000, China*

Correspondence should be addressed to Xingang Meng; 15885007970@163.com

Received 20 December 2021; Accepted 5 March 2022; Published 22 March 2022

Academic Editor: Ajaya Kumar Singh

The purposes of this study were to explore the systemic properties of vanisulfane in tobacco plant and to provide a reference for the rational use of vanisulfane in the field. After the tobacco plants were treated by hydroponics and foliar spraying, the contents of vanisulfane in root and stem leaf were detected by high-performance liquid chromatography tandem high-resolution mass spectrometry (UPLC-HRMS), and the position of vanisulfane in root and stem leaf was real-time observed through fluorescence two-photon confocal microscope. UPLC-HRMS results showed that the contents of vanisulfane in root and stem leaf gradually increased with the extension of processing time, and after 12 h treatment, the contents of vanisulfane in root and stem leaf reached the maximum levels of 31.95 and 0.215 mg/kg, respectively. In addition, fluorescence two-photon confocal microscope results showed that vanisulfane could observe in the root and stem leaf. These results showed that vanisulfane had excellent upward and downward of systemic in tobacco plants, which is helpful to guide a reference for the rational use of vanisulfane in the field.

1. Introduction

Vanisulfane, 2,2′-(((4-((4-chlorobenzyl)oxy)-3-methoxyphenyl) methylene) bis-(2-hydroxyethyl) dithioacetal (Figure 1), is a novel antiviral agent that exhibits pronounced protection and curative activities against cucumber mosaic virus (CMV) with the half-maximal effective concentration (EC_{50}) values of 186.2 and 206.3 μg/mL, respectively, which are superior to those of the commercial agents, such as ribavirin (766.5 and 858.2 μg/mL, respectively), dufulin (465.4 and 471.2 μg/mL, respectively), and ningnanmycin (405.3 and 426.1 μg/mL, respectively) [1]. Vanisulfane, whose CAS registry number and patent number are 2088490-79-1 and CN106467478A, was developed as a new dithioacetal class of antiviral agent. The patent of vanisulfane (CN106467478A) has been granted by the State Intellectual Property Office, the People's Republic of China in March 2017.

In the last decades, many studies have reported the fluorescent label detection of other drugs [2–5]. Because farmers lack the means to carry out in situ assessment of leaf cover in real-time, they often overuse pesticides in order to prevent pests due to insufficient leaf coverage. In order to replace the excessive use of pesticides, a fluorescence method has been developed that can be quickly evaluated and used in the field to detect pesticides on plant leaves [6]. Ivy leaves were selected to study the fluorescence method for quickly assessing the coverage of pesticides and to overcome the matrix effects related to plant fluorescence emission and physiologicalspectral interferences. The results showed that fluorescent labeling agents in nano- and microcrystallites forms can be used to overcome matrix effects. By studying the characteristics of fluorescence quenching/enhancement, spectral shifts, and fluorescence lifetimes, it can be found that these spectral features are adequate for mapping the

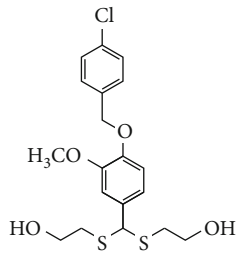

Vanisulfane

Figure 1: The structure of vanisulfane.

pesticides on plant surfaces to assess their coverage [7]. Compared to other fluorophores, development of quantum dot (QD) based excellent and unique optical properties and have high fluorescence quantum yields has gained momentum in recent years. Their applications as fluorescent probes in the detection of pesticides in different media (including water, fruits, and vegetables) were studied. The low detection limits reported demonstrate the potential use of these methods as alternatives to expensive and time-consuming conventional techniques [8]. The fluorescence analysis method for detecting three organophosphorus pesticides using magnetic-assisted FAM-aptamer as probes was studied. The results showed that choosing 37°C and 150 min as the best combination temperature and time, respectively, the developed method exhibited a higher selectivity for organophosphorus pesticides (OPs) whose aptamers had the common sequence and trueness of the MA-FA method [9]. Many studies have shown that naringenin is a key signaling molecule in the control of root nodulation, a prerequisite for the plant nitrogen fixation. In this experiment, the appropriate positions of fluorescent labeling were found at the six chemically available positions of the flavonone core of naringenin. Fluorescence labeling was used to detect the bindings of naringenin to nod-D after its entry into Rhizobium cells. In the corresponding fluorescence imaging experiments, it was observed that the entry of naringin into living Rhizobium cells was clear [10]. Methods with fluorescent labels have the potential to achieve the low limits of detection (LOD) imposed by legislation when interferences resulting from the sample matrix are reduced. In heterogeneous test formats, the background fluorescence inherent to real samples is reduced by means of a physical separation step shows that it is feasible to detect and accurately determine pesticides in low-limit real environmental samples [11]. Obviously, literature studies have shown that fluorescent labeling plays an important role in drug detection [12–14].

In addition, there is no literature report on the systemic conduction of vanisulfane in plants. Therefore, we investigated the systemic transmission of other drugs in plants as a reference [15–17]. The present investigation indicates that lignin is the most important sorbent responsible for the adsorption of pesticides in the apoplast. The adsorption of five labeled systemic fungicides and one herbicide, on ligins (stems of pepper plants and cotton plants, 120 and 90 days old, were used for lignin preparations) from three kinds of plant stems and on other components of plant tissue, was investigated. The dual character of carbendazim-lignin binding is further corroborated adsorption of systemic fungicides by plant tissues by its decreased adsorption on lignin in the presence of mineral salts, on the one hand, and its increased binding to methylated cellulose on the other hand [18]. With the advent of industrialization, a variety of used chemicals and their derivatives will eventually enter the soil and pose a threat to plants. Some papers focus on the plant uptake capacity of various contaminants of emerging concern (CEC) in soil, such as pesticides [19–21] and pharmaceutical [22, 23]. The results of some researchers indicated that the bioaccumulation of CEC in roots was higher than that in shoots. In addition, various plant species, pollutant types, and microbial interactions will affect the overall absorption [24]. The root pathway and seed pathway of maize seedlings during the growth and development process were studied. Experiments showed that the absorption and transportation of pesticides by these two pathways occurred at the same time. Compared with seeds, the root system has a stronger ability to absorb and transport pesticides. It has a greater contribution to the absorption and transport behavior of the coating agent [25]. The study using nanoparticle-immersed paper imprinting mass spectrometry imaging technology immersed in nanoparticles revealed the carrier-mediated systemic and transmission mechanism of modified chlorantraniliprole in plants. The results showed that the modified chlorantraniliprole was applied after foliar application. It has two-way conductivity in cabbage plants, and when the concentration of chlorantraniliprole in the phloem is too high, it can be transmitted to the xylem and then migrate to the leaves through the xylem [26].

To the best of our knowledge, there were only some researches on its synthesis, bioactivity, and the application methods of vanisulfane residues [27–29]. However, the fluorescent label detection and systemic conduction of vanisulfane in plants have not been reported yet. The fluorescent label detection and systemic conduction of vanisulfane was of great significance to the current situation in the field and scientific medication. Fluorescent labeling was a key technology, which was widely used in biological processes of cell and biochemistry. The two photon confocal technology undertakes the real-time observation and determination of the fluorescent molecular position. It can visually display the conduction of drugs in plants. In view of these considerations, this experiment took tobacco plants as the experimental object, using UPLC-HRMS [30] and fluorescent dual-light sub-confocal real-time imaging technology [10, 31, 32] to carry out the systemic conduction study of vanisulfane in the plant.

The purpose was to accurately and intuitively study the internal absorption and conduction performance of vanisulfane on tobacco plants, so as to provide a certain reference for the scientific and rational mode of administration of vanisulfane in the field. The objectives of the present study are as follows: (I) to synthesize fluorescent-labeled vanisulfane and compare the activity difference between vanisulfane and fluorescent-labeled vanisulfane, (II) to quantitative and

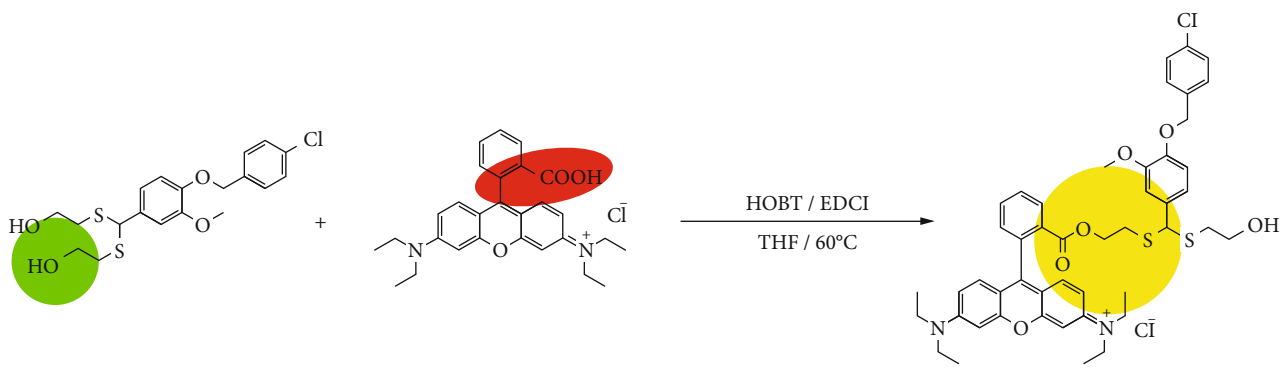

Figure 2: Synthetic route of vanisulfane with fluorescent label.

Table 1: Experiments of adding and recovering vanisulfane in tobacco root, stem leaf.

Sample	Add level (mg/kg)	Recovery rate (%), RSD_r^a (%) ($n = 5$)						RSD_R^b (%) ($n = 15$)
		First day		Second day		Third day		
Tobacco root and stem leaf	0.0005	102.12	1.34	99.98	3.22	101.03	2.56	2.23
	0.0010	77.93	1.89	80.21	3.78	81.11	3.56	2.37
	0.0100	86.69	5.05	85.55	3.45	84.32	3.41	4.32
	0.1000	82.10	1.60	83.29	3.21	80.23	2.41	1.92

Note: [a]intraday coefficient of variation; [b]intraday coefficient of variation.

qualitative analysis vanisulfane in tobacco by UPLC-HRMS, and (III) to real-time imaging of vanisulfane in tobacco by fluorescent two-photon confocal.

2. Materials and Methods

2.1. Reagents and Instruments. Vanisulfane standard sample (99.6% purity) was provided by the Key Laboratory of Green Pesticide and Agricultural Bioengineering, Guizhou University (Guiyang, China). Methanol and acetonitrile (chromatographic grade) were purchased from Tedia High Purity Solvents (Darmstadt, Germany). Sodium chloride (analytical purity) was purchased from LookChem (Beijing, China), anhydrous sodium sulfate (analytical purity) was purchased from Jinshan Chemical Reagent Co. (Chengdu, China). Distilled water was obtained from Watsons Co. Ltd. (Dongguan, China).

Thermo Scientific UltiMate 3000 high-performance liquid chromatography and Thermo Scientific Q Exactive high-resolution mass spectrometer were purchased from Thermo Fisher Scientific, Inc. (Waltham, USA). BUCHI R-210 rotary evaporator was purchased from BUCHI Labortechnik AG (Flawil, Switzerland). ALC-210.4 Electronic Balance was purchased from Sartorius (Darmstadt, Germany). MTV-100 Multitube Vortex Mixer was purchased from Hangzhou Allsheng Instruments Co., Ltd. (Hangzhou, China). TGL-20B centrifuge was purchased from Shanghai Anting Scientific Instrument Factory (Shanghai, China). KQ-100B Ultrasonic cleaner was purchased from Kunshan Ultrasonic Instruments Co., Ltd (Kunshan, China). Fluorescent Two-photon Confocal microscope Olympus FV 3000 was purchased from Olympus (Olympus, Japan).

2.2. The Absorption and Conduction of Vanisulfane in Tobacco

2.2.1. Internal Suction and Upward Conduction Test (Hydroponic Method). Vanisulfane aqueous solution (100 mL) with the concentration of 100 mg/L was added to 250 mL Erlenmeyer flask. The tobacco seedlings at the 3-4 leaf stage were dug out with roots and then washed away the soil with water. After that, the tobacco seedlings were inserted into a triangular flask for cultivation in a greenhouse (18-25°C) under natural light. The stems and leaves were cut off at 4, 8, 12, 24, 36, 48, 72, and 96 h, respectively, and then stored at -20°C for later test use.

2.2.2. Inward Suction Downward Conduction Test (Spray Method). Vanisulfane aqueous solution (100 mg/L) was uniformly sprayed on the leaf surface of the 3-4 leaf stage tobacco seedlings. Then, the leaf surface was sprayed with fresh-keeping film to prevent pollution. The plant samples were cultivated in a greenhouse (18-25°C) under natural light. The roots were cut and rinsed at 4, 8, 12, 24, 36, 48, 72, 96, and 120 h, respectively, and stored at -20°C for later test use.

2.3. Qualitative Analysis of Vanisulfane by UPLC-HRMS

2.3.1. Instrumental Method

(1) Liquid Condition. UPLC separations were obtained using a Thermo scientific Hypersll Gold C8 1.9 μm (2.1 × 100 mm) operating at 40°C in the isocratic elution mode. The mobile phase was component A (60% water with 0.1% formic acid): component D (40% acetonitrile). The flow rate was 0.3 mL/min, and the sample injection volume was 2 μL.

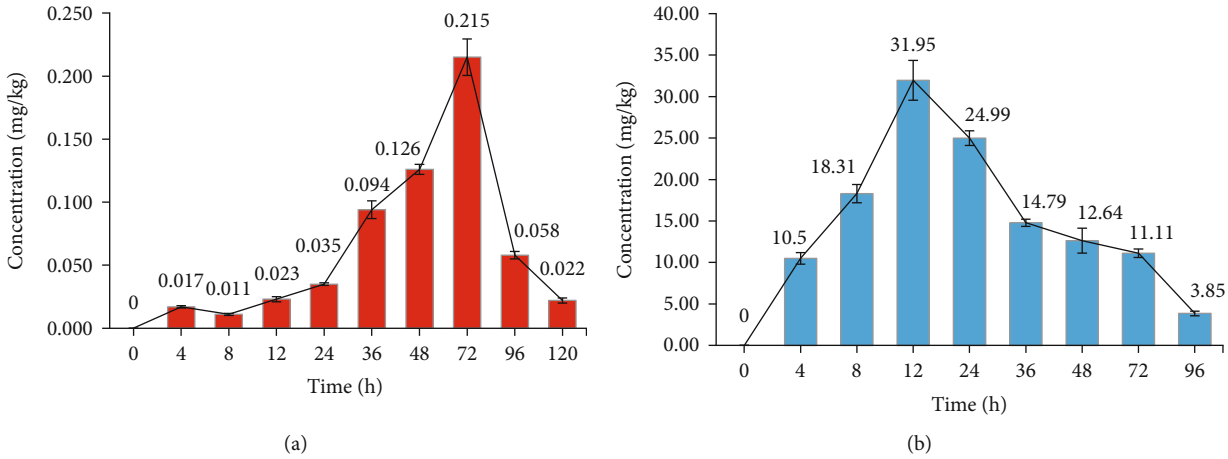

Figure 3: Systemic inhalation of vanisulfane in tobacco, conducts downward (a) and upward (b).

(2) Mass Spectrum Condition. ESI; negative ion mode; aux gas heater temperature at 300°C; capillary temperature at 300°C; and spray voltage at 3.0 kV, sheath gas, sweep gas, and auxiliary gas flow rates at 30, 3, and 10 a.u., respectively. Qualitative and quantitative ion: [M + $HCOO^-$], 459.07083 m/z.

2.3.2. Extraction Method of Vanisulfane from Tobacco Roots, Stems, and Leaves. In the experiment, 5 g of fresh tobacco (including roots, stems, and leaves) was accurately weighed into 50 mL centrifuge tubes, and vanisulfane standard samples were added to make the additive levels in tobacco are 0.0005, 0.01, 0.1, and 1 mg/kg, respectively. After the solvent evaporates, acetonitrile (20 mL), NaCl (2 g), and anhydrous Na_2SO_4 (3 g) were added to the centrifuge tubes. The homogenate was extracted for 3 minutes and centrifuged at 6000 r/min for 5 minutes. After that, 10 mL of the supernatant was sucked out and spin-dried. The dried sample was dissolved in 1 mL of methanol, and the content was determined by UPLC-HRMS. The additive recovery experiment was carried out for 3 consecutive days, and 6 parallels were performed for each additive level.

2.4. Synthesis of Fluorescent Labels of Vanisulfane. In order to further prove the law of internal absorption and conduction of vanisulfane in plants, the fluorescent-labeled of vanisulfane (Figure 2) was synthesized. Using rhodamine B as raw material, 1-ethyl-3-(3-dimethylaminopropyl) carbodiimide hydrochloride (EDCI, 0.55 g), rhodamine B (0.92 g), 1-hydroxybenzotriazole (HOBt, 0.32 g), and tetrahydrofuran (20 mL) were added into a 50 mL three mouth flask and refluxed at 60°C for 0.5 h. After that, vanisulfane (1 g) dissolved in 10 mL tetrahydrofuran was slowly added and stirred at 60°C. After completion of reaction, the vanisulfane with fluorescent label was purified by column chromatography (Vethyl acetate : Vdichloromethane : Vmethanol = 2 : 5 : 1) and characterized the structure by ^{1}H NMR, ^{13}C NMR, and HRMS. The ^{1}H NMR, ^{13}CNMR, and HRMS data are shown below. ^{1}H NMR (500 MHz, $CDCl_3$, ppm) δ 8.26 (d, J = 7.5 Hz, 1H), 7.72 (dd, J = 11.9, 7.2 Hz, 2H), 7.28 (d, J = 13.0 Hz, 3H), 7.23 (d, J = 7.2 Hz, 1H), 7.07–6.91 (m, 4H), 6.88–6.63 (m, 6H), 5.09–4.87 (m, 3H), 4.13–4.03 (m, 2H), 3.86–3.16 (m, 14H), 2.72–2.44 (m, 4H), 1.25 (t, J = 6.7 Hz, 12H); ^{13}C NMR (125 MHz, $CDCl_3$, ppm) δ 165.00, 158.55, 157.86, 157.84, 155.63, 155.57, 149.79, 147.65, 135.70, 133.76, 133.64, 133.44, 133.06, 131.65, 131.36, 131.32, 130.54, 130.21, 130.07, 128.77, 128.74, 120.12, 118.17, 114.38, 114.27, 113.81, 113.61, 113.59, 111.49,

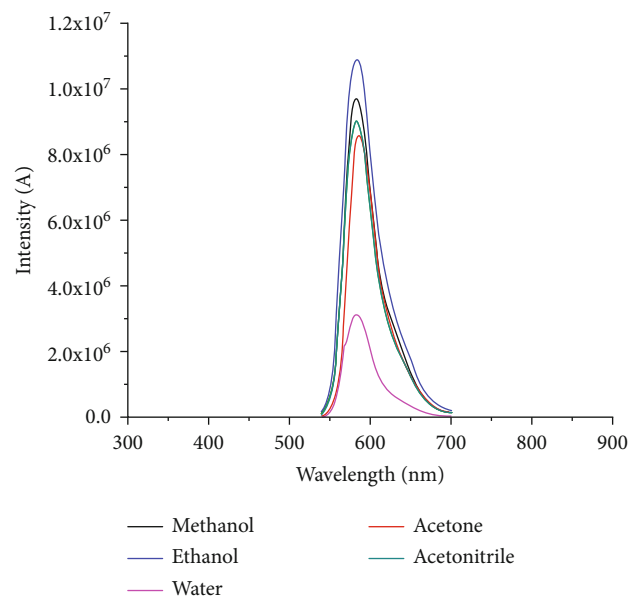

Figure 4: Fluorescence intensity of vanisulfane fluorescent label compounds in different solvents.

Table 2: The anti-CMV activity of vanisulfane and vanisulfane with fluorescent label.

Compound name	Curative activity (%)	Protection activity (%)
Vanisulfane	50.53 ± 6.12	51.42 ± 5.32
Vanisulfane with fluorescent label	51.23 ± 4.12	53.12 ± 6.45

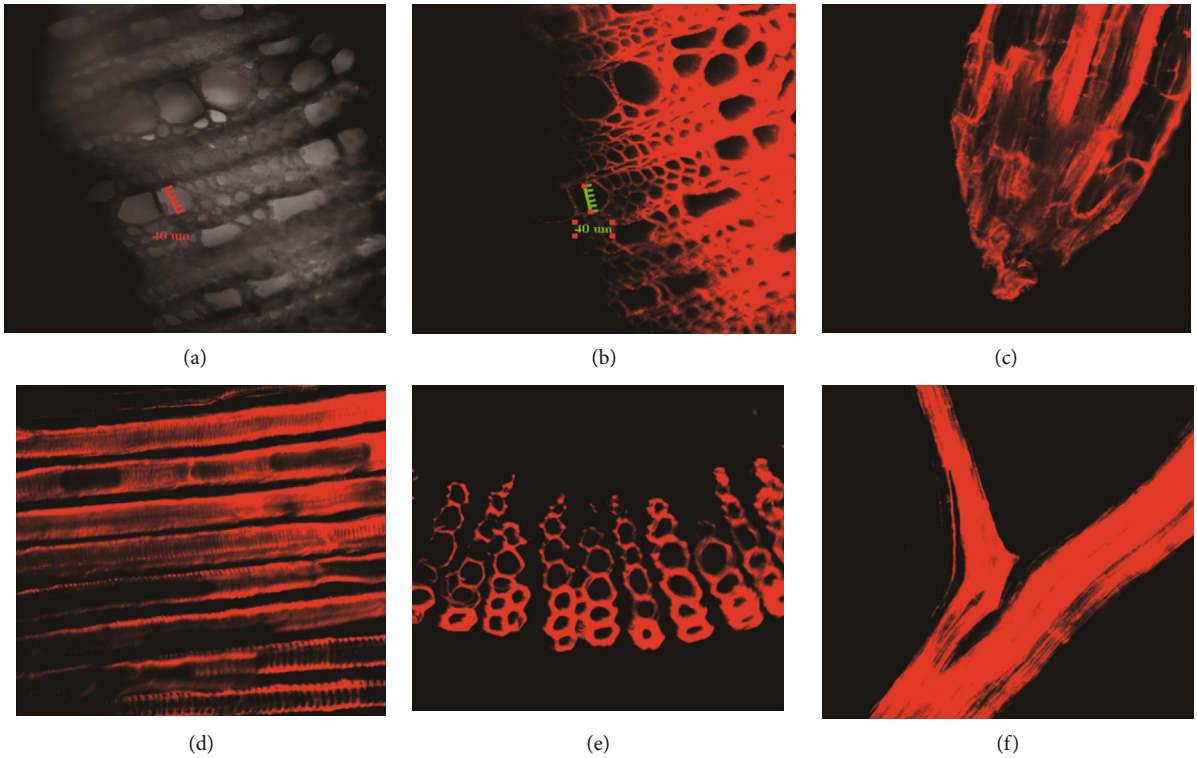

Figure 5: Fluorescence imaging of vanisulfane in tobacco plants ((a) the bright field of the cross-section of the stem; (b) the fluorescence field of the cross-section of the stem; (c) the fluorescence field of the vertical section of the root; (d) the fluorescence field of the vertical section of the stem; (e) fluorescence field of leaf vein cross-section; (f) fluorescence field of leaf vein vertical section).

96.56, 96.54, 70.44, 64.33, 61.58, 56.18, 53.26, 46.19, 46.17, 35.16, 31.03, 12.73; HRMS (ESI) theoretical value: m/z $C_{47}H_{52}O_6N_2ClS_2$ = 839.29498, measured value: m/z 839.29431, mass error, -0.79988 ppm (Shown in Supplementary Materials (available here).

2.5. Bioactivity Test of Vanisulfane with Fluorescent Label. Whether the CMV activity of vanisulfane after fluorescent labeling has changed remains to be determined. Therefore, the CMV activities of vanisulfane and vanisulfane with fluorescent label were determined and compared in this experiment. The curative and protection activity against CMV of the vanisulfane with fluorescent label at the concentration of 500 mg/L was tested by the half-leaf dead spot method [1]. Methods: vanisulfane and vanisulfane with fluorescent label were accurately weighed 2 mg, respectively. The weighed samples were dissolved in 20 μL N,N-dimethylformamide (DMF), and 4 mL of 1% Tween water was added to prepare the compound to a concentration of 500 μg/mL. The anti-CMV activity of the compound was tested by the half-leaf dead spot method.

2.6. Real-Time Observation of Fluorescent Labels in Tobacco. The excitation and emission wavelength of the synthesized vanisulfane fluorescent label were measured. The detection wavelength of the two-photon confocal was set according to the measured excitation and emission wavelengths. According to the method of 2.2.1., the obtained tobacco plants were sliced, and the treated slices were observed under two-photon confocal microscope. The sampling time of fluorescence real-time imaging was the same as that of the hydroponic method.

3. Results and Discussion

3.1. Accuracy and Precision. According to the extraction method of vanisulfane in tobacco in 2.3.2, the experiments were carried out with different concentrations of vanisulfane, each with 5 mass concentrations in parallel, and the extraction was added for three consecutive days. As shown in Table 1, the recovery rate was 77.93-102.12%, and the coefficient of variation RSD was 1.34-5.05%. The experimental results showed that the accuracy and precision of the extraction method meet the requirements of pesticide residue analysis and detection [33].

3.2. The Quantitative Detection of Vanisulfane by UPLC-HRMS. The quantitative detection of the content of vanisulfane in tobacco at different times was carried out through design experiments using UPLC-HRMS. Figure 3(a) indicated that vanisulfane can be absorbed and transmitted downward to the root, and the conduction is slow. The content of vanisulfane in the sample reaches the maximum value of 0.215 mg/kg after 72 h of treatment. After that, the content gradually decreased with the extension of sampling time. At the end of sampling at 120 h, the content of vanisulfane in the sample was 0.022 mg/kg. It can be seen from Figure 3(b) that vanisulfane can be sucked inward and

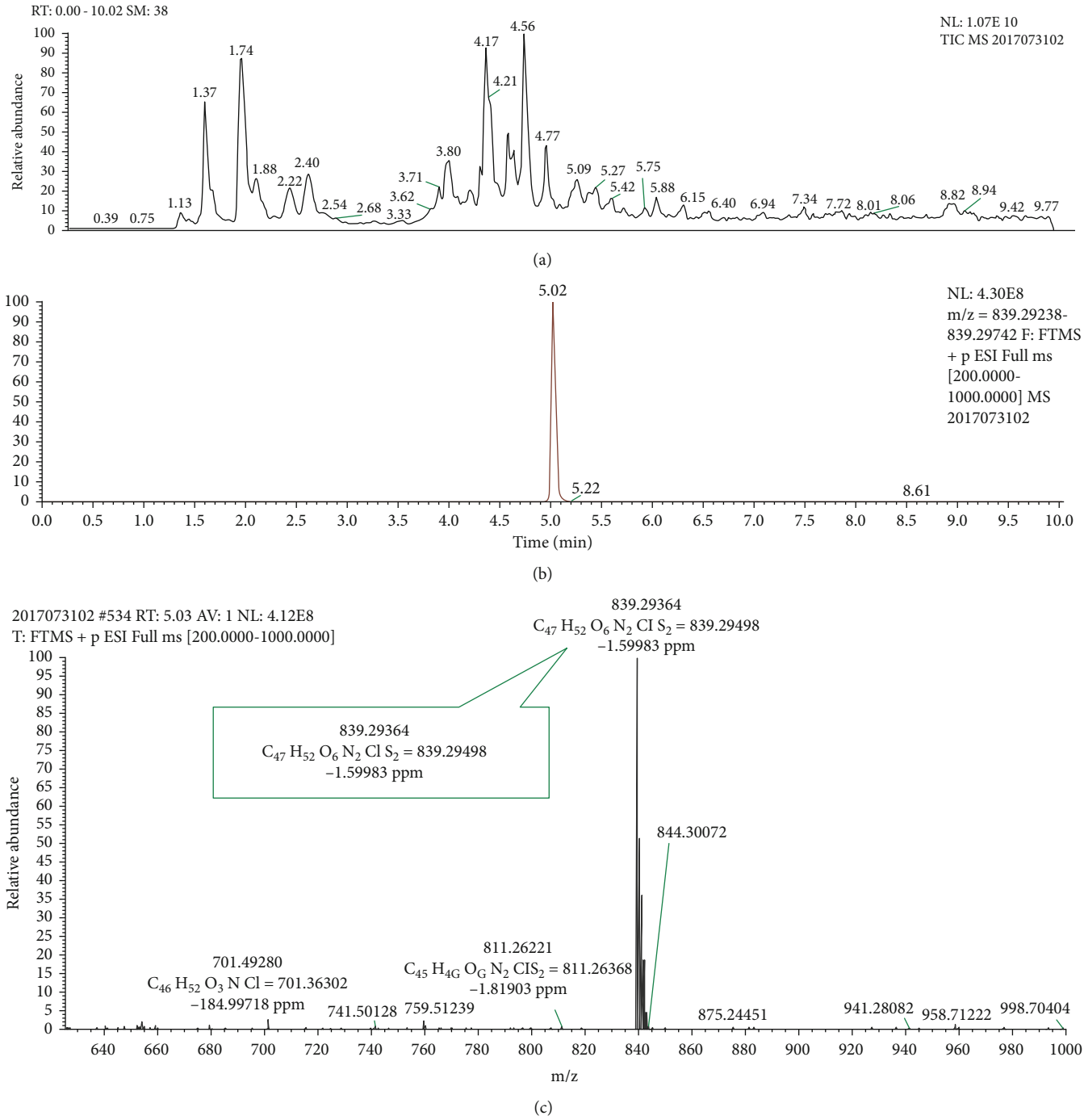

Figure 6: High-resolution mass spectrum of vanisulfane after the fluorescent label ((a) total ion chromatogram TIC; (b) mass range graph; (c) mass range graph).

uploaded to the stems and leaves. With the extension of treatment time, the content gradually increases. After 12 h of treatment, the content of vanisulfane in the sample reaches the maximum, which was 31.95 mg/kg. With the extension of sampling time, the content gradually decreased. At the end of 96 h, the content of vanisulfane in the sample was 3.85 mg/kg. According to the experimental data, vanisulfane can be conducted in tobacco, the process of downward conduction is slower than that of upward conduction, and the content is also lower. Many systemic pesticides can be transported up and down in plants [34–37]. It can be known that vanisulfane was a systemic agricultural antiplant virus agent.

3.3. Real-Time Fluorescence Two-Photon Confocal Imaging of Vanisulfane in Tobacco

3.3.1. Wavelength Determination of Vanisulfane Fluorescent Label. The excitation and emission wavelengths of vanisulfane with fluorescent label were determined by FLUOROMAX-4

spectrofluorometer. The excitation wavelength was 568 nm, and the emission wavelength was 583 nm. The fluorescence intensity of vanisulfane fluorescent label compounds was different in different solvents. The determination results were shown in Figure 4. According to the measured excitation and emission wavelengths, the detection wavelength of the two-photon confocal was set 1165 nm.

3.3.2. Verification of the CMV Activity of Vanisulfane with Fluorescent Label. As shown in Table 2, the curative and protection activities against CMV of vanisulfane with fluorescent label were 51.23% and 53.12%, respectively, which were equal to those of vanisulfane (50.53% and 51.42%, respectively), demonstrating that there was no significant effect on the anti-CMV activity after connecting the fluorescent label.

3.3.3. Real-Time Imaging of Vanisulfane with Fluorescent Label in Tobacco. It can be seen from the results of two-photon confocal imaging Figure 5 that the fluorescence of fluorescent-labeled vanisulfane can be clearly observed in the root, stem leaf vein of tobacco in real-time. The excitation wavelength of two-photon was 1165 nm when the excitation wavelength of real-time imaging was 568 nm. Rhodamine B was selected as the fluorophore to avoid the interference of plant fluorescence [38, 39], such as the coincidence of chlorophyll fluorescence (the excitation wavelength of chlorophyll was 439, and the excitation wavelength of two-photon was 915 nm). Figures 5(a) and 5(b) were comparison diagrams of tobacco stem cross-sections under bright field and fluorescent field positioning after partial magnification, and the fluorescent substance can be observed intuitively. The large number of fluorescent clusters was found in the xylem of tobacco root, which was transmitted along the xylem conduit (Figure 5(c)). The vessel of the plant can be clearly seen in the vertical section of the stem of tobacco, and the fluorescent substances were transmitted to all parts of the plant along the vessel (Figure 5(d)). In Figure 5(e), the fluorescence conduction can be clearly seen from the cross-section of the leaf vein. Figure 5(f) was shown that the presence of fluorescence can also be clearly seen on the leaf veins of tobacco.

Through two-photon confocal imaging, vanisulfane labeled with fluorescent can observe its internal absorption conduction in tobacco in real-time, which further verifies that vanisulfane has internal absorption conductivity in tobacco, which was consistent with the qualitative and quantitative results of high-resolution mass spectrometry. Both fluorescence two-photon confocal and UPLC-HRMS showed that vanisulfane had endothermic conductivity in tobacco plants.

3.3.4. Qualitative Determination of Vanisulfane with Fluorescent Label in Tobacco. Whether vanisulfane after being attached with a fluorescent tag was conducted in tobacco plants in addition to observing the conduction of fluorescence with two-photon confocal, whether vanisulfane after being fluorescently tagged was changed in plants remains to be determined. We therefore developed a high-resolution mass spectrometric qualitative assay of fluorescently tagged vanisulfane in tobacco (Figure 6).

Experimentally determined qualitatively by high-resolution mass spectrometry of the conducted fluorescently tagged vanisulfane in tobacco, mass range 839.29498 m/z peak pattern was able to be extracted in the total ion chromatogram (TIC), from which it was observed that the theoretical mass spectrum of fluorescently tagged vanisulfane had a peak at 839.29498 m/z, found 839.29364 m/z, which was -1.59983 ppm from the theoretical value, and was accurate in the 3 ppm range. The results of the experiment proved that the vanisulfane following the attached fluorescent tags was conducted in tobacco plants in vivo, but not the conduction of fluorescein itself in tobacco.

4. Conclusion

In this paper, the UPLC-HRMS technology was used to qualitatively and quantitatively analyze the internal absorption and conduction content of vanisulfane in tobacco plants after two treatments: hydroponics and foliar spraying. The properties of vanisulfane systemic upward and downward conduction in tobacco have been studied. The results showed that vanisulfane had good internal and upward conductance in tobacco plants. In addition, through fluorescent labeling of vanisulfane, using fluorescent two-photon confocal real-time imaging technology, we observed that vanisulfane can absorb and conduct in tobacco plants in real-time. The results can provide some reference for the scientific and rational drug use of vanisulfane in the field.

Data Availability

The data that support the findings of this study are available from the corresponding author upon reasonable request.

Conflicts of Interest

None of the authors have any professional or financial conflicts of interest.

Acknowledgments

This study was supported by Key Project of Science and Technology Research of Jiangxi Provincial Education Department (GJJ202803) and Subject Construction Project of Jingdezhen Science and Technology Plan (20202GYZD015-07). Thank you Huang Qian for supporting my research work.

Supplementary Materials

Vanisulfane with fluorescent label. The synthesized Vanisulfane fluorescent compound label has been characterized by ^{1}H NMR,^{13}C NMR and high resolution mass spectrometry. ^{1}H NMR,^{13}C NMR and high resolution mass spectrometry. HRMS *(Supplementary Materials)*

References

[1] J. Zhang, L. Zhao, C. Zhu et al., "Facile synthesis of novel vanillin derivatives incorporating a bis(2-hydroxyethyl)dithhioacetal

moiety as antiviral agents," *Journal of Agricultural and Food Chemistry*, vol. 65, no. 23, pp. 4582–4588, 2017.

[2] L. Bian, X. Ji, and W. Hu, "A novel single-labeled fluorescent oligonucleotide probe for silver(I) ion detection in water, drugs, and food," *Journal of Agricultural and Food Chemistry*, vol. 62, no. 21, pp. 4870–4877, 2014.

[3] O. S. Wolfbeis, "Nanoparticle-enhanced fluorescence imaging of latent fingerprints reveals drug abuse," *Angewandte Chemie International Edition*, vol. 48, no. 13, pp. 2268-2269, 2009.

[4] Y. Yang, H. Niu, and H. Zhang, "Direct and highly selective drug optosensing in real, undiluted biological samples with quantum-dot-labeled hydrophilic molecularly imprinted polymer microparticles," *ACS Applied Materials & Interfaces*, vol. 8, no. 24, pp. 15741–15749, 2016.

[5] B. Priem, C. Tian, J. Tang, Y. Zhao, and W. J. M. Mulder, "Fluorescent nanoparticles for the accurate detection of drug delivery," *Expert Opinion on Drug Delivery*, vol. 12, no. 12, pp. 1881–1894, 2015.

[6] R. Ben-Zur, H. Hake, S. Hassoon, V. Bulatov, and I. Schechter, "Optical analytical methods for detection of pesticides," *Reviews in Analytical Chemistry*, vol. 30, no. 3-4, pp. 123–139, 2011.

[7] H. Hake, R. Ben-Zur, I. Schechter, and A. Anders, "Fast optical assessment of pesticide coverage on plants," *Analytica Chimica Acta*, vol. 596, no. 1, pp. 1–8, 2007.

[8] S. A. Nsibande and P. B. C. Forbes, "Fluorescence detection of pesticides using quantum dot materials - a review," *Analytica Chimica Acta*, vol. 945, pp. 9–22, 2016.

[9] M. Jiang, C. Chen, J. He, H. Zhang, and Z. Xu, "Fluorescence assay for three organophosphorus pesticides in agricultural products based on magnetic-assisted fluorescence labeling aptamer probe," *Food Chemistry*, vol. 307, article 125534, 2020.

[10] L. Chen, F. Q. Li, B. H. Hou, G. F. Hong, and Z. J. Yao, "Site-specific fluorescent labeling approaches for naringenin, an essential flavonone in plant nitrogen-fixation signaling pathways," *The Journal of Organic Chemistry*, vol. 73, no. 21, pp. 8279–8285, 2008.

[11] U. Schobel, C. Barzen, and G. Gauglitz, "Immunoanalytical techniques for pesticide monitoring based on fluorescence detection," *Fresenius' Journal of Analytical Chemistry*, vol. 366, no. 6-7, pp. 646–658, 2000.

[12] M. Xie, F. Zhao, Y. Zhang, Y. Xiong, and S. Han, "Recent advances in aptamer-based optical and electrochemical biosensors for detection of pesticides and veterinary drugs," *Food Control*, vol. 131, article 108399, 2022.

[13] P. Hazarika, S. M. Jickells, K. Wolff, and D. . A. Russell, "Imaging of latent fingerprints through the detection of drugs and metabolites," *Angewandte Chemie International Edition*, vol. 47, no. 52, pp. 10167–10170, 2008.

[14] M. Ramezani, N. M. Danesh, P. Lavaee, K. Abnous, and S. M. Taghdisi, "A selective and sensitive fluorescent aptasensor for detection of kanamycin based on catalytic recycling activity of exonuclease III and gold nanoparticles," *Sensors and Actuators B: Chemical*, vol. 222, pp. 1–7, 2016.

[15] D. J. Wright, A. R. K. Blyth, and P. E. Pearson, "Behaviour of the systemic nematicide oxamyl in plants in relation to control of invasion and development of Meloidogyne incognita," *Annals of Applied Biology*, vol. 96, no. 3, pp. 323–334, 1980.

[16] T. Yang, Y. Qu, M. Hickey et al., "Mapping of pesticide transmission on biological tissues by surface enhanced Raman microscopy with a gold nanoparticle mirror," *ACS Applied Materials & Interfaces*, vol. 11, no. 47, pp. 44894–44904, 2019.

[17] D. Jianchang and Z. Xing, "The review of transmission and translocation of pesticide in wood plant," *Acta Universitatis Agriculturalis Boreali-occidentalis*, vol. 29, no. 4, pp. 128–134, 2001.

[18] E. Barak, A. Dinoor, and B. Jacoby, "Adsorption of systemic fungicides and a herbicide by some components of plant tissues, in relation to some physicochemical properties of the pesticides," *Pesticide Science*, vol. 14, no. 3, pp. 213–219, 1983.

[19] J. Sun, X. Ge, X. Wu, C. Dai, and N. Yang, "Identification of pesticide residues in lettuce leaves based on near infrared transmission spectroscopy," *Journal of Food Process Engineering*, vol. 41, no. 6, article e12816, 2018.

[20] M. Wu, J. Sun, B. Lu, X. Ge, X. Zhou, and M. Zou, "Application of deep brief network in transmission spectroscopy detection of pesticide residues in lettuce leaves," *Journal of Food Process Engineering*, vol. 42, no. 3, article e13005, 2019.

[21] J. Kaushal, M. Khatri, and S. K. Arya, "A treatise on organophosphate pesticide pollution: current strategies and advancements in their environmental degradation and elimination," *Ecotoxicology and Environmental Safety*, vol. 207, article 111483, 2021.

[22] K. Buckley and P. Matousek, "Recent advances in the application of transmission Raman spectroscopy to pharmaceutical analysis," *Journal of Pharmaceutical and Biomedical Analysis*, vol. 55, no. 4, pp. 645–652, 2011.

[23] M. Zhang, J. Zuo, X. Yu, X. Shi, L. Chen, and Z. Li, "Quantification of multi-antibiotic resistant opportunistic pathogenic bacteria in bioaerosols in and around a pharmaceutical wastewater treatment plant," *Journal of Environmental Sciences*, vol. 72, pp. 53–63, 2018.

[24] V. L. R. Pullagurala, S. Rawat, I. O. Adisa, J. A. Hernandez-Viezcas, J. R. Peralta-Videa, and J. L. Gardea-Torresdey, "Plant uptake and translocation of contaminants of emerging concern in soil," *Science of the Total Environment*, vol. 636, pp. 1585–1596, 2018.

[25] Y. Cohen and U. Gisi, "Uptake, translocation and degradation of [^{14}C]cymoxanil in tomato plants," *Crop Protection*, vol. 12, no. 4, pp. 284–292, 1993.

[26] X. Wu, R. Qin, H. Wu et al., "Nanoparticle-immersed paper imprinting mass spectrometry imaging reveals uptake and translocation mechanism of pesticides in plants," *Nano Research*, vol. 13, no. 3, pp. 611–620, 2020.

[27] K. Mastovska, K. J. Dorweiler, S. J. Lehotay, J. S. Wegscheid, and K. A. Szpylka, "Pesticide multiresidue analysis in cereal grains using modified QuEChERS method combined with automated direct sample introduction GC-TOFMS and UPLC-MS/MS techniques," *Journal of Agricultural and Food Chemistry*, vol. 58, no. 10, pp. 5959–5972, 2009.

[28] T. Kovalczuk, O. Lacina, M. Jech, J. Poustka, and J. Hajšlová, "Novel approach to fast determination of multiple pesticide residues using ultra-performance liquid chromatography-tandem mass spectrometry (UPLC-MS/MS)," *Food Additives and Contaminants*, vol. 25, no. 4, pp. 444–457, 2008.

[29] Z. Q. Kong, F. S. Dong, J. Xu et al., "Determination of difenoconazole residue in tomato during home canning by UPLC-MS/MS," *Food Control*, vol. 23, no. 2, pp. 542–546, 2012.

[30] T. Cai, H. Ting, and L. Z. Jin, "Novel identification strategy for ground coffee adulteration based on UPLC- HRMS

oligosaccharide profiling," *Food Chemistry*, vol. 190, pp. 1046–1049, 2016.

[31] Z. W. Lei, J. Wang, Y. X. Tian, G. Song, G. Zhao, and H. Xu, "Synthesis and application of clickable and biocompatible fluorescent glycosyl labels," *Dyes and Pigments*, vol. 113, pp. 627–633, 2015.

[32] R. I. Benhamou, M. Bibi, K. B. Steinbuch et al., "Real-time imaging of the azole class of antifungal drugs in live Candida cells," *ACS Chemical Biology*, vol. 12, no. 7, pp. 1769–1777, 2017.

[33] E. C. D. Watch, "OECD guidelines," *Accessed on*, vol. 28, 2020https://www.somo.nl/wp-content/uploads/2012/06/OECD-Watch-brochure.pdf.

[34] A. Veres, K. A. G. Wyckhuys, J. Kiss et al., "An update of the Worldwide Integrated Assessment (WIA) on systemic pesticides. Part 4: alternatives in major cropping systems," *Environmental Science and Pollution Research*, vol. 27, no. 24, pp. 29867–29899, 2020.

[35] B. Łozowicka, P. Kaczyński, P. Mojsak et al., "Systemic and non-systemic pesticides in apples from Kazakhstan and their impact on human health," *Journal of Food Composition and Analysis*, vol. 90, article 103494, 2020.

[36] R. Bundschuh, M. Bundschuh, M. Otto, and R. Schulz, "Food-related exposure to systemic pesticides and pesticides from transgenic plants: evaluation of aquatic test strategies," *Environmental Sciences Europe*, vol. 31, no. 1, pp. 1–13, 2019.

[37] D. Zhang, P. Liang, J. Ye et al., "Detection of systemic pesticide residues in tea products at trace level based on SERS and verified by GC–MS," *Analytical and Bioanalytical Chemistry*, vol. 411, no. 27, pp. 7187–7196, 2019.

[38] D. Wu, A. C. Sedgwick, T. Gunnlaugsson, E. U. Akkaya, J. Yoon, and T. D. James, "Fluorescent chemosensors: the past, present and future," *Chemical Society Reviews*, vol. 46, no. 23, pp. 7105–7123, 2017.

[39] E. Fodor and F. Ayaydin, *Fluorescent probes and live imaging of plant cells*, Springer, Cham, 2018.

Hindawi
Journal of Chemistry
Volume 2022, Article ID 5354088, 7 pages
https://doi.org/10.1155/2022/5354088

Research Article

Synthesis and Bioactivity Evaluation of Novel Thiochroman-4-One Derivatives Incorporating Carboxamide and 1, 3, 4-Thiadiazole Thioether Moieties

Lu Yu,[1] **Lingling Xiao**,[1] **Pei Li**,[1,2] **Jiyan Chi**,[1] **Jie Li**,[1] **and Shuming Tan**[1]

[1]*School of Liquor and Food Engineering, Guizhou University, Guiyang 50025, China*
[2]*Qiandongnan Engineering and Technology Research Center for Comprehensive Utilization of National Medicine, Kaili University, Kaili 556011, China*

Correspondence should be addressed to Pei Li; pl19890627@126.com and Shuming Tan; smtan@gzu.edu.cn

Received 11 January 2022; Accepted 3 February 2022; Published 26 February 2022

Academic Editor: Ajaya Kumar Singh

A series of novel thiochroman-4-one derivatives incorporating carboxamide and 1, 3, 4-thiadiazole thioether moieties were synthesized. Bioassay results indicated that the EC_{50} values of compound 6-chloro-*N*-(5-(methylthio)-1, 3, 4-thiadiazol-2-yl)-4-oxothiochromane-2-carboxamide (5a) against *Xanthomonas oryzae* pv. *Oryzae* (*Xoo*) and *Xanthomonas axonopodis* pv. *Citri* (*Xac*) were 24 and 30 μg/mL, respectively, which were even better than those of bismerthiazol and thiadiazole copper. Meanwhile, compound 6-methyl-4-oxo-*N*-(5-(propylthio)-1, 3, 4-thiadiazol-2-yl)thiochromane-2-carboxamide (5m) showed a better antifungal activity against *Botrytis cinerea* (*B. cinerea*), with an inhibition rate of 69%, than carbendazim. As far as we know, this is the first report on the antibacterial and antifungal activities of this series of novel thiochroman-4-one derivatives incorporating carboxamide and 1, 3, 4-thiadiazole thioether moieties.

1. Introduction

Global food safety/security will remain a worldwide concern for the next 50 years and beyond. Bacterial and fungal diseases of plants have been an enormous impact on the food safety/security at various stages of the food chain from primary production to consumption and have presented serious threats in agricultural production and caused enormous economic losses each year worldwide [1]. Although pesticide application has been a conventional methodology used in plant protection, frequent use of conventional chemical pesticides has resulted in problems in resistance to bacteria and fungi populations, environmental contamination, and human health [2]. With the improvement of human living standards and human health, the demand for high-quality agricultural products as foods makes it necessary to limit the use of conventional chemical pesticides and challenges the control of plant bacterial and fungal diseases [3]. Therefore, the current paradigm of relying almost exclusively on conventional chemical pesticides for bacterial and fungal diseases of plants control may need to be reconsidered.

Natural product pesticides of using innate disease-resistant plants against resist pests and diseases is an innovative stratagem in sustainable agricultural development because these pesticides are safer than the conventional chemical pesticides due to their low toxicity to natural enemies, humans, and other mammals [4–7]. Therefore, natural products can either be used directly in bacterial and fungal control or develop novel synthetic analogs with favorable biological properties. Thiochroman-4-one, an important natural product which is widely found in many plants, showed extensive bioactivities, including antifungal [8], herbicidal [9], insecticidal [10], and antibacterial [11–14] properties. In our previous study, we disclosed a series of novel thiochroman-4-one derivatives (Figure 1) which showed moderate to good antibacterial and antifungal activities [11–14].

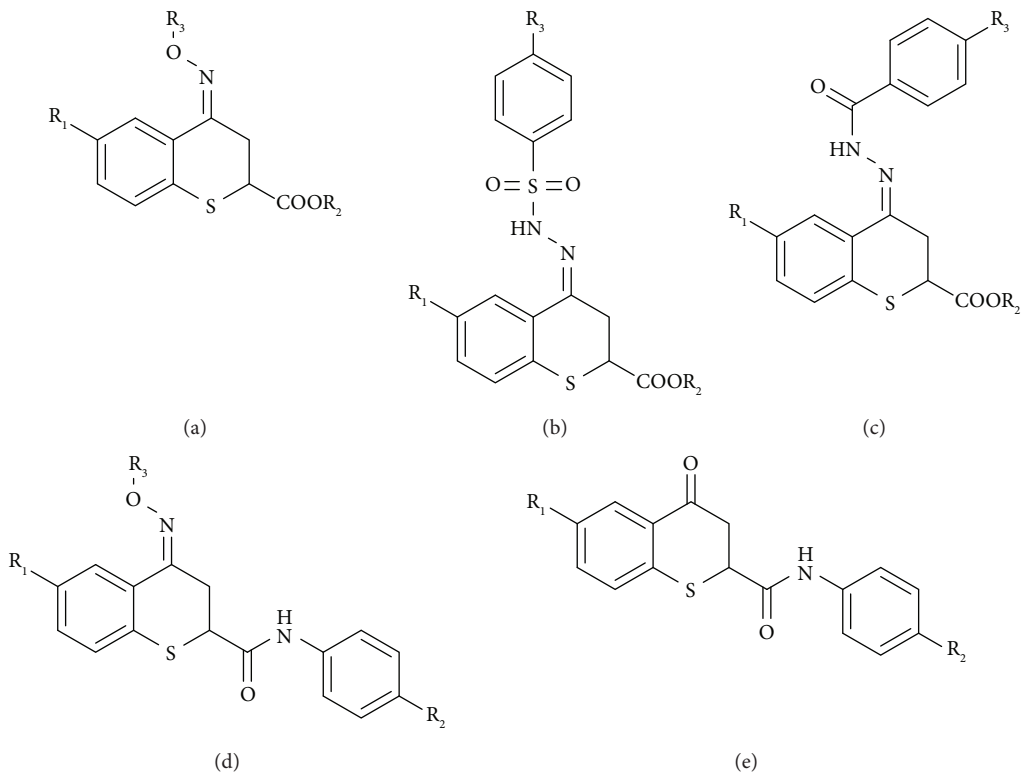

Figure 1: Structures of the target compounds reported in our previous work.

The carboxamide moiety, an important functional group in pesticide chemistry, had attracted more and more attention to the researchers due to its broad spectrum of pesticidal bioactivities, for example, antibacterial [15, 16], antifungal [17, 18], antiviral [19–21], insecticidal [22, 23], and herbicidal [24] properties. Over the past few decades, many new pesticides containing carboxamide moiety, such as fluxapyroxad, penflufen, and isoflucypram, had been developed. Meanwhile, 1, 3, 4-thiadiazole thioether unit had played an important role in the field of agricultural chemistry, including antibacterial [16, 25], antifungal [26, 27], antiviral [28–31], insecticidal [32], and herbicidal [33] properties.

In view of these facts mentioned above, we aim to replace the benzene ring with a 1, 3, 4-thiadiazole thioether group (Figure 2) to build a series of novel thiochroman-4-one derivatives incorporating carboxamide and 1, 3, 4-thiadiazole thioether moieties, and then their in vitro antibacterial activity against *Xanthomonas oryzae* pv. *Oryzae* (*Xoo*) and *Xanthomonas axonopodis* pv. *Citri* (*Xac*) as well as antifungal activity against *Verticillium dahliae* (*V. dahliae*), *Botrytis cinerea* (*B. cinerea*), and *Fusarium oxysporum* (*F. oxysporum*) were determined.

2. Materials and Methods

2.1. Preparation Procedure of the Target Compounds 5a–5o. As shown in Scheme 1, the key intermediates 2 and 4 were prepared according to our previously reported literature [11–14, 16].

Intermediate 2 (0.022 mol), intermediate 4 (0.02 mol), 1-(3-dimethylaminopropyl)-3-ethylcarbodiimide hydrochloride (EDCI, 0.03 mol), dimethylaminopyridine (DMAP, 0.0002 mol), and N, N-dimethylformamide (DMF, 50 mL) were added to a 50 mL three-necked round-bottomed flask and then reacted overnight at room temperature. Upon completion, the reaction mixture was quenched by pouring into 100 mL distilled water. The residues were recrystallized from methanol to give the pure target compounds 5a–5o. The structures of the target compounds were characterized using a DRX-400 ^{1}H and ^{13}C nuclear magnetic resonance (NMR; Bruker, Rheinstetten, Germany) and a Waters Xevo G2-S QTOF high-resolution mass spectrum (HRMS; Waters, MA, USA).

2.2. Bioactivity Evaluation. The antibacterial activity against *Xoo* and *Xac* and the antifungal activity against *B. cinerea*, *V. dahliae*, and *F. oxysporum* of the target compounds were determined according to the reported methods [34, 35]. Meanwhile, the EC_{50} values of some of the target compounds against *Xoo* and *Xac* were also evaluated and calculated using SPSS 17.0 software.

3. Results and Discussion

3.1. Chemistry. Using different substituted thiols and 2-amino-5-mercapto-1, 3, 4-thiadiazole as the starting materials, as shown in Scheme 1, a series of novel thiochroman-4-one derivatives incorporating carboxamide and 1, 3, 4-thiadiazole thioether moieties were synthesized. The physical

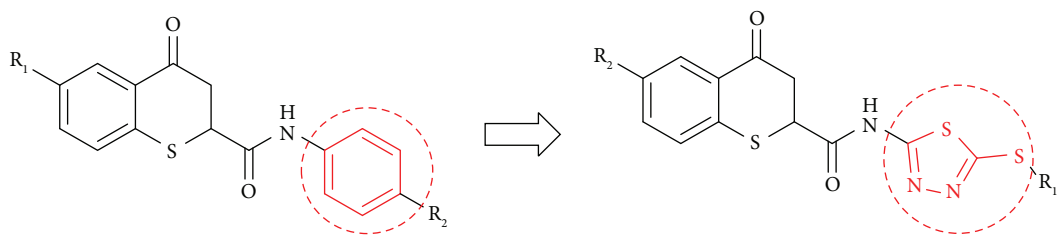

Figure 2: Design route of the target compounds 5a–5o.

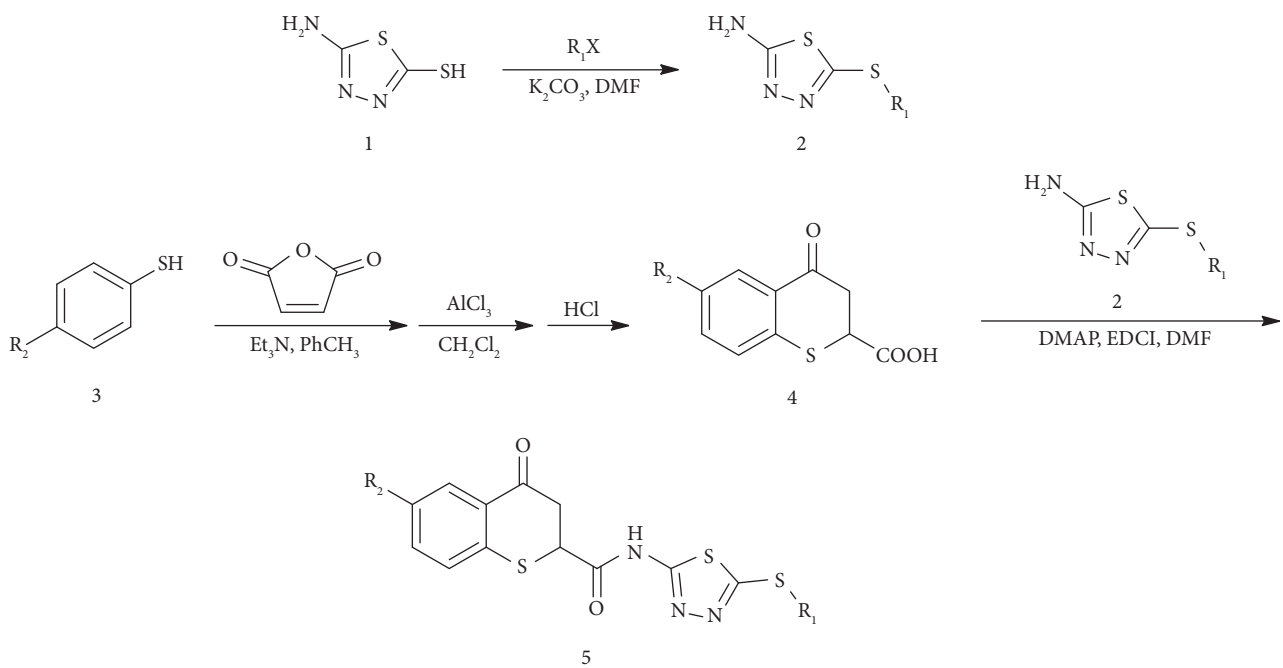

5a: $R_1 = CH_3$, $R_2 = Cl$
5b: $R_1 = CH_2CH_3$, $R_2 = Cl$
5c: $R_1 = CH_2CH_2CH_3$, $R_2 = Cl$
5d: $R_1 = PhCH_2$, $R_2 = Cl$
5e: $R_1 = 4\text{-F-}PhCH_2$, $R_2 = Cl$
5f: $R_1 = CH_3$, $R_2 = F$
5g: $R_1 = CH_2CH_3$, $R_2 = F$
5h: $R_1 = CH_2CH_2CH_3$, $R_2 = F$
5i: $R_1 = PhCH_2$, $R_2 = F$
5j: $R_1 = 4\text{-F-}PhCH_2$, $R_2 = F$
5k: $R_1 = CH_3$, $R_2 = CH_3$
5l: $R_1 = CH_2CH_3$, $R_2 = CH_3$
5m: $R_1 = CH_2CH_2CH_3$, $R_2 = CH_3$
5n: $R_1 = PhCH_2$, $R_2 = CH_3$
5o: $R_1 = 4\text{-F-}PhCH_2$, $R_2 = CH_3$

Scheme 1: Synthetic route of the target compounds 5a–5o.

characteristics, ^{1}H NMR, ^{13}C NMR, and HRMS data for all the target compounds are shown as follows. The ^{1}H NMR, ^{13}C NMR, and HRMS spectra for all the target compounds can be found in the Supplementary Materials (available here).

Data for compound 6-chloro-*N*-(5-(methylthio)-1, 3, 4-thiadiazol-2-yl)-4-oxothiochromane-2-carboxamide (5a). White solid; mp 228–230°C; yield 67%; ^{1}H NMR (400 MHz, DMSO-d_6, ppm) δ: 12.99 (s, 1H, CONH), 7.90 (d, J = 4.0 Hz, 1H, Ph-H), 7.55 (dd, J1 = 4.0 Hz, J2 = 16.0 Hz, 1H, Ph-H), 7.39 (d, J = 8.0 Hz, 1H, Ph-H), 4.46 (t, J = 4.0 Hz, 1H, SCH), 3.23 (qd, J1 = 4.0 Hz, J2 = 16.0 Hz, 2H, CH_2), 2.68 (s, 3H, CH_3); ^{13}C NMR (100 MHz, DMSO-d_6, ppm) δ: 191.17, 169.58, 161.60, 158.42, 136.53, 133.80, 130.88, 129.91, 127.22, 41.12, 40.41, 16.48; HRMS (ESI) $[M + Na]^+$ calcd. for $C_{13}H_{10}ClN_3O_2S_3$: 369.95509, found 369.95619.

Data for compound 6-chloro-*N*-(5-(ethylthio)-1, 3, 4-thiadiazol-2-yl)-4-oxothiochromane-2-carboxamide (5b). White solid; mp 236–237°C; yield 60%; ^{1}H NMR (400 MHz, DMSO-d_6, ppm) δ: 13.00 (s, 1H, CONH), 7.90 (d, J = 4.0 Hz, 1H, Ph-H), 7.55 (dd, J1 = 4.0 Hz, J2 = 8.0 Hz, 1H, Ph-H), 7.39 (d, J = 8.0 Hz, 1H, Ph-H), 4.47 (t, J = 4.0 Hz, 1H, SCH), 3.31–3.15 (m 4H, CH_2, CH_2CH_3), 1.31 (t, J = 8.0 Hz, 3H, CH_2CH_3); ^{13}C NMR (100 MHz, DMSO-d_6, ppm) δ: 191.16, 169.61, 159.86, 158.74, 136.52, 133.80, 131.77, 130.89, 129.91, 127.22, 41.10, 40.41, 28.59, 15.17; HRMS (ESI) $[M + Na]^+$ calcd. for $C_{14}H_{12}ClN_3O_2S_3$: 383.97074, found 383.97183.

Data for compound 6-chloro-4-oxo-*N*-(5-(propylthio)-1, 3, 4-thiadiazol-2-yl)thiochromane-2-carboxamide (5c). White solid; mp 191–193°C; yield 58%; ^{1}H NMR (400 MHz, DMSO-d_6, ppm) δ: 13.00 (s, 1H, CONH), 7.90 (d, J = 4.0 Hz, 1H, Ph-H), 7.55 (dd, J1 = 4.0 Hz, J2 = 8.0 Hz, 1H, Ph-H), 7.39

(d, J = 8.0 Hz, 1H, Ph-H), 4.46 (t, J = 4.0 Hz, 1H, SCH), 3.31–3.14 (m, 4H, CH_2, $CH_2CH_2CH_3$), 1.71–1.62 (m, 2H, $CH_2CH_2CH_3$), 0.95 (t, J = 8.0 Hz, 3H, $CH_2CH_2CH_3$); ^{13}C NMR (100 MHz, DMSO-d_6, ppm) δ: 191.19, 169.68, 159.96, 158.88, 136.59, 133.80, 131.78, 130.86, 129.91, 127.22 41.17, 40.41, 36.03, 22.86, 13.37; HRMS (ESI) $[M-H]^+$ calcd. for $C_{15}H_{14}ClN_3O_2S_3$: 397.98639, found 397.98782.

Data for compound *N*-(5-(benzylthio)-1, 3, 4-thiadiazol-2-yl)-6-chloro-4-oxothiochromane-2-carboxamide (5d). White solid; mp 234–235°C; yield 69%; ^{1}H NMR (400 MHz, DMSO-d_6, ppm) δ: 13.00 (s, 1H, CONH), 7.90 (d, J = 4.0 Hz, 1H, Ph-H), 7.55 (dd, J1 = 4.0 Hz, J2 = 8.0 Hz, 1H, Ph-H), 7.44–7.38 (m, 3H, Ph-H), 7.13 (t, J = 8.0 Hz, 2H, Ph-H), 4.47 (d, J = 4.0 Hz, 3H, SCH, $PhCH_2$), 3.23 (qd, J1 = 4.0 Hz, J2 = 16.0 Hz, 2H, CH_2); ^{13}C NMR (100 MHz, DMSO-d_6, ppm) δ: 191.19, 163.16, 160.74, 159.26, 159.03, 136.54, 133.81, 133.45, 133.43, 131.76, 131.47, 131.39, 130.89, 129.91, 127.23, 115.91, 115.70, 41.17, 40.41, 37.13; HRMS (ESI) $[M+Na]^+$ calcd. for $C_{19}H_{14}ClN_3O_2S_3$: 465.98289, found 465.99061.

Data for compound 6-chloro-*N*-(5-((4-fluorobenzyl) thio)-1, 3, 4-thiadiazol-2-yl)-4-oxothiochromane-2-carboxamide (5e). White solid; mp 220–222°C; yield 62%; ^{1}H NMR (400 MHz, DMSO-d_6, ppm) δ: 12.99 (s, 1H, CONH), 7.90 (d, J = 4.0 Hz, 1H, Ph-H), 7.55 (dd, J1 = 4.0 Hz, J2 = 8.0 Hz, 1H, Ph-H), 7.43–7.38 (m, 3H, Ph-H), 7.16–7.11 (m, 2H, Ph-H), 4.46 (d, J = 8.0 Hz, 3H, SCH, $PhCH_2$), 3.22 (qd, J1 = 4.0 Hz, J2 = 16.0 Hz, 2H, CH_2); ^{13}C NMR (100 MHz, DMSO-d_6, ppm) δ: 191.19, 169.63, 161.95 (d, J = 242.0 Hz), 159.05, 136.53, 133.82, 133.45 (d, J = 3.0 Hz), 131.76, 131.48, 131.39, 130.89, 129.92, 127.23, 115.86 (d, J = 5.0 Hz), 41.13, 40.41, 37.12; HRMS (ESI) $[M-H]^+$ calcd. for $C_{19}H_{13}ClFN_3O_2S_3$: 463.97697, found 463.97829.

Data for compound 6-fluoro-*N*-(5-(methylthio)-1, 3, 4-thiadiazol-2-yl)-4-oxothiochromane-2-carboxamide (5f). White solid; mp 220–222°C; yield 62%; ^{1}H NMR (400 MHz, DMSO-d_6, ppm) δ: 12.98 (s, 1H, CONH), 7.69 (d, J = 8.0 Hz, 1H, Ph-H), 7.41 (d, J = 4.0 Hz, 2H, Ph-H), 4.45 (s, 1H, SCH), 3.23 (qd, J1 = 4.0 Hz, J2 = 16.0 Hz, 2H, CH_2), 2.68 (s, 3H, CH_3); ^{13}C NMR (100 MHz, DMSO-d_6, ppm) δ: 191.37, 169.63, 161.81, 161.56, 158.91 (d, J = 95.0 Hz), 133.13, 132.11, 132.05, 130.14 (d, J = 7.0 Hz), 121.83 (d, J = 23.0 Hz), 113.98 (d, J = 23.0 Hz), 41.13, 40.40, 16.47; HRMS (ESI) $[M-H]^+$ calcd. for $C_{13}H_{10}FN_3O_2S_3$: 353.98464, found 353.98612.

Data for compound *N*-(5-(ethylthio)-1, 3, 4-thiadiazol-2-yl)-6-fluoro-4-oxothiochromane-2-carboxamide (5g). White solid; mp 261–262°C; yield 76%; ^{1}H NMR (400 MHz, DMSO-d_6, ppm) δ: 12.98 (s, 1H, CONH), 7.70–7.67 (m, 1H, Ph-H), 7.41 (dd, J1 = 4.0 Hz, J2 = 8.0 Hz, 2H, Ph-H), 4.45 (t, J = 4.0 Hz, 1H, SCH), 3.30–3.15 (m, 4H, CH_2, CH_2CH_3), 1.30 (t, J = 4.0 Hz, 3H, CH_2CH_3); ^{13}C NMR (100 MHz, DMSO-d_6, ppm) δ: 196.11, 174.39, 172.91, 165.57 (d, J = 198.0 Hz), 164.13, 163.53, 137.88, 137.86, 136.82 (d, J = 6.0 Hz), 134.91 (d, J = 7.0 Hz), 126.61 (d, J = 23.0 Hz), 118.73 (d, J = 17.0 Hz), 45.85, 40.41, 33.34, 19.93; HRMS (ESI) $[M+Na]^+$ calcd. for $C_{14}H_{12}FN_3O_2S_3$: 391.99678, found 391.99632.

Data for compound 6-fluoro-4-oxo-*N*-(5-(propylthio)-1, 3, 4-thiadiazol-2-yl)thiochromane-2-carboxamide (5h). White solid; mp 226–228°C; yield 70%; ^{1}H NMR (400 MHz, DMSO-d_6, ppm) δ: 12.98 (s, 1H, CONH), 7.69 (d, J = 8.0 Hz, 1H, Ph-H), 7.41 (t, J = 4.0 Hz, 2H, Ph-H), 4.44 (t, J = 4.0 Hz, 1H, SCH), 3.30–3.14 (m, 4H, CH_2, $CH_2CH_2CH_3$), 1.67 (m, 2H, CH_2, $CH_2CH_2CH_3$), 0.95 (t, J = 8.0 Hz, 3H, $CH_2CH_2CH_3$); ^{13}C NMR (100 MHz, DMSO-d_6, ppm) δ: 191.37, 169.67, 160.91 (d, J = 179.0 Hz), 159.38, 133.14 (d, J = 3.0 Hz), 132.06 (d, J = 6.0 Hz), 130.15 (d, J = 8.0 Hz), 121.97, 121.74, 114.09, 113.86, 41.10, 40.41, 36.02, 22.85, 13.36; HRMS (ESI) $[M-H]^+$ calcd. for $C_{15}H_{14}FN_3O_2S_3$: 382.01594, found 382.01732.

Data for compound *N*-(5-(benzylthio)-1, 3, 4-thiadiazol-2-yl)-6-fluoro-4-oxothiochromane-2-carboxamide (5i). White solid; mp 212–214°C; yield 73%; ^{1}H NMR (400 MHz, DMSO-d_6, ppm) δ: 12.99 (s, 1H, CONH), 7.69 (d, J = 8.0 Hz, 1H, Ph-H), 7.41–7.23 (m, 7H, Ph-H), 4.44 (t, J = 4.0 Hz, 3H, SCH, $PhCH_2$), 3.22 (qd, J1 = 4.0 Hz, J2 = 16.0 Hz, 2H, CH_2); ^{13}C NMR (100 MHz, DMSO-d_6, ppm) δ: 191.40, 169.66, 160.60 (d, J = 243.0 Hz), 159.24, 159.12, 137.05, 133.14, 132.08, 130.16 (d, J = 7.0 Hz), 129.38, 129.01, 128.04, 121.86 (d, J = 23.0 Hz), 113.99 (d, J = 22.0 Hz), 41.14, 40.40, 38.01; HRMS (ESI) $[M-H]^+$ calcd. for $C_{19}H_{14}FN_3O_2S_3$: 430.01594, found 430.01700.

Data for compound 6-fluoro-*N*-(5-((4-fluorobenzyl) thio)-1, 3, 4-thiadiazol-2-yl)-4-oxothiochromane-2-carboxamide (5j). White solid; mp 225–227°C; yield 70%; ^{1}H NMR (400 MHz, DMSO-d_6, ppm) δ: 12.98 (s, 1H, CONH), 7.68 (d, J = 8.0 Hz, 1H, Ph-H), 7.42 (dd, J1 = 4.0 Hz, J2 = 8.0 Hz, 4H, Ph-H), 7.13 (t, J = 8.0 Hz, 2H, Ph-H), 4.44 (t, J = 4.0 Hz, 3H, SCH, $PhCH_2$), 3.22 (qd, J1 = 4.0 Hz, J2 = 16.0 Hz, 2H, CH_2); ^{13}C NMR (100 MHz, DMSO-d_6, ppm) δ: 191.19, 169.63, 161.95 (d, J = 242.0 Hz), 159.05, 136.53, 133.82, 133.45 (d, J = 3.0 Hz), 131.76, 131.48, 131.39, 130.89, 129.92, 127.23, 115.81 (d, J = 22.0 Hz), 41.13, 40.41, 34.12; HRMS (ESI) $[M-H]^+$ calcd. for $C_{19}H_{13}F_2N_3O_2S_3$: 448.00652, found 448.00777.

Data for compound 6-methyl-*N*-(5-(methylthio)-1, 3, 4-thiadiazol-2-yl)-4-oxothiochromane-2-carboxamide (5k). White solid; mp 269–270°C; yield 79%; ^{1}H NMR (400 MHz, DMSO-d_6, ppm) δ: 12.94 (s, 1H, CONH), 7.79 (s, 1H, Ph-H), 7.30 (dd, J1 = 4.0 Hz, J2 = 8.0 Hz, 1H, Ph-H), 7.20 (d, J = 8.0 Hz, 1H, Ph-H), 4.41 (t, J = 4.0 Hz, 1H, SCH), 3.17 (qd, J1 = 4.0 Hz, J2 = 16.0 Hz, 2H, CH_2); 2.67 (s, 3H, CH_3), 2.29 (s, 3H, CH_3); ^{13}C NMR (100 MHz, DMSO-d_6, ppm) δ: 192.17, 169.72, 161.46, 158.44, 135.61, 135.03, 134.10, 130.34, 128.29, 127.68, 41.19, 40.41, 20.83, 16.47; HRMS (ESI) $[M-H]^+$ calcd. for $C_{14}H_{13}N_3O_2S_3$: 350.00971, found 350.01051.

Data for compound *N*-(5-(ethylthio)-1, 3, 4-thiadiazol-2-yl)-6-methyl-4-oxothiochromane-2-carboxamide (5l). White solid; mp 227–228°C; yield 76%; ^{1}H NMR (400 MHz, DMSO-d_6, ppm) δ: 12.97 (s, 1H, CONH), 7.80 (s, 1H, Ph-H), 7.30 (dd, J1 = 4.0 Hz, J2 = 8.0 Hz, 1H, Ph-H), 7.20 (d, J = 8.0 Hz, 1H, Ph-H), 4.42 (t, J = 4.0 Hz, 1H, SCH), 3.25–3.11 (m, 4H, CH_2, CH_2CH_3), 2.30 (s, 3H, CH_3), 1.31 (t, J = 8.0 Hz, 3H, CH_2CH_3); ^{13}C NMR (100 MHz, DMSO-d_6, ppm) δ: 192.16, 169.77, 159.70, 158.84, 135.60, 135.03, 134.11, 130.33, 128.29, 127.67, 41.20, 40.41, 28.59, 20.83, 15.18; HRMS (ESI) $[M-H]^+$ calcd. for $C_{15}H_{15}N_3O_2S_3$: 364.02536, found 364.02620.

Data for compound 6-methyl-4-oxo-*N*-(5-(propylthio)-1, 3, 4-thiadiazol-2-yl)thiochromane-2-carboxamide (5m). White solid; mp 198–200°C; yield 72%; ^{1}H NMR (400 MHz, DMSO-d_6, ppm) δ: 13.00 (s, 1H, CONH), 7.90 (d, J = 4.0 Hz, 1H, Ph-H), 7.39 (d, J = 8.0 Hz, 1H, Ph-H), 4.46 (t, J = 4.0 Hz, 1H, SCH), 3.31–3.14 (m, 4H, CH_2, $CH_2CH_2CH_3$), 2.29 (s, 3H, CH_3), 1.69–1.64 (m, 2H, $CH_2CH_2CH_3$), 0.95 (t, J = 8.0 Hz, 3H, $CH_2CH_2CH_3$); ^{13}C NMR (100 MHz, DMSO-d_6, ppm) δ: 191.19, 169.68, 159.96, 158.88, 136.59, 133.80, 131.78, 130.86, 129.91, 127.22, 41.17, 40.41, 39.57, 36.03, 22.86, 13.37; HRMS (ESI) $[M-H]^+$ calcd. for $C_{15}H_{14}ClN_3O_2S_3$: 397.98639, found 397.98782.

Data for compound *N*-(5-(benzylthio)-1, 3, 4-thiadiazol-2-yl)-6-methyl-4-oxothiochromane-2-carboxamide (5n). White solid; mp 224–226°C; yield 76%; ^{1}H NMR (400 MHz, DMSO-d_6, ppm) δ: 12.94 (s, 1H, CONH), 7.79 (s, 1H, Ph-H), 7.43–7.11 (m, 7H, Ph-H), 4.45 (s, 2H, $PhCH_2$), 4.41 (s, 1H, SCH), 3.17 (qd, J1 = 4.0 Hz, J2 = 16.0 Hz, 2H, CH_2), 2.29 (s, 3H, CH_3); ^{13}C NMR (100 MHz, DMSO-d_6, ppm) δ: 192.19, 169.80, 159.13, 158.92, 137.07, 135.62, 134.11, 133.48, 131.39, 130.32, 129.37, 129.02, 128.31, 128.04, 127.68, 115.92, 115.70, 41.23, 38.02, 37.14, 20.83; HRMS (ESI) $[M+Na]^+$ calcd. for $C_{20}H_{17}N_3O_2S_3$: 450.03751, found 450.03614.

Data for compound *N*-(5-((4-fluorobenzyl)thio)-1, 3, 4-thiadiazol-2-yl)-6-methyl-4-oxothiochromane-2-carboxamide (5°). White solid; mp 230–232°C; yield 76%; ^{1}H NMR (400 MHz, DMSO-d_6, ppm) δ: 12.97 (s, 1H, CONH), 7.79 (s, 1H, Ph-H), 7.38 (dd, J1 = 8.0 Hz, J2 = 16.0 Hz, 4H, Ph-H), 7.30 (d, J = 8.0 Hz, 1H, Ph-H), 7.20 (d, J = 8.0 Hz, 1H, Ph-H), 4.45 (s, 2H, $PhCH_2$), 4.41 (t, J = 4.0 Hz, 1H, SCH), 3.17 (qd, J1 = 4.0 Hz, J2 = 16.0 Hz, 2H, CH_2), 2.29 (s, 3H, CH_3); ^{13}C NMR (100 MHz, DMSO-d_6, ppm) δ: 192.19, 169.80, 159.04 (d, J = 50.0 Hz), 136.42, 135.61, 135.05, 134.11, 132.60, 131.23, 128.96, 128.30, 127.68, 41.21, 37.13, 20.83; HRMS (ESI) $[M+Na]^+$ calcd. for $C_{20}H_{16}FN_3O_2S_3$: 468.09808, found 468.09825.

3.2. Bioassay Activity Test. As shown in Table 1, compounds 5a–5g displayed 74–100% and 60–94% in vitro antibacterial activity against *Xoo* at 200 and 100 μg/mL, respectively, which were better than those of bismerthiazol and thiadiazole copper. Meanwhile, compounds 5a–5h revealed 60–90% and 48–78% in vitro antibacterial activity against *Xac* at 200 and 100 μg/mL, respectively, which were better than those of bismerthiazol and thiadiazole copper. Table 2 shows that the EC_{50} values of compounds 5a, 5b, 5c, 5f, and 5g against *Xoo* and *Xac* were 24–54 and 30–61 μg/mL. In particular, compound 6-chloro-*N*-(5-(methylthio)-1, 3, 4-thiadiazol-2-yl)-4-oxothiochromane-2-carboxamide (5a) had the lowest EC_{50} values against *Xoo* (24 μg/mL) and *Xac* (30 μg/mL) than bismerthiazol and thiadiazole copper. The structure-activity relationship (SAR) analysis was analyzed on the basis of the antibacterial activity values shown in Tables 1 and 2. First, compared with the same substituent at R_1 substituent groups, the presence of the –Cl group at R_2 substituent group showed better in vitro antibacterial activity in the order of 5a > 5f and 5b > 5g. Second, compared with the same substituent at R_2 substituent group, the $-CH_3$ at R_1 substituent group could cause an increase in the antibacterial activity followed the order 5a > 5b and 5f > 5g.

Table 1: Preliminary antibacterial activity of the target compounds against Xoo and Xac at 200 and 100 μg/mL.

Compounds	Inhibition rate (%)			
	Xoo		Xac	
	200 μg/mL	100 μg/mL	200 μg/mL	100 μg/mL
5a	100 ± 2.13	94 ± 1.25	90 ± 0.28	78 ± 1.01
5b	92 ± 1.14	78 ± 2.07	86 ± 2.22	70 ± 1.27
5c	81 ± 2.19	70 ± 1.64	74 ± 2.08	61 ± 2.21
5d	60 ± 1.95	44 ± 1.47	51 ± 1.18	40 ± 1.27
5e	64 ± 1.54	50 ± 1.99	57 ± 3.12	45 ± 2.19
5f	90 ± 1.17	75 ± 1.54	80 ± 2.21	61 ± 1.31
5g	74 ± 1.41	60 ± 2.17	68 ± 1.14	54 ± 1.29
5h	68 ± 1.54	54 ± 0.59	60 ± 1.24	48 ± 2.20
5i	51 ± 1.19	38 ± 1.02	47 ± 1.14	31 ± 2.01
5j	54 ± 2.08	41 ± 1.28	51 ± 1.98	39 ± 1.52
5k	45 ± 2.21	32 ± 1.59	40 ± 1.21	30 ± 2.06
5l	37 ± 1.27	28 ± 2.28	32 ± 0.98	20 ± 0.94
5m	30 ± 1.08	20 ± 2.21	25 ± 1.26	14 ± 2.19
5n	24 ± 1.26	16 ± 1.21	16 ± 1.24	8 ± 1.54
5o	28 ± 1.11	18 ± 1.24	21 ± 1.59	12 ± 2.20
Bismerthiazol	70 ± 0.89	52 ± 1.62	57 ± 5.56	35 ± 6.76
Thiadiazole copper	63 ± 2.71	45 ± 2.65	35 ± 4.31	15 ± 2.11

Table 2: The EC_{50} values of some of the target compounds against Xoo and Xac.

Compounds	EC_{50} (μg/mL)	
	Xoo	Xac
5a	24 ± 2.25	30 ± 2.18
5b	32 ± 1.65	40 ± 2.49
5c	45 ± 2.05	51 ± 2.65
5f	26 ± 1.54	35 ± 2.65
5g	54 ± 1.94	61 ± 2.27
Bismerthiazol	84 ± 2.89	145 ± 2.65
Thiadiazole copper	109 ± 3.01	230 ± 2.46

The preliminary antifungal activity results at 50 μg/mL (Table 3) showed that compound 5m displayed a favorable antifungal activity (69%) than carbendazim against *B. cinerea*. Meanwhile, compound 6-methyl-4-oxo-*N*-(5-(propylthio)-1, 3, 4-thiadiazol-2-yl)thiochromane-2-carboxamide (5m) revealed the best antifungal activity against *V. dahliae* (54%) and *F. oxysporum* (40%), and it was still lower than that of carbendazim. The SAR analysis was analyzed on the basis of the antifungal activity values shown in Table 3. First, compared with the same substituent at R_1 substituent groups, the presence of the $-CH_3$ group at the R_2 substituent group showed better in vitro antifungal activity in the order of 5m > 5h and 5l > 5g. Second, compared with the same substituent at the R_2 substituent group, the $-CH_2CH_2CH_3$ at the R_1 substituent group could cause an increase in the antifungal activity following the order 5m > 5l > 5k and 5h > 5g > 5f.

Table 3: The antifungal activity of the target compounds 5a–5o against *B. cinerea*, *V. dahliae*, and *F. oxysporum* at 50 μg/mL.

Compounds	Inhibition rate (%)		
	B. cinerea	*V. dahliae*	*F. oxysporum*
5a	0	0	2 ± 1.01
5b	17 ± 3.26	8 ± 1.21	5 ± 1.65
5c	21 ± 1.14	15 ± 2.96	12 ± 1.26
5d	0	2 ± 1.32	0
5e	0	0	0
5f	0	0	0
5g	48 ± 4.02	24 ± 1.69	16 ± 2.21
5h	55 ± 1.29	36 ± 2.95	26 ± 1.54
5i	0	0	0
5j	0	0	0
5k	0	12 ± 1.56	0
5l	61 ± 1.23	45 ± 1.95	32 ± 1.65
5m	69 ± 2.24	54 ± 1.25	40 ± 1.65
5n	0	0	0
5o	9 ± 1.94	6 ± 2.67	
Carbendazim	57 ± 2.19	79 ± 3.18	100

4. Conclusion

In conclusion, a total of 15 novel thiochroman-4-one derivatives incorporating carboxamide and 1, 3, 4-thiadiazole thioether moieties were synthesized. Bioassay results showed that compound 6-chloro-*N*-(5-(methylthio)-1, 3, 4-thiadiazol-2-yl)-4-oxothiochromane-2-carboxamide (5a) revealed the best antibacterial activity against *Xoo* and *Xac*. Meanwhile, 6-methyl-4-oxo-*N*-(5-(propylthio)-1, 3, 4-thiadiazol-2-yl) thiochromane-2-carboxamide (5m) showed a better antifungal activity against *B. cinerea*. This study demonstrated that this series of thiochroman-4-one derivatives incorporating carboxamide and 1, 3, 4-thiadiazole thioether moieties can be used to develop potential agrochemicals.

Data Availability

All data included in this study are available upon request by contact with the corresponding author.

Conflicts of Interest

The authors declare that they have no conflicts of interest.

Authors' Contributions

The authors Lu Yu and Lingling Xiao contributed equally to the article.

Acknowledgments

This research was funded by the National Natural Science Foundation of China (grant no. 32102267), Science and Technology Foundation of Guizhou Province (grant numbers ZK[2021]137 and [2020]1Y130), and Kaili University Doctoral Program (grant no. BS201811).

Supplementary Materials

The supporting information contained 1H NMR, ^{13}C NMR, and HRMS spectra for all the target compounds 5a–5o. (*Supplementary Materials*)

References

[1] R. Bhattacharjee and U. Dey, "An overview of fungal and bacterial biopesticides to control plant pathogens/diseases," *African Journal of Microbiology Research*, vol. 8, pp. 1479–1762, 2014.

[2] N. Patel, P. Desai, N. Patel, A. Jha, and H. K. Gautam, "Agronanotechnology for plant fungal disease management: a review," *International Journal of Current Microbiology and Applied Sciences*, vol. 3, pp. 71–84, 2014.

[3] E. T. Alori and O. O. Babalola, "Microbial inoculants for improving crop quality and human health in africa," *Frontiers in Microbiology*, vol. 9, p. 2213, 2018.

[4] R. S. Mann and P. E. Kaufman, "Natural product pesticides: their development, delivery and use against insect vectors," *Mini-Reviews in Organic Chemistry*, vol. 9, no. 2, pp. 185–202, 2012.

[5] D. A. Dias, S. Urban, and U. Roessner, "A historical overview of natural products in drug discovery," *Metabolites*, vol. 2, no. 2, pp. 303–336, 2012.

[6] L. G. Copping and S. O. Duke, "Natural products that have been used commercially as crop protection agents," *Pest Management Science*, vol. 63, no. 6, pp. 524–554, 2007.

[7] I. Ujváry, "Natural product pesticides," *Encyclopedia of Agrochemicals*, vol. 3, 2003.

[8] Y. F. Zhong, X. Y. Han, S. B. Li, H. Qi, Y. L. Song, and X. Q. Qiao, "Design, synthesis, antifungal activity and molecular docking of thiochroman-4-one derivatives," *Chemical and Pharmaceutical Bulletin*, vol. 65, pp. 904–910, 201.

[9] S. S. Szucs, "Thiono-thiochroman and -dihydrobenzothiophene compounds as herbicidal agents," *PCT International Applied WO*, Article ID 2001029033, 2001.

[10] G. Steiner, T. Schmidt, M. Kordes et al., "Amino-substituted benzo(hetero)cyclic derivatives, particularly 1-Alkyl-4-benzo(hetero)cyclicsubstituted π-perazines, useful ass insecticides, Acaricides, and nematocides, and their preparation, uses, and compositions," *PCT International Applied WO*, Article ID 2004080170, 2004.

[11] L. Yu, J. Chi, L. Xiao et al., "Novel thiochromanone derivatives containing a sulfonyl hydrazone moiety: design, synthesis, and bioactivity evaluation," *Molecules*, vol. 26, no. 10, Article ID 2925, 2021.

[12] J. Chi, L. Yu, P. Li et al., "Design, synthesis, and antibacterial activity of novel thiochromanone derivatives containing an acylhydrazone moiety," *Phosphorus, Sulfur, and Silicon and the Related Elements*, vol. 197, no. 1, pp. 13–17, 2021.

[13] L. Yu, L. Xiao, J. Chi et al., "Design, synthesis, and bioactivity evaluation of novel thiochromanone derivatives containing an oxime or oxime ether moiety," *Journal of Heterocyclic Chemistry*, vol. 58, no. 11, pp. 2124–2131, 2021.

[14] L. Xiao, L. Yu, P. Li et al., "Design, synthesis, and bioactivity evaluation of new thiochromanone derivatives containing a carboxamide moiety," *Molecules*, vol. 26, no. 15, Article ID 4391, 2021.

[15] M. Chen, D. Lu, X. Zhang et al., "Synthesis and biological activities of novel S-β-D-glucopyranoside derivatives of 1,2,4-triazole," *Phosphorus, Sulfur, and Silicon and the Related Elements*, vol. 196, no. 7, pp. 679–684, 2021.

[16] J. Chen, C. Yi, S. Wang et al., "Novel amide derivatives containing 1, 3, 4-thiadiazole moiety: design, synthesis, nematocidal and antibacterial activities," *Bioorganic & Medicinal Chemistry Letters*, vol. 29, no. 10, pp. 1203–1210, 2019.

[17] M. Chen, X. Zhang, D. Lu et al., "Synthesis and bioactivities of novel 1, 3, 4-thiadiazole derivatives of glucosides," *Frontiers of Chemistry*, vol. 9, Article ID 645876, 2021.

[18] X.-J. Du, X.-J. Zhao, R.-Q. Zhao, W.-G. Zhao, W.-L. Dong, and X.-H. Liu, "Design, synthesis and antifungal activity of threoninamide carbamate derivatives via pharmacophore model," *Journal of Enzyme Inhibition and Medicinal Chemistry*, vol. 35, no. 1, pp. 682–691, 2020.

[19] X. Tang, C. Zhang, M. Chen, Y. Xue, T. Liu, and W. Xue, "Synthesis and antiviral activity of novel myricetin derivatives containing ferulic acid amide scaffolds," *New Journal of Chemistry*, vol. 44, no. 6, pp. 2374–2379, 2020.

[20] Z. Yang, P. Li, and X. Gan, "Novel pyrazole-hydrazone derivatives containing an isoxazole moiety: design, synthesis, and antiviral activity," *Molecules*, vol. 23, no. 7, Article ID 1798, 2018.

[21] Z.-B. Yang, P. Li, and Y.-J. He, "Design, synthesis, and bioactivity evaluation of novel isoxazole-amide derivatives containing an acylhydrazone moiety as new active antiviral agents," *Molecules*, vol. 24, no. 20, Article ID 3766, 2019.

[22] B. Wang, H. Wang, H. Liu et al., "Synthesis and structure-insecticidal activity relationship of novel phenylpyrazole carboxylic acid derivatives containing fluorine moiety," *Chinese Chemical Letters*, vol. 31, no. 3, pp. 739–745, 2020.

[23] X. Hua, C. Liu, S. Zhou et al., "Design, synthesis and insecticidal evaluation of novel N-pyridylpyrazolecarboxamide derivatives containing isoxazole, isoxazoline and 1, 3, 4-thiadiazole rings," *Chemical Research in Chinese Universities*, vol. 33, no. 6, pp. 882–889, 2017.

[24] X. Sun, Z. Ji, S. Wei, and Z. Ji, "Design, synthesis and herbicidal activity of 5-cyclopropyl-N-phenylisoxazole-4-carboxamides," *Journal of Molecular Structure*, vol. 1220, Article ID 128628, 2020.

[25] X. Ruan, C. Zhang, S. Jiang et al., "Design, synthesis, and biological activity of novel myricetin derivatives containing amide, thioether, and 1, 3, 4-thiadiazole moieties," *Molecules*, vol. 23, no. 12, p. 3132, 2018.

[26] X. Wang, W.-G. Duan, G.-S. Lin, M. Chen, and F.-H. Lei, "Synthesis, antifungal activity and 3D-QSAR study of novel nopol-based 1, 3, 4-thiadiazole-thioether compounds," *Research on Chemical Intermediates*, vol. 47, no. 10, pp. 4029–4049, 2021.

[27] C. Wang, H. Song, W. Liu, and C. Xu, "Design, synthesis and antifungal activity of novel thioureas containing 1, 3, 4-thiadiazole and thioether skeleton," *Chemical Research in Chinese Universities*, vol. 32, no. 4, pp. 615–620, 2016.

[28] W.-M. Xu, S.-Z. Li, M. He, S. Yang, X.-Y. Li, and P. Li, "Synthesis and bioactivities of novel thioether/sulfone derivatives containing 1,2,3-thiadiazole and 1, 3, 4-oxadiazole/thiadiazole moiety," *Bioorganic & Medicinal Chemistry Letters*, vol. 23, no. 21, pp. 5821–5824, 2013.

[29] L. Yu, X. Gan, D. Zhou, F. He, S. Zeng, and D. Hu, "Synthesis and antiviral activity of novel 1,4-Pentadien-3-one derivatives containing a 1, 3, 4-thiadiazole moiety," *Molecules*, vol. 22, no. 4, 658 pages, 2017.

[30] X. Zhong, X. Wang, L. Chen et al., "Synthesis and biological activity of myricetin derivatives containing 1, 3, 4-thiadiazole scaffold," *Chemistry Central Journal*, vol. 11, no. 1, p. 106, 2017.

[31] W.-N. Wu, A.-Q. Tai, Q. Chen, and G.-P. Ouyang, "Synthesis and antiviral bioactivity of novel 2-substituted methlthio-5-(4-amino-2-methylpyrimidin-5-yl)-1, 3, 4-thiadiazole derivatives," *Journal of Heterocyclic Chemistry*, vol. 53, no. 2, pp. 626–632, 2016.

[32] R. G. Yang, M. Y. Han, J. P. Fan et al., "Development of novel (+)-Nootkatone thioethers containing 1, 3, 4-oxadiazole/thiadiazole moieties as insecticide candidates against three species of insect pests," *Journal of Agricultural and Food Chemistry*, vol. 69, 2021.

[33] X. Ding, Z. Zhai, L. Lv, Z. Sun, and X. Liu, "Design, synthesis, biological activity and density function theory study of pyrazole derivatives containing 1, 3, 4-thiadiazole moiety," *Frontiers of Chemical Science and Engineering*, vol. 11, no. 3, pp. 379–386, 2017.

[34] P. Dalgaard, T. Ross, L. Kamperman, K. Neumeyer, and T. A. McMeekin, "Estimation of bacterial growth rates from turbidimetric and viable count data," *International Journal of Food Microbiology*, vol. 23, no. 3-4, pp. 391–404, 1994.

[35] K. C. Tarun and D. J. Prem, "Antifungal activity of 4-methyl-6-alkyl-2H-pyran-2-ones," *Journal of Agricultural and Food Chemistry*, vol. 54, pp. 2129–2133, 2006.

Hindawi
Journal of Chemistry
Volume 2021, Article ID 1036199, 10 pages
https://doi.org/10.1155/2021/1036199

Research Article

Research on Crystal Structure and Fungicidal Activity of the Amide Derivatives Based on the Natural Products Sinapic Acid and Mycophenolic Acid

Zhanfang Chen,[1] Hongbin Fang,[1] Xuewen Hua,[1] Wenrui Liu,[1] Yi Liu,[1] Chenmeng Xue,[1] Bingxiang Wang,[2] Dzmitry Bazhanau,[1] Xiaohe Zhu,[1] Man Yuan,[1] Jing Ru,[3] and Pengfei Chu[1]

[1]*College of Agriculture, Liaocheng University, Liaocheng 252000, China*
[2]*College of Pharmacy, Liaocheng University, Liaocheng 252000, China*
[3]*College of Chemistry and Chemical Engineering, Liaocheng University, Liaocheng 252000, China*

Correspondence should be addressed to Xuewen Hua; huaxuewen906@163.com, Bingxiang Wang; wangbingxiang@lcu.edu.cn, and Pengfei Chu; chupengfei@lcu.edu.cn

Received 9 November 2021; Accepted 30 November 2021; Published 21 December 2021

Academic Editor: Wenneng Wu

Structural optimization based on natural products is an important and effective way to discover new green pesticides. Here, two series of amide derivatives based on sinapic acid and mycophenolic acid were designed in combination with the fungicidal natural product piperlongumine and synthesized by preparing the carboxylic acid into acyl chloride and then reacting with the corresponding aromatic amines, respectively. The resulting structures were successively characterized by ^{1}H NMR, ^{13}C NMR, and HRMS. The crystal structures of molecules **I-4** and **II-5** were analyzed for structure validation. The in vitro inhibitory activity indicated that most of the target products exhibited fungicidal activity equivalent to or even better than fluopyram against *Physalospora piricola*. The in vivo fungicidal activity demonstrated that the compounds **I-5** and **II-4** displayed almost the same preventative activity as carbendazim and fluopyram at 200 μg mL^{-1}. The TEM observation revealed that the fungicidal activity of the target molecules against *Physalospora piricola* may be due to the influence on the mitochondria in the cell structure. These results will provide valuable theoretical guidance for developing the new green fungicides.

1. Introduction

Agrochemicals are important production materials for agricultural production, and their development plays an important role in ensuring national food security, agricultural product quality, ecological environment safety, and public health [1]. However, the continuous application of traditional chemical fungicides has produced many negative effects including ecological environment pollution, pathogen resistance, and poison for beneficial insects and microorganisms [2, 3]. Therefore, the development of efficient, safe, low residual, and environmentally friendly green fungicides has become the inevitable trend for pesticide innovation [4, 5].

The discovery of lead compounds and the exploration of mechanism of action are the key to the development and innovation of fungicides. Structural optimization based on natural products has become an effective way to develop new green fungicides, which has important guiding significance for practicing new development concepts and promoting green development of agrochemicals [6–11]. For example, coumoxystrobin was successfully developed based on natural products strobilurin and coumarin (Figure 1) [12]. Moreover, natural product strobilurin A-derived

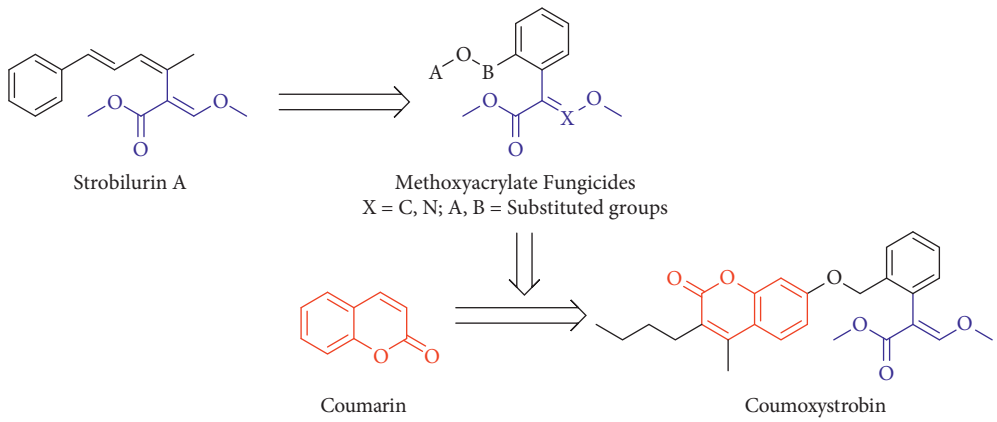

Figure 1: Methoxyacrylate fungicides and coumoxystrobin successfully developed based on natural product strobilurin A.

methoxyacrylate fungicides have occupied the top position in the market sales of fungicides [6].

Mycophenolic acid (MPA) was discovered by Gosio in 1893 in a strain of *Penicillium* fungus and was found to possess broad biological activity such as antifungal, antiviral, anticancer, and antipsoriasis properties [13, 14]. Sinapic acid is widely distributed in the plants and belongs to hydroxycinnamic acid. Furthermore, commercial fungicides dimethomorph, pyrimorph, and flumorph were successively developed based on natural product cinnamic acid (Figure 2) [15–18]. In this project, combined with the structure of fungicidal natural product piperlongumine [19, 20], two series of amide compounds based on natural products sinapic acid and mycophenolic acid were designed, synthesized, and evaluated their fungicidal activity against the common agricultural pathogens (Figure 3).

2. Experimental Materials and Methods

2.1. Materials and Equipment. The materials and reagents used in the organic synthesis reactions were of analytical grade and purchased from Energy Chemical and Bide Pharmatech Ltd. Melting points were measured on a X-5 binocular microscope (Yuhua Co., Ltd., China). ^{1}H NMR and ^{13}C NMR were provided on a AVANCE NEO-500 MHz spectrometer (Bruker, Germany). HRMS was recorded on a Xevo G2-XS QTof spectrometer (Waters, USA). X-ray crystal structure was determined on a D8 Venture diffractometer (Bruker, Germany). The purification of target compounds was performed by the column chromatography on silica gel (200–300 mesh).

2.2. Preparation of the Target Molecules. (*E*)-2,6-dimethoxy-4-(3-oxo-3-(phenylamino)prop-1-en-1-yl)phenyl acetate (**I-1**) was synthesized as follows. Thionyl chloride (2.38 g, 20.0 mmol) was added dropwise to a mixture of (E)-3-(4-acetoxy-3,5-dimethoxyphenyl) acrylic acid (1.06 g, 4.0 mmol) and DMF (3drops) in DCM (20 mL). The reaction was stirred for 6 h at room temperature and concentrated in vacuo to sufficiently remove the solvent and excess thionyl chloride. The resulting acyl chloride was immediately dissolved in anhydrous DCM (3 mL) and then added dropwise at room temperature to a mixture of aniline (0.45 g, 4.8 mmol) and trimethylamine (0.81 g, 8.0 mmol) in anhydrous DCM (25 mL). The reaction was stirred overnight and poured into a mixture of DCM and water (150 mL, v/v = 1/1). The DCM layer was separated by extraction and washed successively with dilute hydrochloric acid and potassium carbonate aqueous solution. The obtained solution was dried over anhydrous sodium sulfate, filtered, and concentrated. The provided residue was purified by silica gel chromatography using petroleum ether/ethyl acetate (v/v = 1/1) as eluent to provide **I-1** (yield 68%). Molecules **I-2**–**I-5** and **II-1**–**II-5** were prepared similarly.

(*E*)-2,6-dimethoxy-4-(3-oxo-3-(phenylamino)prop-1-en-1-yl)phenyl acetate (**I-1**): white solid, yield 68%, m.p. 125–127°C. ^{1}H NMR (500 MHz, $CDCl_3$) δ 7.67 (s, 1H, NH), 7.63–7.57 (m, 3H, Ph-H, and CH), 7.34 (t, J = 7.9 Hz, 2H, Ph-H), 7.12 (t, J = 7.4 Hz, 1H, Ph-H), 6.68 (s, 2H, Ph-H), 6.39 (d, J = 15.4 Hz, 1H, CH), 3.78 (s, 6H, $(OCH_3)_2$), 2.37 (s, 3H, $COCH_3$). ^{13}C NMR (126 MHz, $CDCl_3$) δ 169.0, 163.8, 152.3, 141.7, 138.2, 133.2, 130.1, 129.1, 124.4, 121.4, 119.8, 104.7, 56.2, 20.5. Found, *m/z*: 342.1333 $[M+H]^+$. $C_{19}H_{20}NO_5$. Calculated, *m/z*: 342.1336.

(*E*)-2,6-dimethoxy-4-(3-oxo-3-((2-(trifluoromethyl) phenyl)amino)prop-1-en-1-yl)phenyl acetate (**I-2**): white solid, yield 60%, m.p. 143–145°C. ^{1}H NMR (500 MHz, $CDCl_3$) *d* 8.37 (d, J = 7.9 Hz, 1H, Ph-H), 7.68 (d, J = 15.4 Hz, 1H, CH), 7.66–7.57 (m, 3H, NH, and Ph-H), 7.27–7.24 (m, 1H, Ph-H), 6.80 (s, 2H, Ph-H), 6.47 (d, J = 15.4 Hz, 1H, CH), 3.87 (s, 6H, $(OCH_3)_2$), 2.36 (s, 3H, $COCH_3$). ^{13}C NMR (126 MHz, $CDCl_3$) δ 168.6, 163.8, 152.5, 143.2, 135.4, 135.4, 133.0, 132.6, 130.4, 126.1 (q, $J_{C\text{-}F}$ = 5.4 Hz), 124.5, 124.4, 124.2 (q, $J_{C\text{-}F}$ = 273.4 Hz), 120.5, 104.7, 56.3, 20.5. Found, *m/z*: 410.1208 $[M+H]^+$. $C_{20}H_{19}F_3NO_5$. Calculated, *m/z*: 410.1210.

(*E*)-4-(3-((2,3-dichlorophenyl)amino)-3-oxoprop-1-en-1-yl)-2,6-dimethoxyphenyl acetate (**I-3**): white solid, yield 64%, m.p. 114–116°C. ^{1}H NMR (500 MHz, $CDCl_3$) δ 8.49 (dd, J = 7.5, 2.2 Hz, 1H, Ph-H), 7.89 (s, 1H, NH), 7.67 (d, J = 15.4 Hz, 1H, CH), 7.27–7.23 (m, 2H, Ph-H), 6.78 (s, 2H, Ph-H), 6.53 (d, J = 15.4 Hz, 1H, CH), 3.86 (s, 6H, $(OCH_3)_2$), 2.36 (s, 3H, $COCH_3$). ^{13}C NMR (126 MHz, $CDCl_3$) δ 168.6,

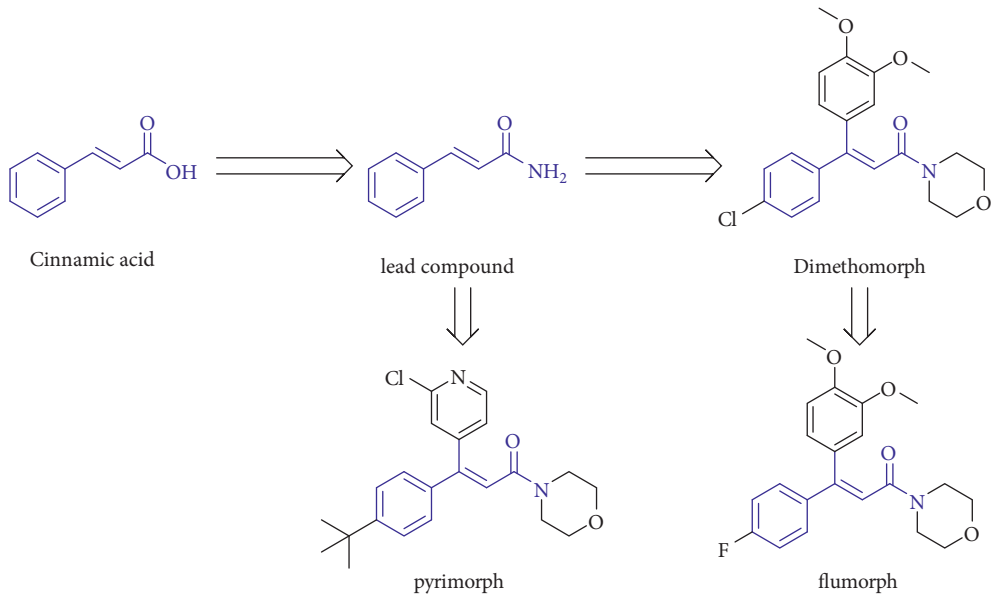

Figure 2: Cinnamic acid amide fungicides successfully developed based on natural product cinnamic acid.

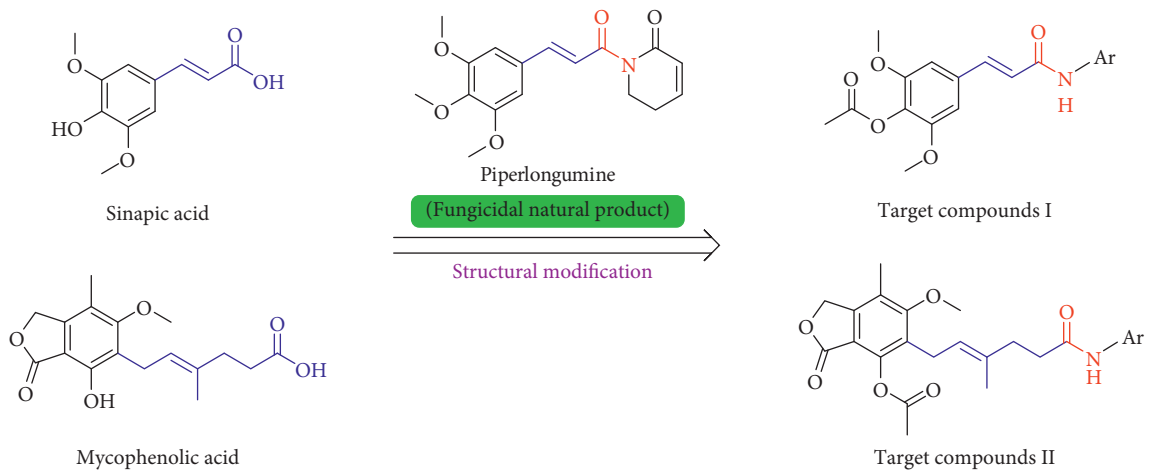

Figure 3: Molecular design strategy in this project.

163.7, 152.4, 143.2, 136.4, 132.8, 132.6, 130.4, 127.9, 125.3, 121.2, 120.6, 119.6, 104.7, 56.2, 20.5. Found, *m*/*z*: 410.0555 $[M+H]^+$. $C_{19}H_{18}Cl_2NO_5$. Calculated, *m*/*z*: 410.0557.

(*E*)-2,6-dimethoxy-4-(3-((2-methoxy-5-methylphenyl) amino)-3-oxoprop-1-en-1-yl)phenyl acetate (**I-4**): white solid, yield 72%, m.p. 153–155°C. ^{1}H NMR (500 MHz, $CDCl_3$) δ 8.35 (s, 1H, NH), 7.93 (s, 1H, Ph-H), 7.65 (d, J = 15.4 Hz, 1H, CH), 6.86 (dd, J = 8.2, 1.4 Hz, 1H, Ph-H), 6.80–6.78 (m, 3H, Ph-H), 6.52 (d, J = 15.4 Hz, 1H, CH), 3.89 (s, 3H, OCH_3), 3.87 (s, 6H, $(OCH_3)_2$), 2.35 (s, 3H, $COCH_3$), 2.33 (s, 3H, Ph-CH_3). ^{13}C NMR (126 MHz, $CDCl_3$) δ 168.6, 163.4, 152.4, 145.9, 141.6, 133.2, 130.8, 130.1, 127.5, 124.1, 121.7, 120.7, 109.8, 104.6, 56.2, 55.9, 21.0, 20.5. Found, *m*/*z*: 386.1594 $[M+H]^+$. $C_{21}H_{24}NO_6$. Calculated, *m*/*z*: 386.1598.

(*E*)-4-(3-((3-isopropoxyphenyl)amino)-3-oxoprop-1-en-1-yl)-2,6-dimethoxyphenyl acetate (**I-5**): white solid, yield 68%, m.p. 122–124°C. ^{1}H NMR (500 MHz, $CDCl_3$) δ 7.61 (d, J = 15.4 Hz, 1H, CH), 7.51 (s, 1H, Ph-H), 7.41 (s, 1H, NH), 7.21 (t, J = 8.1 Hz, 1H, Ph-H), 7.03 (d, J = 7.8 Hz, 1H, Ph-H), 6.71 (s, 2H, Ph-H), 6.67 (dd, J = 8.2, 1.8 Hz, 1H, Ph-H), 6.40 (d, J = 15.4 Hz, 1H, CH), 4.57 (hept, J = 6.1 Hz, 1H, $\underline{CH}(CH_3)_2$), 3.81 (s, 6H, $\underline{(OCH_3)_2}$), 2.36 (s, 3H, $COCH_3$), 1.34 (d, J = 6.1 Hz, 6H, $CH\underline{(CH_3)_2}$). ^{13}C NMR (126 MHz, $CDCl_3$) δ 168.9, 163.7, 158.6, 152.3, 149.3, 141.9, 139.3, 133.1, 130.1, 129.7, 121.3, 112.3, 111.8, 104.6, 70.0, 56.2, 22.1, 20.5. Found, *m*/*z*: 400.1753 $[M+H]^+$. $C_{22}H_{26}NO_6$. Calculated, *m*/*z*: 400.1755.

(*E*)-6-methoxy-7-methyl-5-(3-methyl-6-oxo-6-(phenylamino)hex-2-en-1-yl)-3-oxo-1,3-dihydroisobenzofuran-4-yl acetate (**II-1**) : white solid, yield 66%, m.p. 160–162°C. ^{1}H NMR (500 MHz, $CDCl_3$) δ 7.53 (s, 1H, NH), 7.33 (d, J = 7.8 Hz, 2H, Ph-H), 7.18 (t, J = 7.9 Hz, 2H, Ph-H), 7.01 (t,

$J = 7.4$ Hz, 1H, Ph-H), 5.15 (t, $J = 6.9$ Hz, 1H, CH), 5.01 (s, 2H, OCH_2Ph), 3.70 (s, 3H, OCH_3), 3.35 (d, $J = 7.1$ Hz, 2H, $PhCH_2$), 2.40 (s, 3H, $COCH_3$), 2.38–2.35 (m, 4H, CH_2CH_2), 2.06 (s, 3H, Ph-CH_3), 1.81 (s, 3H, CH_3). ^{13}C NMR (126 MHz, $CDCl_3$) δ 170.9, 169.9, 168.4, 162.6, 146.1, 145.5, 138.1, 134.6, 129.2, 128.5, 123.7, 123.0, 122.5, 119.6, 113.2, 68.4, 61.2, 36.1, 34.4, 23.5, 20.8, 16.8, 11.7. Found, *m/z*: 438.1907 $[M+H]^+$. $C_{25}H_{28}NO_6$. Calculated, *m/z*: 438.1911.

(*E*)-6-methoxy-7-methyl-5-(3-methyl-6-oxo-6-((2-(trifluoromethyl)phenyl) amino)hex-2-en-1-yl)-3-oxo-1,3-dihydroisobenzofuran-4-yl acetate (**II-2**): white solid, yield 70%, m.p. 93–95°C. ^{1}H NMR (500 MHz, $CDCl_3$) δ 8.09 (d, $J = 7.6$ Hz, 1H, Ph-H), 7.58 (d, $J = 7.8$ Hz, 1H, Ph-H), 7.51 (t, $J = 7.8$ Hz, 1H, Ph-H), 7.38 (s, 1H, NH), 7.21 (t, $J = 7.6$ Hz, 1H, Ph-H), 5.19 (t, $J = 6.4$ Hz, 1H, CH), 5.11 (s, 2H, OCH_2Ph), 3.77 (s, 3H, OCH_3), 3.36 (d, $J = 6.8$ Hz, 2H, $PhCH_2$), 2.51–2.44 (m, 2H, CH_2), 2.41 (t, $J = 7.4$ Hz, 2H, CH_2), 2.37 (s, 3H, $COCH_3$), 2.19 (s, 3H, Ph-CH_3), 1.83 (s, 3H, CH_3). ^{13}C NMR (126 MHz, $CDCl_3$) δ 170.9, 169.0, 168.2, 162.6, 146.2, 145.9, 135.2, 134.3, 132.8, 129.1, 126.0 (q, $J_{C\text{-}F} = 5.4$ Hz), 125.1, 124.8, 124.5, 122.9, 122.8, 113.5, 68.3, 61.2, 36.1, 34.7, 23.6, 20.5, 16.3, 11.8. Found, *m/z*: 506.1781 $[M+H]^+$. $C_{26}H_{27}F_3NO_6$. Calculated, *m/z*: 506.1785.

(*E*)-5-(6-((2,3-dichlorophenyl)amino)-3-methyl-6-oxohex-2-en-1-yl)-6-methoxy-7-methyl-3-oxo-1,3-dihydroisobenzofuran-4-yl acetate (**II-3**): white solid, yield 67%, m.p. 149–151°C. ^{1}H NMR (500 MHz, $CDCl_3$) δ 8.24 (dd, $J = 6.5$, 2.9 Hz, 1H, Ph-H), 7.67 (s, 1H, NH), 7.18 (s, 1H, Ph-H), 7.17 (dd, 1H, $J = 8.5$, 3.5 Hz, Ph-H), 5.20 (td, $J = 6.9$, 1.1 Hz, 1H, CH), 5.12 (s, 2H, OCH_2Ph), 3.74 (s, 3H, OCH_3), 3.36 (d, $J = 6.8$ Hz, 2H, $PhCH_2$), 2.51 (t, $J = 7.6$ Hz, 2H, CH_2), 2.42 (t, $J = 7.4$ Hz, 2H, CH_2), 2.39 (s, 3H, $COCH_3$), 2.16 (s, 3H, Ph-CH_3), 1.84 (s, 3H, CH_3). ^{13}C NMR (126 MHz, $CDCl_3$) δ 170.8, 169.1, 168.2, 162.6, 146.2, 145.9, 136.2, 134.2, 132.6, 129.0, 127.7, 125.1, 122.9, 119.7, 113.5, 68.3, 61.1, 36.2, 34.6, 23.6, 20.6, 16.5, 11.8. Found, *m/z*: 506.1129 $[M+H]^+$. $C_{25}H_{26}Cl_2NO_6$. Calculated, *m/z*: 506.1132.

(*E*)-6-methoxy-5-(6-((2-methoxy-5-methylphenyl) amino)-3-methyl-6-oxohex-2-en-1-yl)-7-methyl-3-oxo-1,3-dihydroisobenzofuran-4-yl acetate (**II-4**): white solid, yield 74%, m.p. 113–115°C. ^{1}H NMR (500 MHz, $CDCl_3$) δ 8.14 (s, 1H, NH), 7.69 (s, 1H, Ph-H), 6.79 (dd, $J = 8.2$, 1.1 Hz, 1H, Ph-H), 6.71 (d, $J = 8.3$ Hz, 1H, Ph-H), 5.16 (t, $J = 6.4$ Hz, 1H, CH), 5.10 (s, 2H, OCH_2Ph), 3.81 (s, 3H, OCH_3), 3.76 (s, 3H, OCH_3), 3.35 (d, $J = 6.8$ Hz, 2H, $PhCH_2$), 2.46–2.38 (m, 4H, CH_2CH_2), 2.37 (s, 3H, $COCH_3$), 2.27 (s, 3H, Ph-CH_3), 2.17 (s, 3H, Ph-CH_3), 1.83 (s, 3H, CH_3). ^{13}C NMR (126 MHz, $CDCl_3$) δ 170.5, 169.0, 168.3, 162.6, 146.1, 145.9, 145.7, 134.7, 130.4, 129.2, 127.3, 123.6, 122.9, 122.3, 120.4, 113.4, 109.6, 68.3, 61.2, 55.7, 36.4, 34.8, 23.6, 20.9, 20.5, 16.5, 11.8. Found, *m/z*: 506.1129 $[M+H]^+$. $C_{27}H_{32}NO_7$. Calculated, *m/z*: 506.1132.

(*E*)-5-(6-((3-isopropoxyphenyl)amino)-3-methyl-6-oxohex-2-en-1-yl)-6-methoxy-7-methyl-3-oxo-1,3-dihydroisobenzofuran-4-yl acetate (**II-5**): white solid, yield 58%, m.p. 89–91°C. ^{1}H NMR (500 MHz, $CDCl_3$) δ 7.45 (s, 1H, NH), 7.12 (s, 1H, Ph-H), 7.05 (t, $J = 8.1$ Hz, 1H, Ph-H), 6.75 (dd, $J = 8.0$, 0.9 Hz, 1H, Ph-H), 6.56 (dd, $J = 8.2$, 1.8 Hz, 1H, Ph-H), 5.15 (t, $J = 6.9$ Hz, 1H, CH), 5.05 (s, 2H, OCH_2Ph), 4.48 (dt, $J = 12.1$, 6.1 Hz, 1H, OCH), 3.71 (s, 3H, OCH_3), 3.35 (d, $J = 7.1$ Hz, 2H, $PhCH_2$), 2.41 (s, 3H, $COCH_3$), 2.40–2.31 (m, 4H, CH_2CH_2), 2.08 (s, 3H, Ph-CH_3), 1.81 (s, 3H, CH_3), 1.30 (d, $J = 6.1$ Hz, 6H, $CH(\underline{CH_3})_2$). ^{13}C NMR (126 MHz, $CDCl_3$) δ 170.9, 169.8, 168.4, 162.5, 158.2, 146.2, 145.6, 139.2, 134.6, 129.2, 129.1, 123.0, 122.5, 113.2, 111.8, 111.6, 107.1, 70.0, 68.4, 61.2, 36.2, 34.4, 23.5, 22.0, 20.8, 16.8, 11.7. Found, *m/z*: 496.2326 $[M+H]^+$. $C_{28}H_{34}NO_7$. Calculated, *m/z*: 496.2330.

2.3. X-Ray Crystal Structure Determination. The crystals of the target compounds **I-4** and **II-5** were cultivated from a mixed solvent of methanol, ethyl acetate, and n-hexane, respectively. All measurements were made on a Bruker D8 Venture diffractometer with *Mo-Kα* radiation ($\lambda = 0.71073$ Å). The crystal data of the compound **I-4** were collected at 298 K, and the colorless crystal is of monoclinic system, space group *C 2/c*, with $a = 28.208$ (3), $b = 11.1670$ (12), $c = 14.0948$ (14) Å, $\alpha = 90°$, $\beta = 114.242$ (4)°, $\gamma = 90°$, $V = 4048.3$ (7) Å^3, $Z = 8$, $F(000) = 1712$, density (calculated) = 1.324 g/cm^3, and linear absorption coefficient 0.100 mm^{-1}. All of the non-H atoms were refined anisotropically by full-matrix least-squares to give the final $R = 0.0493$ and $wR = 0.1153$ ($w = 1/[\sigma^2(F_o^2) + (0.0465P)^2 + 2.2020P]$, where $P = (F_o^2 + 2F_c^2)/3$) with $S = 1.064$ using the SHELXL program. The crystal data of the compound **II-5** were collected at 298(2) K, and the colorless crystal is of monoclinic system, space group $P2_1/n$, with $a = 15.3461$ (16), $b = 10.3766$ (11), $c = 16.0494$ (17) Å, $\alpha = 90°$, $\beta = 95.683$ (2)°, $\gamma = 90°$, $V = 2543.2$ (5) Å^3, $Z = 4$, $F(000) = 1056$, density (calculated) = 1.294 g/cm^3, and linear absorption coefficient 0.093 mm^{-1}. All of the non-H atoms were refined anisotropically by full-matrix least-squares to give the final $R = 0.0625$ and $wR = 0.1565$ ($w = 1/[\sigma^2(F_o^2) + (0.0001P)^2 + 0.9874P]$, where $P = (F_o^2 + 2F_c^2)/3$) with $S = 1.044$ using the SHELXL program. The crystal structures were solved by direct methods with SHELXS-2014/6 program.

2.4. Fungicidal Activity Measurement. With fluopyram and carbendazim as positive controls, the mycelial growth inhibition method was used to determine the in vitro inhibitory activities of the target compounds against common agricultural pathogens according to the previously reported procedures [21, 22], and each treatment was repeated at least three times. The tested pathogens include *Rhizoctonia solani* (RS), *Gibberella zeae* (GZ), *Botrytis cinerea* (BC), *Physalospora piricola* (PP), *Cercospora circumscissa Sacc.* (CS), *Colletotrichum capsici* (CC), *Alternaria kikuchiana Tanaka* (AK), and *Alternaria* sp. (AS). The in vivo fungicidal activity of compounds **I-5** and **II-4** against *Physalospora piricola* was performed on apples referring to literature methods [23]. The target molecule (5.0 mg) was dissolved in dimethyl sulfoxide (30 μL) and diluted with 0.1% Tween-80 aqueous solution to provide the test stock solution (200 μg·mL^{-1}), which was sprayed with the same volume on healthy apples. Subsequently, the fungi cake containing *Physalospora piricola* with a diameter of 7 mm was inoculated. After cultivation at 25°C for 5 days, the average lesion area was

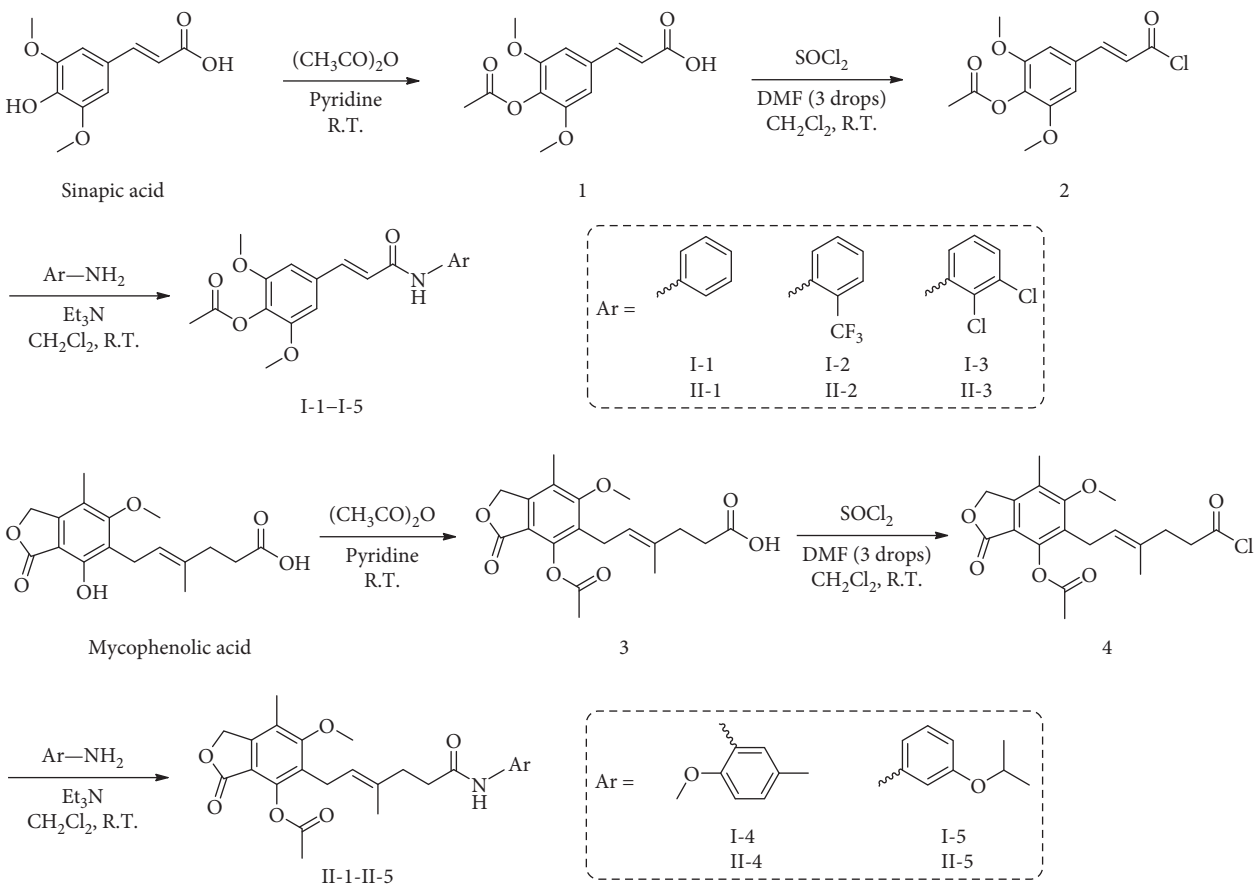

Scheme 1: The synthetic procedures for the target molecules **I** and **II**.

measured to calculate the preventative activity. Each in vivo fungicidal activity screening was carried out for at least five repeats.

2.5. Transmission Electron Microscope (TEM) Investigation. *Physalospora piricola* hyphae were obtained by incubation in PDB medium at 25°C for 72 h and centrifugation at 7000 rpm for 3 min, which were then resuspended in PDB medium to treat with compounds **I-5** and **II-4** (200 μg $\cdot$mL^{-1}) for 24 h, respectively. Subsequently, the treated hyphae were provided by centrifugation and fixed with 2.5% glutaraldehyde. The ultrastructure observation of the hyphae treated with compounds **I-5** and **II-4** (200 μg$\cdot$mL^{-1}) was performed by Shiyanjia Lab on a TEM according to the standard procedures.

3. Results and Discussion

3.1. Organic Synthesis. Herein, the important intermediates and target molecules **I-1**–**I-5** and **II-1**–**II-5** were provided referring to the reported procedures (Scheme 1). In the preparation of target compound **I-1**–**I-5**, the phenolic hydroxyl group in sinapic acid was firstly reacted with acetic anhydride to produce (*E*)-3-(4-acetoxy-3,5-dimethoxyphenyl)acrylic acid [24], which was further reacted with thionyl chloride under the catalyzed condition of DMF (3 drops) to provide (*E*)-3-(4-acetoxy-3,5-dimethoxyphenyl) acrylic chloride. Finally, the target compound **I-1**–**I-5** was synthesized by reacting the acyl chloride **2** with the corresponding aromatic amines, respectively. In addition, the condensing reagents such as EDCI-HOBt, HATU-DIEA, or TBTU-DIEA were also taken to explore the condensation of the carboxylic acid **1** and substituted aromatic amines; however, the yields of the products were low. The target compound **II-1**–**II-5** was obtained according to the same steps described above. Subsequently, the obtained structures were identified and characterized by ^{1}H NMR, ^{13}C NMR, and HRMS.

3.2. Crystal Structure Analysis. The crystal structure analysis is beneficial in investigating the physical and chemical properties of the molecules. In this study, several crystal structure characteristics were also illustrated through the crystal structures and packing of molecules **I-4** and **II-5** (Figure 4, CCDC numbers 2095769 and 2095768). The selected bond lengths and angles are presented in Table 1, and the selected dihedral angles are shown in Table 2. From the data, the sum of bond angles C(4)–C(3)–H(3), C(2)–C(3)–C(4), and C(2)–C(3)–H(3) in compound **I-4** was 360°, indicating the sp^2 hybridization state of atom C(3). Similarly, the atoms C(2) in **I-4** and C(17) in **II-5** also adopted sp^2 hybridization state. The torsion angle of C(8)–C(7)–O(3)–

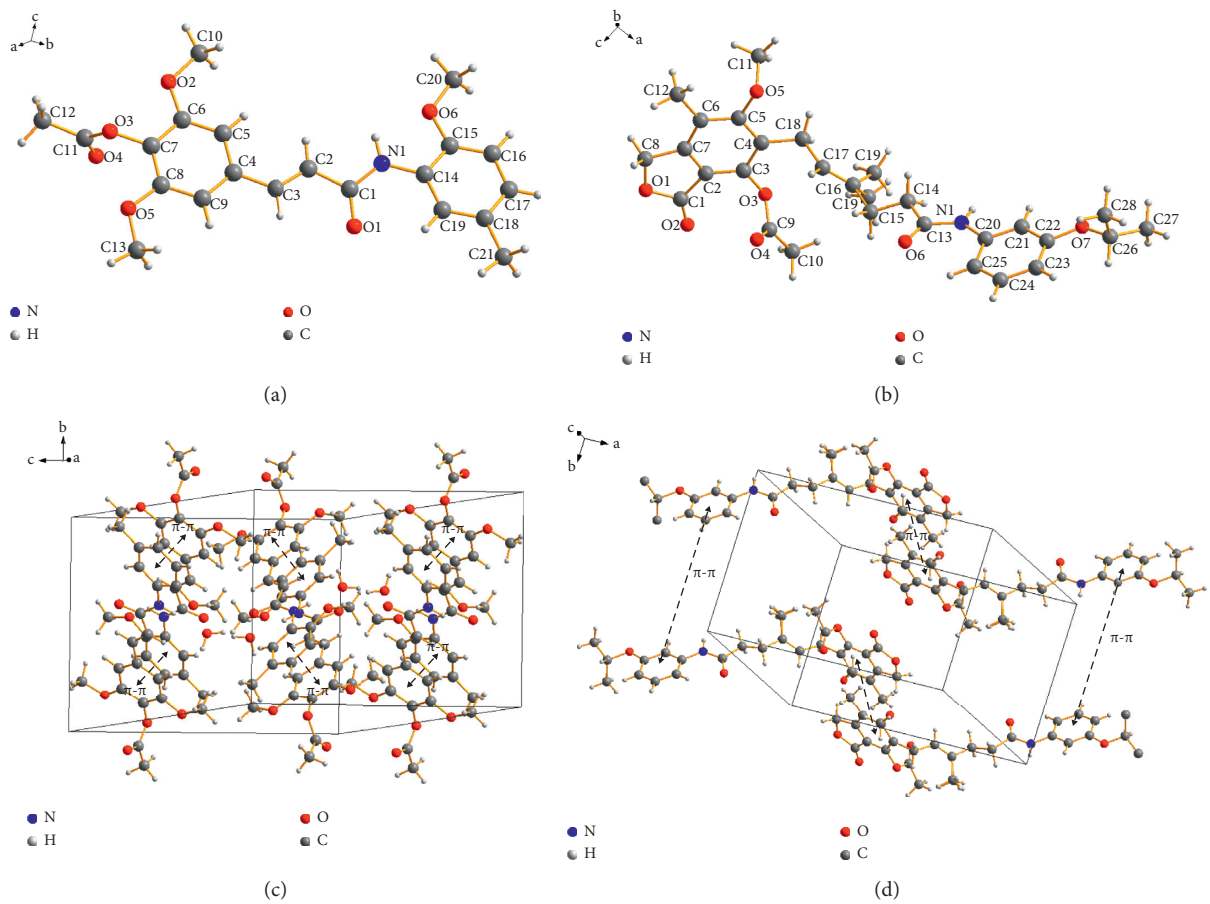

Figure 4: Crystal structures of I-4 (a) and II-5 (b), and crystal packing of I-4 (c) and II-5 (d).

Table 1: Selected bond lengths (Å) and bond angles (°) for the compounds I-4 and II-5.

Compound I-4		Compound II-5	
Bond	Dist.(Å)	Bond	Dist.(Å)
C(1) = O(1)	1.209(3)	C(1) = O(2)	1.193(4)
C(1)–N(1)	1.332(3)	C(1)–O(1)	1.339(4)
C(11) = O(4)	1.182(3)	C(3)–O(3)	1.385(4)
C(11)–O(3)	1.327(3)	C(9) = O(4)	1.175(5)
C(2) = C(3)	1.309(3)	C(9)–O(3)	1.354(4)
C(8)–O(5)	1.351(3)	C(13) = O(6)	1.200(4)
C(15)–O(6)	1.351(3)	C(13)–N(1)	1.339(4)
C(4) = C(5)	1.376(3)	C(5)–O(5)	1.367(4)
C(1)–C(2)	1.456(3)	N(1)–C(20)	1.390(4)
C(3)–C(4)	1.444(3)	C(4) = C(5)	1.394(4)
C(4) = C(9)	1.378(3)	C(22)–O(7)	1.364(3)
C(14) = C(15)	1.383(3)	C(16) = C(17)	1.285(4)
C(14) = C(19)	1.369(3)	C(17)–C(18)	1.482(4)
C(18)–C(21)	1.484 (4)	C(15)–C(16)	1.478(5)
Bond angles	(°)	Bond angles	(°)
C(1)–C(2)–C(3)	121.6(2)	O(1)–C(1)–C(2)	108.4(3)
C(2)–C(3)–C(4)	127.0(2)	O(2)–C(1)–C(2)	130.1(3)
C(4)–C(5)–C(6)	120.2(2)	C(1)–C(2)–C(7)	108.1(3)
C(14)–C(15)–C(16)	119.3(3)	C(16)–C(17)–C(18)	129.0(3)
O(3)–C(11)–O(4)	122.6(2)	C(15)–C(16)–C(17)	122.4(3)

Table 1: Continued.

Compound I-4		Compound II-5	
Bond	Dist.(Å)	Bond	Dist.(Å)
O(1)–C(1)–N(1)	122.9(2)	O(6)–C(13)–N(1)	123.7(3)
O(1)–C(1)–C(2)	122.1(2)	C(13)–N(1)–C(20)	129.6(3)
N(1)–C(1)–C(2)	114.9(2)	C(20)–C(21)–C(22)	120.9(3)
C(8)–O(5)–C(13)	117.7(2)	C(2)–C(3)–C(4)	120.7(3)
C(6)–O(2)–C(10)	117.7(2)	C(4)–C(18)–C(17)	114.2(3)
C(15)–O(6)–C(20)	119.2(2)	C(5)–O(5)–C(11)	115.1(3)
C(3)–C(4)–C(5)	121.7(2)	C(22)–O(7)–C(26)	120.4(3)

Table 2: Selected dihedral angles (°) for the compounds I-4 and II-5.

Compounds	Groups		Dihedral angles (°)
I-4	Benzene ring {C(4)–C(9)}	Benzene ring {C(14)–C(19)}	6.505 (76)
I-4	Benzene ring {C(4)–C(9)}	Ester group {C(11) = O(4)}	88.750 (188)
I-4	Benzene ring {C(4)–C(9)}	Amide group {C(1)–N(1)}	12.563 (176)
I-4	Benzene ring {C(14)–C(19)}	Ester group {C(11) = O(4)}	82.625 (197)
I-4	Benzene ring {C(14)–C(19)}	Amide group {C(1)–N(1)}	19.106 (166)
II-5	Benzene ring {C(2)–C(7)}	Benzene ring {C(20)–C(25)}	84.911 (77)
II-5	Benzene ring {C(2)–C(7)}	Ester group {C(1) = O(2)}	0.106 (338)
II-5	Benzene ring {C(2)–C(7)}	Ester group {C(9) = O(4)}	74.962 (214)
II-5	Benzene ring {C(2)–C(7)}	Amide group {C(13)–N(1)}	89.604 (240)
II-5	Benzene ring {C(20)–C(25)}	Ester group {C(1) = O(2)}	84.918 (219)
II-5	Benzene ring {C(20)–C(25)}	Ester group {C(9) = O(4)}	73.317 (318)
II-5	Benzene ring {C(20)–C(25)}	Amide group {C(13)–N(1)}	12.284 (211)

C(11) in compound **I-4** was −92.8(3)°, revealing that the plane of ester group was clearly vertical with the adjacent benzene ring. In compound **II-5**, the ester group plane consisted of O(1)-C(1)-O(2) was coplanar with the adjacent benzene ring, resulting in the existing conjugation effect between these two planes. However, the ester group plane composed of O(3)-C(9)-O(4) and the adjacent benzene ring were apparently nonplanar, with a dihedral angle of 74.830(111)°. The dihedral angle between the two benzene rings in compound **I-4** was 6.505(75)°, indicating that these two benzene rings were approximately coplanar. However, the two benzene rings in compound **II-5** were nearly vertical, with a dihedral angles of 84.911(77)°. In addition, the amide plane was almost coplanar with the two benzene rings in compound **I-4**, with the dihedral angles of 13.111(183)° and 19.106(159)°, respectively. In compound **II-5**, the dihedral angle between the amide plane and the benzene ring consisted of C(20)-C(25) was 12.284(189)°, while the amide plane and the benzene ring consisted of C(2)-C(3) were obviously vertical with the dihedral angle of 89.604(238)°. From the crystal packing, the π-π interactions occurred between the benzene rings of the adjacent molecules, which strengthen the integration of the crystal molecules (Figures 4(c) and 4(d)).

3.3. Fungicidal Inhibitory Activity. The in vitro inhibitory activities of the target compounds against the common agricultural pathogens were investigated, and the results are shown in Table 3. From the data, most of the target compounds exhibited weak-to-moderate fungicidal activity against *Gibberella zeae*, *Rhizoctonia solani*, *Botrytis cinerea*, *Cercospora circumscissa Sacc*, *Alternaria kikuchiana Tanaka*, *Colletotrichum capsici,* and *Alternaria* sp. However, all compounds showed moderate-to-good fungicidal activity against *Physalospora piricola*, even better than fluopyram. For example, compounds **I-1**, **I-4,** and **I-5** exhibited higher inhibitory activity than fluopyram, with the inhibitory rates of 76.2%, 73.3%, and 73.5%, respectively. It can be concluded that the compounds **I-1**–**I-5** and **II-1**–**II-5** displayed high selectivity for the fungicidal activity against *Physalospora piricola*. In terms of the relationship between the structures and the initial inhibitory activity, the structural modification had different effects on the inhibitory activities of target compounds against the different pathogens. For example, compared with the electron-withdrawing trifluoromethyl and chlorine groups, the introduction of the electron-donating methyl, methoxy, or isopropoxy group at the benzene ring was beneficial to improving the fungicidal activity of **I-4** and **I-5** against *Physalospora piricola*. For instance, the inhibition rates of compounds **I-4** and **I-5** were 73.3% and 73.5%, respectively, which were apparently higher than those of compounds **I-2** and **I-3**. However, this structural modification had no significant effects on the inhibitory activity of the compounds **II-2**–**II-5** against *Physalospora piricola*. To further investigate the fungicidal activity of the target compounds against *Physalospora piricola*, the EC_{50} values were measured and the results are exhibited in Table 4. It could be found that most of the target compounds exhibited fungicidal activity equivalent to or even better than

Table 3: In vitro inhibitory activity of the target compounds at 50 $\mu g \cdot mL^{-1}$.

Compounds	Inhibition rate (%)							
	GZ	RS	BC	CS	PP	AK	CC	AS
I-1	12.9 ± 0.28**	7.0 ± 0.61**	24.7 ± 0.25	36.5 ± 0.59**	76.2 ± 0.66**	27.9 ± 0.34	14.5 ± 0.81**	17.2 ± 0.46**
I-2	11.8 ± 0.51**	7.4 ± 0.41**	22.2 ± 0.50	19.7 ± 0.51**	53.9 ± 0.83**	31.0 ± 0.43	1.7 ± 0.64**	12.1 ± 0.77
I-3	29.9 ± 0.32**	3.2 ± 0.30**	4.2 ± 0.55**	20.1 ± 0.81**	54.8 ± 0.79**	29.1 ± 0.67	7.5 ± 0.71**	16.2 ± 0.35**
I-4	41.7 ± 0.42**	2.7 ± 0.13**	22.2 ± 0.32	22.5 ± 0.60**	73.3 ± 0.85**	38.5 ± 0.32**	10.1 ± 0.61**	20.1 ± 0.46**
I-5	24.6 ± 0.55**	8.3 ± 0.31**	14.0 ± 0.51**	24.3 ± 0.65**	73.5 ± 0.56**	34.4 ± 0.34**	5.5 ± 0.71**	16.5 ± 0.55**
II-1	36.1 ± 0.38**	9.4 ± 0.61**	23.6 ± 0.26	17.3 ± 0.51**	45.2 ± 0.11**	31.1 ± 0.34	8.8 ± 0.59**	15.8 ± 0.46**
II-2	28.2 ± 0.57**	21.9 ± 0.52**	27.4 ± 0.25	23.0 ± 0.60**	55.9 ± 0.39**	28.5 ± 0.24	3.3 ± 0.81**	16.5 ± 0.35**
II-3	16.8 ± 0.48**	19.0 ± 0.31**	24.4 ± 0.25	19.7 ± 0.51**	55.3 ± 0.59**	25.6 ± 0.83	13.7 ± 0.71**	26.9 ± 0.54**
II-4	35.9 ± 0.38**	19.5 ± 0.57**	20.1 ± 0.51**	14.1 ± 0.40**	57.2 ± 0.39**	41.1 ± 0.67**	3.3 ± 0.30**	25.9 ± 0.58**
II-5	19.8 ± 0.30**	24.8 ± 0.44**	13.8 ± 0.76**	19.5 ± 0.56**	56.1 ± 0.43**	18.8 ± 0.49**	5.6 ± 0.38**	10.3 ± 0.47**
Fluopyram	100	56.6 ± 0.31**	100.0**	85.5 ± 0.51**	53.2 ± 0.73**	100**	60.1 ± 0.31**	100**
Carbendazim	100	100	24.6 ± 0.74	27.8 ± 0.47	100	27.1 ± 0.34	100	12.4 ± 0.49

GZ, *Gibberella zeae*; RS, *Rhizoctonia solani*; BC, *Botrytis cinerea*; CS, *Cercospora circumscissa Sacc.*; PP, *Physalospora piricola*; AK, *Alternaria kikuchiana Tanaka*; CC, *Colletotrichum capsici*; AS, *Alternaria* sp. Asterisk (*) means significant differences among different treatments. *, significant at the $p < 0.05$ level, and **, significant at the $p < 0.01$ level compared with carbendazim.

Table 4: Medium effective concentration (EC_{50}, $\mu g \cdot mL^{-1}$) values of the target compounds against *Physalospora piricola*.

Compounds	Regression equation	Correlation coefficient (r)	EC_{50} (95% confidence interval)
I-1	$y = 1.26x + 3.35$	0.9918	20.4 (17.7–23.7) **
I-2	$y = 1.00x + 3.51$	0.9903	30.7 (26.2–36.0) **
I-3	$y = 1.52x + 2.81$	0.9911	27.3 (23.5–31.7) **
I-4	$y = 1.83x + 2.33$	0.9908	28.6 (24.6–33.3) **
I-5	$y = 1.27x + 3.42$	0.9876	17.4 (14.4–21.0) **
II-1	$y = 1.78x + 1.67$	0.9824	74.2 (54.1–101.7) **
II-2	$y = 1.90x + 1.83$	0.9993	46.9 (44.8–49.2) **
II-3	$y = 1.10x + 3.44$	0.9835	25.7 (20.9–31.5) **
II-4	$y = 1.54x + 2.88$	0.9919	23.9 (20.8–27.6) **
II-5	$y = 2.46x + 1.41$	0.9823	28.8 (23.2–35.7) **
Fluopyram	$y = 1.07x + 3.42$	0.9951	30.4 (27.2–34.0) **
Carbendazim			<3.125

Asterisk (*) means significant differences among different treatments. *, significant at the $p < 0.05$ level, and **, significant at the $p < 0.01$ level compared with carbendazim.

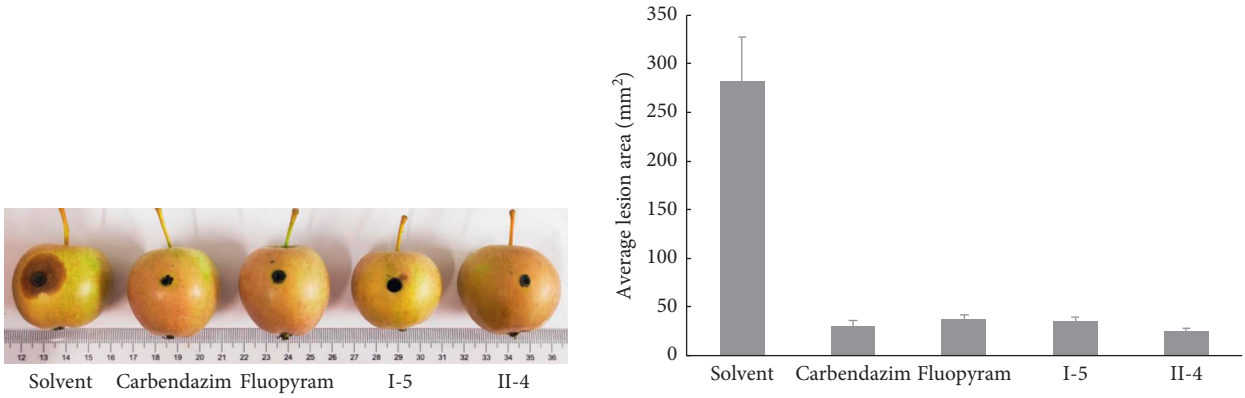

Figure 5: In vivo fungicidal activity of compounds **I-5** and **II-4** against *Physalospora piricola*-infected apples at 200 $\mu g \cdot mL^{-1}$.

fluopyram, with the EC_{50} values of compounds **I-1**, **I-5,** and **II-4** to 20.4 $\mu g \cdot mL^{-1}$, 17.4 $\mu g \cdot mL^{-1}$, and 23.9 $\mu g \cdot mL^{-1}$, respectively.

Subsequently, the in vivo fungicidal activity of sinapic amide **I-5** and mycophenolic amide **II-4** against *Physalospora piricola* was performed on apples at 200 $\mu g \cdot mL^{-1}$, and the results are displayed in Figure 5. From the data, the compounds **I-5** and **II-4** exhibited almost the same preventative activity as carbendazim and fluopyram at 200 $\mu g \cdot mL^{-1}$, with the inhibition rates of carbendazim,

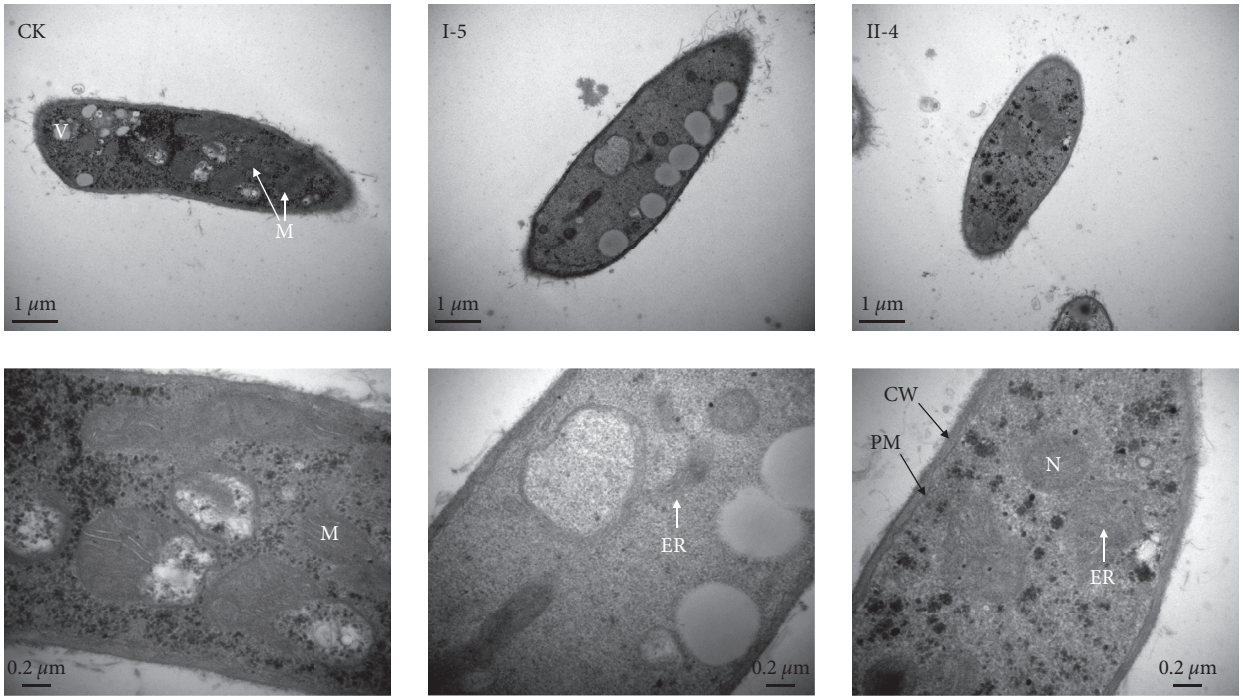

Figure 6: TEM investigation of *Physalospora piricola* hyphae treated with I-5 and II-4. CW: cell wall; PM: plasma membrane; N: nucleus; V: vacuole; M: mitochondria; ER: endoplasmic reticulum.

fluopyram, **I-5,** and **II-4** to 90.8%, 86.9%, 87.6%, and 91.1%, respectively.

3.4. TEM Observation. To further explore the effects of molecules **I-5** and **II-4** on the hyphae, the ultrastructure of *Physalospora piricola* hyphae treated with distilled water, compounds **I-5** and **II-4** (200 μg·mL^{-1}), was observed on a TEM, and the results are illustrated in Figure 6. From the data, the cell wall and plasma membrane of the cell structures in the control and tested groups were normal, and mitochondria could be clearly observed in the control group. However, the mitochondria in the cell structure treated with **I-5** and **II-4** were blurred or even disappeared. Based on this, it could be speculated that the fungicidal activity of the target compounds against *Physalospora piricola* may be due to the influence of **I-1**–**I-5** and **II-1**–**II-5** on the mitochondria in the cell structure.

4. Conclusion

In summary, two series of sinapic acid-derived and mycophenolic acid-derived amide derivatives were designed and synthesized. The obtained structures were characterized by ^{1}H NMR, ^{13}C NMR, HRMS, and X-ray crystal diffraction. The in vitro and in vivo fungicidal activity screening indicated that compared with other tested pathogens, most of the target compounds exhibited excellent fungicidal activity against *Physalospora piricola*, of which the compounds **I-5** and **II-4** displayed almost the same preventative activity as carbendazim and fluopyram at 200 μg·mL^{-1}. The TEM observation further revealed that the fungicidal activity of the target compounds against *Physalospora piricola* may be due to the influence on the mitochondria in the cell structure.

Data Availability

The data used to support the findings of this study are included within the article and the supplementary information file(s). Crystallographic data for the structures reported in this manuscript have been deposited with the Cambridge Crystallographic Data Centre under the CCDC numbers: 2095769 (compound I-4) and 2095768 (compound II-5). Copies of these data can be obtained free of charge from http://www.ccdc.cam.ac.uk/data_request/cif.

Conflicts of Interest

There are no conflicts of interest to declare.

Acknowledgments

This research was supported by the National Natural Science Foundation of China (No. 32001929), Shandong Provincial Agricultural Science and Technology Project (Park Indus-try Upgrade Project) (No. 2019YQ037), the National Innovation and Entrepreneurship Training Program for College Students (No. 202110447013, 202110447032), and the Innovation and Entrepreneurship Training Program for College Students of Liaocheng University (No. CXCY2020Y116).

Supplementary Materials

The supporting information contained X-ray crystal data of the compounds **I-4** and **II-5**, and ^{1}H NMR, ^{13}C NMR, and

HRMS spectra of target compounds **I-1**–**I-5** and **II-1**–**II-5**. (*Supplementary Materials*)

References

[1] C. Yan, J. Dong, Y. Liu, Y. Li, and Q. Wang, "Target-directed design, synthesis, antiviral activity, and SARs of 9-substituted phenanthroindolizidine alkaloid derivatives," *Journal of Agricultural and Food Chemistry*, vol. 69, no. 27, pp. 7565–7571, 2021.

[2] M. Kabbage, J. S. Piotrowski, E. Thill et al., "Poacic acid suppresses dollar spot and snow mould in amenity turfgrass," *Plant Pathology*, vol. 69, no. 1, pp. 112–119, 2020.

[3] J.-K. Zhu, J.-M. Gao, C.-J. Yang et al., "Design, synthesis, and antifungal evaluation of neocryptolepine derivatives against phytopathogenic fungi," *Journal of Agricultural and Food Chemistry*, vol. 68, no. 8, pp. 2306–2315, 2020.

[4] J. G. Zheng, T. T. Liu, Z. X. Guo et al., "Fumigation and contact activities of 18 plant essential oils on Villosiclava virens, the pathogenic fungus of rice false smut," *Scientific Reports*, vol. 9, pp. 1–10, 2019.

[5] S. X. Guo, F. He, B. A. Song, and J. Wu, "Future direction of agrochemical development for plant disease in China," *Food and Energy Security*, vol. 10, pp. e293-1–e293-16, 2021.

[6] X. Hua, W. Liu, Y. Chen et al., "Synthesis, fungicidal activity, and mechanism of action of pyrazole amide and ester derivatives based on natural products l-serine and waltherione alkaloids," *Journal of Agricultural and Food Chemistry*, vol. 69, no. 38, pp. 11470–11484, 2021.

[7] J. W.-H. Li and J. C. Vederas, "Drug discovery and natural products: end of an era or an endless frontier?" *Science*, vol. 325, no. 5937, pp. 161–165, 2009.

[8] T. Rodrigues, D. Reker, P. Schneider, and G. Schneider, "Counting on natural products for drug design," *Nature Chemistry*, vol. 8, no. 6, pp. 531–541, 2016.

[9] L. W. K. Moodie, K. Sepčić, T. Turk, R. Frangež, and J. Svenson, "Natural cholinesterase inhibitors from marine organisms," *Natural Product Reports*, vol. 36, no. 8, pp. 1053–1092, 2019.

[10] D. J. Newman and G. M. Cragg, "Natural products as sources of new drugs over the nearly four decades from 01/1981 to 09/2019," *Journal of Natural Products*, vol. 83, no. 3, pp. 770–803, 2020.

[11] J. Liu, S. Lu, J. Feng et al., "Enantioselective synthesis and antifungal activity of C18 polyacetylenes," *Journal of Agricultural and Food Chemistry*, vol. 68, no. 7, pp. 2116–2123, 2020.

[12] C. L. Liu, A. Y. Guan, Z. N. Li et al., "Preparation and application of benzopyrone compounds with insecticidal and fungicidal activity," vol. 6, 2007 in Chinese, Article ID 200310105079.

[13] S. Anand and P. Srivastava, "Optimization strategies for purification of mycophenolic acid produced by *Penicillium brevicompactum*," *Applied Biochemistry and Biotechnology*, vol. 191, no. 2, pp. 867–880, 2020.

[14] R. Freedman, R. Yu, A. W. Sarkis, and L. Hedstrom, "A structural determinant of mycophenolic acid resistance in eukaryotic inosine 5′-monophosphate dehydrogenases," *Protein Science*, vol. 29, no. 3, pp. 686–694, 2020.

[15] P. Chen, C. Liu, J. Hu, H. Zhang, and R. Sun, "Design, synthesis and fungicidal activity studies of 3-ferrocenyl-N-acryloylmorpholine," *Journal of Organometallic Chemistry*, vol. 854, pp. 113–121, 2018.

[16] W. C. Liu and C. L. Liu, "Novel fungicide flumorph (SYP-L190) with high activity," *Pesticides*, vol. 41, pp. 8–11, 2002, in Chinese.

[17] C. W. Mu, H. Z. Yuan, N. Li et al., "Synthesis and fungicidal activities of a novel series of 4-[3-(pyrid-4-y1)-3-substituted phenyl acryloyl]morpholine," *Chemical Journal of Chinese Universities*, vol. 28, pp. l902–l906, 2007.

[18] Y. Xiao, X. Yang, B. Li et al., "Design, synthesis and antifungal/insecticidal evaluation of novel cinnamide derivatives," *Molecules*, vol. 16, no. 11, pp. 8945–8957, 2011.

[19] S. E. Lee, N. E. Mahoney, and B. C. Campbell, "Inhibition of aflatoxin B1 biosynthesis by piperlongumine isolated from Piper longum L." *Journal of Microbiology and Biotechnology*, vol. 12, pp. 679–682, 2002.

[20] Y. S. Moon, W. S. Choi, E. S. Park et al., "Antifungal and antiaflatoxigenic methylenedioxy-containing compounds and piperine-like synthetic compounds," *Toxins*, vol. 8, pp. 240-1–240-10, 2016.

[21] X. Hua, N. Liu, S. Zhou et al., "Design, synthesis, and biological activity of novel aromatic amide derivatives containing sulfide and sulfone substructures," *Engineering*, vol. 6, no. 5, pp. 553–559, 2020.

[22] W. R. Liu, X. W. Hua, S. Zhou et al., "Design, synthesis and biological activity of *N*-sulfonyl aromatic amide derivatives," *Chinese Journal of Structural Chemistry*, vol. 40, pp. 666–674, 2021.

[23] X. Hua, W. Liu, Y. Su et al., "Studies on the novel pyridine sulfide containing SDH based heterocyclic amide fungicide," *Pest Management Science*, vol. 76, no. 7, pp. 2368–2378, 2020.

[24] F. Allais, P.-H. Ducrot, and S. Martinet, "Straightforward total synthesis of 2-O-Feruloyl-l-malate, 2-O-Sinapoyl-l-malate and 2-O-5-Hydroxyferuloyl-l-malate," *Synthesis*, vol. 2009, no. 21, pp. 3571–3578, 2009.

Hindawi
Journal of Chemistry
Volume 2021, Article ID 9951949, 9 pages
https://doi.org/10.1155/2021/9951949

Research Article

Establishment of Tissue Culture System of *Actinidia deliciosa* Cultivar "Guichang"

Weimin Zhong,[1] Junliang Zhou,[1] Dongmei Tang,[1] Yaxin Huang,[2] Futao Liu,[1] Min Zhang,[1] Guoli Wang,[2] Sufang Wu,[2] Yue He,[2] and Jingwen Tang[2]

[1]*Institute of Fruit Science, Guizhou Academy of Agricultural Sciences, Guiyang 550006, China*
[2]*Agricultural Bureau of Xiuwen County, Xiuwen 550200, China*

Correspondence should be addressed to Dongmei Tang; tdmemail@126.com

Received 11 November 2021; Revised 30 November 2021; Accepted 2 December 2021; Published 16 December 2021

Academic Editor: Wenneng Wu

In order to breed virus-free plantlets of the kiwifruit cultivar "Guichang," which belongs to *Actinidia deliciosa*, in this study, stem segments with buds were used as explants, the establishment of a tissue culture rapid propagation system was carried out, and then the virus status of tissue culture plantlets was detected via the real-time reverse transcription-polymerase chain reaction (RT-qPCR) method. The tissue culture rapid propagation system proved that the contamination and browning rates could be controlled below 20% and the survival rate could be exceeded by 70% when the single bud stem segment of "Guichang" kiwifruit was sterilized with 70% alcohol for 30–60 s and 15% NaClO for 15 min, respectively. Meanwhile, we screened the hormone concentration to get better results, and the appropriate medium for adventitious bud induction was MS + 6-BA (1.0 mg/L) + IBA (0.2 mg/L); for proliferation, it was MS + 6-BA (1.0 mg/L) + IBA (0.1 mg/L); and for rooting, it was 1/2 MS + IBA (0.3 mg/L), and the efficiency of induction, proliferation, and rooting could reach 74.07%, 79.63%, and 85.18%, respectively. In addition, the RT-qPCR results demonstrated that the infection rate of 9 viruses: *apple stem grooving virus* (ASGV), *cucumber mosaic virus* (CMV), *Actinidia virus X* (AVX), *cucumber necrosis virus* (CNV), *ribgrass mosaic virus* (RMV), *citrus leaf blotch virus* (CLBV), *Actinidia virus B* (AcVB), *Pelargonium zonate spot virus* (PZSV), and *cherry leaf roll virus* (CLRV) in the "Guichang" kiwifruit tissue culture plantlets was 0. This study could lay a foundation for the production of "Guichang" kiwifruit tissue culture seedlings, and the medium formula provided in this study was useful for the industrial rapid propagation of "Guichang" plantlets.

1. Introduction

Kiwifruit (*Actinidia* spp.), an important and economically substantial fruit in China, has long been known as "the king of fruits" because of its high vitamin C content and balanced nutritional composition of minerals and other health-promoting metabolites [1, 2]. Kiwifruit cultivar "Guichang" (*Actinidia deliciosa* var. *deliciosa*), one excellent cultivar with the characteristics of excellent quality, beautiful appearance, strong resistance, and high yields from wild resources, developed by the Institute of Fruit Science, Guizhou Academy of Agricultural Sciences in 1979, has become the main cultivar in Guizhou province [3]. By 2018, the cultivation area of "Guichang" kiwifruit in Guizhou was nearly 16,000 hectares.

As most species of *Actinidia* are dioecious and have a long juvenile period, it is difficult to identify the gender of young plants [4, 5]. Due to the limited number of branches, the traditional cutting and grafting methods make it difficult to cultivate large numbers of plantlets in a short time. Therefore, the tissue culture had gradually become the main method to produce numerous plantlets rapidly, which had the advantages of stable inheritance, maintaining good traits, no time and space restrictions, and a high reproduction coefficient. Since the 1970s, tissue culture rapid propagation has become an important breeding method. Recently, more and more research studies on the establishment of kiwifruit rapid propagation systems have been performed [6–9]. However, in the process of in vitro rapid propagation of kiwifruit, serious browning and diseases of explants in

primary culture have become a major obstacle [10, 11]. In recent years, some literature has reported that many viruses, including *apple stem grooving virus* (ASGV), *cucumber mosaic virus* (CMV), *Actinidia virus X* (AVX), *cucumber necrosis virus* (CNV), *ribgrass mosaic virus* (RMV), *Actinidia virus B* (AcVB), *Actinidia virus A* (AcVA), *Actinidia virus* 1 (AcV-1), *alfalfa mosaic virus* (AMV), *cherry leaf roll virus* (CLRV), *tomato necrotic spot associated virus* (TNSaV), *tomato zonate spot virus* (TZSV), *Pelargonium zonate spot virus* (PZSV), *citrus leaf blotch virus* (CLBV), *Actinidia chlorotic ringspot-associated virus* (AcCRaV), *turnip vein clearing virus* (TVCV), and *Actinidia seed-borne latent virus* (ASbLV), can infect kiwifruit plants through pollen, grafting, or artificial inoculation [12–19]. Once infected, viruses cause a detrimental effect on the growth and development of kiwifruit plants, and the fruits will be deformed and the yields will be reduced, with huge economic loss. However, the traditional cutting and grafting methods had a good chance of spreading viruses to the other branches and thus expanding the spread of viral diseases. Therefore, it is urgent to develop the rapid propagation technology of "Guichang" kiwifruit.

In order to breed virus-free plantlets of "Guichang" kiwifruit, in this study, the establishment of a tissue culture rapid propagation system was carried out, and then detected the virus status via the real-time reverse transcription-polymerase chain reaction (RT-qPCR) method. To our knowledge, this is the first report on the rapid production of "Guichang" kiwifruit tissue culture plantlets. This study provides scientific guidance for large-scale factory production and boosts the healthy development of the kiwifruit industry in China.

2. Materials and Methods

2.1. Experimental Materials. The materials were taken from the kiwifruit demonstration area (north latitude: 26.816339, east longitude: 106.492149) of Gubao township, Xiuwen county, Guizhou province, China, in June 2015. Plants with robust growth and good comprehensive performance were selected as the sampled parent plants. New shoots were removed from the tops with the base semilignified, and leaf blades that had not fully developed were used as explants for in vitro culture. The young leaves of the parent plant were hydropically cultured to accelerate budding, and the young leaves cultured by tissue culture were taken as test materials for virus detection.

2.2. Sterilization of the Explants. For sterilization of the explants, the petioles, which were removed from the leaves, were cut into 5–6 cm long pieces, rinsed with tap water several times, soaked in detergent water for 30 min, and rinsed with tap water for 1–2 h. Then, the explants were soaked with 70% alcohol for 10, 30, and 60 s, respectively, and soaked with 15% sodium hypochlorite (NaClO) for 10, 15, and 20 min, respectively. After that, the explants were washed with sterile water 3–4 times, sucked dry with sterile paper, cut into 1.5–2.0 cm segments with a single bud, and inoculated on Murashige and Skoog (MS) culture medium without adding hormones. After 20 days of inoculation with an illumination intensity of 2000 Lx and at 25°C with a light/dark cycle of 16/8 h, the contamination, browning, and survival rates were calculated as the following equations:

Contamination rate (%) = (number of browning explants/number of inoculated explants) × 100

Browning rate (%) = (number of contaminated explants/number of inoculated explants) × 100

Survival rate (%) = (number of the survival explants/number of inoculated explants) × 100

2.3. Proliferation Culture. The disinfected explants were inoculated on the MS culture medium with 6-benzyl aminopurine (6-BA, 0 mg/L) + indolebutyric acid (IBA, 0.2 mg/L), 6-BA (0.5 mg/L) + IBA (0.2 mg/L), 6-BA (1.0 mg/L) + IBA (0.2 mg/L), 6-BA (1.5 mg/L) + IBA (0.2 mg/L), and 6-BA (2.0 mg/L) + IBA (0.2 mg/L), respectively. The inducement rate of the axillary buds was calculated after 30 days of inoculation with an illumination intensity of 2000 Lx, a temperature of 25°C, and light/dark cycles of 16/8 h: inducement rate (%) = (number of explants in axillary bud germination/number of inoculated explants) × 100.

For subculture, the sterile new single shoots that grow on the primary culture medium were cut into 0.5–1.0 cm long stem segments and then inoculated on the proliferation MS culture medium with 6-BA (0 mg/L) + IBA (0.1 mg/L), 6-BA (0.5 mg/L) + IBA (0.1 mg/L), 6-BA (1.0 mg/L) + IBA (0.1 mg/L), 6-BA (1.5 mg/L) + IBA (0.1 mg/L), and 6-BA (2.0 mg/L) + IBA (0.1 mg/L), respectively. The growth of tube plantlets was observed, and the proliferation coefficients were calculated after 30 days of inoculation with an illumination intensity of 2000 Lx, a temperature of 25°C, and light/dark cycles of 16/8 h.

Proliferation rate (%) = (number of regeneration buds/number of inoculated buds) × 100

Proliferation coefficients = number of regeneration buds/number of inoculated buds

2.4. Rooting and Transplantation Culture. The sterile new single shoots produced by adventitious buds were cut into 0.5–1.0 cm long stem segments and then inoculated on the rooting culture medium (1/2 MS culture medium) with 0.1, 0.3, 0.5, and 0.7 mg/L of IBA, respectively. The rooting rate and root number were counted after 30 days of inoculation with an illumination intensity of 2000 Lx, a temperature of 25°C, and light/dark cycles of 16/8 h: rooting rate (%) = (number of rooting explants/number of inoculated explants) × 100.

Tissue culture plantlets, with a height of more than 4 cm, 3–5 leaves, and more than 3 roots, were selected and placed into the greenhouse (23–25°C and 90% relative humidity (RH)) to harden the plantlets for 7 days, then the plantlets were transplanted into the paper cups with the matrix containing perlite, vermiculite, and peat (1 : 1:2, v/v) and then transferred the paper cups into the greenhouse with

natural lighting, a temperature of 23–25°C, and RH to reduce the gradient from 90% to indoor humidity. Meanwhile, the plantlets were regularly irrigated with the 1/8 MS nutrient solution and a pesticide, such as carbendazim, that prevents young plants from rotting. The plantlets were grown for about 30 days, and then the survival rate was calculated using the following equation: survival rate (%) = (number of the transplanting survival/number of transplanting explants) × 100.

2.5. RNA Extraction and RT-qPCR Detection. A total of 9 kinds of viruses, including ASGV, CMV, AVX, CNV, RMV, CLBV, AcVB, PZSV, and CLRV, were detected via the RT-qPCR method [18, 19]. The RNA of the "Guichang" kiwifruit leaves was extracted using the total RNA extraction kit (Qiagen, Hilden, Germany). The purity (OD_{260}/OD_{280}) and concentration of the extracted RNA were detected by an ultraviolet spectrophotometer (Beckman Instruments, Inc., Fullerton, CA). RNA was reverse-transcribed using a cDNA kit (TaKaRa, Dalian, China) according to the manufacturer's instructions. The primers used for RT-qPCR amplification are listed in Table 1. The RT-qPCR amplification was carried out according to the method reported by Huang et al. [2]. After that, the electrophoresis of the RT-qPCR products was performed with a 1.2% agarose gel (Bio Tech Corporation, Beijing, China).

2.6. Statistical Analysis. SPSS 17.0 (SPSS Inc., Chicago, USA) was used for statistical analysis. Statistical analysis was conducted by ANOVA with software SPSS 17.0 (SPSS Inc., Chicago, USA). Different lowercase letters indicate a significant difference ($p < 0.05$) among different treatment groups.

3. Results

3.1. Sterilization of the Explants. Table 2 shows that, with the prolonged sterilization time of 70% alcohol and 15% NaClO, the contamination rate of explants gradually decreased while the browning rate gradually increased, and the survival rate increased first and then decreased. Meanwhile, Table 2 shows that the contamination and browning rates could be controlled below 20% and the survival rate could be exceeded by 70% when the single bud stem segments of "Guichang" kiwifruit were sterilized with 70% alcohol for 30–60 s and 15% NaClO for 15 min, respectively.

3.2. Induction, Proliferation, and Rooting Culture. As shown in Table 3, with the increase of 6-BA concentration, the germination rate of axillary buds first increased and then decreased; especially, using MS + 6-BA (1.0 mg/L) + IBA (0.2 mg/L) as the induction medium, the inducement rate reached 74.07% and the plantlets were robust with almost no callus at the base.

Table 4 shows that all the tested concentrations of 6-BA could enhance the proliferation rate; especially, using MS + 6-BA (1.0 mg/L) + IBA (0.1 mg/L) as the proliferation medium, the proliferation rate and proliferation coefficient reached the highest values of 79.63% and 5.06, respectively. Meanwhile, the plants were robust with green leaves and longer internodes.

Table 5 shows that all the tested concentrations of IBA could enhance the rooting rate, especially taking 1/2 MS + IBA (0.3 mg/L) as the optimum rooting medium, the rooting rate and average rooting number were 85.18% and 4.90, respectively, and the rooting number was 2–6 with more and longer fibrous roots and basically no callus. After that, the tissue culture plantlets with a height of more than 4 cm, 3–5 leaves, and more than 3 roots were selected and placed into the greenhouse. The survival rate exceeded 90%.

3.3. Virus Detection. A total of 9 kinds of viruses in tissue culture plantlets, including ASGV, CMV, AVX, CNV, RMV, CLBV, AcVB, PZSV, and CLRV, were detected via the RT-qPCR method, and the results (Figure 1) demonstrated that the infection rate of 9 kinds of viruses in tissue culture plantlets was 0. Therefore, the in vitro tissue culture rapid propagation system established in this study could obtain the virus-free plantlets of "Guichang" kiwifruit.

4. Discussion

China is the major source of wild kiwifruit and the world's largest producer and planting area [20]. It has an important significance to study the rapid propagation technology of kiwifruit, which is helpful to promote its development. In the sterilization process of in vitro rapid propagation, many scholars used alcohol and mercury chloride as the disinfecting agents, while only a few scholars used alcohol and NaClO [20, 21]. In this study, the single bud stem segment of the "Guichang" kiwifruit was disinfected with 70% alcohol and 15% NaClO, and the results showed that the contamination and browning rates could be controlled below 20% and the survival rate could be exceeded by 70% when the single bud stem segment of the Guichang kiwifruit was sterilized with 70% alcohol for 30–60 s and 15% NaClO for 15 min, respectively.

There are many reports on the combination of plant growth regulators in different stages of tissue culture of kiwifruit, and the selection of appropriate auxin types and concentrations is the key role of plant tissue culture. A previous study found that there are some differences in the morphology of tissue culture plantlets induced by different auxin combinations [21]. Yu et al. [22] and Long et al. [23] successfully established the kiwifruit stem culture using MS + 6-BA (1.0 mg/L) + naphthylacetic acid (NAA, 0.1 mg/L) medium. It was also found that different concentrations of plant growth regulators could affect the growth and browning of kiwifruit, and the auxin IBA could delay the synthesis of polyphenols and reduce browning [24–26]. Based on the results of previous literature, this experiment studied the effects of IBA at different concentrations on the induction and proliferation of "Guichang" kiwifruit stem segments. As for the effective buds and proliferation coefficients induced in the first generation, when using

Table 1: Primers used for RT-qPCR amplification of 9 viruses.

No.	Virus	Primers	Primer sequence (5′-3′)	Product size (bp)
1	ASGV	F	CCTGAATTGAAAACCTTTGCTGCCACTT	456
		R	TAGAAAAACCACACTAACCCGGAAATGC	
2	CMV	F	CTTTCTCATGGATGCTTCTC	855
		R	GCCGTAAGCTGGATGGAC	
3	AVX	F	AAGTCCGCAACACCTACCTG	175
		R	GGACAGACGATAGCAGCCTT	
4	CNV	F	AAGGGTAAGGATGGTGAGGA	587
		R	TTTGGTAGGTTGTGGAGTGC	
5	RMV	F	AGACAGCAATTCTCAAACTTGT	223
		R	CGGTCGCATCATCAACAC	
6	CLBV	F	AGCCATAGTTGAACCATTCCTC	425
		R	GCAGATCATTCACCACATGC	
7	AcVB	F	AATTCGGACCACTCCTGAGGC	529
		R	CTCATTCTCCAMCCRCARAAGAG	
8	PZSV	F	GATAAATTCAGAGCTCTCGG	997
		R	ATCTCTGCAGATTGTGTTCC	
9	CLRV	F	TGGCGACCGTGTAACGGCA	416
		R	GTCGGAAAGATTACGTAAAAGG	

Table 2: Comparison of sterilization effects of different disinfection treatments.

Treatment	Disinfection		Contamination rate (%)*	Browning rate (%)*	Survival rate (%)*
	70% alcohol (s)	15% NaClO (min)			
1		10	74.07a	7.41c	18.52e
2	10	15	46.30b	22.22bc	31.48bcde
3		20	25.93cde	44.44a	29.63de
4		10	40.74bc	11.11c	48.15bcd
5	30	15	14.81def	9.30c	75.93a
6		20	11.11ef	29.63b	59.26ab
7		10	29.63cd	18.52bc	51.85bc
8	60	15	9.30f	18.52bc	72.22a
9		20	7.41f	53.70a	38.89bcde

* Different lowercase letters indicate a significant difference ($p < 0.05$ among different treatment groups.

Table 3: Effect of different concentrations of 6-BA on inducing axillary bud sprouting.

Treatment	Concentration (mg/L)		Inducement rate (%)*	Growth conditions
	6-BA	IBA		
1	0	0.2	25.93c	Plantlets robust, no callus at the base
2	0.5	0.2	42.59bc	Plantlets robust, almost no callus at the base
3	1.0	0.2	74.07a	Plantlets robust, almost no callus at the base
4	1.5	0.2	53.70ab	Plantlets robust, a few small clusters of calluses at the base
5	2.0	0.2	42.59c	Plantlets robust, small clusters of calluses at the base

* Different lowercase letters indicate a significant difference ($p < 0.05$) among different treatment groups.

MS + 6-BA (1.0 mg/L) + IBA (0.2 mg/L) as the optimum induction medium, the inducement rate was 74.07% and the plantlets were almost robust with no callus at the base (Figure 2(a)). Meanwhile, using MS + 6-BA (1.0 mg/L) + IBA (0.1 mg/L) as the optimum proliferation medium, the proliferation rate reached 79.63%, the proliferation coefficient was greater than 5, and the plants were robust with green leaves and longer internodes (Figure 2(b)). MS medium is an important substrate for plant tissue culture, and the selection of an appropriate medium type is crucial to the success or failure of plant tissue culture [27]. Regarding the root culture of kiwifruit, a large body of literature showed that 1/2 MS medium with a low salt content is more conducive to the rooting of kiwifruit tissue culture plantlets [28]. Meanwhile, the use of auxins in MS medium for in vitro rooting stage has also been reported by many other researchers [29]. In addition, it has also been reported that IBA induced lateral rooting better than IAA and NAA [20]. In this study, using 1/2 MS + IBA (0.3 mg/L) as the optimum rooting medium, the rooting rate and average rooting number reached 85.18%

Table 4: Effect of different concentrations of 6-BA on the proliferation of culture plantlets.

Treatment	Concentration (mg/L)		Proliferation rate (%)*	Proliferation coefficient*	Growth conditions
	6-BA	IBA			
1	0	0.1	42.59b	4.12b	Plants robust, leaves green, internodes short, and taproot >2
2	0.5	0.1	64.81ab	4.58ab	Plants robust, leaves green, and internodes short
3	1.0	0.1	79.63a	5.06a	Plants robust, leaves green, and internodes longer
4	1.5	0.1	81.48a	5.06a	Plants weaker, leaves green, internodes longer, and individual callus produced
5	2.0	0.1	66.67ab	4.63ab	Plants weak, bud clumps, leaves green, vitrification, and few calluses produced

* Different lowercase letters indicate a significant difference ($p < 0.05$) among different treatment groups.

Table 5: Effect of different concentrations of IAA on rooting of culture plantlets.

Treatment	IBA concentration (mg/L)	Rooting rate (%)*	Average rooting number*	Rooting situation
1	0	42.59c	3.35d	2–5 roots, a small amount of fibrous root, and no callus
2	0.1	81.48ab	4.13bc	2–5 roots, more fibrous roots, and no callus
3	0.3	85.18a	4.90a	2–6 roots, more and longer fibrous roots, and basically no callus
4	0.5	85.18a	4.48ab	2–6 roots, few fibrous roots, and small callus at base
5	0.7	62.96b	3.78cd	2–5 roots, no fibrous roots, and few calluses at base

* Different lowercase letters indicate a significant difference ($p < 0.05$) among different treatment groups.

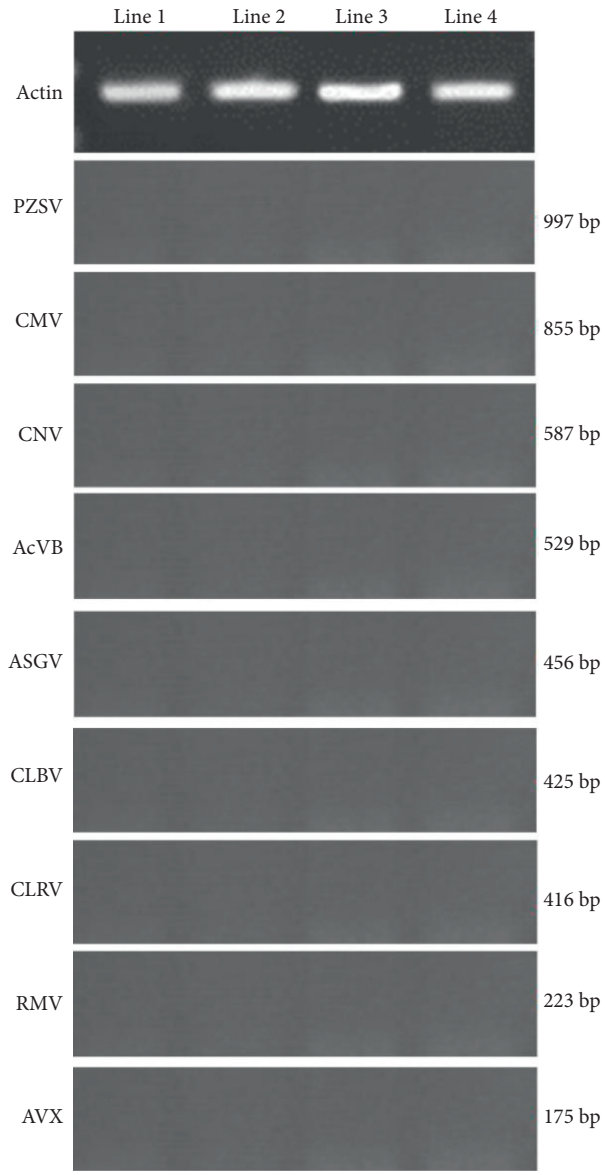

Figure 1: The electrophoresis results of the RT-qPCR products.

and 4.90, respectively, and the rooting number was 2–6 with more and longer fibrous roots and basically no callus (Figure 2(c)). After that, the tissue culture plantlets were transplanted into the greenhouse, and the survival rate exceeded 90% (Figure 2(d)).

Virus disease is a kind of disease with a long incubation period and a great production so hidden trouble. In recent years, many works of literature have reported that kiwifruit virus diseases, especially the pathogenic viruses CLRV and PZSV, which can be spread through pollen, grafting, or

(a) (b) (c) (d)

Figure 2: The rapid in vitro propagation of "Guichang" kiwifruit by tissue culture techniques. (a) Induction culture, (b) proliferation culture, (c) rooting culture, and (d) transplantation culture.

mechanical inoculation, are common in preserved kiwifruit germplasm resources and cultivated kiwifruit plants [30, 31]. Meanwhile, during the cultivation and promotion of "Guichang" kiwifruit for several decades, the virus disease in the main "Guichang" kiwifruit producing areas seriously affected the fruit appearance and commodity value, causing huge economic losses to the kiwifruit industry. In this study, a total of 9 kinds of viruses, including ASGV, CMV, AVX, CNV, RMV, CLBV, AcVB, PZSV, and CLRV, in tissue culture plantlets were detected via the RT-qPCR method, and the results demonstrated that the infection rate of 9 kinds of viruses in tissue culture plantlets was 0. Therefore, this study could lay the foundation for the production of breed virus-free plantlets of "Guichang" kiwifruit.

5. Conclusions

In this study, the establishment of a tissue culture rapid propagation system of "Guichang" kiwifruit was carried out and then detected virus status via the RT-qPCR method. The tissue culture rapid propagation system proved that MS + 6-BA (1.0 mg/L) + IBA (0.2 mg/L), MS + 6-BA (1.0 mg/

L) + IBA (0.1 mg/L), and 1/2 MS + IBA (0.3 mg/L) were the optimal induction, proliferation, and rooting mediums, respectively. In addition, the RT-qPCR results demonstrated that the infection rate of ASGV, CMV, AVX, CNV, RMV, CLBV, AcVB, PZSV, and CLRV in the tissue culture plantlets was 0. This study could lay the foundation for the production of "Guichang" kiwifruit tissue culture plantlets and the industrial rapid propagation of plantlets.

Data Availability

The datasets used and analyzed during the current study are available from the corresponding author on reasonable request.

Conflicts of Interest

The authors declare that they have no conflicts of interest.

Authors' Contributions

Weimin Zhong and Junliang Zhou contributed equally to this work.

Acknowledgments

This work was supported by the Guizhou Province Science and Technology Plan Project Natural Science ([2016]2528), Agricultural Science and Technology Cooperation Projects of Guiyang City, Guizhou Academy of Agricultural Sciences ([2015]002), Foundation of Guizhou Province (LH[2014] 7710), and China Agriculture Research System of MOF and MARA.

References

[1] I. Nishiyama, Y. Yamashita, M. Yamanaka, A. Shimohashi, T. Fukuda, and T. Oota, "Varietal difference in vitamin C content in the fruit of kiwifruit and other *Actinidia* species," *Journal of Agricultural and Food Chemistry*, vol. 52, no. 17, pp. 5472–5475, 2004.

[2] S. Huang, J. Ding, D. Deng et al., "Draft genome of the kiwifruit *Actinidia chinensis*," *Nature Communications*, vol. 4, no. 1, p. 2640, 2013.

[3] F. L. Jin, M. Li, and C. M. Han, "Biological characteristic of Guichang Chinese gooseberry and its cultivation technique with high yield and quality in Qianbei areas," *Guizhou Agricultural Sciences*, vol. 31, pp. 1001–3601, 2003.

[4] R. C. Gardner, "Genetic engineering of kiwifruit," in *Proceedings of the NZ kiwifruit Authority National Research Conference*, pp. 27-28, Hamilton, New Zealand, December 1986.

[5] Y. Lv, "Main characteristics of Hongyang kiwifruit," *Northwest Horticulture*, vol. 3, pp. 37-38, 2001.

[6] J. Chai, Y. Gao, Y. Dong, L. Kong, and Y. Zhang, "Browning treatment in tissue culture of "hongyang" kiwifruit," *IOP Conference Series: Materials Science and Engineering*, vol. 452, Article ID 022075, 2018.

[7] X. H. Wu, Y. L. Zhang, and Y. Zhou, "Establishment of high frequency and direct regeneration system from leaf of "Hayward" kiwifruit [*Actinidia deliciosa* (A. Chev.) C. F. Liang et A. R. Ferguson]," *Plant Physiology Journal*, vol. 49, pp. 759–763, 2013.

[8] X. P. Zhao, K. M. Luo, Y. Zhou, X. H. Wen, L. Yang, and S. H. Tang, "Establishment of high frequency regeneration via leaf explants of 'Red Sun' kiwifruit (*Actinidia chinensis*)," *Chinese Journal of Biotechnology*, vol. 29, pp. 1599–1606, 2013.

[9] F. Yu, "Establishment of tissue culture and rapid propagation system of kiwi," *Chinese Horticulture Abstract*, vol. 6, pp. 17–30, 2017.

[10] G. X. Gao, "Browning in plant tissue culture," *Plant Physiology Communications*, vol. 35, pp. 501–506, 1999.

[11] J. H. Wu, "Establishment of in vitro culture systems for breeding new types of kiwifruit and forActinidiagenomics studies," *Acta Horticulturae*, vol. 1224, pp. 195–202, 2018.

[12] A. G. Blouin, M. N. Pearson, R. R. Chavan et al., "Viruses of kiwifruit (*Actinidia* species)," *Journal of Plant Pathology*, vol. 95, pp. 221–235, 2013.

[13] A. G. Blouin, R. R. Chavan, M. N. Pearson, R. M. Macdiarmid, and D. Cohen, "Detection and characterisation of two novel vitiviruses infecting Actinidia," *Archives of Virology*, vol. 157, no. 4, pp. 713–722, 2012.

[14] Y. X. Wang, N. Hong, G. P. Wang, Z. K. Yang, L. P. Wang, and L. Li, "First report of the Tospovirus tomato necrotic spot associated virus infecting kiwifruit (*Actinidia* sp.) in China," *Plant Disease*, vol. 100, no. 12, p. 2539, 2016.

[15] D. Wang, X. X. Liu, T. T. Li et al., "First report of *Cucumber mosaic virus* infection in kiwifruit (*Actinidia chinensis*) in China," *Plant Disease*, vol. 102, no. 6, p. 1180, 2018a.

[16] Y. Zheng, B. Navarro, G. Wang et al., "Actinidia chlorotic ringspot-associated virus: a novel emaravirus infecting kiwifruit plants," *Molecular Plant Pathology*, vol. 18, no. 4, pp. 569–581, 2017.

[17] S. Veerakone, L. W. Liefting, J. Tang, and L. I. Ward, "The complete nucleotide sequence and genome organisation of a novel member of the family *Betaflexiviridae* from *Actinidia chinensis*," *Archives of Virology*, vol. 163, no. 5, pp. 1367–1370, 2018.

[18] H. Liu, S. Song, W. Wu et al., "Distribution and molecular characterization of *Citrus leaf blotch virus* from *Actinidia* in Shaanxi province, China," *European Journal of Plant Pathology*, vol. 154, no. 3, pp. 855–862, 2019.

[19] S. D. Card, M. N. Pearson, and G. R. G. Clover, "Plant pathogens transmitted by pollen," *Australasian Plant Pathology*, vol. 36, no. 5, pp. 455–461, 2007.

[20] H. Ma, *Studies on Tissue Culture and Rapid Propagation of Kiwifruit Seedlings*, Anhui Agricultural University, Hefei, China, 2015.

[21] D. P. Wang, "The effect of hormone combination with different concentrations on the callus induction and bud differentiation of kiwifruit," *Journal of Anhui Agricultural Sciences*, vol. 35, pp. 11761–11821, 2007.

[22] H. M. Yu, M. Z. Zhao, Y. M. Qian, J. Wang, J. Xia, and F. H. Pang, "Tissue culture and rapid propagation of bud stem segments of kiwifruit in Heyward," *Jiangsu Agricultural Sciences*, vol. 42, pp. 78-79, 2014.

[23] Q. J. Long, Y. J. Wu, and M. Xie, "Tissue culture and rapid propagation of "Hongyang" kiwifruit leaves and bud stem segments," *Acta Agriculturae Zhejiangensis*, vol. 22, pp. 1004–1524, 2010.

[24] M. Irshad, B. He, S. Liu et al., "In vitro regeneration of Abelmoschus esculentus L. cv. Wufu: influence of anti-browning additives on phenolic secretion and callus formation frequency in explants," *Horticulture, Environment, and Biotechnology*, vol. 58, no. 5, pp. 503–513, 2017.

[25] D. Rani and P. K. Dantu, "Sustained shoot multiplication and method for overcoming in vitro browning in medicinally important plant, *Piper chaba* Hunt," *Proceedings of the National Academy of Sciences, India Section B: Biological Sciences*, vol. 86, no. 2, pp. 407–413, 2016.

[26] I. Verstraeten and D. Geelen, "Adventitious rooting and browning are differentially controlled by auxin in rooting-recalcitrant *Elegia capensis* (Burm. f.) Schelpe," *Journal of Plant Growth Regulation*, vol. 34, no. 3, pp. 475–484, 2015.

[27] P. Bhattacharyya, S. Kumaria, and P. Tandon, "High frequency regeneration protocol for Dendrobium nobile: a model tissue culture approach for propagation of medicinally important orchid species," *South African Journal of Botany*, vol. 104, pp. 232–243, 2016.

[28] M. X. Gao, X. Feng, R. L. Lai, W. G. Chen, and Y. T. Chen, "Optimization of tissue culture system of *Actinidia deliciosa* cv," *"Miliang-1". Southeast Horticulture*, vol. 4, pp. 1–5, 2017.

[29] L. Kong, R. Wang, Q. Song, Y. Xie, and Y. Zhang, "Establishment of rapid propagation system of "xu Xiang" kiwifruit," *IOP Conference Series: Earth and Environmental Science*, vol. 252, no. 5, Article ID 052027, 2019.

[30] R. Wang, D. Zhou, J. Luo, and J. B. Fang, "Progress report on viruses of kiwifruit," *Journal of Fruit Science*, vol. 34, pp. 1043–1050, 2017.

[31] Y. Z. Zheng, G. P. Wang, J. F. Zhou et al., "The detection of *Actinidia virus A* and *Actinidia virus B* by RT-PCR and their molecular variation analysis," *Acta Horticulturae Sinica*, vol. 42, pp. 665–671, 2015.

Hindawi
Journal of Chemistry
Volume 2021, Article ID 2166775, 11 pages
https://doi.org/10.1155/2021/2166775

Research Article

Comparative Transcriptomic Analysis of Root Cadmium Responses in Two Chinese Rice Cultivars Yuzhenxiang and Xiangwanxian 12

Shangdu Zhang,[1,2] **Zhenliang Luo**,[3] **Xiang Wu**,[2] **Bangzhi Shi**,[2] **Huidan Jiang**,[4] **Leliang Zhou**,[2] **and Lianyang Bai**[1,4]

[1]*Long Ping Branch of Graduate School, Central South University, Changsha, Hunan 410125, China*
[2]*Guizhou Rice Research Institute, Guizhou Academy of Agricultural Sciences, Guiyang, Guizhou 550006, China*
[3]*Hunan Rice Research Institute, Hunan Academy of Agricultural Sciences, Changsha, Hunan 410125, China*
[4]*Hunan Agricultural Biotechnology Research Institute, Hunan Academy of Agricultural Sciences, Changsha, Hunan 410125, China*

Correspondence should be addressed to Lianyang Bai; lybai@hunaas.cn

Received 4 November 2021; Revised 25 November 2021; Accepted 27 November 2021; Published 13 December 2021

Academic Editor: Wenneng Wu

Cadmium (Cd) pollution in paddy soil is an increasingly serious issue in rice production. It has been reported that there is a higher or lower grain Cd accumulation in the rice cultivars Yuzhenxiang (YZX) or Xiangwanxian 12 (XWX), respectively. To better manage the Cd pollution problem, the genes that might play vital roles in governing the difference in root Cd responses between these two rice cultivars were examined. In this study, the results of RNA sequencing (RNA-seq) showed that there were 341 and 161 differentially expressed genes in the roots of YZX and XWX after Cd exposure, respectively. Among these genes, 7 genes, such as Os06g0196300 (OsJ_019618), Os07g0570700 (OsJ_24808), ADI1, GDCSH, HSFB2C, PEX11-4, and CLPB1, possessed higher degree nodes with each other, through interaction analysis by the STRING (search tool for the retrieval of interacting genes/proteins) software, suggesting that they might play vital roles in Cd response. Based on GO enrichment analysis, 41 differently expressed genes after Cd treatment in YZX or XWX were identified to be related to Cd response. Through comparative transcriptomic analysis, 257 genes might be associated with the root Cd response difference between YZX and XWX. Furthermore, we supposed that ADI1, CFBP1, PEX11-4, OsJ_019618, OsJ_24808, GDCSH, CLPB1, LAC6, and WNK3 might be implicated in Cd response based on the combined analysis of RT-qPCR, interaction, and GO annotation analysis. In conclusion, the numerous genes that might be related to Cd stress response and root Cd response difference between YZX and XWX at the booting stage may be of benefit for the development of rice varieties with low Cd consumption.

1. Introduction

Rice (*Oryza sativa* L.) is the primary source of calorie intake in plenty of countries, including China, and the staple food of over half of the world's population [1, 2]. To meet the food demand of increasing world populations, it is imperative to improve the rice yield [3]. However, the sustainability and productivity of the rice production system are constantly threatened by multiple factors, such as environmental pollution, climate change, and excessive use of pesticides and fertilizers [2].

Heavy metal pollution is the predominant type in all soil contaminants, and cadmium (Cd) contamination ranks the first among heavy metal contaminants in China [4, 5]. Cd contamination, mainly caused by mining, e-waste, and overuse of nitrogen and phosphate fertilizers, has been found in large-scale agricultural soil in China [6, 7]. Cd is readily absorbed by rice plants and easily transferred to food chains [8]. Moreover, it is often accumulated in rice grains and human bodies due to its long half-life of up to 25–30 years [8, 9]. Excessive Cd exposure not only can inhibit the

growth of rice plants but also can decrease the quality/nutrients/yields of rice grains [7]. Additionally, the intake of Cd-contaminated rice can markedly increase the risks of multiple diseases, such as cancer, osteoporosis, and liver/kidney injury, as well as nervous system diseases [9–11]. To reduce the potential harm of Cd on human health, it is imperative to screen out the genes that play vital roles in Cd response in rice plants [7].

It has been reported that there is a notable difference in Cd content in the grains of different rice cultivars, which might be caused by the genotypic and environmental diversities among rice cultivars [12, 13]. More specifically, rice Cd concentration is closely associated with heading time, soil pH, mutation/dysregulation/diversity of multiple genes, or quantitative trait locus related to Cd response (absorption, translocation, and accumulation) among different rice subspecies and cultivars [12, 13]. Over the past decades, high-throughput RNA sequencing (RNA-seq) in combination with function annotation/enrichment and bioinformatics prediction analysis has been widely used to decipher or speculate the essential genes/biological processes/pathways under different conditions at the transcriptomic level and gain a deep and comprehensive understanding of molecular basis underlying the phenotypic/biological differences in plants including rice [14–16].

In this study, RNA-seq-based transcriptomic analysis of root samples of YZX and XWX with or without Cd treatment at the booting stage was performed to identify key genes in root Cd response in Yuzhenxiang (YZX, a high Cd accumulation rice cultivar) and Xiangwanxian 12 (XWX, a low Cd accumulation rice cultivar) and genes associated with root Cd accumulation difference between YZX and XWX. RNA-seq results showed that 341 and 161 transcripts were differentially expressed in the roots of YZX or XWX rice after Cd treatment. Moreover, the protein-protein interaction (PPI) networks of dysregulated transcripts in response to Cd exposure in YZX or XWX were established by the STRING database and 7 genes that might play vital roles in the response to Cd pollution were screened out based on the node degrees of proteins in the PPI networks. Additionally, 41 transcripts that function as crucial players in Cd response were filtered out based on GO annotation analysis. Furthermore, 257 transcripts that might be associated with the difference in root Cd response between YZX or XWX were screened out by comparative transcriptomic analysis. Also, we further examined the expression patterns of 10 genes (ferredoxin-1 (ADI1), fructose-1, 6-bisphosphatase (CFBP1), glycine cleavage system H protein (GDCSH), laccase-6 (LAC6), peroxiredoxin Q (Os06g0196300), ribosome-recycling factor (Os07g0570700), peroxisomal membrane protein 11–4 (PEX11-4), probable serine/threonine-protein kinase WNK3, chaperone protein CLPB1, and heat stress transcription factor B-2c (HSFB2C)) by RT-qPCR assay and filtered some key genes related to Cd stimulation based on RNA-seq/RT-qPCR/interaction/GO enrichment/GO annotation analysis together with previous study outcomes.

2. Materials and Methods

2.1. Plant Materials and Treatment. Two *Indica* rice cultivars (i.e., YZX and XWX) were cultivated in the LT-36VL climatic growth chamber (Percival, Perry, IA, USA) at the Hunan Agricultural Biotechnology Research Institute (Changsha, China). In the preliminary tests, YZX and XWX rice at 4 different growth phases (i.e., seedling, tillering, booting, and grain-filling stages) were cultivated in a hydroponic system containing 2 mg/L of Cd under low-temperature (15–20°C), moderate-temperature (22–27°C), and high-temperature (30–35°C) condition for 48 h. Cd concentration was determined according to the instructions in the Chinese National Standard GB 5009.15–2014.

2.2. RNA Sequencing. In the RNA-seq and real-time quantitative reverse transcription PCR (RT-qPCR) validation experiments, YZX and XWX rice were grown at 22–27°C (moderate temperature) in the hydroponic system with or without 2 mg/L of Cd exposure for 48 h. Next, rice root samples were collected. The samples were divided into 4 groups: AMD group (YZX group with Cd treatment), AMK group (YZX group without Cd treatment), BMD group (XWX group with Cd addition), and BMK group (XWX group without Cd exposure). Each group contains 3 root samples.

RNA was extracted from the root samples using the TRIzol reagent (Thermo Scientific, Waltham, MA, USA) according to the protocols of the manufacturer. The concentration, purity, and quality of RNA were examined by NanoDrop 2000 spectrophotometer (Thermo Scientific). RNA sequencing was carried out as previously described [17]. The cDNA library was constructed using the TruSeq RNA sample preparation kit (Illumina, San Diego, CA, USA) following the protocols of the manufacturer. The mRNA with poly-A structure was enriched by Poly-T oligo-attached magnetic beads (Illumina). The cDNA library was sequenced using the PE150 strategy by Biomarker Technologies Co., Ltd. (Beijing, China). Raw sequencing data were processed and filtered into high-quality clean data. Next, the clean data were aligned to the reference genome of *Oryza sativa* L. subsp. *Indica* using HISAT2 and then assembled and quantified using StringTie. The genome version used in the sequence assembly was ASM465v1. (http://plants.ensembl.org/Oryza_indica/Info/Index).

2.3. Differential Expression Analysis. Differential expression analysis was performed using the DESeq R package. Genes were defined to be differentially expressed at the fold change ≥2 and FDR <0.01.

2.4. Gene Enrichment Analysis. KEGG enrichment analysis was performed using the KOBAS3 database (http://kobas.cbi.pku.edu.cn/kobas3/genelist/). $P < 0.05$ represented that the terms were significantly enriched.

2.5. Interaction Network Construction. The interaction networks of gene-coding proteins were constructed by the STRING database (https://www.string-db.org/).

2.6. RT-qPCR Assay. RNA was reversely transcribed into first-strand cDNA without genomic DNA contamination using TransScript One-Step gDNA Removal and cDNA Synthesis SuperMix (TransGen Biotech Co., Ltd, Beijing, China). Briefly, RNA was coincubated with Oligo (dT) 18 primer for 5 min at 65°C and then immediately placed on an ice bath for 2 min. Then, the reaction mixture was coincubated with TS Reaction Mix, TransScript RT/RI Enzyme Mix, and gDNA Remover at 42°C for 30 min and then terminated at 85°C for 5 min. Next, cDNA was amplified and quantified using the ChamQ Universal SYBR qPCR Master Mix (Vazyme Biotech Co., Ltd., Nanjing, China) and specific quantitative primers under the following thermocycling conditions: 95°C for 3 min, 40 cycles of 95°C for 10 s, and 60°C for 30 s. 18sRNA served as the housekeeping gene to normalize the expression of other genes. RT-qPCR was performed on Roche LightCycler 480 II Real-Time PCR Detection System (Basel, Sweden). The quantitative primer sequences are presented in Table 1. The RNA samples in the RT-qPCR assay were identical to those used in RNA-seq experiments.

2.7. Statistical Analysis. Data analysis was performed using GraphPad Prism 7 software (GraphPad Software, Inc., San Diego, CA, USA). Results were displayed as mean ± standard deviation. The difference among groups was examined using one-way ANOVA and Dunnett post hoc test. Statistically significant differences were set at $P < 0.05$.

2.8. Accession Numbers. The raw data of RNA-seq reads were deposited in the National Center for Biotechnology Information (NCBI) database under the accession number (Submission ID: SUB10609471, BioProject ID: PRJNA777353). Biosample accessions were as follows: SAMN22851327, SAMN22851328, SAMN22851329, SAMN22851330, SAMN22851331, SAMN22851332, SAMN22851333, SAMN22851334, SAMN22851335, SAMN22851336, SAMN22851337, and SAMN22851338.

3. Results

3.1. Cd Accumulation Difference in the Roots of YZX and XWX at Four Different Growth Stages. Previous studies have reported that there is a higher Cd accumulation in the first node under panicle, panicle node, and grains of YZX cultivar compared to XWX cultivar [16, 18]. We supposed that the difference in grain Cd accumulation in these two rice cultivars might be caused by the discrepancy of root Cd absorptive ability. Moreover, root Cd uptake capacity has been found to be varied at different growth temperatures and growth stages in rice [19–21]. To identify the optimal conditions under which the difference of Cd concentration in the roots of YZX and XWX was the most prominent, the concentrations of Cd in the roots of these two rice cultivars at the seedling/tillering/booting/grain-filling stage under low/moderate/high temperature and 2 mg/L of Cd stress were measured. Results showed that there was a noticeable difference in root Cd content at the booting stage when these two rice cultivars were cultured under the moderate-temperature condition (Figure 1). Hence, YZX and XWX rice were cultivated at moderate temperature and 2 mg/L of Cd stress for 48 h to explore the gene expression alterations in response to Cd treatment in the following experiments.

3.2. Identification of Differentially Expressed Transcripts after Cd Treatment in YZX and XWX. In this study, RNA-seq technology was used to identify Cd response-related transcripts in YZX and XWX and investigate genes that might play vital roles in governing the difference in root Cd accumulation between YZX and XWX. The statistics information of clean data after filtration of RNA-seq raw data is shown in Table 2. The GC content of clean data was approximately 50% (Table 2). Moreover, more than 94% of bases have a recognition accuracy of over 99.9% in the clean data (Table 2). Differential expression analysis showed that 341 transcripts were differentially expressed (206 downregulated and 135 upregulated) in the AMD vs. AMK group (Supplementary Figure 1(a) and Supplementary Table 1). Also, 75 downregulated transcripts and 86 upregulated transcripts were identified in the BMD vs. BMK group (Supplementary Figure 1(b) and Supplementary Table 2). Moreover, 18 dysregulated transcripts (i.e., BGIOSGA022091, BGIOSGA007908, BGIOSGA007302, BGIOSGA029201, BGIOSGA022060, BGIOSGA023662, BGIOSGA026675, BGIOSGA001422, BGIOSGA025476, BGIOSGA030712, BGIOSGA004724, BGIOSGA018872, BGIOSGA010590, BGIOSGA001025, BGIOSGA016478, BGIOSGA020263, BGIOSGA001117, and BGIOSGA 000917) in the AMD vs. AMK group and 6 dysregulated transcripts (i.e., BGIOSGA004809, BGIOSGA030712, BGIOSGA034657, BGIOSGA012380, BGIOSGA018872, and BGIOSGA020584) in the BMD vs. BMK group were identified to be involved in inorganic ion transport and metabolism based on COG_class and KOG_class annotation analyses in Supplementary Tables 1 and 2. These transcripts might play vital roles in governing the difference in root Cd accumulation in YZX and XWX.

3.3. Construction of PPI Networks of Dysregulated Genes in the AMD vs. AMK and BMD vs. BMK Groups. Next, the STRING database was used to investigate the relationships of proteins encoded by the abovementioned differentially expressed genes. The interaction networks of the dysregulated genes in the AMD vs. AMK group are presented in Supplementary Figure 2(a) and Supplementary Table 3. Similarly, the interaction relationships of the differentially expressed genes in the BMD vs. BMK group are shown in Supplementary Figure 2(b) and Supplementary Table 4. Additionally, the node degree (number of interacted proteins) of each protein in the PPI network of Supplementary Figures 2(a) and 2(b) was analyzed and is displayed in Supplementary Tables 5 and

Table 1: Quantitative primer sequences of 10 interested genes.

Gene ID	Primer name	Primer (5′-3′)
18s rRNA	18s rRNA-F1 18s rRNA-R1	CTACGTCCCTGCCCTTTCTACA ACACTTCACCGGACCATTCAA
BGIOSGA029403	HSFB2C–F1 HSFB2C-R1	ACAACTTCTCCAGCTTCGTG ACCTTCCGGCGGTGTATATC
BGIOSGA016829	PEX11-4-F1 PEX11-4-R1	TCGTGAGCTGTTCCAACTCT TGCCAGTGAGCTGTTCAGTA
BGIOSGA017714	CLPB1-F1 CLPB1-R1	GTTCGAAGAACGGCTCAAGG ACGAGGTGTATCTCGTCGAT
BGIOSGA015634	WNK3–F1 WNK3-R1	CGTCGACTTCATGTCATCGG TGCAAATGCTGCTCCTCTTC
BGIOSGA033278	GDCSH-F1 GDCSH-R1	AGGACGGGTGGATGATCAAG AGAGCCTAGTGAGCGTCTTC
BGIOSGA004865	CFBP1–F1 CFBP1-R1	GGGAAGTATTGCGTGTGCTT AGGCTGTAACACGTCCTCAA
BGIOSGA027798	ADI1-F1 ADI1-R1	TCATCGAGACCCACAAGGAG AGCATAGGGACGACGACATT
BGIOSGA004807	LAC6-F1 LAC6-R1	TGTCAGCCAGGGAATACGAG GGACTGTCACGTTGTATGGC
BGIOSGA025975	Os07g0570700-F1 Os07g0570700-R1	GTTCCAGAACGCCCAAACAT GGCATGCCTCAATACTGCTC
BGIOSGA021734	Os06g0196300-F1 Os06g0196300-R1	ACAAGGTGAGGAAGGAGTGG GGAGGATCTTGAGGGTCTCG

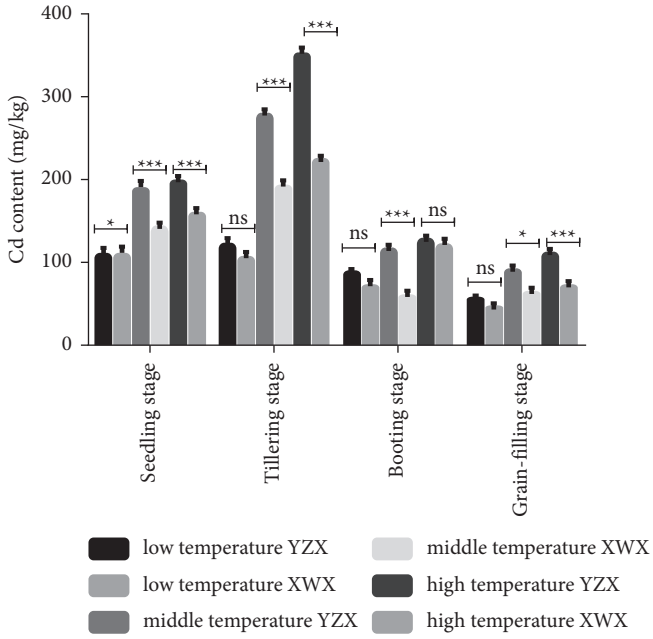

Figure 1: Cd accumulation difference in the roots of YZX and XWX at 4 different growth stages under different temperatures and the same Cd stress. YZX and XWX rice at different growth stages (i.e., seedling, tillering, booting, and grain-filling stages) were cultured for 48 h under different temperatures (low temperature (15–20°C), moderate temperature (22–27°C), or high temperature (30–35°C)) and 2 mg/L of Cd stress. Next, Cd concentrations in the roots of these two rice cultivars were determined.

6, respectively. Genes with greater node degrees might play central roles in the response to Cd. Among genes with higher node degrees, 7 genes (Os06g0196300 (OsJ_019618), Os07g0570700 (OsJ_24808), ADI1, GDCSH, HSFB2C, PEX11-4, and CLPB1) were screened out for further RT-qPCR validation. Moreover, interaction analysis of dysregulated genes in the AMD vs. AMK group revealed that there was a complex interaction among OsJ_019618, OsJ_24808, ADI1, GDCSH, and PEX11-4. For instance, OsJ_019618 could interact with OsJ_24808, ADI1, GDCSH,

Table 2: The statistics information of clean data.

Sample no.	Clean reads	Clean bases	GC content (%)	% ≥Q30
AMD-1	28,320,921	8,469,123,354	52.51	94.89
AMD-2	24,166,384	7,224,223,020	52.62	95.04
AMD-3	23,919,699	7,147,482,544	52.16	95.05
AMK-1	25,675,783	7,673,764,994	52.99	94.99
AMK-2	24,904,107	7,449,500,706	51.75	95.23
AMK-3	23,973,697	7,172,841,032	52.79	94.77
BMD-1	30,635,040	9,159,932,340	53.28	96.41
BMD-2	21,090,058	6,311,270,668	51.64	94.84
BMD-3	23,708,848	7,088,906,522	51.67	94.81
BMK-1	25,223,039	7,541,950,044	52.28	94.88
BMK-2	37,274,481	11,138,840,832	53.13	96.36
BMK-3	27,498,859	8,216,506,798	52.49	96.44

Notes. Clean reads: the total number of paired-end reads in clean data; clean bases: the total number of bases in clean data; GC content: the percentages of G and C bases in clean data; ≥Q30%: the percentage of bases with the quality value ≥ 30 (base identification accuracy ≥ 99.9%).

or PEX11-4 (Supplementary Tables 3 and 5). ADI1 could interact with OsJ_019618, GDCSH, or PEX11-4 (Supplementary Tables 3 and 5). Moreover, there was a potential interaction between OsJ_24808 and OsJ_019618 or GDCSH (Supplementary Tables 3 and 5).

3.4. Comparative Analysis of Cd-Responsive Genes in XWX and YZX. GO annotation analysis of the 341 differentially expressed transcripts in the AMD vs. AMK group showed that 37 transcripts were involved in the response to Cd (Supplementary Table 7). Moreover, 23 of the 161 differentially expressed transcripts in the BMD vs. BMK group were identified to be implicated in Cd response based on GO annotation analysis of dysregulated transcripts in the BMD vs. BMK group (Supplementary Table 8). Among these Cd-responsive transcripts, 19 common elements were found in AMD vs. AMK and BMD vs. BMK groups (Figure 2(a) and Supplementary Table 9). These common transcripts had the same alteration trends in the AMD vs. AMK and BMD vs. BMK groups (Supplementary Table 9). And 18 or 4 transcripts were found to be differentially expressed only in the AMD vs. AMK group or BMD vs. BMK group, respectively (Figure 2(a) and Supplementary Table 9). These 22 transcripts might have crucial roles in regulating the difference in root Cd accumulation between YZX and XWX at the booting stage. Additionally, we noticed that 43 transcripts were differentially expressed only in the BMD vs. BMK group, but not notably altered in the AMD vs. AMK group (Supplementary Table 10). Also, 214 transcripts were found to be markedly upregulated or downregulated in the AMD vs. AMK group, whereas the difference in the expression of these 214 transcripts was not significant in the BMD vs. BMK group (Supplementary Table 11). The 257 transcripts in Supplementary Tables 10 and 11 are integrated into Supplementary Table 12. We believed that these transcripts might also be related to the difference in root Cd accumulation between XWX and YZX. Also, transcripts with notably different upregulated or downregulated ratios in the BMD vs. BMK and AMD vs. AMK groups might be implicated in root Cd accumulation difference between two rice cultivars, which were not analyzed in our project. KEGG enrichment analysis showed that the transcripts in Supplementary Table 12 mainly participated in the regulation of metabolic pathways, biosynthesis of secondary metabolites, carbon fixation in photosynthetic organisms, carbon metabolism, glutathione metabolism, fructose and mannose metabolism, glycolysis/gluconeogenesis, starch and sucrose metabolism, and glycerophospholipid metabolism (Supplementary Table 13 and Figure 2(b)). For instance, 23, 16, 5, 7, or 5 differentially expressed genes were significantly enriched in KEGG pathways related to metabolism, biosynthesis of secondary metabolites, carbon fixation in photosynthetic organisms, carbon metabolism, or glutathione metabolism, respectively (Supplementary Table 13). The top 20 KEGG pathways are shown in Figure 2(b).

3.5. Expression Analysis of 10 Interested Genes by RT-qPCR Assay. Next, 10 genes including the 7 abovementioned genes with greater node degrees in the PPI networks, 1 interested gene (LAC6), and 2 genes related to heavy metal stress tolerance (WNK3 and CFBP1) (detailed information is shown in the Discussion section) were selected for further RT-qPCR validation. RT-qPCR results showed that the expression levels of ADI1, CFBP1, GDCSH, LAC6, Os06g0196300, Os07g0570700, PEX11-4, and WNK3 were notably downregulated in both AMD vs. AMK and BMD vs. BMK groups (Figure 3(a), 3(b), 3(d), and 3(f)–3(j)). CLPB1 and HSFB2C were highly expressed in the AMD vs. AMK group, but not notably changed in the BMD vs. BMK group (Figures 3(c) and 3(e)). Comparative analysis of RT-qPCR and RNA-seq outcomes disclosed that the alteration trends of these 10 genes were consistent in response to Cd treatment in YZX and XWX rice cultivars, although some differences were not statistically significant (Figures 3(a)–3(j)).

3.6. Interaction and Enrichment Analysis of These 10 Genes. The relationships of these 10 genes were further deciphered by PPI analysis via the STRING database. Results suggested that 7 gene-encoded proteins (ADI1, CFBP1, PEX11-4, OsJ_019618, OsJ_24808, GDCSH, and CLPB1) could form a potential regulatory network (Figure 4). The interaction

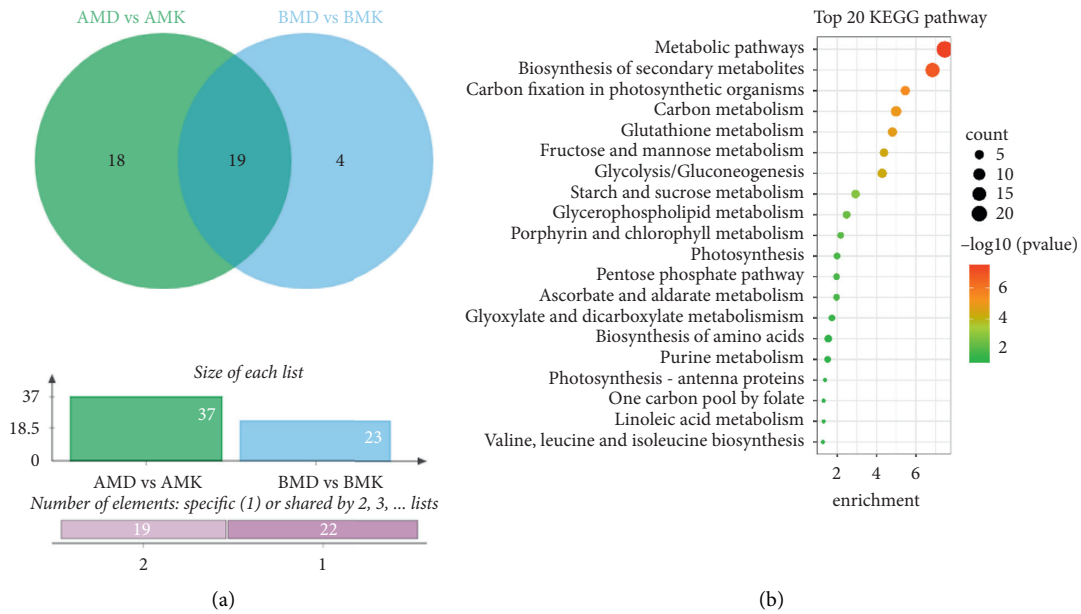

Figure 2: Comparative analysis of Cd-responsive genes in XWX and YZX. (a) Venn analysis for transcripts in Supplementary Tables 7 and 8. AMD vs. AMK list: differentially expressed transcripts related to Cd response in the AMD vs. AMK group based on GO annotation analysis of dysregulated transcripts in the AMD vs. AMK group. BMD vs. BMK list: differentially expressed transcripts related to Cd response in the BMD vs. BMK group based on GO annotation analysis of dysregulated transcripts in the BMD vs. BMK group. Upper subfigure: Venn diagrams showing a number of differentially expressed transcripts related to Cd response in the AMD vs. AMK and BMD vs. BMK groups, as well as the number of overlapping genes. Middle subfigure: number of transcripts in the AMD vs. AMK and BMD vs. BMK lists. Bottom subfigure: number of specific (1) and shared (2) transcripts in the AMD vs. AMK and BMD vs. BMK lists. (b) The top 20 KEGG pathways enriched by the transcripts in Supplementary Table 12. The circle size denotes the number of transcripts in corresponding KEGG pathway terms. The circle color represents the "$-\log_{10}$ (P value)".

analysis of these 10 proteins is shown in sheet 1 of Supplementary Table 14. Moreover, GO enrichment analysis revealed that 7 genes (LAC6, CFBP1, OsJ_019618, WNK3, OsJ_24808, ADI1, and GDCSH) were enriched in the metabolic process (Supplementary Table 14, sheet 2). Additionally, 6 genes (LAC6, CFBP1, CLPB1, WNK3, OsJ_24808, and ADI1) had a potential ion binding activity (Supplementary Table 14, sheet 3). Furthermore, annotation analysis revealed that 3 genes (LAC6, OsJ_019618, and PEX11-4) were involved in the regulation of the response to oxidative stress (Supplementary Table 14, sheet 4).

3.7. Correlation Analysis of These 10 Genes and Cd Response. As shown in Supplementary Table 5, OsJ_019618, OsJ_24808, ADI1, GDCSH, PEX11-4, CLPB1, and HSFB2C could interact with 59, 44, 36, 29, 17, 6, and 6 genes in the interaction network of dysregulated genes in the AMD vs. AMK group, respectively. And CLPB1, PEX11-4, and HSFB2C could interact with 6, 5, and 3 genes in the BMD vs. BMK group, respectively (Supplementary Table 6). To explore the association of these genes and Cd response, Venn analysis of genes that could interact with the 10 above-mentioned genes and GO-annotated Cd-related genes in Supplementary Tables 7 and 8 was performed. Results showed that OsJ_019618 could interact with 4 genes related to the Cd response (i.e., APX2, HCF136, GLN2, and ALDP). ADI1 could interact with 2 Cd-related genes (i.e., ALDP and GLN2). OsJ_24808, GDCSH, or CLPB1 could interact with Cd-responsive gene TPI, GLN2, or HSP17.4, respectively. These data further suggested the close association of these genes and Cd response.

4. Discussion

Rice is a big reservoir of potentially toxic heavy metals in paddy soil-rice systems [22, 23]. The contamination of heavy metals in soil not only influences rice growth and grain yields but also seriously threatens the health of animals and humans that consume rice [22–24]. In this study, genes related to Cd response and root Cd content difference between YZX and XWX were further examined in the roots of these two rice cultivars with different grain Cd accumulation.

Both RT-qPCR and RNA-seq outcomes suggested that 10 genes (i.e., PEX11-4, CLPB1, HSFB2C, LAC6, CFBP1, OsJ_019618, WNK3, OsJ_24808, ADI1, and GDCSH) might play vital roles in the response to Cd in both YZX and XWX. Moreover, interaction analysis suggested that 7 genes (ADI1, CFBP1, PEX11-4, OsJ_019618, OsJ_24808, GDCSH, and CLPB1) could form a potential regulatory network in rice. Additionally, OsJ_019618 could interact with 4 GO-annotated genes related to Cd response (i.e., APX2, HCF136, ALDP, and GLN2). Moreover, there was a potential interaction between ADI1 and GO-annotated Cd-related gene ALDP or GLN2. OsJ_24808, CLPB1, or GDCSH could interact with GO-annotated Cd-responsive gene TPI, HSP17.4, or GLN2, respectively. Furthermore, APX2

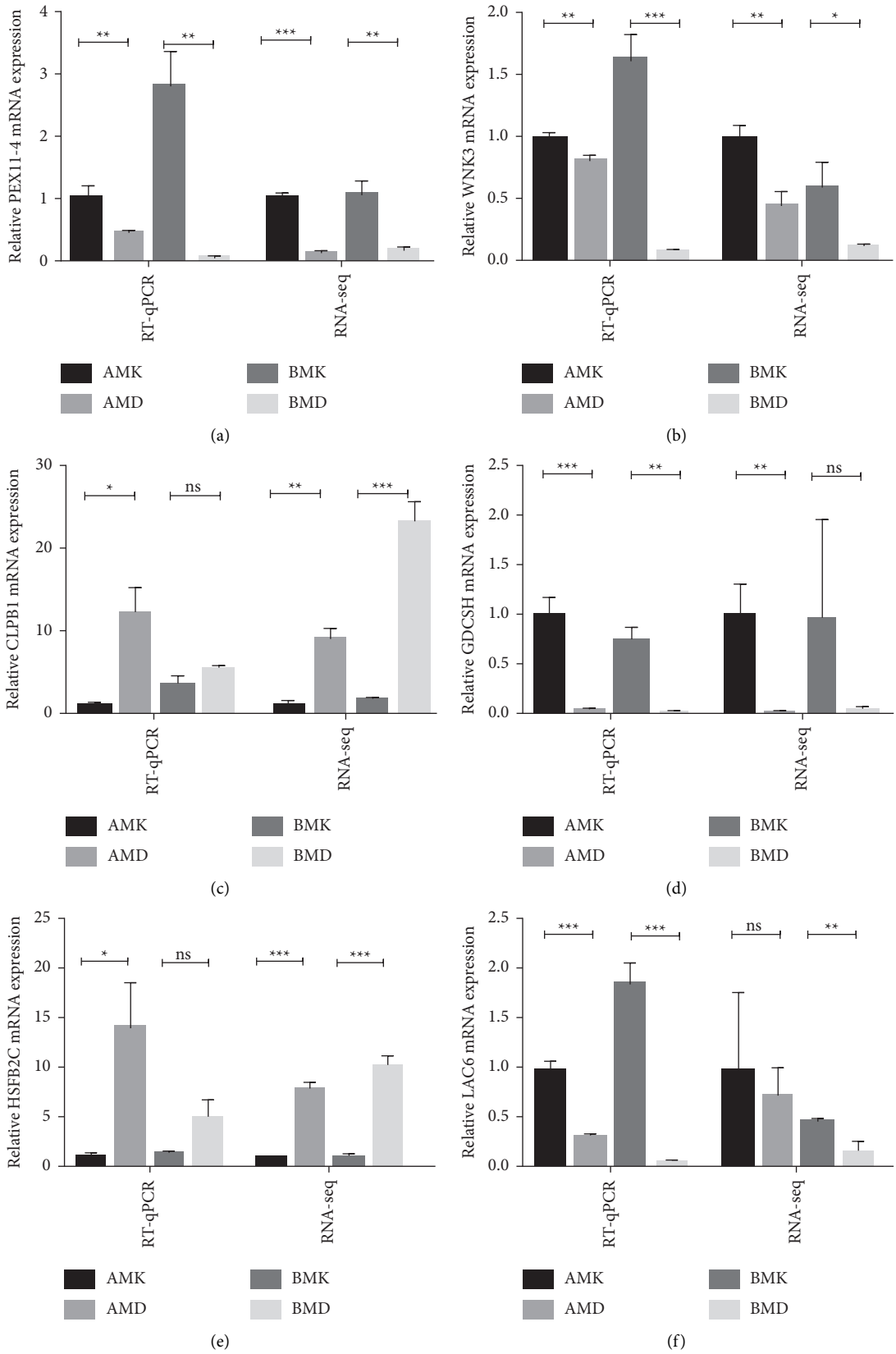

Figure 3: Continued.

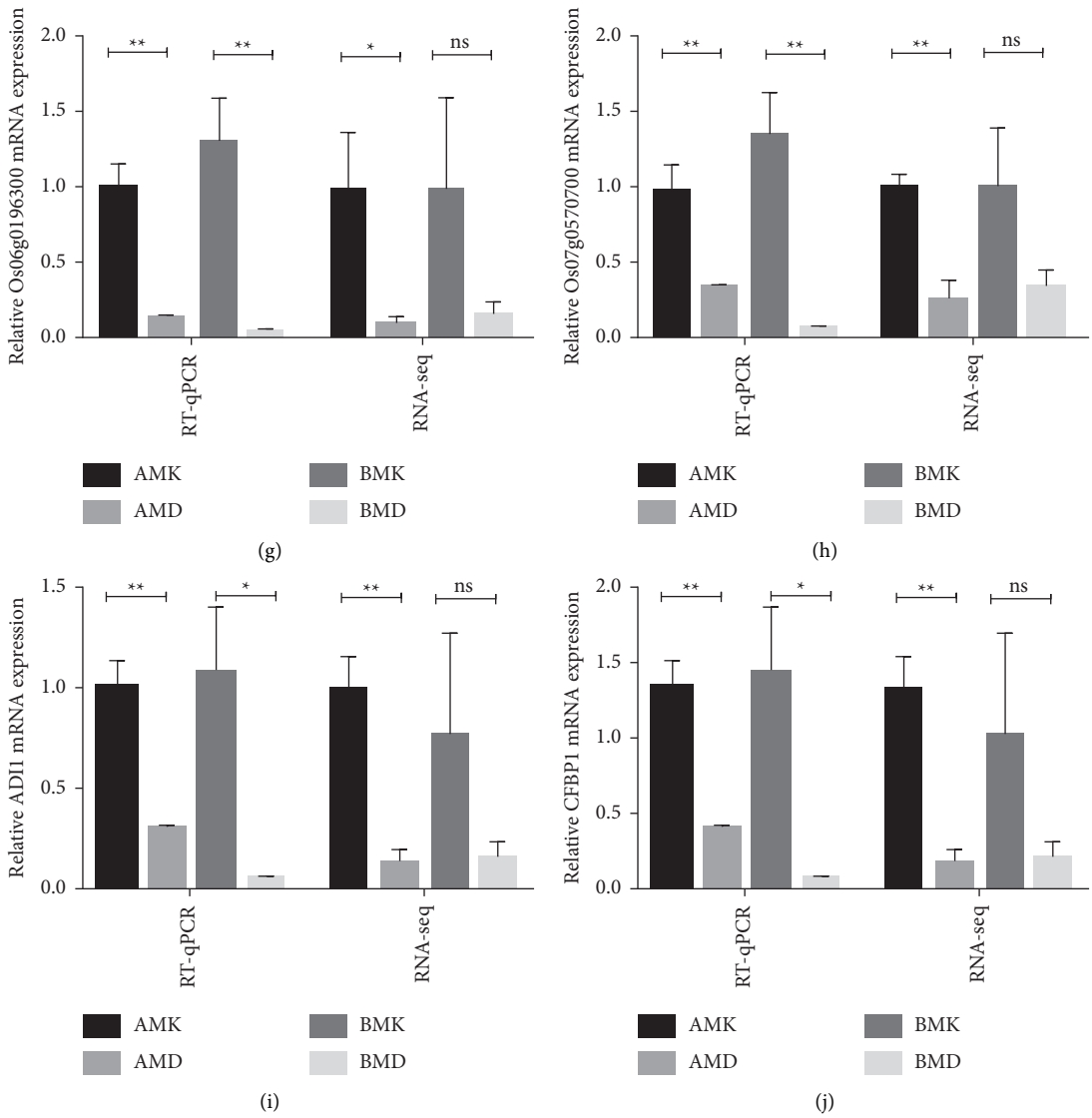

Figure 3: Comparative analysis of RT-qPCR and RNA-seq outcomes of expression patterns of 10 interested genes (i.e., PEX11-4 (a), WNK3 (b), CLPB1 (c), GDCSH (d), HSFB2C (e), LAC6 (f), Os06g0196300 (g), Os07g0570700 (h), ADI1 (i), and CFBP1 (j)) in roots of XWX and YZX.

[25, 26], HCF136 [27], ALDP [28], TPI [29, 30], and HSP17.4 [31] have been found to be implicated in Cd response. ADI1 has also been reported to be related to Cd stress in *Agaricus brasiliensis* [32]. Cd exposure could lead to the increase of CLPB expression level and delay of cell division in *Escherichia coli* [33, 34]. Additionally, our analysis revealed that 6 genes (LAC6, CFBP1, CLPB1, WNK3, OsJ_24808, and ADI1) had a potential ion binding activity. Probable serine/threonine-protein kinase WNK3 belongs to the WNK family, which plays vital roles in plant growth and development and stress responses [35, 36]. A recent study showed that WNK9 (a member of the WNK family) overexpression could improve arsenite (a heavy mental) tolerance in transgenic Arabidopsis [37]. Furthermore, annotation analysis revealed that 3 genes (LAC6, OsJ_019618, and PEX11-4) were related to oxidative stress. Oxidative stress has been found to be closely linked with Cd tolerance and Cd-induced injury and toxicity [38–40]. For instance, molybdenum could relieve Cd-induced toxicity and potentiate Cd tolerance by restricting Cd uptake, reducing oxidative stress, and improving antioxidant defense responses [41]. These data suggested that these genes might function as crucial players in the response to Cd stress.

Cao et al. showed that 706 transcripts were specially expressed in the roots of the mutant *Indica* rice (Icd1 group), which had an extremely low Cd accumulation in root and shoot under Cd exposure [42]. Moreover, 987 transcripts were specially expressed in the roots of wild-type rice (WT group) under Cd exposure [42]. These transcripts might be implicated in the difference in Cd accumulation in wild-type and mutant-type Icd1 rice. Combined with our data and Cao's outcomes, we found that 4 transcripts (BGIOSGA004865 (CFBP1),

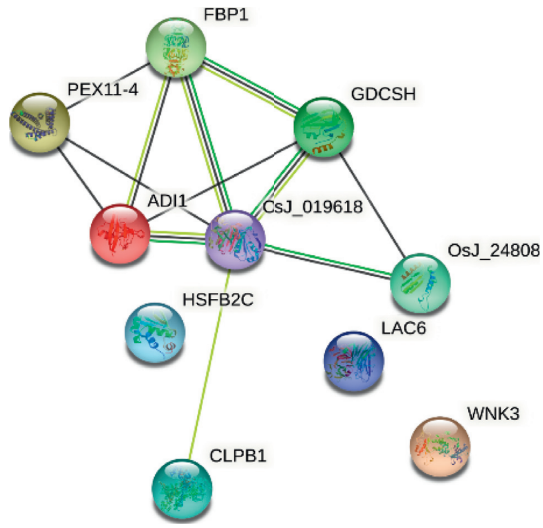

Figure 4: Interaction network of 10 interested genes. The yellow line represents that the potential interaction between proteins was obtained by text mining. The black line denotes that the potential interaction between proteins was identified by coexpression analysis. The green line means that the potential interaction between proteins was predicted based on gene neighborhood relationships. PPI analysis suggested that PEX11-4 could interact with CFBP1 (FBP1), ADI1, and Os06g0196300 (OsJ_019618). There was a potential interaction between CFBP1 (FBP1) and PEX11-4/ADI1/Os06g0196300 (OsJ_019618)/GDCSH. GDCSH coud interact with CFBP1 (FBP1)/ADI1/Os06g0196300 (OsJ_019618)/Os07g0570700 (OsJ_24808). Os07g0570700 (OsJ_24808) could interact with GDCSH/Os06g0196300 (OsJ_019618). Os06g0196300 (OsJ_019618) could interact with ADI1/PEX11-4/CFBP1 (FBP1)/GDCSH/Os07g0570700 (OsJ_24808)/CLPB1. ADI1 could interact with PEX11-4/CFBP1 (FBP1)/GDCSH/Os06g0196300 (OsJ_019618). CLPB1 could interact with Os06g0196300 (OsJ_019618).

BGIOSGA017856 (Os05g0480200), BGIOSGA031509 (GSTU6), and BGIOSGA033278 (GDCSH)) that were specially expressed in the Icd1 group were differentially expressed in the AMD vs. AMK group. Also, 11 transcripts (BGIOSGA000239 (SPS1), BGIOSGA000945 (LEA14), BGIOSGA001233 (ABCG36), BGIOSGA005931 (YSL2), BGIOSGA006919 (SAT1), BGIOSGA007802 (CKX6), BGIOSGA011045 (HSP17.4), BGIOSGA014421 (AOX1B), BGIOSGA021670 (OPR1), BGIOSGA033315 (GSTU6), and BGIOSGA033325 (GSTU6)) or 6 transcripts (BGIOSGA000239 (SPS1), BGIOSGA006919 (SAT1), BGIOSGA009154 (HSP18.6), BGIOSGA011045 (HSP17.4), BGIOSGA021670 (OPR1), and BGIOSGA033325 (GSTU6)) that were specially expressed in the WT group were differentially expressed in the AMD vs. AMK or BMD vs. BMK group, respectively. Among these genes, 2 genes (GSTU6 and HSP17.4) were annotated to be involved in Cd response by the GO database. Moreover, GSTU6 has been found to be notably upregulated in roots of rice under Cd stress [43]. HSP17.4 expression was markedly increased in *Arabidopsis thaliana* roots after Cd exposure [31]. SPS1 was notably downregulated in response to Cd exposure in *Chlorella sorokiniana* [44]. ABCG36 (PDR9) expression was markedly increased in the roots of rice after a short exposure to Cd [45, 46]. ABCG36 knockout promoted root Cd accumulation and potentiated Cd sensitivity in rice [45]. The YSL2 expression level was noticeably increased in the root and shoot of rice in response to Cd stress and YSL2 might be related to Cd uptake transport [47, 48]. These transcripts might play vital roles in the response to Cd stress in rice.

5. Conclusion

Taken together, a host of Cd response-related transcripts were identified in the roots of YZX and XWX at the booting stage. Some transcripts that might be associated with the difference in the root Cd-responsive ability of these two rice cultivars were screened out. Moreover, our data suggested that ADI1, CFBP1, PEX11-4, OsJ_019618, OsJ_24808, GDCSH, CLPB1, and WNK3 might play vital roles in regulating Cd response and Cd tolerance. An in-depth insight into the genetic and molecular mechanisms underlying root Cd stress response difference in YZX and XWX at the booting stage might contribute to the development of new strategies that can improve rice yield and reduce Cd harm to rice and humans.

Data Availability

The data supporting these results are available from the corresponding author upon request.

Conflicts of Interest

The authors declare that they have no conflicts of interest.

Acknowledgments

This research was financially supported by the National Natural Science Foundation of China (no. 41907032), the Science and Technology Support Project of Guizhou

Province (nos. 2018.2295 and 2019.2305), and the Key Scientific and Technological Special Project of Changsha City in China (no. kq200602019.230526).

Supplementary Materials

Supplementary Table 1: differentially expressed transcripts in the AMD vs. AMK group. Supplementary Table 2: differentially expressed transcripts in the BMD vs. BMK group. Supplementary Table 3: interaction of proteins encoded by differentially expressed genes in the AMD vs. AMK group. Supplementary Table 4: interaction of proteins encoded by differentially expressed genes in the BMD vs. BMK group. Supplementary Table 5: the node degree of each gene in Supplementary Table 3. Supplementary Table 6: the node degree of each gene in Supplementary Table 4. Supplementary Table 7: differentially expressed transcripts related to Cd responses in the AMD vs. AMK group, which was annotated by the GO database. Supplementary Table 8: GO-annotated Cd-responsive transcripts, which were also differentially expressed in the BMD vs. BMK group. Supplementary Table 9: Venn analysis outcomes for differentially expressed transcripts related to Cd responses in the AMD vs. AMK and BMD vs. BMK groups. Supplementary Table 10: transcripts that were markedly upregulated or downregulated in the BMD vs. BMK group, but not in the AMD vs. AMK group. Supplementary Table 11: transcripts that were notably upregulated or downregulated in the AMD vs. AMK group, but not in the BMD vs. BMK group. Supplementary Table 12: the information of transcripts in Supplementary Tables 10 and 11. Supplementary Table 13: KEGG enrichment analysis for genes in Supplementary Table 12. Supplementary Table 14: the interaction, enrichment, and annotation analysis of 10 interested genes. Supplementary Figure 1: identification of differentially expressed transcripts in AMD vs. AMK and BMD vs. BMK groups. (A) The heat map of differentially expressed transcripts in the AMD vs. AMK group. (B) The heat map of differentially expressed transcripts in the BMD vs. BMK group. Supplementary Figure 2: construction of interaction networks of dysregulated genes. (A) Interaction networks of differentially expressed genes in the AMD vs. AMK group. (B) Interaction networks of differentially expressed genes in the BMD vs. BMK group. (*Supplementary Materials*)

References

[1] C. Marco, D. L. Maria, G. Cádiz, and S. C. Antonio, "Xtraction and analysis of phenolic compounds in rice: a review," *Molecules*, vol. 23, no. 11, p. 2890, 2018.

[2] L. Nie and S. Peng, "Rice production in China," *Rice Production Worldwide*, , pp. 33–52, Springer, 2017.

[3] N. Li, R. Xu, P. Duan, and Y. Li, "Control of grain size in rice," *Plant Reproduction*, vol. 31, no. 3, pp. 237–251, 2018.

[4] P. Wang, H. Chen, P. M. Kopittke, and F.-J. Zhao, "Cadmium contamination in agricultural soils of China and the impact on food safety," *Environmental Pollution*, vol. 249, pp. 1038–1048, 2019.

[5] Q. Yang, Z. Li, X. Lu, Q. Duan, L. Huang, and J. Bi, "A review of soil heavy metal pollution from industrial and agricultural regions in China: pollution and risk assessment," *The Science of the Total Environment*, vol. 642, pp. 690–700, 2018.

[6] M. Zou, S. Zhou, Y. Zhou, Z. Jia, T. Guo, and J. Wang, "Cadmium pollution of soil-rice ecosystems in rice cultivation dominated regions in China: a review," *Environmental Pollution*, vol. 280, Article ID 116965, 2021.

[7] J. Chen, W. Zou, L. Meng, X. Fan, G. Xu, and G. Ye, "Advances in the uptake and transport mechanisms and QTLs mapping of cadmium in rice," *International Journal of Molecular Sciences*, vol. 20, no. 14, p. 3417, 2019.

[8] W.-E. Song, S.-B. Chen, J.-F. Liu, L. Song, N. Li, and B. Liu, "Variation of Cd concentration in various rice cultivars and derivation of cadmium toxicity thresholds for paddy soil by species-sensitivity distribution," *Journal of Integrative Agriculture*, vol. 14, no. 9, pp. 1845–1854, 2015.

[9] G. Genchi, M. S. Sinicropi, G. Lauria, A. Carocci, and A. Catalano, "The effects of cadmium toxicity," *International Journal of Environmental Research and Public Health*, vol. 17, no. 11, p. 3782, 2020.

[10] B. Hussain, M. N. Ashraf, R. Shafeeq-ur-Rahman, A. Abba, and M. Farooq, "Cadmium stress in paddy fields: effects of soil conditions and remediation strategies," *The Science of the Total Environment*, vol. 754, Article ID 142188, 2021.

[11] J. J. V. Branca, G. Morucci, and A. Pacini, "Cadmium-induced neurotoxicity: still much ado," *Neural Regeneration Research*, vol. 13, no. 11, pp. 1879–1882, 2018.

[12] L. Sun, X. Xu, Y. Jiang et al., "Genetic diversity, rather than cultivar type, determines relative grain Cd accumulation in hybrid rice," *Frontiers of Plant Science*, vol. 7, p. 1407, 2016.

[13] G. Duan, G. Shao, Z. Tang et al., "Genotypic and environmental variations in grain cadmium and arsenic concentrations among a panel of high yielding rice cultivars," *Rice*, vol. 10, no. 1, p. 9, 2017.

[14] S. Naidoo, E. A. Visser, L. Zwart, Y. D. Toit, V. Bhadauria, and L. S. Shuey, "Dual RNA-sequencing to elucidate the plant-pathogen duel," *Current Issues in Molecular Biology*, vol. 27, pp. 127–142, 2018.

[15] S. Jones, A. Baizan-Edge, S. MacFarlane, and L. Torrance, "Viral diagnostics in plants using next generation sequencing: computational analysis in practice," *Frontiers of Plant Science*, vol. 8, p. 1770, 2017.

[16] A. Liu, Z. Zhou, Y. Yi, and G. Chen, "Transcriptome analysis reveals the roles of stem nodes in cadmium transport to rice grain," *BMC Genomics*, vol. 21, no. 1, p. 127, 2020.

[17] H. Chen, X. Chen, J. Tian et al., "Development of gene-based SSR markers in rice bean (*vigna umbellata* L.) based on transcriptome data," *PLoS One*, vol. 11, no. 3, Article ID e0151040, 2016.

[18] M. Israël Prince, M. François, S. Sun, and X. Lin Fan, "Effects of alkaline fertilizer and rice cultivation (*Oryza sativa* L.) on remediation of soils polluted with cadmium (Cd)," *Journal of Applied Biosciences*, vol. 157, pp. 16182–16193, 2021.

[19] L. Ge, L. Cang, J. Yang, and D. Zhou, "Effects of root morphology and leaf transpiration on Cd uptake and translocation in rice under different growth temperature," *Environmental Science and Pollution Research*, vol. 23, no. 23, pp. 24205–24214, 2016.

[20] L.-Q. Ge, L. Cang, H. Liu, and D.-M. Zhou, "Effects of warming on uptake and translocation of cadmium (Cd) and copper (Cu) in a contaminated soil-rice system under Free Air Temperature Increase (FATI)," *Chemosphere*, vol. 155, pp. 1–8, 2016.

[21] H. Zhou, W. Zhu, W.-T. Yang et al., "Cadmium uptake, accumulation, and remobilization in iron plaque and rice

tissues at different growth stages," *Ecotoxicology and Environmental Safety*, vol. 152, pp. 91–97, 2018.

[22] W. Ali, K. Mao, H. Zhang et al., "Comprehensive review of the basic chemical behaviours, sources, processes, and endpoints of trace element contamination in paddy soil-rice systems in rice-growing countries," *Journal of Hazardous Materials*, vol. 397, Article ID 122720, 2020.

[23] R. Khanam, A. Kumar, A. K. Nayak et al., "Metal(loid)s (As, Hg, Se, Pb and Cd) in paddy soil: bioavailability and potential risk to human health," *The Science of the Total Environment*, vol. 699, Article ID 134330, 2020.

[24] S. Sharma, I. Kaur, and A. K. Nagpal, "Contamination of rice crop with potentially toxic elements and associated human health risks-a review," *Environmental Science and Pollution Research*, vol. 28, no. 10, pp. 12282–12299, 2021.

[25] M. Y. Lee and H. W. Shin, "Cadmium-induced changes in antioxidant enzymes from the marine alga Nannochloropsis oculata," *Journal of Applied Phycology*, vol. 15, no. 1, pp. 13–19, 2003.

[26] M. Jozefczak, S. Bohler, H. Schat et al., "Both the concentration and redox state of glutathione and ascorbate influence the sensitivity of arabidopsis to cadmium," *Annals of Botany*, vol. 116, no. 4, pp. 601–612, 2015.

[27] W.-L. Huang, F.-L. Wu, H.-Y. Huang et al., "Excess copper-induced alterations of protein profiles and related physiological parameters in citrus leaves," *Plants*, vol. 9, no. 3, p. 291, 2020.

[28] R. Yu, Y. Ma, Y. Li, X. Li, C. Du, and G. Shi, "Comparative transcriptome analysis revealed key factors for differential cadmium transport and retention in roots of two contrasting peanut cultivars," *BMC Genomics*, vol. 19, no. 1, p. 938, 2018.

[29] Z.-W. Cheng, Z.-Y. Chen, X. Yan, Y.-W. Bian, X. Deng, and Y.-M. Yan, "Integrated physiological and proteomic analysis reveals underlying response and defense mechanisms of Brachypodium distachyon seedling leaves under osmotic stress, cadmium and their combined stresses," *Journal of Proteomics*, vol. 170, pp. 1–13, 2018.

[30] C.-L. Ge, Z.-G. Wang, D.-Z. Wan et al., "Proteomic study for responses to cadmium stress in rice seedlings," *Rice Science*, vol. 16, no. 1, pp. 33–44, 2009.

[31] M. Weber, A. Trampczynska, and S. Clemens, "Comparative transcriptome analysis of toxic metal responses in *Arabidopsis thaliana* and the Cd2+-hypertolerant facultative metallophyte Arabidopsis halleri," *Plant, Cell and Environment*, vol. 29, no. 5, pp. 950–963, 2006.

[32] P.-H. Liu, Z.-X. Huang, X.-H. Luo et al., "Comparative transcriptome analysis reveals candidate genes related to cadmium accumulation and tolerance in two almond mushroom (*Agaricus brasiliensis*) strains with contrasting cadmium tolerance," *PLoS One*, vol. 15, no. 9, Article ID e0239617, 2020.

[33] Z. Khan, M. A. Nisar, S. Z. Hussain, M. N. Arshad, and A. Rehman, "Cadmium resistance mechanism in *Escherichia coli* P4 and its potential use to bioremediate environmental cadmium," *Applied Microbiology and Biotechnology*, vol. 99, no. 44, pp. 10745–10757, 2015.

[34] A. Wang and D. E. Crowley, "Global gene expression responses to cadmium toxicity in *Escherichia coli*," *Journal of Bacteriology*, vol. 187, no. 9, pp. 3259–3266, 2005.

[35] R. Manuka, A. A. Saddhe, and K. Kumar, "Genome-wide identification and expression analysis of WNK kinase gene family in rice," *Computational Biology and Chemistry*, vol. 59, no. Pt A, pp. 56–66, 2015.

[36] A. A. Saddhe, S. B. Karle, T. Aftab, and K. Kumar, "With no lysine kinases: the key regulatory networks and phytohormone cross talk in plant growth, development and stress response," *Plant Cell Reports*, vol. 40, no. 11, pp. 2097–2109, 2021.

[37] R. Manuka, A. A. Saddhe, A. K. Srivastava, K. Kumar, and S. Penna, "Overexpression of rice OsWNK9 promotes arsenite tolerance in transgenic Arabidopsis plants," *Journal of Biotechnology*, vol. 332, pp. 114–125, 2021.

[38] S. Nemmiche, "Oxidative signaling response to cadmium exposure," *Toxicological Sciences: An Official Journal of the Society of Toxicology*, vol. 156, no. 1, pp. 4–10, 2017.

[39] C. Loix, M. Huybrechts, J. Vangronsveld, M. Gielen, E. Keunen, and A. Cuypers, "Reciprocal interactions between cadmium-induced cell wall responses and oxidative stress in plants," *Frontiers of Plant Science*, vol. 8, p. 1867, 2017.

[40] A. Cuypers, M. Plusquin, T. Remans et al., "Cadmium stress: an oxidative challenge," *Biometals*, vol. 23, no. 5, pp. 927–940, 2010.

[41] M. Imran, S. Hussain, M. A. El-Esawi et al., "Molybdenum supply alleviates the cadmium toxicity in fragrant rice by modulating oxidative stress and antioxidant gene expression," *Biomolecules*, vol. 10, no. 11, p. 1582, 2020.

[42] Z. Z. Cao, X. Y. Lin, Y. J. Yang, M. Y. Guan, P. Xu, and M. X. Chen, "Gene identification and transcriptome analysis of low cadmium accumulation rice mutant (lcd1) in response to cadmium stress using MutMap and RNA-seq," *BMC Plant Biology*, vol. 19, no. 1, p. 250, 2019.

[43] Y. Huang, H. Chen, J. R. Reinfelder et al., "A transcriptomic (RNA-seq) analysis of genes responsive to both cadmium and arsenic stress in rice root," *The Science of the Total Environment*, vol. 666, pp. 445–460, 2019.

[44] N. Ding, L. Wang, Y. Kang et al., "The comparison of transcriptomic response of green microalga Chlorella sorokiniana exposure to environmentally relevant concentration of cadmium(II) and 4-n-nonylphenol," *Environmental Geochemistry and Health*, vol. 42, no. 9, pp. 2881–2894, 2020.

[45] S. Fu, Y. Lu, X. Zhang et al., "The ABC transporter ABCG36 is required for cadmium tolerance in rice," *Journal of Experimental Botany*, vol. 70, no. 20, pp. 5909–5918, 2019.

[46] A. Moons, "Ospdr9, which encodes a PDR-type ABC transporter, is induced by heavy metals, hypoxic stress and redox perturbations in rice roots1," *FEBS Letters*, vol. 553, no. 3, pp. 370–376, 2003.

[47] T. Guha, S. Barman, A. Mukherjee, and R. Kundu, "Nanoscale zero valent iron modulates Fe/Cd transporters and immobilizes soil Cd for production of Cd free rice," *Chemosphere*, vol. 260, Article ID 127533, 2020.

[48] X. Li, D. Chen, B. Li, Y. Yang, and Y. Yang, "Combined transcriptomic, proteomic and biochemical approaches to identify the cadmium hyper-tolerance mechanism of turnip seedling leaves," *Environmental Science and Pollution Research*, vol. 28, no. 18, pp. 22458–22473, 2021.

Hindawi
Journal of Chemistry
Volume 2021, Article ID 6238893, 12 pages
https://doi.org/10.1155/2021/6238893

Research Article

Study of the Physiological Dynamics of Cadmium Accumulation in Two Varieties of Rice with Different Cadmium-Accumulating Properties

Shangdu Zhang,[1,2] **Xiang Wu**,[2] **Ju Peng**,[2] **Xiufei Meng**,[2] **Bangzhi Shi**,[2] **Leliang Zhou**,[2] **and Lianyang Bai**[1,3]

[1]*Long Ping Branch of Graduate School, Central South University, Changsha, Hunan 410125, China*
[2]*Guizhou Rice Research Institute, Guizhou Academy of Agricultural Sciences, Guiyang, Guizhou 550006, China*
[3]*Hunan Agricultural Biotechnology Research Institute, Hunan Academy of Agricultural Sciences, Changsha, Hunan 410125, China*

Correspondence should be addressed to Lianyang Bai; lybai@hunaas.cn

Received 8 November 2021; Accepted 28 November 2021; Published 10 December 2021

Academic Editor: Wenneng Wu

This study focused on cadmium (Cd) uptake by two rice varieties, Yuzhenxiang (YZX) and Xiangwanxian 12 (XWX), which differ in their capacity to accumulate Cd, i.e., XWX > YZX. Treatments with three different gradients of soil Cd concentrations showed that with the increase in soil Cd concentration gradient, the Cd content in each rice plant organ also increased, i.e., Cd-3 > Cd-2 > Cd-1. The trend in the Cd content of each organ was such that the farther the organ from the root, the lower its Cd content, i.e., root > stem and sheath > leaf > grain. We observed that for all four growth stages, the booting stage is the key stage in terms of Cd absorption, where the highest levels of accumulation are observed, that is, booting stage > full heading stage > tillering stage > maturity stage. Of the two cultivars, XWX had higher SOD, POD, and CAT activities but lower MDA content. In contaminated soils, SOD, POD, and CAT activities increased gradually with the increase in Cd concentration, while MDA content decreased, which indicated that the low Cd variety XWX had an advantage over the high Cd variety YZX. Through the comparative analysis of photosynthetic physiology, it was found that the low-Cd-accumulating rice variety XWX appeared more tolerant to Cd, while the high-Cd-accumulating rice YZX was more sensitive. Therefore, the low Cd rice variety XWX was more suitable for planting safe rice in Cd-polluted paddy fields.

1. Introduction

Rice (*Oryza sativa* L.) is the main food crop in China, with more than half of the population consuming rice as their staple food. The rapid development following industrialization in China has not only provided huge economic benefits but also caused a large amount of environmental pollution, including numerous types of heavy metals that have entered into the agricultural soil. Heavy metal pollution in agricultural soil mainly includes cadmium (Cd), chromium (Cr), mercury (Hg), lead (Pb), and nickel (Ni) [1]. According to the National Soil Pollution Investigation Bulletin jointly published by the Ministry of Environmental Protection and the Ministry of Land and Resources in 2014 [2], the above-standard rate of heavy metal pollution in China's cultivated soil reached 19.4%. Cd is the number one contaminant in heavy metal pollution, and the threshold rate beyond which the standard is exceeded is 7.0%. Cd is a toxic heavy metal element with strong biological activity and is a nonessential element for plants, whose growth and development are hindered by excessive accumulation [3]. Cd can be transferred from rice to the human body through the food chain, thus causing harm to human health [4].

Following the occurrence of Cd stress, plants will activate evolved self-protection defense mechanisms, such as increasing the activity of superoxide dismutase (SOD),

peroxidase (POD), catalase (CAT), and other antioxidant enzymes and reducing the accumulation of membrane lipid malondialdehyde (MDA). These mechanisms can effectively reduce the damage to plants caused by Cd stress [5–7].

Cd stress will inhibit plant photosynthesis, and the degree of inhibition is related to plant species, growth period, environmental conditions, Cd stress concentration, time, and many other factors. The inhibition of plant photosynthesis by heavy metals is due to their effects on electron transport in the process of photosynthesis and in destroying chloroplast integrity [8]. Cd stress damages plant photosynthesis mainly through disruption of physiological processes such as photosynthesis rate (Photo, Pn), stomatal conductance (Gs), intercellular CO_2 concentration (Ci), and transpiration rate (Trmmol, Tr) [9].

A low concentration of Cd in soil generally has no effect on rice yield, given that rice has a high capacity for Cd adsorption; when the soil Cd content is higher, however, Cd stresses affect rice plant physiological and biochemical metabolism, causing a series of changes in these characteristics, which induces disorders in cell metabolism and ultimately inhibits rice growth and development. In studies of medium and high concentrations of Cd pollution stress, there are currently few reports describing the characterization of Cd content, antioxidant enzyme activity, and photosynthesis parameters in various organs of rice. In order to provide a theoretical basis for the breeding of new Cd-tolerant rice varieties, this study took Yuzhenxiang (YZX) and Xiangwanxian 12 (XWX) as the research objects, based on their different patterns of Cd accumulation, and analyzed their physiological and biochemical characteristics under treatment with different concentrations of soil Cd, so as to provide a theoretical basis for the breeding of new Cd-tolerant rice varieties.

2. Materials and Methods

2.1. Materials

2.1.1. Experimental Material. The experimental materials were the high-Cd-accumulating variety YZX and the low-Cd-accumulating variety XWX, which are the result of selection by predecessors over many years and many points of pot cultivation and field verification [10]. The two rice varieties were bred and provided by Hunan Rice Research Institute and were suitable for the double cropping of late rice in the rice growing area of Hunan Province, with a growth period of 115 ± 2 d.

2.1.2. Summary of the Test Site. The experiment was conducted in the Spring Science Research Base of the Hunan Academy of Agricultural Sciences—the breeding and identification base of rice varieties with low Cd accumulation (113°26′57″E, 28°29′36″N) in Chunhua Town, Changsha County, Changsha City. The experimental site is located in a typical section of the middle subtropical region, with an average annual temperature of 17.2°C and an average annual rainfall of 1361 mm, belonging to the double-cropping rice production area.

In this experiment, the pool planting identification area of the breeding and identification base of rice varieties with low Cd accumulation was selected, and the irrigation and drainage design was adopted to control the uniformity of factors such as soil Cd content, pH, and water content in the tank, and the high-precision soil moisture, pH, and temperature monitoring system and remote control system were matched.

2.1.3. Test Treatment and Method. The two tested rice varieties were sown on June 13, 2018, and two grain seedlings were transplanted on July 1, 2018. Six rows were planted in each plot, with 14 stumps for each row. The spacing between plants and rows was 17×20 cm, with a protection row set between. Samples were taken at the tillering (August 4, 2018), booting (August 16, 2018), full heading (September 14, 2018), and maturity stages (September 20, 2018) of rice. The pool identification area contains natural Cd concentration-treated soil, and according to the Cd concentration, the soil was divided into Cd-1, Cd-2, and Cd-3 gradients. Fertilizer management: no basal fertilizer, urea (60 kg/ha), and potassium chloride (30 kg/ha) were applied for tillering. Water management: flooding in the early stage, moist irrigation after heading, dry soil naturally in the week before harvest, and other management aspects are the same as in the field. In the above four growth stages of rice, the Cd content in roots, stem sheath, leaves, and grains was measured. The photosynthetic parameters, Pn, Gs, Ci, and Tr, of the top leaves were measured. The activity of the antioxidant enzymes SOD, POD, and CAT and the content of MDA were measured in the top leaves.

2.2. Determination Items and Methods

2.2.1. Soil Physical and Chemical Properties Detection. The soil of 0–20 cm in the tillage layer of the paddy field was taken before rice transplantation, and the physical and chemical indexes were detected. The soil was air-dried to remove rock and animal and plant residues, then crushed through a 100-target sieve, and sealed for use. The method was repeated three times for each sample. Soil physical and chemical indexes and determination methods are as follows: Soil total Cd (ST-Cd) was determined by atomic spectrophotometry [11], and soil effective Cd (SE-Cd) was determined by atomic absorption spectrometry [12]. Total nitrogen (TN) was determined using the Kjeldahl method [13], available nitrogen (AN) was determined by the alkali-hydrolytic diffusion method [14], and total phosphorus (TP) was determined by the perchloric acid-sulfuric acid method [15]. Available phosphorus (AP) was determined by spectrophotometry [16], and total potassium (TK) was determined by sodium hydroxide melting [17]. Available potassium (AK) was determined by flame spectrophotometry [18], and pH was determined using the potentiometric method [19]. Soil organic matter (SOM) was determined by REDOX colorimetry [20].

Soil samples were taken from rice fields of Cd-1, Cd-2, and Cd-3, each with different Cd concentrations, for the characterization of physical and chemical indicators. Samples were taken from each tested variety area of each treatment, for which there were three replicates. These results are shown in Table 1.

Table 1: Physical and chemical properties of soil samples.

Test item	Soil treatment		
	Cd-1	Cd-2	Cd-3
ST-Cd (mg/kg)	0.16 ± 0.00c	0.56 ± 0.00b	0.89 ± 0.00a
SE-Cd (mg/kg)	0.05 ± 0.00c	0.27 ± 0.00b	0.53 ± 0.00a
TN (g/kg)	0.85 ± 0.02c	1.55 ± 0.02b	1.69 ± 0.01a
AN (mg/kg)	71.33 ± 0.88 b	118.67 ± 0.88a	118.33 ± 1.20a
TP (g/kg)	0.35 ± 0.01c	0.45 ± 0.01b	0.49 ± 0.01a
AP (mg/kg)	4.30 ± 0.06c	6.47 ± 0.09a	5.37 ± 0.03b
TK (g/kg)	11.80 ± 0.15b	11.87 ± 0.09b	13.40 ± 0.10a
AK (mg/kg)	40.67 ± 1.20b	33.67 ± 1.20c	51.33 ± 0.88a
pH	6.54 ± 0.00b	7.03 ± 0.01a	6.09 ± 0.01c
SOM (g/kg)	11.17 ± 0.03c	27.17 ± 0.09a	25.80 ± 0.12b

Note. The data in the table are mean ± standard error. ST-Cd, soil total Cd; SE-Cd, soil effective Cd; TN, total nitrogen; AN, available nitrogen; TP, total phosphorus; AP, available phosphorus; TK, total potassium; AK, available potassium; SOM, soil organic matter.

2.2.2. Determination of Cd Content in Rice. After the rice plants were cleaned, they were washed with deionized water, and the water on the surface was absorbed using absorbent paper. The roots, stems and sheathing, leaves, and rice were decomposed into paper bags and numbered, then placed into the oven at 110°C for 30 minutes, and dried at 80°C until the weight was constant. The root system, stem sheath, leaves, and husked rice (husked using a huller with a polyurethane roller to prevent metal contamination) were pulverized and screened over a 100-point sieve before being stored in a dryer. Cd content in the samples was determined by ICP-OES and repeated three times [21].

2.2.3. Antioxidant Enzyme Index Determination. At the tillering, booting, full heading, and maturity stages of rice, the upper leaves were taken in the field, wrapped with tin foil paper and numbered, and then placed in the liquid nitrogen tank for snap-freezing. After returning to the laboratory, liquid nitrogen was added for grinding, weighing (approximately 0.2 g per serving), and tube loading (2 mL centrifuge tube); then, the samples were numbered and placed in the refrigerator at −80°C for reserve.

The SOD, POD, and CAT activities and MDA content were measured using the corresponding kits (Nanjing Jiancheng Bioengineering Institute, Nanjing, China).

2.2.4. Determination of Photosynthetic Index. At the same time as the determination of antioxidant enzymes, the LI-6400 portable photosynthetic system analyzer was used to determine the top leaves of rice in the four growth periods from 09:00 to 11:00 in the morning on sunny days. The determination of Pn, Gs, Ci, and Tr was repeated three times, and the average value was taken. The light intensity was set to 1000 μmol·m^{-2}·s^{-1}, and the gas flow rate was 600 μmol·s^{-1}.

2.3. Data Processing. The data obtained were statistically analyzed using Microsoft Excel 2007 software, an OVA was analyzed using DPS software, and the significance test of mean was conducted using Duncan's new complex range method ($P < 0.05$). Origin 7.5 and Adobe Illustrator CS5 were used for illustrations.

3. Results

3.1. Effects of Cd Stress on Antioxidant Enzymes of Rice. Under different Cd concentrations, the activity of antioxidant enzymes (SOD, POD, and CAT) and MDA content in the leaves of the two tested rice varieties at different growth stages are shown in Table 2.

3.1.1. Comparison of Responses between Different Rice Varieties. The results show that the SOD activity of YZX was significantly lower than that of XWX, accounting for 66.7%, and the difference was significant except in the full heading stage Cd-2 and mature stage Cd-3 (accounting for 16.7%). There was no significant difference in POD activity between YZX and XWX at the booting, full heading, and maturity stages in Cd-1 treatment. However, the POD activity of YZX was significantly lower than that of XWX at the tillering stage. Under Cd-2 treatment, the POD activity of XWX was significantly higher than that of YZX at the tillering, full heading, and maturity stages, but there was no significant difference between the POD activity of XWX and YZX at the booting stage. In Cd-3 treatment, the POD activity of XWX was significantly higher than that of YZX in all four growth stages. The comparison of CAT activity showed the same, and the CAT activity in YZX was mostly significantly lower than that of XWX. The MDA content of YZX was significantly higher than that of XWX for most stages and treatments. There was no significant difference in MDA content between the full heading stage in Cd-1 treatment and maturity stage in Cd-2 and Cd-3 treatments.

3.1.2. Comparison of Responses to Different Concentrations of Cd Pollution in Soils. There were significant differences in SOD, POD, and CAT activities between the two rice varieties grown in soils with different Cd concentrations, which also showed similar trends of increasing with the increase in Cd concentration, that is, Cd-3 > Cd-2 > Cd-1. The MDA content was significantly different, though it showed a similar but opposite trend of decreasing with the increase in Cd pollution concentration, that is, Cd-1 > Cd-2 > Cd-3.

3.1.3. Comparison of Responses according to Different Growth Stages. There was no significant difference in SOD activity between the two rice varieties at different growth stages, but the enzyme activity fluctuated significantly between different rice varieties under different soil Cd concentrations. The highest values of SOD activity for Cd-1 and Cd-2 were observed at the booting stage, and the highest values for Cd-3 were at the full heading stage. With prolongation of the growth period, the POD activity showed an obvious decreasing trend, that is, tillering stage > booting stage > full heading stage > maturity stage, but the significance of the difference varied by rice variety and soil Cd concentration. There were significant differences in CAT activity, but the

Table 2: Antioxidant enzymes activity and MDA of two tested rice varieties under Cd pollution treatment at different growth period.

Rice growth period	Soil treatment	YZX				XWX			
		SOD (U/g)	POD (U/g)	CAT (U/g)	MDA (nmol/mg)	SOD (U/g)	POD (U/g)	CAT (U/g)	MDA (nmol/mg)
Tillering stage	Cd-1	1814.3 ± 23.3a(b)*	42.4 ± 5.7a(a)	44.4 ± 9.6a(b)	5.5 ± 0.2a(c)	1825.6 ± 23.2a(c)	47.7 ± 4.3a(a)	64.5 ± 14.6a(c)	5.5 ± 0.2a(d)
	Cd-2	2114.3 ± 10.7a(ab)**	49.5 ± 4.4b(a)	138.7 ± 9.4 b(b)	4.9 ± 0.8ab(c)	2049.3 ± 16.7 b(c)	57.1 ± 5.0a(a)	160.5 ± 10.7a(b)	4.5 ± 0.5ab(b)
	Cd-3	2143.2 ± 11.7 b(c)	60.9 ± 5.7b(a)	162.5 ± 10.4 c(c)	4.3 ± 0.8b(c)	2183.5 ± 11.1c(c)	59.2 ± 4.3b(a)	174.2 ± 11.7b(c)	3.5 ± 0.8b(c)
Booting stage	Cd-1	1822.7 ± 25.2a(a)**	33.7 ± 6.1b(a)	46.1 ± 9.6 a(b)	7.8 ± 0.6a(b)	1917.5 ± 17.4a(a)	40.0 ± 5.4a(ab)	76.8 ± 8.5 a(c)	6.6 ± 0.8a(c)
	Cd-2	2159.2 ± 13.3b(a)	45.6 ± 5.4b(a)	144.0 ± 8.5b(b)	5.6 ± 0.8b(c)	2177.5 ± 14.6b(a)	46.9 ± 6.6a(b)	158.4 ± 10.9a(b)	4.3 ± 0.1b(b)
	Cd-3	2292.4 ± 24.8c(c)**	58.2 ± 6.4a(ab)	165.6 ± 9.6 c(c)*	4.3 ± 0.4b(c)	2375.8 ± 13.8 c(b)	52.4 ± 8.3a(a)	174.5 ± 13.6b(bc)	3.9 ± 0.4b(c)
Full heading stage	Cd-1	1925.5 ± 20.9a(b)**	24.9 ± 5.4a(b)	101.2 ± 9.3a(a)	9.9 ± 0.4a(a)**	2039.8 ± 37.8a(b)	30.1 ± 4.9a(b)	109.0 ± 9.4a(a)	8.6 ± 0.1a(b)
	Cd-2	2087.4 ± 15.3b(bc)	35.8 ± 4.8ab(b)	259.4 ± 9.5b(a)	7.6 ± 0.8b(b)	2088.4 ± 14.4b(b)	40.3 ± 4.9a(b)	267.6 ± 10.8b(a)	7.8 ± 0.6b(a)
	Cd-3	2146.6 ± 18.2 c(a)*	41.4 ± 7.9b(b)	339.4 ± 15.4c(a)	7.3 ± 0.4b(b)*	2218.3 ± 14.1b(a)	45.0 ± 5.1 b(b)	344.7 ± 7.8c(a)	6.6 ± 0.1c(b)
Maturity stage	Cd-1	1873.3 ± 22.6a(b)	22.9 ± 5.6a(b)	68.9 ± 9.9 a(b)**	10.8 ± 0.7a(a)	1881.8 ± 15.8a(d)	26.9 ± 4.5a(b)	87.6 ± 10.7a(b)	10.4 ± 0.5a(a)
	Cd-2	2044.5 ± 25.0b(c)	32.5 ± 5.7ab(b)	152.1 ± 9.5a(b)	9.6 ± 0.5ab(a)	2069.6 ± 20.9b(bc)	39.1 ± 4.4a(b)	154.9 ± 8.3b(b)	8.8 ± 0.7b(a)
	Cd-3	2122.4 ± 23.2c(b)	38.8 ± 6.8b(b)	160.7 ± 9.3b(b)	8.9 ± 0.6b(a)	2106.9 ± 14.0c(b)	43.6 ± 6.4b(b)	195.9 ± 9.4c(b)	8.0 ± 0.1b(a)

Note. The data in the table are mean ± standard error. The difference between different treatments of soil Cd concentration is shown outside the brackets, and the difference between different growth stages is shown inside brackets. *The difference between the two varieties at the 0.05 level, and ** the difference between the two varieties at 0.01 level. SOD, superoxide dismutase; POD, peroxidase (POD); CAT, catalase (CAT); MDA, malondialdehyde.

enzyme activity fluctuated significantly between different soil Cd treatments and varieties, and no obvious trend was found. The variation trend in CAT values for the two tested varieties was consistent in Cd-1 and Cd-2, with the value peaking at the full heading stage and then decreasing. CAT values in Cd-3 showed a gradual upward trend with the extension of the growth period, with the highest value at the maturity stage. The trend of MDA content was opposite to that of POD activity, both of which showed an obvious trend of increasing with the prolongation of growth period, that is, tillering stage < booting stage < full heading stage < maturity stage.

3.2. Changes of Photosynthetic Parameters in Cd Environment. Through data processing, it was found that there were significant differences among the photosynthetic parameters Pn, Gs, Ci, and Tr of leaves according to differing Cd concentration pollution treatments, rice variety, and growth and development stages (Table 3).

3.2.1. Comparison of Photosynthetic Parameters at Different Growth Stages. For Pn, there was a significant effect on Pn between the two varieties. For Gs, there were no obvious trends or significant differences observed. For Ci, after the tillering stage of growth, the effects of both varieties on Ci were consistent. For Tr, in the Cd-1 and Cd-3 treatments, there was a significant difference in the performance of the two varieties in terms of Tr, while there was no significant difference in the Tr of the two varieties in the Cd-2 treatment (Table 3).

3.2.2. Comparison of Photosynthetic Parameters for the Treatment of Different Cd Soils. The Pn and Gs values of the two tested varieties were significantly affected by different Cd soil treatments, and there was an obvious trend in the change. The values for Cd-2 were the highest, while the values for Cd-1 and Cd-3 were lower. In other words, the Pn was higher in Cd-2 than in the other Cd soil treatments at different growth stages, and the Pn of Cd-1 and Cd-3 varied greatly with the change in growth stage. The Ci values differed significantly with different Cd treatments, but the trends were not consistent between YZX and XWX. In most growth periods, the effects of Cd soil treatment on Tr were consistent in both varieties. With the increase in the Cd concentration in soil, all Tr values were increased, i.e., Cd-3 > Cd-2 > Cd-1.

3.2.3. Comparison among Four Growth Stages. Pn variation trend: No significant effect on Pn was found for the tillering stage of both cultivars, but a significant effect on Pn was observed at booting, full heading, and maturity stages. Hence, the Pn value was significantly affected by different growth stages, and there was an obvious trend in the change. Under Cd-1 and Cd-3 treatments, the two varieties showed a gradual decrease in Pn with the extension of the growth period. However, the lowest Pn value was observed for Cd-2 at the booting stage, which then gradually increased, and in each case, the Pn value was higher under Cd-2 than the corresponding Cd-1 and Cd-3 for each growth stage. The variation trend in Gs was as follows: The Gs value gradually decreased with the extension of the growth stage, that is, tillering stage > booting stage > full heading stage > maturity stage. The effects of Cd-1 and Cd-3 on Gs were consistent; there was no significant difference between the tillering and booting stages, but their effects were significantly greater than those of the full heading and mature stages. At Cd-2, the Gs value at tillering stage was significantly higher than that at the other growth stages, and there was no significant difference between the booting and full heading stages, but the value was significantly higher than that at maturity stage. For example, Cd-2 and Cd-3 had the same effect on Gs in XWX, and there was no significant difference among the tillering, booting, and full heading stages, but the effect was significantly greater than that at the maturity stage. At Cd-2, the Gs value at the tillering stage was significantly higher than that at the other growth stages, and there was no significant difference between the booting and full heading stages, but it was significantly higher than that at the maturity stage. Ci variation trend: The Ci value of Cd-1 decreased gradually with the growth period, reaching the lowest value at the full heading stage and then eventually rose again. The Ci values of Cd-2 and Cd-3 decreased gradually with the extension of the growth period. The change trend of Tr was as follows: booting stage > full heading stage > tillering stage > maturity stage. The difference between the two varieties was that the lowest value was different; that is, the lowest value of Cd-1 appeared at the full heading stage, while the lowest value of Cd-2 and Cd-3 appeared at the booting stage.

3.3. Cd Uptake Trend of Two Rice Varieties in Cd-Contaminated Fields. Through data processing, it was found that there were significant differences in Cd content among different Cd concentration pollution treatments, genotypes of rice varieties, and organs (root system, stem sheath, and leaf) at different growth and development stages (Table 4).

3.3.1. Determination of Cd Content in Roots, Stems, Sheaths, and Leaves of Rice. The Cd content in the root system, stem sheath, leaf, and brown rice of YZX was higher than that of XWX (Table 4). The Cd content was significantly affected by different soil concentrations of Cd, and there was an obvious trend in change. The Cd content in the root system, stem sheath, leaf, and brown rice of both YZX and XWX increased with the increase in the Cd concentration in soil, that is, Cd-3 > Cd-2 > Cd-1.

The Cd content in roots, stem sheaths, and leaves was significantly affected by different concentrations of Cd, which increased with the increase in Cd concentration, that is, booting stage > full heading stage > tillering stage > maturity stage.

3.3.2. Determination of Cd Content in Rice Grains. The Cd content in the grains of the two tested varieties increased with the increase in soil Cd concentration (Table 5), that is,

Table 3: Photosynthetic index results of cultivars at different growth stages under Cd pollution treatment.

Rice growth period	Soil treatment	YZX				XWX			
		Pn (μmol·m^{-2}·s^{-1})	Gs (μmol·m^{-2}·s^{-1})	Ci (μmolCO$_2$·mol^{-1})	Tr (mmol·m^{-2}·s^{-1})	Pn (μmol·m^{-2}·s^{-1})	Gs (μmol·m^{-2}·s^{-1})	Ci (μmolCO$_2$·mol^{-1})	Tr (mmol·m^{-2}·s^{-1})
Tillering stage	Cd-1	23.7 ± 0.7b(a)	1.0 ± 0.0a(a)	329.3 ± 2.1a(b)	7.7 ± 0.1c(a)	24.5 ± 0.9ab(a)	1.2 ± 0.1b(a)	333.9 ± 4.3a(a)	8.4 ± 0.3c(a)*
	Cd-2	26.4 ± 0.7a(a)	1.2 ± 0.0a(a)	319.4 ± 2.6b(a)	9.1 ± 0.2b(a)	25.8 ± 0.6a(b)	1.5 ± 0.1a(a)**	325.8 ± 0.8 b(a)*	9.0 ± 0.2b(a)
	Cd-3	24.4 ± 0.6b(a)	1.1 ± 0.1a(a)	322.8 ± 3.0b(a)	10.0 ± 0.2a(a)	23.7 ± 1.2b(a)	1.4 ± 0.1ab(a)	337.1 ± 4.0a(a)**	10.4 ± 0.1a(a)
Booting stage	Cd-1	20.9 ± 0.7b(b)	0.9 ± 0.1a(a)	328.6 ± 0.2a(b)	5.8 ± 0.2a(b)	23.1 ± 0.5a(b)*	0.7 ± 0.2b(b)	322.6 ± 1.4a(b)*	5.5 ± 0.4a(b)
	Cd-2	23.7 ± 0.5a(b)	1.0 ± 0.0a(b)	315.5 ± 5.5b(ab)	6.2 ± 0.6a(c)	23.6 ± 0.1a(c)	1.1 ± 0.0a(b)**	321.7 ± 6.7a(a)	5.6 ± 0.1a(c)
	Cd-3	23.1 ± 0.4a(b)	0.9 ± 0.0a(a)	313.4 ± 2.0b(a)	6.5 ± 0.1a(d)	21.1 ± 0.1b(b)*	1.0 ± 0.1a(b)	319.0 ± 12.6a(ab)	6.0 ± 0.1a(c)**
Full heading stage	Cd-1	19.4 ± 0.1b(c)	0.6 ± 0.0b(b)	325.4 ± 6.2a(b)	4.8 ± 0.2c(c)	21.8 ± 0.1b(c)**	0.6 ± 0.0b(b)*	306.0 ± 5.4a(c)**	4.8 ± 0.2c(c)
	Cd-2	25.7 ± 0.7a(a)	0.9 ± 0.1a(b)	308.8 ± 2.8a(b)	6.6 ± 0.1b(c)	24.0 ± 0.5a(c)	0.8 ± 0.1a(c)	304.0 ± 5.0a(b)	6.7 ± 0.4 b(b)
	Cd-3	17.5 ± 0.9c(c)	0.5 ± 0.2b(b)	302.6 ± 24.4a(a)	7.6 ± 0.5a(c)	19.9 ± 0.7c(b)*	0.6 ± 0.1b(c)	303.5 ± 5.1a(b)	7.7 ± 0.3a(b)
Maturity stage	Cd-1	19.3 ± 0.3b(c)	0.5 ± 0.0a(b)	338.7 ± 1.0a(a)	7.6 ± 0.1c(a)	18.8 ± 0.6b(d)	0.6 ± 0.1a(b)	318.7 ± 1.5a(b)**	8.8 ± 0.1b(a)**
	Cd-2	25.9 ± 0.7a(a)	0.5 ± 0.0a(c)	278.8 ± 6.5b(c)	8.1 ± 0.2b(b)	29.0 ± 0.3a(a)**	0.6 ± 0.1a(d)	278.4 ± 15.8 b(c)	8.9 ± 0.6ab(a)
	Cd-3	14.9 ± 0.3c(d)	0.4 ± 0.1b(b)	298.9 ± 19.0b(a)	9.2 ± 0.4a(b)	19.7 ± 1.1b(b)**	0.5 ± 0.3a(c)	295.2 ± 24.3ab(b)	10.5 ± 1.3a(a)

Note. The data in the table are mean ± standard error. The soil difference of Cd is shown outside the brackets, while the growth period difference is shown inside the brackets. *There was significant difference between the two varieties at the 0.05 level, and ** a significant difference at 0.01 level. Pn (Photo), photosynthesis rate; Gs, stomatal conductance (Gs); Ci, intercellular CO_2 concentration; Tr (Trmmol), transpiration rate.

Table 4: Cd enrichment of rice under different soil Cd concentrations (mg/kg).

Rice growth period	Soil treatment	YZX				XWX			
		Roots	Stems and sheaths	Leaves	Average	Roots	Stems and sheaths	Leaves	Average
Tillering stage	Cd-1	1.03 ± 0.09b(c)[a]	0.27 ± 0.04c(b)[b]	0.07 ± 0.01c(b)[c]	0.45	0.44 ± 0.05c(b)[a]**	0.18 ± 0.05c(ab)[b]	0.04 ± 0.01c(b)[c]*	0.22
	Cd-2	1.29 ± 0.06b(b)[a]	0.72 ± 0.06b(c)[b]	0.25 ± 0.04b(b)[c]	0.75	1.23 ± 0.01b(b)[a]	0.50 ± 0.05b(a)[b]**	0.12 ± 0.02b(a)[c]**	0.62
	Cd-3	2.05 ± 0.22a(c)[a]	1.13 ± 0.27a(b)[b]	0.42 ± 0.01a(b)[c]	1.20	1.74 ± 0.13a(c)[a]	0.75 ± 0.04a(c)[b]	0.23 ± 0.01a(b)[c]**	0.91
	Average	1.46	0.71	0.25	0.80	1.14	0.48	0.13	0.58
Booting stage	Cd-1	1.54 ± 0.06c(a)[a]	0.42 ± 0.05c(a)[b]	0.11 ± 0.02c(a)[c]	0.69	0.55 ± 0.03c(a)[a]**	0.20 ± 0.05c(ab)[b]	0.08 ± 0.01c(a)[c]	0.28
	Cd-2	2.10 ± 0.10b(a)[a]	1.70 ± 0.09b(a)[b]	0.33 ± 0.02b(a)[c]	1.38	1.36 ± 0.06b(a)[a]**	0.56 ± 0.05b(a)[b]**	0.14 ± 0.01b(a)[c]**	0.69
	Cd-3	4.86 ± 0.17a(a)[a]	3.61 ± 0.10a(a)[b]	0.54 ± 0.02a(a)[c]	3.00	4.71 ± 0.20a(a)[a]	1.40 ± 0.05a(a)[b]**	0.37 ± 0.01a(a)[c]**	2.16
	Average	2.83	1.91	0.33	1.69	2.21	0.72	0.20	1.04
Full heading stage	Cd-1	1.21 ± 0.06b(b)[a]	0.37 ± 0.04c(a)[b]	0.06 ± 0.01c(b)[c]	0.55	0.28 ± 0.07c(c)[a]**	0.10 ± 0.04b(b)[b]**	0.04 ± 0.01b(b)[b]	0.14
	Cd-2	1.26 ± 0.06b(b)[a]	0.91 ± 0.06b(b)[b]	0.19 ± 0.02b(c)[c]	0.79	1.15 ± 0.02b(c)[a]*	0.20 ± 0.05b(b)[b]**	0.06 ± 0.01b(b)[c]**	0.47
	Cd-3	2.98 ± 0.19a(b)[a]	1.12 ± 0.05a(b)[b]	0.39 ± 0.02a(b)[c]	1.50	2.21 ± 0.19a(b)[a]**	1.00 ± 0.08a(b)[b]	0.22 ± 0.01a(b)[c]**	1.14
	Average	1.82	0.80	0.21	0.94	1.22	0.43	0.11	0.58
Maturity stage	Cd-1	0.16 ± 0.03c(d)[a]	0.06 ± 0.01c(c)[b]	0.04 ± 0.01c(b)[b]	0.08	0.12 ± 0.03b(d)[a]	0.05 ± 0.02c(b)[b]	0.03 ± 0.01b(b)[b]	0.07
	Cd-2	0.77 ± 0.06b(c)[a]	0.35 ± 0.06 b(d)[b]	0.14 ± 0.01b(d)[c]	0.42	0.76 ± 0.04a(d)[a]	0.18 ± 0.05b(b)[b]*	0.05 ± 0.01b(b)[c]**	0.33
	Cd-3	2.03 ± 0.22a(c)[a]	0.62 ± 0.07a(c)[b]	0.32 ± 0.01a(c)[c]	0.99	0.99 ± 0.22a(d)[a]**	0.37 ± 0.05a(d)[b]**	0.18 ± 0.01a(c)[b]**	0.51
	Average	0.99	0.34	0.17	0.50	0.62	0.20	0.09	0.30

Note. The data in the table are mean ± standard error. Outside the brackets are the differences between different Cd treatments in the soil, inside the brackets are the differences between different growth stages, [] is the differences between different organs in rice. *There was significant difference between the two varieties at the 0.05 level, and ** a significant difference at 0.01 level.

Table 5: Cd content in grain under soil treatment with different Cd concentrations.

Rice organs	Soil treatment	Cd content (mg/kg)	
		YZX	XWX
Grain	Cd-1	0.02 ± 0.00c	0.01 ± 0.00b
	Cd-2	0.04 ± 0.01b	0.02 ± 0.00b**
	Cd-3	0.12 ± 0.00a	0.10 ± 0.01a*
	Average	0.06	0.04

Note. Different letters indicated significant differences among soil Cd treatments. *The differences among varieties at the level of 0.05, and **a significant difference at 0.01 level.

Cd-1 < Cd-2 < Cd-3 (Figure 1), and there were significant differences between YZX and XWX under three different soil Cd concentrations. Under the Cd concentration of each soil, the Cd content in the grains of YZX was higher than that of XWX but was lower than 0.2 mg/kg in all cases; that is, they did not exceed the threshold value for Cd content in food set by the National Food Safety Standard for Limits of Pollutants in Food [22].

Under the same soil Cd concentration, the Cd content in the grains of YZX was higher than that of XWX, and there was a significant difference. The average values of Cd in the three soils were 0.06 and 0.04 mg/kg, respectively. Comparatively, the low Cd accumulation in XWX in terms of the Cd content in rice grains is favorable to that of YZX. Therefore, the higher the initial Cd content in soil, the higher the Cd content in rice grains.

4. Discussion

4.1. Effects of Cd Pollution on Antioxidant Enzyme Indices of Rice

4.1.1. SOD Activity. The SOD activities in leaves for YZX and XWX differed according to variety, Cd concentration, and treatment time. The SOD activity of XWX was significantly higher than that of YZX (66.7%), which indicates that the capacity of XWX to respond to Cd stress is higher than that of YZX. In each growth period, the SOD activity increased with the increase in Cd concentration, and the differences among different Cd treatments were significant and consistent in trend.

With the increase in the soil Cd concentration, the SOD activity of rice leaves firstly increased and then decreased; that is, the key growth period of rice leaves was the reproductive growth period, and the SOD activity was more sensitive to Cd at this time. These results indicated that the protective system of antioxidant enzymes was activated when the concentration of Cd in the environment reached a certain threshold. The change pattern of the enzyme showed an initial increase followed by a decrease, which indicates that the enzyme has a greater potential to allow tolerance of Cd stress, which is consistent with the research results on the entire regeneration forests [23].

4.1.2. POD Activity. POD is an important antioxidant enzyme in plants that can degrade H_2O_2 in plants and allow them to avoid damage [24]. In this experiment, with the increase in the Cd pollution concentration, the changes in POD and SOD activities of YZX and XWX were consistent in trend. This is mainly due to the fact that in the life course of rice, the enzymes of the antioxidant system are affected by external factors, such as heavy metal Cd and the internal metabolic process of plant aging [25].

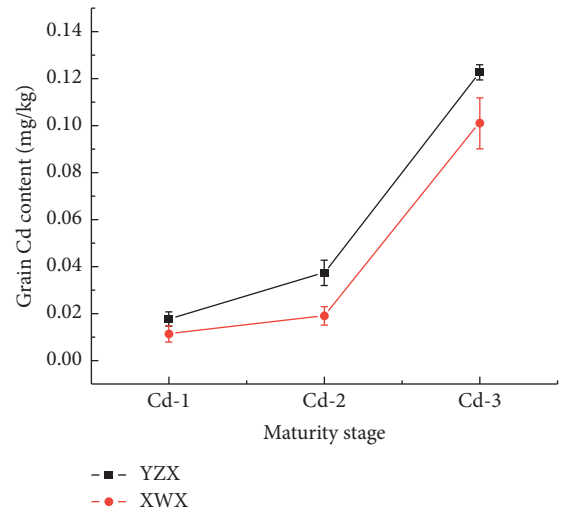

Figure 1: Variation trend of Cd content in seeds at maturity stage.

Both varieties tested POD vigor, as the extension of the growth period showed a significantly smaller tendency, namely, the tillering stage > booting stage > full panicle stage of maturity; POD plays a clearly defined free radical role in rice, and the effect of POD activity decreased with the decrease in the mean antioxidant protection ability; this may be due to the level of Cd stress under the condition of active oxygen free radicals. In other words, the capacity of the enzyme to handle Cd stress was reached.

4.1.3. CAT Activity. When plants are stressed by heavy metals, CAT activity increases, indicating that CAT can enhance plant resistance [26]. In this experiment, the CAT activity of XWX was higher than that of YZX, and the situation was similar regarding POD activity. With the increase in Cd pollution concentration, CAT activity increased, which is consistent with previous research results [27].

The CAT activity of YZX and XWX showed a significant difference at different growth stages under the same soil Cd concentration, and the biggest decrease was observed at the full heading stage, indicating that Cd stress had a great influence on the CAT activity of YZX and XWX under the conditions tested in this experiment. The two varieties showed an increasing trend with the growth period of the two cultivars, and there were significant differences among the growth periods. This indicates that Cd stress changes greatly as the aging of the plant affects their metabolism. With the extension of the growth period, the adaptability of rice to Cd is enhanced, the antioxidant protection ability is enhanced, and the difference in CAT activity is gradually reduced.

4.1.4. MDA Content. MDA can change the fluidity and permeability of the cell membrane, and its content can reflect the degree of damage to the plant membrane system and indicate the ability of the plant to resist stress [28]. In this experiment, the MDA content of YZX and XWX increased with the increase in soil Cd concentration and the prolongation of treatment time (i.e., growth process). The accumulation of MDA indicated that rice was experiencing stress due to H_2O_2, $O^{2-}\cdot$, OH·, and other reactive oxygen radicals, which cause the peroxidation of rice leaf cell membranes [29].

It can be seen from the above results that the growth of rice is affected under soil Cd pollution, and the trend is consistent between the varieties. The MDA content in rice leaves increases significantly, and with the increase in soil Cd concentration, the increase in MDA becomes more obvious [30]. Hence, in response to the increase in soil Cd concentration in this experiment, the activities of SOD, POD, and CAT showed a gradual upward trend, while the MDA concentration showed an opposite or downward trend [31]. There were significant differences in the activities of antioxidant enzymes in different rice varieties under the same and different soil Cd concentrations. It was found that the activities of SOD, POD, and CAT decreased with the increase in Cd concentration in soil.

4.2. Effects of Cd Stress on Photosynthetic Parameters of Rice

4.2.1. Comparison of Photosynthetic Parameters between Varieties. The Pn, Gs, Ci, and Tr of XWX were higher than those of YZX, and the Pn, Gs, and Ci decreased gradually with the prolongation of the growth period; only Tr was the lowest at the full heading stage and then eventually rose again. The results of this experiment showed that between the two rice varieties with different Cd tolerance, XWX had a lower variation range of photosynthetic parameters than YZX. Comparatively, XWX had a stronger tolerance to Cd in the soil than YZX [32], which could protect itself from environmental damage.

4.2.2. Comparison of Photosynthetic Parameters with Different Cd Concentrations. The Pn, Gs, Ci, and Tr of different varieties were highest in Cd-2, followed by Cd-3, and the lowest in Cd-1, that is, Cd-2 > Cd-3 > Cd-1. In addition, Pn, Gs, and Ci decreased gradually with the prolongation of the growth period, and Tr was the lowest at the full heading stage and then eventually rose again.

Previous studies have shown that Cd stress in rice seedlings leads to decreased photosynthetic parameters (such as photosynthetic rate, transpiration rate, and stomatal conductance) in leaves. The Tr of rice photosynthesis is negatively correlated to Cd concentration, i.e., the higher the Cd concentration, the lower the Tr [33]. In this experiment, the Pn and Gs of YZX and XWX had a promoting effect on the photosynthesis of rice plants under the low-concentration treatment. When the Cd concentration increases to a certain threshold, the photosynthetic rate peaks and then gradually declines [34]. The change trends were the same for both varieties. The Tr value of XWX was higher than that of YZX, but the difference was not significant, indicating that for XWX in a certain period, the transpiration of water per unit leaf area was slightly higher than that of YZX, so as to cope with the damage caused by Cd pollution to the plants. Throughout the entire rice growth period, Pn and Gs present a decreasing trend with increases in the soil Cd concentration, and the research results of Chen [35] and also of Xiao [36], which show that stomatal openness affects the efficiency of gas exchange, support our results in the rice heading stage. In contrast to Pn and Gs, Ci first decreased and then increased, which was different from the results of Wang et al. [37] and James [38] that indicated the rise and fall of Pn were caused by nonstomatal restriction. This may be due to the restriction of RuBP carboxylation, photosynthetic activity, and inorganic phosphorus, which hinders CO_2 utilization [39]; this is consistent with the research results of Zhang et al. [40]. In general, there was a positive correlation among Pn, Gs, and Tr and a negative correlation with Ci. At the same time, the high concentration of Cd inhibited Pn and Gs, both of which decreased simultaneously, while Ci and Tr increased, indicating that nonstomatal limiting factors led to a decrease in Tr.

4.2.3. Trend in the Variation of Photosynthetic Parameters among Different Growth Stages. The four indexes of Pn, Gs, Ci, and Tr of both varieties showed the following values in four growth stages: tillering stage > booting stage > full heading stage > maturity stage. Both Pn and Gs showed that Cd-2 was higher than Cd-1 and Cd-3, presenting a "pyramid" trend. Ci decreased with the increase in soil Cd concentration, while Tr and Ci showed the opposite trend; that is, they increased with the increase in soil Cd concentration.

4.3. Cd Uptake by Two Rice Varieties in Cd-Contaminated Rice Fields

4.3.1. Comparison of Cd Accumulation between Two Rice Varieties. Studies [41] have shown that, under the same Cd stress, different rice varieties have different performances in Cd absorption, accumulation, and distribution in paddy soil due to interspecific (different species and genera) and intraspecific (different varieties or varieties) differences. For the same growth period of the same rice organs under the same Cd soil concentration, most of the experimental treatments showed that the Cd content of YZX was significantly higher than that of XWX; only a small number of experimental treatments showed no significant difference between the two varieties, namely, only the organs (root, stem sheath, and leaf) of Cd-1 at the maturity stage. There was no significant difference in the Cd content in the roots of rice varieties at the Cd-2 tillering and Cd-3 booting stages (a total of five treatments, accounting for 13.89% of the total treatments), but the Cd content in YZX was significantly higher than that in XWX. Relatively, YZX absorbs Cd more easily than XWX.

4.3.2. Comparison of Cd Accumulation under Three Cd Concentration Gradients. The Cd content of rice increased significantly with the increase in the soil Cd concentration for the same growth period and the same rice variety in the same rice organ. Taking the tillering stage as an example, the root Cd content of Cd-3 was (2.05 mg/kg) > Cd-2 (1.29 mg/kg) > Cd-1 (1.03 mg/kg), and the Cd content of Cd-3 was significantly higher than that of Cd-1 and Cd-2, but there was no significant difference between Cd-1 and Cd-2. When reaching the booting stage, the root Cd content of Cd-3 was (4.86 mg/kg) > Cd-2 (2.10 mg/kg) > Cd-1 (1.54 mg/kg), and there were significant differences among different treatments. Therefore, the higher the original Cd content in the soil, the more the Cd absorbed by rice.

4.3.3. Change Trend in Cd Accumulation among Different Growth Periods. The accumulation of Cd differs greatly depending on the growth stages of rice. Zhao et al. [42] examined the whole growth period and found that the Cd uptake trend of different organs of different varieties was inconsistent at each growth period. The Cd content in the roots, stems, and leaves of rice at the booting stage was significantly higher than that at the other growth stages, while the Cd content in various organs of rice at other growth stages fluctuated. The average Cd content of three kinds of soil at different growth stages was as follows: booting stage (1.69 mg/kg) > full heading stage (0.94 mg/kg) > tillering stage (0.80 mg/kg) > maturity stage (0.50 mg/kg); in XWX, booting stage (1.04 mg/kg) > full heading stage (0.58 mg/kg) = tillering stage (0.58 mg/kg) > maturity stage (0.30 mg/kg). Therefore, the booting stage is the key stage in rice, where Cd absorption is highest. However, fluctuation was observed in both the root and leaf, and no obvious trend was found. In XWX, there was no correlation with the growth stage, but the highest Cd content was found in all organs at the booting stage (average value was 1.05 mg/kg). Peng et al. [43] used hydroponic experiments to add exogenous Cd at different growth stages of rice, and the results showed that Cd exposure at the booting and heading stages contributed significantly to Cd accumulation in rice. Under the condition of high Cd, Tang et al. [44] found that the biomass of rice with high Cd accumulation increased gradually with the extension of the growth period, and there was a positive correlation between Cd accumulation in shoots of rice with high Cd accumulation and the whole plant, and the Cd accumulation rate in the shoots and the whole plant reached the maximum at the filling stage.

4.3.4. Analysis of Cd Accumulation in Different Rice Organs. As the most important nutrient-acquiring organ, the rice root absorbs and accumulates minerals and other nutrient elements while introducing Cd into the system. Its ability to introduce Cd into the system depends on the Cd content in the environment and the transport efficiency of metal ion channels in the root system [45–48]. Ju et al. [49] found that nutrient elements in roots, stems, and leaves enter grains via the cob, and the final Cd content in grains is determined by the Cd concentration in the cob, which is highly positively correlated [50]. In this experiment, the Cd content in the roots of rice was significantly higher than that in stems, sheaths, and leaves under the same soil Cd concentration for the same variety and growth period. The Cd content of the stem sheath was significantly higher than that of the leaf in most experimental treatments. Taking the tillering stage as an example, the average Cd contents in different organs of three soils under the Cd concentration were as follows: root (1.46 mg/kg), stem sheath (0.71 mg/kg), and leaf (0.25 mg/kg). Therefore, the root system of rice is the most important organ to absorb Cd. The Cd content in all organs of the rice plant is highest in the root system, followed by the stem and sheath leaves, and the least in the grain, that is, root > stem and sheath > leaf > grain, which is consistent with the previous research results of screening varieties or breeding intermediate materials with low Cd absorption or low accumulation in the grain by artificially adding Cd [51–54]. The Cd content of YZX was higher than that of XWX but was lower than 0.2 mg/kg in all cases and does not exceed the levels specified in the safety standard for Cd intake in food.

5. Conclusions

The activity of SOD, POD, and CAT of XWX was higher than that of YZX, but the content of MDA was the opposite. SOD, POD, and CAT all increased with the increase in Cd concentration, while the MDA content decreased in the three contaminated soils with different Cd concentrations. Through the comparative analysis of photosynthetic physiology, it was found that the low-Cd-accumulating rice, XWX, was more tolerant to Cd in the Cd-polluted soil, while the high-Cd-accumulating rice, YZX, was more sensitive. The Cd absorption trend of the two tested varieties was consistent: the booting stage is the key stage of Cd absorption of all four growth stages, in which Cd levels peak. Under different soil Cd concentrations, the Cd content in all organs of rice plants increased with the increase in soil Cd concentrations. The trend in Cd content for all organs is that the farther away they are from the root, the lower the Cd content.

Data Availability

The data supporting these results are available from the corresponding author upon request.

Conflicts of Interest

The authors declare that they have no conflicts of interest.

Acknowledgments

This research was financially supported by the National Natural Science Foundation of China (No. 41907032), the Science and Technology Support Project of Guizhou Province (Nos. 2018.2295 and 2019.2305), and the Key Scientific and Technological Special Project of Changsha City in China (No. kq200602019.230526).

References

[1] W. X. Chen, Q. Li, Z. Wang, and Z. J. Sun, "Spatial distribution characteristics and pollution evaluation of heavy metals in arable Land soil of China," *Environmental Sciences*, vol. 41, no. 6, pp. 2822–2833, 2020.

[2] Ministry of Environmental Protection and Ministry of Land and Resources, "National soil pollution survey bulletin," 2014, http://www.gov.cn/foot/site1/20140417/782bcb88840814ba158d01.pdf.

[3] D.-F. Huang, L. L. Xi, L. N. Yang, Z. Q. Wang, and J. C. Yang, "Comparisons in agronomic and physiological traits of rice genotypes differing in cadmium-tolerance," *Acta Agronomica Sinica*, vol. 34, no. 5, pp. 809–817, 2008.

[4] J. Guo, Y. Yao, X. X. Zhao, J. P. Liu, and T. Wang, "Pollution status of lead and cadmium ions in grain and its harm to human," *Grain science and technology and economy*, vol. 43, no. 3, pp. 33–35, 2018.

[5] G. Arindam, C. Palak, and W. Wolfram, "Metabolomics in plant stress physiology," *Plant Genetics and Molecular Biology*, vol. 164, pp. 187–236, 2018.

[6] X. R. Shen, M. Y. Dong, C. Y. Wang, J. Wang, and Q. Zhou, "Effects of high manganese stress on the mineral element absorption and photosynthetic system of vetiver grass," *Journal of Agro-Environment Science*, vol. 38, no. 10, pp. 2297–2305, 2019.

[7] S. Y. Yang, X. Y. Chen, W. K. Hui, Y. Ren, and L. Ma, "Progress in responses of antioxidant enzyme systems in plant to environmental stresses," *Journal of Fujian Agriculture and Forestry University (Natural Science Edition)*, vol. 45, no. 5, pp. 481–489, 2016.

[8] S. Chen, Q. Wang, H. Lu et al., "Phenolic metabolism and related heavy metal tolerance mechanism in Kandelia Obovata under Cd and Zn stress," *Ecotoxicology and Environmental Safety*, vol. 169, pp. 134–143, 2019.

[9] C. G. Sanbon, L. Yaniv, and M. Menachem, "Quantitative and comparative analysis of whole-plant performance for functional physiological traits phenotyping: new tools to support pre-breeding and plant stress physiology studies," *Plant Science*, vol. 282, pp. 49–59, 2019.

[10] Y. Z. Zhang, B. H. Fang, Z. N. Teng, G. H. Chen, and Y. Liu, "Screening and verification of rice varieties with low cadmium accumulation," *Agricultural Science and Technology*, vol. 20, no. 3, pp. 1–10, 2019.

[11] Ministry of Environmental Protection of the People's Republic of China, *Soil Quality-Determination of Lead, Cadmium-Graphite Atomic Absorption Spectrophotometry*, China Standards Press, Beijing, China, 1997.

[12] General Administration of Quality Supervision, Inspection and Quarantine of the People's Republic of China, *Soil Quality-Analysis of Available Lead and Cadmium Contents in Soils-Atmic Absorption spectrometry*, China Standards Press, Beijing, China, 2009.

[13] Ministry of Environmental Protection of the People's Republic of China, *Soil Quality-Determination of Total Nitrogen-Modified Kjeldahl method*, China Standards Press, Beijing, China, 2015.

[14] Sichuan Provincial Bureau of Quality and Technical Supervision, *Soil-Determination of Alkali-Hydrolyzable nitrogen*, Sichuan Standards Press, Chengdu, China, 2015.

[15] The Ministry of Agriculture of the People's Republic of China, *Method for Determination of Soil Total phosphorus*, China Standards Press, Beijing, China, 1988.

[16] The Ministry of Agriculture of the People's Republic of China, *Soil Testing-Part 7: Method for Determination of Available Phosphorus in Soil*, China Standards Press, Beijing, China, 2014.

[17] The Ministry of Agriculture of the People's Republic of China, *Method for Determination of Total Potassium in soils*, China Standards Press, Beijing, China, 1988.

[18] The Ministry of Agriculture of the People's Republic of China, *Determination of Exchangeable Potassium and Non-exchangeable Potassium Content in soil*, China Standards Press, Beijing, China, 2004.

[19] The Ministry of Agriculture of the People's Republic of China, *Soil Testing Part 2: Method for Determination of Soil pH*, China Standards Press, Beijing, China, 2006.

[20] The Ministry of Agriculture of the People's Republic of China, *Soil Testing Part 6: Method for Determination of Soil Organic matter*, China Standards Press, Beijing, China, 2006.

[21] L. Sun, X. Xu, Y. Jiang et al., "Genetic diversity, rather than cultivar type, determines relative grain Cd accumulation in hybrid rice," *Frontiers of Plant Science*, vol. 7, p. 1407, 2016.

[22] National Health and Family Planning Commission of the People's Republic of China and National Food and Drug Administration of the People's Republic of China, *Food Safety National Standard Limits of Contaminants in food*, China Standards Press, Beijing, China, 2017.

[23] Q. L. Dai, *Ariety differences of Zea mays in response to cadmium(Cd) or lead(Pb) stress and mechanisms*, Ph.D. thesis, Sun Yat-sen University, Guangzhou, China, 2005.

[24] X. L. Jiang, Z. X. Li, and Z. S. Kang, "The recent progress of research on peroxidase in plant disease resistance," *Journal of Northwest Forestry University*, vol. 6, pp. 124–129, 2001.

[25] F. M. Yu, K. H. Liu, H. Liu, H. Deng, and Z. M. Zhou, "Antioxidative responses to cadmium stress in the leaves of Oryza saliva L. in different growth period," *Ecology and Environmental Sciences*, vol. 21, no. 1, pp. 88–93, 2012.

[26] Z. Y. Chen, X. Y. Fei, F. Sun, and X. Y. Cui, "Effects of saline-alkali stress on activities and gene expression of antioxidant enzymes of transgenic *Lc-CDPK* rice," *Journal of Northwest Forestry University*, vol. 47, no. 5, pp. 15–22, 2019.

[27] A. Z. Yang, S. M. Duan, W. G. Wu, and G. Chen, "Effects of drought stress at booting stage on physiological index and yield of super rice," *Molecular Plant Breeding*, vol. 15, no. 2, pp. 685–691, 2017.

[28] X. H. Song, "The effect of Cd sang Cd+ high temperature stress to the growth and the antioxidant system of the double antioxidase transgenic rice," Master's thesis, Shandong Normal University, Jinan, China, 2008.

[29] F. Liu, C. Qu, Y. Wang, and G. H. Chen, "Effects of drought rewatering at heading stage on antioxidant enzyme activity and root activity of machine-transplanted rice," *Journal of Southern Agriculture*, vol. 51, no. 1, pp. 65–71, 2020.

[30] J. D. Chen, *Research on difference and mechanism of rice response under cadmium stress and regulation*, Ph.D. thesis, Yangzhou Nuiversity, Yangzhou, China, 2013.

[31] T. Z. Li, A. T. Chen, C. Li, D. Yang, and N. He, "Effects of silicon on growth and physiological responses of rice seedlings under cadmium stress," *Journal of Agro-Environment Science*, vol. 37, no. 6, pp. 1072–1078, 2018.

[32] Z. N. Teng, B. H. Fang, Y. Liu, Y. He, and J. Yang, "Effects of Cd on photosynthesis of different rice varieties," *Chinese Journal of Agrometeorology*, vol. 37, pp. 538–544, 2016.

[33] F. Gao, Y.-J. Lin, J.-L. Zhang et al., "Effects of cadmium stresses on physiological characteristics, pod yield, and seed

quality of peanut," *Acta Agronomica Sinica*, vol. 37, no. 12, pp. 2269–2276, 2012.

[34] Y. L. Sun, H. M. Liu, and Q. G. Xu, "Effect of cadmium stress on photosynthetic characteristics and physiological and biochemical traits during seedling stage of different rice cultivars," *Acte Agriculturae Boreali-Simica*, vol. 32, pp. 176–181, 2017.

[35] Y. W. Chen, "The study of the infect of photosynthetic characteristics and the absorption of related nutritents of rice materials and hybrids under cadumium stress," Master's thesis, Agricultural University of Sichuan, Chengdu, China, 2011.

[36] Q. T. Xiao, "Physiogical response in rice (Oryza sative L.) under cadmium stress conditions," Master's thesis, Fujian Agriculture and Forestry University, Fuzhou, China, 2011.

[37] H. Wang, S. Yan, H. Xin et al., "A subsidiary cell-localized glucose transporter promotes stomatal conductance and photosynthesis," *The Plant Cell*, vol. 31, no. 6, pp. 1328–1343, 2019.

[38] A. B. James, "Effects of pulses of elevated carbon dioxide concentration on stomatal conductance and photosynthesis in wheat and rice," *Physiologia Plantarum*, vol. 149, no. 2, pp. 214–221, 2013.

[39] C. Z. Li, Y. L. Sun, H. M. Liu, and Q. G. Xu, "The difference of seedling growth and photosynthetic performance of different rice varieties under cadmium stress," *Journal of Hunan Agricultural University*, vol. 47, no. 2, pp. 147–152, 2021.

[40] X. Y. Zhang, Y. Cao, J. Meng, G. C. Zhou, and H. N. Zhang, "Effects of biochar on growth and photosynthetic yield of rice under cadmium environment," *Jiangsu Agricultural Sciences*, vol. 44, no. 5, pp. 97–101, 2016.

[41] C. G. Yang, X. Y. Liao, X. F. Zhang, Z. W. Zhu, and M. X. Chen, "Genotypic difference in cadmium accumulation in Brown rice," *Chinese Journal of Rice Science*, vol. 20, pp. 660–662, 2006.

[42] J. L. Zhao, S. H. Zhang, T. F. Yang, J. F. Dong, and Q. Liu, "Phenotype evaluation of Cd accumulation of 181 diverse indica germplasm at seedling and mature stages," *Molecular Plant Breeding*, vol. 16, no. 18, pp. 6080–6087, 2018.

[43] O. Peng, B. Q. Tie, C. C. Ye, M. Zhang, and X. L. Liu, "The key period of cadmium accumulation in rice," *Journal of Agricultural and Resource Economics*, vol. 34, no. 3, pp. 272–279, 2017.

[44] H. Tang, T. X. Li, X. Z. Zhang, H. Y. Yu, and G. D. Chen, "Cadmium accumulation in high cadmium-accumulating rice cultivars at different growth stages," *Journal of Agriculture and Environment Science*, vol. 34, no. 3, pp. 471–477, 2015.

[45] F. F. Nocito, C. Lancilli, B. Dendena, G. Lucchini, and G. A. Sacchi, "Cadmium retention in rice roots is influenced by cadmium availability, chelation and translocation," *Plant, Cell and Environment*, vol. 34, no. 6, pp. 994–1008, 2011.

[46] S. Akimasa, N. Yamaji, K. Yokosho, and J. F. Ma, "Nramp5 is a major transporter responsible for manganese and cadmium uptake in rice," *The Plant Cell Online*, vol. 24, no. 5, pp. 2155–2167, 2012.

[47] Z. W. Zhu, C. X. Chen, R. X. Mou, Z. Y. Cao, and W. X. Zhang, "Advances in research of cadmium metabolism and control in rice plants," *Scientia Agricultura Sinica*, vol. 47, no. 18, pp. 3633–3640, 2014.

[48] G. Deng, G. Wang, M. F. Sun, and J. W. Peng, "Accumulation and distribution of Cadmium in different rice varieties under cadmium stress," *Journal of Zhejiang Agricultural Sciences*, vol. 57, no. 4, pp. 468–471, 2016.

[49] X. H. Ju, C. B. Zhang, Z. G. Song, L. N. Han, and Z. Y. Lu, "Changes in cadmium accumulation in rice organs during grain development and their relationship with genotype and cadmium levels in soil," *Plant Physiology Journal*, vol. 50, no. 5, pp. 634–640, 2014.

[50] Q. L. Cai, D. S. Lin, G. Wang, and D. Wang, "Differences in cadmium accumulation and transfer capacity among different types of rice cultivars," *Journal of Agriculture and Environment Science*, vol. 35, no. 6, pp. 1028–1033, 2016.

[51] Y. H. Chen, J. G. Li, T. Yang, J. Xie, and L. G. Wei, "Research on accumulation characteristic and correlation of cadmium in various rice varieties," *Acta Agriculturae Jiangxi*, vol. 29, no. 9, pp. 10–14, 2017.

[52] X. L. Long, X. C. Xiang, Y. F. Xu, W. L. Su, and C. F. Liao, "Absorption, transfer and distribution of Cd in indica and japonica rice under Cd stres," *Chinese Journal of Rice Science*, vol. 28, no. 2, pp. 177–184, 2014.

[53] J. Liu, M. Qian, G. Cai, J. Yang, and Q. Zhu, "Uptake and translocation of Cd in different rice cultivars and the relation with Cd accumulation in rice grain," *Journal of Hazardous Materials*, vol. 143, no. 1-2, pp. 443–447, 2007.

[54] X. D. Hu, "Effects of soil cadmium pollution and p H on cadmium accumulation in different rice varieties," Master's thesis, Agricultural University of Hunan, Changsha, China, 2018.

Hindawi
Journal of Chemistry
Volume 2021, Article ID 1416925, 12 pages
https://doi.org/10.1155/2021/1416925

Research Article

Physiological Responses and Proteomic Analysis on the Cold Stress Responses of Annual Pitaya (*Hylocereus* spp.) Branches

Junliang Zhou, Lijuan Wang, Tujian Xiao, Zhuang Wang, Yongya Mao, and Yuhua Ma

Guizhou Fruit Institute, Guizhou Academy of Agricultural Sciences, Guiyang 550006, China

Correspondence should be addressed to Yuhua Ma; m_yh79@163.com

Received 17 October 2021; Revised 28 October 2021; Accepted 30 October 2021; Published 22 November 2021

Academic Editor: Wenneng Wu

In this study, the physiological response of the annual branches of three varieties of pitaya (Xianmi, Fulong, and Zihonglong) in cold stress was investigated using a multivariate statistical method. Physiological change results showed that cold stress could decrease the moisture and chlorophyll contents, on the contrary, increase the relative electric conductivity, the contents of malonadehyde, soluble protein, soluble sugar, and free proline, and enhance the enzyme activities of peroxidase, superoxide dismutase, and catalase. Meanwhile, a comparative proteomic approach was also conducted to clarify the cold resistance-related proteins and pathways in annual pitaya branches. Proteomics results concluded that the cold tolerance of annual pitaya branches could be improved by modulating autophagy. Therefore, we hypothesized that an increased autophagy ability may be an important characteristic of the annual pitaya branches in response to cold stress conditions. Our results provide a good understanding of the physiological responses and molecular mechanisms of the annual pitaya branches in response to cold stress.

1. Introduction

Pitaya (*Hylocereus* spp.), a member of the family Cactaceae, is a perennial climbing cactus plant which is rich in anthocyanins, betanin, and plant albumin [1, 2]. Because of the ability of pitaya to resist prolonged drought, it is considered to have a high potential for agricultural development, especially in the drought areas [3, 4]. Therefore, pitaya has been a thriving fruit and large-scale commercial cultivation in the karst regions of southwest China, such as Guangxi, Yunnan, and Guizhou provinces, which are frequently exposed to severe drought stress. However, low temperature is also found to be the most important environmental factor which can limit the development of pitaya production [5]. Literature has reported that most pitaya cultivars can tolerate 0°C, which may lead the pitaya fruits and its young buds, shoots, and even some mature branches to death [6]. The lower the temperature with the longer the duration, the more serious the effect on the pitaya yield and quality [7].

Meanwhile, literature has reported that cold stress (classified as chilling (0 to 15°C) or freezing (<0°C) stress) can affect agricultural production [8]. When exposed to low temperature, to adapt to the cold stress, plants require physiological response and cold resistance to survive, which is known as 'cold acclimation' [9]. In the past few years, significant progress in many plants, such as pitaya fruit [7], cassava [10, 11], alfalfa [12], petunia seedlings [13], castor seeds [14], rice [15], and grape [16], has been made in understanding the molecular mechanisms under cold stress.

In recent years, literatures reported that the moisture content, chlorophyll content, relative electric conductivity (REC), malonadehyde (MDA) content, soluble sugar content, soluble protein content, free proline content, catalase (CAT) activity, peroxidase (POD) activity, and superoxide dismutase (SOD) activity can be used as the indices to identify the cold resistance [11, 17–21]. Different pitaya varieties have different adaptabilities to the cold resistance, and the cold resistance among different pitaya varieties could be determined by the multi-index comprehensive evaluation [22]. Meanwhile, in the past few years, the comparative proteomic approach has been become a promising tool that is crucial for plants' stress response

[23–27]. However, to date, our understanding of cold stress mechanisms in pitaya branch is limited.

In this study, the annual branches of three varieties of pitaya (Xianmi (XM), Fulong (FL), and Zihonglong (ZHL)) were selected, and a multivariate statistical method and a comparative proteomic approach were used to investigate the tolerance to cold stress of the annual pitaya branches.

2. Materials and Methods

2.1. Plant Material, Growth Condition, and Cold Treatments. The annual branches of three varieties of pitaya (XM, FL, and ZHL) with basically the same cultivation management measures and similar growth potential (approximately 50 cm length and 10 cm width without fruits and flowers) were selected from the pitaya demonstration garden of Luodian experimental station of Guizhou Fruit Institute in Dec. 2020. The branches are required to be complete and smooth, with no obvious disease spots on the surface and no obvious mechanical injury or freezing damage. The annual branches of three varieties of pitayas were transferred to a chamber for pretreatment for 1 day at 25°C. After that, the temperature of the chamber was dropped to 0°C with the gradient of 5 °C/h for cold treatment with light/dark cycles of 16/8 h. The annual branches were exposed to 0°C for 0, 1, 3, 5, and 7 days, respectively, and then frozen at −80°C. The branches in the chamber maintained at 25°C for 7 days were used as negative controls (CK).

2.2. Physiological Response Analyses. To analyze the physiological responses of the annual pitaya branches under cold stress, the REC, the contents of moisture, chlorophyll, MDA, soluble protein, soluble sugar, and free proline, and the enzyme activities of POD, SOD, and CAT were measured in this study.

2.2.1. Moisture Content Determination. The moisture contents of the annual branches of the three varieties of pitayas were determined according to AOAC official method 934.06 and calculated using formula (1).

$$\text{Moisture content } (\%) = \frac{(m_a - m_b)}{m_a} \times 100. \quad (1)$$

In this formula, m_a and m_b are the qualities of samples before and after drying at 70°C, respectively [28].

2.2.2. Chlorophyll Content Determination. The chlorophyll contents of the annual branches of the three varieties of pitaya were determined by a reported method with some modifications [29]. Each test sample (50 mg) was placed in a 5 mL precooling mixture solution with 85% acetone and 85% ethanol (v/v = 1/1) to be homogenized and incubated in a chamber for 0.5 h at 25°C. Then, the supernatant was obtained by centrifuging at 6,500 g for 15 min. The OD_{663} and OD_{645} values of the supernatant were monitored by using a Multiskan Sky 1530 microplate reader (Thermo Scientific, Poland). The contents of chlorophyll a (C_a), chlorophyll b (C_b), and total chlorophyll (C_t) were calculated using the following equations:

$$C_a\,(\text{mg/L}) = 0.0127\text{OD}_{663} - 0.00269\text{OD}_{645}, \quad (2)$$

$$C_b\,(\text{mg/L}) = 0.0229\text{OD}_{645} - 0.00468\text{OD}_{663}, \quad (3)$$

$$C_t\,(\text{mg/L}) = C_a + C_b. \quad (4)$$

2.2.3. REC Determination. The REC was determined according to Wang's method [30]. Each test sample (2 g) was placed in 30 mL distilled water at room temperature for 3 h to determine the value of electrical conductivity (EC_1). After that, the test sample was boiled for about 20 min and then quenched to room temperature to determine the EC_2 value. EC_0 value was the electrical conductivity value of the distilled water. REC was calculated using the following equation:

$$\text{REC}\,(\%) = \frac{(\text{EC}_1 - \text{EC}_0)}{(\text{EC}_2 - \text{EC}_0)} \times 100. \quad (5)$$

2.2.4. Determination of the Contents of Soluble Protein, Soluble Sugar, Free Proline, and MDA. The soluble sugar contents were identified according to Solarbio kits (Solarbio, Beijing, China). Coomassie brilliant blue G250 was used to measure the content of soluble protein [31]. The contents of free proline and MDA were measured using the proline and MDA content determination kits (Nanjing Jiancheng Bioengineering Institute, Nanjing, China).

2.2.5. Determination of the Enzyme Activities of CAT, SOD, and POD. The enzyme activities of CAT, SOD, and POD were measured with the corresponding enzyme assay reagent kits (Suzhou Comin Bioengineering Institute, Suzhou, China).

2.2.6. Fuzzy Synthetic Evaluation. The cold resistance abilities of the annual branches of the three varieties of pitaya were evaluated using the fuzzy mathematics method [32]. The positive subordinate function values, such as REC, the contents of MDA, soluble protein, soluble sugar, and free proline, and the activities of SOD, POD, and CAT, were calculated as equation (6); meanwhile, the negative subordinate function values, such as moisture and chlorophyll contents, were calculated as equation (7):

$$f(X_{ij}) = \frac{(X_{ij} - X_{\min})}{(X_{\max} - X_{\min})}, \quad (6)$$

$$f(X_{ij}) = 1 - \frac{(X_{ij} - X_{\min})}{(X_{\max} - X_{\min})}, \quad (7)$$

where $f(X_{ij})$ is the value of the i pitaya variety of the j item, X_{ij} is the value of the i pitaya variety of the j item, and $X_{\max}$ and $X_{\min}$ are the maximum and minimum values of the j item, respectively.

2.3. Recovery Growth of Annual Pitaya Branches after Cold Treatment. In order to investigate the recovery growth of the annual pitaya branches after cold treatment at 0°C for 7 days, we transplanted the precooling treated annual pitaya branches into the greenhouse with the temperature increased from 0 to 25°C by 5°C/h, light/dark cycles of 16/8 h, and 90% relative humidity. The survival rate and germination rate were counted after 60 days.

2.4. Proteomics Analysis

2.4.1. Protein Extraction and LC-MS/MS Analysis. The annual branches of the three varieties of pitaya, preexposed to 0°C for 7 days, were used as the test samples for proteomics analysis. In each experiment, about 1.5 g fine powder samples were suspended in a 10 mL precooling acetone solution containing 0.15% trichloroacetic acid, 10% polyvinylpyrrolidone, and 0.07% β-mercaptoethanol. The solution was stored at −20°C overnight and centrifuged at 8,000 g and 4°C for 30 min. The precipitate was washed using 10 mL precooled acetone three times and then dissolved in 5 mL of precooled protein extraction buffer (40 mM dithiothreitol, 0.1 M KCl, 0.7 M sucrose, 50 mM EDTA, and 0.5 M Tris-HCl (pH 7.5)). The protein solution was collected by centrifugation at 12,000 g and 4°C for 15 min. The polypeptide, digested to polypeptide with trypsin at 37°C overnight, was dissolved in 50 μL of HPLC-grade H_2O containing 0.1% formic acid and detected using an AB SCIEX Triple TOF 5600 mass spectrometer (Foster City, CA, USA). The parameters of MS were set according to the manufacturer's recommendations.

2.4.2. Sequence Database Searching and Bioinformatics Analysis. MS/MS spectra (Wiff. files) were analyzed and quantified using the MaxQuant software and searched against the *Cactaceae* proteome by the reported methods [33, 34]. The raw data were uploaded in iPorX (http://www.iprox.org) with the accession number of IPX0001296003. The differentially expressed proteins (DEPs) (the expression level > 2-fold and p value < 0.01) at the Gene Ontology (GO) term, named cellular components (CC), biological processes (BP), and molecular function (MF), were calculated. Then, the pathway enrichment of DEPs was identified from the Kyoto Encyclopedia of Genes and Genomes (KEGG) database.

2.5. Statistical Analysis. GraphPad Prism 5 software (GraphPad Software, Inc., San Diego, CA, USA) was used to analyze the significant difference at $p < 0.05$.

3. Results and Discussion

3.1. Physiological Changes with Cold Treatment. Low temperature can affect the growth and development of many plants, especially originating from tropical and subtropical origins. Due to the time and region of domestication, different varieties of pitaya have different cold resistance. Therefore, in this study, the annual branches of the three varieties of pitaya were selected and the physiological responses on the cold resistance abilities of annual pitaya branches were investigated. The dynamic changes results of moisture and chlorophyll contents in cold stress are listed in Figure 1. Figure 1 shows that compared with the control group (0 day), the moisture content (Figure 1(a)) and chlorophyll content (Figure 1(b)) of the annual branches of the three varieties of pitaya have a tendency to decrease from 1 to 7 days under the cold treatment. In the previous study, the relationship between plant moisture content and cold resistance under low temperature was studied, and the results revealed that the cold resistance was positively correlated with the moisture content [35]. In this study, we found that the cold resistance could decrease the moisture content in annual pitaya branches which are in accord with the previous report [35]. Meanwhile, previous studies showed that the chlorophyll content, which is closely related to photosynthesis, has been proved to be an effective parameter for evaluating plant cold resistance [36–39]. In this study, our results showed that cold stress could significantly decrease the chlorophyll contents in the annual branches of the three varieties of pitaya, which are in accord with the previous reports [40, 41].

Compared with the control group (0 day), the REC (Figure 2(a)) and MDA content (Figure 2(b)) of the annual pitaya branches were increased under cold stress from 0 to 7 days. Overall, with the time extension of cold treatment from 0 to 7 days, the REC and MDA contents of ZHL were consistently lower than those of FL and XM. REC, which was used to research the cytoplasmic membrane damage, is a physiological parameter for evaluating plant cold resistance [42, 43]. In the previous study, Wang et al. [44] and Li et al. [45] found that the REC of corn seedling and tea leaf could increase under cold stress. In our study, we found that the REC of the annual pitaya branches increases under cold stress, proving that cold stress can increase the membrane permeability of the annual pitaya branches. MDA, an important physiological and biochemical index, can reduce the content of antioxidants to inhibit the activity of cell protective enzymes and accelerate the process of membrane lipid peroxidation [46]. Yin et al. [47] found that the low-temperature stress had a little effect on the content of MDA in cassava in the early period, but with the extension of stress time, large amounts of MDA were accumulated due to severe peroxidation of membrane lipids. Therefore, determination of MDA content and its dynamics in a plant can reflect the strength of cold resistance of the plant to low-temperature stress. This study results demonstrated that cold stress can increase the MDA content in annual pitaya branches. Similar results were also obtained in the previous studies about cassava [48], maize [49], peach [50], pineapple [51], tomato [52], and rapeseed [53].

Compared with the control group (0 day), the contents of soluble protein (Figure 3(a)), soluble sugar (Figure 3(b)), and free proline (Figure 3(c)) of the annual pitaya branches were enhanced with the extension of the cold stress time from 0 to 7 days. Soluble protein can increase the water content in the cell to reduce the cold injury [54]. In the present study, we demonstrated that the soluble protein

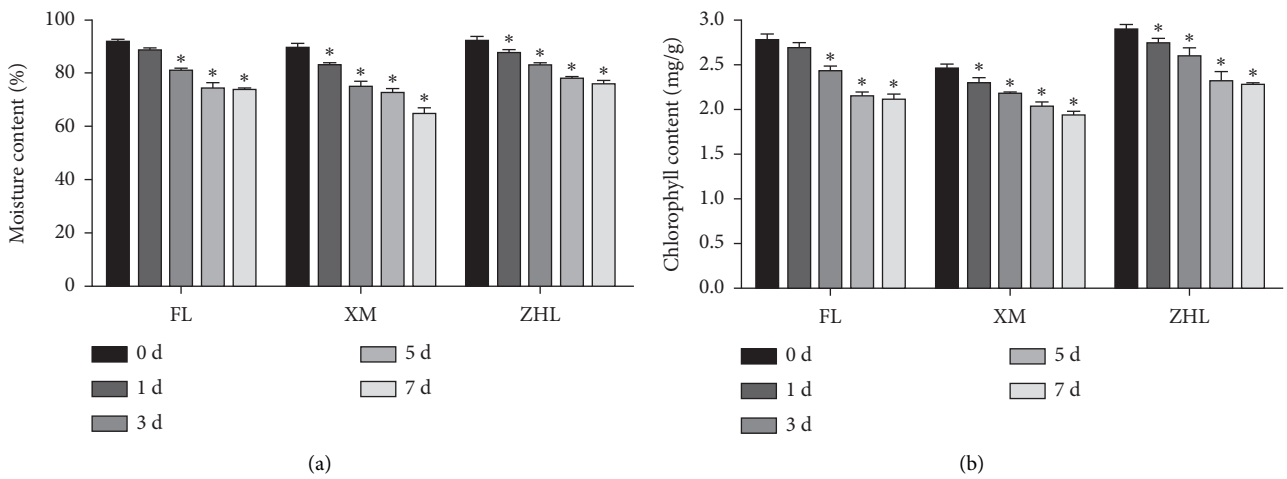

Figure 1: The changes of moisture content (a) and chlorophyll content (b) of the annual branches of the three varieties of pitaya with cold treatment. "∗" indicates the changes of moisture content and chlorophyll content with a significant difference at $p < 0.05$ compared with the control group.

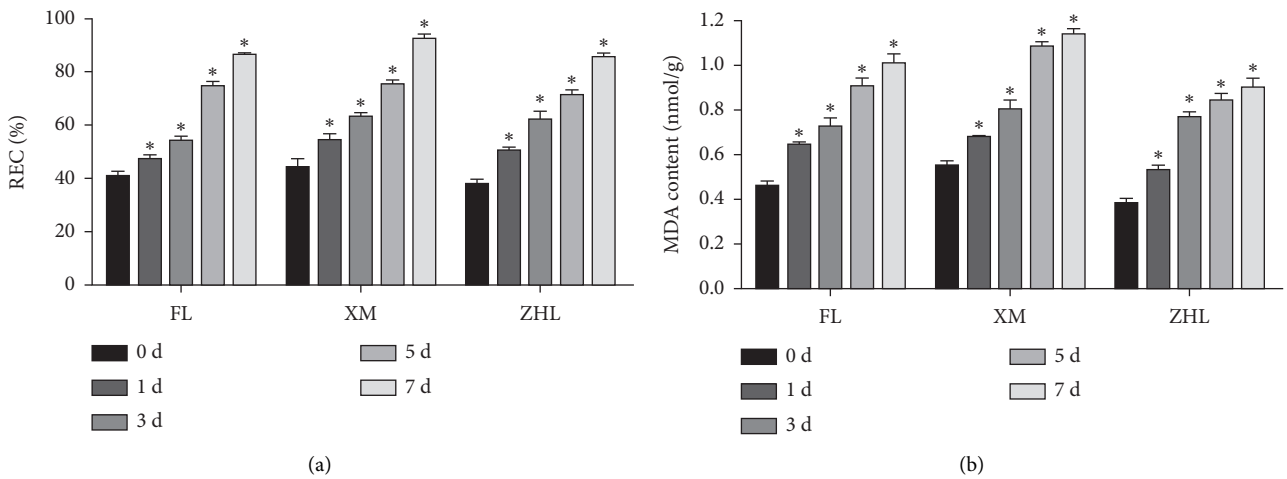

Figure 2: The changes of REC (a) and MDA content (b) of the annual branches of the three varieties of pitaya with cold treatment. "∗" indicates the changes of moisture content and chlorophyll content with a significant difference at $p < 0.05$ compared with the control group.

content and cold resistance revealed a positive correlation, and similar results were also obtained by Wallis et al. [55]. Meanwhile, soluble sugar is an important osmotic substance in plant cells, and it can increase the content of intracellular solute. The increase of soluble sugar content is beneficial to the increase of osmotic pressure, thus enhancing the water retention ability of plant cells [55]. This study showed that the soluble sugar content in annual pitaya branches could increase to again be conducive to cold stress.

With the extension time of cold treatment from 0 to 7 days, the antioxidant enzyme activities, including SOD, POD, and CAT, exhibited an increasing trend under cold stress (Figure 4). In the rise trend, the SOD, POD, and CAT activities of ZHL were consistently higher than those of FL and XM. Antioxidant enzymes had an important role in protecting the membrane system for maintaining the normal physiological activities of plants [56]. SOD is a key factor in eliminating reactive oxygen species (ROS) to decrease the ability to minimize oxidative damage under cold stress [57]. Meanwhile, POD can induce the salicylic acid (SA) pathway to promote cell-wall reinforcement, thus activating the systemic acquired resistance (SAR) to cold stress [58, 59]. In addition, CAT can protect plant cells from oxidative damage under cold stress by catalyzing H_2O_2 to decompose to water and oxygen [60]. Therefore, our results demonstrated that cold stress may improve cold resistance of plants in the form of antioxidant enzymes.

The cold resistance abilities of the annual branches of the three varieties of pitaya were evaluated using the fuzzy mathematics method, and the results are shown in Table 1. The higher cold resistance abilities have higher value of synthetic evaluation values [61]. Table 1 shows that the synthetic evaluations of cold resistance indicator of the annual branches of XM, FL, and FHL were 0.495, 0.515, and 0.545, respectively, demonstrating that the cold resistance abilities of the annual branches of the three varieties of pitaya were ranked in the order of ZHL > FL > XM.

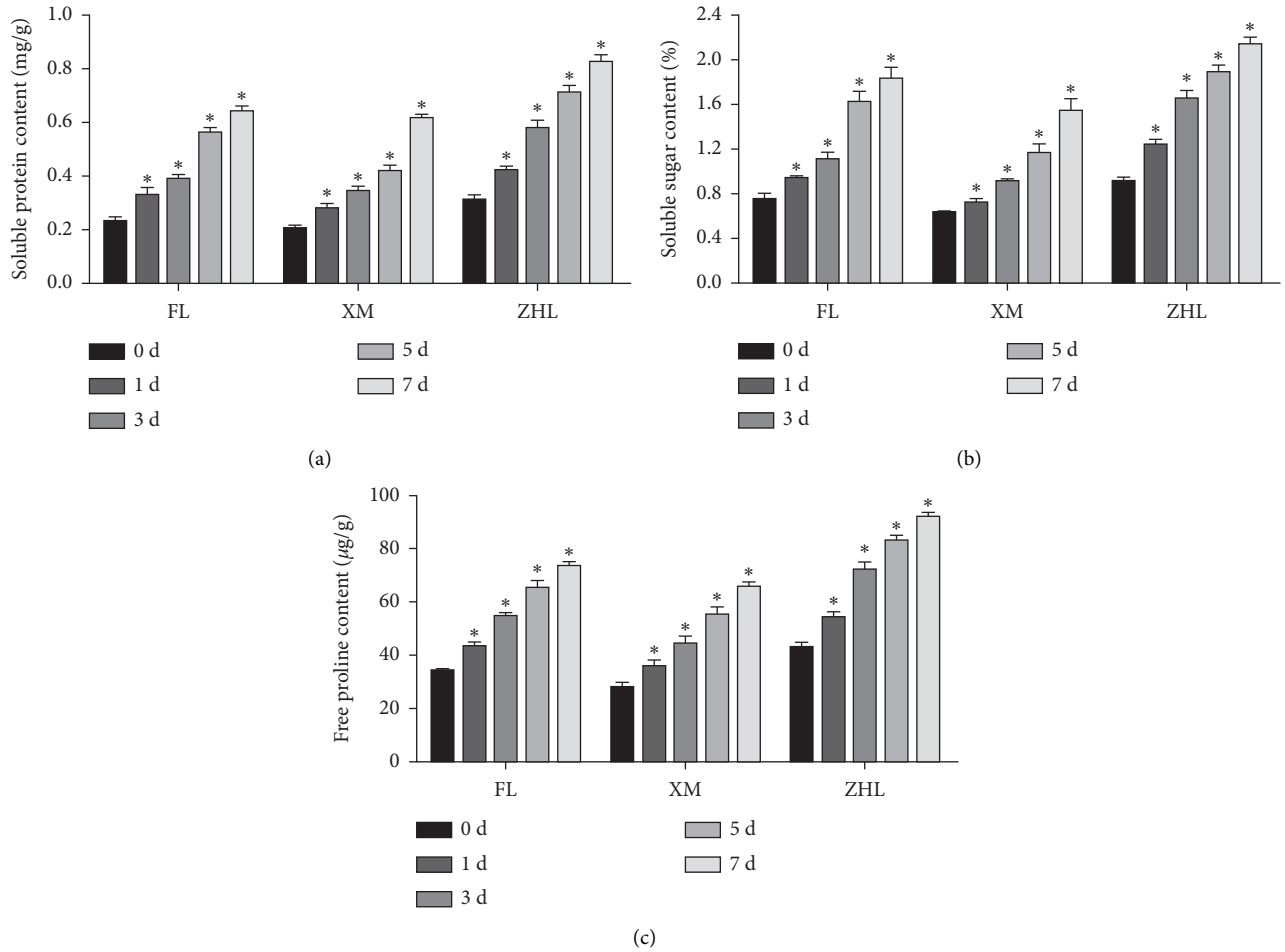

Figure 3: The changes of soluble protein content (a), soluble sugar content (b), and free proline content (c) of the annual branches of three varieties of pitaya with cold treatment. "$*$" indicates the changes of soluble protein content, soluble sugar content, and free proline content with a significant difference at $p < 0.05$ compared with the control group.

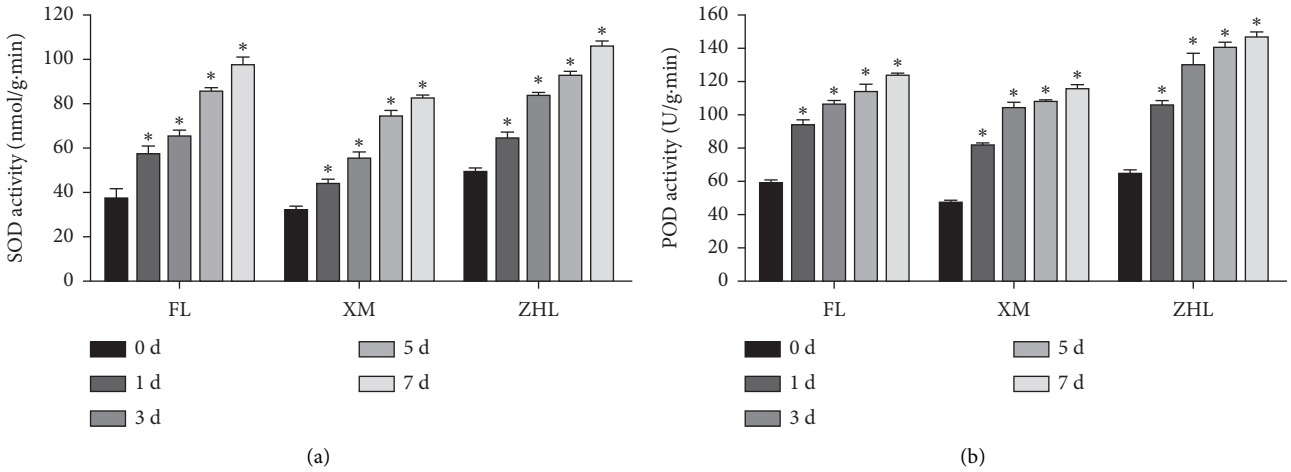

Figure 4: Continued.

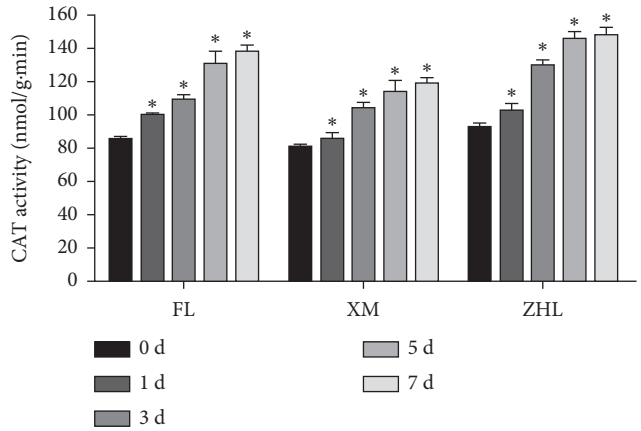

(c)

Figure 4: The changes of enzyme activities of SOD (a), POD (b), and CAT (c) of the annual branches of the three varieties of pitaya with cold treatment. "∗" indicates the enzyme activity changes of SOD, POD, and CAT with a significant difference at $p < 0.05$ compared with the control group.

3.2. Recovery Growth of Annual Pitaya Branches after Cold Treatment. After 60 days of recovery growth, the results, as shown in Table 2, showed that ZHL had the best survival rate (45.25%) and germination rate (39.16%), followed by FL (35.16% and 31.58%, respectively) and XM (26.62% and 21.49%, respectively), showing that the cold resistance abilities of the annual branches of the three varieties of pitaya were in the order of ZHL > FL > XM.

3.3. Label-Free Proteomics Analysis. The proteomics technique was used to analyze the cold stress responses of the annual branches of the three varieties of pitaya. A total of 2798 proteins were identified in the annual branches of the three varieties of pitaya, and the results are listed in Table S1, of which 1900, 2099, and 2023 proteins were identified in the annual branches of ZHL, FL, and XM, respectively. Meanwhile, the box plot (Figure 5(a)) and normal distribution (Figure 5(b)) of the protein expression of the three varieties of pitaya indicated that compared with FL and XM, ZHL had the highest protein expression abundance.

As shown in Figure 6(a) and Table S1, the numbers of identified proteins of ZHL vs. XM showing up- and downregulation were 699 and 450, respectively. Figure 6(b) and Table S1 show that the up- and downregulated proteins of ZHL vs. FL were 494 and 784, respectively. Figure 6(c) and Table S1 also show that the up- and downregulated proteins of FL vs. XM were 492 and 390, respectively. Meanwhile, to clarify the cold resistance ability-related proteins in the annual branches of the three varieties of pitaya, the numbers of in turn up- (mode = 1) and downregulated (mode = −1) expression proteins were also investigated, and the results are listed in Figure 7 and Table S2. As shown in Figure 7 and Table S2, the numbers of in turn up- and downregulated expression proteins in XM, FL, and ZHL were 479 and 261, respectively.

The functions of the in turn up- and downregulated expression proteins were annotated by GO analysis and further classified into the categories of MF, CC, and BP. GO term enrichment analysis of the in turn up- and downregulated expression proteins revealed that main CC involved ribosome (GO:0005840), cytoplasm (GO:0005737), membrane (GO: 0016020), mitochondrion (GO:0005739), and chloroplast (GO: 0009507); main BP involved translation (GO:0006412), carbohydrate metabolism (GO:0005975), small-molecule metabolism (GO:0044281), response to stress (GO:0006950), and transport (GO:0006810); and main MF involved structural molecule activity (GO:0005198), lyase activity (GO:0016829), rRNA binding (GO:0019843), oxidoreductase activity (GO: 0016491), and ligase activity (GO:0016874). Meanwhile, KEGG analysis results, shown in Table S3, showed that the in turn up- and downregulated expression proteins identified in XM, FL, and ZHL were mainly related to autophagy (path:ko04138), carbon fixation pathways in prokaryotes (path:ko00720), fluid shear stress and atherosclerosis (path:ko05418), Epstein–Barr virus infection (path:ko05169), and biosynthesis of amino acids (path:ko01230). It is worth noting that the pathway with the highest enrichment was autophagy (path:ko04138). Autophagy, a major process of protein degradation, can recycle nutrient contents to remove the damaged proteins when exposed to the environmental stress conditions [62, 63]. Recent studies had divulged that autophagy is extremely important in environmental stress and plant development [64–69]. Therefore, our results demonstrated that autophagy may play a key role in response to cold stress in annual pitaya branches, and we concluded that the pitaya branches could be improve tolerance to cold stress by modulating autophagy to clean up the damaged cellular structures caused by cold stress conditions for recycling of nutrients.

Table 1: Synthetic evaluation of the cold resistance indicator of the annual branches of the three varieties of pitaya.

Pitaya variety	Subordinate function value[a]										
	Moisture content	Chlorophyll content	REC	MDA content	Soluble protein content	Soluble sugar content	Free proline content	SOD activity	POD activity	CAT activity	Synthetic evaluation[a]
XM	0.508 ± 0.05	0.532 ± 0.08	0.451 ± 0.11	0.510 ± 0.04	0.470 ± 0.05	0.408 ± 0.01	0.399 ± 0.02	0.521 ± 0.07	0.507 ± 0.16	0.646 ± 0.01	0.495 ± 0.04 A
FL	0.548 ± 0.04	0.520 ± 0.10	0.435 ± 0.04	0.526 ± 0.01	0.510 ± 0.11	0.485 ± 0.02	0.462 ± 0.02	0.519 ± 0.09	0.520 ± 0.05	0.625 ± 0.01	0.515 ± 0.08B
ZHL	0.542 ± 0.02	0.534 ± 0.62	0.493 ± 0.14	0.585 ± 0.02	0.528 ± 0.06	0.501 ± 0.04	0.532 ± 0.03	0.564 ± 0.04	0.528 ± 0.04	0.645 ± 0.03	0.545 ± 0.10 C

[a]Experiments were repeated three times. Different uppercase letters indicate the values of synthetic evaluation with a significant difference among different pitaya varieties at $p < 0.05$.

Table 2: The survival rate and germination rate of the annual branches of the three varieties of pitaya.

Pitaya varieties	Survival rate (%)[a]	Germination rate (%)[a]
ZHL	45.25 ± 3.65 A	39.16 ± 2.65 A
FL	35.16 ± 2.95B	31.58 ± 4.16B
XM	26.62 ± 5.26 C	21.49 ± 1.98 C

[a]Experiments were repeated three times. Different uppercase letters indicate the values of survival rate and germination rate with a significant difference among different pitaya varieties at $p < 0.05$.

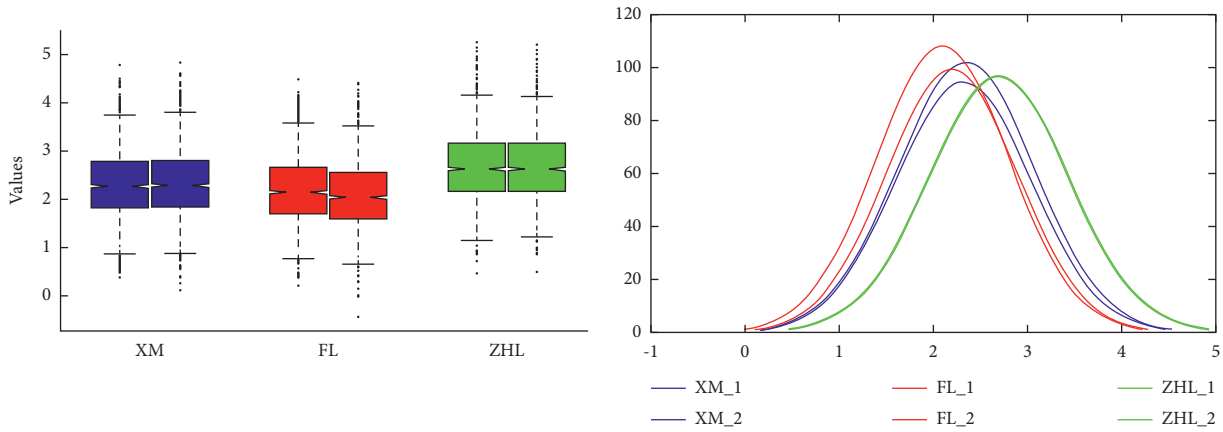

(a) (b)

Figure 5: The box plot (a) and normal distribution (b) of the protein expression of the annual branches of the three varieties of pitaya.

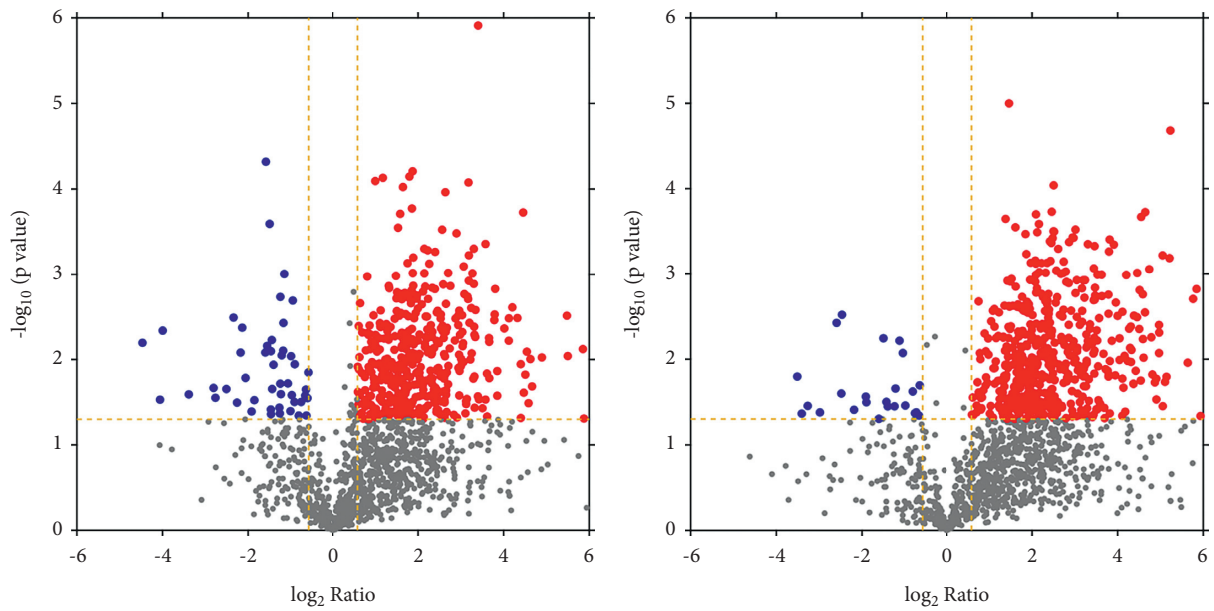

(a) (b)

Figure 6: Continued.

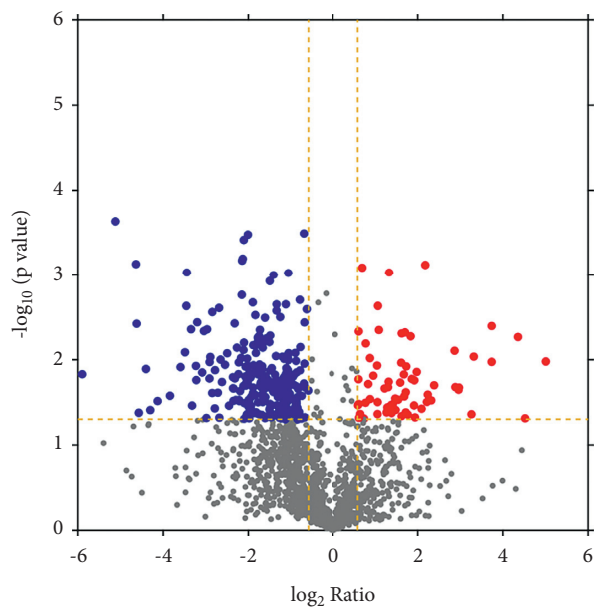

Figure 6: Volcano plot of the relative protein abundance changes in the annual branches of the three varieties of pitaya. (a) ZHL vs. XM, (b) ZHL vs. FL, and (c) FL vs. XM. The green and red dots are the up- and downregulated DEPs, respectively.

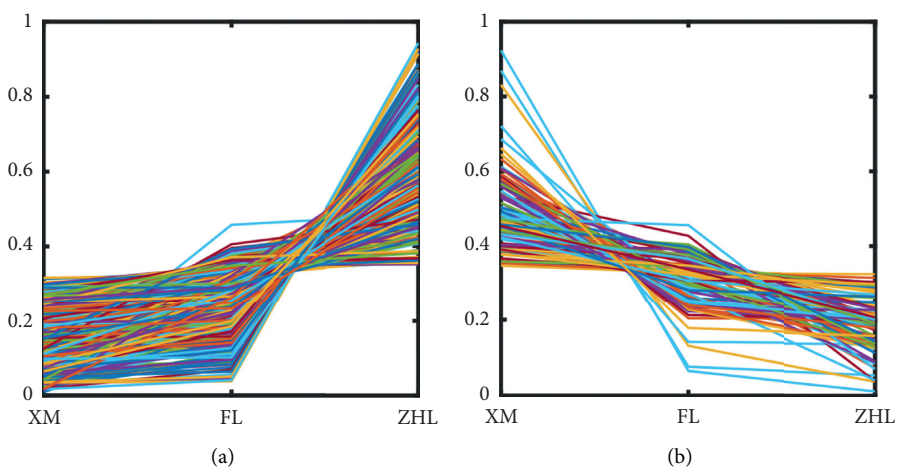

Figure 7: The in turn up- (a) and downregulated (b) expression proteins in the annual branches of the three varieties of pitaya.

4. Conclusions

In conclusion, the physiological and proteome dynamic changes in the annual branches of the three varieties of pitaya were investigated using a multivariate statistical method and a comparative proteomic approach, respectively. Physiological response results showed that the contents of moisture and chlorophyll decreased, in contrast with the REC and the contents of MDA, soluble protein, soluble sugar, and free proline increased, and the enzyme activities of SOD, POD, and CAT enhanced in annual pitaya branches under cold stress. Meanwhile, proteomic analysis results concluded that the pitaya branches could improve tolerance to cold stress by modulating autophagy. In addition, the physiological and proteome dynamic changes results demonstrated that the cold resistance of the annual branches of the three varieties of pitaya should be in the order of FHL > FL > XM which are in accord with the cold resistance ability in agricultural production under the natural environment condition. Our results provide a better understanding of how the annual pitaya branches respond and survive under low temperatures.

Data Availability

The datasets used and analyzed during the current study are available from the corresponding author on reasonable request.

Conflicts of Interest

The authors declare no conflicts of interest.

Authors' Contributions

Junliang Zhou and Lijuan Wang contributed equally to this work.

Acknowledgments

This research was funded by the National Natural Science Foundation of China, grant no. 31560547; Guizhou Provincial Talent Base Project, grant no. [2018]3, and Special Funds for Innovation Capacity Building of Research Institutions, grant no. [2019]4002.

Supplementary Materials

Table S1: list of identified proteins in the annual branches of XM, FL, and FHL; Table S2: the in turn up- and downregulated expression proteins in the annual branches of XM, FL, and FHL; Table S3: the KEGG analysis results of the in turn up- and downregulated expression proteins in the annual branches of XM, FL, and FHL. (*Supplementary Materials*)

References

[1] K. Mahattanatawee, J. A. Manthey, G. Luzio, S. T. Talcott, K. Goodner, and E. A. Baldwin, "Total antioxidant activity and fiber content of select Florida-grown tropical fruits," *Journal of Agricultural and Food Chemistry*, vol. 54, no. 19, pp. 7355–7363, 2006.

[2] N. Sengkhamparn, N. Chanshotikul, C. Assawajitpukdee, and T. Khamjae, "Effects of blanching and drying on fiber rich powder from pitaya (Hylocereus undatus) peel," *International Food Research Journal*, vol. 20, no. 4, pp. 1595–1600, 2013.

[3] B. Rodriguez-Jimenez, J. Dominguez-Ortega, A. Ledesma, B. Cava-Sumner, and C. Kindelan-Recarte, "Generalized urticaria due to yellow pitahaya (Selenicereus megalanthus)," *Journal of Investigational Allergology and Clinical Immunology*, vol. 24, no. 2, pp. 124-125, 2014.

[4] G. Jiménez, G. Gómez, A. M. Pérez, and A. Blanco-Metzler, "Estimation of glycaemic index of peach palm (Bactris gasipaes) cooked fruits and chips, and pitahaya (Hylocereus spp.) pulp," *Archivos Latinoamericanos de Nutricion*, vol. 62, no. 3, pp. 242–248, 2012.

[5] R. J. Deng, J. X. Fan, Y. Q. Wang, J. F. Jin, and T. Liu, "Semilethal temperature of Pitaya under low temperature stress and evaluation on their cold resistance," *Plant Physiology Journal*, vol. 50, no. 11, pp. 1742–1748, 2014.

[6] R. J. Deng, J. X. Fan, B. Wang, and Y. Q. Cai, "Preliminary study on determination of chilling-resistance in pitaya (Hylocereus spp.)," *Plant Physiology Communications*, vol. 45, no. 10, pp. 1023–1026, 2009.

[7] J. Corrales-García and E. Canche-Canche, "Physical and physiological changes in low-temperature-stored pitahaya fruit (Hylocereus undatus)," *Journal of the Professional Association for Cactus Development*, vol. 10, pp. 108–119, 2008.

[8] R.-j. Feng, L.-l. Zhang, J.-y. Wang et al., "Proteomic analysis of cold stress responses in banana leaves," *Journal of the American Society for Horticultural Science*, vol. 140, no. 3, pp. 214–222, 2015.

[9] M. F. Thomashow, "Plant cold acclimation: freezing tolerance genes and regulatory mechanisms," *Annual Review of Plant Physiology and Plant Molecular Biology*, vol. 50, no. 1, pp. 571–599, 1999.

[10] W. Zhang, T. Yi, Y. Wu, and Y. Song, "Research progress of cold resistance mechanism of cassava," *Agricultural Science & Technology*, vol. 18, no. 9, pp. 1607–1614, 2017.

[11] F. An, G. Li, Q. X. Li et al., "The comparatively proteomic analysis in response to cold stress in cassava plantlets," *Plant Molecular Biology Reporter*, vol. 34, no. 6, pp. 1095–1110, 2016.

[12] J. Chen, G. Han, C. Shang et al., "Proteomic analyses reveal differences in cold acclimation mechanisms in freezing-tolerant and freezing-sensitive cultivars of alfalfa," *Frontiers of Plant Science*, vol. 6, p. 105, 2015.

[13] W. Zhang, H. Zhang, L. Ning, B. Li, and M. Bao, "Quantitative proteomic analysis provides novel insights into cold stress responses in petunia seedlings," *Frontiers of Plant Science*, vol. 7, p. 136, 2016.

[14] X. Wang, M. Li, X. M. Liu, L. Zhang, Q. Duan, and J. Zhang, "Quantitative proteomic analysis of castor (Ricinus communis L.) seeds during early imbibition provided novel insights into cold stress response," *International Journal of Molecular Sciences*, vol. 20, no. 2, p. 355, 2019.

[15] K. A. Neilson, M. Mariani, and P. A. Haynes, "Quantitative proteomic analysis of cold-responsive proteins in rice," *Proteomics*, vol. 11, no. 9, pp. 1696–1706, 2011.

[16] Z. M. Wu, X. Z. Yuan, H. Li et al., "Heat acclimation reduces postharvest loss of table grapes during cold storage – analysis of possible mechanisms involved through a proteomic approach," *Postharvest Biology and Technology*, vol. 105, pp. 26–33, 2015.

[17] G. Wang, J. Wang, X. Xue, L. U. Chao, and P. Nie, "Research progress and identification method of apple stress resistance," *Agricultural Science & Technology*, vol. 18, no. 10, pp. 1413–1416, 2013.

[18] B. Q. Zhang, L. T. Yang, and Y. R. Li, "Physiological and biochemical characteristics related to cold resistance in sugarcane," *Sugar Tech*, vol. 17, pp. 49–58, 2015.

[19] X. Li, J. P. Wei, E. R. Scott et al., "Exogenous melatonin alleviates cold stress by promoting antioxidant defense and redox homeostasis in Camellia sinensis L," *Molecules*, vol. 23, no. 1, p. 165, 2018.

[20] X. F. Zhang, W. Shen, and S. Gurunathan, "Biologically synthesized gold nanoparticles ameliorate cold and heat stress-induced oxidative stress in *Escherichia coli*," *Molecules*, vol. 21, no. 6, p. 731, 2016.

[21] Y. Z. Yang, G. Chen, F. R. Peng et al., "Differences in water and osmoregulation substance contents in Toona sinensis from different provenances under low temperature stress and their correlation to cold tolerance," *Journal of Plant Resources and Environment*, vol. 23, no. 4, pp. 47–54, 2014.

[22] G. Zhang, J. Bai, M. Xi et al., "Soil quality assessment of coastal wetlands in the Yellow River Delta of China based on the minimum data set," *Ecological Indicators*, vol. 66, pp. 458–466, 2016.

[23] K. K. Meena, A. M. Sorty, U. M. Bitla et al., "Abiotic stress responses and microbe-mediated mitigation in plants: the omics strategies," *Frontiers of Plant Science*, vol. 8, p. 172, 2017.

[24] M. J. Li, D. X. Li, F. J. Feng et al., "Proteomic analysis reveals dynamic regulation of fruit development and sugar and acid

accumulation in apple," *Journal of Experimental Botany*, vol. 67, no. 17, pp. 5145–5157, 2016.

[25] S. L. Xu, R. J. Chalkley, J. C. Maynard et al., "Proteomic analysis reveals O-GlcNAc modification on proteins with key regulatory functions in Arabidopsis," *Proceedings of the National Academy of Sciences USA*, vol. 114, no. 8, pp. E1536–E1543, 2017.

[26] A. Aroca, J. M. Benito, C. Gotor, and L. C. Romero, "Persulfidation proteome reveals the regulation of protein function by hydrogen sulfide in diverse biological processes in Arabidopsis," *Journal of Experimental Botany*, vol. 68, no. 17, pp. 4915–4927, 2017.

[27] Z. Y. Shan, X. L. Luo, M. G. Wei et al., "Physiological and proteomic analysis on long-term drought resistance of cassava (Manihot esculenta Crantz)," *Scientific Reports*, vol. 8, p. 17982, 2018.

[28] M. Fouskaki, K. Karametsi, and N. A. Chaniotakis, "Method for the determination of water content in sultana raisins using a water activity probe," *Food Chemistry*, vol. 82, no. 1, pp. 133–137, 2003.

[29] J. Zhao, J. J. Zhou, Y. Y. Wang, J. W. Gu, and X. Z. Xie, "Positive regulation of phytochrome B on chlorophyll biosynthesis and chloroplast development in rice," *Rice Science*, vol. 20, no. 4, pp. 243–248, 2013.

[30] Y. X. Wang, Y. Hu, B. H. Chen et al., "Physiological mechanisms of resistance to cold stress associated with 10 elite apple rootstocks," *Journal of Integrative Agriculture*, vol. 17, no. 4, pp. 857–866, 2018.

[31] J. J. Sedmak and S. E. Grossberg, "A rapid, sensitive, and versatile assay for protein using Coomassie brilliant blue G250," *Analytical Biochemistry*, vol. 79, no. 1–2, pp. 544–552, 1977.

[32] N. Wang, M. L. Yuan, and F. Yang, "Physiological changes and cold tolerance of three camphor species during natural winter temperature fluctuations," *Journal of Northwest A & F University*, vol. 21, pp. 7–16, 2014.

[33] J. Cox, N. Neuhauser, A. Michalski et al., "Andromeda: a peptide search engine integrated into the MaxQuant environment," *Journal of Proteome Research*, vol. 10, no. 4, pp. 1794–1805, 2011.

[34] L. Yu, W. L. Wang, S. Zeng et al., "Label-free quantitative proteomics analysis of Cytosinpeptidemycin responses in southern rice black-streaked dwarf virus-infected rice," *Pesticide Biochemistry and Physiology*, vol. 147, pp. 20–26, 2018.

[35] W. Yamori, K. Hikosaka, and D. A. Way, "Temperature response of photosynthesis in C3, C4, and CAM plants: temperature acclimation and temperature adaptation," *Photosynthesis Research*, vol. 119, pp. 101–117, 2014.

[36] E. Ghasemie, M. Kazempour, and F. Padasht, "Isolation and identification of Xathomonas oryzae pv. oryzae the causal agent of bacterial blight of rice in Iran," *Journal of Plant Protection Research*, vol. 48, no. 1, pp. 53–62, 2008.

[37] B. Ehlert and D. K. Hincha, "Chlorophyll fluorescence imaging accurately quantifies freezing damage and cold acclimation responses in Arabidopsis leaves," *Plant Methods*, vol. 4, p. 12, 2008.

[38] F. Rizza, D. Pagani, A. Stanca, and L. Cattivelli, "Use of chlorophyll fluorescence to evaluate the cold acclimation and freezing tolerance of winter and spring oats," *Plant Breeding*, vol. 120, no. 5, pp. 389–396, 2001.

[39] A. Aghaee, F. Moradi, H. Zare-Maivan et al., "Physiological responses of two rice (Oryza sativa L.) genotypes to chilling stress at seedling stage," *African Journal of Biotechnology*, vol. 10, no. 39, pp. 7617–7621, 2011.

[40] C. J. Zhang, J. X. Liu, Y. Y. Zhang et al., "Overexpression of SlGMEs leads to ascorbate accumulation with enhanced oxidative stress, cold, and salt tolerance in tomato," *Plant Cell Reports*, vol. 30, pp. 389–398, 2011.

[41] W. Y. Liu, K. M. Yu, T. F. He, D. X. Zhang, and J. X. Liu, "The low temperature induced physiological responses of Avena nuda L., a cold-tolerant plant species," *Science World Journal*, vol. 2013, pp. 1–7, Article ID 658793, 2013.

[42] L. J. Chen, H. Z. Xiang, Y. Miao et al., "An overview of cold resistance in plants," *Journal of Agronomy and Crop Science*, vol. 200, no. 4, pp. 237–245, 2014.

[43] R. E. Blankenship, *Molecular Mechanisms of Photosynthesis*, pp. 149–151, Blackwell Sci, Oxford, UK, 2002.

[44] R. Wang, F. M. Ma, C. F. Li, S. Y. Chen, and J. Hou, "Effect of low temperature stress on proline, malondialdehyde contents and electric conductivity of maize seedling," *Journal of Northwest A & F University*, vol. 39, pp. 20–23, 2008.

[45] Y. Y. Li, L. Pang, Q. W. Chen, Y. Q. Zhou, and C. J. Jiang, "The influence of physiological characteristics of tea tree leaf on low temperature stress," *Journal of Northwest A & F University*, vol. 40, pp. 134–145, 2012.

[46] W. Zhang, T. Yi, Y. Wu, and Y. Song, "Research progress of cold resistance mechanism of cassava," *Agricultural Science & Technology*, vol. 18, no. 9, pp. 1607–1614, 2017.

[47] C. X. Yin, R. X. Yao, and A. M. Qiao, "The response to cold stress and evaluation of cold resistance of five cassava varieties," *Guangdong Agricultural Science*, vol. 39, pp. 30–33, 2012.

[48] Q. F. Huang, X. L. Luo, C. L. Wang, X. L. Lai, and C. L. Wei, "Effects of low temperature stress on physiological and biochemical characteristics of cassava seedling," *Chinese Agricultural Science Bulletin*, vol. 26, no. 17, pp. 172–177, 2010.

[49] M. P. Zunino and J. A. Zygadlo, "Effect of monoterpenes on lipid oxidation in maize," *Planta*, vol. 219, pp. 303–309, 2004.

[50] L. Zhou, K. Liao, L. Wang, Z. Xu, and W. Y. Yang, "Study on resistance to coldness of Prunus divaricate," *Journal of Xinjiang Agricultural University*, vol. 29, no. 1, pp. 47–50, 2006.

[51] X. H. Lu, G. M. Sun, and C. H. Ye, "Changes of membrane permeability, malondialdehyde and chlorophyll content in pineapple seedlings under low temperature stress," *Journal of Anhui Agricultural University*, vol. 38, no. 16, pp. 8374-8375, 2010.

[52] J. Zhang and W. M. Zhu, "Effects of chilling stress on contents of chlorophyll and malondialdehyde in tomato seedlings," *Acta Agriculture Shanghai*, vol. 28, no. 3, pp. 74–77, 2012.

[53] S. L. Wang, H. Y. Huang, J. Tang, R. Q. Wang, and X. Q. Wang, "Effects of low temperature stress on the content of malondialdehyde in rape seedlings," *Hubei Agricultural Sciences*, vol. 51, no. 20, pp. 4467–4469, 2012.

[54] Y. Gao, X. H. Qi, J. H. Yang, and M. F. Zhang, "The response mechanism of cold stress in higher plants," *Northern Horticulture*, vol. 10, pp. 58–61, 2007.

[55] J. G. Wallis, H. Wang, and D. J. Guerra, "Expression of a synthetic antifreeze protein in potato reduces electrolyte release at freezing temperatures," *Plant Molecular Biology*, vol. 35, pp. 323–330, 1997.

[56] T. Gechev, H. Willekens, M. Van Montagu et al., "Different responses of tobacco antioxidant enzymes to light and chilling stress," *Journal of Plant Physiology*, vol. 160, no. 5, pp. 509–515, 2003.

[57] M. Hermes-Lima, "Oxygen in biology and biochemistry: role of free radicals," in *Functional Metabolism: Regulation and Adaptation*, K. B. Storey, Ed., pp. 319–368, John Wiley & Sons Inc., Hoboken, NJ, USA, 2004.

[58] J. C. M. S. Moura, C. A. V. Bonine, J. De Oliveira Fernandes Viana, M. C. Dornelas, and P. Mazzafera, "Abiotic and biotic stresses and changes in the lignin content and composition in plants," *Journal of Integrative Plant Biology*, vol. 52, no. 4, pp. 360–376, 2010.

[59] R. L. Nicholson and R. Hammerschmidt, "Phenolic compounds and their role in disease resistance," *Annual Review of Phytopathology*, vol. 30, pp. 369–389, 1992.

[60] Y. Y. Du, P. C. Wang, J. Chen, and C. P. Song, "Comprehensive functional analysis of the catalase gene family in *Arabidopsis thaliana*," *Journal of Integrative Plant Biology*, vol. 50, no. 10, pp. 1318–1326, 2008.

[61] G. F. Xu, C. Y. Zhang, and Z. X. Xiang, "Comprehensive evaluation of cold resistance on four Lysimachia plants by subordinate function values analysis," *Journal of Northwest Forestry University*, vol. 24, no. 3, pp. 24–26, 2009.

[62] K. Yoshimoto, Y. Takano, and Y. Sakai, "Autophagy in plants and phytopathogens," *FEBS Letters*, vol. 584, no. 7, pp. 1350–1358, 2010.

[63] Y. F. Zhai, M. Guo, H. Wang et al., "Autophagy, a conserved mechanism for protein degradation, responds to heat, and other abiotic stresses in Capsicum annuum L," *Frontiers of Plant Science*, vol. 7, p. 131, 2016.

[64] S. Slavikova, S. Ufaz, T. Avin-Wittenberg, H. Levanony, and G. Galili, "An autophagy-associated Atg8 protein is involved in the responses of Arabidopsis seedlings to hormonal controls and abiotic stresses," *Journal of Experimental Botany*, vol. 59, no. 14, pp. 4029–4043, 2008.

[65] Y. M. Liu, Y. Xiong, and D. C. Bassham, "Autophagy is required for tolerance of drought and salt stress in plants," *Autophagy*, vol. 5, pp. 954–963, 2009.

[66] J. H. Shin, K. Yoshimoto, Y. Ohsumi, J. S. Jeon, and G. An, "OsATG10b, an autophagosome component, is needed for cell survival against oxidative stresses in rice," *Molecules and Cells*, vol. 27, pp. 67–74, 2009.

[67] D. Kuzuoglu-Ozturk, O. C. Yalcinkaya, B. A. Akpinar et al., "Autophagy–related gene, TdAtg8, in wild emmer wheat plays a role in drought and osmotic stress response," *Planta*, vol. 236, pp. 1081–1092, 2012.

[68] D. Pei, W. Zhang, H. Sun et al., "Identification of autophagy-related genes ATG4 and ATG8 from wheat (*Triticum aestivum* L.) and profiling of their expression patterns responding to biotic and abiotic stresses," *Plant Cell Reports*, vol. 33, pp. 1697–1710, 2014.

[69] L. Chen, B. Liao, H. Qi et al., "Autophagy contributes to regulation of the hypoxia response during submergence in *Arabidopsis thaliana*," *Autophagy*, vol. 11, no. 12, pp. 2233–2246, 2015.